UNIVERSITAT POLITÈCNICA DE VALÈNCIA

Departamento de Ingeniería del Terreno
Escuela Tecnica Superior de Ingenieros
de Caminos, Canales y Puertos

The effects of the structure on the mechanical behaviour of young Holocene alluvial materials from the Bormida River (Italy) and Turia River (Spain)

PhD Thesis

by

Miguel Ángel Carrión Carmona

Supervisor

Professor Matthew R. Coop

Co-supervisor

Professor José Joaquín Celma Giménez

January 2016

To my parents

Abstract

The understanding of the mechanical behaviour of natural intact soils is central to engineers when designing new structures. The research carried in this thesis focused on investigating the effects of the naturally occurring in-situ structure on the mechanical behaviour of two shallow recently deposited Holocene alluvial materials, the Bormida River silts (BRS) from Italy and the Valencia silty soils (VSS) from the alluvial plains of the Turia River, Spain. These types of deposits are frequently characterised by highly heterogeneous in-situ structures.

A large range of soils with different size distributions from sands to silty clays were investigated. Oedometer and triaxial tests were carried out on intact, slurry and compacted samples. The first step was to characterise the behaviour of the materials at their reconstituted state to define the reference framework for investigating the effect of the in-situ structure of the intact specimens. The effects of the sample preparation technique on the mechanical behaviour were examined, in particular its influence on the uniqueness of the normal compression line and critical state line. The initial structure created during the preparation of the specimens was totally removed after compression and shearing regardless of the sample preparation method. Only one soil displayed a clear effect of the sample preparation technique, the oedometer compression lines of which remained parallel to each other even at a very high stress levels for the case of the slurry samples. This result showed that contrary to what is stated in the literature the sample preparation technique can created very robust initial structures resulting in a transitional behaviour.

Clears effects of the in-situ structure of the intact samples of the BRS and VSS were observed on the oedometer compression behaviour even at very high stress levels with stress sensitivity values still larger than unity at the end of the tests. It appeared that the effects were more noticeable as the degree of heterogeneity inside the specimens increased at a meso-structure level as it was the case of some samples of the VSS materials which exhibited a certain layering. Small effects of the in-situ structure were seen at large shearing strains and only on the wet side of the critical state.

Resumen

El conocimiento del comportamiento mecánico de los suelos en su estado natural es de importancia capital para los ingenieros a la hora de diseñar nuevas obras. La investigación desarrollada en esta Tesis se centra en descubrir los efectos que tiene la estructura del suelo en su estado natural en la respuesta mecánica de dos suelos aluviales holocenos, depositados superficialmente: los limos del río Bormida (BRS) en Italia y los suelos limosos provenientes de la llanura aluvial del río Turia (VSS) en España. Este tipo de suelos se caracterizan frecuentemente por una estructura inicial altamente heterogénea.

Se ha ensayado una gran variedad de muestras con diferentes granulometrías, desde arenas a arcillas limosas en las que se han realizado ensayos edométricos y triaxiales en muestras intactas, compactadas y en muestras reconstituidas (slurry). En una primera etapa de la investigación se caracterizó la respuesta del material en su estado reconstituido para definir un marco de referencia con el que poder comparar la respuesta de las muestras intactas tomadas in situ y que preservan su estructura natural (inalteradas). Se ha analizado la influencia del modo de preparación de las muestras en su comportamiento mecánico, y, en particular, en la unicidad de las curvas de compresión noval y de estado critico. Se ha comprobado que la estructura inicial inducida durante el proceso de preparación desaparece completamente tras someter la muestra a compresión y corte, independientemente del método de preparación utilizado. Únicamente un suelo mostró, de un modo nítido, el efecto de la técnica de preparación, de modo que las líneas de compresión edométrica se mantuvieron paralelas incluso a niveles de tensión elevados en el caso de muestras reconstituidas (slurry). Este resultado demostró, contrariamente a la opinión aceptada en la bibliografía, que el sistema de preparación de la muestra puede crear una potente estructura inicial dando lugar a un comportamiento de tipo transicional.

En los ensayos de compresión edométrica se ha podido comprobar un claro efecto positivo de la estructura inicial de las muestras intactas, incluso a niveles altos de tensión, observándose índices de sensitividad tensional superiores a uno al final de los ensayos, de modo que para igualdad de índice de huecos, la tensión efectiva vertical de la muestra intacta es superior a la correspondiente en la muestra reconstituida. Aparentemente, este efecto es tanto más significativo cuanto mayor

es el grado de heterogeneidad interno de la muestra a nivel de meso-estructura, como se pudo observar en algunas muestras de los suelos (VSS) que presentaban niveles de laminación horizontal. En los ensayos de corte la influencia de la estructura intacta fue relativamente pequeña y únicamente en el lado húmedo del estado critico.

Resum

Conèixer el comportament mecànic dels sòls en el seu estat natural és d'importància capital per als enginyers a l'hora de dissenyar noves obres. La investigació desenvolupada en aquesta Tesi se centra a descobrir els efectes de l'estructura del sòl en el seu estat natural en la resposta mecànica de dos sòls al · luvials holocens, dipositats superficialment: els llims del riu Bormida (BRS) a Itàlia i els sòls llimosos provinents de la plana al · luvial del riu Túria (VSS) a Espanya. Aquests tipus de sòls es caracteritzen sovint per una estructura inicial altament heterogènia. S'ha assajat una gran varietat de mostres amb diferents granulometries, des d'arenes fins a argiles llimoses amb les quals s'han realitzat assajos edomètrics i triaxials en mostres intactes, compactades i en mostres reconstituïdes (slurry).

En una primera etapa de la investigació es va caracteritzar la resposta del material en el seu estat reconstituït per a definir un marc de referència amb el qual poder comparar la resposta de les mostres intactes preses in situ i que preserven la seua estructura natural (inalterades). S'ha analitzat la influència del mètode de preparació de les mostres en el seu comportament mecànic i en particular, en la unicitat de les corbes de compressió noval i d'estat crític. S'ha comprovat que l'estructura inicial induïda al llarg del procés de preparació desapareix completament després de sotmetre la mostra a compressió i tall, independentment del mètode de preparació utilitzat. Únicament un sòl va mostrar clarament l'efecte de la tècnica de preparació, de manera que les línies de compressió edomètrica es van mantenir paral · leles fins i tot a nivells de tensió elevats en el cas de mostres reconstituïdes (slurry).

Aquest resultat va demostrar, contràriament a l'opinió acceptada en la bibliografia, que el sistema de preparació de la mostra pot crear una potent estructura inicial donant lloc a un comportament de tipus transicional. Als assajos de compressió edomètrica s'ha pogut comprovar un clar efecte positiu de l'estructura inicial de les mostres intactes, inclús a nivells alts de tensió, observant-se índexs de sensitivitat tensional superiors a la unitat al final dels assajos, de manera que per a igualtat d'índex de buits, la tensió efectiva vertical de la mostra intacta és superior a la corresponent en la mostra reconstituïda. Aparentment, aquest efecte és més significatiu quant major és el grau d'heterogeneïtat intern de la mostra a nivell de

meso-estructura, com es va poder observar en algunes mostres dels sòls (VSS) que presentaven nivells de laminació horitzontal. Als assajos de tall la influència de l'estructura intacta va ser relativament petita i únicament en el costat humit de l'estat crític.

Acknowledgements

I want to express my profound gratitude to my supervisor, Professor Matthew Coop, and to my co-supervisor, Professor Joaquín Celma Giménez. Both have taught me an immense amount about Soils Mechanics, how to do research, and more importantly, they have also taught me about life. I am proud to consider them friends as well as colleagues.

I am deeply in debt to Professor Matthew Coop for so many things. He supported my research at every stage; in particular he provided me the support to carry out all the experimental work of this research at the laboratories of the Imperial College. During my trips to Hong Kong, where I travelled to consolidate my research and write up my thesis, he and Dr. Beatrice Baudet treated me like a member of their family. Thank you Matthew and thank you Beatrice.

I am also in debt with Professor Joaquín Celma. I still remember when I told him that I wanted to go to Imperial College to do my PhD, but that I needed someone to help me with my teaching duties at the Technical University of Valencia. He immediately replied that he would take over of all my classes. Unfortunately things were not that easy! But still, here I am writing these acknowledgments. What would I have done without you, Chimo?

I also wish to express my gratitude to all the academic staff of the Soils Mechanics section at Imperial College. Their friendly hospitality made my stay in London highly enjoyable. I also want to thank Dr. Alessandra Nocilla for providing me the block sample of the Bormida River silts and for her instructive discussions. It goes without saying that an experimental thesis such as this requires the help of great technicians to make it possible. Special thanks are due to Mr. Steve Ackerly for his mentorship in the lab. I am also grateful to Mr. Alan Bolsher for his invaluable help. Mr Graham Keefe provided valuable support at crucial moments.

My studies enabled me to befriend wonderful people from all over the world. All of them helped me in different ways, and without them it would not have been possible to complete this journey. I hope I have the good fortune to cross paths with you again.

Finally, a special thank you is to my family for their support and encouragement.

Table of Contents

Abstract **5**
Resumen **7**
Resum **9**
Acknowledgements **11**
Table of Contents **13**
List of Figures **17**
List of tables **31**
Nomenclature **33**
Chapter1 Introduction **37**
1.1 Background 37
1.2 Objectives of this research 38
1.3 Thesis layout 39
Chapter 2 Literature review **41**
2.1 Introduction 41
2.2 Soil structure and definition of reconstituted and remoulded states 41
2.2.1 Fabric 42
2.2.2 Bonding 42
2.2.3 Reconstituted and remoulded states 42
2.3 Mechanical behaviour of reconstituted/remoulded sands 43
2.3.1 Compression behaviour 44
2.3.2 Shearing behaviour at large strains 52
2.4 Mechanical behaviour of intermediate graded soils 69
2.4.1 Packing in intermediate graded soils 69
2.4.2 Effect on the compression line of adding fines to granular soils 74
2.4.3 Effects on the critical state line of adding fines to granular soils 76
2.4.4 Effects of sample preparation technique on the NCL and CSL/SSL 80
2.5 Transitional soil behaviour 81
2.5.1 Definition of transitional soil behaviour 82
2.5.2 Previous investigations of transitional soils 85
2.5.3 Effect of sample preparation method on transitional behaviour 93
2.6 Summary on the behaviour of reconstituted/remoulded soils 100
2.7 Mechanical behaviour of natural soils 103
2.7.1 One-dimensional compression behaviour of natural clays 103
2.7.2 Sedimentation and post-sedimentation structure 106

2.7.3 The sensitivity framework 107
2.7.4 Stability of structure after gross yield 109
2.7.5 Summary 114
Chapter 3 Laboratory equipment, sample preparation and testing procedures 117
3.1 Introduction 117
3.2. Oedometer apparatus 117
3.3 Triaxial apparatus 119
3.3.1. Introduction 119
3.3.2 Bishop & Wesley triaxial apparatus 119
3.3.3 7MPa triaxial apparatus 120
3.4 Instrumentation to measure stress and strain 121
3.4.1 Stress measurements 121
3.4.2 Strain measurements 122
3.5 Control and data logging system 124
3.6 Calibration 125
3.7 Sample preparation and testing procedures 125
3.7.1 Oedometer tests 125
3.7.2 Triaxial tests 130
Chapter 4 The Bormida River Silts 137
4.1 Introduction 137
4.2 The Bormida River silts 137
4.2.1 Characterization of the Bormida River silts: index properties 140
4.2.2 Summary of the index properties of the Bormida River silts 148
4.3 Previous investigations of the mechanical behaviour of the BRS 149
4.3.1 Previous investigations on the BR 149
4.3.2 Previous investigations of the mechanical behaviour of the silty soils from the Po River 150
4.4. Summary of soils reviewed 166
Chapter 5 Mechanical behaviour of the Bormida River Silts 169
5.1 Introduction 169
5.2 Oedometric compression behaviour 169
5.2.1 Calculation of the initial void ratio 170
5.2.2 Compression behaviour of the Bormida clayey silt (BRS-B) 171
5.2.3 Compression behaviour of the Bormida sandy silt (BRS-E) 189
5.2.4 Influence of the initial structure on the compression behaviour of the BRS soils 193
5.2.5 Summary of the compression behaviour 199
5.3 Triaxial behaviour of the Bormida River clayey silt (BRS-B) 201
5.3.2 Compression behaviour of slurry and compacted samples 204
5.3.3 Shearing behaviour of the slurry and compacted samples 219

5.3.4 Compression behaviour of intact samples 232
5.3.5 Shearing behaviour of intact samples 236
5.3.6 Stiffness data 246
Chapter 6 The Valencia Silty Soils 257
6.1 Introduction 257
6.2 The Valencia silty soils 257
6.2.1 Characterization of the Valencia silty soils: index properties 259
6.2.2 Summary of the index properties of the Valencia silty soils 268
6.3 Previous investigations on the mechanical behaviour of the Valencia silty soils 269
Chapter 7 The mechanical behaviour of the Valencia Silty Soils 271
7.1 Introduction 271
7.2 Oedometric behaviour 271
7.2.1 Oedometric behaviour of the Valencia silty clay soil (VMClay) 272
7.2.2 Oedometric behaviour of the Valencia silty sand (VMSand) 283
7.2.3 Oedometric behaviour of the Valencia sandy silt/clay (VSSilt) 289
7.2.4 Summary 291
7.3 Triaxial behaviour of the Valencia silty clay (VMClay 293
7.3.1 Compression behaviour of the slurry samples 293
7.3.2 Large strain behaviour of the slurry samples 298
7.3.3 Compression behaviour of the intact samples 304
7.3.4 Large shearing behaviour of the intact samples 307
7.3.5 Stiffness data 317
Chapter 8 Discussion 323
8.1 Introduction 323
8.2 Index properties 324
8.3 Oedometric compression behaviour 326
8.3.1 Slurry and compacted behaviour 327
8.3.2 Intact behaviour 331
8.4 Shearing behaviour at large strains 335
8.4.1 Slurry and compacted behaviour 342
8.4.2 Intact behaviour 344
8.5 Shearing behaviour at small strains 347
Chpater 9 Conclusions and recommendations for future work 353
9.1 Conclusions 353
9.2 Recommendations for future work 358
References 359

List of Figures

Figure 2.1 Isotropic compression behaviour of three different sands (Coop & Lee, 1993) 45
Figure 2.2 (a) Isotropic and (b) one-dimensional compression behaviour of Dogs Bay sand (Coop, 1990) 46
Figure 2.3 Conceptual model of first loading and unloading of freshly deposited cohesionless soils (Pestana & Whittle, 1995) 47
Figure 2.4 Definition of relative breakage (Br) base don Hardin (1985) (redrawn by Coop et al., 2004) 48
Figure 2.5 Compression behaviour of Ottawa sand (Mesri & Vardhanabhuti, 2009) 48
Figure 2.6 Comparison of $(\sigma'_v)_{MC}$ and $(\sigma'_v)_{Mmax}$ (Mesri & Vardhanabhuti, 2009) 49
Figure 2.7 Compression behaviour of Toyura sand (a) one-dimensional compression (b) isotropic compression (Mesri & Vardhanabhuti, 2009) 50
Figure 2.8 Particle breakage (Br) for (a) Dogs Bay sand (b) decomposed granite and (c) Ham River sand (Coop & Lee, 1993) 51
Figure 2.9 Isotropic compression of Erksak sand. First loading (Jefferies & Been, 2000) 53
Figure 2.10 Expanded views of Figure 2.9. Isotropic behaviour showing loading and unloading paths (Jefferies & Been, 2000) 53
Figure 2.11 Consolidation characteristics of samples prepared by: (a) moist placement (b) dry deposition (c) water sedimentation (Ishihara, 1993) 54
Figure 2.12 Comparison of critical state (CS) – steady state (SS) from drained and undrained tests on Erksak sand (Been et al., 1991) 55
Figure 2.13 State diagram evaluated from both drained and undrained triaxial tests on Toyura sand (Verdugo & Ishihara, 1996) 55
Figure 2.14 Effect of initial state on the crtitical state (Been et al., 1991) 56
Figure 2.15 Effect of sample preparation method on the critical state line for Erksak sand (Been et al., 1991) 57
Figure 2.16 Steady state line established from two kinds of samples prepared by different methods (Ishihara, 1993) 57
Figure 2.17 Critical state lines of three sands (Coop & Lee, 1993) 58
Figure 2.18 Effect of stress path on the critical state line of Erksak sand (extension versus compression) (Been et al., 1991) 59

Figure 2.19 Effect of stress path on the critical state line of Toyura sand (extension versus compression) (Been et al., 1991) 59
Figure 2.20 Steady state lines from undrained simple shear testing compared to SSLs in undrained compression and extension tests (Riemer & Seed, 1997) 60
Figure 2.21 Influence of the initial density and compression history on the critical state for (a) masonry and (b) concrete sands (Finno & Rechenmacher, 2003) 61
Figure 2.22 End points of constant p' shearing tests on assemblies of agglomerates; effect of precompression on final state (Data from Cheng et al., 2005) (redrawn by Muir Wood, 2008) 62
Figure 2.23 Fractal limiting particle size distribution and definition of grading state index I_G (Muir Wood & Maeda, 2008) 63
Figure 2.24 Critical state surface in v:logp':I_G space (Muir Wood & Maeda, 2008) 63
Figure 2.25 Critical state lines for Dogs Bay sand after second shearing stage (Bandini & Coop, 2011) 65
Figure 2.26 Critical state line for reconstituted samples of Dogs Bay sand with the same grading as the pre-sheared ones (Bandini & Coop, 2011) 65
Figure 2.27 NCL and CSL of the original and damaged OT sand (Sadrekarimi & Olson, 2011) 66
Figure 2.28 NCL and CSL of the original and damaged IR sand (Sadrekarimi & Olson, 2011) 66
Figure 2.29 Relative breakage of Dogs Bay sand in ring shear tests under different normal stresses (Coop et al., 2004) 67
Figure 2.30 Evolution of mobilised shear strength angle with shear strain (Coop et al., 2004) 68
Figure 2.31 Idealised critical state line for a sand (Konrad, 1998) 68
Figure 2.32 General critical state line shape for sands (Russell & Khalili, 2004) 69
Figure 2.33 Ideal packings of uniform spheres: (a) simple cubic, (b) cubic tetrahedral, (c) tetragonal sphenoidal, (d) pyramidal and (e) tetrahedral (Mitchell, 1993) 70
Figure 2.34 Theoretical variation of minimum void ratio in a binary packing with % fines (Lade et al., 1998) 71
Figure 2.35 Influence of adding non-plastic fines on the maximum and minimum void ratios of Ottawa sand (Lade & Yamamuro, 1997) 71
Figure 2.36 Intergranular classification (Thevanayagam et al., 2002) 72
Figure 2.37 Isotropic compression of samples with and without fines (Coop & Atkinson, 1993) 74
Figure 2.38 One-dimensional compression behaviour of silt and sand mixtures (Carrera et al., 2011) 75
Figure 2.39 One-dimensional compression curves of three different mixtures considering the equivalent intergranular specific volume (Carrera et al., 2011) 76
Figure 2.40 Steady state lines for Kogyuk 350 sand with different silt contents (Been & Jefferies, 1985) 77

Figure 2.41 Grain size distributions for F55 Foundry sand mixed with fines at different proportions (Thevanayagam et al., 2002) 78
Figure 2.42 Steady state lines for F55 Foundry sand mixed with fines at different proportions (Thevanayagam et al., 2002) 78
Figure 2.43 Steady state lines for triaxial tests on samples prepared by different techniques and at different fines contents (Naeini & Baziar, 2003) 81
Figure 2.44 One-dimensional compression tests on compacted and remoulded (slurry) samples of the Metramo silty sand (Santucci de Magistris et al., 1998) 82
Figure 2.45 Schematic illustration of the compression behaviour of clays, clean sands and transitional soils 83
Figure 2.46 Schematic illustration of the CSL of clays, clean sands and transitional soils 84
Figure 2.47 Grain size distributions of BRS and SK soils (Martins et al., 2001) 85
Figure 2.48 One-dimensional compression lines of BRS soil (a) slurry samples (b) air pluviated and compacted samples (Martins et al., 2001) 86
Figure 2.49 One-dimensional compression lines of BRS and SK samples (Martins et al., 2001) 86
Figure 2.50 One-dimensional compression tests on remoulded and reconstituted samples of BRS (Ferreira & Bica, 2006) 87
Figure 2.51 Critical state line of natural intact samples of BRS (Ferreira & Bica, 2006) 87
Figure 2.52 Critical state lines of remoulded samples of BRS (Ferreira & Bica, 2006) 88
Figure 2.53 Grading curves of an Italian silt with different clay contents (NS25: natural sample; O: reconstituted samples after oedometer testing to 14 MPa; T: reconstituted sample after triaxial testing from p_0' = 600 kPa) (Nocilla et al., 2006) 89
Figure 2.54 One-dimensional compression lines of an Italian silt (a) 45% clay content (b) 25% clay content (c) 8% clay content (d) 3.5% clay content (Nocilla et al., 2006) 89
Figure 2.55 Isotropic NCL and critical state lines for reconstituted/remoulded samples of and Italian silt (a) 45% clay content (b) 25% clay content (Nocilla et al., 2006) 90
Figure 2.56 Critical states for reconstituted/remoulded samples of silts with 8% of clay content (Nocilla et al., 2006) 91
Figure 2.57 One-dimensional compression lines of the plastic and non-plastic transitional soil mixtures (Shipton, 2010) 91
Figure 2.58 Isotropic and one-dimensional compression behaviour of the non-plastic transitional mixture (Shipton, 2010) 92
Figure 2.59 Isotropic compression paths, end of shearing points and assumed CSLs for the groups of triaxial test samples with similar initial densities for the plastic transitional soil (Shipton, 2010) 92

Figure 2.60 Grading curves for soils that displayed transitional behaviour (Shipton, 2010) 93
Figure 2.61 One-dimensional compression curves of Italian silty soil with 8% of clay content (a) dry and wet compaction samples (b) slurry samples (redrawn from Nocilla et al., 2006) 97
Figure 2.62 One-dimensional compression curves of Italian silty soil with 3.5% of clay content (a) dry and wet compaction samples (b) slurry samples (redrawn from Nocilla et al., 2006) 98
Figure 2.63 One-dimensional compression curves of Botucatu sandstone (a) air-dry and wet compaction samples (b) slurry samples (redrawn from Ferreira and Bica, 2006) (redrawn from Nocilla et al., 2006) 98
Figure 2.64 One-dimensional compression curves of Italian silt (a) air-dry and wet compaction samples (b) slurry samples (redrawn form Radici, 2006) 99
Figure 2.65 One-dimensional compression curves for the non-plastic transitional soil mixture consisted of 75% Redhill sand and 25% crushed quarz silt: dry and wet compaction samples (NP01, NP03, NP05); slurry samples (NP02, NP04) (Shipton, 2010) 99
Figure 2.66 State parameters that relate the current state to the critical state line (Mitchell & Soga, 2005) 101
Figure 2.67 Sedimentation compression curves for normally consolidated argillaceous sediments (Skempton, 1970) 104
Figure 2.68 Intrinsic compression line and sedimentation compression line (Burland, 1990) 105
Figure 2.69 Responses of clays under one-dimensional compression: (a) sedimentation structure (b) post-sedimentation structure (Cotecchia & Chandler, 2000) 106
Figure 2.70 Idealized sensitivity framework in the Iv:logσ'_v plane (Cotecchia & Chandler, 2000) 107
Figure 2.71 Idealized sensitivity framework in the q:p':v space for a clay with a sedimentation structure (Cotecchia & Chandler, 2000) 108
Figure 2.72 Normilized oedometer compression behaviour of structurally complex clays and clay shales (Fearon & Coop, 2002) 109
Figure 2.73 Normilized oedometer compression behaviour of structurally complex scaly clays and bentonite samples (Vitone & Cotecchia, 2011) 109
Figure 2.74 Oedometer compression behaviour of structurally complex soils: (a) meta-stable structure in Bothkennar clay (Smith et al., 1992) (b) stable structure in Sibari clay (Coop & Cotecchia, 1995) 111
Figure 2.75 Oedometer compression behaviour of Pisa upper clay layer B "Pancone clay" (Rampello & Callisto, 1998; data from Callisto, 1996) 112
Figure 2.76 Normilised oedometer compression behaviour of Pisa clayey silts from layer A1 (Rampello & Callisto, 1998) 112

Figure 2.77 Normilised shearing behaviour of the Bothkennar clay after gross yield (Smith et al., 1992) 113
Figure 2.78 Normilised shearing behaviour of the Sibari clay after gross yield (Coop & Cotecchia, 1995) 113
Figure 2.79 Normilised behaviour of the scaly clay SCM (Vitone & Cotecchia, 2011) 114
Figure 3.1 Modified oedometer cell to flush water through the sample from the bottom to the top under a pressure of 10kPa 118
Figure 3.2 Schematic diagram of the Bishop & Wesley triaxial apparatus (modified from Qarimi, 2005) 120
Figure 3.3 The 7MPa triaxial apparatus 121
Figure 3.4 Imperial College inclinometers (Kuwano, 1990, adapted from Jardine et al., 1984) 123
Figure 3.5 Local LVDTs for measuring axial and radial strains of samples 124
Figure 3.6 Imperial College volume gauge (modified from Head, 1985) 124
Figure 3.7 Equipment used for the static compaction 128
Figure 3.8 Schematic representation of the equipment used for creating the vertical holes in the compacted samples 128
Figure 3.9 Oedometer sample after holes were drilled 128
Figure 3.10 38mm diameter floating ring consolidometer 131
Figure 3.11 (a) Large consolidometer cell with a diameter of 230mm (b) “cake” sample after being removed from consolidometer 131
Figure 3.12 Trimming procedure of the (a) BRS and (b) VSS intact samples 132
Figure 3.13 Schematic drawing of the load cell connection using a suction cap (modified from Carrera, 2006) 134
Figure 4.1 (a) Castellazo Bormida, Alessandria province, Italy (b) Enlargement of the Geological map of the Alessandria region 138
Figure 4.2 Po River main stream and tributary rivers 139
Figure 4.3 Sampling process of the BRS (modified from Radici, 2006) 139
Figure 4.4 Particle size distributions of the BRS soils. Six samples taken from different parts of the block (BRS-B) and two samples of the excavated material (BRS-E) 140
Figure 4.5 Schematic diagram of the QicPic apparatus (http://www.sympatec.com) 141
Figure 4.6 Particle size distributions; comparison between sieving and QicPic analyses for the sandy fraction of the BRS-B sample 142
Figure 4.7 Digital microscope photo of the BRS-B; material retained on the 63μm sieve after washing 143
Figure 4.8 Digital microscope photos of; (a) the BRS-B sample, particle size 180μm<D<300μm and (b) the BRS-E sample, particle size 160μm<D<400μm 143
Figure 4.9 Digital microscope photos of the material passing the 63μm sieve: (a) BRS-B sample and (b) BRS-E sample 143

Figure 4.10 Interlayer particle of illite and smectite (Altaner & Ylagan, 1997).... 145
Figure 4.11 Casagrande plasticity chart for samples of the BRS in Table 4.4..... 146
Figure 4.12 Plant root in a sample of the BRS-B..... 147
Figure 4.13 One-dimensional compression curves of intact samples of the BRS-B (redrawn from Radici, 2006)..... 150
Figure 4.14 Particle size distributions range of the materials commonly used in the construction of the Po River embankments (redrawn from Colombo, 1965) 152
Figure 4.15 X-ray diffraction patterns comparison of a powder sample of (a) clayey silt with 25% of clay (Nocilla et al., 2006) and (b) BRS-B. Axis x is in lin (counts) and y is 2θ 152
Figure 4.16 Free swelling tests results of the laboratory compacted silty samples at the standard Proctor energy (Colleselli et al., 1980) 154
Figure 4.17 Oedometer compression curves for in-situ and laboratory compacted silty samples from the Po River (Colleselli et al., 1980)..... 154
Figure 4.18 CIU triaxial tests on in-situ and laboratory compacted silty samples from the Po River (Colleselli et al., 1980) 155
Figure 4.19 Oedometer compression behaviour of a silty soil from the Po River embankments at Viadana (Sciotti and Jommi, 2003)..... 157
Figure 4.20 Oedometer compression curves for intact samples of a clayey/sandy silt from the Po River at Viadana (redrawn from De'Angelis & Molteni, 2004)..... 158
Figure 4.21 Comparison of the oedometer compression behaviour of the silty soils from the Po River at Viadana 159
Figure 4.22 Soil profile and location of the experimental embankment constructed inside the Po River channel at Viadana, Lombardia region (AIPO, 2004) 159
Figure 4.23 Particle size distributions of layer T2 (data from AIPO, 2004 and Nocilla et al., 2006)..... 160
Figure 4.24 Stress paths of a silty soil with a clay content of: (a) 45% (b) 25% (c) 8% and (d) 3.5% (Nocilla et al., 2006) 161
Figure 4.25 Stress-dilatancy plot for drained triaxial tests of a silty soil with diffrent clay contents (Nocilla et al., 2006)..... 161
Figure 4.26 Normalised stress paths for drained and undrained triaxial tests on a silty soil with a clay content of: (a) 45% (b) 25% and(c) 8% (Nocilla et al., 2006) 162
Figure 4.27 Triaxial and oedometer data for intact silty samples with clay contents of: (a) 39-53.3% (b) 29-30% (c) 20-25.5% and (d) 13-16% (Nocilla & Coop, 2008) 164
Figure 4.28 Influence of the clay content on: (a) the location of the CSL in the compression plane and (b) the M value for the intact silty samples (Nocilla & Coop, 2008)..... 164
Figure 4.29 Particle size distributions of soils with same fine content (data from AIPO, Final Report, 2004 and Nocilla et al., 2006) 165

Figure 4.30 Comparison of the compression curves of the intact silty samples with the same fine content tested by Nocilla et al. (2006) and AIPO (2004) 165
Figure 4.31 Comparison of the compression behaviour of the intact and slurry samples of the silty soils retrieved from Viadana. Quantification of the effect of the in-situ structure 166
Figure 5.1 Oedometer compression of the slurry samples of the clayey silt (BRS-B) 172
Figure 5.2 Oedometer compression behaviour of the slurry sample BRS-B-OS4 during unload-reload cycles..... 173
Figure 5.3 Oedometer tangent moduli (M_{oed}) of the slurry samples of the BRS-B soil..... 175
Figure 5.4 Oedometer tangent moduli (M_{oed}) and oedomerter compression curve of the slurry sample BRS-B-OS4 175
Figure 5.5 Comparison of oedometer compression curves of sample BRS-B-OS7 prepared with the original grading of the BRS-B material, with sample BRS-B-OS9 preparaed by re-using the same soil of tests BRS-B-OS7 and BRS-B-OS8 after being one-dimendionally compressed to 12.5MPa..... 176
Figure 5.6 Oedometer compression of the remoulded compacted samples of the BRS-B 179
Figure 5.7 Oedometer compression of the remoulded compacted samples of the BRS-B with holes..... 180
Figure 5.8 Oedometer compression lines of all the remoulded compacted samples of the BRS-B soil 181
Figure 5.9 Correlation between initial void ratio after soaking anf yield stress for all the remoulded compacted samples of the BRS-B 182
Figure 5.10 Oedometer tangent moduli (M_{oed}) of the remoulded compacted samples of the BRS-B..... 183
Figure 5.11 Oedometer compression of the intact samples of the BRS-B 185
Figure 5.12 Oedometer compression of a sample saturated by flooding the oedometer cell (BRS-B-OI4) and another sample saturated by circulating a back pressure of 10kPa for one week (BRS-B-OI8)..... 185
Figure 5.13 Comparison of the one-dimensional compression behaviour of an intact sample (BRS-B-OI1) with a compacted sample (BRS-B-OC5) 186
Figure 5.14 Correlation between the initial void ratio after soaking and the yield stress for all the remoulded compacted and intact samples of the BRS-B 187
Figure 5.15 Oedometer tangent moduli (M_{oed}) of the intact samples of the BRS-B 188
Figure 5.16 Oedometer tangent moduli (M_{oed}) of the intact samples of the BRS-B. Effect of initial sweeling on the compression behaviour 188
Figure 5.17 Oedometer compression of the slurry samples of the BRS-E 190
Figure 5.18 Comparison of the oedometer compression lines of the slurry samples of the clayey silt (BRS-B) and sandy silt (BRS-E) 190

Figure 5.19 Oedometer compression of the compacted samples of the BRS-E..... 192
Figure 5.20 Oedometer tangent moduli (M_{oed}) of the slurry and compacted samples of the BRS-E..... 192
Figure 5.21 Comparison between the intrinsic compression line 1D-ICL* of the BRS-B and the ICL proposed by Burland (1990) 193
Figure 5.22 Comparison between the normalized compression lines of the BRS-B intact samples, the measured 1D-ICL* and the SCL 194
Figure 5.23 Comparison between the normalized compression lines of the BRS-B intact samples and two other Holocene natural materials (data from Burland, 1990; Smith, 1992 and Coop & Cotecchia, 1995) 195
Figure 5.24 Comparison between the normalized compression lines of the BRS-B compacted samples, the measured 1D-ICL* and the SCL 196
Figure 5.25 Comparison of the oedometric tangent moduli (M_{oed}) for intact and slurry samples of the BRS-B..... 197
Figure 5.26 Comparison of the oedometric tangent moduli (M_{oed}) for remoulded compacted and slurry samples of the BRS-B..... 197
Figure 5.27 Effect of the sample preparation method on the uniqueness of the normal compression lines of the BRS-E sandy silt 198
Figure 5.28 Comparison of the oedometric tangent moduli for the clayey silt (BRS-B), the sandy silt (BRS-E) and soils from the Venice lagoon (data redrawn from Simonini et al., 2007) 199
Figure 5.29 Deformation mechanisms during shearing of (a) slurry sample BRS-B-TS7 (b) slurry sample BRS-B-TS8-ko (c) compacted sample BRS-B-TC2 (d) intact sample BRS-B-TI7 (e) intact sample BRS-B-TI4 and (f) intact sample BRS-B-TI9 204
Figure 5.30 Isotropic compression of the slurry samples of the BRS-B clayey silt 206
Figure 5.31 Strain ratio measured during the isotropic compression of the slurry samples BRS-B-TS4, BRS-B-TS5 and BRS-B-TS6 207
Figure 5.32 Estimated isotropic intrinsic compression line (ICL*) of the slurry samples of the BRS-B clayey silt 209
Figure 5.33 Isotropic compression lines of the slurry and compacted samples of the BRS-B clayey silt 209
Figure 5.34 Anisotropic stress path under ko conditions of (a) slurry sample BRS-B-TS8-ko and (b) compacted sample BRS-B-TC5-ko 210
Figure 5.35 ko compression stress path of slurry sample BRS-B-TS8-ko and compacted sample BRS-B-TC5-ko..... 211
Figure 5.36 Radial strains measured during ko compression of slurry sample BRS-B-TS8-ko and compacted sample BRS-B-TC5-ko 211
Figure 5.37 Variation of the coefficient of earth pressure at rest during the anisotropic normal compression of slurry sample BRS-B-TS8-ko and compacted sample BRS-B-TC5-ko..... 212

Figure 5.38 Anisotropic stress path under ko conditions of slurry sample BRS-B-TS8-ko in the planes (a) q:p' and (b) v:p' 213
Figure 5.39 Unload-reload stress paths under ko conditions of slurry sample BRS-B-TS8-ko in the planes (a) η:p'/p'$_{max(NC)}$ and (b) η:log(p'/p'$_{max(NC)}$) 215
Figure 5.40 Variation of the coefficient of earth pressure at rest with p' for slurry sample BRS-B-TS8-ko 216
Figure 5.41 Variation of the coefficient of earth pressure plotted against the OCR for slurry sample BRS-B-TS8-ko (a) unload-reload cycle (b) comparison of computed and experimental data 217
Figure 5.42 ko and isotropic compression lines of the slurry and compacted samples of the BRS-B clayey silt. Comparison with the estimated ICL* and 1D-ICL* 218
Figure 5.43 Normalized swelling lines of isotropic BRS-B-TS6 and anisotropic BRS-B-TS8-ko samples 219
Figure 5.44 Variation of (a) deviator stress and increment of pwp and (b) mean effective stress during undrained shearing of BRS-B slurry samples 221
Figure 5.45 Undrained and drained stress paths of slurry samples of the BRS-B. 222
Figure 5.46 Variation of deviator stress and volume strain during drained shearing of samples BRS-B-TS4 and BRS-B-TS5 223
Figure 5.47 Normalized stress-strain behaviour for the slurry samples of the BRS-B 224
Figure 5.48 Shearing stress paths in the v:logp' palne for the slurry samples of the BRS-B 225
Figure 5.49 Relationship between undrained shear strength and specific volume for the slurry samples of the BRS-B 226
Figure 5.50 Normalized triaxial shearing data of slurry samples of the BRS-B using equivalent pressures on the intrinsic critical state line (CSL*) 226
Figure 5.51 Variation of (a) deviator stress and increment of pwp and (b) mean effective stress during undrained shearing of compacted samples of the BRS-B ... 228
Figure 5.52 Undrained stress paths of compacted samples of the BRS-B 230
Figure 5.53 Normalized stress-strain behaviour for the compacted samples of the BRS-B 230
Figure 5.54 Unique critical state line for the slurry and compacted samples of the BRS-B 231
Figure 5.55 Relationship between undrained shear strength and specific volume for the slurry and compacted samples of the BRS-B 232
Figure 5.56 Isotropic compression lines for the intact samples of the BRS-B 233
Figure 5.57 Isotropic compression lines of the intact samples of the BRS-B. Comparison with the isotropic ICL* defined by the slurry samples 235
Figure 5.58 Strain ratios measured during isotropic compression of two intact samples BRS-B-TI2 and BRS-B-TI3. Comparison with slurry sample BRS-B-TS4 236

Figure 5.59 Variation of (a) deviator stress and increment of pwp and (b) mean effective stress during undrained shearing of intact samples of the BRS-B 237
Figure 5.60 Variation of (a) deviator stress and increment of pwp and (b) mean effective stress during undrained shearing of intact samples of the BRS-B at high confining stresses..... 239
Figure 5.61 Variation of deviator stress and volume strain during drained shearing of intact sample BRS-B-TI10..... 240
Figure 5.62 Undrained and drained stress paths of intact samples of the BRS-B at lower confining stresses..... 241
Figure 5.63 Undrained and drained stress paths of intact samples of the BRS-B. 242
Figure 5.64 Normalized stress-strain behaviour for the intact samples of the BRS-B 243
Figure 5.65 Compression and shearing stress paths in the v:logp' plane for the intact samples of the BRS-B..... 244
Figure 5.66 Normalized triaxial shearing data of intact samples of the BRS-B using the equivalent pressure on the intrinsic critical state line (CSL*) 245
Figure 5.67 Degradation of undrained secant Young's modulus with strain for the normally consolidated slurry samples BRS-B-TS1, BRS-B-TS7 and overconsolidated sample BRS-B-TS6 sheared at different mean effective stress levels 247
Figure 5.68 Effect of the OCR on the normalized undrained secant Young's modulus for the slurry samples of the BRS-B 248
Figure 5.69 Effect of the OCR on the undrained compression stiffness (Jardine,1995) 249
Figure 5.70 Degradation of undrained secant Young's modulus with strain for the normally consolidated compacted samples BRS-B-TC1 and BRS-B-TC4 sheared at different mean effective stress levels 249
Figure 5.71 Comaprison of the normalized undrained Young's modulus between normally consolidated slurry (TS) and compacted (TC) samples of the BRS-B... 250
Figure 5.72 Degradation of undrained secant Young's modulus with strain for the intact samples of the BRS-B sheared at different mean effective stress levels 251
Figure 5.73 Effect of the in-situ structure on the stiffness of the BRS-B. Comaprison between intact (TI), compacted (TC) and slurry (TS) samples sheared at p'=400kPa 252
Figure 5.74 Effect of the in-situ structure on the stiffness of the BRS-B. Comaprison between intact (TI), compacted (TC) and slurry (TS) samples sheared at p'=200kPa and p'=500kPa 253
Figure 5.75 Undrained secant Young's modulus as a function of the current mean effective stress at various strsin levels for the slurry, compacted and intact normally consolidated samples of the BRS-B 255
Figure 6.1 Geomorphological map of the Turia River coastal plains (Carmona & Ruiz, 2011)..... 258

Figure 6.2 Geomorphological map of the Turia River coastal flood plains and location where the block and remoulded samples of the VSS tested in this research project were retrieved (modified Carmona & Ruiz, 2011) 258
Figure 6.3 Soil profile at the General Urrutia underground station where the block sample of the VSS was retrived 259
Figure 6.4 Sampling process of the intact block of the VSS obtained from the excavation works of the T2 underground line extension to the south of the city of Valencia at the General Urrutia underground station 260
Figure 6.5 Particle size distributions of the Valencia silty soils tested in this research project 261
Figure 6.6 Samples of the aggregates of cemented particles found in the clayey silt block sample 262
Figure 6.7 Back scattered electron microscopy image of an aggregate of particles cemented by calcium carbonate with EDX analysis locations 262
Figure 6.8 Energy dispersive X-ray spectroscopy (EDX) analysis of the aggregate shown in Figure 6.7 at different locations: (a) silt particle (location 1) and (b) calcium carbonate cement (location 2) 263
Figure 6.9 Comparison of digital microscope photos of soil particles with 180μm<D<300μm: (a) Italian clayey silt (BRS-B) and (b) Valencia silty sand (VMSand) 264
Figure 6.10 Comparison of digital microscope photos of soil particles passing 63μm sieve: (a) Italian clayey silt (BRS-B) and (b) Valencia silty sand (VMSand) 264
Figure 6.11 Casagrande plasticity chart of the Valencia silty soils for the samples included in Table 6.3 266
Figure 6.12 Electron microscopy images of silt particles nonded by calcium carbonate found in an intact sample of the silty clay soil (VMClay) from the block 267
Figure 7.1 Oedometer compression of the slurry samples of the Valencia silty clay (VMClay) 273
Figure 7.2 Comparison of the compression of the slurry (OS), cake (OSC) and compacted (OC) samples of the VMClay 274
Figure 7.3 Oedometric tangent moduli (M_{oed}) of the slurry samples of the VMClay 275
Figure 7.4 Comparison between oedometric tangent moduli (M_{oed}) of the slurry, cake and compacted samples of the VMClay 276
Figure 7.5 Oedometer compression of the intact samples of the VMClay 278
Figure 7.6 Oedometer compression of some intact samples of the VMClay with different grading curves 279
Figure 7.7 Comparison between the oedometer compression of the intact and slurry samples of the VMClay 280
Figure 7.8 Normalized data (a) oedometer compression of the intact samples and (b) in-situ states of the VMClay 281

Figure 7.9 Oedometric tangent moduli (M_{oed}) of the intact samples of the VMClay 284
Figure 7.10 Oedometer compression of the compacted samples of the Valencia silty sand (VMSand). Notation OWC: oedometer wet compaction; ODC: oedometer air-dried compaction..... 285
Figure 7.11 Particle breakage of the VMSand: (a) grading curves before and after the oedometer test and (b) relative breakage based on Hardin (1985) definition . 287
Figure 7.12 Oedometric tangent moduli (M_{oed}) of the compacted samples of the VMSand 288
Figure 7.13 Oedometer compression lines of the slurry (OS) and compacted (OWC) samples of the Valencia sandy silt/clay (VSSilt)..... 290
Figure 7.14 Oedometric tangent moduli (M_{oed}) of the slurry and compacted samples of the VSSilt 290
Figure 7.15 Unique normal compression lines of the Valencia silty soils (VSS).... 292
Figure 7.16 Oedometric tangent moduli (M_{oed}) of the Valencia silty soils (VSS).. 292
Figure 7.17 Isotropic compression of the slurry cake samples of the VMClay 294
Figure 7.18 Strain ratio measured during isotropic loading and unloading stress increments of the slurry cake samples of the VMClay 295
Figure 7.19 Anisotropic compression stress paths under ko conditions of two slurry cake samples of the VMClay..... 296
Figure 7.20 Comparison between the isotropic, ko and oedometric compression paths of the slurry cake samples of the VMClay..... 297
Figure 7.21 Variation of (a) deviator stress and increment of pwp and (b) mean effective stress during undrained shearing of the slurry cake samples of the VMClay 299
Figure 7.22 Undrained stress paths of the slurry cake samples of the VMClay 300
Figure 7.23 Normalized stress-strain behaviour of the slurry cake samples of the VMClay..... 301
Figure 7.24 Undrained shearing stress paths and critical state line in the v:logp' plane of the slurry cake samples of the VMClay 302
Figure 7.25 Comparison of the undrained shear strengths predicted by the Cam clay model and the experimental results for the slurry cake samples of the VMClay 303
Figure 7.26 Normalized undrained shearing stress paths of the slurry cake samples of the VMClay using an equivalent pressure on the intrinsic critical state line (CSL*) 303
Figure 7.27 Isotropic compression of the intact samples of the VMClay 305
Figure 7.28 Strain ratios measured during isotropic loading stress increments for the intact samples of the VMClay..... 307
Figure 7.29 Shear mechanisms of (a) slurry sample VMClay-TSC1 (b) slurry sample VMClay-TSC2 (c) and (d) intact sample VMClay-TIV4..... 308

Figure 7.30 Variation of (a) deviator stress and increment of pwp and (b) mean effective stress during undrained shearing of the intact samples of the VMClay..309
Figure 7.31 Variation of (a) deviator stress and increment of pwp and (b) mean effective stress during undrained shearing of the intact sample VMClay-TIV2 at a high confining pressure 310
Figure 7.32 Normalized increment of pore water pressure during undrained shearing of the intact samples of the VMClay 311
Figure 7.33 Undrained stress paths of all the samples of the VMClay. Sample VMClay-TIV2 is not included in this plot..... 312
Figure 7.34 Undrained stress paths of all the samples of the VMClay..... 313
Figure 7.35 Normalized stress-strain behaviour of all the samples of the VMClay314
Figure 7.36 Undrained shearing stress paths in the v:logp' plane for the intact samples of the VMClay 315
Figure 7.37 Normalized undrained shearing stress paths of all the samples of the VMClay using the equivalent pressure on the intrinsic critical state line (CSL*) 316
Figure 7.38 Normalized undrained secant Young's modulus degradation curves for the slurry samples of the VMClay compressed isotropically 317
Figure 7.39 Normalized undrained secant Young's modulus degradation curves for the slurry samples of the VMClay compressed under ko conditions. Comaprison with the isotropically compressed specimen VMClay-TSC2..... 318
Figure 7.40 Normalized undrained secant Young's modulus degradation curves for the intact samples of the VMClay 319
Figure 7.41 Comparison of the normalized undrained secant Young's modulus degradation curves for the vertical and horizontal intact samples of the VMClay320
Figure 7.42 Undrained secant Young's modulus as a function of the current mean effective stress at various strain levels for the slurry and intact samples of the VMClay..... 321
Figure 8.1 Particle size distributions of (a) the BRS, VSS and Nocilla et al. (2006) and (b) soils that displayed transitional behaviour (Shipton, 2010) 325
Figure 8.2 One-dimensional normal compression lines of the BRS and VSS..... 327
Figure 8.3 One-dimensional compression lines of slurry and compacted samples of the BRS-E..... 329
Figure 8.4 Normalized one-dimensional compression behaviour of the compacted samples of the BRS-B 330
Figure 8.5 Normalized one-dimensional compression behaviour of the intact samples of the BRS-B and VMClay 332
Figure 8.6 Comparison of the normalized one-dimensional compression behaviour of the intact samples of the BRS-B, VMClay, Sibari clay and Pisa clay (Sibari and Pisa clay data redrawn from Coop & Cotecchia, 1995 and Rampello & Callisto, 1998 respectively)..... 334
Figure 8.7 Electron microscopy images of a slurry sample of the BRS-B 336
Figure 8.8 Electron microscopy images of an intact sample of the BRS-B 337

Figure 8.9 Electron microscopy images of a compacted sample of the BRS-B..... 338
Figure 8.10 Electron microscopy images of a slurry sample of the VMClay 339
Figure 8.11 Electron microscopy images of an intact sample of the VMClay 340
Figure 8.12 Electron microscopy images of silty particles bonded by calcium carbonate taken from two intact samples of the VMClay 341
Figure 8.13 Isotropic ICLs* and CSLs* for samples of the BRS-B and VMClay.. 342
Figure 8.14 Normalized shearing data for the slurry samples of the (a) VMClay and (b) BRS-B 343
Figure 8.15 Intrinsic local state boundary surfaces (LBS*) of the VMClay and BRS-B 345
Figure 8.16 Normalized shearing data of the slurry and intact samples of the (a) VMClay and (b) BRS-B 346
Figure 8.17 Undrained secant Young's modulus as a function of the current mean effective stress at different strain levels for samples of the (a) BRS-B and (b) VMClay..... 348
Figure 8.18 Comaprison of the undrained secant Young's modulus as a function of the current mean effective stress at different strain levels for samples of the BRS-B and VMClay..... 349
Figure 8.19 Comparison of the variation of the effective stress level exponent of stiffness (n) with axial strain for the VMClay and BRS-B 349
Figure 8.20 Effect of the sample preparation method and in-situ structure on the stiffness at different strain levels of the slurry, compacted and intact specimens of the BRS-B..... 350
Figure 8.21 Undrained secant Young's modulus as a function of the current mean effective stress at different strain levels for vertically and horizontally intact cut samples of the VMClay..... 352

List of tables

Table 2.1 Index properties of Erksak, Toyura and Leighton Buzzard sands (Been et al., 1991)……52
Table 2.2 Index properties of masonry and concrete sands (Finno & Rechenmacher, 2003)……61
Table 2.3 Transitional fines contents reported by different authors……79
Table 2.4 Summary of soil characteristics for materials that showed transitional behaviour and for those that did not display transitional behaviour (Shipton, 2010)……94
Table 2.5 Summary of soil characteristics for materials that showed transitional behaviour and for those that did not display transitional behaviour (Shipton, 2010)……95
Table 2.6 Summary of soil characteristics for materials that showed transitional behaviour and for those that did not display transitional behaviour (Shipton, 2010)……96
Table 4.1 Average contents of clay-sized, silt and sand particles and median particle size (D_{50}) according to the British Standard classification system……141
Table 4.2 X-ray diffraction results from (a) whole sample (b) soil fraction< 4μm144
Table 4.3 Specific gravity values of the BRS-B and BRS-E. Oedometer (O) and triaxial (T) samples……145
Table 4.4 Atterberg limits and estimated activity of some oedometer (O) and triaxial (T) samples of the BRS……146
Table 4.5 Organic matter content measured for one oedometer (O) and two triaxial (T) samples of the BRS-B……148
Table 4.6 Summary of the selected references on the Po River materials……151
Table 4.7 Summary of the material properties and possible transitional behaviour of the soils analysed……167
Table 5.1 Summary of the oedometer tests carried out on slurry samples of the Bormida clayey silt (BRS-B)……171
Table 5.2 Summary of the oedometer tests carried out on remoulded compacted samples of the clayey silt (BRS-B). *Measured swelling of samples after flooding the cell with water once the initial vertical load was applied. **Samples were soaked after applying this stress. ***Maximum vertical stress applied during static compaction……177

Table 5.3 Summary of the oedometer tests carried out on intact samples of the BRS-B. *Measured swelling of samples after flooding the cell with water once the initial vertical load was applied. **Samples were soaked after applying this stress. ***Water flushed throughout sample OI8 during 1 week under a back pressure of 10kPa after applying first load……184
Table 5.4 Summary of the oedometer tests carried out on slurry samples of Bormida sandy silt (BRS-E)……189
Table 5.5 Summary of the oedometer tests carried out on compacted samples of the BRS-E.*Measured swelling of samples after flooding the cell with water once the initial vertical load was applied.**Samples were soaked after applying this stress191
Table 5.6 Summary of the triaxial tests carried out on slurry (TS) and remoulded compacted (TC) samples of the BRS-B clayey silt.*Maximum vertical stress applied to the slurry samples in the floating ring consolidometer……205
Table 5.7 Summary of the triaxial tests carried out on intact samples of the BRS-B clayey silt……233
Table 6.1 Average content of clay-sized, silt and sand particles and median particle size (D_{50}) according to MIT classification systems. *Part of the sand content corresponds to the aggregates of cemented particles with the size of sand……261
Table 6.2 Specific gravity values of the Valencia silty soils VMClay, VMSand and VSSilt……264
Table 6.3 Atterberg limits and liquidity index measured on some intact oedometer (O) and triaxial (T) samples and on a slurry cake (Cake) samples of the Valencia silty soils ……265
Table 6.4 Content of calcium carbonate ($CaCO_3$) measured on samples of the Valencia silty soils……267
Table 7.1 Summary of the oedometer tests carried out on slurry samples of the Valencia silty clay (VMClay)……272
Table 7.2 Summary of the oedometer tests carried out on intact samples of the Valencia silty clay (VMClay). *Samples were soaked after applying this stress. **Water flushed throughout the sample during 24h under a back pressure of 10kPa after applying first load……277
Table 7.3 Summary of the oedometer tests carried out on compacted samples of the Valencia silty sand (VMSand) (notation OWC: oedometer wet compaction; ODC: oedometer air-dried compaction)……284
Table 7.4 Summary of the oedometer tests carried out on slurry and compacted samples of the Valencia sandy silt/clay (VSSilt)……289
Table 7.5 Summary of the triaxial tests carried out on slurry cake samples of the Valencia silty clay (VMClay). *Maximum vertical stress applied to the slurry cake sample in the consolidometer when the cake was consolidated……293
Table 7.6 Summary of the triaxial tests carried out on intact samples of the block of the Valencia silty clay (VMClay)……304
Table 8.1 Summary of index properties of the BRS and VSS……326

Nomenclature

1D-ICL*	Intrinsic one-dimensional normal compression line
A	Activity
A_0	Initial cross-sectional area of the sample
A_c	Current cross-sectional area of the sample
B	Skempton's pore water pressure parameter
b	Proportion of fine grains which contribute to the active granular contact
B_p	Breakage potential
B_r	Relative breakage
BRS	Bormida River Silts
BRS-B	Intact block sample of the Bormida River Silts
BRS-E	Remoulded sample of the Bormida River Silts
B_t	Total breakage
C^*_c	Intrinsic compression index
C^*_c	Intrinsic swell index
C_c	Compression index
CF	Clay fraction
CID	Isotropically Consolidated Drained triaxial test
CIU	Isotropically Consolidated Undrained triaxial test
CRS	Constant Rate of Strain
CRSP	Constant Rate of Strain Pump
CS	Critical State
C_s	Swell index
CSL	Critical State Line
CSL*	Intrinsic Critical State Line
CSSM	Critical State Soil Mechanics
C_u	Coefficient of uniformity
D_0	Initial sample diameter
D_{50}	Mean diameter
DEM	Discrete Element Method
DIC	Digital Image Correlation
d_{large}	Diameter of larger uniform particles
d_{min}	Diameter of smaller uniform particles
D_r	Relative density

e	Void ratio
e^*_{100}	Intrinsic void ratio corresponding to a vertical effective stress of 100kPa
e^*_{1000}	Intrinsic void ratio corresponding to a vertical effective stress of 1000kPa
e_c	Granular void ratio
e_f	Fin void ratio
e_{LL}	Void ratio at the liquid limit
e_{max}	Maximun void ratio
$e_{max,HF}$	Maximum void ratio of host silt
e_{min}	Minumum void ratio
e_N	Void ratio at a vertical effective stress of 1kPa in the e:logσ'_v plane
Eu	Undrained Young's modulus
Eu_{secant}	Undrained secant Young's modulus
fc	Fines content
FC_L	Limiting fines content
FC_{th}	Threshold fine grains content
G_s	Relative specific gravity of particles
ICL	Intrinsic Compression Line
I_g	Grading state index
I_L	Liquidity index
I_p	Plasticity index
Iv	Void index
ko – NCL	One-dimensional Normal Compression Line
ko	Coefficient of earth pressure at rest
L_0	Initial sample length of the sample
LBS	Local Boundary Surface
LBS*	Intrinsic Local Boundary Surface
LCC	Limiting Compression Curve
LVDT	Linear Variable Diffrential Transformer
m	Inverse of the gradient of the unloading stress path in the η:ln(p'/p'$_{(NC)}$) plane
M	Slope of critical state line in a q:p' plane
M*	Intrinsic slope of critical state line in a q:p' plane
M_{oed}	Oedometric tangent modulus
n	Effective stress level exponent of stiffness
N	Porosity
N	Specific volume of normal compression line at p'=1kPa in v:Lnp' plane
NC	Normally consolidated
NCL	Normal Compression Line
OC	Overconsolidated

OCR	Overconsolidation Ratio
OM	Organic matter content
p'	Mean effective stress
p'_0	Maximum mean effective stress at the start of triaxial shearing
p'_{cs}	Mean effective stress at the critical state line
q	Cambridge deviator stress
q_{cs}	Cambridge deviator stress at the critical state
R_d	Grain size disparity ratio
s	Spacing between fine grains
S_σ	Stress sensitivity
SBS	State Boundary Surface
SBS*	Intrinsic State Boundary Surface
SCC	Sedimentation Compression Curve
SCL	Sedimentation Compression Line
SEM	Scanning Electron Microscope
S_r	Saturation degree
S_s	Swell sensitivity
SS	Steady State
SSL	Steady State Line
S_t	Strength sensitivity
s_u	Undrained shear strength
TFC	Transitional fines content
u	Pore water pressure
v	Specific volume
V_0	Initial volume of the sample
VMClay	Intact block sample of the Valencia Silty Soils
VMSand	Remoulded silty sand material from the Valencia Silty Soils
VSS	Valencia Silty Soils
VSSilt	Remoulded silt/clay with sand from the Valencia Silty Soils
w_l	Liquid limit
w_n	Natural water content
w_p	Plastic limit
YSR	Yield Stress Ratio
η	Stress ratio on the q:p' plane
λ	Slope of normal compression line in v:Lnp' plane
κ	Slope of swelling line in v:Lnp' plane
Γ	Specific volume at mean effective stress of p'=1kPa in v:Lnp'
$(\sigma'_v)_{MC}$	Effective vertical stress at the point of maximum curvature of compression curve in an e:Log σ'_v plane
$(\sigma'_v)_{Mmax}$	Effective vertical stress at the yield point defined at the first inflection point of compression curve in a e:σ'_v plane
λ^*	Intrinsic slope of normal compression line in v:Lnp' plane

κ^*	Intrinsic slope of swelling line in v:Lnp' plane
Γ^*	Intrinsic specific volume at mean effective stress of p'=1kPa in v:Lnp'
σ'	Current effective stress
μ'	Poisson's ratio
ϕ'_{cs}	Critical state angle of shear strength
σ'_e	Equivalent vertical effective pressure
σ'_p	Preconsolidation stress
σ'_r	Reference effective stress at e=1
σ'_v	Effective vertical stress
σ'_y	Yield stress
ε_1	Maximum principal strain
ε_2	Intermediate principal strain
ε_3	Minimum principal strain
ε_a	Axial strain
σ_a	Axial stress
ρ_b	Bulk density of soil
ρ_c	Slope of LCC
$(e_c)_{eq}$	Equivalent intergranular contact void ratio
$(e_f)_{eq}$	Equivalent interfine void ratio
ε_r	Radial strain
σ_r	Radial stress
ρ_s	Density of solid particles
ε_s	Shear strain
ε_v	Volumetric strain
ρ_w	Density of water

Chapter 1
Introduction

1.1 Background

Large areas around the world are covered by "recently" deposited alluvial materials where cities are founded. In these environments the materials are characterised by a complex layering system of sands to silty clays with a high variability from site to site and, in many occasions with a complex in-situ structure. The development and expansion of urban areas on these shallow heterogeneous materials requires a rigorous characterization of their geotechnical properties for reliable support to engineers in designing new structures. In particular the effect of the naturally occurring in-situ structure on the mechanical behaviour of natural soils is of paramount importance.

Traditionally much of the research carried out to investigate the natural structure of soils has been focused on geologically old materials but less attention has been paid to young Holocene deposits. The research carried out in this thesis is intended to provide more knowledge about the mechanical behaviour of young Holocene deposits by testing natural intact samples of two alluvial soils. These soils were recently deposited and retrieved from the alluvial plains of the Bormida River at Castellazo Bormida, Italy and Turia River at Valencia, Spain where the fluvial dynamics at each location was different.

The effects of the structure of natural intact samples on the soil behaviour have been evaluated routinely by comparing the intact soil response to its reconstituted

state (e.g. Burland, 1990; Leroueil & Vaughan, 1990). In this comparison it is assumed that there exists a unique normal compression line (NCL) and a unique critical state line (CSL) for the reconstituted soil state from which the intrinsic parameters can be obtained. The key point of this comparison is whether the NCL and CSL are unique for a given reconstituted soil state.

The non-uniqueness of the NCL and CSL has been found in a large range of materials with very different gradings and mineralogy for reconstituted and compacted samples (e.g. Martins et al., 2001; Nocilla et al., 2006, Altuhafi & Coop, 2011; Shipton & Coop, 2012, 2015) and for natural samples (e.g. Nocilla & Coop, 2008). The term "transitional" has been used to refer to this mode of behaviour in reconstituted/remoulded materials where the initial structure of the soil dominates its compression and shearing response even at high stresses and large strains. Transitional soils represent a clear example of the robustness of the initial structure during compression and shearing, where the term "intrinsic" properties defined by the reconstituted samples lacks any practical meaning.

Soils of similar gradings and mineralogy retrieved from close locations to those tested in this thesis, in particular the Italian silts from the Bormida River, displayed transitional behaviour (Nocilla & Coop, 2006; 2008). A priori, this finding makes the Bormida River silts (BRS) a potential transitional soil which could invalidate the possibility of evaluating its natural in-situ structure in the traditional way.

1.2 Objectives of this research

The materials tested in this research project consist of Holocene silty alluvial soils, recently deposited and retrieved from the alluvial plains of the Bormida River at Castellazo Bormida, Italy and Turia River at Valencia, Spain. These materials are named Bormida River silts (BRS) and Valencia silty soils (VSS). An intact block specimen was excavated at each site together with remoulded samples.

The main objective of this research project was to investigate the effects of the naturally occurring in-situ structure of these two young alluvial materials on their mechanical behaviour. In doing so, triaxial and oedometer tests were performed firstly to characterise the mechanical behaviour of these materials in their reconstituted state, the response of which was compared with the behaviour of the natural intact samples. Special attention was paid in investigating the influence of the sample preparation technique in the uniqueness of the NCL and CSL, as it will be shown in Chapter 2, it appears that the sample preparation technique triggered

the transitional behaviour observed in a few soils, including those with the same mineralogy and gradings as the BRS.

1.3 Thesis layout

The work carried out in this thesis is presented in nine chapters including this introductory chapter.

Chapter 2 presents a review of the most relevant references found in the literature, paying special attention to the factors that could affect the uniqueness of the NCL and CSL. The term *transitional soil behaviour* is addressed together with a review, from previous investigations, of soils which exhibited this behaviour. Finally the effects of the natural structure of soils on the mechanical behaviour are also reviewed, paying special attention on young Holocene alluvial materials.

A detailed description of the laboratory equipment used and the testing procedures followed during this research project are presented in Chapter 3. All the apparatus used in this research belongs to the Soil Mechanics section at Imperial College, London, where the author of this thesis carried out all the laboratory tests.

Chapters 4 and 6 present a detailed characterisation of the index properties of the Bormida River silts (BRS) and Valencia silty soils (VSS). Additionally, a specific literature review of previous investigations on these materials is carried out. The mechanical behaviour of the BRS and VSS soils tested in this thesis is described in Chapters 5 and 7 respectively, including the analysis and interpretation of the results from the experiments performed. A comparison between the mechanical behaviour of the BRS and the VSS is carried out in Chapter 8.

Finally, Chapter 9 summarises the main conclusions derived from this research project and presents recommendations for future work.

Chapter 2
Literature review

2.1 Introduction

Critical State Soil Mechanics (CSSM) has been used as a reference framework to describe the behaviour of clays and also clean sands with a few modifications. Recent research on the behaviour of clean sands, intermediate and well graded soils has shown contradictory findings in terms of the uniqueness of the NCL and CSL. In this chapter a review of the factors that could affect the uniqueness of the NCL and CSL is presented; the term *transitional soil behaviour* is described together with a review, from previous investigations, of soils which exhibited this behaviour and finally the possible influence of sample preparation methods on the transitional behaviour is analysed. Finally the effects of the in-situ structure on the mechanical behaviour of natural soils are reviewed.

2.2 Soil structure and definition of reconstituted and remoulded states

The term "structure" in soils is defined as a combination of particles arrangement "fabric" and inter-particle forces "bonding" (Mitchell, 1976). The structure of a natural material is formed and evolves during and after deposition. Many factors such as mineralogy of the solid phase, water chemistry, environmental conditions and physical and chemical processes can affect the structure during its formation.

The effect of the natural structure on the soil behaviour is investigated by comparing the response of the natural material with that of its reconstituted state. It is obvious that to make this comparison possible there should exist a unique NCL and CSL for the reconstituted state. Reported effects of this comparison showed that the natural structure enhances the strength of the soil, allowing it to exist at a higher specific volume than that of its reconstituted state for a given stress level (e.g. Burland, 1990; Leroueil & Vaughan, 1990; Cuccovillo & Coop, 1997 and 1999). This "extra" strength represents a positive effect of the natural structure. However, other researchers showed negative effects of the natural structure, where the strength is weaker than that of the reconstituted soil (e.g. Fearon & Coop, 2002; Vitone & Cotecchia, 2011). Consequently, the structure of a natural soil represents another important parameter to be added to the traditional void ratio (e) and stress history in controlling the soil behaviour.

2.2.1 Fabric

As mentioned above, fabric is that part of the structure which represents the spatial arrangement of particles in a soil mass. Fabric is created mainly through physical processes and is influenced by many factors like size distribution, shape and mineralogy of the particles, electrochemistry of the water (for fine grain soils), organic content, mode and rate of deposition and stillness of the water. Burland (1990) pointed out that for clays; low rate of deposition creates fabrics which are more open and sensitive than those produced by rapid deposition.

2.2.2 Bonding

The term bonding refers to all the inter-particle forces that are not of a purely frictional nature (Cotecchia & Chandler, 1997). Bonding is related to the physico-chemical interaction between the solid and liquid phases of a soil which clearly means that it is not always a solid link. Changes in the nature of any of the phases will influence the bonding and therefore the structure of the soil. Cementation is also a source of bonding between particles which represents a solid link associated to processes like precipitation, dissolution and recrystallisation. Carbonates are one of the most common cementing minerals together with iron oxides.

2.2.3 Reconstituted and remoulded states

According to Burland (1990) a reconstituted soil is created by mixing the natural sample with water to form a slurry at a water content of between the liquid limit (w_l) and 1.5 times w_l, preferably $1.25w_l$. The water chemistry should be similar to that of the in-situ pore fluid. The slurry should then be compressed one-

dimensionally to define the "intrinsic" parameters which he stated to be unique and inherent for a given material. During this research project the terms slurry and reconstituted soil have the same meaning.

Although it is common to find in the literature the term remoulded equivalent to that of reconstituted, from the point of view of the author of this thesis they represent different structures as a consequence of the sample preparation procedure followed in each case. The term remoulded soil defines a state where the initial natural structure is broken down to produce a more homogeneous structure. Different levels of structure are created depending on the energy applied during the remoulding process, which might influence the soil behaviour like for natural materials with complex structure (e.g. Dumbleton, 1967; Fearon & Coop, 2000; Atkinson et al., 2003; Carrion, 2006; Madhusudhan & Baudet, 2014). As will be described in Chapter 3, in this thesis the term remoulded state is used for samples whose initial intact structure is broken down by the action of a spatula and then compacted statically or dynamically.

What is clear from the above discussion is that reconstituted and remoulded samples have an initial and different structure, depending on the sample preparation technique. Moreover, and contrary to what was originally thought that a reconstituted/slurry sample was "destructured", it has in fact a structure, which depends on the initial water content. In this case, the bonding related to cementation, considered as a solid link, is unlikely to have any significant effect on the structure, but for fine grained materials there still a clear physico-chemical interaction between particles and water which generates a certain bonding.

So the questions are; what is the effect of the initial structure of a slurry sample on the soil behaviour? Is there a unique response regardless of the initial water content or conversely it influences the behaviour? These are very important questions to answer because they could invalidate the concept of the slurry structure as a reference material for interpreting the behaviour of natural intact structures, which in fact is one of the main objectives of this research project.

2.3 Mechanical behaviour of reconstituted/remoulded sands

Depositional density in sands, and in general in granular materials, is a key parameter that controls the soil behaviour within the engineering stress range (<1MPa). For reconstituted/remoulded samples, it is assumed that any possible cementation between particles is destroyed during the sample preparation process and consequently the term structure is equivalent to fabric due to the lack of

physico-chemical interaction between particles and water. The initial density is associated with an initial fabric that could be completely erased if the soil ever reaches a unique NCL and CSL. In this section a review of the factors that could influence the compression and shearing behaviour of reconstituted/remoulded sand specimens is carried out.

2.3.1 Compression behaviour

Volumetric compression of all soils is achieved by means of particle rearrangement into a denser packing. In clays, physico-chemical interaction between particles controls the compression behaviour whereas in granular soils the mechanical and gravitational interaction between particles controls the soil's response. Focusing on granular soils, particle rearrangement into a more dense configuration is achieved by overcoming inter-particle friction through inter-particle slip and rotation (elastic components), by overcoming particle strength through different levels of particle damage (plastic components), or by both (e.g. Roberts & DeSouza, 1958; Hardin, 1985; Coop, 1990; Pestana & Whittle, 1995; Chuhan et al., 2003; Mesri & Vardhanabhuti, 2009).

Jefferies & Been (2000) pointed out that while a unique NCL is accepted for clays, the debate about what comprises a NCL for sands continues. There are two main arguments in the literature:

I. A unique NCL exists for any particular sand and it only occurs at the onset of particle breakage at high stress level (e.g. Robert & DeSouza, 1958; Vesic & Clough, 1968; Coop, 1990; Coop & Lee, 1993; Pestana & Whittle, 1995).

II. For a given sand there exist many different NCLs, each one corresponding to a different initial density regardless of the stress level (e.g. Ishihara et al., 1975; Jefferies & Been, 2000).

In support of the first argument, Coop & Lee (1993) investigated the behaviour of three different sands under high stresses. The soils tested were a carbonate sand (Dogs Bay sand), a decomposed granite and a silica sand (Ham River sand). Very loose samples were prepared by pluviation and denser samples by moist tamping in layers. The isotropic compression behaviour of the three sands is shown in Figure 2.1. Although the mineralogy, grading and particle shape were quite different for each soil, they all showed a similar behaviour. Samples starting from different initial specific volumes (v) converged towards a unique NCL at high stresses in the v:lnp' plane, where particle breakage was controlling the soil response. The NCL

was linear and the compression behaviour can be described by Equation 2.1, where λ is the slope of the NCL, N is the specific volume extrapolated to a mean effective stress of p'=1kPa and v and p' are the current specific volume and mean effective stress.

$$v = N - \lambda \cdot \mathrm{Ln}p' \qquad 2.1$$

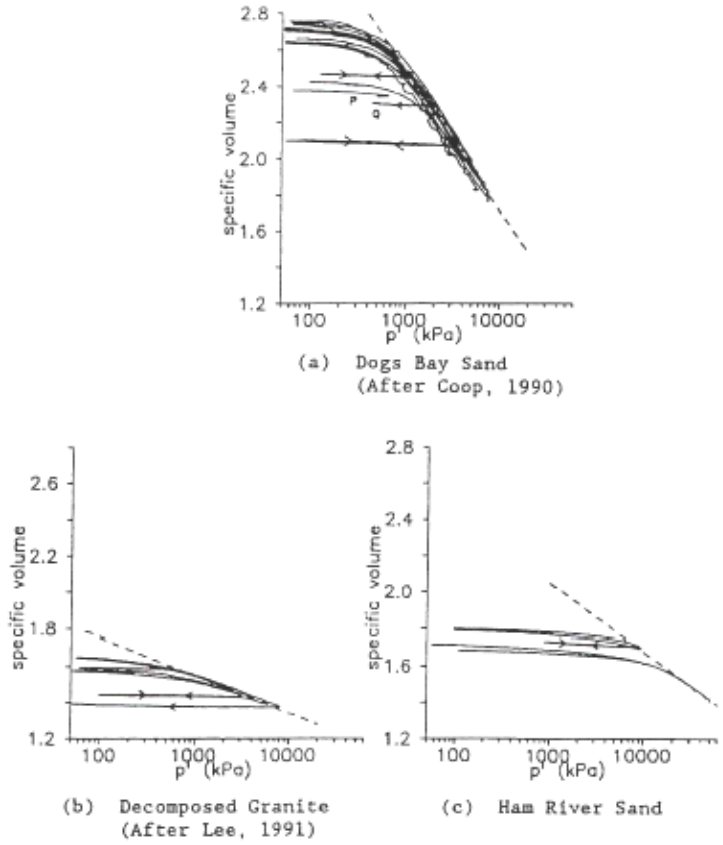

Figure 2.1 Isotropic compression behaviour of three different sands (Coop & Lee, 1993)

Coop (1990) investigated the one-dimensional behaviour of the Dogs Bay sand in the triaxial apparatus and showed that the one-dimensional normal compression line (1D-NCL) was located below and parallel to the isotropic NCL as it would do for clays and as expected from the critical state framework (Figure 2.2).

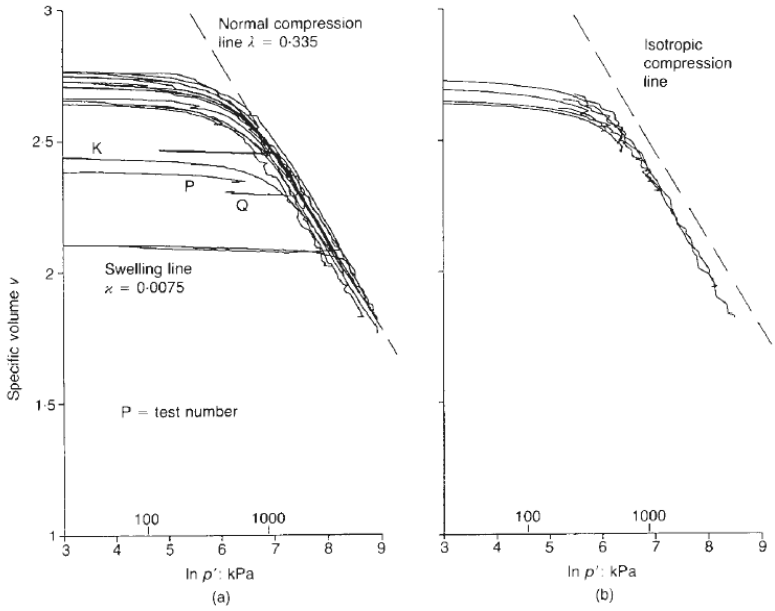

Figure 2.2 (a) Isotropic and (b) one-dimensional compression behaviour of Dogs Bay sand (Coop, 1990)

Pestana & Whittle (1995) proposed a simple elasto-plastic compression model for freshly deposited cohesionless soils to describe the behaviour under one-dimensional and isotropic compression. The model assumes that samples of sand tested in compression from different initial formation densities approach a unique response at high stress levels called the *Limiting Compression Curve* (LCC) where particle breakage is the principal component of deformation (Figure 2.3). Assuming a double logarithmic void ratio versus effective stress space, the LCC is linear and the compression behaviour can be described by Equation 2.2.

$$e = \left(\frac{\sigma'}{\sigma'_r} \right)^{-\rho_c} \qquad 2.2$$

where ρ_c is the slope of the LCC, σ'_r is the reference effective stress at a void ratio of 1.0 and e and σ' are the current void ratio and effective stress respectively.

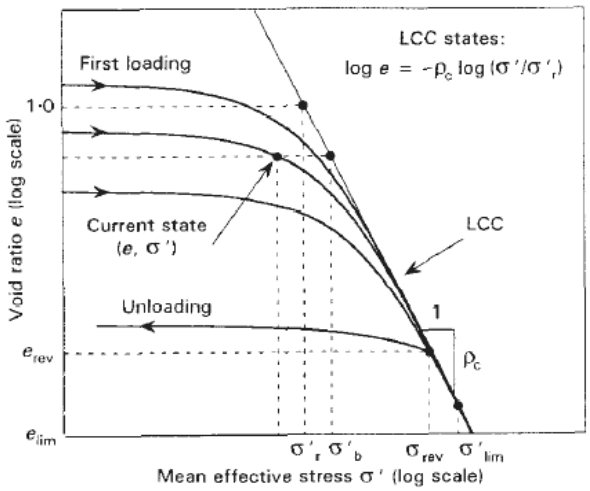

Figure 2.3 Conceptual model of first loading and unloading of freshly deposited cohesionless soils (Pestana & Whittle, 1995)

The yielding stress in soils has been considered as the point of inflection where compressibility increases abruptly and plastic deformation takes place. For reconstituted/remoulded cohesive soils, where particle breakage is not a factor, the yielding stress is generally associated with the preconsolidation pressure (σ'_p) which is related to the stress history of the sample. In freshly deposited granular materials yield generally occurs at the onset of major particle breakage (e.g. Coop & Lee, 1993; Pestana & Whittle, 1995; McDowell & Bolton, 1998). According to Pestana & Whittle (1995), during compression, the main factors affecting the particle breakage of granular soils and therefore the yielding stress are:

- ✓ Initial depositional density and fabric
- ✓ Mineralogy
- ✓ Physical properties; angularity, particle size distribution
- ✓ Applied boundary stress conditions; isotropic and one-dimensional compression
- ✓ Time-dependent behaviour
- ✓ Interstitial fluids

In order to quantify the amount of particle breakage, Hardin (1985) proposed a method to measure the relative breakage (Br) by comparing the grading curves above the 74μm sieve before and after testing (Figure 2.4).

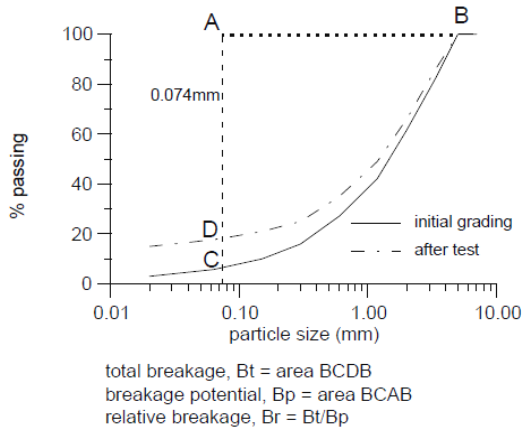

Figure 2.4 Definition of relative breakage (Br) based on Hardin (1985) (redrawn by Coop et al., 2004)

The importance of particle breakage, initial depositional density, mineralogy and physical properties such as angularity and grading can be seen in Figures 2.1, 2.5 and 2.6. For example, the weak shelly particles of calcium carbonate from the Dogs Bay sand started breaking at around 0.8MPa while the stronger quartz particles of Ham River sand started breaking at around 10MPa (Figure 2.1). The effect of initial density, and therefore initial fabric, on the compression behaviour of sub-rounded quartz particles of Ottawa sand is shown in Figure 2.5. It can be seen that the loose sample yielded at a lower stress compared to the dense one and eventually they arrive at a unique NCL at high stresses. This behaviour can be explained because the coordination number, which is the number of contacts with neighbouring particles, increased for the dense sample and therefore reduced the interparticle stresses which decreased the probability of particle breakage (McDowell et al., 1996).

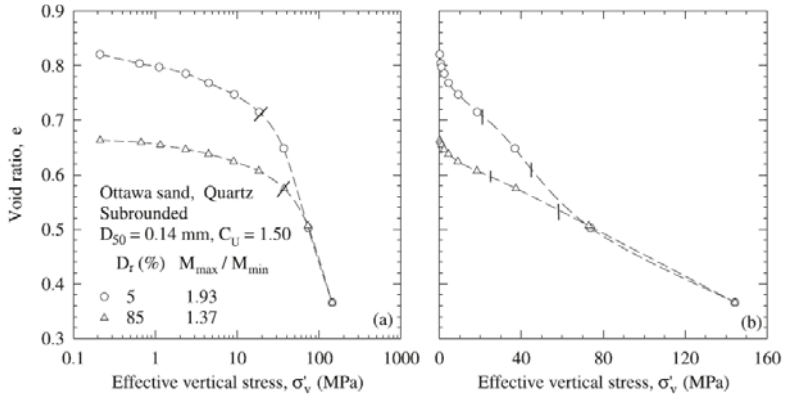

Figure 2.5 Compression behaviour of Ottawa sand (Mesri & Vardhanabhuti, 2009)

Mesri & Vardhanabhuti (2009) examined the compression data for over 100 sands. They defined the yield stress $(\sigma'_v)_{MC}$ as the effective vertical stress at the point of maximum curvature of the compression curve in an e:logσ'_v plane and $(\sigma'_v)_{Mmax}$ as the vertical effective stress at the yield point defined at the first inflection point of the compression curve in an e:σ'_v plane (Figure 2.5). Figure 2.6 shows that the yielding stress may range from less than 0.4MPa for an angular biogenic carbonate sand to 30MPa for a well-rounded quartz sand.

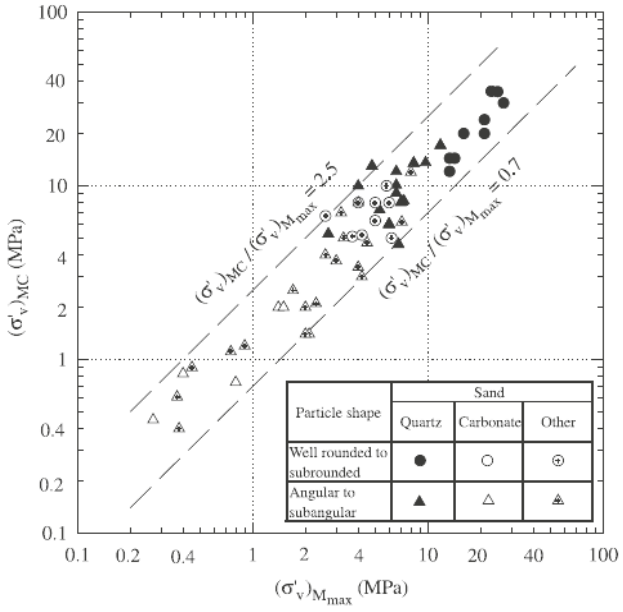

Figure 2.6 Comparison of $(\sigma'_v)_{MC}$ and $(\sigma'_v)_{Mmax}$ (Mesri & Vardhanabhuti, 2009)

The effect of the applied stress boundary conditions on the onset of particle breakage is shown in Figures 2.7 and 2.8. Mesri & Vardhanabhuti (2009) compared the one-dimensional and isotropic compression behaviour of Toyoura sand samples tested by Kwag et al. (1999). They showed that the yield effective stress was higher in isotropic compression than in one-dimensional compression for a similar initial density as can be seen in Figure 2.7. For example, the yield stress of a sample with an initial relative density (Dr) of 80% was around 20MPa for one-dimensional compression compared to 100MPa for isotropic conditions. The differences in behaviour are due to the induced shear stresses in the sample during one-dimensional compression, which contribute to a significant increase in particle breakage compared to those in isotropic compression for the same p' (e.g. Coop & Lee, 1993; Pestana & Whittle, 1995).

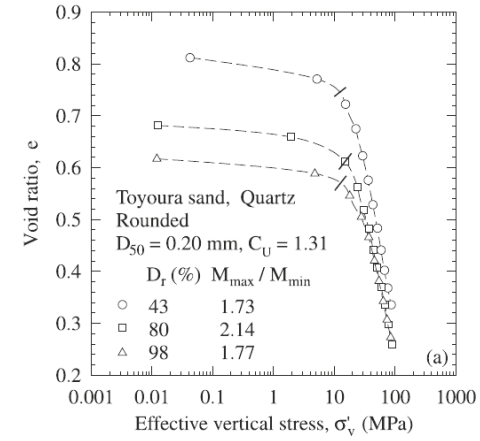

(a) one-dimensional compression

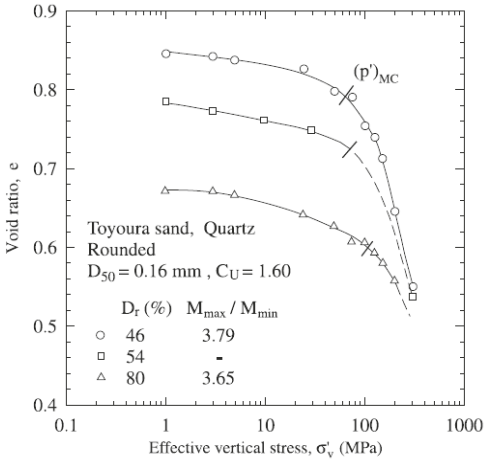

(b) isotropic compression

Figure 2.7 Compression behaviour of Toyura sand (a) one-dimensional compression (b) isotropic compression (Mesri & Vardhanabhuti, 2009)

Coop & Lee (1993) quantified the particle breakage (Br) of three different soils in compression and shearing stages (Figure 2.8). They observed that at any given p', the values of Br in isotropic compression were lower than those achieved in shearing, reinforcing the influence of the applied stress conditions on the extent of particle breakage. They also concluded that at high stresses there exists a unique linear relationship between Br and lnp' which appears to be independent of the stress path followed to reach the critical state. More recently Altuhafi & Coop (2011) carried out a research to examine the effect of initial grading and density on the one-dimensional compression behaviour of three sands with distinct mineralogy. Contrary to the initial hypothesis of Coop & Lee (1993), Altuhafi & Coop concluded that the amount of breakage is not unique for a given stress level when

the soil reaches the NCL and that it also depends on the initial density of the sample.

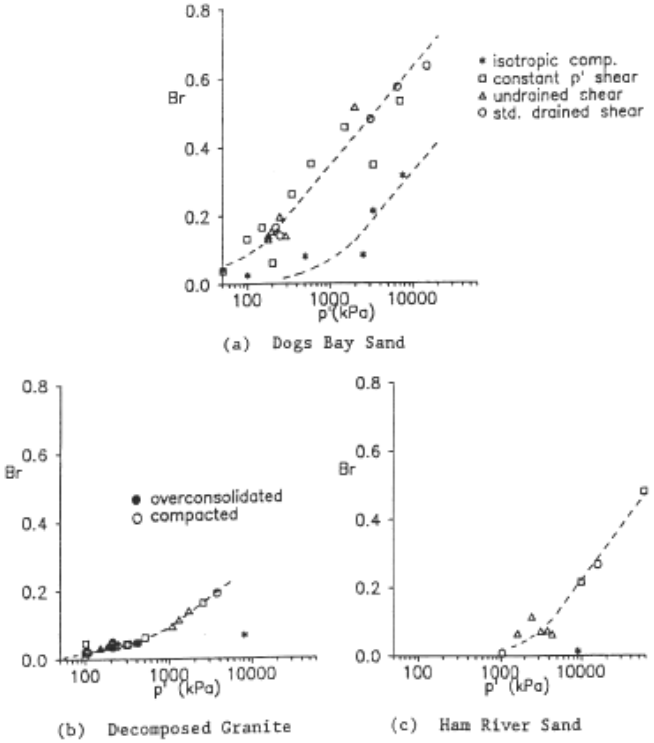

Figure 2.8 Particle breakage (Br) for (a) Dogs Bay sand (b) decomposed granite and (c) Ham River sand (Coop & Lee, 1993)

According to what has been presented in the previous paragraph, it seems to be clear that for any particular sand, and regardless of its initial density and sample preparation technique, there is a unique NCL that occurs at the onset of major particle breakage at high stress levels. It is also clear that at low stress levels, initial density controls the compression behaviour for a given sand and the compression paths run approximately parallel to each other. The question is, are these compression paths at low stress levels real NCLs and if so, does a range of NCLs exist, each one corresponding to a different initial density or are the recompression paths similar to that of an overconsolidated soil?

Jefferies & Been (2000) analyzed the isotropic compression behaviour of Erksak sand. Samples were prepared by wet pluviation and moist tamping and compressed isotropically in the triaxial apparatus over a stress range of 20kPa to 2000kPa. The index properties of Erksak sand are shown in Table 2.1 and compared to those of Toyoura and Leighton Buzzard sands. The compression behaviour for Erksak sand is shown in Figures 2.9 and 2.10. They concluded that each compression path

should be regarded as a true NCL because of two factors; the first is that, the samples were never overconsolidated and secondly, the unload-reload loop indicated that plastic deformation occurred as can be seen in Figure 2.10. Therefore at lower stresses, an infinite number of NCLs exist for a given sand. This interpretation is in agreement with what was shown by Ishihara et al. (1975). They tested samples of Fuji River and Niigata sands in the triaxial apparatus. Loose and dense specimens were prepared by air-pluviation and mechanical vibration and tamping respectively. They showed that when a sample has been compacted to any possible initial density and is subjected to stresses, it displays plastic deformation from the beginning of loading and therefore each initial density state defines a true NCL. It seems reasonable to think that for a given sand there should be two limiting NCLs associated to the maximum and minimum void ratio that can be achieved by any sample preparation method. Ishihara (1993) showed that the range of initial void ratios that can be attained depends on the sample preparation method (Figure 2.11). The widest and the narrowest ranges in initial void ratio can be obtained by the moist placement and water sedimentation methods respectively.

	Erksak 330/0·7	Toyoura	Leighton Buzzard
Mineralogy			
Quartz: %	73	75	—*
Feldspar: %	22	25	
Other: %	5	0	
Median grain size D_{50}: mm	0·330	0·160	0·120
Effective grain size D_{10}: mm	0·190	0·120	0.095
Uniformity coefficient D_{60}/D_{10}	1·8	1·5	1·5
Passing 200 sieve: %	0·7	0	5
Specific gravity	2·66	2·65	2·65
Minimum density: kg/m^3	1517	1338	1310
Maximum density: kg/m^3	1742	1648	1592

* X-ray diffractometry was not carried out on Leighton Buzzard sand in this study. The sand consists mainly of quartz, by visual inspection.

Table 2.1 Index properties of Erksak, Toyura and Leighton Buzzard sands (Been et al., 1991)

2.3.2 Shearing behaviour at large strains

The classical definition of Critical State (CS) is the state at which the soil continues to deform at constant effective stress and constant void ratio (Roscoe et al., 1958). It can be assumed that when soils reach the CS, any initial structure will have been erased by continuing shear deformations. Muir Wood (2008) proposed that if CS has been reached it should be expected that all aspects of the fabric should, on average, have arrived at steady state, including particle orientations, contact orientations, and particle grading, if particle breakage occurred.

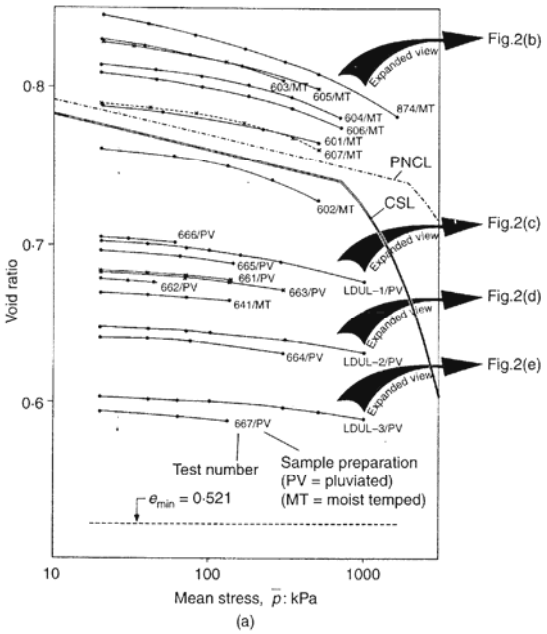

Figure 2.9 Isotropic compression of Erksak sand. First loading (Jefferies & Been, 2000)

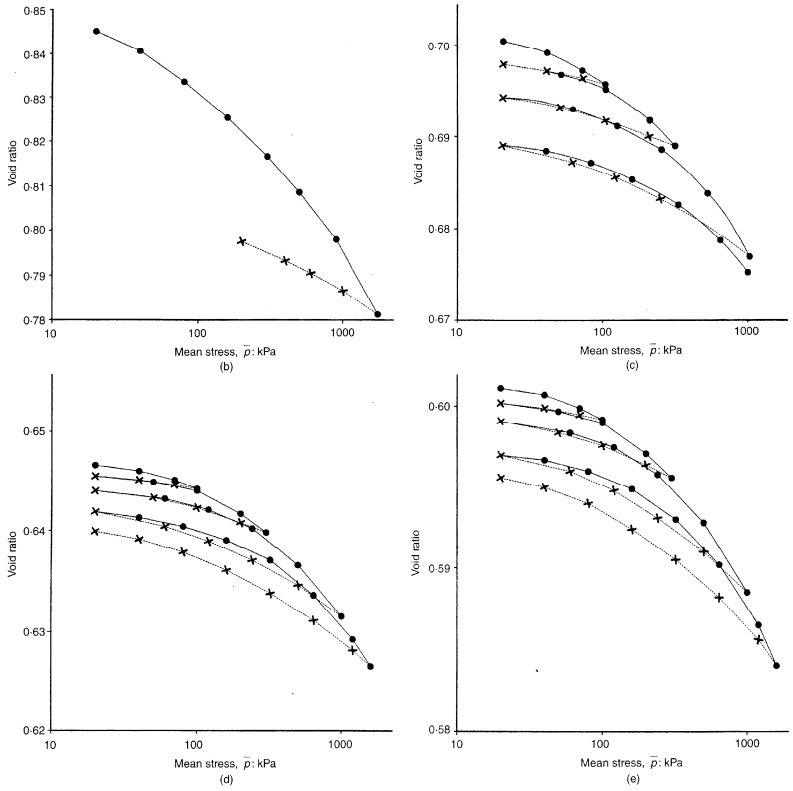

Figure 2.10 Expanded views of Figure 2.9. Isotropic behaviour showing loading and unloading paths (Jefferies & Been, 2000)

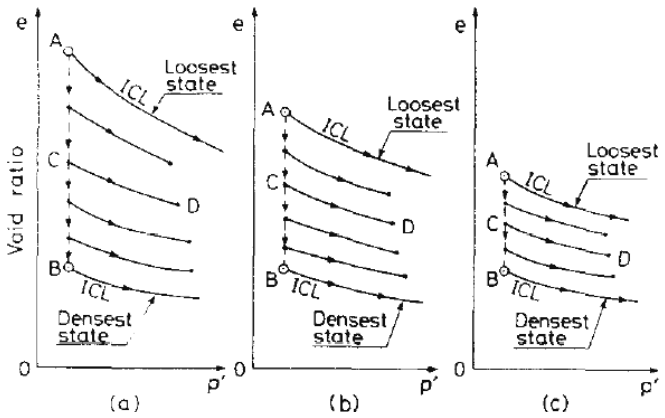

Figure 2.11 Consolidation characteristics of samples prepared by: (a) moist placement (b) dry deposition (c) water sedimentation (Ishihara, 1993)

Poulos (1981) defined the Steady State (SS) of a sand as:

> *"The steady state of deformation for any mass of particles is that state in which the mass is continuously deforming at constant volume, constant normal effective stress, constant shear stress and constant velocity. The steady state of deformation is achieved only after all particle orientation has reached a statically steady state condition and after all particle breakage, if any, is complete, so that the shear stress needed to continue deformation and velocity of deformation remains constant".*

Been et al. (1991) pointed out that there are several basic questions about the critical state line (CSL) or steady state line (SSL) of sands that are not satisfactorily answered:

- Are the CSL and SSL the same?
- Is the CSL/SSL unique for any particular sand, or does it depends on initial fabric and stress path of the test?
- What is the shape of the CSL/SSL over a wide range of stresses?

Recent research on the shearing behaviour of sands showed the importance of particle breakage on the position and slope of the CSL/SSL in the compression plane (e.g. Cheng et al., 2005; Muir Wood & Maeda, 2008; Muir Wood, 2008). Therefore it seems to be logical to extend the questions proposed by Been et al. (1991) and include:

- How does particle breakage influence the position of CSL/SSL in the compression plane?

All these questions are reviewed in the following paragraphs.

- **Are the CSL and SSL the same?**

Traditionally, for sands, the CS has been determined by means of drained triaxial tests while the SS has been measured by testing undrained samples (Been at al., 1991). Although the CS and SS represent slightly different concepts on comparison of their definitions, many authors including Poulos et al. (1988), Poorooshab (1989), Been et al. (1991) and Verdugo & Ishihara (1996) have shown that the CS and SS are the same (Figures 2.12 and 2.13).

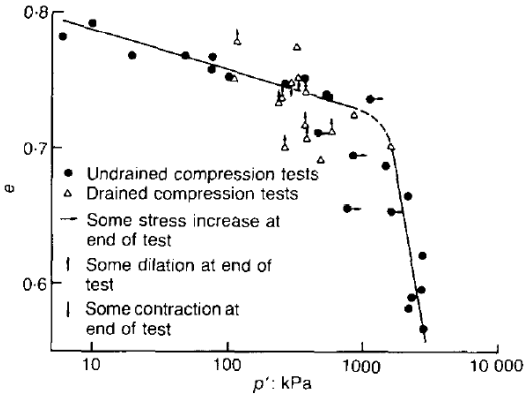

Figure 2.12 Comparison of critical state (CS) – steady state (SS) from drained and undrained tests on Erksak sand (Been et al., 1991)

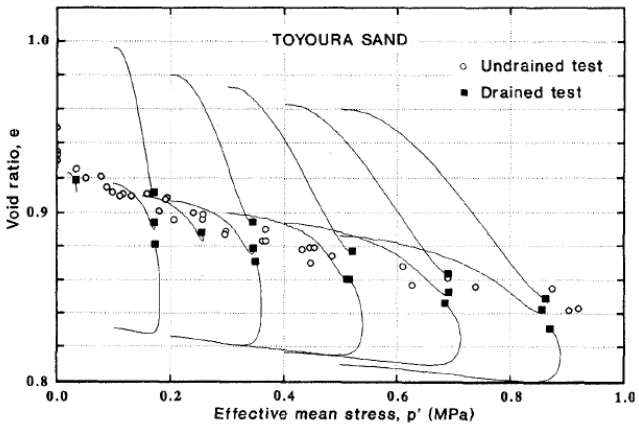

Figure 2.13 State diagram evaluated from both drained and undrained triaxial tests on Toyura sand (Verdugo & Ishihara, 1996)

Verdugo & Ishihara (1996) noted that even though there is a good agreement between the final state from both undrained and drained tests, the scatter in the data points for the final state is much more significant for drained tests compared to undrained ones (Figure 2.13). Therefore they suggested evaluating the SSL with undrained tests. Moreover, Been et al. (1991) pointed out that the definition of the CSL with tests on dense drained samples is poor because the samples are generally still dilatant at the end of the test and shear band localization occurs (Figure 2.14).

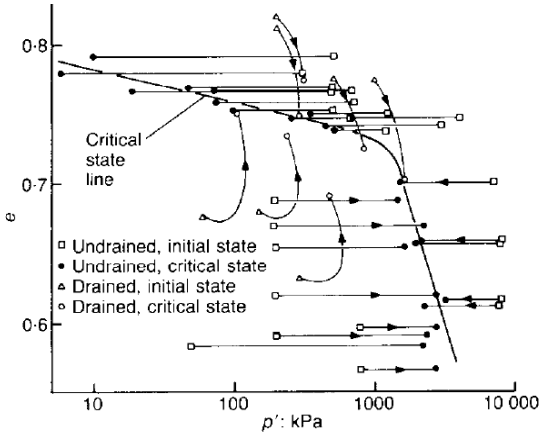

Figure 2.14 Effect of initial state on the crtitical state (Been et al., 1991)

- **Is the CSL/SSL unique for any particular sand, or does it depend on initial fabric and the stress path of the test?**

Before starting to review whether the CSL/SSL is unique or not for a given sand, it is very important to distinguish between different initial fabrics created in soil specimens by means of different sample preparation techniques, and initial fabrics produced with the same sample preparation method but different densities. This clarification will be used to separate the possible effects of sample preparation technique on the uniqueness of CSL/SSL when the data are available.

Been et al. (1991) investigated the effect of sample preparation method on the CSL for Erksak sand specimens prepared by wet pluviation and moist compaction techniques. They showed that at high stresses, the sample preparation method appeared to have no effect on the CSL and that a unique CSL/SSL was found in an e:logp' plane for different samples regardless of the preparation method (Figure 2.15). They also pointed out that the fact that at high stress levels the sample preparation method does not have any apparent effect on CSL does not necessarily mean that it has no effect at low stress levels.

Ishihara (1993) showed a unique SSL in an e:logp' plane for samples of Toyoura sand created by moist placement and dry deposition (Figure 2.16). He concluded that if the sand is deformed to a strain of more than 20% in reaching a steady state, then the initial fabric is erased completely and the CSL is unique irrespective of the method by which the sample is prepared. On the contrary, other authors have suggested that the position of CSL in the compression plane could be affected by the sample preparation technique (e.g. Alarcon & Leonards, 1988; Dennis, 1988; DeGregorio, 1990).

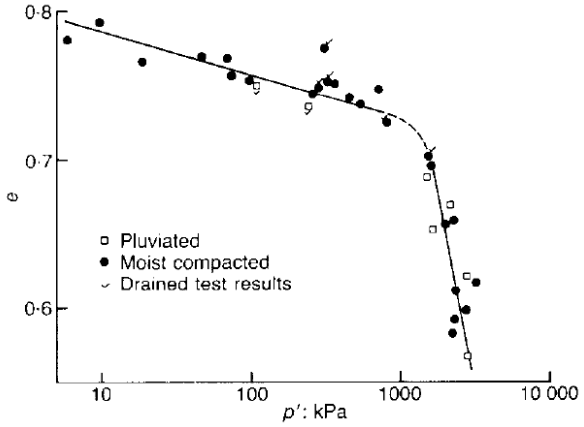

Figure 2.15 Effect of sample preparation method on the critical state line for Erksak sand (Been et al., 1991)

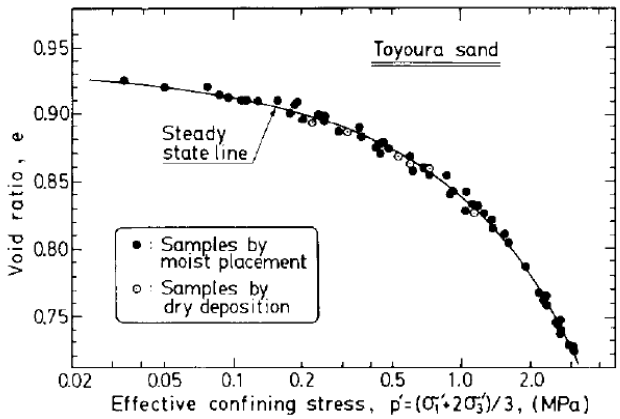

Figure 2.16 Steady state line established from two kinds of samples prepared by different methods (Ishihara, 1993)

Coop & Lee (1993) identified a unique CSL in a v:lnp' plane for the three different sands tested in the triaxial cell at high stress levels (Figure 2.17). Loose samples were prepared by wet pluviation and dense samples by wet tamping. They

concluded that as seen for the NCL, particle breakage controls the behaviour at the CSL. They also pointed out that the slope of the CSL depends on the mineralogy of the sand and that its NCL is parallel to the CSL and located above it as expected from the critical state framework.

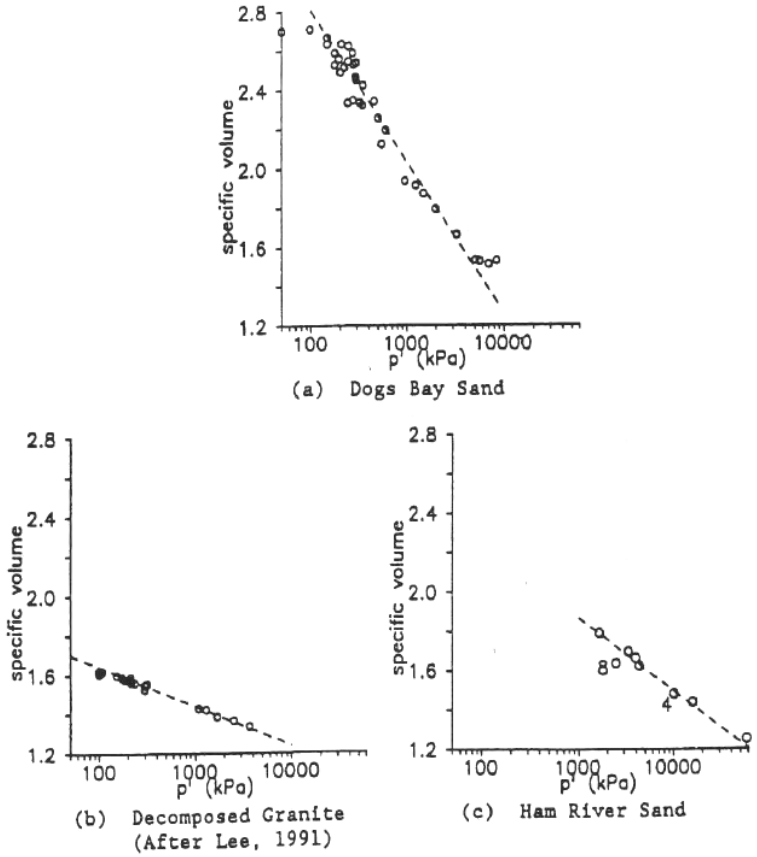

Figure 2.17 Critical state lines of three sands (Coop & Lee, 1993)

The effect of the stress path on the uniqueness of the CSL/SSL has been investigated by different authors (e.g. Alarcon-Guzman, 1988; Coop, 1990; Vaid et al., 1990; Been et al., 1991; Negussey & Islam, 1994; Riemer & Seed, 1997). Been et al. (1991) showed that the CSL is independent of the stress path for the Erksak and Toyoura sands (Figures 2.18 and 2.19). Contrary to the findings of Been et al., Vaid et al. (1990) concluded that the SSL of a given sand is not unique in the e:logp' plane and depends on the stress path (compression versus extension). Riemer and Seed (1997) investigated the effect of different factors affecting the position of the SSL for the Monterey #0 sand. Very loose specimnes were created by moist tamping. Four factors were analysed; level of consolidation stress, drainage conditions during shearing, stress path to which the sand is subjected during shearing and mode of deformation of the soil specimen during shearing.

They concluded that the factor which controls the position of the SSL in the e:logp' plane appears to be the mode of deformation or strain path of the sample (Figure 2.20). All the tests in which cylindrical specimens deform in axial compression yield the same SSL for a given material regardless of the effective stress path, while specimens that deform in another mode (cylindrical axial extension or simple shear) all produced different SSLs.

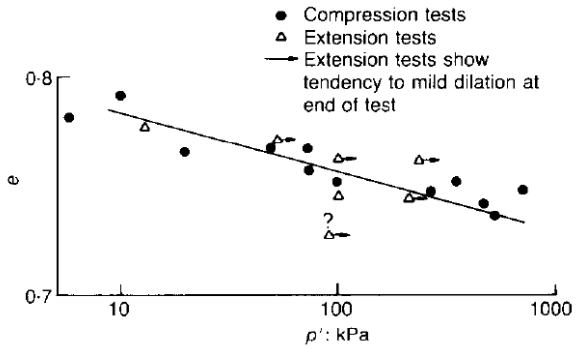

Figure 2.18 Effect of stress path on the critical state line of Erksak sand (extension versus compression) (Been et al., 1991)

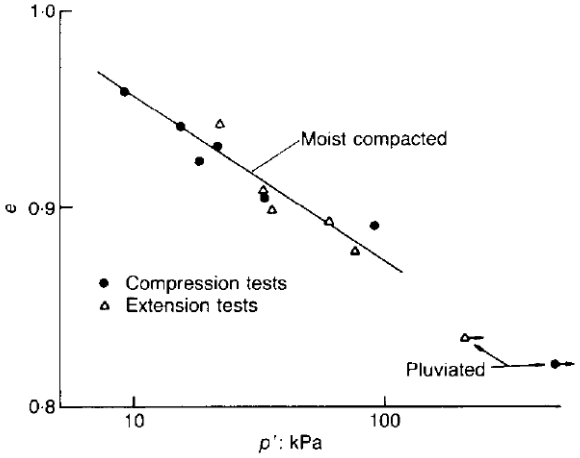

Figure 2.19 Effect of stress path on the critical state line of Toyura sand (extension versus compression) (Been et al., 1991)

Most of the research carried out to investigate the uniqueness of CSL/SSL involved tests on loose samples of sands. Dense specimens of sand develop shear bands after peak strength is achieved (e.g. Been et al. 1991) and therefore a non-homogeneous deformation of the samples is expected. Traditionally, the CS in dense samples has been determined measuring global strain but this may not reflect the true response in the soil. Casagrande (1936) concluded that it is not possible to determine the

critical void ratio of dense sands from global measurements from triaxial tests due to the formation of shear bands.

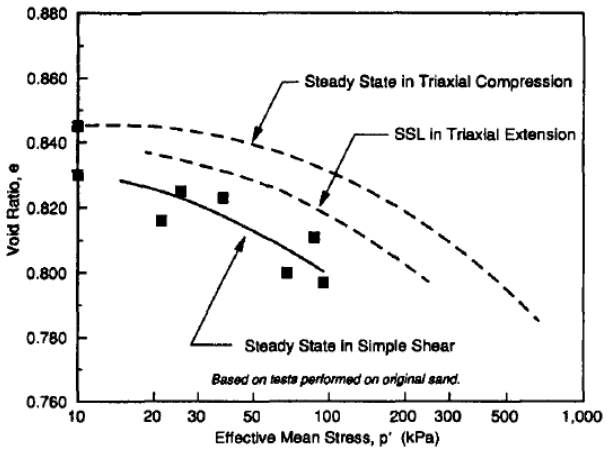

Figure 2.20 Steady state lines from undrained simple shear testing compared to SSLs in undrained compression and extension tests (Riemer & Seed, 1997)

As mentioned in previous paragraphs, Been et al. (1991) noted that the definition of the CSL with tests on dense drained specimens is poor because the samples are generally still dilatant at the end of the test and shear band localization occurs (Figure 2.14). Many authors have tried to quantify the evolution of the local void ratio within the shear band using different techniques including stereophotogrammetry, X-ray tomography, Digital Image Correlation (DIC) (e.g. Roscoe, 1970; Desrues et al., 1996; Finno et al., 1996; Mooney, 1997; Finno & Rechenmacher, 2003). Although these methods provide an excellent view of the shear band within the sample, it should be noted that there are limitations on the resolution that can be achieved for local volume measurements.

Finno & Rechenmacher (2003) conducted a series of drained plane strain compression tests on dense specimens of mansory and concrete sands to study the influence of initial density and subsequent consolidation history on the relationship of the void ratio and effective stress at the critical state. The index properties of the two sands are given in Table 2.2. All the masonry sand samples were prepared by dry pluviation at different initial densities. The concrete sand specimens were also prepared by dry pluviation except for three samples that were prepared by vibratory compaction (C27, C28 and C29). The complete stress-strain behaviour for each test was computed combining the pre-peak global specimen response and the post-peak shear band response. The volumetric and shear strains within the shear band were determined by using Digital Image Correlation (DIC) together with a linear regression technique to formulate a displacement function. Figure 2.21 shows the CSLs for each sand tested together with the SSL derived by Finno et al.

(1996) from undrained plane strain compression tests on loose masonry sand samples and the CSL measured on loose samples of concrete sand by Riemer et al. (1990). They concluded that the CSL is a function of the initial density of the sand and its subsequent consolidation history. Moreover all the CSLs are parallel.

Property	Masonry sand	Concrete sand
D_{50}	0.32 mm	0.62 mm
C_u (D_{60}/D_{10})	1.3	3.8
C_c ($D_{30}^2/[D_{10}\times D_{60}]$)	1.02	0.67
e_{max}	0.875	0.72
e_{min}	0.60	0.47
G_s	2.68	2.73

Table 2.2 Index properties of masonry and concrete sands (Finno & Rechenmacher, 2003)

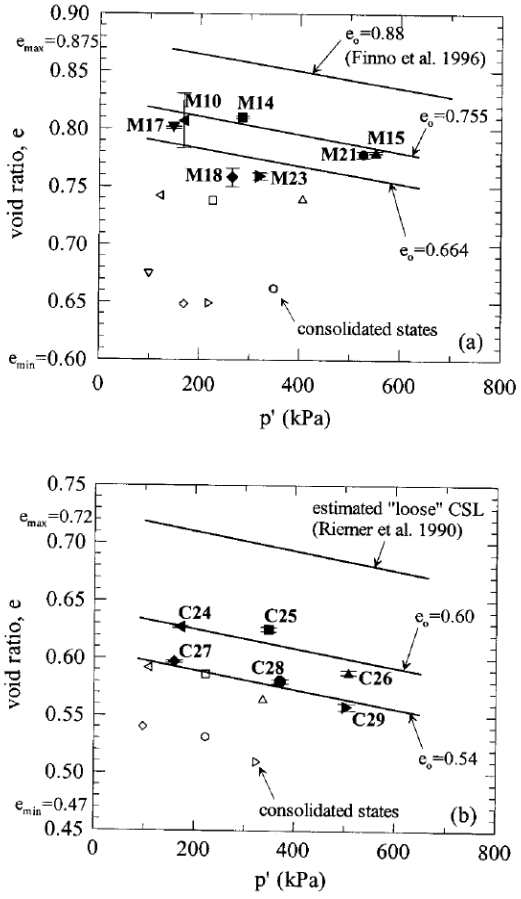

Figure 2.21 Influence of the initial density and compression history on the critical state for (a) masonry and (b) concrete sands (Finno & Rechenmacher, 2003)

The same behaviour was observed by Monney et al. (1998) for masonry sand specimens tested in drained plane compression. They concluded that there is not a

unique critical state void ratio for a given mean effective stress. These cases represent a situation where a non-unique CSL can be identified for samples prepared by the same method. Looking at Figure 2.21, the maximum effective stress reached during compression was p'≤400kPa in all the specimens tested, therefore it could be argued that no particle breakage was taking place in the quartz sands because of the low stress level applied. It would have been interesting to see what would have been the response at higher stress levels when the compression behaviour is controlled by particle breakage.

- **How does particle breakage influence the position of CSL/SSL in the compression plane?**

As mentioned above, recent research on the shearing behaviour of sands, based on experimental and numerical analysis using the Discrete Element Method (DEM), has shown the importance of particle breakage on the position and slope of the CSL/SSL in the compression plane (e.g. Cheng et al., 2005; Muir Wood & Maeda, 2008; Muir Wood, 2008).

Using DEM, Cheng et al. (2005) carried out simulations involving agglomerates of spherical particles that were able to break during compression and shearing. They showed that the CSL for test simulations starting on the virgin compression line for both denser and looser samples is unique in the compression plane. On the contrary, specimens that had been taken to the virgin compression line and then unloaded to various stresses for shearing, reach a different unique CSL compared to the samples that are not unloaded (Figure 2.22).

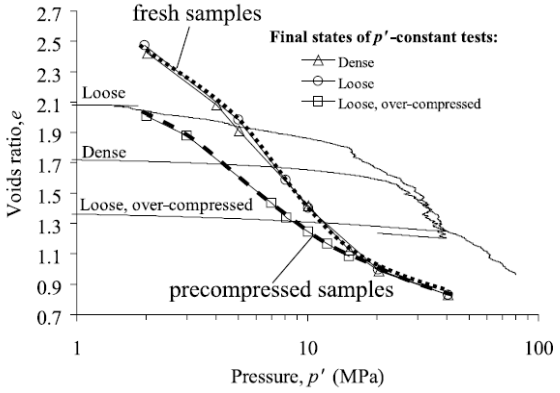

Figure 2.22 End points of constant p' shearing tests on assemblies of agglomerates; effect of precompression on final state (Data from Cheng et al., 2005) (redrawn by Muir Wood, 2008)

Muir Wood (2008) pointed out that once recompression reaches a sufficiently high stress level, the amount of particle breakage equals that in the compressed samples and the CSL conditions coalesce. Assuming that there is a limiting grading distribution for a given soil due to particle breakage during compression and shearing (e.g. McDowell & Bolton, 1998; Coop et al., 2004; Altuhafi et al., 2010), Muir Wood & Maeda (2008) proposed the *grading state index* (I_G) which is defined as the ratio of the area under the current grading ABC to the area under the limiting grading ABD (Figure 2.23). Using DEM Muir Wood & Maeda demonstrated that the location of the CSL changes in the compression plane as the grading changes (I_G increases) (Figure 2.24).

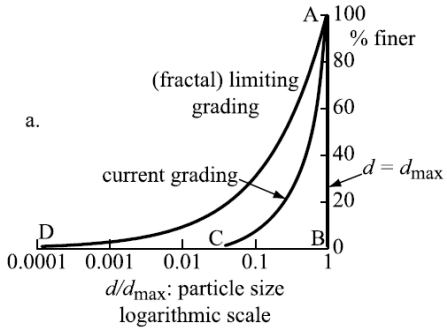

Figure 2.23 Fractal limiting particle size distribution and definition of grading state index I_G (Muir Wood & Maeda, 2008)

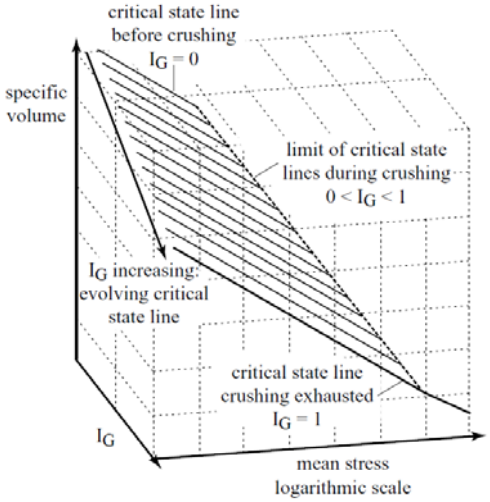

Figure 2.24 Critical state surface in v:logp':I_G space (Muir Wood & Maeda, 2008)

The CSLs are linear and the compression behaviour can be described by Equation 2.3, where $\lambda(I_G)$ and $\Gamma(I_G)$ are the slope of the CSL and the specific volume at a mean effective stress of p'=1kPa for a given value of I_G, and v and p' are the current specific volume and mean effective stress. They also proposed that the change in slope of the CSL is small as I_G increases and therefore it could be assumed that the CSLs are all parallel to one another (Figure 2.24). This approach contrasts with earlier experimental work in which a unique critical state line was assumed for a given soil regardless the particle breakage. The main difference between the two approaches is the question of whether the soil "knows" about the breakage that it has undergone during compression and shearing.

$$v = \Gamma(I_G) - \lambda(I_G) \cdot \mathrm{Ln}p' \qquad 2.3$$

Bandini & Coop (2011) carried out a series of triaxial tests to investigate the effect of particle breakage on the current location of the critical state line for samples of Dogs Bay sand. They used two different shearing stages. The first one was intended to produce particle breakage and the second one to see if the material "remembers" the original state when it was sheared again. They concluded that the CSL does move vertically in the compression plane with particle breakage and so the soil does "remember" about the particle breakage that has occurred before the final shearing to reach the CS. They also showed that the effect of particle breakage is not only to move the CSL vertically but also to rotate it (Figure 2.25). In addition, Bandini & Coop conducted more triaxial tests on reconstituted specimens with the same grading as the pre-sheared samples in order to compare them. They concluded that the CSL of the same soil when reconstituted is found to be very different to that resulting from prior breakage with no reconstitution (Figure 2.26). This finding does not support the hypothesis made by Muir Wood & Maeda (2008) which involves the assumption that the soil "knows" what its current grading is and therefore the behaviour of the soil that has undergone some breakage would be the same as that of the same soil that had been reconstituted at the new grading. Therefore, this confirms that although the soil does have some "knowledge" of its current grading, its behaviour is still largely a function of its initial grading.

Probably the most important contribution by Bandini & Coop was to emphasise that large amounts of particle breakage are required to create a significant shift in the position of the CSL. They pointed out that in most of the engineering applications much smaller amounts of particle breakage would be expected. Consequently the effect of particle breakage on the position of the CSL in the compression plane might be irrelevant and therefore a unique CSL could be adopted in a simple constitutive model.

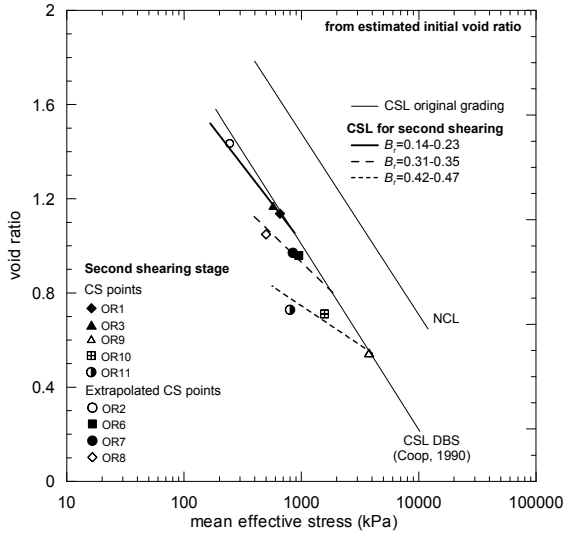

Figure 2.25 Critical state lines for Dogs Bay sand after second shearing stage (Bandini & Coop, 2011)

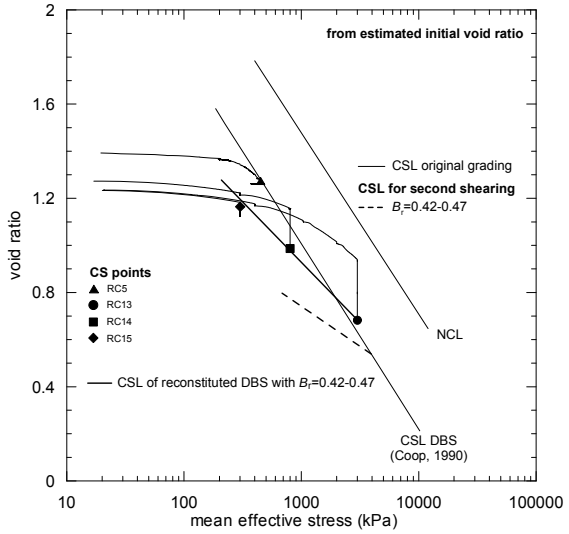

Figure 2.26 Critical state line for reconstituted samples of Dogs Bay sand with the same grading as the pre-sheared ones (Bandini & Coop, 2011)

Sadrekarimi & Olson (2011) also studied the influence of particle breakage on the position of the CSL in the e:logσ'_n compression plane for three selected sands: OT, IR and MR. They used a new ring shear device (Sadrekarimi & Olson, 2009) and constant volume ring shear (RS) tests were performed. The OT and IR sands were medium-grained, clean pure quartz sands with rounded to sub-rounded particles, while MR was a silty sand. Focusing on the behaviour of the clean sand, Figures 2.27 and 2.28 show the CSLs and NCLs for the original samples before particle damage, CSL_0 and NCL_0, and after particle damage was complete, CSL_c and NCL_c.

It is understood that the meaning of "complete" indicates a certain degree of particle breakage and not that samples have reached a limiting grading distribution where breakage is exhausted. The NCL_c were obtained from oedometer tests on sand collected from the shear band of the RS tests. They concluded that particle damage changes the position and increases the slope of the CSL_c and NCL_c in the compression plane. Moreover, they pointed out that the CSL and NCL are parallel. Looking again at Figures 2.27 and 2.28, it is very important to notice that the space between the CSLc and NCLc is very much larger than has been seen previously in other soils and therefore the conclusions drawn from these results should be interpreted carefully.

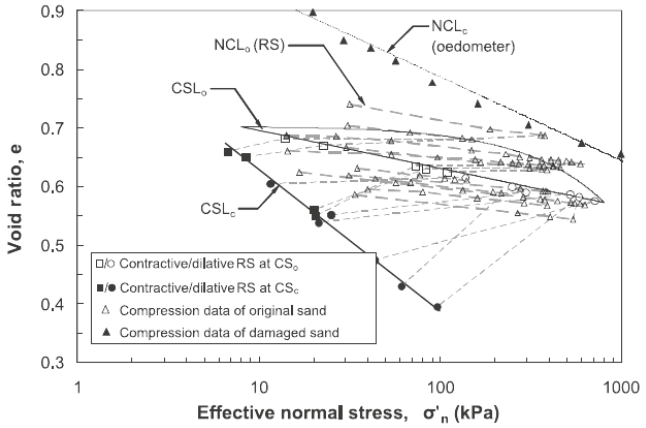

Figure 2.27 NCL and CSL of the original and damaged OT sand (Sadrekarimi & Olson, 2011)

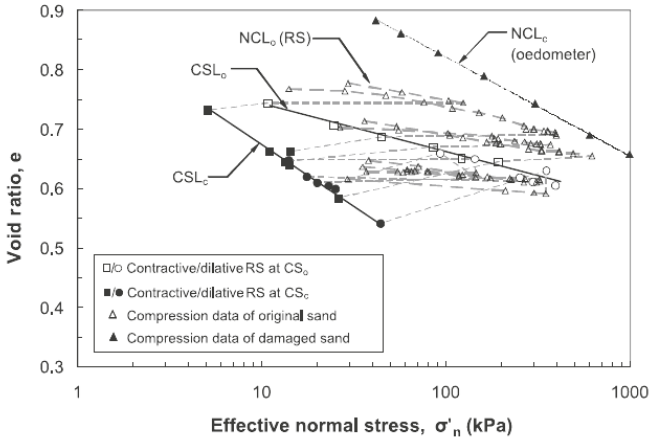

Figure 2.28 NCL and CSL of the original and damaged IR sand (Sadrekarimi & Olson, 2011)

The conclusions obtained by Sadrekarimi & Olson (2011) are partially in agreement with Bandini & Coop (2011). In both studies it has been demonstrated that

particle breakage changes the position of the CSL in the compression plane but while in Bandini & Coop the slope of the CSL decreases in Sadrekarimi & Olson it increases. In any case, these findings clearly show that the CSL slope changes as I_G increases and the evidence does not support the hypothesis made by Muir Wood & Maeda (2008) where they assumed that the CSL slope changes are of a second order compared to its position.

Throughout the discussion presented above, it is assumed that the soil being tested reaches a final critical state where deformation continues at constant effective stress and constant void ratio. Coop et al. (2004) showed, through a series of ring shear tests, that the particle breakage and volume change continue to very large strains, far beyond those reached in triaxial tests (Figure 2.29). They concluded that the apparent critical state or constant volume seen in a triaxial test for a sand is not rigorous and it represents a transient state of constant volume due to the counteracting dilative strain from particle rearrangement and compressive strain from particle breakage. This behaviour is in agreement with the assumption made by Chandler (1985) although his model is for particle deformation instead of particle breakage.

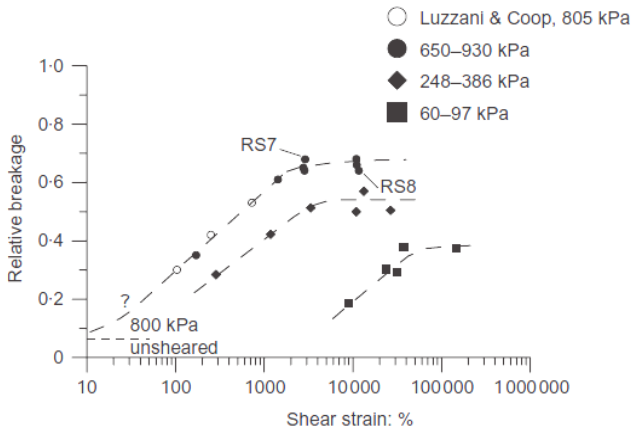

Figure 2.29 Relative breakage of Dogs Bay sand in ring shear tests under different normal stresses (Coop et al., 2004)

The angle of shearing resistance at the critical state (ϕ'_{cs}) depends on the uniformity of particles, their shape and mineralogy. However, particle breakage appears to have no measurable effects on ϕ'_{cs} (e.g. Coop, 1990; Coop et al., 2004). Coop et al. (2004) showed that the ϕ'_{cs} is reached well before particle breakage is complete and that continued shearing at very large strains has no effect on it (Figures 2.29 and 2.30).

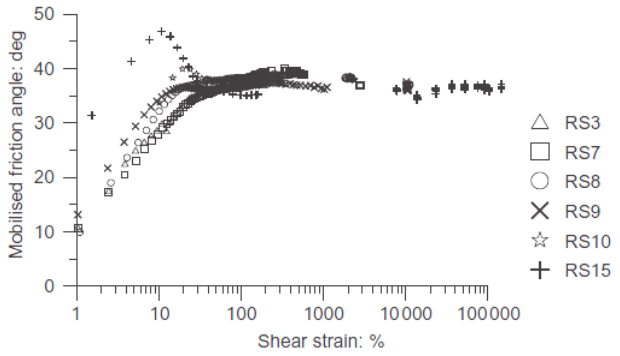

Figure 2.30 Evolution of mobilised shear strength angle with shear strain (Coop et al., 2004)

- **What is the shape of the CSL/SSL over a wide range of stresses?**

Many authors have shown that the CSL for a given sand can be modelled in the compression plane as bi-linear (e.g. Been & Jefferies, 1985; Konrad, 1998) (Figure 2.15), or curved (e.g. Verdugo & Ishihara, 1996) (Figure 2.16). Figure 2.31 shows the bi-linear nature of the CSL proposed by Konrad (1998). The change in the slope of the CSL is assumed to correspond to the onset of particle breakage during shearing at high stresses. At lower stress levels it is supposed that particle breakage is negligible and only some damage is taking place (e.g. abrasion or grinding of particle surface asperities). The break point in the CSL is expected to be dependent on sand mineralogy, stress conditions (isotropic, anisotropic) and initial density.

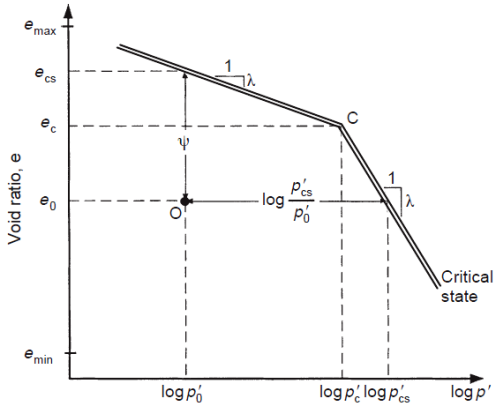

Figure 2.31 Idealised critical state line for a sand (Konrad, 1998)

Russell & Khalili (2004) proposed a three part critical state line in their bounding surface plasticity model for sands exhibiting particle crushing (Figure 2.32). Each part of the curve corresponds to a different mechanism. The response between

point A and B is due to rearrangement of particles in the form of sliding and rotation. At point B the onset of particle breakage starts to be important and a steeper line is observed between B and C. Finally the response between C and D is controlled by pseudoelastic behaviour and particle breakage is complete.

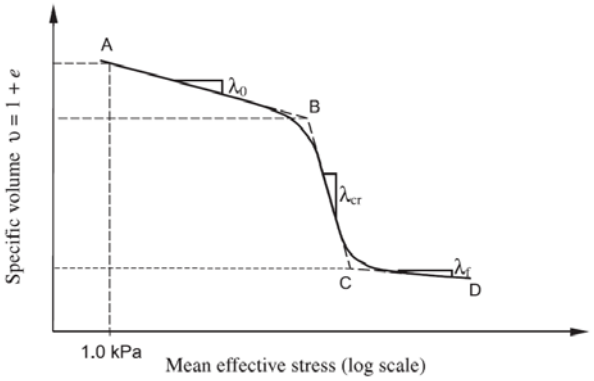

Figure 2.32 General critical state line shape for sands (Russell & Khalili, 2004)

2.4 Mechanical behaviour of intermediate graded soils

Traditionally, research into the behaviour of granular material has been mainly concentrated on clean sands. However, intermediate graded soils are more widely encountered either as natural or as reconstituted material and are also more commonly used in earth construction practice. These soils represent a class of geomaterials with gradings in between those of clays and sands. Adding a small amount of fines to a clean sand can change its behaviour dramatically (e.g. Been & Jefferies, 1985; Coop & Atkinson, 1993).

2.4.1 Packing in intermediate graded soils

The possible regular packing arrangements of spheres of the same size are shown in Figure 2.33 (Mitchell, 1993). It can be demonstrated that the limiting void ratios of idealized spherical particles are e=0.34 and e=0.91 which are independent of particle size. In real soils, particle size is more varied and therefore smaller particles can occupy the pore spaces between larger ones. Therefore, it follows that adding smaller particles into an arrangement of larger uniform particles will alter the limiting void ratios (e.g. Kuerbis et al., 1988; Lade & Yamamuro, 1997; Lade et al., 1998). Many factors such as particle shape and diameter ratio (d_{large}/d_{small}) can influence the maximum and minimum void ratios that can be obtained (e.g. Fraser, 1935; McGeary, 1961).

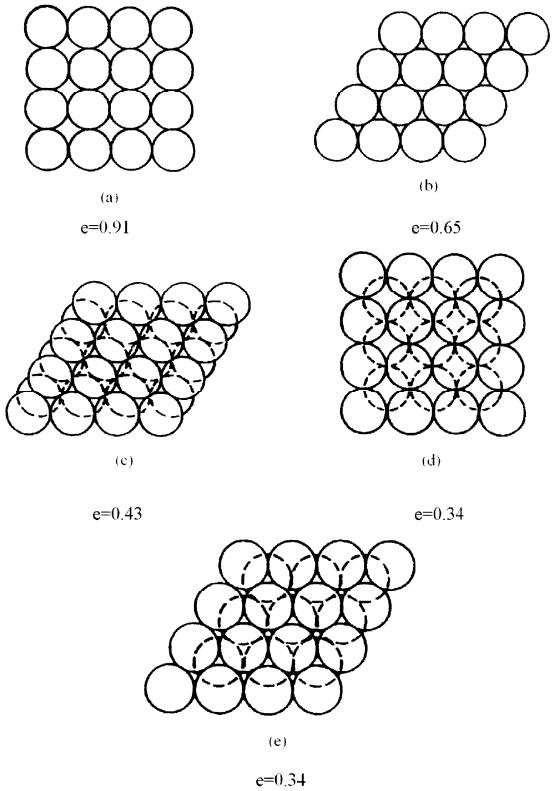

Figure 2.33 Ideal packings of uniform spheres: (a) simple cubic, (b) cubic tetrahedral, (c) tetragonal sphenoidal, (d) pyramidal and (e) tetrahedral (Mitchell, 1993)

Lade et al. (1998) investigated the theoretical variation of minimum void ratio with the percentage fines (soil particles of diameter less that 0.075mm) for a binary packing (fabric) of two grain sizes of uniform spheres. If the diameter ratio is large enough (more than 7, MacGeary, 1961) the larger particles will not be pushed apart when one single smaller particle is inserted into the primary packing (initial fabric) of the larger one (Figure 2.34). It can be seen that the minimum void ratio decreases as the % fines increases until a minimum void ratio (e_{min}) is reached. This e_{min} represents a point in the e:%fines plane where all the available voids in the primary packing are filled with fines. If the % fines continues to increase the larger particles are pushed apart and the behaviour of the binary packing will be mainly controlled by the fines.

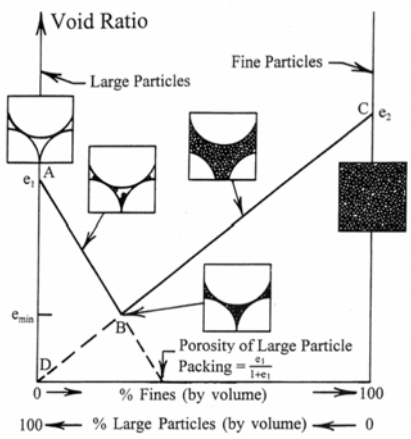

Figure 2.34 Theoretical variation of minimum void ratio in a binary packing with % fines (Lade et al., 1998)

Assuming that the specific gravity of the particles (G_s) is constant, it can be demonstrated that the % fines at which e_{min} is reached can be obtained from Equation 2.4 (Lade et al., 1998):

$$\% \text{ fines} = \frac{n_1 \cdot \frac{n_2}{e_2}}{\frac{n_1}{e_1} + n_1 \cdot \frac{n_2}{e_2}} \cdot 100 \qquad 2.4$$

where n and e are the minimum porosity and minimum void ratio for the larger and the smaller spheres. This expression can be extended for the tertiary and quaternary packings (Lade et al., 1998). Figure 2.35 shows an example of the influence of adding non-plastic fines to samples of Ottawa 50/200 sand on the variation of maximum and minimum void ratios (Lade & Yamamuro, 1997).

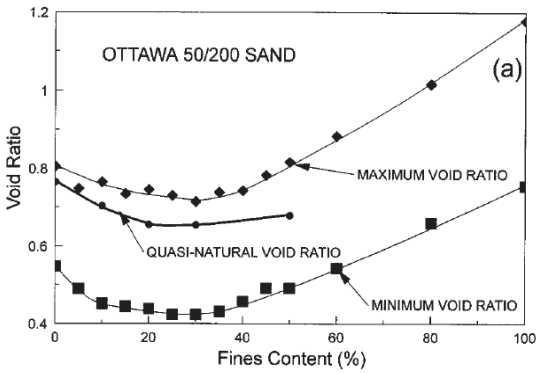

Figure 2.35 Influence of adding non-plastic fines on the maximum and minimum void ratios of Ottawa sand (Lade & Yamamuro, 1997)

Traditionally, void ratio (e) has been one of the most important parameters used to describe soil behaviour. The fabric of a granular mix can be very complex as shown schematically in Figure 2.36 (Thevanayagam et al., 2002). Many authors (e.g. Mitchell, 1976; Vaid, 1994; Thevanayagam, 1998) realised that e is not a suitable parameter to characterise the behaviour of mixed soils such as those in Figure 2.36 which led them to introduce two new void ratios, the granular void ratio (e_c) and fine void ratio (e_f), which are defined as follows:

$$e_c = \frac{e + fc}{1 - fc} \qquad 2.5$$

$$e_f = \frac{e}{fc} \qquad 2.6$$

where fc is the fines content, defined as the volume of fines divided by the total volume of solids.

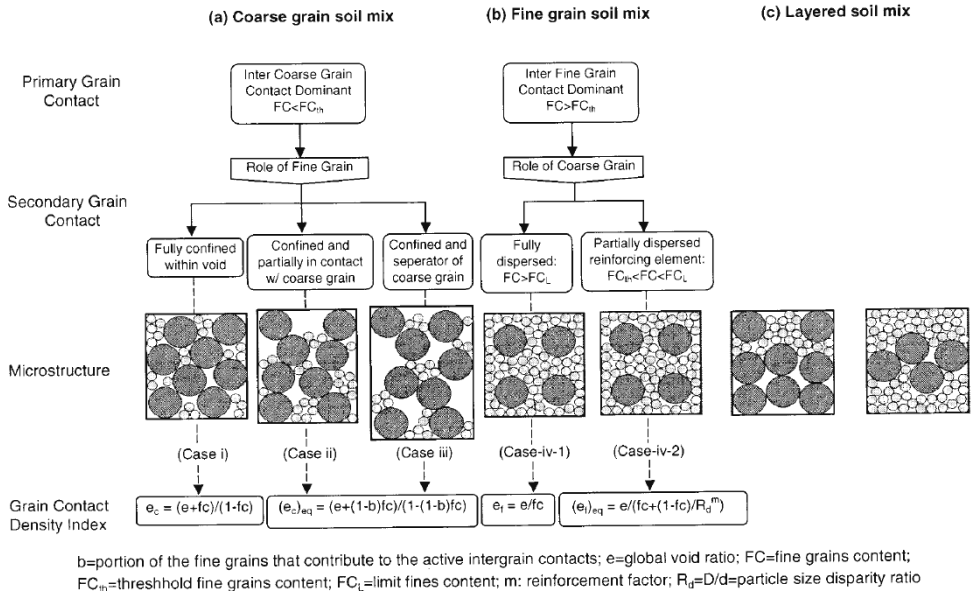

Figure 2.36 Intergranular classification (Thevanayagam et al., 2002)

Thevanayagam (2000a) defined a threshold fines content (FC_{th}) as:

$$FC_{th} \le \frac{100 \cdot e_c}{1 + e_c + e_{max,HF}}\% = \frac{100 \cdot e}{e_{max,HF}}\% \qquad 2.7$$

where $e_{max,HF}$ is the maximum void ratio of the pure silt above which it has no appreciable strength. He proposed that when the fine grain content ($FC = fc \cdot 100$) is

lower than FC_{th} the coarse grain contacts play a primary role in the soil behaviour with the fines offering a secondary contribution. If $FC>FC_{th}$, the fine grain contacts begin to play a greater role as the coarse grains begin to disperse and provide a secondary reinforcement effect until they are separated sufficiently. This implies a limiting fines content (FC_L), above which the fines control soil behaviour. Therefore it was suggested that a transition zone exists between the FC_{th} and FC_L where the soil is not completely governed by the content of fine grains. The FC_L is defined by:

$$FC_L \geq 100 \cdot \left[1 - \frac{\pi \cdot (1+e)}{6 \cdot s^3}\right]\% = 100 \cdot \left[\frac{6 \cdot s^3 - \pi}{6 \cdot s^3 + \pi \cdot e_f}\right]\% \geq FC_{th} \qquad 2.8$$

where $e_f \leq e_{max,HF}$ and where $s=1+a/Rd$ is the spacing between fine grains, $Rd=D/d$ is the size disparity ratio (defined before as diameter ratio) and $a=10$.

For $FC<FC_{th}$, Thevanayagam et al. (2002) introduced a new parameter, b, to represent the portion of fine grains that contributes to the active intergrain contacts and proposed an equivalent intergranular contact void ratio $(e_c)_{eq}$ as follows:

$$(e_c)_{eq} = \frac{e + fc \cdot (1-b)}{1 - fc \cdot (1-b)} \qquad 2.9$$
$$0 < b < 1$$

They suggested that the value of b should be between 1 and 0. If b=0, the fines have no effect on soil behaviour and if b=1, all the fine grains actively participate in supporting the soil skeleton and $(e_c)_{eq}$ reduces to e_c. Ni et al. (2004) pointed out that the plasticity of the fines could influence the b value and found that the limits for b appear to be $-\infty \leq b \leq 0$ for plastic fines and $0 \leq b \leq 1$ for non-plastic fines.

When $FC_L>FC>FC_{th}$ they suggested there would be a reinforcement effect of coarse grains and proposed an equivalent interfine void ratio $(e_f)_{eq}$ as follows:

$$(e_f)_{eq} = \frac{e}{fc + \frac{(1-fc)}{R_d^m}} < e_f \qquad 2.10$$

where $0<m<1$ and $m=a$ is a coefficient that depends on grain characteristics and fine grain packing.

Thevanayagam et al. (2002) also suggested that when $FC>FC_{th}$, the fine grains will control the soil behaviour and e_f could be used as a first approximation for grain contacts in the soil matrix. Moreover, when $FC<FC_{th}$, the coarse grains dominate and e_c could be used to represent the interparticle contacts.

2.4.2 Effect on the compression line of adding fines to granular soils

Coop & Atkinson (1993) investigated the effect of fines on the location of the NCL for the Dogs Bay sand (DBS) at high stresses. They added a quantity of 24% non-plastic fines to a reconstituted sample of Dogs Bay sand. The non-plastic fines were gypsum or calcium carbonate. Figure 2.37 shows how the addition of fines causes a reduction in the specific volume and a flattening of the NCL. They concluded that the change in grading rather than in mineralogy influences the behaviour of the soil.

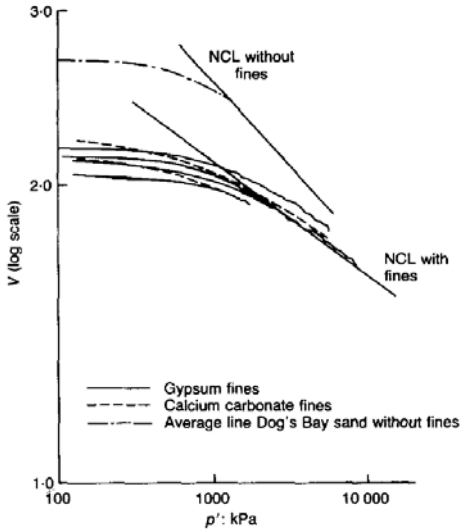

Figure 2.37 Isotropic compression of samples with and without fines (Coop & Atkinson, 1993)

Been & Jefferies (1985) examined the effect of adding fines to the Kogyuk sand which is a uniform, medium quarztzitic sand. They pointed out that the compressibility increases with increasing fines content. The differences in behaviour of these two mixtures investigated may be related to the stress level at which the compression behaviour was analysed. While Coop & Atkinson (1993) investigated the effects of fines at high stresses, where particle breakage controls the soil behaviour, Been & Jefferies (1985) studied the compression behaviour at stress levels before the onset of particle breakage. Looking at Figure 2.37, and focusing on

the behaviour at lower stresses it can be seen that the compressibility of the samples with fines is higher than that of samples without fines, especially for the calcium carbonate fines. This behaviour at low stresses supports the conclusion of Been & Jefferies (1985).

More recently, Altuhafi & Coop (2011) showed that adding fines to a uniformly graded sample of DBS reduces the slope of the NCL at high stresses for each grading and therefore well-graded sands will have a lower compression index. They also pointed out that the particle breakage in well-graded mixtures of DBS was smaller compared to a uniformly graded one. Moreover, Altuhafi & Coop noted that with the reduction of breakage for well-graded sands the NCL is not unique for a given grading even at very high stresses and a *transitional* behaviour was observed.

Carrera et al. (2011) studied the one-dimensional compression behaviour of silt and sand mixtures in different proportions. It was found that as the fines content increases the specific volume reduces and the NCL flattens (Figure 2.38). It was also observed that as the fines content increases the NCL moves downwards and reaches a minimum at fines contents between 50% and 70%. It is interesting to see how the NCL for the pure silt moves upwards again and its position approximately corresponds to the NCL for the 30% fines content sample. Another important aspect to note is that once the fines content reaches a value of 30% the slope of the NCL hardly changes. This behaviour shows the transition from pure sand to pure silt response.

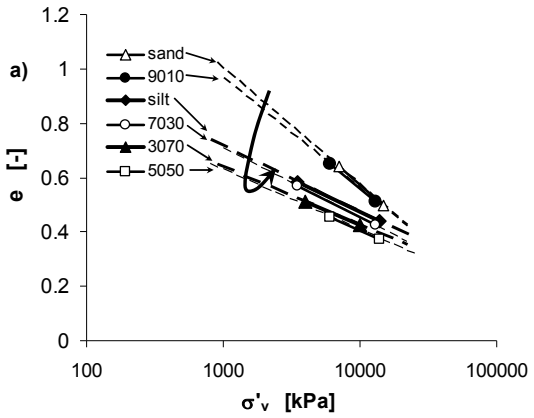

Figure 2.38 One-dimensional compression behaviour of silt and sand mixtures (Carrera et al., 2011)

Carrera et al. (2011) used the equivalent intergranular contact void ratio $(e_c)_{eq}$ to characterise the behaviour of three mixtures of soils of different fines contents and

with the parameter b equal to 0.8. The results were compared to the compression behaviour of a pure sand sample (Figure 2.39). An apparent convergence towards a unique NCL can be seen for mixtures containing 10% and 30% of fines and the pure sand whereas the compression curve for the 50% fines content mixture is flatter and tends to cross the NCL of the others samples. It seems that there is a transitional fines content between 30% and 50% where the fines start to control the soil's behaviour which might be the reason why the $(e_c)_{eq}$ could not be used to characterise the response at high fines contents.

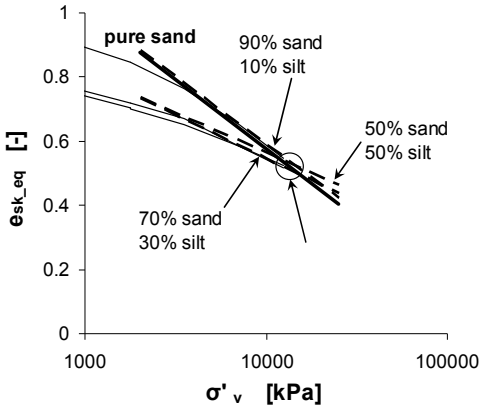

Figure 2.39 One-dimensional compression curves of three different mixtures considering the equivalent intergranular specific volume (Carrera et al., 2011)

In the cases presented above only non-plastic fines were used. One question immediately arises; what would be the effect of plastic fines on compression behaviour? Yin (1999) studied the influence of fines content on the properties of Hong Kong marine deposits with mixtures of silica silt and sand with different clay contents. He correlated the plasticity index (I_p) with compressibility and showed that an increase in I_p resulted in an increase in the compression index (C_c) at stresses lower than 1MPa.

2.4.3 Effects on the critical state line of adding fines to granular soils

The effects of adding fines on the critical state line of sands were first investigated by Been & Jefferies (1985). They examined the effect of fines on the location of the steady state line at stress levels below the onset of particle breakage (Figure 2.40). They found that the slope of the SSL increases with increasing fines content. The same tendency has been seen in the in the idealized effects of fines content on SSL presented by Bouckovalas et al. (2003).

A number of studies of the influence of fines content on the undrained monotonic response of sands have been published (e.g. Zlatovic & Ishihara, 1995; Lade & Yamamuro, 1997; Thevanayagam, 1998; Thevanayagam & Mohan, 2000; Thevanayagam et al., 2002; Ni et al., 2004; Yang et al., 2006; Murthy et al. 2007; Rahman & Gnanendran, 2008).

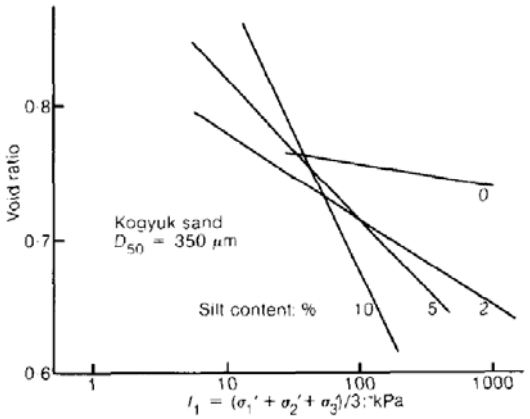

Figure 2.40 Steady state lines for Kogyuk 350 sand with different silt contents (Been & Jefferies, 1985)

Thevanayagam et al. (2002) carried out an experimental programme to investigate the effects of fines on the shear behaviour of the F55 silica Foundry sand mixed with different amounts of non-plastic crushed silica fines. Figure 2.41 shows the grain size distribution for each of the mixes tested. All the samples were prepared by air-dry deposition or the moist tamping method. They found a unique steady state line for each grading and also that all the SSLs are parallel to one another (Figure 2.42a). As the silt content increases towards 40%, the position of the SSLs moves downwards and with a further increase of fines the position of the SSL changes direction, moving upwards until the silt content reaches 100%. The same behaviour has been reported by other authors. For example Zlatovic & Ishihara (1995) found that the SSLs for mixtures of Toyoura sand and non-plastic silt moves downwards until the silt content increases to approximately 30% and then the SSLs move upwards to represent the behaviour of the pure silt.

Figures 2.42(b), (c) and (d) show the steady state data from the tests of Thevanayagam et al. (2002) plotted against the new void ratios e_c, $(e_c)_{eq}$ and $(e_f)_{eq,}$. At low fines contents, where $FC<FC_{th}$, the intercourse grain friction is the dominant mechanism affecting the mechanical response of the mixtures. Figure 2.42(c) shows that the behaviour of all the silty sand specimens is similar to that of the host sand. On the other hand, at high fines contents, where $FC>FC_{th}$ the

mechanism that controls the behaviour is the interfine contacts and all the sandy silt specimens respond similarly to the host silt (Figure 2.42d).

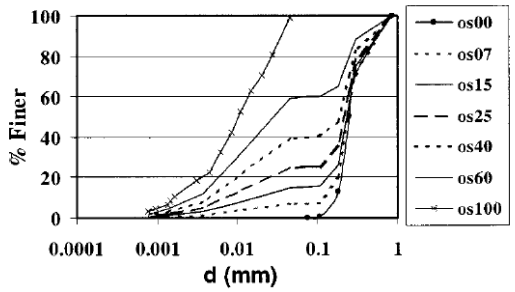

Figure 2.41 Grain size distributions for F55 Foundry sand mixed with fines at different proportions (Thevanayagam et al., 2002)

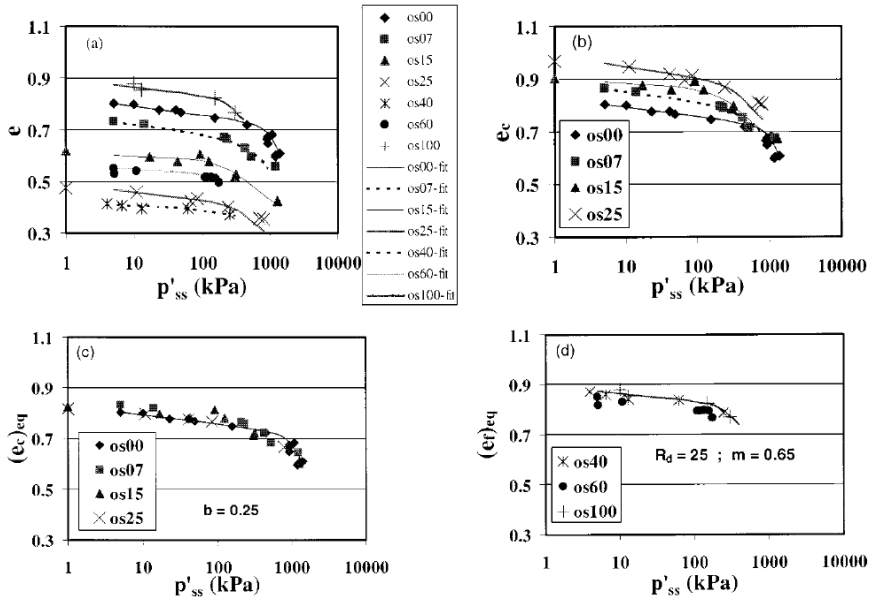

Figure 2.42 Steady state lines for F55 Foundry sand mixed with fines at different proportions (Thevanayagam et al., 2002)

It has been noted that there exists a fines content when the soil behaviour changes from a coarse-grain dominated mode to a fine-grain dominated one. This fines content has been named by different authors as; the limiting silt content (Polito & Martin, 2001), the threshold fines content, FC_{th} (Thevanayagam et al., 2002) as presented above, the transitional fines content, TFC (Yang et al., 2006). A summary of previous reported transitional fines contents from the literature is presented in Table 2.3. Mitchell (1993) shows that for water contents usually encountered in practice, the clay fraction needed to dominate soil behaviour of a mixture of clay and granular particles is about 30%. This quantity is sufficient to prevent any granular particle contact.

Source	Host Sand	Host Fines	Transitional fines content (%)
Zlatovic & Ishihara (1995)	Toyoura	Milled Toyoura sand	30
Polito (1999)	Yalesville	Yalesville silt	37
Polito & Martin (2001)	Monterey 0/30	Yalesville silt	32
Thevanayagam et al. (2002)	F55 Foundry	Sil co sil N_0 40	25
Naemi & Baziar (2004)	Ardebil	Silt	35
Carrera et al. (2011)	Stava tailings		50-70
Yang et al. (2006)	Hokksund	Chengbei	30

Table 2.3. Transitional fines contents reported by different authors

It can be concluded that, based on available reported data in the literature, part of which has been reviewed here, there are two main hypotheses with regard to the influence of fines content on the CSL/SSL for sand-silt mixtures:

- The slope of the CSL/SSL changes with increasing fines content (e.g. Been & Jefferies, 1985; Bouckovalas et al., 2003)
- The CSLs/SSLs are more or less parallel to one another. Moreover, as the fines content increases, the position of the CSL/SSL moves downwards up to a certain quantity of fines when the position of the CSL/SSL changes direction, moving upwards until the fines content reaches 100% (e.g. Zlatovic & Ishihara, 1995; Lade & Yamamuro, 1997; Thevanayagam, 1998; Thevanayagam & Mohan, 2000; Thevanayagam et al., 2002; Ni et al., 2004; Yang et al., 2006; Murthy et al. 2007; Rahman & Gnanendran, 2008).

Finally it is also important to mention that based on the analysed data, a unique CSL/SSL can be identified in each case for a given sand-silt grading irrespective of the argument presented above.

2.4.4 Effects of sample preparation technique on the NCL and CSL/SSL

In Section 2.3.1 and 2.3.2 it was noted that the sample preparation method does not affect the position of the NCL and CSL/SSL for clean sands. Naeini & Baziar (2003) carried out an investigation to study the influence of fines content and sample preparation method on the position of the SSL for mixed and layered samples of Ardebil sand with silt. Samples were prepared in their loosest state by means of water sedimentation and using compaction techniques. Three types of samples were prepared; (a) a predetermined amount of a sand-silt mixture was dropped into water and left for enough time to assure that all the particles were completely settled. This process was repeated until the sample was created. As expected, this method induced segregation and the sand particles were deposited at the bottom of each layer (b) under compacted samples were prepared by compaction of moist sand-silt mixtures in layers (c) layered samples were formed by compacting alternate layers of sand and silt. This method was used to simulate the layered samples created by water sedimentation techniques.

Figure 2.43 shows the results obtained by Naeini & Baziar from undrained triaxial tests. For samples prepared by the same method, it can be seen that an increase in fines content moves the SSL downwards and all of them are parallel to one another which is in agreement with the second hypothesis presented above. On the other hand, for a given fines content, the SSL is not unique and depends on the sample preparation technique. It appears that segregation during sample preparation might lower the position of the CSL/SSL with respect to a more homogeneous sample prepared by compaction for any given mixture. This behaviour clearly shows the influence of sample preparation method, and therefore initial fabric, on the uniqueness of the SSL. In agreement with this, Chang et al. (2011) showed that the CSL of slurries, moist tamped and undisturbed samples of gold tailings is non-unique in the e:logp' plane and depends on the initial fabric. They also noted that the samples reach a unique stress ratio M irrespective of the sample preparation technique.

Coop & Cotecchia (1995) and (1997) carried out a series of compression and triaxial tests on sediments from the archeological site of Sibari, Italy. They found that the NCL and CSL for naturally layered structure of the samples tested were located above the intrinsic NCL and CSL. This conclusion disagrees with the results shown in Figure 2.43 where the position of the CSL is lower for layered samples compared to the more homogeneous one.

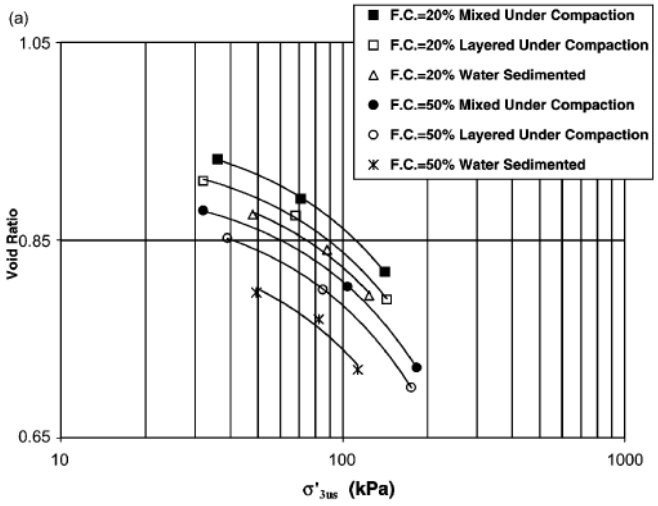

Figure 2.43 Steady state lines for triaxial tests on samples prepared by different techniques and at different fines contents (Naeini & Baziar, 2003)

Santucci de Magistris et al. (1998) investigated the mechanical behaviour of artificially prepared samples of the Metramo silty sand derived from the weathering of a granite rock. Two sample preparation methods were used: slurry and dynamic compaction. Figure 2.44 shows the compression behaviour of two specimens prepared at different initial densities and by different methods. It can be seen that the compression curve for a compacted sample intersects that of a remoulded one and there is no tendency for convergence onto a single NCL. The authors attributed the differences in compressibility to the initial different fabrics that result from the different sample preparation methods. They also concluded that at high stresses the initial fabric can not be removed and some differences remain. In terms of shearing behaviour at large strains, the results showed that a unique CSL/SSL exists in the v:lnp' plane in the stress range of 50–800kPa where the samples were tested. In this case the different initial fabrics are erased by shearing the sample to large strains.

2.5 Transitional soil behaviour

In previous sections the discussion has been focused on the mechanical behaviour at large strains of clean sands and intermediate graded soils. Many authors have pointed out that some factors including structure might have a large influence on soil behaviour. Only a few of these authors have recognized the consequences of a non-unique NCL and/or CSL/SSL for a given soil in using the critical state soil mechanics theory as a reference framework. In this section the definition of *transitional* soil behaviour is presented together with a summary of soils that

exhibited this behaviour. Attention is paid to the factors which could influence this soil response and to the consequences of applying the CSSM framework. Much of the research published in the literature on transitional soil behaviour has been carried out under the supervision of Professor Matthew Coop.

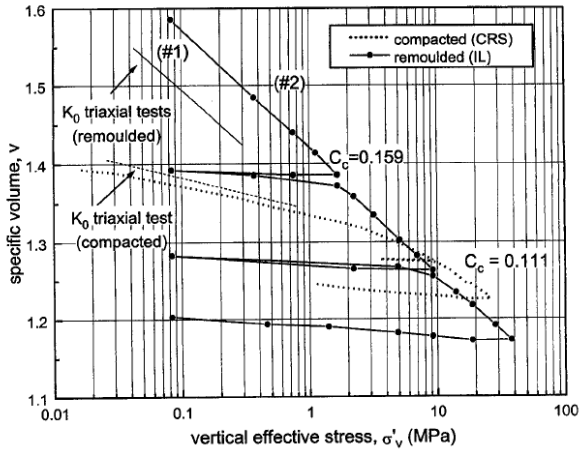

Figure 2.44 One-dimensional compression tests on compacted and remoulded (slurry) samples of the Metramo silty sand (Santucci de Magistris et al., 1998)

2.5.1 Definition of transitional soil behaviour

Traditionally, critical state soil mechanics has been used to describe the behaviour of clays and clean sands as shown schematically in Figures 2.45 and 2.46. For reconstituted clays, initial differences in specific volume (v) are erased at very low stresses (<100kPa) well below the range typically encountered in field and all compression lines converge towards a unique NCL. In terms of shearing to large strains, a unique CSL can also be defined. These unique NCL and CSL, which are parallel to each other, represent the intrinsic properties of a given clay and can be used as a basic frame of reference for interpreting the corresponding characteristics of the natural clay at its in-situ state (Burland, 1990).

On the other hand, volume changes of clean sands are achieved by overcoming interparticle friction through interparticle slip and rotation (elastic component), by overcoming particle strength through different levels of particle damage (plastic component), or both. At lower stresses, initial density controls the compression behaviour and an infinity of NCLs can be defined for each initial density (e.g. Jefferies & Been, 2000). These NCLs could be possibly better called “approaching compression lines”. At higher stresses all the compression lines converge towards a unique NCL at the onset of major particle breakage. A unique CSL/SSL can be defined with an abrupt change in the slope due to the onset of major particle

breakage. It is important to mention that some clastic soils that have a unique NCL and curved CSL like sands showed an insignificant quantity of breakage (e.g. Carrera et al., 2011). Various state parameters have been proposed in literature to characterize the stiffness and strength properties of sands (e.g. Wroth & Basset, 1965; Been & Jefferies, 1984; Ishihara et al., 1998; Wang et al., 2002), using the uniqueness of the CSL/SSL as a reference state for comparison with the current state of the soil. From the discussions in previous sections it can be concluded that there are still contradictory findings regarding the uniqueness of the CSL in the compression plane for a given sand, but little attention has been paid to this.

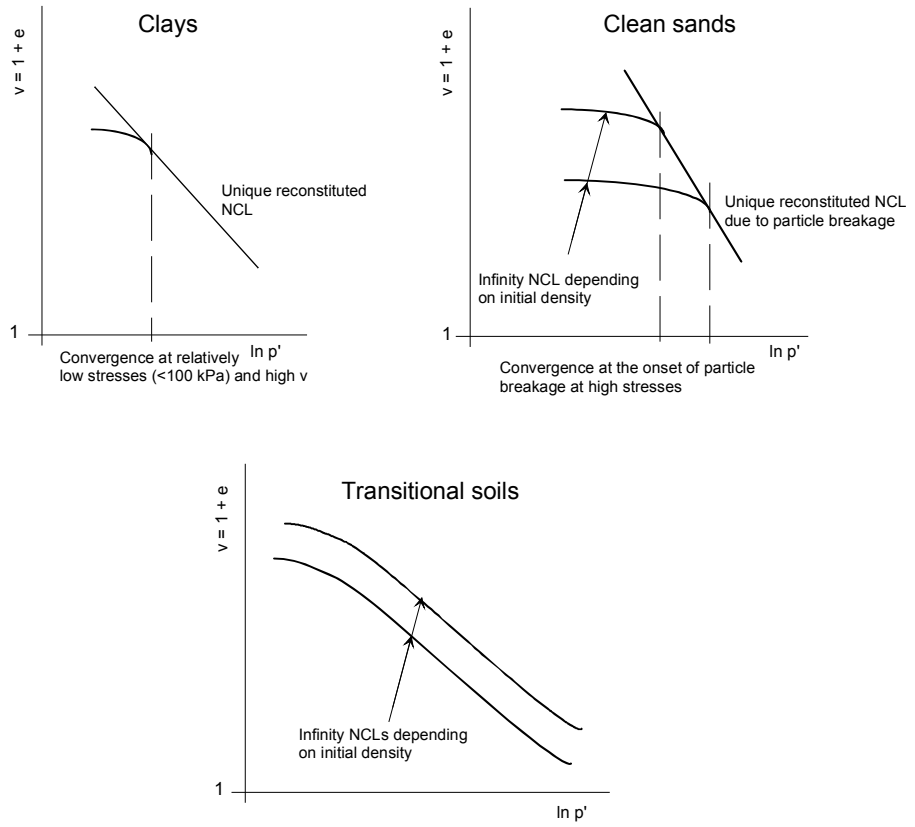

Figure 2.45 Schematic illustration of the compression behaviour of clays, clean sands and transitional soils

A transitional soil is defined as one which has a mode of behaviour between that of clean sands and of clays, where a non-unique NCL and/or CSL/SSL can be identified even at high stress and strain levels (e.g. Nocilla et al., 2006) (Figures 2.45 and 2.46). The lack of convergence towards a unique NCL and/or CSL/SSL from different initial densities must be associated with the stability of the initial

strcuture that can not be removed by compression and shearing alone. This means that the soil "remembers" its initial structure during compression and shearing stages even at large strains.

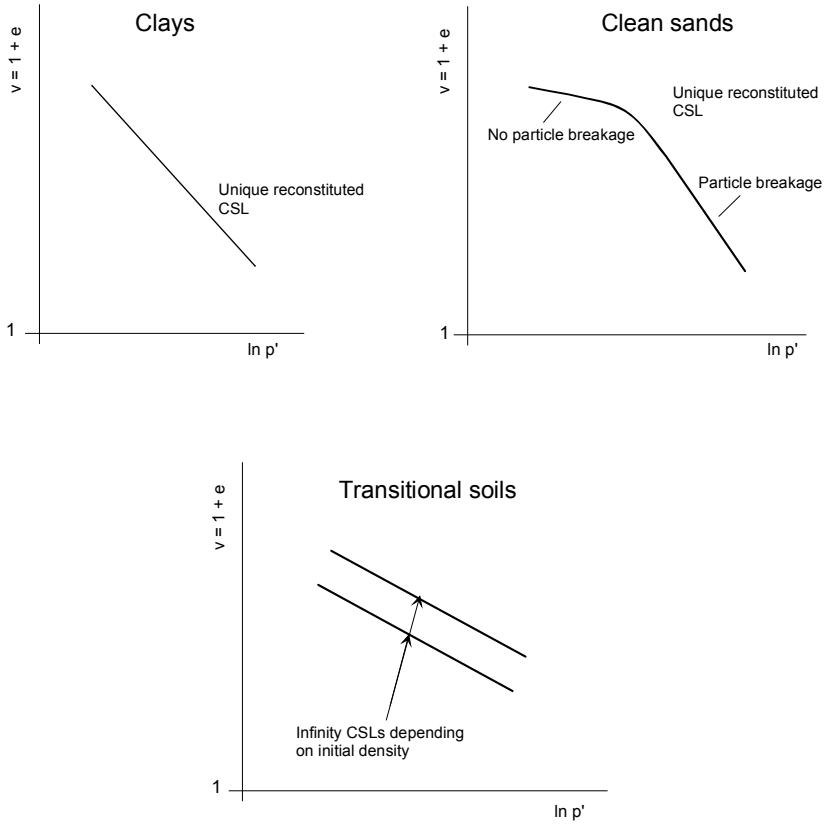

Figure 2.46 Schematic illustration of the CSL of clays, clean sands and transitional soils

Transitional soil behaviour completely breaks down traditional concepts of the uniqueness of NCL and CLS lines for reconstituted samples that have been used as a reference framework for interpreting soil response since the mid 1960's when the critical state theory was conceived at Cambridge University.

The term transitional behaviour should not be confused with the transitional fines content (TFC) discussed previously in Section 2.4.3, which represents a fines content when soil behaviour changes from a coarse-grain dominated mode to a fine-grain dominated one (e.g. Yang et al., 2006). Moreover the use of the intergranular void ratio or the interfine void ratio to try to make the compression and shearing behaviour converge will not be successful because in the case of transitional behaviour the soil has the same grading.

2.5.2 Previous investigations of transitional soils

The first study carried out to address transitional soil behaviour was by Martins et al. (2001). They investigated the effect of plastic fines content on the compression behaviour of reconstituted samples of a gap-graded Botucatu residual sandstone (BRS) and a model clay-sand mixture (SK). The BRS sandstone consisted of mainly quartz grains of sand and fine grains of kaolin with Atterberg limits of w_l=49%, w_p=34% and I_p=5%. The SK soil was used for comparison with the results of the naturally occurring BRS. The Atterberg limits of SK were w_l=39%, w_p=30% and I_p=9%. Figure 2.47 shows the grading curves for both soils. Different types of specimens were created including slurries, air pluviated and compacted samples.

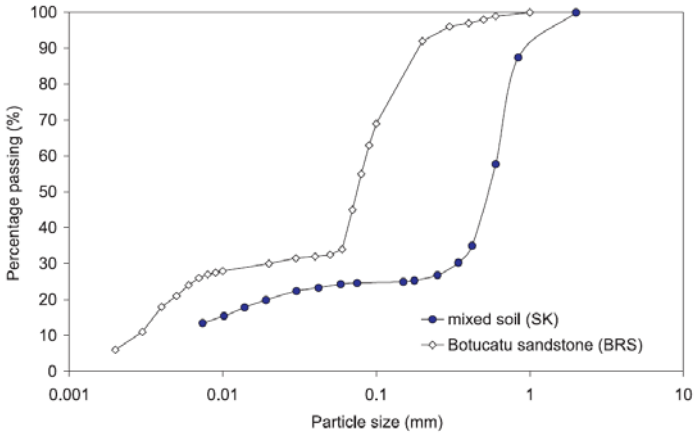

Figure 2.47 Grain size distributions of BRS and SK soils (Martins et al., 2001)

The compression lines of the BRS are shown in Figure 2.48. It can be seen that a non-unique NCL can be identified and all curves remain parallel to one another, even at high stress levels. The same behaviour was seen with samples of SK as observed in Figure 2.49. Ferreira & Bica (2006) carried out further tests and confirmed the non-convergence of reconstituted and remoulded samples of BRS at even higher stresses (Figure 2.50). Martins et al. (2001) concluded that this transitional soil behaviour is a characteristic of gap-graded soils and not a consequence of the complex mineralogy of the BRS. For each initial void ratio there is a NCL and its position is related to the initial structure which can not be erased by compression.

Ferreira & Bica (2006) also tested natural intact samples of BRS at different initial void ratios and found that a unique NCL can be identified. In terms of CSL, they found that a unique CSL can be defined for intact samples whereas a non-unique CSL is identified for reconstituted/remoulded samples (Figures 2.51 and 2.52).

They concluded that it is impossible to evaluate the effect of the natural intact sample's structure on the soil response because of the non-uniqueness of the NCL and CSL for the reconstituted/remoulded samples.

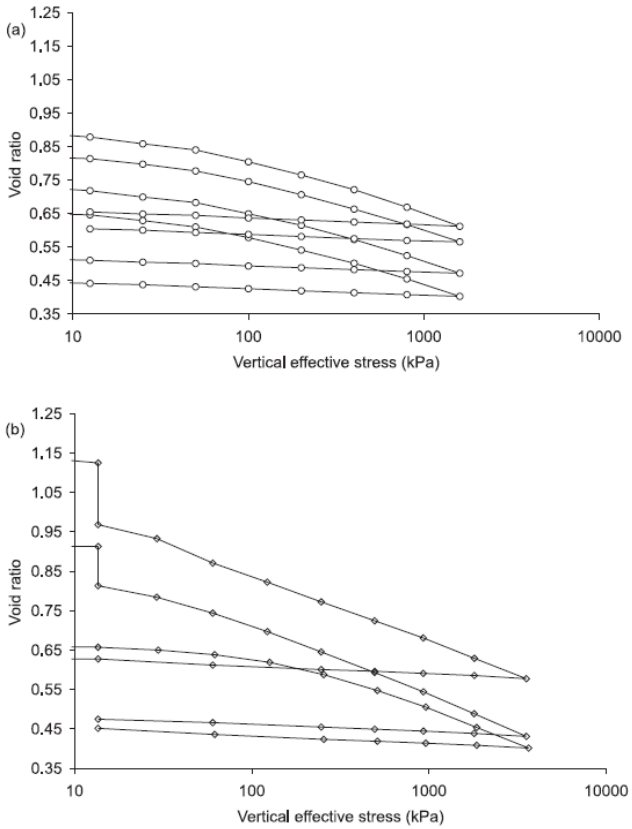

Figure 2.48 One-dimensional compression lines of BRS soil (a) slurry samples (b) air pluviated and compacted samples (Martins et al., 2001)

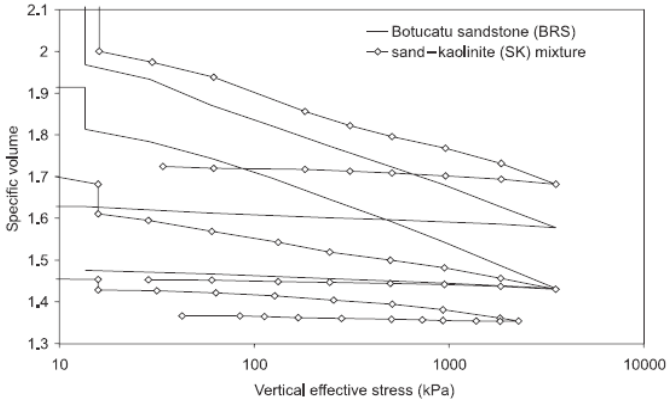

Figure 2.49 One-dimensional compression lines of BRS and SK samples (Martins et al., 2001)

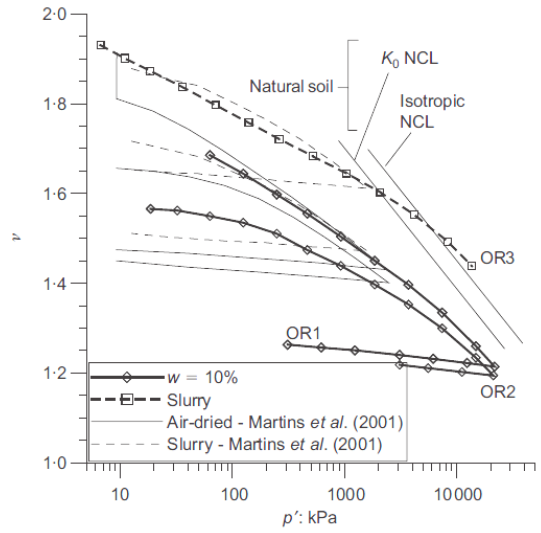

Figure 2.50 One-dimensional compression tests on remoulded and reconstituted samples of BRS (Ferreira & Bica, 2006)

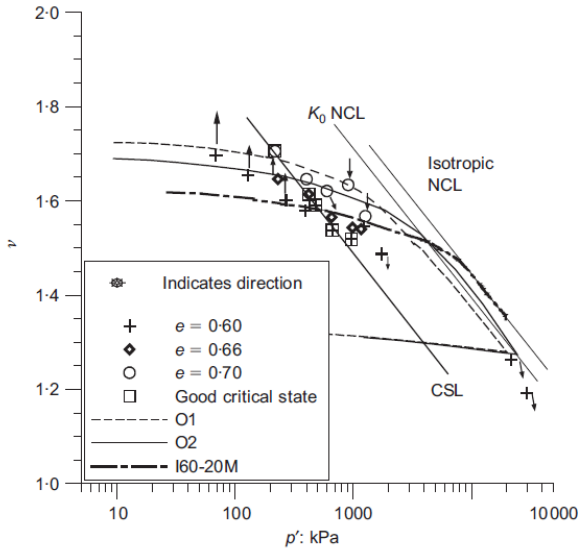

Figure 2.51 Critical state line of natural intact samples of BRS (Ferreira & Bica, 2006)

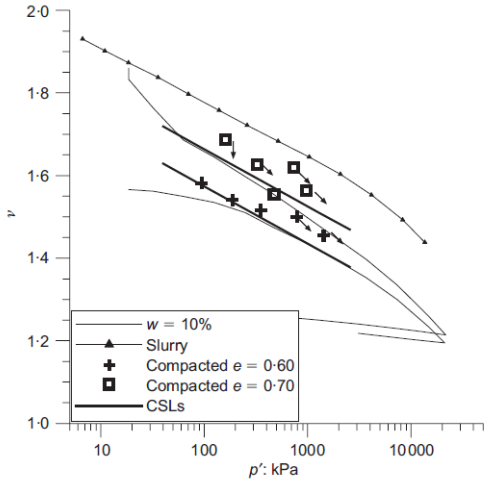

Figure 2.52 Critical state lines of remoulded samples of BRS (Ferreira & Bica, 2006)

As mentioned before, it was believed that transitional behaviour is a characteristic feature of gap-graded soils (e.g. Martins et al., 2001) but recent investigations have shown that this type of behaviour can also be seen in other soil gradings, including well-graded materials (e.g. Nocilla et al., 2006; Shipton, 2010).

Nocilla et al. (2006) investigated the possible transitional behaviour of a well-graded Italian silt from the embankments of the Po River. Slurry and compacted samples of different gradings were tested (Figure 2.53). The one-dimensional compression lines of the silty soils of different clay contents are shown in Figure 2.54. It can be seen that as the clay content is reduced the convergence of the NCLs is less clear and a non-unique NCL is found for the 8% and 3.5% clay content samples. Triaxial tests were also carried out to investigate the shearing behaviour. While for the 45% and 25% clay content samples unique CSLs can be found, as the clay content reduced the samples do not define a unique CSL for the 8% clay content (Figures 2.55 and 2.56).

More recently, Shipton (2010) carried out an extensive investigation to try to understand clearly the fundamental behaviour of transitional soils by testing two fabricated gap-graded mixtures; a plastic transitional soil consisting of 75% Thames Valley sand and 25% kaolin and a non-plastic transitional soil with 75% Redhill sand and 25% crushed quartz silt. The one-dimensional compression behaviour of both mixtures showed the non-uniqueness of the NCLs (Figure 2.57). It was suggested that the NCLs are probably curving towards a unique NCL but that it would only exist at exceptionally high stresses.

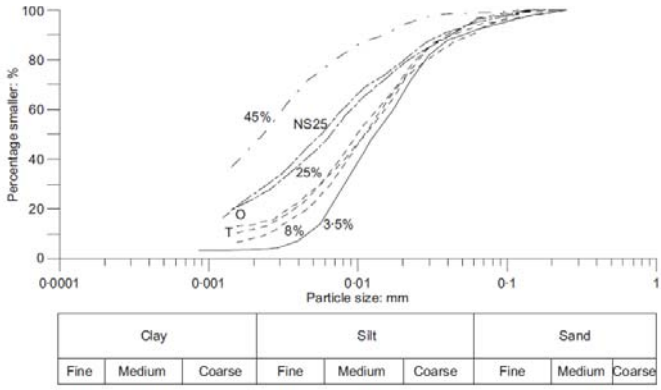

Figure 2.53 Grading curves of an Italian silt with different clay contents (NS25: natural sample; O: reconstituted samples after oedometer testing to 14 MPa; T: reconstituted sample after triaxial testing from p_0' = 600 kPa) (Nocilla et al., 2006)

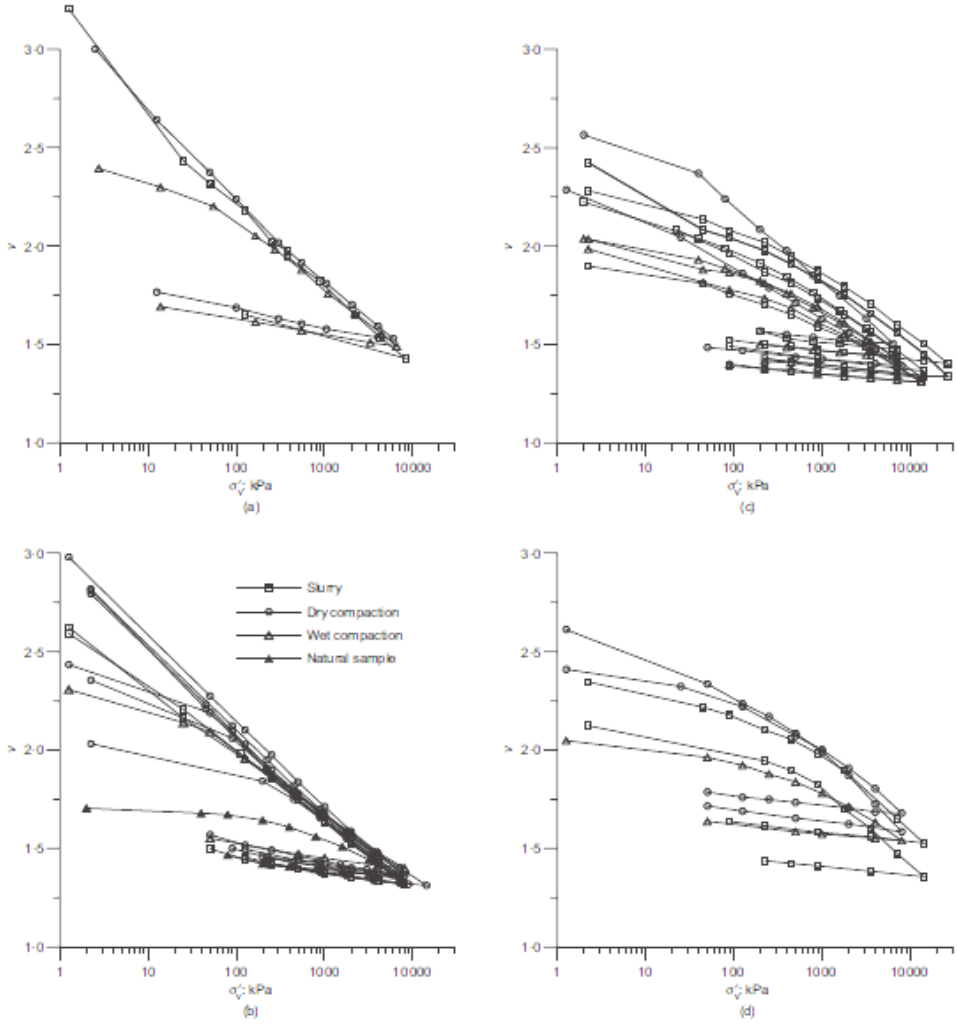

Figure 2.54 One-dimensional compression lines of an Italian silt (a) 45% clay content (b) 25% clay content (c) 8% clay content (d) 3.5% clay content (Nocilla et al., 2006)

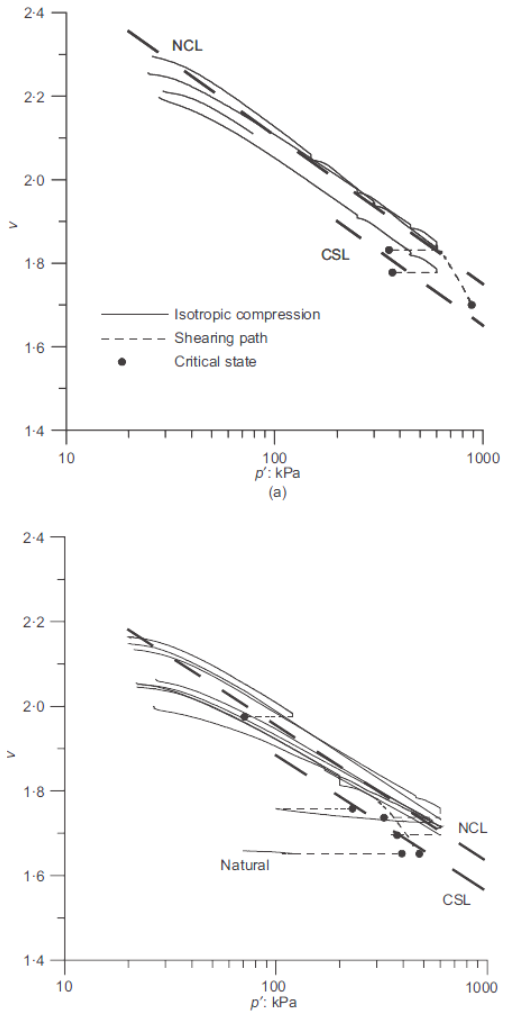

Figure 2.55 Isotropic NCL and critical state lines for reconstituted/remoulded samples of and Italian silt (a) 45% clay content (b) 25% clay content (Nocilla et al., 2006)

When comparing the one-dimensional and isotropic compression paths, it can be shown that the one-dimensional compression lines are steeper than the isotropic ones (Figure 2.58). Shipton concluded that the difference in the slope of NCLs is not likely to be a result of particle breakage. The shearing behaviour was also investigated. Unique critical state lines were not identified for either of the mixtures tested. Figure 2.59 shows the shearing behaviour of the plastic mixture. It can be seen that a unique CSL exists for each group of similar initial density and which are parallel to one another. Shipton (2010) also carried out tests where samples were sheared twice. She concluded that the CSL for each initial density is unique and independent of the number of times the sample was pre-sheared or pre-compressed. This demonstrates the robustness of the initial structure.

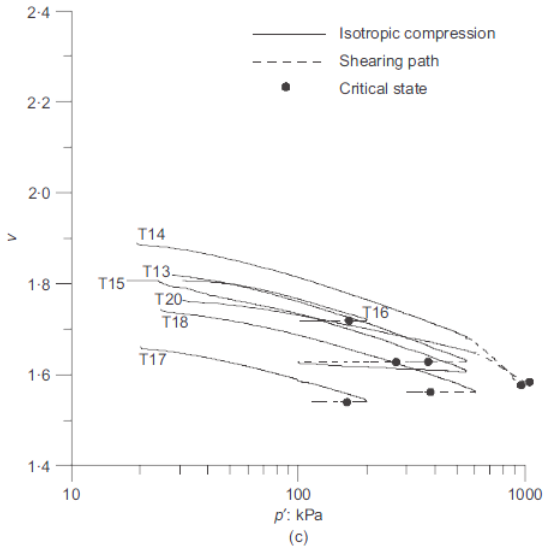

Figure 2.56 Critical states for reconstituted/remoulded samples of silts with 8% of clay content (Nocilla et al., 2006)

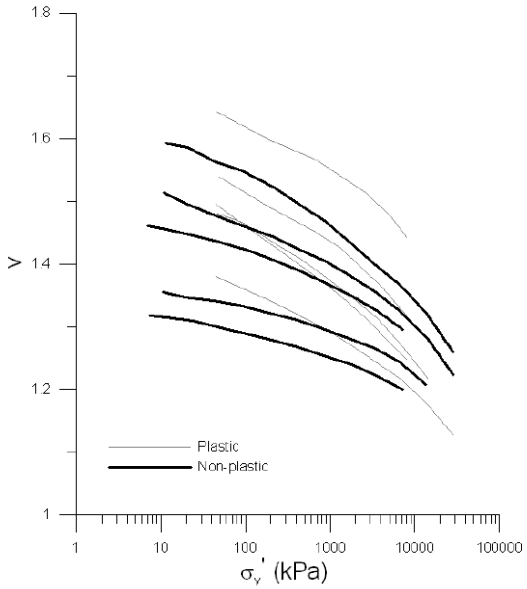

Figure 2.57 One-dimensional compression lines of the plastic and non-plastic transitional soil mixtures (Shipton, 2010)

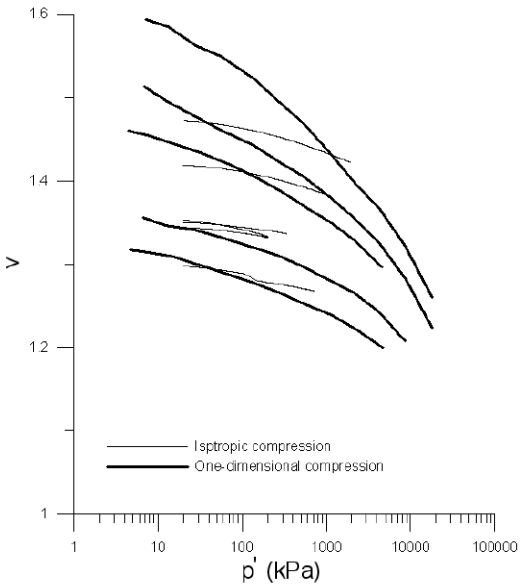

Figure 2.58 Isotropic and one-dimensional compression behaviour of the non-plastic transitional mixture (Shipton, 2010)

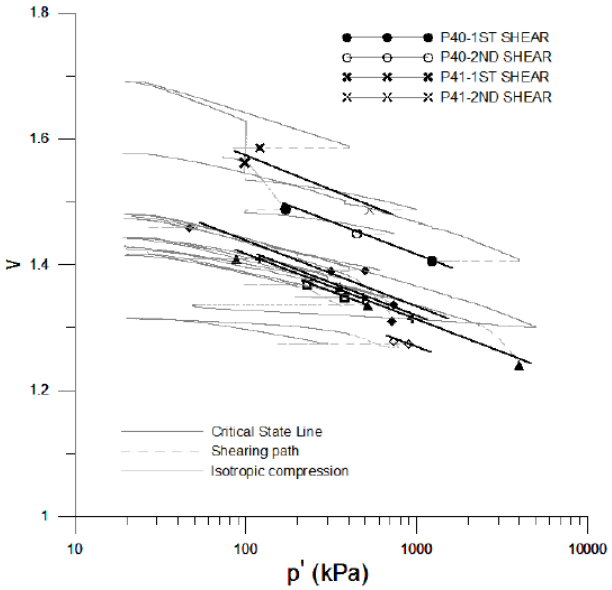

Figure 2.59 Isotropic compression paths, end of shearing points and assumed CSLs for the groups of triaxial test samples with similar initial densities for the plastic transitional soil (Shipton, 2010)

Shipton (2010) made an extensive review of soils that were previously investigated by other authors, looking for transitional behaviour. Some other soils found in the literature that showed possible transitional behaviour were also investigated although this special response had not been taken into consideration. A summary

of soil characteristics for the soils reviewed by Shipton is presented in Tables 2.4 to 2.6. Based on previous investigations, it was believed, that gap-graded materials and soils with clay contents less than around 20% to 25% might display transitional behaviour. Contrary to this belief, Shipton (2010) showed that transitional behaviour can be found in a wide range of soil gradings and is therefore much more widespread that had been thought (Figure 2.60).

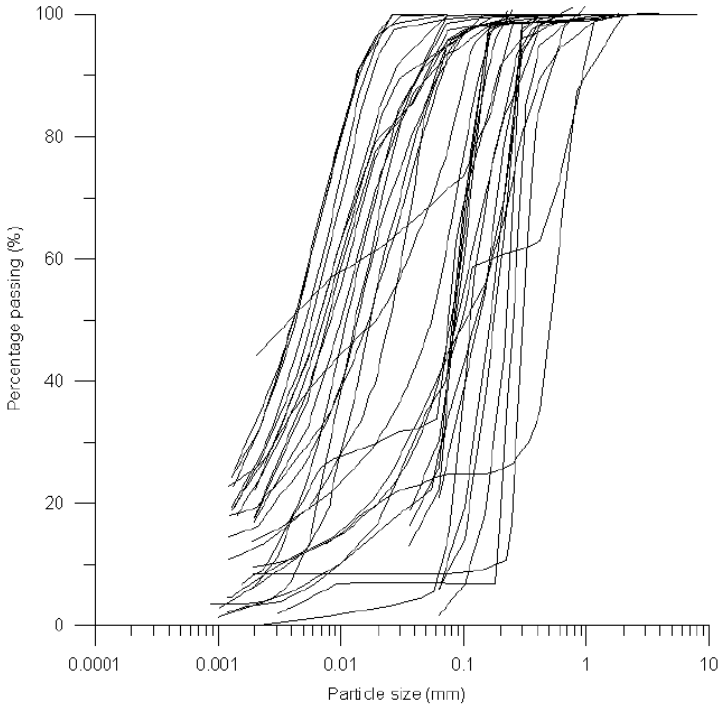

Figure 2.60 Grading curves for soils that displayed transitional behaviour (Shipton, 2010)

2.5.3 Effect of sample preparation method on transitional behaviour

Previous researchers have concluded that the sample preparation method alone does not produce different structures which can result in a non-convergence of the compression paths and therefore they pointed out that the sample preparation method has no effect on transitional soil behaviour (e.g. Martins et al., 2001; Nocilla, 2006; Ferreira & Bica, 2006; Shipton, 2010). In order to confirm this conclusion a more detailed study was carried out to analyse the compression behaviour for some of the soils that displayed a clear transitional behaviour. The compression curves have been redrawn grouping samples prepared by the same method (Figures 2.61 to 2.63). Figures 2.61 to 2.63 show that the compression curves of samples prepared by air-dried and wet compaction converge towards a unique NCL.

Soil	Reference	Origin	Mineralogy	D_{50} / C_u (mm)	Transitional
Botucatu sandstone (BRS)	Martins et al. (2001)	Residual aeolian	Quartz/feldspar	0.070 / 35	YES
SK[1] (75%sand:25%kaolin)	Martins et al. (2001)	Manufactured	Quartz/kaolin	0.520 / -	YES
Natural BRS	Ferreira and Bica (2006)	Residual aeolian	Quartz/feldspar	0.180 / 100	YES
Reconst. silt (45% clay)	Nocilla et al. (2006)	Fluvial	Quartz/calcite/...	0.001 / -	NO
Reconst. silt (25% clay)	Nocilla et al. (2006)	Fluvial	Quartz/calcite/...	0.006 / -	NO (?)
Reconst. silt (8% clay)	Nocilla et al. (2006)	Fluvial	Quartz/calcite/...	0.012 / 6	YES
Reconst. silt (3.5% clay)	Nocilla et al. (2006)	Fluvial	Quartz/calcite/...	0.013 / 4	YES
Natural silt (39–53% clay)	Nocilla and Coop (2008)	Fluvial	Quartz/calcite/...	0.002 / -	NO (?)
Natural silt (29–30% clay)	Nocilla and Coop (2008)	Fluvial	Quartz/calcite/...	0.006 / -	?
Natural silt (20–26% clay)	Nocilla and Coop (2008)	Fluvial	Quartz/calcite/...	0.018 / -	YES (?)
Natural silt (13–16% clay)	Nocilla and Coop (2008)	Fluvial	Quartz/calcite/...	0.020 / -	YES (?)
Venice Lagoon silty-sands	Sanzeni (2006)	Shallow marine	Quartz/dolmite/...	- / -	YES
Silty Thanet sand	Ventouras (2005)	Shallow marine	Quartz/clay	0.083 / -	YES
Gullfaks clayey-sand	Georgiannou et al. (1991)	Marine	Quartz/illite	0.078 / 45	YES (?)

[1] SK: Sand-kaolin mixture

Table 2.4 Summary of soil characteristics for materials that showed transitional behaviour and for those that did not display transitional behaviour (Shipton, 2010)

Soil	Reference	Origin	Mineralogy	D_{50} / C_u (mm)	Transitional
Silty loess	Lee (2004)	Aeolian	Calcite	0.018 / 6	YES
Reconst. chalk	Tam (2005)	Marine	Calcite	- / -	NO
Reconst. sandstone	Tam (2005)	-	Quartz	- / -	NO
Copper tailings	Kwok (2006)	Man made	-	- / -	YES
Copper tailings	Sivakanthan (2005)	Man made	-	0.120 / 17	YES
Magna Copper tailings	Tan (2004)	Man made	-	0.008 / -	YES
Morenci Copper tailings	Tan (2004)	Man made	-	0.060 / -	?
Chino Copper tailings	Tan (2004)	Man made	-	4.3 / 529	NO
Gold tailings	Sivakanthan (2005)	Man made	-	0.100 / 27	YES
Gold tailings	Fourie and Papageorgiou (2001)	Man made	-	- / -	?
Stava Silty tailings	Tan (2004)	Man made	-	0.005/ -	YES
Stava Silty tailings	Carrera et al. (2010)	Man made	Quartz/calcite/fluorite	0.024 / 8	NO
Stava Sandy tailings	Tan (2004)	Man made	-	0.130 / 6	NO
Stava Sandy tailings	Carrera et al. (2010)	Man made	Quartz/calcite/fluorite	0.180 / 2	NO

Table 2.5 Summary of soil characteristics for materials that showed transitional behaviour and for those that did not display transitional behaviour (Shipton, 2010)

Soil	Reference	Origin	Mineralogy	D_{50} / C_u (mm)	Transitional
HPF4 (Crushed silt)	Lee (2004)	Manufactured	Quartz	0.040 / 10	YES
HPF4 (Crushed silt)	Chapter 7	Manufactured	Quartz	0.094 / 1	NO
Reconst. London Clay	Wilson (2008)	Shallow marine	Kaolinite	<0.001 / -	NO
Reconst. Oxford Clay	Wilson (2008)	Shallow marine	Illite/quartz/...	- / -	NO
Kaolin	Wilson (2008)	Manufactured	Kaolin	- / -	NO
Kaolin	Hui (2006)	Manufactured	Kaolin	- / -	NO
75%kaolin:25%sand	Hui (2006)	Manufa./river ter.	Kaolin/quartz	- / -	NO
50%kaolin:50%sand	Hui (2006)	Manufa./river ter.	Kaolin/quartz	- / -	NO
10%kaolin:90%sand	Hui (2006)	Manufa./river ter.	Kaolin/quartz	- / -	YES
HK[1] (7%kaolin:93%sand)	Lee (2004)	Manufa./river ter.	Kaolin/quartz	0.220 / 2	YES
40%DBS[2]:60%silt	Tam (2005)	Shallow mar./manufa.	Carbonate/quartz	0.10 / 11	YES
30%DBS:70%sand	Lau (2007)	Shallow mar./riv. ter.	Carbonate/quartz	- / -	YES
10%DBS:90%sand	Lau (2007)	Shallow mar./riv. ter.	Carbonate/quartz	0.220 / 2	?
KSS[3]	Lee (2004)	Manufa./river ter.	Kaolin/quartz	0.004 / -	YES

[1] HK: Ham river sand-kaolin mixture

[2] DBS: Dogs Bay sand

[3] KSS: 50% kaolin, 25% crushed quartz silt and 25% quartz sand

Table 2.6 Summary of soil characteristics for materials that showed transitional behaviour and for those that did not display transitional behaviour (Shipton, 2010)

On the contrary the compression paths for slurry samples show no sign of convergence towards a unique NCL and the curves remain parallel to one another. It seems to be clear that sample preparation method has an effect on the initial structure that determines whether the soil displays transitional behaviour or not.

In agreement with these findings Radici (2006) showed that samples of the same Italian silty soil tested by Nocilla et al. (2006), but taken from another place, display transitional behaviour only for slurry samples while the compression curves for compacted samples converge towards a unique NCL (Figure 2.64).

Figure 2.65 shows the compression curves for the non-plastic transitional soil mixture tested by Shipton (2010). In this case, it can be observed that the compression curves for the slurry samples run parallel to one another with no sign of convergence towards a unique NCL as has been seen in the previous cases analysed. On the other hand, in this case the compression curves for the compacted samples show a less clear convergence towards a unique NCL compared to the previous cases.

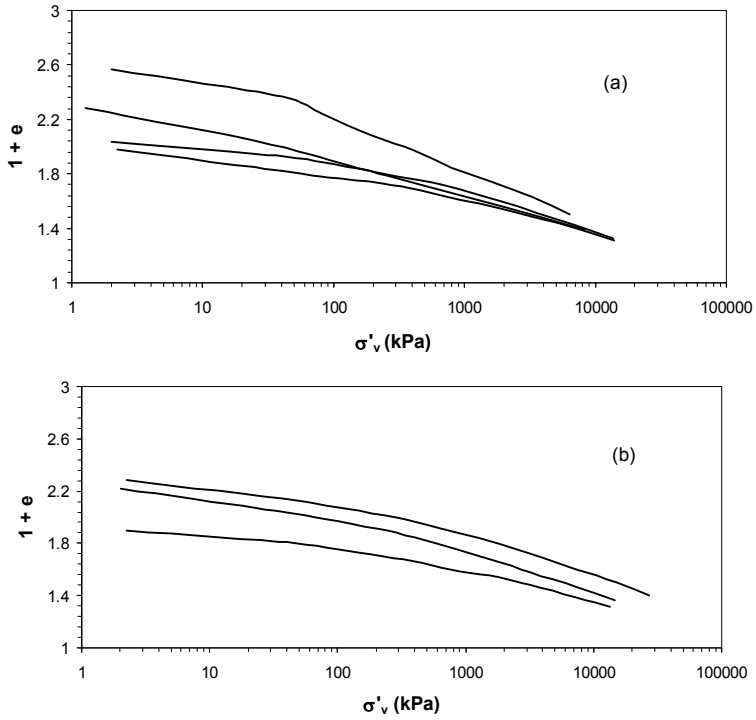

Figure 2.61 One-dimensional compression curves of Italian silty soil with 8% of clay content (a) dry and wet compaction samples (b) slurry samples (redrawn from Nocilla et al., 2006)

Finally, it could be concluded that, even though the results presented above have shown that there is a clear effect of the sample preparation method on the possible transitional behaviour, more tests should be carried out to confirm this finding.

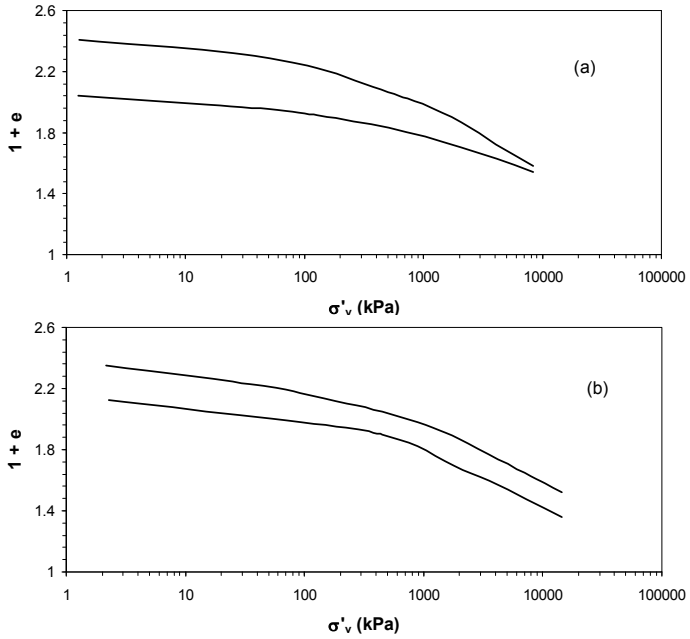

Figure 2.62 One-dimensional compression curves of Italian silty soil with 3.5% of clay content (a) dry and wet compaction samples (b) slurry samples (redrawn from Nocilla et al., 2006)

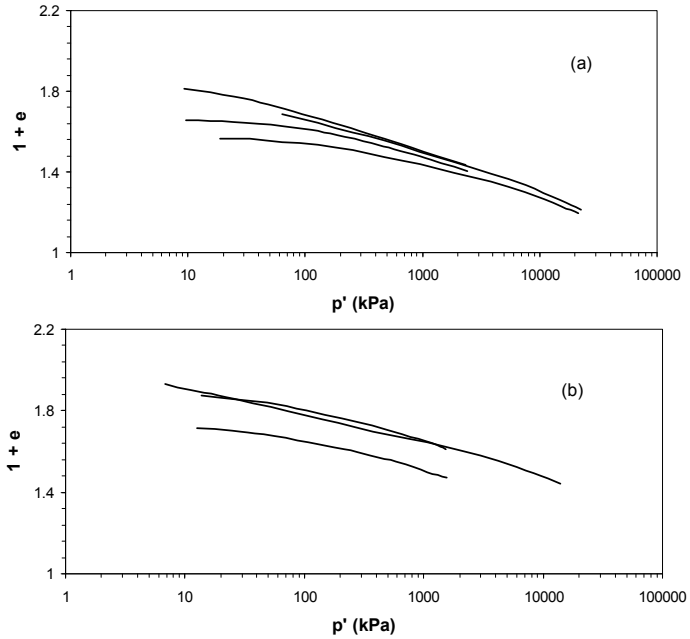

Figure 2.63 One-dimensional compression curves of Botucatu sandstone (a) air-dry and wet compaction samples (b) slurry samples (redrawn from Ferreira and Bica, 2006) (redrawn from Nocilla et al., 2006)

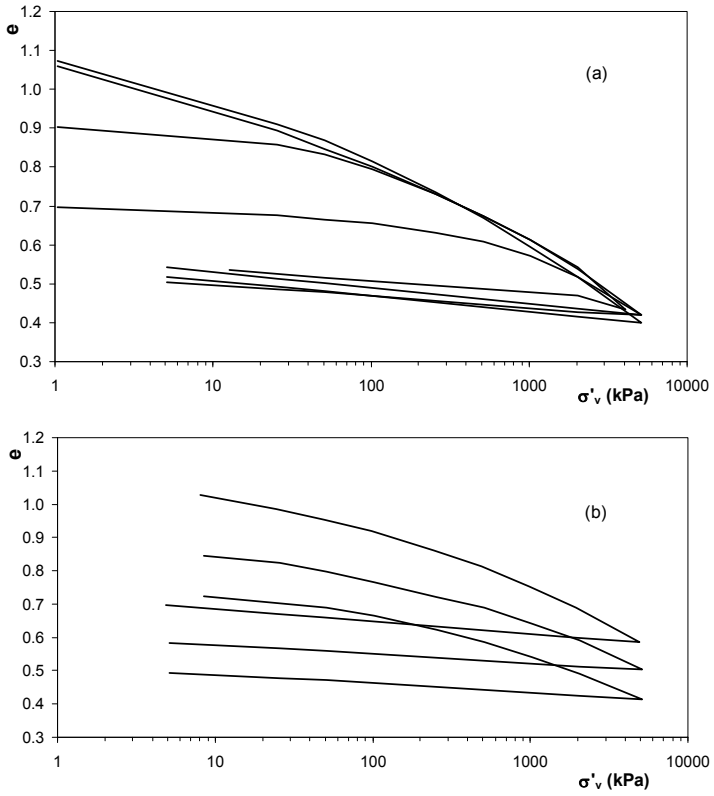

Figure 2.64 One-dimensional compression curves of Italian silt (a) air-dry and wet compaction samples (b) slurry samples (redrawn form Radici, 2006)

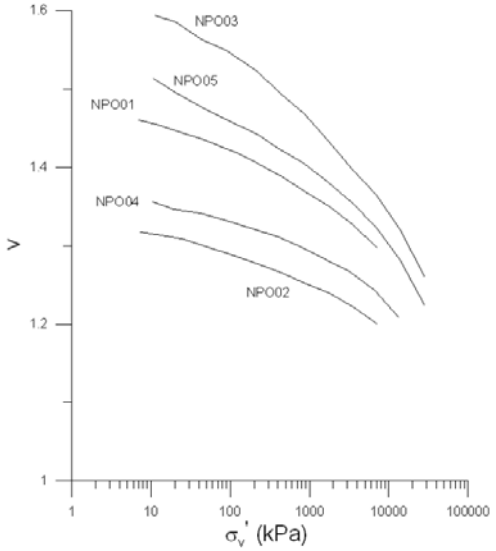

Figure 2.65 One-dimensional compression curves for the non-plastic transitional soil mixture consisted of 75% Redhill sand and 25% crushed quarz silt: dry and wet compaction samples (NP01, NP03, NP05); slurry samples (NP02, NP04) (Shipton, 2010)

2.6 Summary on the behaviour of reconstituted/remoulded soils

- **Clean sands**

According to what has been presented in the previous sections, it seems to be clear that for any particular sand there is a unique NCL that occurs at the onset of major particle breakage at high stress levels, regardless of its initial density and sample preparation technique. It is also clear that at low stress levels, where particle breakage is not a major factor, initial density controls the compression behaviour for a given sand and an infinity of parallel compression lines approaching towards the unique NCL can be identified, each one associated to an initial formation density. Consequently, at low stresses, it seems reasonable to think that for a given sand there should be two limiting approaching compression lines associated to the maximum and minimum void ratios which can be achieved by any sample preparation method.

In terms of critical state/steady state, it can be concluded that there are still contradictory findings about the uniqueness of the CSL in the compression plane for a given sand. While some authors have concluded that for a given sand there exists a unique CSL irrespective of factors such as sample preparation method, stress path followed to reach the critical state, mode of shearing deformation and particle breakage, others have shown that these factors have an important effect on the non-uniqueness of the CSL. Non-uniqueness of the CSL/SSL has been observed in samples tested at low stress levels where little breakage is expected. It would be interesting to see if at high stress levels the non-uniqueness of CSL/SSL still occurs for those materials.

Various state parameters have been proposed in the literature to characterize the stiffness and strength properties of sands (e.g. Been & Jefferies, 1985; Ishihara et al., 1998; Wang et al., 2002) (see Figure 2.66). Probably the most important assumption they made in using state parameters is to assume that the Critical State Line (CSL) - Steady State Line (SSL) is unique for a given sand and so provides a reference state to compare to the current state of the soil. As has been noted in the above paragraphs this assumption can be erroneous, especially at low stress levels, and therefore the state parameters lose their meaning.

- **Intermediate graded soils**

In mixtures of sand with fines, the studies reviewed here have shown that the addition of fines causes a reduction of the specific volume and a flattening of the

unique NCL at high stresses. This might be due to a reduction of the amount of particle breakage due to the presence of fines in the soil matrix. On the other hand, at low stress levels the compressibility of the mixture increases with respect to the compressibility of the sand itself. Moreover, as the fines content increases the NCL moves downwards in the compression plane and it appears to reach a minimum at a transitional fines content that seems to be around 25% to 40%. If the fines content continues to increase above this value it has been observed that the NCL moves upwards. This behaviour might show the transition from pure granular to pure fine soil response in compression. Moreover, it has been noted that the slope of the NCL hardly changes for fines contents higher than this transitional value.

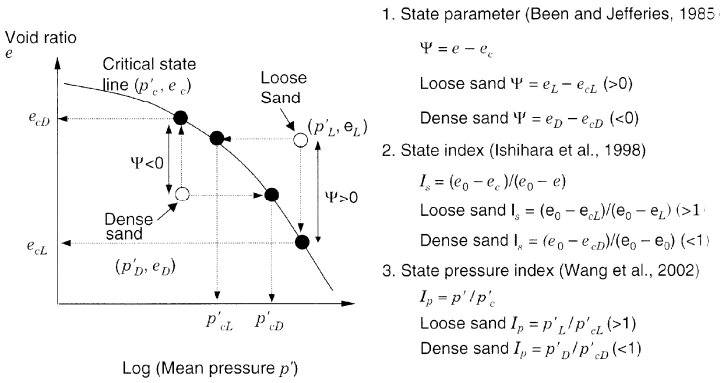

Figure 2.66 State parameters that relate the current state to the critical state line (Mitchell & Soga, 2005)

In terms of critical states/steady states in the compression plane, again there are still contradictory findings about the effect of adding fines to a granular soil. Based on reported data available in the literature, parts of which have been reviewed here, there are two main hypotheses about the influence of fines content on the CSL/SSL for sand-silt mixtures:

- ✓ The slope of the CSL/SSL changes with increasing fines content (e.g. Been & Jefferies, 1985; Bouckovalas et al., 2003)

- ✓ The CSLs/SSLs are more or less parallel to each other and as the fines content increases the position of the CSLs/SSLs moves downwards up to a certain quantity of fines, where the position of the CSLs/SSLs changes direction moving upwards until the fines content reaches 100% (e.g. Zlatovic & Ishihara, 1995; Lade & Yamamuro, 1997; Thevanayagam, 1998; Thevanayagam & Mohan, 2000; Thevanayagam et al., 2002; Ni et al., 2004; Yang et al., 2006; Murthy et al. 2007; Rahman & Gnanendran, 2008).

In both cases a unique CSL/SSL can be identified for a given sand-silt grading.

The effect of the sample preparation method on the position and uniqueness of the NCL and CSL/SSL has been also reviewed. For samples prepared by the same method, an increase in the fines content moves the SSL downwards in the compression plane and all of them are parallel to one another which is in agreement with the second hypothesis presented above. On the other hand, for a given fines content, the SSL is not unique and depends on the sample preparation technique contrary to what has been said above. It has been also seen that the compression curves do not converge towards a unique NCL when samples are prepared by different techniques. This behaviour clearly shows the possible influence of the sample preparation method, and therefore the initial structure, on the uniqueness of the NCL and CSL/SSL indicating that the initial structure can not be removed and some differences should remain during compression and shearing. In these cases, the tests were performed at low stress levels. It would have been interesting to see if at high stress levels the non-uniqueness of CSL/SSL still occurs.

- **Transitional soils**

A transitional soil is defined as one which has a mode of behaviour where a non-unique NCL and/or CSL/SSL could be identified even at high stress and strain levels for a given grading (e.g. Nocilla et al., 2006).

The lack of convergence towards a unique NCL and/or CSL/SSL from different initial densities must be associated with the stability of the initial structure that can not be removed by compression and shearing alone. This means that the soil "remembers" its initial structure during compression and shearing stages even at large strains.

The term transitional behaviour should not be confused with the transitional fines content, which represents a fines content when the soil behaviour changes from a coarse-grain dominated mode to a fine-grain dominated one. The use of the intergranular void ratio or the interfine void ratio to try to make the compression and shearing behaviour to converge can not be successful because in the case of transitional behaviour the soil has the same grading.

Initially, it was believed that transitional behaviour is a characteristic feature of gap-graded soils (e.g. Martins et al., 2001) but recent investigations have shown that this type of behaviour can also be seen in other soil gradings, including well-graded materials and is therefore much more widespread than had been thought (e.g. Nocilla et al., 2006; Shipton, 2010). One of the main objectives of previous

researcher (e.g. Shipton, 2010) was to try to identify special soil characteristics common to all soils that display transitional behaviour, which might help to anticipate this response in other soils. It has been not possible to establish a consistent set of soil characteristics associated with transitional behaviour, leading to difficulties in predicting this response directly from the soil index properties.

Many authors concluded that the sample preparation method alone does not produce different structures which can result in a non-convergence of the compression paths and therefore they pointed out that the sample preparation method has no effect on transitional soil behaviour (e.g. Martins et al., 2001; Nocilla, 2006; Ferreira & Bica, 2006; Shipton, 2010). In order to confirm this conclusion a more detailed study was carried out to analyse the compression behaviour for some of the soils that have displayed a clear transitional behaviour. The compression curves have been redrawn grouping together samples prepared by the same method. In most cases the compression curves of samples prepared by air-dry and wet compaction converge towards a unique NCL. On the contrary the compression paths for slurry samples show no sign of convergence towards a unique NCL and the curves remain parallel to one another. It seems to be possible that sample preparation method has an effect on the initial fabric that determines whether the soil displays transitional behaviour or not. In order to confirm this finding more tests should be carried out.

2.7 Mechanical behaviour of natural soils

As mentioned in Section 2.2 the effects on the mechanical behaviour of the structure of natural soils have been traditionally evaluated by comparing the natural soil response to its reconstituted state. The key factor in this comparison is the assumption of the uniqueness of the NCL and CSL for the reconstituted state of the material investigated. In previous sections it has been shown that some soils displayed transitional response in their reconstituted state which would impede the possibility of quantifying the effects of the natural structure. In general this is not the case and the effects on the mechanical behaviour of the natural structure of soils can be analysed by using the reconstituted response as a reference framework.

2.7.1 One-dimensional compression behaviour of natural clays

Early work by Terzaghi (1941) showed that the compression curve followed by a soil element in-situ is different to that of the same material reconstituted and compressed in an oedometer test. The variation of the in-situ water content of a natural soil plotted against the logarithm of the vertical effective stress was called

the "Sedimentation Compression Curve" (SCC) (Terzaghi, 1941). In 1970 Skempton published a study on the compression of natural normally consolidated clays covering a large range of depths and mineralogy. Figure 2.67 shows the sedimentation compression curves for different argillaceous deposits plotted by Skempton. As can be observed, at a given vertical effective stress the void ratio depends on the nature and amount of the clay minerals and soils with higher liquid limits exhibits higher values of the void ratio. Moreover, and regardless of the mineralogy of the soils, all the compression curves tend to converge at very high stress levels.

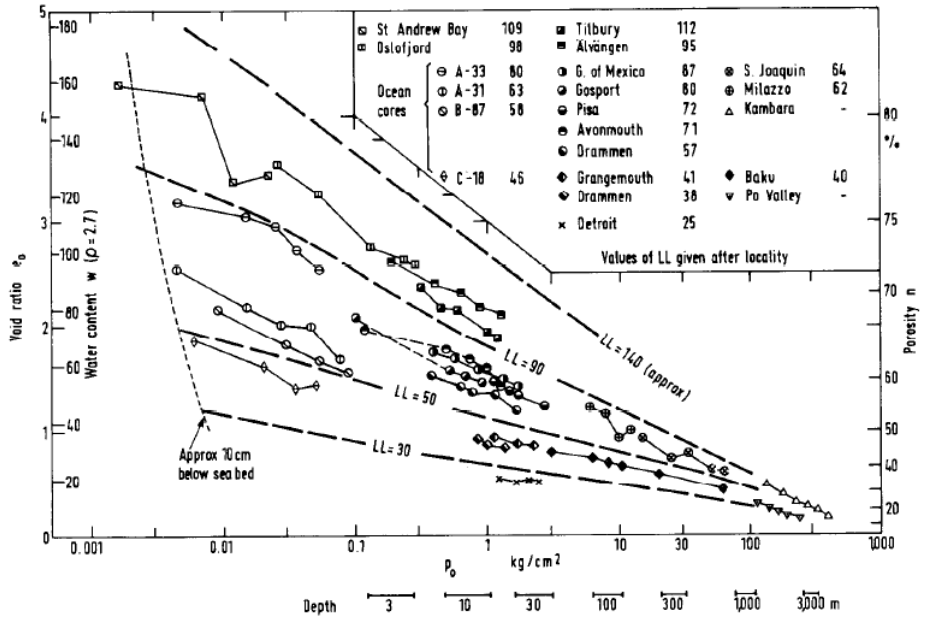

Figure 2.67 Sedimentation compression curves for normally consolidated argillaceous sediments (Skempton, 1970)

Burland (1990) analysed the one-dimensional compression behaviour of different clays in their reconstituted states, the normal compression lines of which were unique for a given material. As described in Section 2.2.3, Burland introduced the concept of "intrinsic" properties to represent the behaviour in the reconstituted soil when the samples were prepared by creating slurries at water contents of between the liquid limit and 1.5 times the liquid limit. The intrinsic properties were denoted by an asterisk. Burland (1990) proposed a normalising parameter called the void index (Iv), Equation 2.11, where e^*_{100} and e^*_{1000} are the intrinsic void ratios corresponding to vertical effective stresses of 100kPa and 1000kPa respectively. The intrinsic compression index (C^*_c) represents the slope of the unique normal compression line measured in the e:logσ'_v plane over the stress range of 100kPa to 1000kPa.

$$Iv = \frac{e - e^*_{100}}{e^*_{100} - e^*_{1000}} = \frac{e - e^*_{100}}{C^*_c} \qquad 2.11$$

The one-dimensional compression behaviour of slurry samples for different soils with a large range of liquid limits was normalised by Burland using the void index. A unique compression line was found regardless of the liquid limit of the soil (Figure 2.68). This unique line was called the "Intrinsic Compression Line" (ICL) which is commonly used as a reference for quantifying the effects of the natural structure of soils.

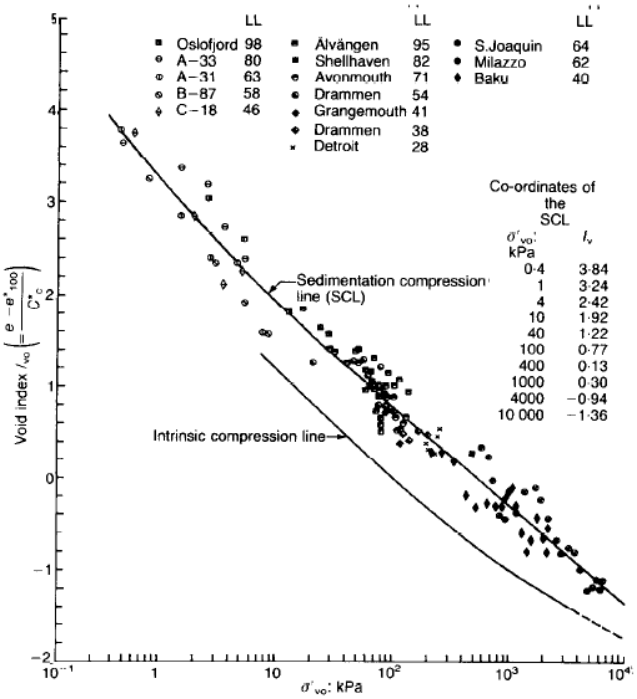

Figure 2.68 Intrinsic compression line and sedimentation compression line (Burland, 1990)

Using the Iv parameter, Burland (1990) normalized the in-situ state data of the normally consolidated samples provided by Skempton (1970), obtaining an average best fit relationship curve called the "Sedimentation Compression Line" (SCL) which is parallel to the ICL over the stress range of 10kPa to 1000kPa. As can be seen in Figure 2.68, the SCL plots to the right of the ICL exhibiting a clear effect of the in-situ structure of the natural soils, enhancing their resistance with respect to the reconstituted state. It is interesting to recall that Skempton omitted in his analysis data highly sensitive clays, clays with a carbonate content of more that 25%, an organic content larger than 5% and diatomaceous clays.

2.7.2 Sedimentation and post-sedimentation structure

Cotecchia & Chandler (2000) separated the different structures which can result from the geological history of clays into two groups; the "sedimentation structure" and the "post-sedimentation structure" (Figure 2.69). The sedimentation structure is that created in-situ during and after deposition as the soil is being slowly compressed one-dimensionally. This type of structure is characteristic of normally consolidated soils and can be associated to different degrees of structure (fabric and bonding). The post-sedimentation structure develops as a result of geological processes such as mechanical unloading, creep, thixotropy, post-deposition bonding and in general diagenesis, which can alter the sedimentation structure of a normally consolidated soil.

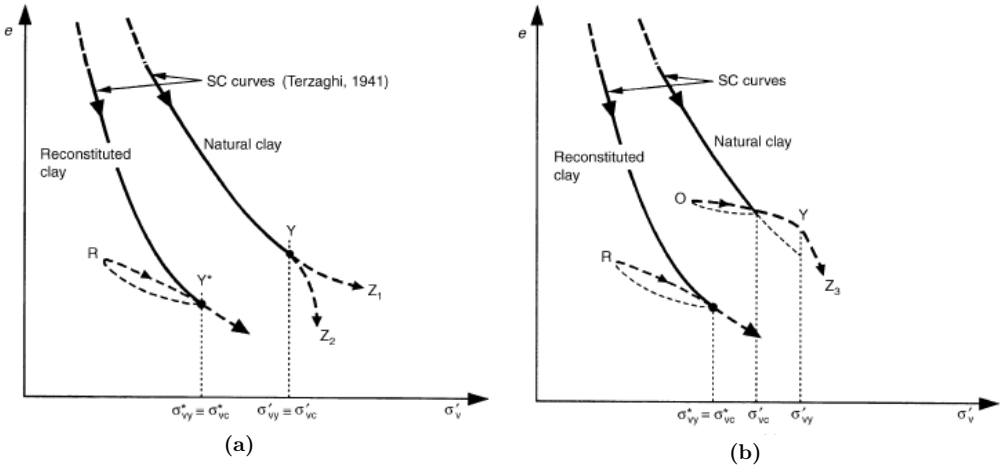

Figure 2.69 Responses of clays under one-dimensional compression: (a) sedimentation structure (b) post-sedimentation structure (Cotecchia & Chandler, 2000)

A soil with a sedimentation structure has a current vertical effective stress (σ'_v) which is equivalent to the preconsolidation pressure (σ'_p), the overconsolidation ratio of which is equal to OCR=σ'_p/σ'_v=1. Moreover the gross yield stress is also the same as the preconsolidation pressure and therefore the yield stress ratio defined by Burland (1990) as YSR=σ'_{vy}/σ'_v is equal to the OCR (Figure 2.69a). However in some normally consolidated clays creep and ageing could be enough to produce YSR ratios in excess to unity (Bjerrum, 1967) and the soil still has a sedimentation structure. In the case of a soil with a post-sedimentation structure, the gross yield stress is higher than the preconsolidation pressure which corresponds to the stress level on the sedimentation compression curve (Figure 2.69b). Consequently for a soil with a post-sedimentation structure the YSR is larger that the OCR. However, Cotecchia & Chandler (2000) pointed out that for geologically recent clays with YSR values of 1.5 it is difficult to confirm if

unloading is the only factor affecting the soil or instead it is the effect of a more complex post-sedimentation structure.

2.7.3 The sensitivity framework

Many sensitivity parameters can be found in the literature to characterize the differences in structure between natural and reconstituted soils. Terzaghi (1944) defined the sensitivity of a natural soil (S_t) as the ratio of the undrained strength of the intact natural soil to the undrained strength of the remoulded soil at the same water content. Schmertmann (1969) introduced another term called swell sensitivity (S_s) as the ratio of the reconstituted swelling index to the intact swelling index $S_s=C^*_s/C_s$. More recently, Cotecchia & Chandler (2000) defined the stress sensitivity (S_σ) as the ratio of the gross yield stress of a natural soil in one-dimensional compression to the equivalent vertical effective pressure on the ICL at the same void ratio, $S_\sigma=\sigma'_{vy}/\sigma'_e$. Figure 2.70 shows the idealized sensitivity framework proposed by Cotecchia & Chandler (2000) in the Iv:logσ'_v plane. As can be observed all the lines are quasi-parallel and, for clays having a sedimentation structure, the sensitivity curves are equivalent to the sedimentation compression curves (SCC) defined by Terzaghi (1941) and Skempton (1970). In fact, the SCL obtained by Burland (1990) and shown in Figure 2.68 represents the average SCC for the normally consolidated soils analysed, the sensitivity values of which ranged from 2 to 9 with an equivalent average value of $S_t\cong5$.

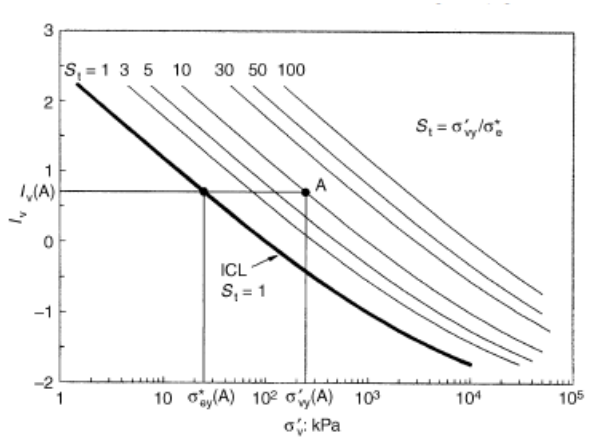

Figure 2.70 Idealized sensitivity framework in the Iv:logσ'_v plane (Cotecchia & Chandler, 2000)

Figure 2.71 shows the sensitivity framework in the q:p':v space for a natural clay with a sedimentation structure. Cotecchia & Chandler (2000) introduced a new definition for the strength sensitivity parameter (S_t) as the ratio between the peak strength (q_{peak}) measured on the state boundary surface of the natural clay (SBS)

and the reconstituted peak strength (q^*_{peak}) measured on the state boundary surface of the reconstituted clay (SBS*) at the same void ratio. Cotecchia & Chandler showed that $S_\sigma = S_t$ for most of the clays with both types of structures and consequently that implies geometric similarity between the SBS and SBS*. Moreover the ratio between the sizes of the SBS and SBS* is the same for clays with equal strength sensitivity.

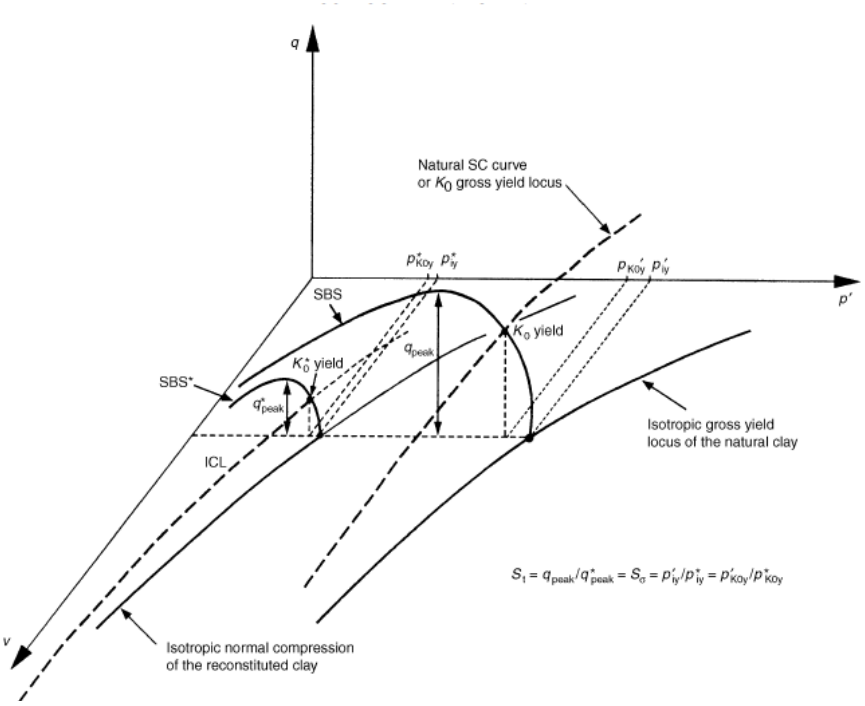

Figure 2.71 Idealized sensitivity framework in the q:p':v space for a clay with a sedimentation structure (Cotecchia & Chandler, 2000)

So far it can be said that for stress sensitivity values higher than unity the micro-structure of the natural soil has a positive effect in enhancing the strength of the soil with respect to that of the reconstituted state. However this is not always the case as shown in Figures 2.72 and 2.73 (Fearon & Coop, 2002; Vitone & Cotecchia, 2011). The oedometer compression curves of these structurally complex clays and clay shales plot below the ICL, the stress sensitivity values of which are lower than unity which implies that the natural structure is weaker than that of the reconstituted material. These soils had a highly heterogeneous structure not only at a microscopic level but also at a mesoscopic scale resulting from tectonic shearing. These meso-structure features are the ones which have the most important effects in controlling the soil behaviour (e.g. Vitone & Cotecchia, 2011).

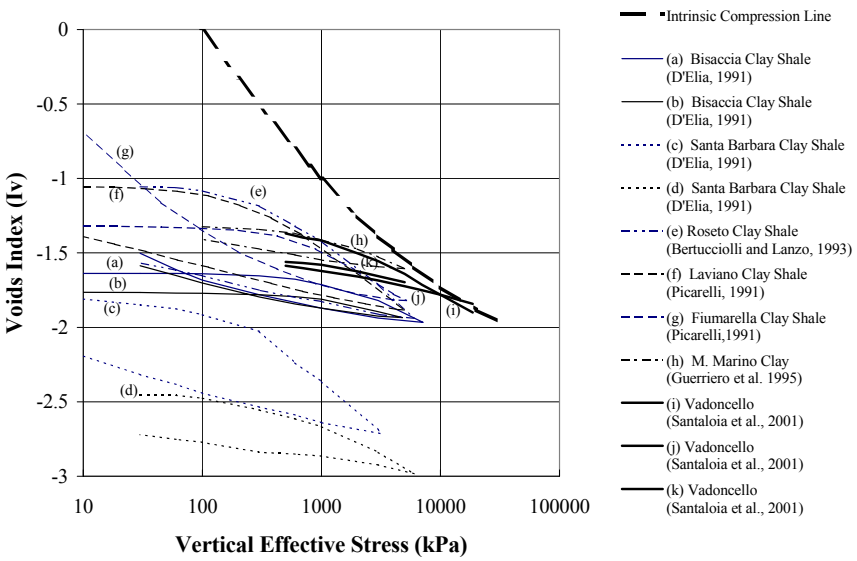

Figure 2.72 Normilized oedometer compression behaviour of structurally complex clays and clay shales (Fearon & Coop, 2002)

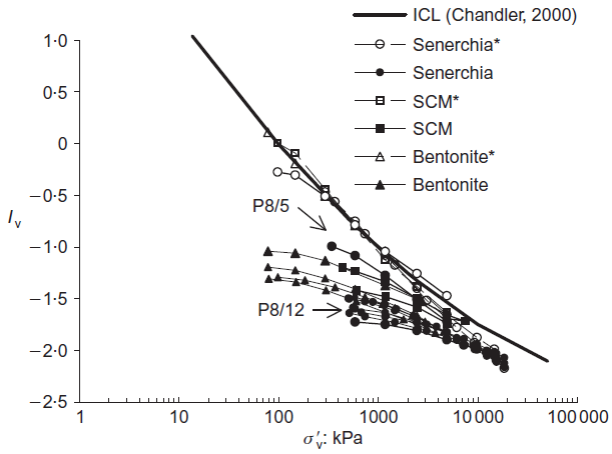

Figure 2.73 Normilized oedometer compression behaviour of structurally complex scaly clays and bentonite samples (Vitone & Cotecchia, 2011)

2.7.4 Stability of structure after gross yield

- **One-dimensional compression behaviour**

The compression behaviour of natural clays after gross yield will depend on the stress sensitivity value and the stability of the initial structure. For values of $S_\sigma>1$, the compression curves of many natural soils after gross yield tend to move towards the ICL as a result of a weakening of the initial structure due to plastic deformations (e.g. Bothkennar clay, Smith et al., 1992) (Figure 2.74a). During

compression the stress sensitivity values reduce with strains after gross yield and, at large strains, some stable elements of the initial structure could remain intact. This type of initial structure has been called meta-stable structure. However in many other soils the compression curves after gross yield remain quasi-parallel to the ICL displaying a clear stable structure that can not be removed by compression even at very high stress levels (e.g. Sibari clay, Coop & Cotecchia, 1995), the stress sensitivity values of which keep constant during compression (Figure 2.74b). Although it is very difficult to determine the different mechanical roles of each component of the structure of a soil, that is, fabric and bonding, Coop et al. (1995) suggested that fabric provides the stable component of the structure whereas bonding represents that part which degrades with strain.

The robust structure observed in Figure 2.74(b) in the one-dimensional compression behaviour of the Sibari clay was attributed to the effect of a very stable fabric that arises from the samples of this normally consolidated young Holocene alluvial material being layered at a meso-structure level. Coop & Cotecchia (1995) also noted that the volumetric offset of the normalised intact compression lines with respect to that of the ICL appeared to increase with the degree of layering.

Other examples of possible meta-stable and stable structures are shown in Figures 2.75 and 2.76. The soils tested are the mid-late Holocene Pisa deposits from the surrounding area of the Leaning Tower of Pisa. Figure 2.75 shows the one-dimensional compression behaviour of a natural sample taken from the Pisa clay unit named as “Pancone”. The Pancone unit consists of clays and silty clays deposited in lagoonal conditions during the mid-Holocene. The soil response during one-dimensional compression is similar to that of the Bothkennar clay where, after gross yield, the initial meta-stable structure of the natural clay was rapidly removed converging to the compression line of the reconstituted sample. Conversely, a more stable structure is found in the behaviour of the more recent Holocene clayey silts from shallow depths (<6m) overlying the Pancone unit (Figure 2.76). In this case the sedimentological features suggested an alluvial depositional environment such as a flood plain (Sarti et al. 2012). The behaviour of these shallower soils is very similar to that of the Sibari clay.

As shown in Figures 2.72 and 2.73, the natural structures of some clays are weaker than those of the reconstituted soils with stress sensitivity values lower than unity ($S_\sigma<1$). After gross yield, the positive hardening strengthens the structure of the soil and the stress sensitivity values increase with plastic deformations. In some cases the compression curves tend to converge towards the ICL but in others very little convergence can be seen. Again some structure elements remain intact even at large strains.

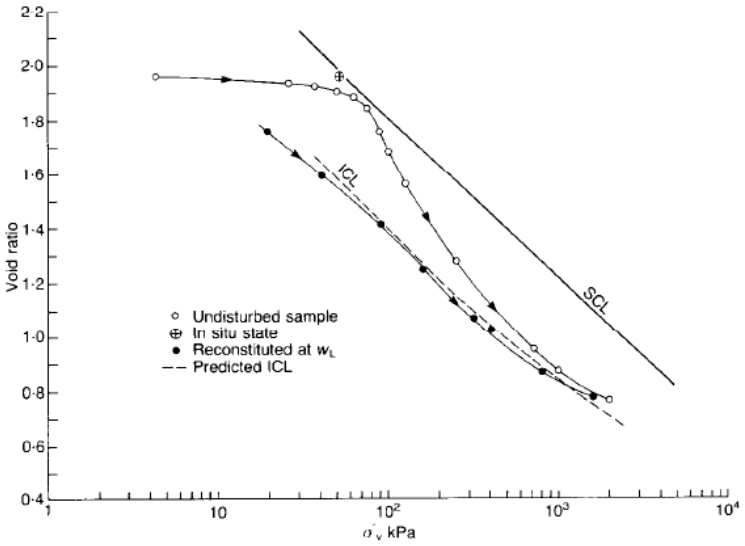

(a)

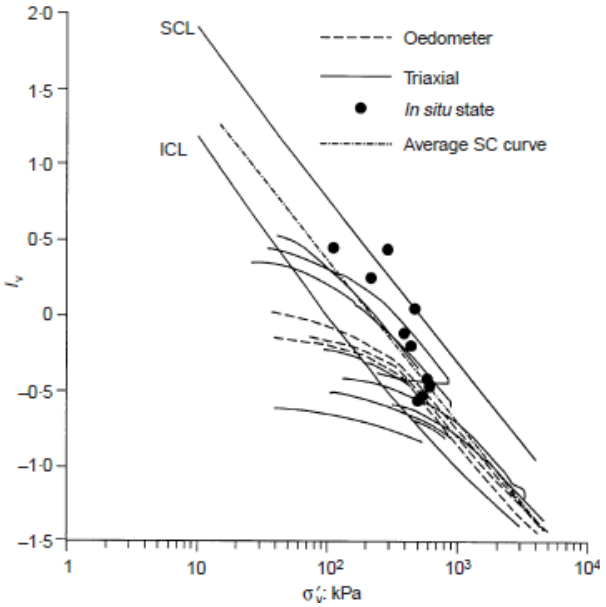

(b)

Figure 2.74 Oedometer compression behaviour of structurally complex soils: (a) metastable structure in Bothkennar clay (Smith et al., 1992) (b) stable structure in Sibari clay (Coop & Cotecchia, 1995)

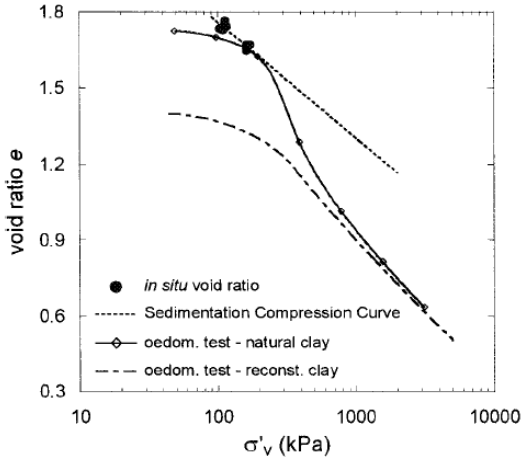

Figure 2.75 Oedometer compression behaviour of Pisa upper clay layer B "Pancone clay" (Rampello & Callisto, 1998; data from Callisto, 1996)

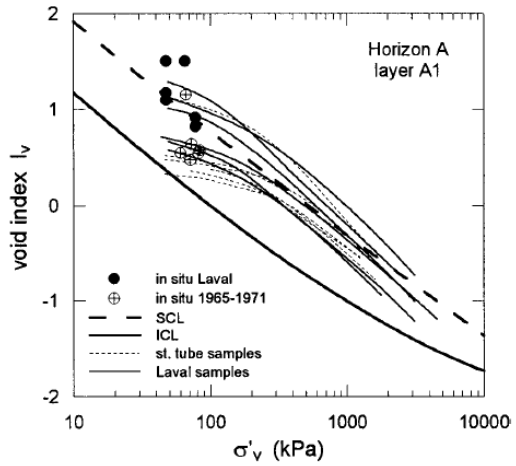

Figure 2.76 Normilised oedometer compression behaviour of Pisa clayey silts from layer A1 (Rampello & Callisto, 1998)

- **Shearing behaviour at large strains**

Figure 2.77 shows the effects of the meta-stable structure of the Bothkennar clay on its shearing behaviour. In the case of this non-fissured medium sensitive clay, the degradation of the natural structure occurs after gross yield. The normalised stress paths move towards the intrinsic state boundary surface (SBS*) after reaching the natural state boundary surface (SBS). As can be observed, at the ends of the tests the shearing deformations were insufficient to erase completely the initial structure of the clay. The shearing behaviour of the low to medium sensitivity Sibari clay is shown in Figure 2.78. As in the case of the one-dimensional compression behaviour (Figure 2.74), the normalised stress paths exhibited little convergence towards the intrinsic response and at the ends of the

tests the state boundary surfaces were still larger than that of the reconstituted soils. Coop & Cotecchia (1995) concluded that the lack of convergence observed in the natural samples was a result of a very robust structure, in particular a stable fabric as a consequence of the soil being layered and not to any meta-stable structure.

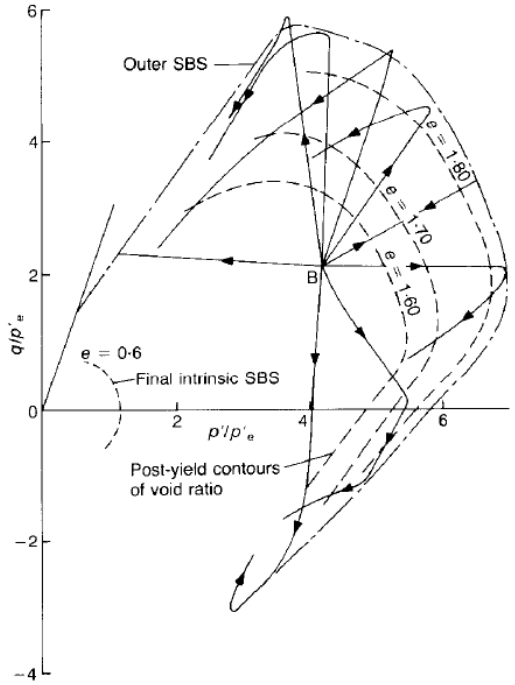

Figure 2.77 Normilised shearing behaviour of the Bothkennar clay after gross yield (Smith et al., 1992)

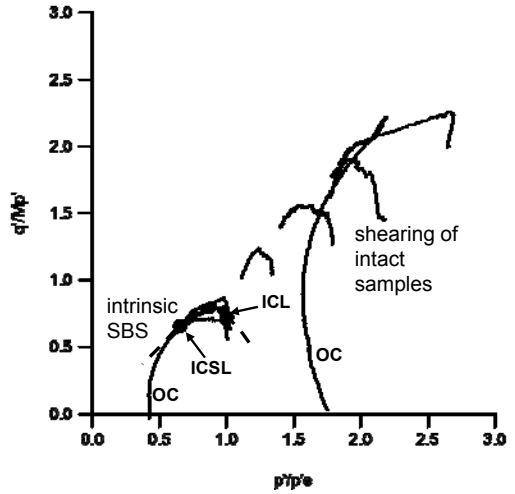

Figure 2.78 Normilised shearing behaviour of the Sibari clay after gross yield (Coop & Cotecchia, 1995)

An example of the shearing behaviour of the scaly clays of Figures 2.72 and 2.73 is represented in Figure 2.79. The stress sensitivity values of these scaly clays were lower than unity. The normalised stress paths for the natural samples compressed beyond gross yield before shearing define state boundary surfaces smaller than that of the reconstituted soils. As can be observed the normalised state boundary surfaces increase in size as the stress sensitivity values increase after gross yield. Vitone & Cotecchia (2011) concluded that the structural changes occurring in these scaly clays after gross yield have a positive effect in increasing the strength of the material. They also proposed to include the S_σ in elasto-plastic hardening of fissured clays as a parameter representing the effect of the natural structure in increasing the size of the state boundary surfaces. The stress sensitivity parameter has already been successfully used in the constitutive model of Baudet & Stallebrass (2004) to take into account the negative hardening effects during the weakening of the initial structure for natural soils with stress sensitivities larger than unity.

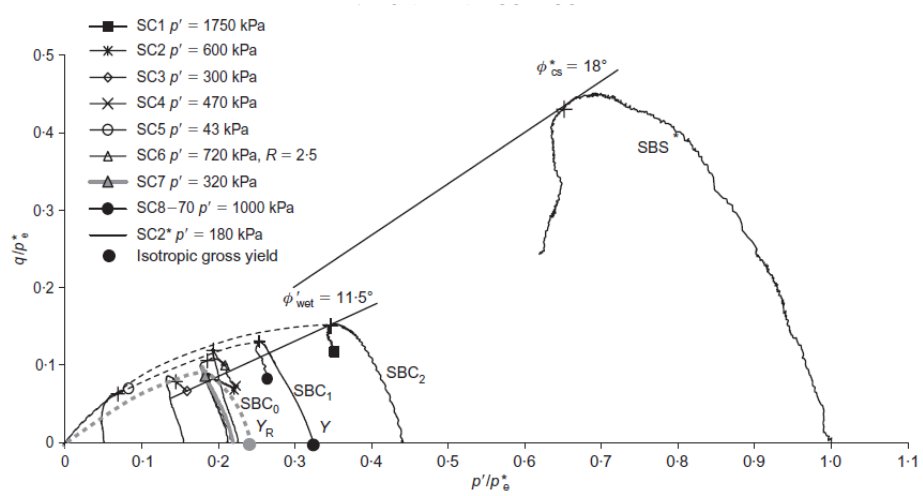

Figure 2.79 Normilised behaviour of the scaly clay SCM (Vitone & Cotecchia, 2011)

2.7.5 Summary

The structure of a natural soil represents another state variable to be added to the traditional void ratio and stress history in controlling the soil behaviour. The stress sensitivity ratio has been successfully used to quantify the effects of natural materials in elasto-plastic hardening models and its application could be extended to the case of stress sensitivity values lower than unity (e.g. Vitone & Cotecchia, 2011).

As has been described above, the naturally occurring structure of many soils could not be completely erased by the strains normally reached in conventional tests

(oedometer and triaxial). These stable structure elements remain intact at the ends of the tests and the non-convergence towards a unique structure similar to that of the reconstituted state does not mean than the natural soil is transitional in behaviour but indicates a clear effect of the different structure between the intact and reconstituted states.

Critical state soil mechanics can be generalised using two axioms implicit in the work of the Cambridge School:

- ✓ *A unique locus exists in the q:p':v space such that a soil can be deformed without limit at constant stress and constant void ratio; this locus is called the critical sate locus (CSL).*

- ✓ *The CSL forms the ultimate condition of all distortional processes in soil, so that all monotonic distortional stress state paths tend to this locus.*

Another key ingredient of the critical state soil mechanics theory is the assumption that there exists a unique NCL for a given reconstituted soil and that it is parallel to the unique CSL. The evaluation and quantification of the effects of the structure of natural soils uses the unique intrinsic compression line and critical state line as a reference framework. The transitional behaviour observed in many soils in their reconstituted state completely breaks down these traditional concepts of the uniqueness of the NCL and CSL lines that have been used as a reference framework for interpreting soil response since the mid 1960's when the critical state theory was conceived at Cambridge University. It is not yet clear how a critical state framework, formulated in a q:p':v space, might be modified to take into account this transitional behaviour. This highlights a new challenge in soil mechanics.

Chapter 3
Laboratory equipment, sample preparation and testing procedures

3.1 Introduction

In this chapter a detailed description of the laboratory equipment used and the testing procedures followed during this research project are presented. The accuracy and calibration scheme of each apparatus is also discussed. All the apparatus used in this research belongs to the Soil Mechanics section at Imperial College, London, where the author of this thesis carried out all the laboratory tests.

3.2. Oedometer apparatus

The oedometer test is probably one of the simplest tests that is routinely carried out in soil mechanics laboratories and at the same time one of the most reliable tests. Moreover, it is a very suitable test to anticipate the possible transitional behaviour of soils in terms of compression. The oedometer test reproduces the one-dimensional compression condition in the laboratory by means of a rigid ring that holds inside a soil sample lying between two porous stones. The top and bottom porous stones allow the sample to drain freely. The test can be either controlled by means of applying a constant rate of strain (CRS) to the sample or stress

controlled by means of applying increments of load in stages using a loading hanger and a lever arm. In this research project all the tests were stress controlled. Calibrations of the oedometer apparatus were carried out routinely to measure the compliance of the system as will be explained in Section 3.6.

The dimensions of the samples used in this investigation were 50mm diameter and 20mm height so that the ratio between diameter and height is greater than two to reduce the side friction effects (Bishop & Henkel, 1957). In some cases a 38 mm diameter ring was used to reach higher stress levels. The vertical displacement of the specimens was measured externally by an axial displacement transducer and the readings were automatically recorded onto a PC (Figure 3.1). In some tests a dial gauge was also used.

Figure 3.1 shows a modified design of some of the oedometer cells in order to ensure the saturation of the sample from the beginning of the test. In this type of cell, water was flushed throughout the sample under a back pressure of around 10kPa. This pressure was generated by connecting a tube to the base of the oedometer cell. This tube was also connected to a perspex container that was filled with distilled water. The difference in height between the container and the base of the oedometer cell was 1m (Figure 3.1). This modified cell was used to compare the results with conventional cells where the oedometer is routinely flooded with water to prevent the drying of the sample and to some extent to saturate it.

Figure 3.1 Modified oedometer cell to flush water through the sample from the bottom to the top under a pressure of 10kPa

3.3 Triaxial apparatus

3.3.1. Introduction

The triaxial test is the most widely used apparatus to investigate the stress-strain behaviour of all types of soil. A large number of stress paths can be applied under conditions of axial symmetry. The triaxial test has the advantages of controlling the drainage condition of the sample and being able to reproduce any axi-symmetric in-situ initial stress state. In this research project two different triaxial apparatus were used; a conventional Bishop & Wesley stress path cell and a modified 7MPa triaxial cell.

3.3.2 Bishop & Wesley triaxial apparatus

The Bishop & Wesley type apparatus is the most extensively used triaxial equipment in the Soil Mechanics laboratories at Imperial College. This type of hydraulic stress path cell is described in detail by Bishop & Wesley (1975). Figure 3.2 shows a schematic diagram of the apparatus.

The Bishop & Wesley triaxial apparatus used in this research were designed to test saturated soil samples with a diameter of 38mm and a height of 76mm. The radial stress/cell pressure (σ_r), axial stress (σ_a) and pore water/back pressure (u) controllers were fed by a main compressor with a minimum delivery air pressure of 850kPa. The air pressure was regulated by electro-manostats and converted to hydraulic pressures through air-water interfaces. The cell pressure interface was linked directly into the cell chamber. The axial stress was applied by means of a vertically moving piston, also known as ram, located at the base of the cell. Axial load was applied to the sample by increasing the ram pressure and therefore pushing the sample top platen against a stationary submersible load cell. The load cell was manufactured by Applied Measurements and had a 5kN capacity. A rubber suction cap (Figure 3.13) (Skinner, 1982) was used in the tests in order to improve the alignment between the sample and the ram piston and also to reduce the local strain measurement errors related to seating and tilting between the load cell and the top platen (Atkinson & Evans, 1985). A connection at the base of the sample pedestal allowed the drainage, the measurement and control of the pore water/back pressure and the measurement of the volume changes. The pore water and cell pressures were measured by Druck pressures transducer of 1.7MPa capacity.

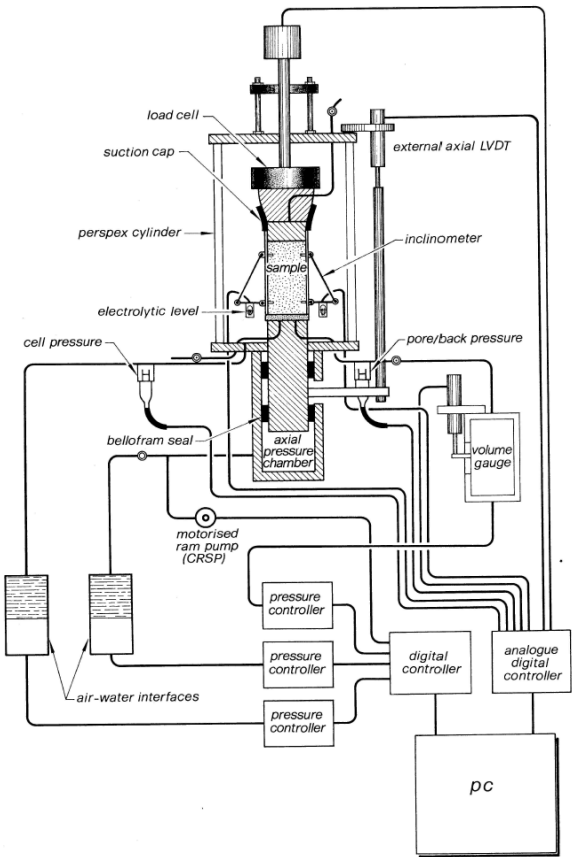

Figure 3.2 Schematic diagram of the Bishop & Wesley triaxial apparatus (modified from Qarimi, 2005)

During the shearing stages, all the tests were carried out by prescribing a constant axial strain rate (strain controlled tests). This was done by-passing the ram pressure interface and using a Imperial College designed constant rate of strain pump (CRSP) that consist of a stepper motor controlled piston that had a pressure capacity of 2MPa. The piston could move up and down. A gear box was used to reduce the torque and increase the number of steps required to produce the desired movement giving better accuracy of control.

3.3.3 7MPa triaxial apparatus

The 7MPa apparatus is a medium pressure triaxial cell capable of reaching higher stresses compared with the Bishop & Wesley cell. This apparatus was used to investigate the compression and shearing behaviour of soils at high stresses. Figure 3.3 shows a photograph of the cell. The cell is made from steel compared to the perspex of the Bishop & Wesley aparatus. This was necessary to be able to withstand the higher pressures. The size of the samples was 50mm in diameter and

100mm in height. For these tests, the connection between the load cell and the sample was done by a half-ball top cap. The volume changes during isotropic compression and shearing were measured by the same Imperial College designed volume gauge used with the Bishop & Wesley cell but in this case with a capacity of 100cc.

Figure 3.3 The 7MPa triaxial apparatus

Another difference between the 7MPa apparatus and the Bishop & Wesley cell was the way in which cell pressure and axial stress were applied to the sample. In this case the cell pressure was generated by a higher capacity CRSP pump which was directly connected to the cell chamber. The axial load was applied by a conventional loading frame by moving the base pedestal that pushed the sample against a stationary submersible load cell at a constant rate. The reaction force was provided by a Wykeham Farrance compression frame as shown in Figure 3.3. The load cell capacity was 25kN.

3.4 Instrumentation to measure stress and strain

3.4.1 Stress measurements

As mentioned before, in the conventional triaxial apparatus, the σ_r and u were measured by Druck pressure transducers with a capacity of 1.7MPa. The pore water pressure was only measured at the base of the sample.

3.4.2 Strain measurements

- **Axial strain**

The axial strain of the specimens was measured using external and internal/local axial displacement devices.

The external axial displacement was measured by using a resistive transducer (MPE) with a maximum movement of 25mm, 2μm resolution and ±0.05mm precision. This transducer measured the axial displacement of the loading piston. Compliance tests on dummy samples were carried out to obtain more accurate measurements of the axial displacement of the sample by correcting the data obtained during tests.

The internal/local axial displacements of the samples were measured using either the Imperial College inclinometers (Jardine et al., 1984) or linear variable differential transformers (LVDTs). The Imperial College inclinometer consisted of an electrolytic liquid sealed in a glass capsule and enclosed in a steel cylinder (Figure 3.4). Three co-planar electrodes protruding into the capsule and partially immersed in the fluid measure the changes in impedance produced when the capsule tilts. The change in the voltage measured by the electrodes is converted into a change in height between the pads on the pivot arms. The linear range of the inclinometers was large, typically 15mm. The resolution was 0.1μm and the precision was ±25 μm. The inclinometers were attached diametrically opposite each other on the sample.

The other type of internal/local axial displacement devices used in this research project was the LVDTs. The LVDTs had a better resolution of 0.02μm. The linear range was 10mm. As well as the inclinometers, they were attached diametrically opposite each other on the sample. Figure 3.5 shows the setting up of the local LVDTs.

- Radial strain

The radial strain of the specimens was measured using an LVDT fixed into a radial strain belt. This strain belt was glued to the membrane of the sample by two metal pads opposite each other (Figure 3.5). The linear range and resolution of this LVDT was the same as those used for axial strain measurements.

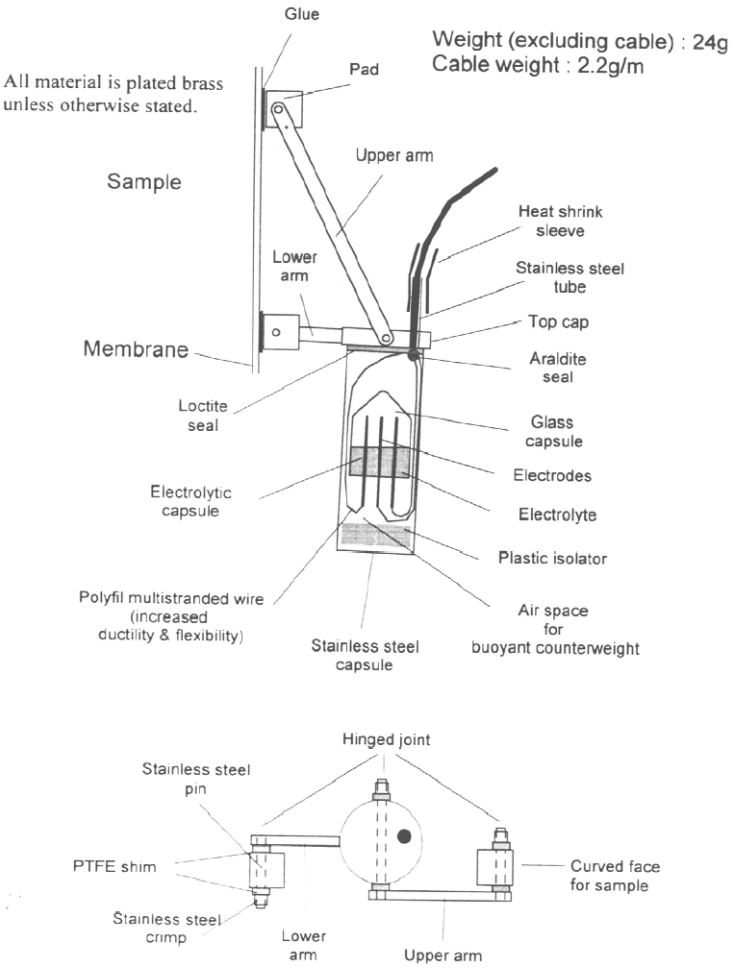

Figure 3.4 Imperial College inclinometers (Kuwano, 1990, adapted from Jardine et al., 1984)

• Volume strain

The volume changes during compression and shearing were measured by Imperial College designed volume gauges (Figure 3.6). This had a capacity of 50cc for the one connected to the Bishop & Wesley triaxial apparatus and 100cc for the 7 MPa triaxial cell. In both cases the resolution was 0.001cc. The sample must be saturated and negligible compliance of the system was required, in order to obtain accurate measurements.

Figure 3.5 Local LVDTs for measuring axial and radial strains of samples

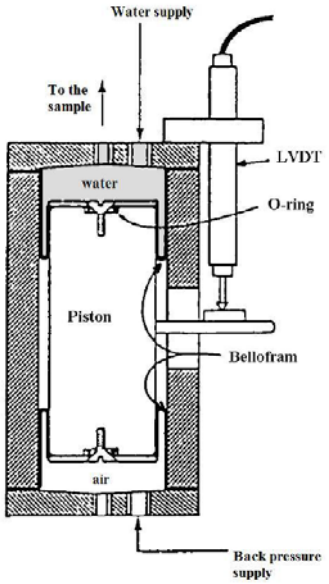

Figure 3.6 Imperial College volume gauge (modified from Head, 1985)

3.5 Control and data logging system

The signals from all the local instrumentation and transducers were data logged by an A/D converter acquisition system manufactured by Measurement Systems Ltd connected to a computer through an RS232 serial port. A computer controlled software called TRIAX was used to monitor the pressures and displacements, and control stresses and strains. The program was written by Professor David Toll at

Durham University. TRIAX allows the user to define a fully automated stress path or strain control stages.

3.6 Calibration

As presented above, a range of apparatus, transducers and specially local instrumentation were used during this research project. Calibration of all the equipment was carried out routinely at the start, during the entire testing programme and at the end. Special attention was paid to the calibration of the load cells in order to check any possible drift in the measurements.

Load cells and pressure transducers were calibrated against a Budenberg dead-weight calibrator. Prior to the calibration of the load cells they were cycled several times reaching 90% of their maximum load capacity. The volume gauges were calibrated using a calibrated Bishop ram. In this case the calibration was carried out applying a back pressure of 200kPa which was the back pressure used in the majority of tests to saturate the samples. The inclinometers and LVDTs were calibrated against a Mitutoyo micrometer mounted in a specially designed device. In all cases a linear regression was used.

For the triaxial cells, it was essential to measure the compliance of the systems, in order to be able to use the readings from the external axial strain transducer. To that end, the calibration was carried out by testing a solid brass dummy sample with perfectly parallel faces. The deformation of the dummy sample was negligible. Curves of load-displacement were obtained after simulating a test with the dummy sample. For the oedometer cells, the same procedure was followed where all the loading and unloading stages during a real test were reproduced again using a solid brass dummy sample.

3.7 Sample preparation and testing procedures

3.7.1 Oedometer tests

• Sample preparation procedures

Three types of oedometer samples were used to investigate the influence of the structure and sample preparation method on the mechanical behaviour of the soils tested; (a) intact, (b) slurry and (c) remoulded samples. As will be seen in the following chapters, two different materials were investigated in this research project: the Bormida River Silts (BRS) from Italy and the Valencia silty soils (VSS), from Spain.

(a) Intact samples

In both cases, intact block samples were carefully excavated and also remoulded material was collected. For each material, the block sample was divided into small pieces large enough to obtain an oedometer or triaxial sample, using a bench saw. The position of each piece within the block was identified to check the homogeneity of the material contained in the block. Intact specimens were trimmed from each piece of material using a sharp knife. The procedure was as follows. The oedometer ring, with a sharp edge, was placed on the top of the material piece and a small pressure was applied on the ring pushing it against the sample at the same time as the trimming was being carried out. Once the sample was inside the ring, the top and bottom parts were trimmed carefully, paying special attention to have a very flat surface on both sides. During the trimming process all the remaining material was collected inside a plastic bag. This material was later used for preparing slurry and remoulded samples to compare their behaviour with the intact ones.

(b) Slurry samples

Slurry specimens were prepared by adding distilled water to the trimmings from the intact samples and mixing thoroughly to achieve a uniform consistency. The soil trimmings were never oven-dried before the mixing with distilled water. After the trimmings were mixed with water the paste was left 24 hours in a tight plastic box to get a homogeneous distribution of the water through the sample. Different samples were prepared by adding different amounts of water. Special attention was paid to the possible segregation of the more sandy material during the mixing process and a limitation on the maximum liquidity index (IL) of 3 was adopted to prevent this. It is important to point out that after the 24 hours curing, the soil sedimented and a very small layer of nearly clear water covered the soil. In all cases the slurry was again re-mixed thoroughly to achieve a homogeneous consistency before placing it inside the oedometer ring.

(c) Remoulded samples

Remoulded samples were prepared by means of static and dynamic compaction methods. The trimmings from the intact specimens were remoulded by hand using a spatula, keeping the initial water content of the intact samples. The samples were compacted inside the oedometer ring either statically or dynamically. The following types of samples were prepared:

Static compaction:

c.1) Samples compacted in one layer
c.2) Samples compacted in two layers
c.3) Samples compacted in one layer with vertical drilled holes
c.4) Samples compacted in one layer with vertical pushed holes
c.5) Samples compacted in layers but with very different values of void ratio for each layer. These samples were called "layered samples"

Dynamic compaction:

c.6) Samples compacted in three layers

The preparation of the statically compacted specimens was carried out using the equipment shown in Figure 3.7. Each sample was compacted inside the ring by applying a constant rate of displacement to the base pedestal. A static flat ended rod connected to a load cell was used to create the reaction to apply the static pressure to the sample. The maximum static load applied during preparation was recorded for all the samples. The flat end of the rod had a slightly smaller diameter compared to the oedemeter ring. As mentioned above, some samples were compacted in layers. In this case, the surface in between each layer was scarified before continuing with the next one to ensure a good continuity in the whole sample. The quantity of material to be added was calculated by knowing the required void ratio, the dimensions of the oedometer ring, the water content of the material and the specific gravity. All the samples were allowed to rest during 5 minutes before placing the oedometer ring in the cell in order to permit them to rebound. Both sides of the samples were flattened before starting the test and the ring plus the wet sample was weighed.

As will be described in Chapter 4, holes and plant roots were often found during the trimming of the BRS intact specimens (Figure 3.12). They were mainly vertical holes and in some cases they extended from the top to the bottom of the sample. In order to reproduce these vertical holes, drilled or pushed holes were artificially created by means of a Carbide Solid steel drill (Figure 3.8). The difference between the two procedures is that the drilled hole was created by extracting material from the sample and the pushed one by displacing the material inside the sample. A top platen was used to avoid any volume change during the drilling and pushing procedures. The number and location of the holes inside the sample was randomly distributed. Figure 3.9 shows an oedometer specimen after the holes were drilled.

Figure 3.7 Equipment used for the static compaction

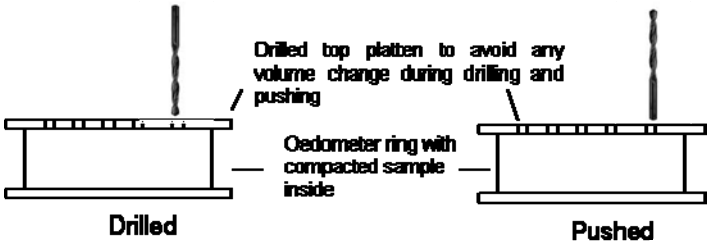

Figure 3.8 Schematic representation of the equipment used for creating the vertical holes in the compacted samples

Figure 3.9 Oedometer sample after holes were drilled

The dynamic compacted samples were prepared by using a steel rod that was dropped by hand. The undercompaction method (Ladd, 1978) was followed in order to obtain homogeneous samples.

- **Test procedures**

As pointed out in Section 3.6, before starting the tests on real samples, all the oedometer cell sets were calibrated using a solid brass dummy sample with perfectly parallel faces. The curves of load-displacement obtained from the calibration were used to correct the displacements measured during the real test. This was especially important when intact samples were tested as the measured displacements are smaller and also for the tests performed at very high stress levels.

For the intact and remoulded specimens an initial load was applied and thereafter the cell was filled with water. The initial load before adding the water varied in order to study the effect of the applied initial stress on the swelling properties of the BRS and VSS soils. After filling the cell with water the samples were left 24 hours before applying the next load. During this time, the swelling behaviour was monitored. It was common to see that the volume change due to swelling stabilise very quickly, although, and as mentioned above, they were all left 24 hours before the next load. The samples were drained on both sides with two porous stones. Filter papers were placed between the porous stones at the top and bottom of the specimens. This was done to avoid the stones becoming clogged with soil particles. The stress was then increased by doubling the load each time when the vertical displacements had become negligible. The samples were then unloaded in stages to a vertical stress of around 8 to 10kPa. Special attention was paid when dismantling the cell at the end of the test, as the water in the cell could be sucked into the sample after the last load was released. To avoid this, all the water that surrounded the sample and porous stones was dried with filter paper before dismantling the cell to minimise the error in measuring the final water content.

Additionally, and as described in Section 3.2, some of the oedometer cells were modified to be able to flush water through the sample, from the bottom to the top, at a pressure of 10kPa. This procedure was applied to some specimens to compare the results with the conventional procedure where the water bath was flooded with water to saturate the sample. This stage was started after the first load increment was applied and the water bath flooded. In each test, the water was flushed for one week and the volume change of the samples was monitored and recorded.

The slurry samples were prepared as explained above and placed directly into the oedometer ring paying special attention so as not to trap any air within them. To this end, it was found that gently hitting the cell with the slurry sample inside was very helpful. This procedure was not applied to the more sandy material to avoid liquefaction. The samples were first loaded under just the weight of the oedometer

top cap, in order to avoid any soil squeezing out from the top of the oedometer ring. After applying the first load the water bath was flooded with water. The loading sequence and the procedure to dismantle the cell were exactly the same as in the case of the intact samples.

3.7.2 Triaxial tests

• Sample preparation procedures

Three types of samples were also prepared in the case of the triaxial tests; (a) slurry (b) intact and (c) remoulded samples.

(a) Slurry samples

The slurry samples were prepared following the same procedure described in Section 3.7.1(b). Initially, once the slurries were created, they were poured into a 38mm diameter floating ring consolidometer (Figure 3.10). The samples were consolidated one-dimensionally up to a required stress to ensure the soil was strong enough to be handled. After the consolidation was complete the samples were extruded and the ends trimmed to create a sample that was 76mm in height. In many cases, during the process of extruding the specimens, it was observed that the perimeter was disturbed generating heterogeneities in the samples. To avoid this problem a newly designed 50mm diameter floating ring consolidometer was used for creating the 38mm samples. The slurries were first consolidated in the 50mm diameter consolidometer and then trimmed to a 38mm using a hand lathe and trimming saws. Following this procedure it was possible to remove the disturbed parts of the samples that were in direct contact with the wall of the consolidometer.

Another method to produce slurry samples was by means of trimming larger pieces of a big "cake" sample (Figure 3.11). This cake sample was prepared by using a large consolidometer which has a diameter of 230mm and a height of 280mm. The soil mixture was placed in this consolidometer and was initially left to consolidate under its own self weight. The cake was then loaded until the same vertical load as the samples consolidated in the small consolidometer. The cake sample was removed from the oedometer ring, once the maximum load was reached and the consolidation finished. To preserve the water content, the cake sample was covered with clingfilm and waxed.

Figure 3.10 38mm diameter floating ring consolidometer

(a)

(b)

Figure 3.11 (a) Large consolidometer cell with a diameter of 230mm (b) "cake" sample after being removed from consolidometer

(b) Intact samples

As described in Section 3.7.1, the block samples of BRS and VSS were cut into small parts, large enough to be able to trim either a 38mm or 50mm diameter sample. The small blocks were reduced in size by using a sharp knife before setting up the samples in the hand lathe. During the trimming of the BRS it was common to find holes and plant roots in the samples (Figure 3.12a). These roots and holes were normally removed from the final sample but in some cases it was impossible. Therefore some samples were tested with holes inside that were observed by visual

inspection. In the case of the VSS, it was also common to find aggregates of cemented particles during the trimming of the samples (Figure 3.12b). In some cases these aggregates were cut by using small saws and in other cases they were removed and the holes were filled with the trimmings of the same sample. Special attention was paid to avoiding the samples drying out during the trimming process. To this end, clingfilm was used to cover the samples.

(a) **(b)**

Figure 3.12 Trimming procedure of the (a) BRS and (b) VSS intact samples

(c) Remoulded samples

Only remoulded triaxial samples created by dynamic compaction were tested in this research project. The samples were compacted in 5 layers following the undercompaction method (Ladd, 1978).

• Test procedures

All the triaxial tests performed in this research project followed the stages described below:

(a) preparation of the cell
(b) setting up of the samples
(c) saturation
(d) consolidation
(e) shearing

(a) Preparation of the cell

Before starting a test, the cells were kept under a pressure of 600kPa during 24 hours. This procedure was carried out to ensure full saturation of the system. Also during this time all the internal transducers were monitored to check any possible malfunction.

(b) Setting up of the sample

Once the sample was prepared it was placed in the triaxial cell. Before this, the weight and dimensions were measured. The local transducers were glued to the specimen immediately after placing it in the triaxial cell (Figure 3.5). Data were started to be recordered during the following procedures which allowed the measuring of any change in the initial dimensions of the sample.

(c) Saturation

The saturation stage is one of the most important procedures for successfully completing a triaxial test on saturated samples. The saturation of a sample guaranties the application of the Terzaghi's effective stress principle. It also assures that the volume changes measured during consolidation and drained shearing are representative.

As mentioned in Section 3.7.2, three types of samples were tested in this research project: intact, slurry and remoulded. Initially, the intact and remoulded samples were partially saturated whereas the slurry were fully saturated. The procedure followed to saturate the samples was to apply increments of back pressure and cell pressure simultaneously in order to maintain the initial effective stress of the sample constant. The degree of saturation was checked by measuring Skempton's pore water pressure parameter (B). The B parameter can be calculated by Equation 3.1, where Δu is the measured pore water pressure increment caused by an increment of the cell pressure $\Delta\sigma_r$ under undrained conditions. Each B test was carried out by applying a cell pressure increment of 50kPa. It was assumed that saturation was satisfactory when the values of B were higher than 0.95.

$$B = \frac{\Delta u}{\Delta \sigma_r} \qquad 3.1$$

(d) Compression

After the saturation stage, all the samples were compressed, mainly isotropically, to reach the target stress value. Before starting the compression stage, and only for

the Bishop & Wesley triaxial cells, a suction cap was connected to the load cell in order to reduce the errors induced by any alignment problems between the load cell and top platen when shearing was started (Figure 3.13). The suction cap consists of a rubber cap that allows connecting the top platen to the submersible load cell trough perspex extension platen. It is recommended to have a mean effective stress of 20kPa in the sample before starting to connect the suction cap to avoid excessive damage to the sample during the connection procedure. To this end, it was necessary to carry out a small compression stage to reach the target mean effective stress of 20kPa before starting to connect the suction cap.

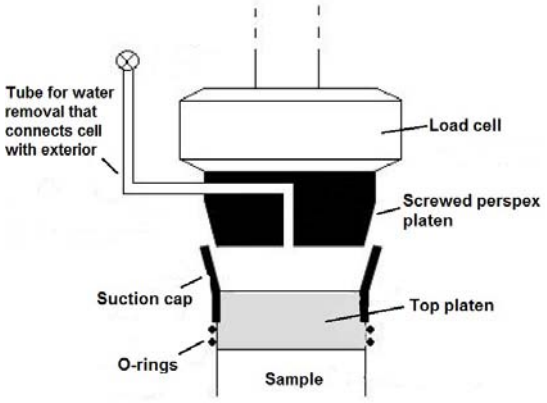

Figure 3.13 Schematic drawing of the load cell connection using a suction cap (modified from Carrera, 2006)

Compression was re-started once the suction cap was connected. During an isotropic compression stage, the back pressure was kept constant while the cell and axial pressures were increased simultaneously to keep the deviatoric stress equal to zero. In the case of a k_0 compression stage the cell and axial pressures were increased in order to have a zero radial strain in the samples. As described in Section 3.4.2, the radial strain of the samples was measured using a LVDT fixed into a radial strain belt. During the compression stage, the rate of increasing the cell pressure was 5kPa/h. At the end of each compression stage, the sample was allowed to dissipate the remaining excess pore water pressure generated during the stage. Radial filter drain was used with all the samples in order to reduce the time for consolidation.

(e) Shearing

The shearing stage was started once the samples had been consolidated to the required mean effective stress and after being allowed to dissipate any remaining excess pore water pressure. It was accepted that the excess pore water pressure was dissipated when the rate of change of the internal axial strain was less than 3% of

the prescribed initial rate of axial strain during shearing. The samples were sheared in either a drained or an undrained condition under strain control. For the undrained tests, the initial rate of shearing was 0.05%/h and was maintained until the small strain region was exceeded. The axial strain rate was then increased in steps up to 0.2%/h in order to complete the tests in a reasonable time. In the case of the drained tests, a series of tests were performed to select a satisfactory shear strain rate to ensure that the test was being carried out in a drained condition. All the tests were sheared to as large strains as possible in order to be able to reach the critical state. As is common in all the Bishop & Wesley triaxial cells, there is a limitation in the maximum axial strain that can be achieved. In this case the majority of the tests reached a final axial strain value of 20% or larger.

Chapter 4
The Bormida River Silts

4.1 Introduction

In this chapter a detailed characterisation of the index properties of the Bormida River silt is presented. In addition, a literature review of previous investigations on the Bormida River silts (BRS) is carried out. The conclusions drawn will be used as a background for the analysis and compared with the results obtained in this research.

4.2 The Bormida River silts

The BRS was the first material investigated in this research project. It was obtained from the foundation level of the Bormida River embankments at Castellazo Bormida, Alexandria region, Italy (Figure 4.1). According to the Geological Map of the Alessandria region (Carta Geologica D'Italia, Foglio 70, scala 1:25000), the BRS consist of postglacial Holocene alluvial deposits.

The Bormida River is a tributary of the Tanaro River (Figure 4.2). The Tanaro in turn is the most significant right-side tributary to the Po in terms of length, size of drainage basin (partly Alpine, partly Apennine) and discharge. Traditionally, the materials dredged from the Bormida River are used for the construction of the embankments. The river environment where the samples were taken could be classified as meandering with a large sinuosity (Figure 4.1b).

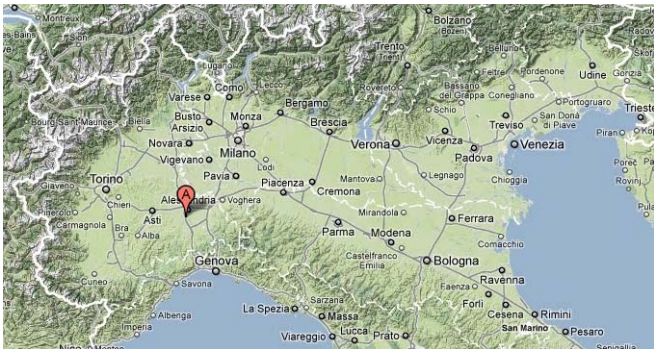

(a)

(b)

Figure 4.1 (a) Castellazo Bormida, Alessandria province, Italy (b) Enlargement of the Geological map of the Alessandria region

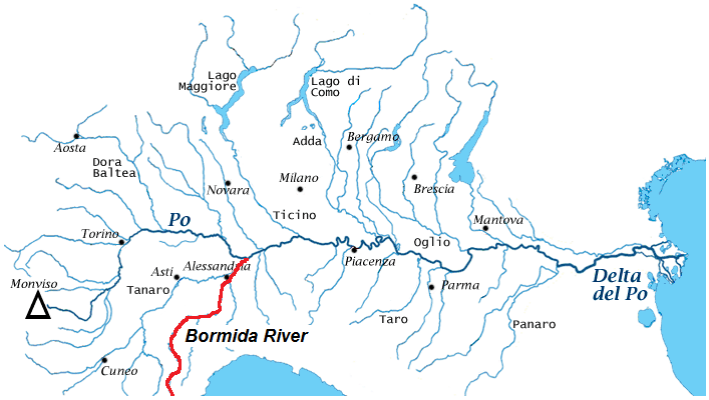

Figure 4.2 Po River main stream and tributary rivers

Figure 4.3 Sampling process of the BRS (modified from Radici, 2006)

The main core of the BRS samples tested during this investigation was trimmed from an intact block sample taken by Radici (2006). The block sample was retrieved from the foundation level of the river embankments at a depth of 1.4m

below ground level. The sampling process is shown in Figure 4.3. During the sampling of the block some of the excavated material was also collected. In order to distinguish between these two types of samples they were named BRS-B for the block and BRS-E for the excavated soil. During this research, only a small quantity of the BRS-E was available. This imposed a limitation in the number of tests that could be carried out.

4.2.1 Characterization of the Bormida River silts: index properties

In this section the index properties of the BRS will be presented. The procedures for their determination followed the British BSI and Spanish UNE standards.

• Particle size distribution

Six samples of the BRS-B from different parts of the block plus two samples of the BRS-E soils were tested in order to obtain the particle size distribution of BRS shown in Figure 4.4. It can be observed that the material contained in the block was very homogeneous in term of size distribution, giving an almost unique grading curve for all the samples tested. This homogeneity can also be seen in the BRS-E specimens. Table 4.1 shows the average content of clay-sized, silt and sand particles, together with the characteristic median particle size (D_{50}), according to the British Standard classification system.

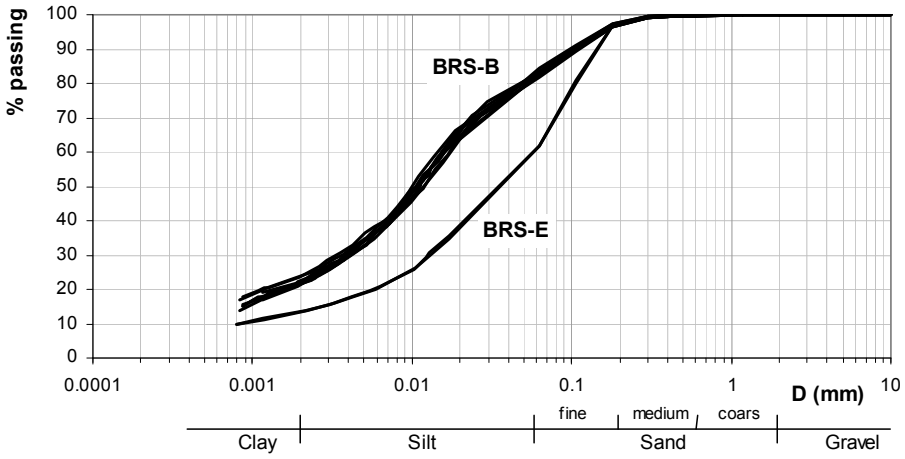

Figure 4.4 Particle size distributions of the BRS soils. Six samples taken from different parts of the block (BRS-B) and two samples of the excavated material (BRS-E)

A new apparatus called QicPic was also used to measure the particle size distribution. The QicPic is a laser image analysis apparatus with a manufacturer's

stated capability of measuring particle sizes between 1µm and 20mm. It uses dynamic image analysis by examining a well dispersed flow of particles passing through the scanning beam emitted by a pulsed laser (Figure 4.5). The camera detector can operate up at to 500 images per second. The Windox software is provided with the apparatus to analyse the images that are taken. Several particle properties can be obtained such as particle size distribution and shape.

Soil	Clay-sized (%)	Silt (%)	Sand (%)	D_{50} (mm)
BRS-B	22	60	18	0.01
BRS-E	13	50	37	0.035

Table 4.1 Average contents of clay-sized, silt and sand particles and median particle size (D_{50}) according to the British Standard classification system.

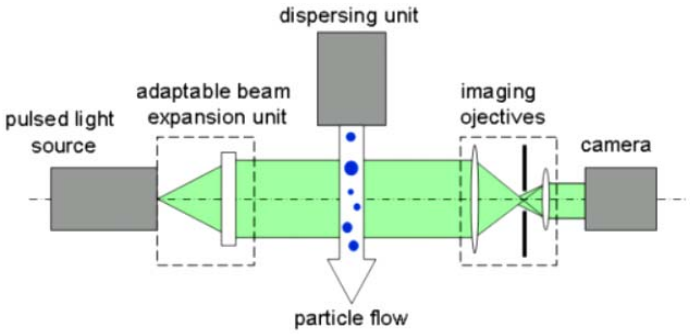

Figure 4.5 Schematic diagram of the QicPic apparatus (http://www.sympatec.com)

Many attempts were made to measure the particle size distribution of the BRS using QicPic. In this case, QicPic was not able to capture the clay-sized particle content in any of the tests carried out, although the manufacturer states that QicPic is capable of measuring particles down to 1µm. This problem might be due to overlapping of the clay-sized particles due to its high clay-sized content. On the other hand the sandy fraction of the sample was tested and the results are compared with the sieving analysis in Figure 4.6. The comparison showed that the sieving method gives higher quantities of sand compared with the QicPic. In both methods a very good repeatability was obtained.

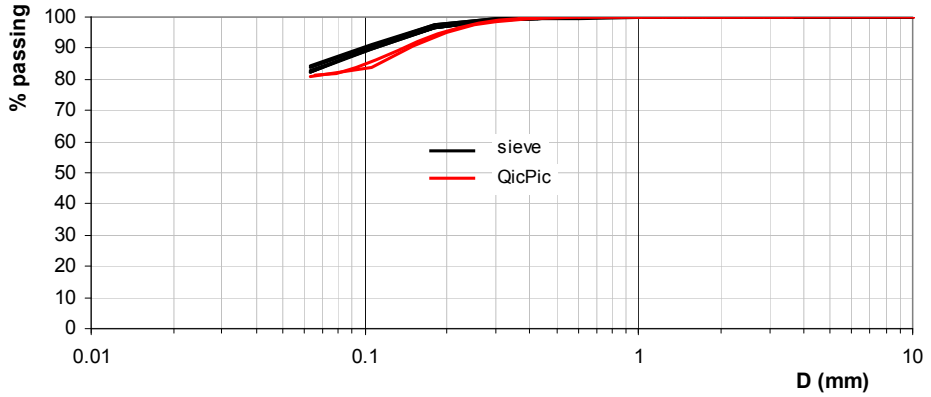

Figure 4.6 Particle size distributions; comparison between sieving and QicPic analyses for the sandy fraction of the BRS-B sample

• Particle shape

The shape of the BRS particles was analysed by means of digital microscope photos taken from samples that had been previously subjected to sieving analysis. An extended focus mode was used to obtain images that are in focus throughout a wide range of focal distances. In general, the shape of the bulk particles is sub-angular to sub-rounded as shown in Figures 4.7 to 4.9. Figure 4.7 shows the material retained on the 63µm sieve after washing one of the BRS-B samples. What can be seen is a range of sands from fine to medium size where the grains are mainly composed of quartz. Detailed photos of the fine to medium sand and silt particles contained in the BRS-B and BRS-E samples are shown in Figures 4.8 and 4.9. Figure 4.9 shows the clastic nature of the silt particles passing the 63 µm. During the microscope analysis a significant quantity of mica particles was observed in both samples.

• Mineralogy

A series of X-ray diffraction tests were performed on different samples of the BRS-B. The tests were carried out by Dr. J. Hugget. A portion of each sample was gently crushed, mixed with distilled water plus a few drops of ammonia as a dispersant and placed in an ultrasonic bath for 30 minutes to release the maximum amount of clay into suspension. The clay suspension was then centrifuged to deposit the entire <2µm fraction, which was filtered (mixed with a little distilled water to make a thick slurry) onto unglazed ceramic tiles. A further portion was ground to a powder in a Tema mill. A few drops of the resulting slurry were allowed to dry on a silicon wafer.

Figure 4.7 Digital microscope photo of the BRS-B; material retained on the 63µm sieve after washing

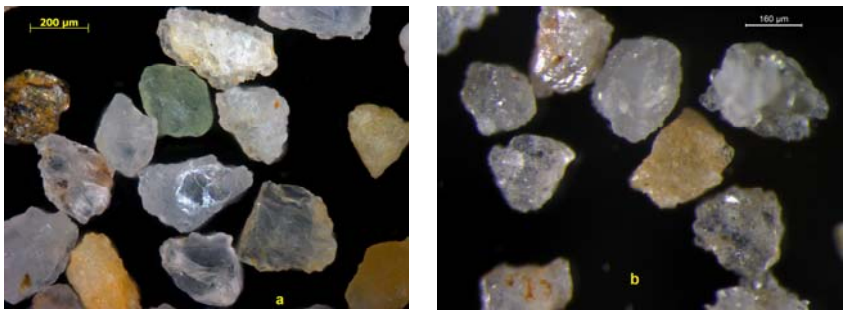

Figure 4.8 Digital microscope photos of; (a) the BRS-B sample, particle size 180µm<D<300µm and (b) the BRS-E sample, particle size 160µm<D<400µm

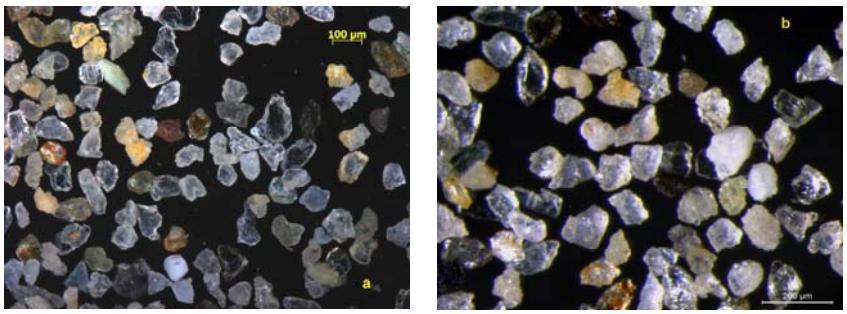

Figure 4.9 Digital microscope photos of the material passing the 63µm sieve: (a) BRS-B sample and (b) BRS-E sample

The samples were scanned on a Phillips 1820 automated X-ray diffractometer using Ni-filtered CuKa radiation. The clay tiles were scanned at a rate of 5 seconds per 0.02° step width, using 0.3mm slits from 2 to 40°2'. The tiles were scanned again after heating at 400°C for 4 hours, after heating at 550°C, also for 4 hours. The

whole rock powder samples were scanned at a rate of 15 seconds per 0.15° step width with a 5° slit, from 5 to 65°2' .

The data were quantified using freeware Macdiff to deconvolute and measure the peak areas. The clay minerals were identified on XRD traces on the basis of the positions of their basal lattice reflections. The reflections used for quantification are ideally free from interference from other mineral reflections. Illite is identified from and measured using the reflection at 10Å (~9°2'), kaolinite with the reflection at 3.57 Å (~24°8'), chlorite with the reflection at 3.54 Å (25°2'). Illite-smectite is identified as the broad reflection(s) on the low angle side of the illite 10 Å reflection.

Table 4.2 shows the results of three different samples tested of the BRS-B. The results appear to be statistically similar and therefore the homogeneity of the whole block in terms of mineralogy was confirmed. As expected from the microscope photos, the clastic fraction (silt and sand) of the BRS-B is mostly quartzitic in nature. The mineralogy of the clay fraction is mainly illite and smectite. Moreover, illite and smectite often occur as part of an interlayer system as shown in Figure 4.10. So although chemically both illite and smectite are present in the BRS-B, they form a single interlayered particle. The exact amounts of illite and smectite are therefore difficult to identify exactly and so often they are divided into three types, illite alone and illite-smectite interlayered particles which can be either illite rich or smectite rich.

Sample	illite & mica	illite-smectite smectite-rich	kaolinite	chlorite	quartz	K feldspar	plagioclase	calcite
1	18 %	18 %	5 %	7 %	40 %	2 %	4 %	6 %
2	16 %	17 %	4 %	7 %	44 %	2 %	5 %	5 %
3	18 %	15 %	5 %	3 %	47 %	2 %	4 %	6 %

(a)

Sample	illite	illite-smectite Smectite-rich	chlorite	kaolinite	illite in illite-smectite
1	19 %	77 %	1 %	2 %	50 %
2	15 %	82 %	2 %	2 %	50 %
3	1 %	95 %	1 %	2 %	45 %

(b)

Table 4.2 X-ray diffraction results from (a) whole sample (b) soil fraction < 4µm.

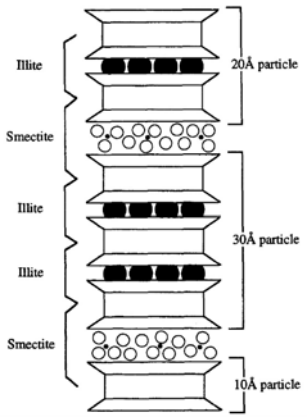

Figure 4.10 Interlayer particle of illite and smectite (Altaner & Ylagan, 1997)

• Specific gravity Gs

The specific gravity of the particles (G_s) was measured on samples from different locations in the block and on specimens from the excavated material. The measured values are shown is Table 4.3. An average value of 2.735 will be used for the analysis of the oedometer and triaxial tests.

Sample	Gs (20°C)
BRS-B-OI4	2.736
BRS-B-TI1	2.735
BRS-B-TI7	2.733
BRS-E	2.739

Table 4.3 Specific gravity values of the BRS-B and BRS-E. Oedometer (O) and triaxial (T) samples.

• Atterberg limits and activity

In this research project, the liquid limit was determined by means of the Casagrande spoon method. The results of the liquid and plastic limit tests are summarised in Table 4.4. The activity of the samples was also estimated and the results are also included in Table 4.4. Figure 4.11 shows the Casagrade plasticity chart with the points associated with the samples in Table 4.4.

Sample	w_l (%)	w_p (%)	I_p (%)	w_n (%)	I_L	Activity (A)
BRS-B-OI1	35.8	25	10.8	19.7	-0.49	0.5
BRS-B-OI4	36.2	24.8	11.4	20.8	-0.35	0.52
BRS-B-TI1	35	25.3	9.7	18.3	-0.72	0.44
BRS-B-TI7	35	24.8	10.2	19.1	-0.55	0.46
BRS-B-TI9	34.2	24.8	9.4	17.2	-0.81	0.42
BRS-E	25.3	21.1	4.2	-	-	0.33

Table 4.4 Atterberg limits and estimated activity of some oedometer (O) and triaxial (T) samples of the BRS.

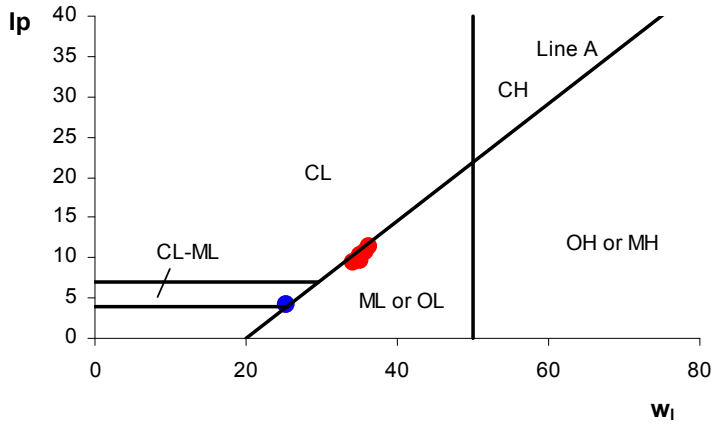

Figure 4.11 Casagrande plasticity chart for samples of the BRS in Table 4.4

According to the Casagrande plasticity chart, the BRS-B can be classified as a medium plasticity inorganic silt (ML) whereas the BRS-E is on the borderline of the zone corresponding to materials represented by a double symbol (CL-ML). The medium to low plasticity values of the BRS could be explained in part by the quartzitic nature of the silt fraction which reduces the plasticity of the soil. The BRS can be also classified as inactive based on the estimated activity values (Skempton, 1948).

• Natural water content

The range of the natural water contents measured on the BRS-B specimens varied from 17 to 21%. Table 4.4 shows the results of some of the samples tested in the triaxial and in the oedometer. In all cases, the natural water content was below the

plastic limit and therefore the liquidity index (I_L) was negative associated with a semi-solid state of the samples. Taking into account that the block sample was taken at a depth of 1.4m, the negative values of the I_L could be associated with a desiccation process.

These values of the natural water content, together with the measured void ratio for all intact samples tested gave a degree of saturation (Sr) that varied from 62 to 80%, with an average of 71%. A few suction measurements were also carried out on two points of the block sample, using the suction probe technique (Ridley & Burland, 1999). The value measured was around 90kPa.

• Organic matter content

Visual inspection of the BRS-B samples showed that organic matter could be found in the form of small roots plant as shown in Figure 4.12. Consequently it was decided to measure the organic content of the samples. The tests were carried out following the Spanish standard UNE 103.204-93. Table 4.5 shows the results obtained. According to some studies (Booth & Dahl, 1986), a minimum quantity of organic matter around 3-4% is necessary to cause a change in soil behaviour. Although there is a bit of dispersion in the results, an average of 1.1% was measured. In any case, the organic matter content is lower than 3% and its effects on the mechanical behaviour of the BRS-B are likely to be insignificant.

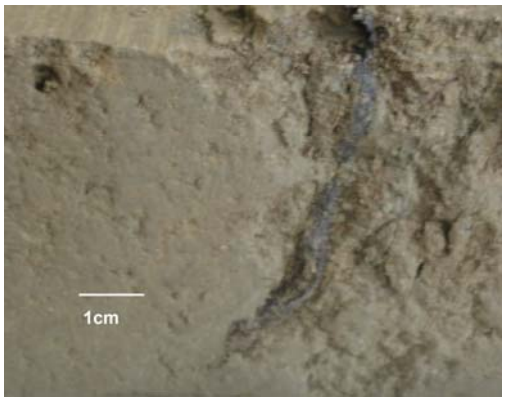

Figure 4.12 Plant root in a sample of the BRS-B

• Carbonate content

A few tests were performed on samples of the BRS-B and BRS-E to determine the carbonate content. The Bernard Calcimeter procedure was followed as specified in the Spanish standard UNE 103.200-93. Average values of 10.4% and 12% of calcium carbonate ($CaCO_3$) were measured for the BRS-B and BRS-E material

respectively. In the case of the BRS-B, the measured value nearly doubles that obtained in the X-ray diffraction analysis where an average of 5.7% was obtained. This difference between the two methods is common considering their different approaches followed to measure the carbonate content. Moreover in the X-ray diffraction analysis there is an estimated error of ±10% in the readings. In any case, the carbonate content of the BRS-B is significant and could be an index parameter to explain any possible cementation in the intact samples.

Sample	OM (%)
BRS-B-OI4	0.78
BRS-B-TI1	1.39
BRS-B-TI7	1.18

Table 4.5 Organic matter content measured for one oedometer (O) and two triaxial (T) samples of the BRS-B.

4.2.2 Summary of the index properties of the Bormida River silts

Based on the results showed in the previous paragraphs, the BRS soils tested in this research project can be classified as follows:

- BRS-B (material from the block sample)

  This soil consist of an inorganic low plasticity clayey silt

  - 22% clay-sized
  - 60% silt
  - 18% fine to medium sand
  - Average w_l= 35.2%
  - Average I_p=10.3%
  - Average liquidity index I_L=-0.6
  - Average A=0.47
  - Average $CaCO_3$=10.4%
  - Unified soil classification system: ML

- BRS-E (excavated material)

  In this case, the soil consist of an inorganic low plasticity sandy silt

  - 13% clay-sized
  - 50% silt

- 37% fine to medium sand
- Average w_l=25.3%
- Average I_p=4.2%
- Activity A=0.33
- Average $CaCO_3$=12%
- Unified soil classification system: CL-ML

For both soils, the bulk particles are mainly composed of quartz with a sub-angular to sub-rounded shape. The mineralogy of the clay fraction was only analysed on samples of the BRS-B. The main clay minerals are illite (mica) with interlayer system of illite-smectite that can be either illite rich or smectite rich. Unfortunately no data are available for the mineralogy of BRS-E but it could be assumed that will be the same as the BRS-B. Finally it could be concluded that the main difference in the index properties between the BRS-B and the BRS-E is the grain size distribution.

4.3 Previous investigations of the mechanical behaviour of the BRS

This section is intended to be a more detailed literature review for the BRS, in particular its possible transitional behaviour, compared to the more general literature review presented in Chapter 2. Unfortunately there is very little information about the mechanical behaviour of the BRS. On the other hand, and as was mentioned in previous paragraphs, the Bormida River is a tributary of the Tanaro River which is the most significant right-side tributary to the Po River (Figure 4.2). Some of the silty soils from the Po River have similar mineralogy and grading to the BRS. Many researchers have carried out investigations on its mechanical response and some of them have focused their research in looking for transitional behavior. For this reason, it was decided to include the silty soils from the Po River in this literature review.

4.3.1 Previous investigations on the BRS

In his MSc thesis Radici (2006) carried out a series of oedometer tests looking for transitional behaviour on samples of the BRS-B and BRS-E. He concluded that the intact samples of the BRS-B showed transitional behaviour during one-dimensional compression due to the lack of convergence of the compression curves towards a unique NCL. From the point of view of the author of this research, it is not clear that the BRS-B shows transitional behaviour. In fact the compression curves tend to converge into a unique NCL as can be observed in Figure 4.13. On the other hand, Radici found that the sample preparation method had an effect on the one-

dimensional compression behaviour of the more silty BRS-E samples. He concluded that the slurry samples showed transitional behaviour whereas the wet and air-dried compacted samples did not show transitional behaviour as shown in Figure 2.62. As was presented in Section 2.4.3, this result contradicts the conclusion of previous researchers who pointed out that the sample preparation method has no effect in triggering transitional behaviour. In this research project this conclusion will be checked and investigated in more detail.

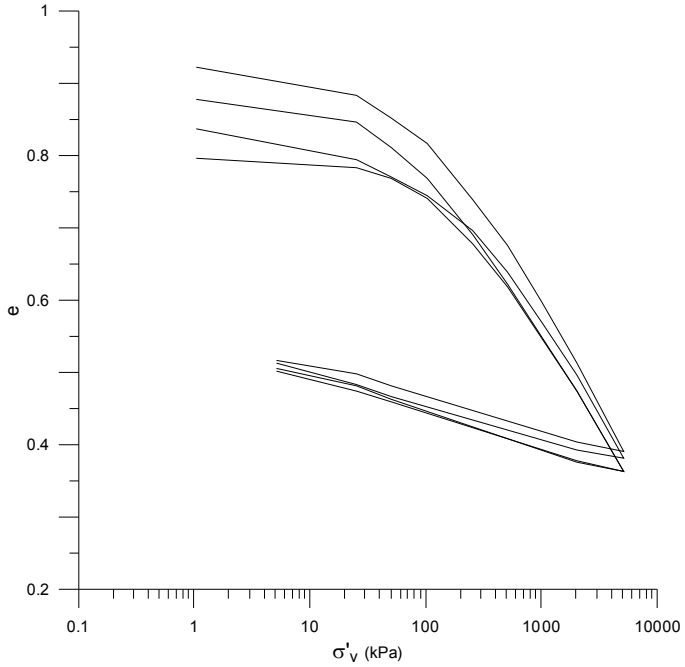

Figure 4.13 One-dimensional compression curves of intact samples of the BRS-B (redrawn from Radici, 2006)

4.3.2 Previous investigations of the mechanical behaviour of the silty soils from the Po River

The silty soils from the Po River flood plain have been traditionally used as a material for constructing the embankments of the river and also as a foundation level. Many researchers and institutions (e.g. Colombo, 1965; Colleselli, 1980; Sciotti & Jommi, 2003; Jommi & Sciotti, 2004; De'Angelis & Molteni, 2004; AIPO, 2004; Nocilla et al., 2006) have carried out studies to characterise the mechanical behaviour of these materials, often in order to provide specifications for the construction and maintenance of the embankments. Table 4.6 shows a summary of the selected references on the Po River materials that will be reviewed together with a description of the type of sample and the location where they were

retrieved. It is important to note that all the samples come from the same location with the exception of the soil tested by Collesselli et al. (1980).

Reference	Sample location	Sample type
Colleselli et al., 1980	Sermide and Carbonara Po municipalities, Lombardy region	In-situ (undisturbed) and laboratory compacted
Sciotti & Jommi, 2003	Viadana, Lombardy region	In-situ (undisturbed) and laboratory compacted
Jommi & Sciotti, 2004	Viadana, Lombardy region	In-situ (undisturbed) and laboratory compacted
De'Angelis & Molteni, 2004	Viadana, Lombardy region	Intact
AIPO: Final report, 2004	Viadana, Lombardy region	Intact
Nocilla et al., 2006	Viadana, Lombardy region	Slurries and laboratory compacted
Nocilla & Coop, 2008	Viadana, Lombardy region	Intact (AIPO samples)

Table 4.6. Summary of the selected references on the Po River materials.

Figure 4.14 shows the particle size distribution range of the materials commonly used in the construction of the Po River embankments (Colombo, 1965). The range varies from fine sandy silts to clayey silts. Nocilla et al. (2006) carried out a series of X-ray diffraction analysis on powder samples of a clayey silt with 25% of clay. The results showed that the soil is composed of quartz, calcite, illite (mica), kaolinite, feldspar, smectite and chlorite. Another analysis was done on the soil fraction passing the 63μm sieve and the result was very similar to the one carried out on the sample as a whole. Nocilla et al. concluded that the similarity of the results indicates that much of the silt-sized particles must be clastic in nature. As pointed out in Table 4.6, practically all the samples analysed in this literature review were retrieved from the same location. Consequently, it could be assumed that the mineralogy of all samples will be very similar and therefore will not impose any important restriction when comparing results from different authors. Moreover, Figure 4.15 shows the comparison between the X-ray diffraction pattern of the clayey silt tested by Nocilla et al. (2006) and the BRS-B. It could be seen that the measured peaks occurred at the same specific angles with little variation in their intensity. These results confirm that the soils included in this literature review are quite similar in their mineralogical components to the BRS.

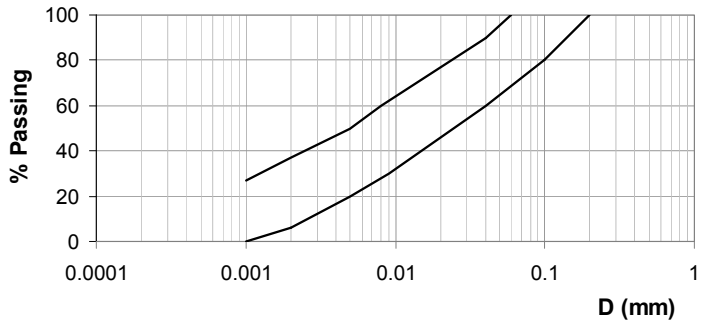

Figure 4.14 Particle size distributions range of the materials commonly used in the construction of the Po River embankments (redrawn from Colombo, 1965)

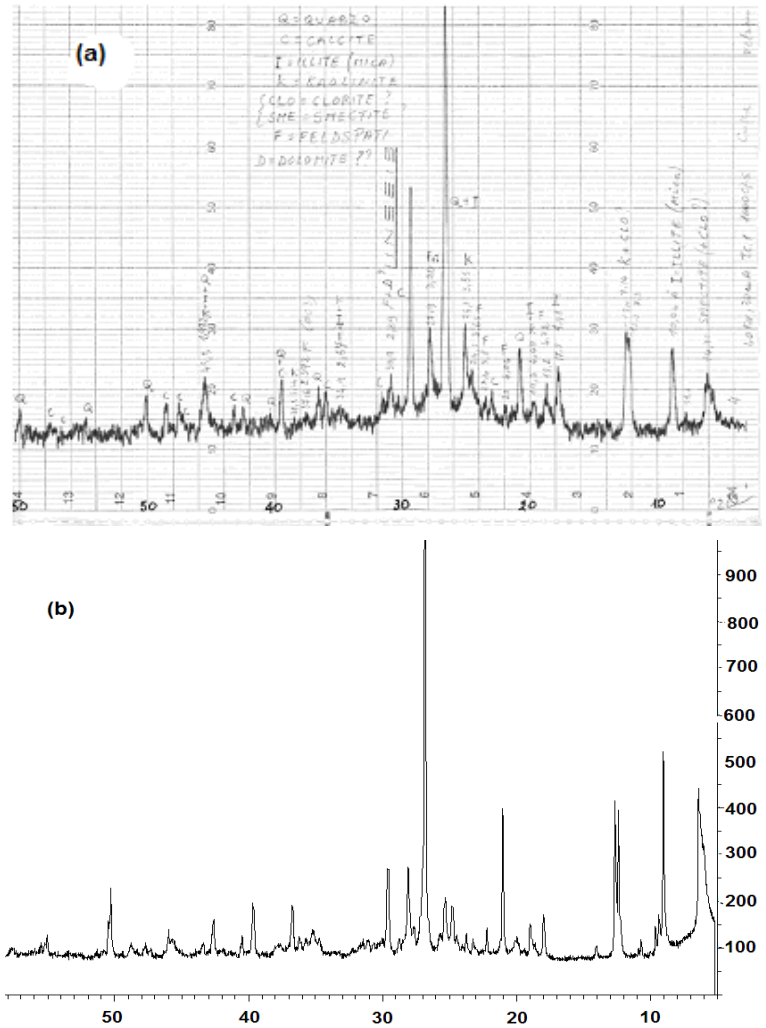

Figure 4.15 X-ray diffraction patterns comparison of a powder sample of (a) clayey silt with 25% of clay (Nocilla et al., 2006) and (b) BRS-B. Axis x is in lin (counts) and y is 2θ

Colleselli et al. (1980) investigated the mechanical behaviour of the silty soils used to construct two embankments of the Sermide Thermal Power Plant located on the right side of the Po River, in the area of Sermide and Carbonara Po municipalities, Lombardy region. The material tested belongs to the range of gradings shown in Figure 4.14 with an average of 15% of sand and 85% of fines (silt and clay). The liquid limit varied from 40 to 44%, with a plasticity index of 20 to 23%. Laboratory compaction tests carried out at the standard Proctor energy showed an optimum water content (w_{opt}) and a maximum dry density (ρ_d) of 18% and 1.73g/cm^3 respectively. The main objective of their investigation was to compare the soil response of "intact" samples compacted in-situ with samples of the same material compacted in the laboratory at the standard Proctor energy. They also looked at the effect of swelling on the compression behaviour of the laboratory compacted samples. In doing so, some of the laboratory samples were compacted at the standard Proctor energy and were allowed to swell freely before starting the loading stages. Four types of samples were tested: (a) intact samples compacted in-situ and retrieved 250 days after the compaction works were finished (non derangés, prelevés après 250 jours), (b) laboratory compacted samples at the standard Proctor energy (compactés á l'énergie standard), (c) laboratory compacted samples at the standard Proctor energy using the same wet material mixed in-situ (compactés humides á l'énergie standard) and (d) laboratory compacted samples at the standard Proctor energy with free swelling (compactés á l'énergie standard, regonflés).

Figure 4.16 shows the results of a series of free swelling tests on the laboratory compacted samples at the standard Proctor energy. It is important to notice that a volume change of 7.5% was measured when the samples were compacted at the optimum water content. This could produce an important change in the initial structure of the samples with its possible effect on the mechanical behaviour. Moreover, for the samples compacted on the wet side of the optimum water content, say w_{opt}+3%, the volume change remained more or less constant at around 2.5% and a less dramatic structure change would be expected.

Figure 4.17 shows the oedometer compression curves of in-situ and laboratory compacted samples. Some of the samples were compacted at the standard Proctor energy at different water contents and allowed to swell before starting the compression test. The volume change measured at the end of the swelling is shown in Figure 4.16. From Figure 4.17, it can be observed that at low stress levels the compressibility of the compacted samples without swelling, either in-situ or in the laboratory, is lower than the compressibility of the samples where free swelling was allowed. Moreover, it can be seen that whereas the compression curves for the compacted samples without swelling tend to converge towards a unique NCL, the compression curves for the samples that were allowed to swell run parallel to one

another showing a sort of transitional behaviour. Consequently, it seems to be that the initial structure created in the samples after swelling is more robust than in the other samples and it could not be easily removed during compression therefore showing no clear convergence towards a unique NCL within the range of stress levels reached. It is worth pointing out that Colleselli et al. did not mention the accuracy on the calculation of the initial void ratio and therefore the apparent non-convergence of the compression curves could be associated to a poor accuracy of the determination of the initial value of e. In any case, what is clear from Figure 4.17 is that the compression behaviour of the compacted samples with swelling is different to the others and this must be associated with a different initial structure. Moreover, although the initial structures of the in-situ and laboratory compacted samples are expected to be different, they show a very similar compression behaviour.

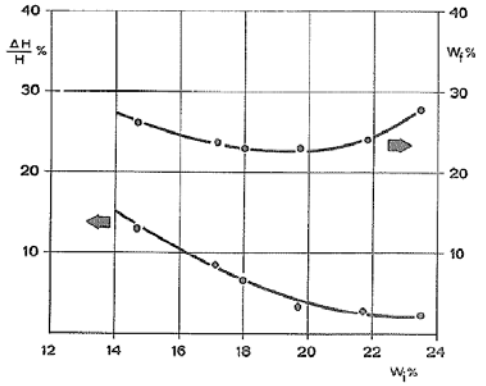

Figure 4.16 Free swelling tests results of the laboratory compacted silty samples at the standard Proctor energy (Colleselli et al., 1980)

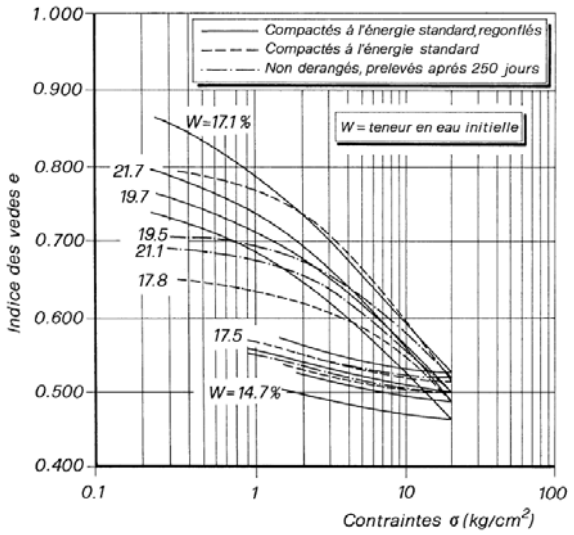

Figure 4.17 Oedometer compression curves for in-situ and laboratory compacted silty samples from the Po River (Colleselli et al., 1980)

Colleselli et al. (1980) also carried out a series of isotropic consolidated undrained triaxial tests (CIU) on in-situ and laboratory compacted samples (Figure 4.18). In this case, the laboratory compacted samples were prepared by two different procedures. The samples that are identified in Figure 4.18 as "compactés humides á l'énergie standard" were compacted in the laboratory at the standard Proctor energy but using the in-situ wet mixed material. On the other hand, the samples identified as "compactés á l'énergie standard" were compacted also in the laboratory but using an oven-dried material and then mixed with the required water content. All the samples were saturated before consolidation was started by applying a back-pressure. Figure 4.18 shows the stress-strain behaviour during undrained shearing. Colleselli et al. concluded that, for the same initial dry density and cell pressure, the undrained strength of the in-situ material is lower but with a higher initial stiffness compared to the laboratory samples.

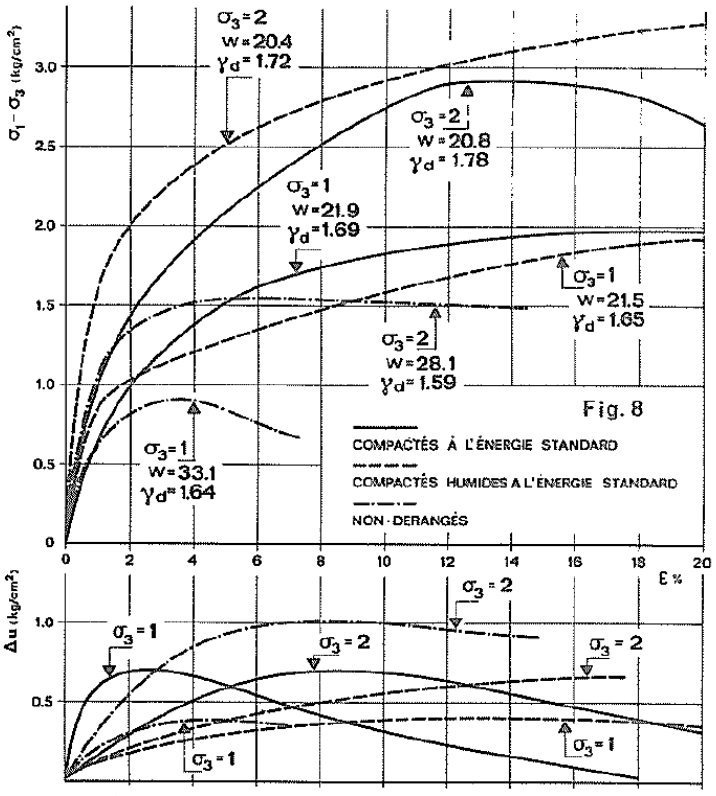

Figure 4.18 CIU triaxial tests on in-situ and laboratory compacted silty samples from the Po River (Colleselli et al., 1980)

They also showed that the critical shear strength angle is the same (28 -30º) regardless of the sample preparation technique. One of the most important features to comment about is the different soil response observed when the two laboratory

compacted samples are compared during shearing. In terms of stress-strain behaviour, and for the same initial dry density and cell pressure, the "compactés á l'énergie standard" samples show a less stiff response at small strains together with a larger increment of the pore water pressure associated with a more contractive behaviour. At larger strains, the initial contractive behaviour changes into a dilatant one where the initial increment of pore water pressure decreases. On the other hand, the "compactés humides á l'énergie standard" samples do not show any dilatant behaviour and the increment of the pore water pressure continuously increases until reaching an apparent critical state. These differences found in the soil response show that the initial structure created in the samples must be different even though all the laboratory samples were compacted at the standard Proctor energy with the difference that in one case the material was oven-dried and the other one was mixed in-situ with water. Unfortunately there was no information about the isotropic compression behaviour to check the uniqueness of the NCL and CSL.

Certainly, and as seen above, the sample preparation method has a great effect on the initial structure of the sample and therefore on the soil behaviour. In this context Jommi & Sciotti (2004) carried out an investigation to asses the reliability of laboratory compacted soils as a reference material for predicting the hydro-mechanical behaviour of the same material compacted in-situ at the same density and water content. Their investigation focused on the study and comparison of the structure created in samples compacted in the laboratory and in-situ, using the scanning electron microscopy (SEM) and mercury intrusion porosimetry (MIP) techniques. Undisturbed samples of a well-graded clayey silt (3% sand, 70% silt and 27% clay) were retrieved from an embankment of the Po River at Viadana seven months after its construction. The liquid limit and plasticity index of the samples were 55% and 27% respectively. Laboratory samples compacted at half of the standard Proctor energy were also prepared for the comparison with those of the undisturbed. Jommi & Sciotti concluded that the undisturbed (in-situ compacted) samples showed more structure levels than the laboratory compacted samples and that their structure was more similar to the original material from the borrow pit used to construct the embankments. On the other hand, they also pointed out that the original structure of the material was more easily erased if the standard procedure for preparing laboratory compacted samples was followed. From the differences observed in the structure of both samples, they suggested that the expected hydro-mechanical response of the in-situ compacted material will be different from that of the laboratory compacted. Consequently, they concluded that the laboratory compacted samples might not represent a reliable reference material for the in-situ compacted earthworks.

Even though it is clear that the laboratory and in-situ compacted specimens showed a different initial structure, Sciotti & Jommi (2003) found a tendency of the compression curves towards a unique NCL regardless of the sample preparation method (Figure 4.19). Sciotti & Jommi also compare the compression behaviour of saturated and partially saturated samples. The saturation of the samples was carried out by flooding the oedometer cell with water once the vertical stress level reached 50kPa. As can be seen in Figure 4.19 the volume change (collapse) due to the saturation is negligible and the compression curves converge towards a unique line regardless of the initial degree of saturation of the sample. On the other hand the initial compressibility is lower for the partially saturated sample, probably due to the effect of the suction in the sample.

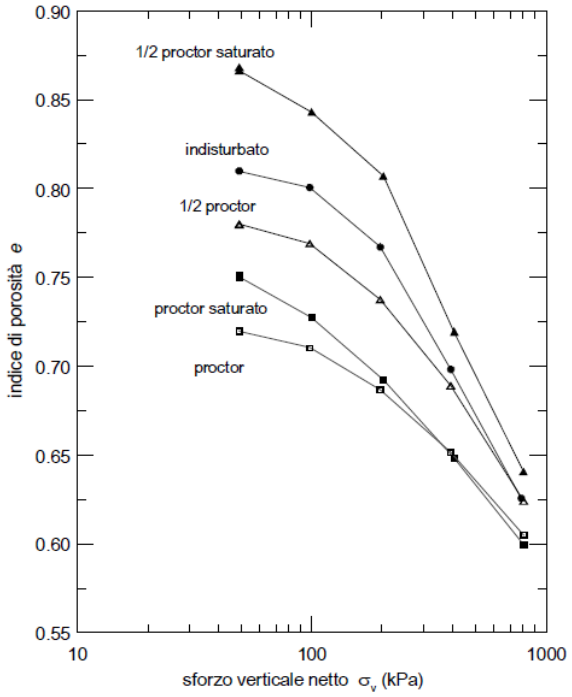

Figure 4.19 Oedometer compression behaviour of a silty soil from the Po River embankments at Viadana (Sciotti and Jommi, 2003)

De'Angelis & Molteni (2004) examined the compression behaviour of partially undisturbed samples of a clayey-sandy silt (20% clay, 60% silt and 20% sand) from a borrow pit adjacent to the Po River at Viadana (Figure 4.20). The mineralogy of this material is the same as that tested by Sciotti & Jommi (2003), with a higher content of sand. Initially, the samples were partially saturated showing different degrees of saturation. The oedometer cell was flooded with water at different vertical stress levels as can be seen in Figure 4.20. At 50kPa, the measured volume

change (collapse) of the samples when the cell was flooded was negligible and around 0.2% at 400kPa, regardless of the initial degree of saturation of the sample. From Figure 4.20, it can be observed that the compression curves run parallel to one another showing no sign of convergence towards a unique NCL in the range of stresses applied, with the exception of sample CGN1 which had the lower initial degree of saturation Sr=65.2%. This sample was expected to had a higher initial suction comparing to CGN1b and therefore its compressibility would be lower as observed in Figure 4.20. What is not clear is why the compression curves do not converge after soaking the samples. Figure 4.21 shows the comparison of the compression curves of these samples with those tested by Sciotti & Jommi (2003). As can be seen, for the same range of stresses applied, a clear tendency towards a unique NCL can be found for the latter specimens contrary to the parallelism showed by the former. The differences found in the compression behaviour between these soils might be explained by the higher content of sand in the material tested by De'Angelis & Molteni that delay or erase the possibility of convergence towards a unique NCL in the range of stress applied. It could be argued that this behaviour is similar to that of sands where the initial density controls the compression response at lower stress levels before particle breakage takes place or alternatively it could be that this material shows a transitional behaviour. Unfortunately, neither of these hypotheses can be confirmed due to the low level of stresses reached during the tests.

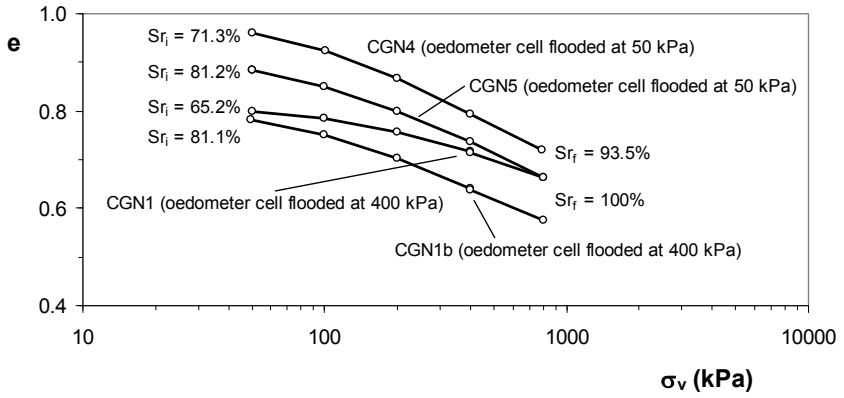

Figure 4.20 Oedometer compression curves for intact samples of a clayey/sandy silt from the Po River at Viadana (redrawn from De'Angelis & Molteni, 2004)

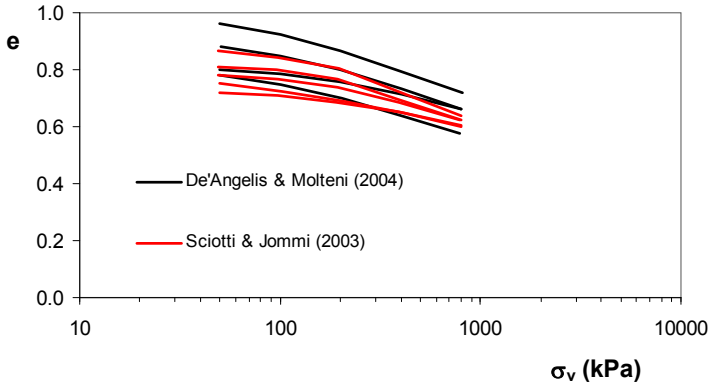

Figure 4.21 Comparison of the oedometer compression behaviour of the silty soils from the Po River at Viadana

The organization of the Magistrato per il Po (AIPO), in collaboration with the Universities of Brescia, Napoli, Parma and Roma, carried out a research programme to study the hydro-mechanical behaviour of an experimental embankment that was constructed inside the Po River channel at Viadana, Lombardia region (Figure 4.22). The material used for the construction of the embankment was obtained from the layer (T2) which consists of soils with a range of gradings showed in Figure 4.23.

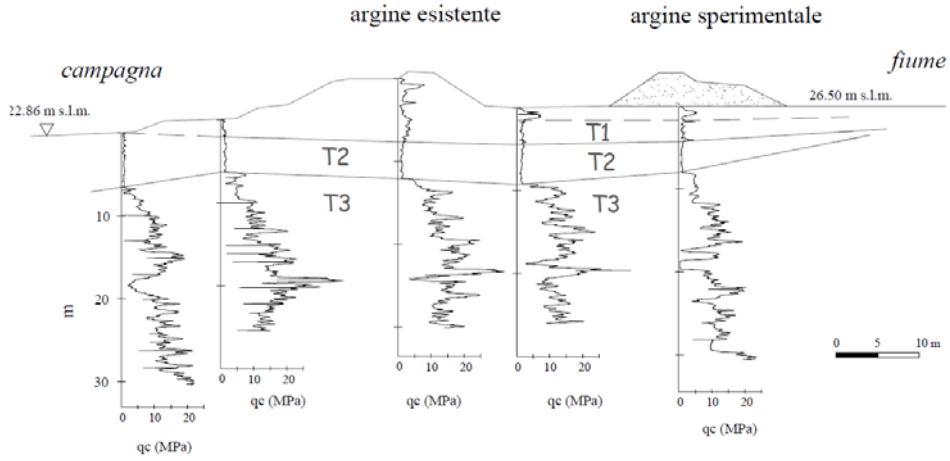

Figure 4.22 Soil profile and location of the experimental embankment constructed inside the Po River channel at Viadana, Lombardia region (AIPO, 2004)

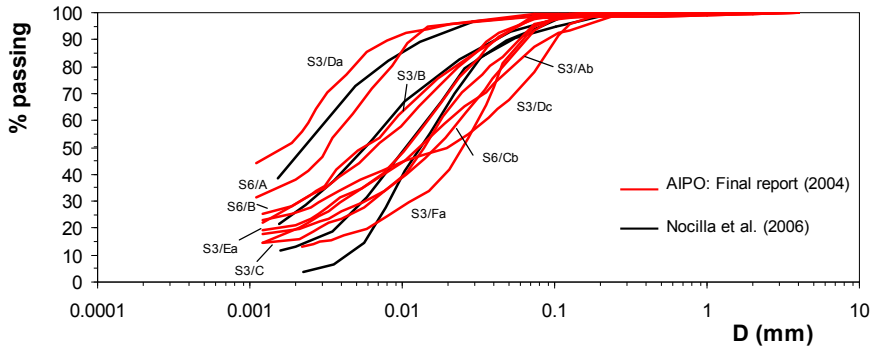

Figure 4.23 Particle size distributions of layer T2 (data from AIPO, 2004 and Nocilla et al., 2006)

Nocilla et al. (2006) carried out research to characterize the mechanical behaviour of the silty soils used for the construction of the experimental embankment mentioned above. The investigation was focused on the effect of the soil grading on the compression and shear behaviour of the material. In doing so, a bulk disturbed sample was retrieved from the dredged material of the estuary. A relatively poor-quality Shelby sample was also obtained from the compacted embankment. This sample will be referred in this review as "Nocilla natural sample" which has a 25% clay content. The bulk sample was used to create artificially four different gradings; 45%, 25%, 8% and 3.5% clay content (Figures 4.23 and 2.53). The compression and shear behaviour for each grading is shown in Figures 2.54 to 2.56. As described in Section 2.4.2, the convergence of the compression curves towards a unique NCL is less clear when the clay content reduces. A clear transitional behaviour was found for clay contents of 8% and 3.5% where there was a different NCL for each initial void ratio. The same conclusion was found for the shearing behaviour, where a non-unique CSL could be found for the 8% and 3.5% clay contents.

Figure 4.24 shows the stress paths during shearing. Nocilla et al. pointed out that although there was insufficient data to identify the critical state line slope (M) with enough accuracy, a value of M=1.3 seemed to agree with the end of the tests for the 45%, 25% and 8% clay contents. As they also noted, this conclusion contradicts the results of the stress-dilatancy plot (Figure 4.25) where only the test on the 8% clay content gave the same M value. Figure 4.26 shows the normalised shearing stress paths for the undrained and drained tests. Normalisation was done using the equivalent pressure on the isotropic NCL. As mentioned above, for the case of 8% clay content there was a different NCL for each initial void ratio and therefore the normalisation was made using each individual NCL. From Figure 4.26 it can be observed that the normalised undrained and drained stress paths were different and therefore Rendulic's principle does not apply.

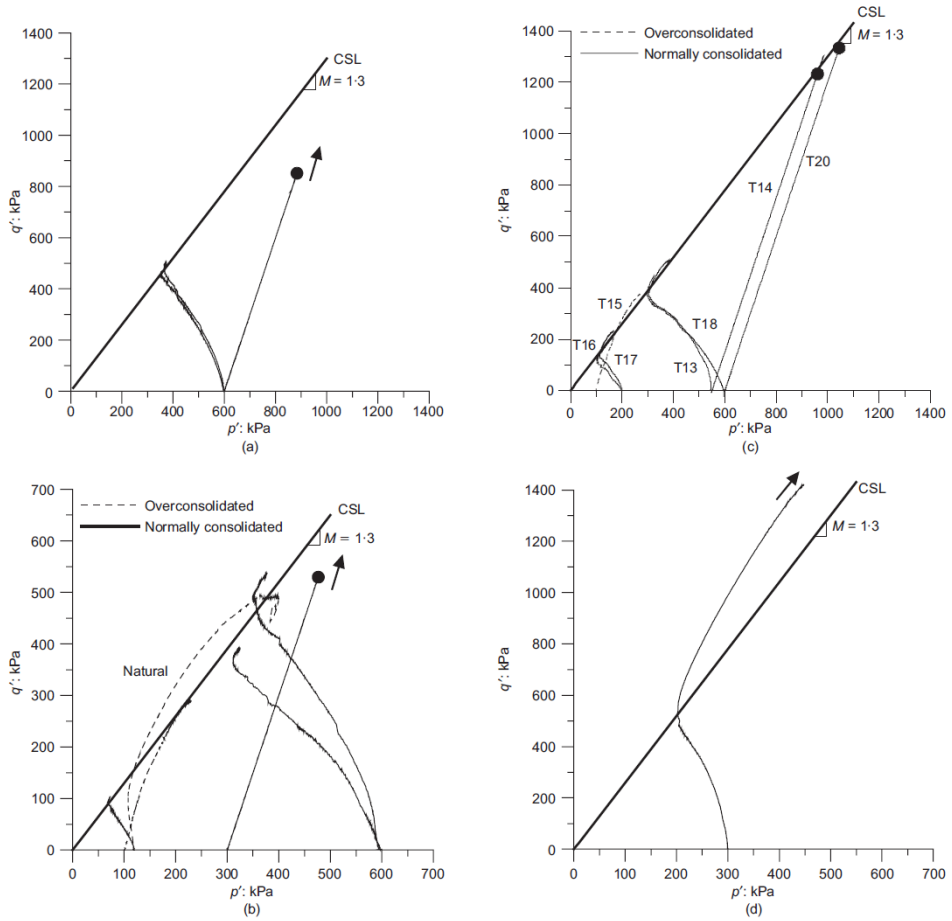

Figure 4.24 Stress paths of a silty soil with a clay content of: (a) 45% (b) 25% (c) 8% and (d) 3.5% (Nocilla et al., 2006)

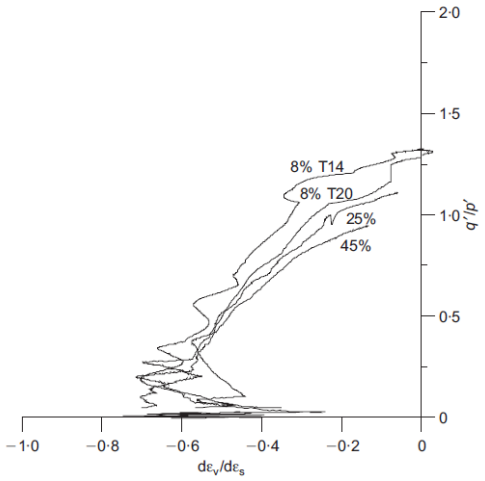

Figure 4.25 Stress-dilatancy plot for drained triaxial tests of a silty soil with diffrent clay contents (Nocilla et al., 2006)

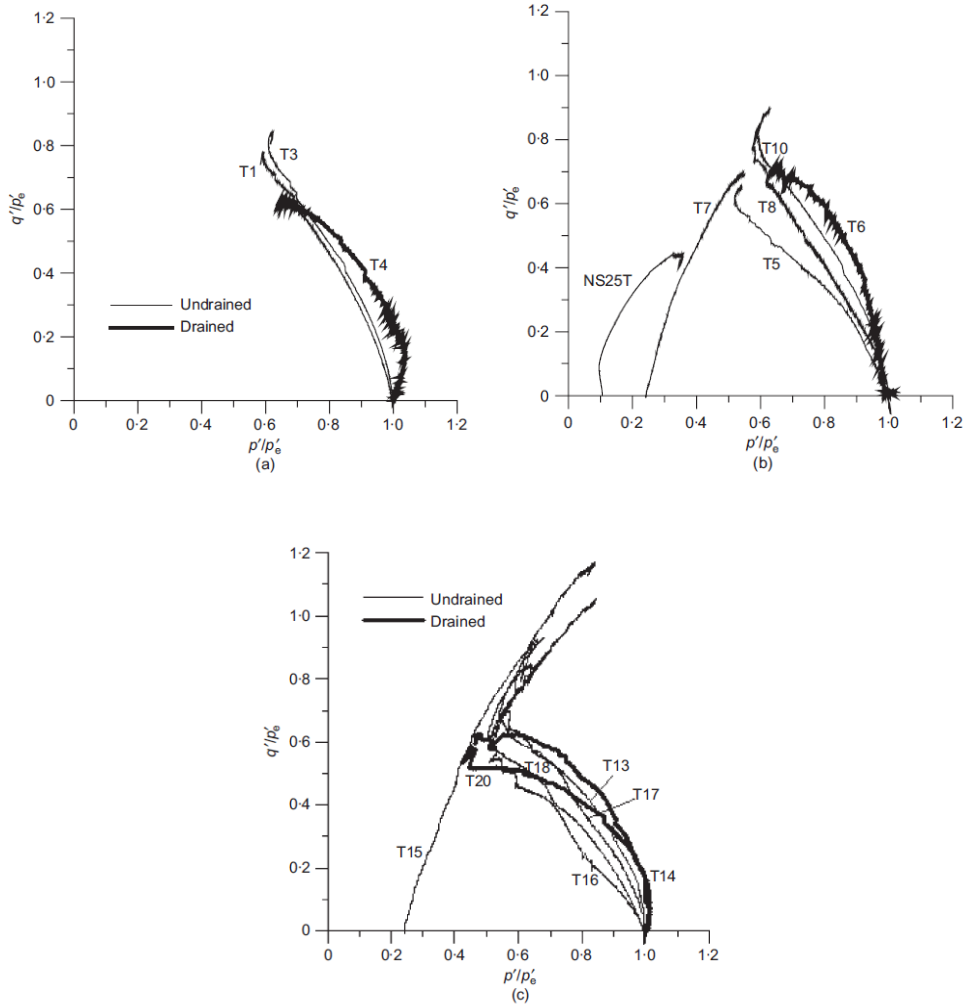

Figure 4.26 Normalised stress paths for drained and undrained triaxial tests on a silty soil with a clay content of: (a) 45% (b) 25% and(c) 8% (Nocilla et al., 2006)

On the other hand, Nocilla et al. (2006) concluded that the transitional behaviour observed in compression for the 8% and 3.5% clay content was not affected by the sample preparation technique. A more detailed analysis of the effect of the sample preparation method was carried out in Section 2.4.3 by the author of this research project. The compression curves for 8% and 3.5% clay contents were redrawn grouping samples prepared by the same method (Figures 2.61 and 2.62). As was pointed out, only the slurry samples showed a transitional behaviour whereas the compression curves for the specimens prepared by wet or dry compaction converge towards a unique NCL. Consequently, it seems to be clear that the preparation method could have an effect on the initial structure that determines whether the

soil displays transitional behaviour or not. It is also important to mention that all the triaxial tests were carried out on slurry samples and as mentioned above the 8% and 3.5% clay contents soils also showed transitional behaviour in shearing. It would have been very interesting to compare the shearing behaviour of slurry and compacted samples to check if they follow the same trend as in compression where the sample preparation technique seems to play an important role in the transitional behaviour.

Nocilla & Coop (2008) analysed the results of a series of triaxial and oedometer tests on intact samples from layer (T2) that were presented in by AIPO, (2004) The main objective of their analysis was to check if transitional behaviour could also be found in intact samples as was observed by Nocilla et al. (2006) for reconstituted samples taken from the same site. In their analysis, Nocilla & Coop grouped the soils according to similar clay contents (Figure 4.27) as Nocilla et al. (2006) did. This grouping criterion was justified because the silt particles were assumed to be clastic in nature. Nocilla & Coop (2008) concluded that when the clay content reduces there is a clear evolution from a clay mode of behaviour, where a unique NCL and CSL can be found (Figure 4.27a), to a transitional mode, where a diffrent unique CSL/NCL can be obtained for each initial void ratio but which are parallel to one another (Figure 4.27c and d). In the case of 20-25.5% clay content they found a transitional behaviour in terms of the CSL but could not confirm the same behaviour in compression because both oedometer tests started at very similar initial void ratios. They also concluded that the different CSL location in the compression plane is not the result of the slight variation in clay content for each sample. For the 13-16% clay content, transitional behaviour was obtained in compression but again the triaxial tests were conducted on samples with very similar initial void ratios and they threrefore could not verify whether a unique CSL occurs or not.

Figure 4.28 shows the location of the CSL in the compression plane and the variation of the critical state line gradient (M) as a function of the clay content. Finally, Nocilla & Coop pointed out that although the tests were not specifically designed to investigate whether the T2 materials show a transitional behaviour or not, it has been possible to identify clear trends and for the first time transitional behaviour had been found in intact samples. This provisional finding has been part of the origin of the main research carried out in this research project, where a specifically designed test programme has been carried out to confirm the transitional behaviour on intact samples of the BRS-B soil which has a similar clay content and grading.

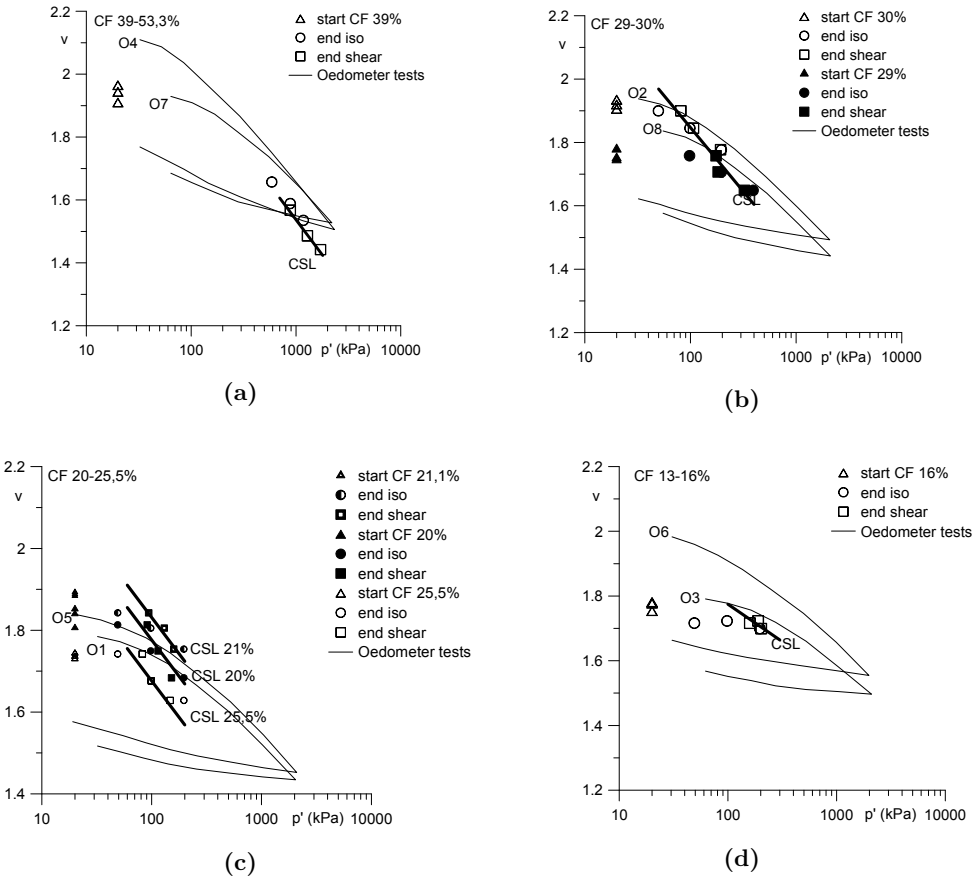

Figure 4.27 Triaxial and oedometer data for intact silty samples with clay contents of: (a) 39-53.3% (b) 29-30% (c) 20-25.5% and (d) 13-16% (Nocilla & Coop, 2008)

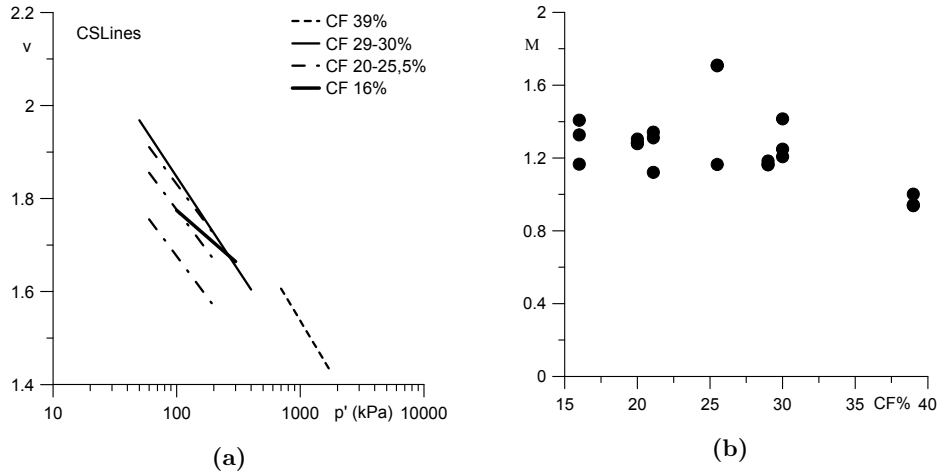

Figure 4.28 Influence of the clay content on: (a) the location of the CSL in the compression plane and (b) the M value for the intact silty samples (Nocilla & Coop, 2008)

As seen above, the grain size distribution has an important effect on the mechanical behaviour of the silty soils from the Po River as expected. Nocilla et al. (2006) and Nocilla & Coop (2008) grouped the soils according to similar clay contents to draw their conclusions. A different, and perhaps more traditional, way of grouping the soils is shown in Figure 4.29. In this case the soils have been grouped according to the same fines content (particles with size smaller than 63μm), in this case 95%. Figure 4.30 shows the compression behaviour of the intact samples tested by the AIPO together with a natural sample tested by Nocilla et al. (2006). It can be seen that, with the exception of sample O2-S3/B, a clear convergence towards a unique NCL can be found for these soils where the clay content varies from 21.1% to 30%. The plasticity index for these samples is very similar except for the natural sample tested by Nocilla et al. (2006) which is higher (Figure 4.30). It is important to recall that the materials tested by Nocilla et al. and AIPO were retrieved from the same place and all of them belong to the T2 layer.

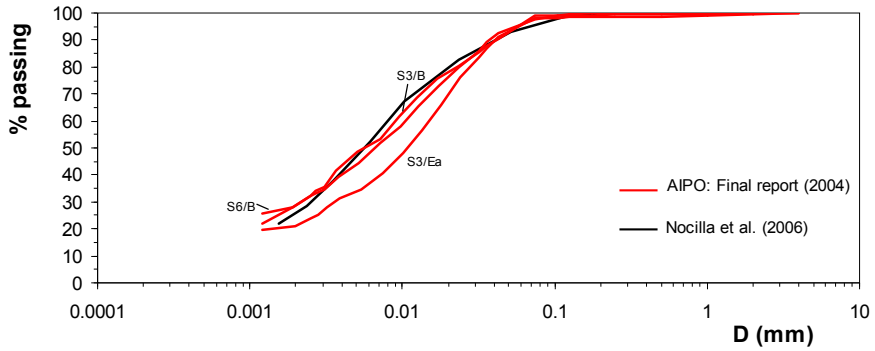

Figure 4.29 Particle size distributions of soils with same fine content (data from AIPO, Final Report, 2004 and Nocilla et al., 2006)

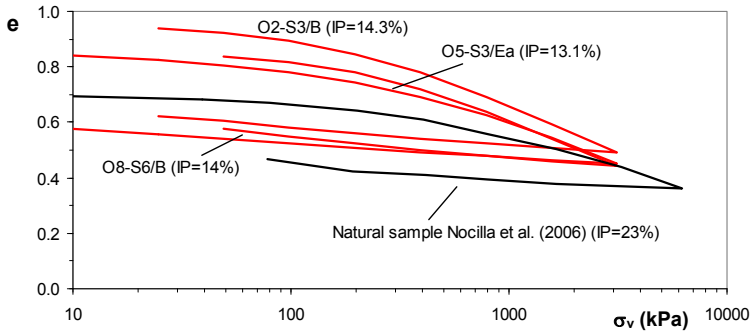

Figure 4.30 Comparison of the compression curves of the intact silty samples with the same fine content tested by Nocilla et al. (2006) and AIPO (2004)

Nocilla et al. (2006) showed that a unique NCL was identified for the reconstituted and remoulded samples of the 25 % clay content material (Figure 2.54). Moreover,

the 25% clay content samples have the same grading as the AIPO intact samples. Consequently, the unique NCL of the 25% clay content material has been used as a reference for comparing with the intact samples in order to quantify the in-situ structure of the soil (Figure 4.31). Although the quality of the intact samples was questioned because they were retrieved by using a piston sampler, it can be observed that the initial structure of the intact sample is easily erased and all of them converge towards to the intrinsic compression line defined by the slurry sample.

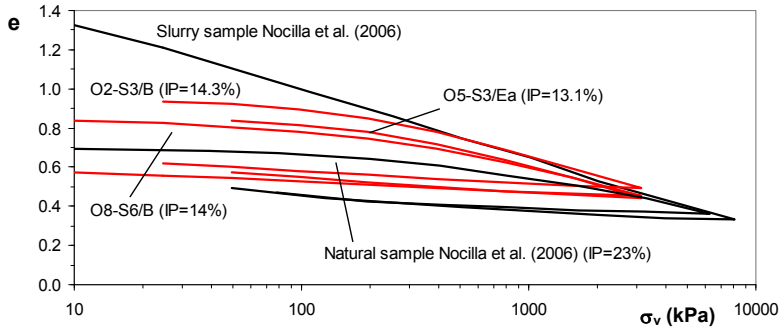

Figure 4.31 Comparison of the compression behaviour of the intact and slurry samples of the silty soils retrieved from Viadana. Quantification of the effect of the in-situ structure

As discussed above, Nocilla & Coop (2008) concluded that the samples with a clay content in the range of 20 to 25.5% showed a transitional behaviour in shearing. These were also expected to have transitional behaviour in compression but this could not be confirmed in their analysis. In this case a unique NCL can be identified for samples with a range of clay contents between 21.1% to 30% (Figure 4.31). This finding could open the possibility of having transitional behaviour in compression and not in shearing or both, in compression and shearing.

4.4. Summary of soils reviewed

In this literature review special attention was given to looking for transitional behaviour, although some of the references analysed were not specifically investigating it. In these cases, the conclusions derived from the review have to be made with caution due to uncertainties like the precision on the calculation of the initial void ratio of the samples, which could invalidate the results. Special interest has been paid to the effect of the sample preparation method on the transitional behaviour. Only the work carried out by Nocilla et al. (2006) and Radici (2006) was specifically designed to look for transitional behaviour. Table 4.7 shows a summary of the material properties and possible transitional behaviour of the soils analysed. The soils have been classified as transitional or not depending on the uniqueness of the NCL and/or CSL.

Reference	sand (%)	silt (%)	Clay (%)	w_l (%)	IP (%)	Type of sample	Transitional behaviour		Effect of sample preparation technique on transitional behaviour
							NCL	CSL	
Colleseli et al. (1980)	15		85		40-44	20-23	In-situ (undisturbed) and laboratory compacted	Yes	-	Yes. Only compacted samples that were allowed to swell freely before compression
Jomi & Sciotti (2004)	3	70		27	55	27	In-situ (undisturbed) and laboratory compacted	No	-	-
De'Angelis & Molteni (2004)	20	60		20	-	-	Intact samples	Yes	-	-
Nocilla et al. (2006)	0	55		45	61	30	Slurry, wet and dry compaction	No	No	No
	5	70		25	47	23		No	No	No
	5	87		8	37	13		Yes	Yes	Yes. Only slurry samples showed transitional behaviour
	5	91.5		3.5	33	10		Yes	Yes	
Radici (2006)	22	58		20	40	14	Intact – block sample	Yes?	-	-
	36	54		10	30	8	Slurry, wet and dry compaction	Yes	-	Yes
Nocilla & Coop (2008)	1-2	45-60		39-53	-	-	Intact samples taking using a piston sampler	No	No	-
	4	66-67		29-30	-	14.3		No	No	-
	4-28	46.5-74.5		20-25.5	-	13.1-20.4		?	Yes	-
	10	74-77		13-16	-	-		Yes	?	-

Table 4.7 Summary of the material properties and possible transitional behaviour of the soils analysed.

Chapter 5
Mechanical behaviour of the Bormida River Silts

5.1 Introduction

The Bormida River silts (BRS) constituted one of the main materials investigated in this research project. As presented in Chapter 4, the BRS studied consisted of a block sample of an inorganic low plasticity clayey silt (BRS-B) and a remoulded material made of an inorganic low plasticity sandy silt (BRS-E). The BRS soils have a similar grading and mineralogy compared with other silty materials that showed transitional behaviour. The aim of this part of the research was to give answers to the following questions: *(a) Is it possible to find a unique NCL for the BRS? (b) Is it possible to find a unique CSL for the BRS? (c) How does the sample preparation technique influence the mechanical behaviour of the BRS in terms of its possible transitional behaviour?* (d) *How does the in-situ structure influence the behaviour of the BRS-B?* In doing so, a specific experimental programme was defined based on a series of oedometer and triaxial tests carried out on intact, compacted and slurry samples.

5.2 Oedometric compression behaviour

The oedometer test has been traditionally used for measuring the compressibility properties of soils and for investigating the effect of the initial structure in their

compression behaviour under one-dimensional conditions. In addition, it is a very suitable test to identify the possible transitional behaviour of soils in terms of compression.

5.2.1 Calculation of the initial void ratio

The calculation of the initial void ratio of a sample is without any doubt the most important task when analysing the results of an oedometer test. Accurate initial values of e are essential when investigating the possible transitional behaviour of soils to ensure the correct location of the compression lines in the e:logσ'_v plane. In this research project Equations 5.1 to 5.4 were used for calculating the initial e value of a sample. Equations 5.2 and 5.3 were only applied for slurries, where the samples were assumed to be fully saturated at the start of the test. Equation 5.4 also implies that the soil was fully saturated during the whole test.

$$e_i = \frac{G_s \cdot \rho_w}{\rho_{di}} - 1 \qquad 5.1$$

$$e_i = G_s \cdot w_i \qquad 5.2$$

$$e_i = \frac{\rho_s - \rho_{bi}}{\rho_{bi} - \rho_w} \qquad 5.3$$

$$e_i = \frac{w_f \cdot G_s + \varepsilon_v}{1 - \varepsilon_v} \qquad 5.4$$

The initial void ratio calculated by Equations 5.1 to 5.4 depends on various measurements which include the specific gravity (G_s), the initial water content (w_i), the initial wet mass ($M_{wet,i}$), the initial height (h_i), the initial diameter (d_i), the final water content (w_f), the final dry mass (M_s) and the volumetric deformation (ε_v) measured during the whole test. The initial dry density (ρ_{di}) and the initial bulk density (ρ_{bi}) were calculated using the initial dimensions of the sample and the dry and wet mass of the soil.

Based on the experience obtained during this research project, it was found that the measurement of the initial height of the samples was a difficult task and an important source of error, especially for the slurry specimens. Therefore, it was extremely important to achieve a high level of accuracy when taking the measurements to reduce the error in the calculated e value. Frequently, when running an oedometer test, another important source of error is the measurements of the final water content of the sample due to the absorption of water from the porous stones when the oedometer cell is removed from the frame. In this investigation, special attention was taken when dismantling the cell at the end of

the test. The water in the cell was removed while the last load was still applied. Before removing the oedometer ring from the cell, all the water that surrounded the sample and porous stones was dried with tissue paper to minimise the error in measuring the final water content. Finally, and after discarding any anomalous values, the initial void ratio was calculated as an average of the remaining values obtained by using the above equations. The estimated maximum error in calculating the initial e values was then less than ±0.03. In general the larger errors were measured on slurry samples.

5.2.2 Compression behaviour of the Bormida clayey silt (BRS-B)

As described in Chapter 4, the material which forms the intact block sample of the Bormida clayey silt (BRS-B) consisted of a low plasticity inorganic clayey silt with sand, classified as ML. The grading distribution of all the samples tested was essentially the same as shown in Figure 4.4. The block was retrieved from the foundation level of the Bormida River embankment at a depth of 1.4m below ground level with and estimated in-situ vertical effective stress of σ'_v=75kPa. The average index properties were summarised in Section 4.2.2. In the following sections the results of the oedometer tests performed on slurry, compacted and intact samples are presented.

- **Slurry samples**

A series of oedometer tests were performed on slurry specimens prepared at different initial water content which varied from 1 to 1.7 times the average liquid limit, using the trimmings from the BRS-B block sample. The objective was to investigate the influence of the initial structure of the slurry samples on the uniqueness of the normal compression line. The procedure followed to create the samples was described in Section 3.7.1. Table 5.1 shows the details of the oedometer tests conducted.

Test	w_i (%)	I_L	$\sigma_{v(max)}$ (kPa)	Comments
BRS-B-OS1	38.4	1.3	8505	
BRS-B-OS2	61.8	3.6	8528	
BRS-B-OS4	40.4	1.5	8529	
BRS-B-OS5	49.6	2.4	8505	
BRS-B-OS7	36.3	1.1	12523	
BRS-B-OS8	39.4	1.4	12523	
BRS-B-OS9	39.4	1.4	12523	Sample prepared using the soil tested in BRS-B-OS7 and BRS-B-OS8
BRS-B-OS10	46.6	2.0	12523	

Table 5.1 Summary of the oedometer tests carried out on slurry samples of the Bormida clayey silt (BRS-B).

Figure 5.1 shows the one-dimensional compression behaviour of the slurry samples. Although it can be observed that there is some scatter in the compression lines, a tendency towards to a unique normal compression line can be seen, regardless of the initial water content and therefore the initial structure of the specimens. The scatter could be associated to the accuracy of measuring the initial void ratio of the samples. An estimation of the unique normal compression line was drawn in Figure 5.1. Following the definition given by Burland (1990), this unique line represents the one-dimensional intrinsic compression line (1D-ICL*) of the BRS-B, whose slope is C^*_c=0.25. During swelling, the behaviour was essentially the same in all the samples with an average swelling index of C^*_s=0.05 which gives a ratio of C^*_s/C^*_c=0.2. The asterisk denotes the intrinsic properties of the material which are inherent to the soil and independent of the initial structure. These intrinsic properties will be used as a reference for assessing the initial structure of the natural intact samples and also the remoulded compacted samples.

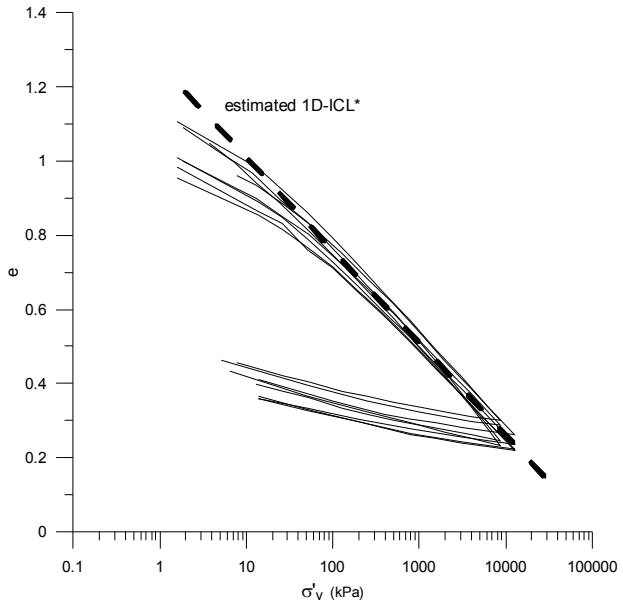

Figure 5.1 Oedometer compression of the slurry samples of the clayey silt (BRS-B)

Burland (1990) proposed Equation 5.5 to correlate the intrinsic compression index (C^*_c) with the void ratio at the liquid limit (e_{LL}), for soils above the A line on the plasticity chart. Although the plasticity characteristics of the BRS-B soil plotted slightly below the A line on the plasticity chart (Figure 4.11), Equation 5.5 was applied and a value of C^*_c=0.21 was obtained, which is slightly lower than that measured directly from the oedometer tests.

$$C^*_c = 0.25 \cdot e_{LL} - 0.04 \qquad 5.5$$

The linear relationship between e and σ'_v along the 1D-ICL* in a semi-logarithmic plane is given by Equation 5.6, where e_N is the extrapolated void ratio of a soil sample at σ'_v=1kPa and e is the void ratio for a given σ'_v stress level.

$$e = e_N - C^*_c \cdot \log_{10} \sigma'_v = 1.27 - 0.25 \cdot \log_{10} \sigma'_v \qquad 5.6$$

Figure 5.2 shows the compression curve of a test performed on sample BRS-B-OS4 where the specimen was unloaded from different preconsolidation stresses (σ'_p) in order to examine its behaviour during unload-reload cycles. It can be observed that the average slope of the unload-reload paths increased with the preconsolidation pressure as expected. Figure 5.2 also shows that the swelling lines were neither parallel nor linear, particularly for larger values of the overconsolidation ratio (OCR). This response is due to the fact that C^*_s depends on the stress level at which the unloading cycle starts and on the OCR. The average values measured for each unloading cycle from Figure 5.2 were C^*_{s1}=0.024, C^*_{s2} =0.037 and C^*_{s3}=0.049. On the other hand, it can be seen that when the soil was reloaded, it remembered the maximum vertical effective stress that was subjected to before the start of each unload-reload cycle so therefore the definition of yield stress (σ'_y) had the same meaning as the preconsolidation pressure. This is the expected behaviour for a material with a standard or reference structure.

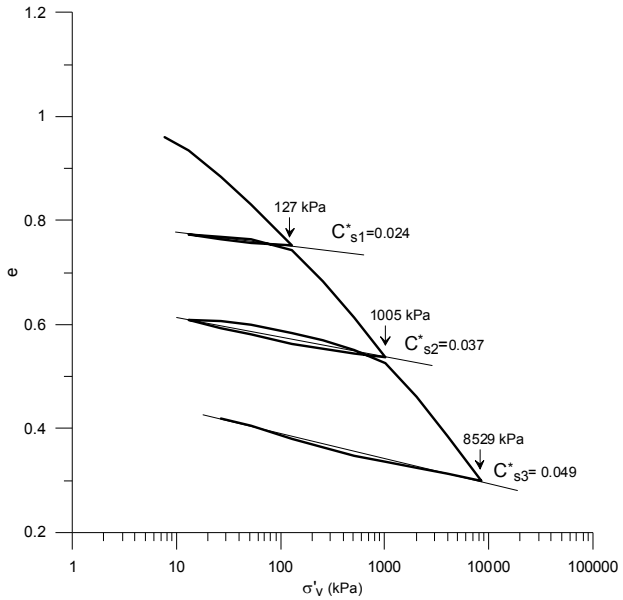

Figure 5.2 Oedometer compression behaviour of the slurry sample BRS-B-OS4 during unload-reload cycles

Traditionally, elastic-hardening plastic models predict that the yield surface will expand as the soil moves along the NCL increasing the linear elastic region (e.g. Cam Clay). As can be observed from Figure 5.2, unloading paths produced not only elastic deformation but also plastic volume changes, where its magnitude depended on the size of the unload-reload cycle and the preconsolidation pressure. This showed that though the elastic region will change in size as the soil moves along the NCL, it is the change in position that will be probably more important. This soil behaviour can be modelled using kinematic hardening models (e.g. Stallebrass, 1990).

Figure 5.3 shows the relationship between the oedometric tangent modulus (M_{oed}) and the vertical effective stress (σ'_v) during loading and unloading stages, plotted on a logarithmic scale, of three slurry samples covering the highest and lowest initial water contents of the specimens tested. It can be seen that for the loading stages the values of M_{oed} converged onto a clear unique line for stresses higher than 20kPa. The differences observed at low stress levels were associated with a denser structure for sample BRS-B-OS6 compared with the other two specimens. During unloading a slightly scatter can be seen on the results. A regression analysis was performed to estimate the M_{oed}-σ'_v relationship. Equations 5.7 and 5.8 express the stiffness for stress levels along the normal compression and swelling lines, where the values of the coefficient of correlation were R^2=0.998 and 0.995 and the MSE=0.0046kPa^2 and 0.02kPa^2 respectively.

$$M_{oed}(NC) = 29.92 \cdot \sigma'_v{}^{0.94} \ (kPa) \qquad 5.7$$

$$M_{oed}(OC) = 35.1 \cdot \sigma'_v{}^{1.15} \ (kPa) \qquad 5.8$$

The M_{oed}-σ'_v relationship for sample BRS-B-OS4 is plotted in Figure 5.4 together with its one-dimensional compression line that was previously shown in Figure 5.2. It is interesting to highlight the observed change in stiffness from a pre-yield to a post-yield state of stress characterised by a maximum value of M_{oed} followed by a sudden decrease, which is typical in slurry/reconstituted overconsolidated soils where the overconsolidation state is only a consequence of an unloading process (e.g. Davison & Atkinson, 1990). Moreover, during the second reloading cycle, and for stresses beyond the first yield stress, it could be seen that the values of M_{oed} increased with a similar slope to the M_{oed}-σ'_v relationship for yield stress ratios equal to unity. This observed compression-stiffness behaviour of a slurry sample represents a reference structure that will be used to asses the effect of the initial structure of the natural intact samples and remoulded compacted samples.

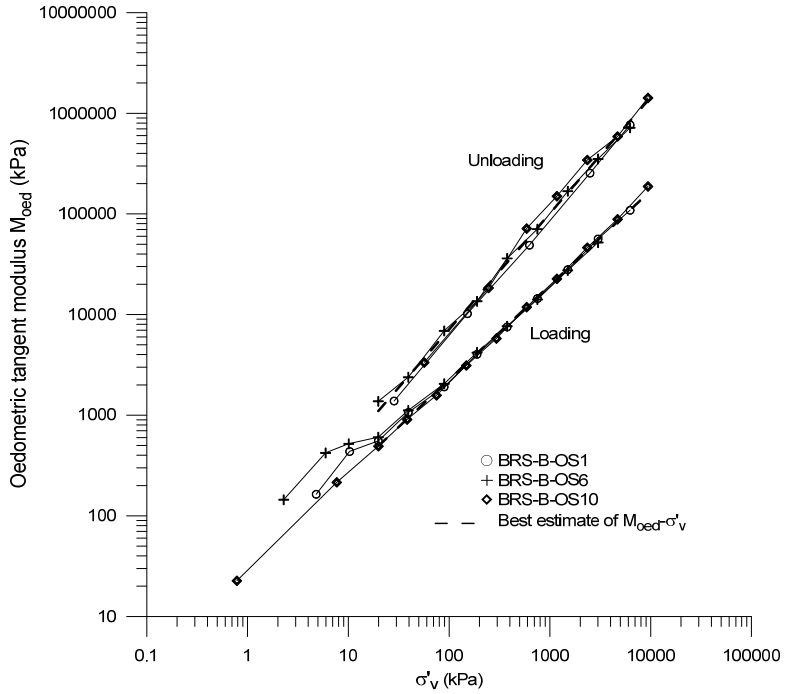

Figure 5.3 Oedometer tangent moduli (M_{oed}) of the slurry samples of the BRS-B soil

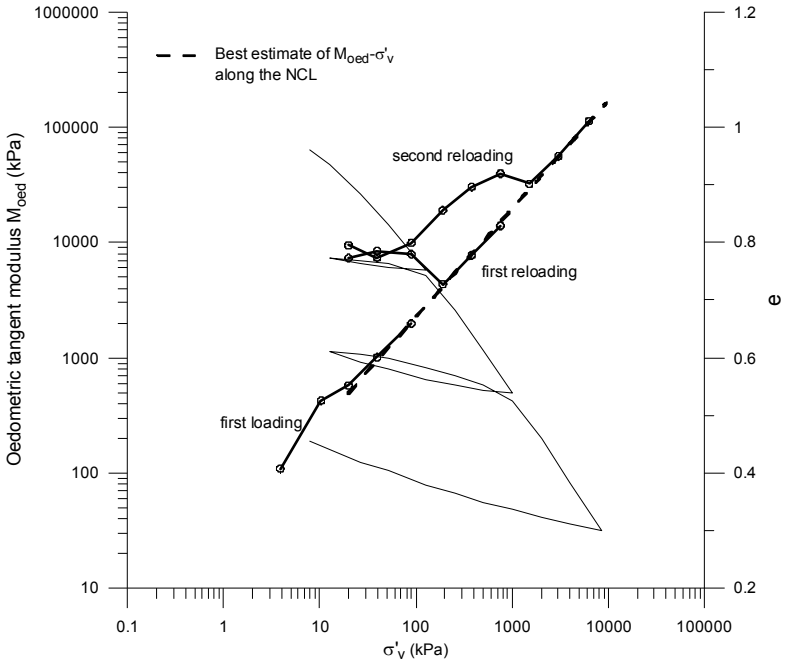

Figure 5.4 Oedometer tangent moduli (M_{oed}) and oedomerter compression curve of the slurry sample BRS-B-OS4

Research on the effect of particle breakage on granular materials has shown that breakage could influence the position and slope of the NCL in the compression plane (e.g. Sadrekarimi & Olson, 2011; Altuhafi & Coop, 2011). Although the breakage of the BRS-B was not measured in this research project, it is expected to be small based on the results obtained by Nocilla et al. (2006) on a material with a very similar grading and mineralogy, which had the same geological origin as the BRS-B. Figure 5.5 shows the comparison of the compression behaviour of a test performed on sample BRS-B-OS7, which had the original grading of the BRS-B material, with another test carried out on sample BRS-B-OS9, which was prepared by re-using the same soil used in tests BRS-OS7 and BRS-B-OS8, which were subjected to a maximum vertical stress of 12.5MPa during one-dimensional compression. It can be observed that both compression curves converged onto the same NCL, showing no apparent effect on the position and slope of the NCL of any possible breakage that could have occurred in the original BRS-B grading at a stress level of 12.5MPa.

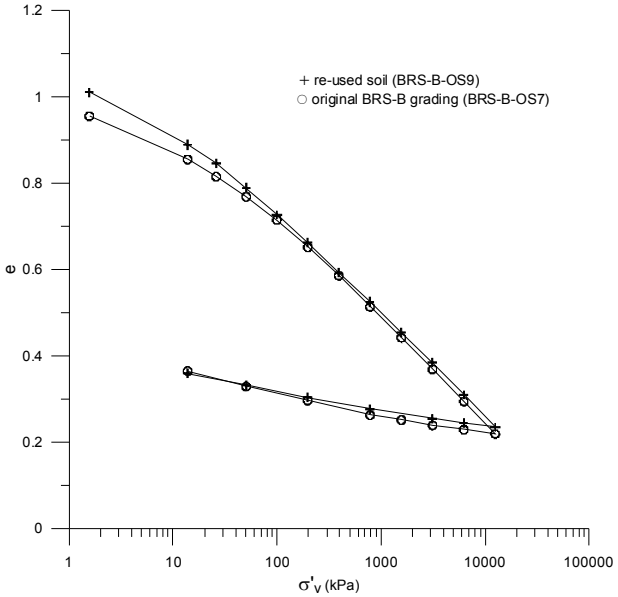

Figure 5.5 Comparison of oedometer compression curves of sample BRS-B-OS7 prepared with the original grading of the BRS-B material, with sample BRS-B-OS9 preparaed by re-using the same soil of tests BRS-B-OS7 and BRS-B-OS8 after being one-dimendionally compressed to 12.5MPa

- **Remoulded compacted samples**

Table 5.2 shows the details of the oedometer tests conducted on compacted samples from the trimmings of the BRS-B block. All the samples were prepared by remoulding the trimmings from the intact specimens, keeping the initial natural

water content constant. The samples were compacted in layers either statically or dynamically depending on the test. For example, samples BRS-B-OCL1 and BRS-B-OCL2 were compacted statically in two and three layers. Each layer was compacted to have a different initial void ratio, as specified in Table 5.2, to create a heterogeneous structure. These samples were called "layered soils". It is important to point out that the definition of a layered soil given here is not the same as the one that can be usually found in the literature, where a layered sample consists of soils with different gradings, e.g. layers of clay and sand such as varved clays. The procedure followed to prepare all the compacted samples was described in Section 3.7.1.

Test	** σ_{vi} (kPa)	$\sigma_{v(max)}$ (kPa)	w_i (%)	e_i	***σ_v (kPa)	σ'_y (kPa)	*swelling (%)	Comments
BRS-B-OC1	12.9	13661	18.6	0.590		840	0.21	Dynamic wet compaction by hand
BRS-B-OC2	8.37	8529	18.6	0.826		130	0.6	Dynamic wet compaction by hand
BRS-B-OC3	6.7	9347	18.8	1.132	86.6	20	0.57	Static wet compaction. 1 layer
BRS-B-OC4	7.8	8505	16.1	0.849	407.5	70	2.04	Static wet compaction. 1 layer
BRS-B-OC5	7.8	8505	17.2	0.790		160	1.82	Static wet compaction. 1 layer
BRS-B-OCL1	7.7	8505	16.2	0.828		170	2.03	Static wet compaction. 2 layers with $e_1 \cong 0.6$ and $e_2 \cong 1$ for each layer

Table 5.2 Summary of the oedometer tests carried out on remoulded compacted samples of the clayey silt (BRS-B). *Measured swelling of samples after flooding the cell with water once the initial vertical load was applied. **Samples were soaked after applying this stress. * Maximum vertical stress applied during static compaction.**

Test	** σ_{vi} (kPa)	$\sigma_{v(max)}$ (kPa)	w_i (%)	e_i	***σ_v (kPa)	σ'_y (kPa)	*swelling (%)	Comments
BRS-B-OCL2	7.7	8505	17.1	0.853		120	1.75	Static wet compaction. 3 layers with $e_1 \cong 0.6$, $e_2 \cong 0.8$ and $e_3 \cong 1$ for each layer
BRS-B-OCH1	7.3	9041	19	0.867		145	1.98	Static wet compaction. 2 layers. 3 vertical drilled holes
BRS-B-OCH2	7.4	8505	18.4	0.828		160	1.76	Static wet compaction. 2 layers. 3 vertical pushed holes
BRS-B-OCH3	6.7	10352	18.9	0.878	407.5	120	1.96	Static wet compaction. 1 layer. 17 vertical drilled holes
BRS-B-OCH4	6.7	3621	18.6	1.102	204	30	0.81	Static wet compaction. 1 layer. 10 vertical drilled holes
BRS-B-OCH5	-	9310	18.8	1.140	86.6	25	-	Static wet compaction. 1 layer. 14 vertical pushed holes

Table 5.2 Continuation

Figure 5.6 shows the one-dimensional compression behaviour of the remoulded compacted BRS-B samples. It can be observed that all the compression curves converged towards a unique NCL regardless of the compaction method used and the number of soil layers created during compaction. Therefore, although the initial structure of each sample was expected to be different, the deformation induced during compression was enough to erase the initial structure to reach the unique NCL. This result was also important in terms of the robustness of the unique NCL

regardless of the heterogeneities created in the specimens during the sample preparation process.

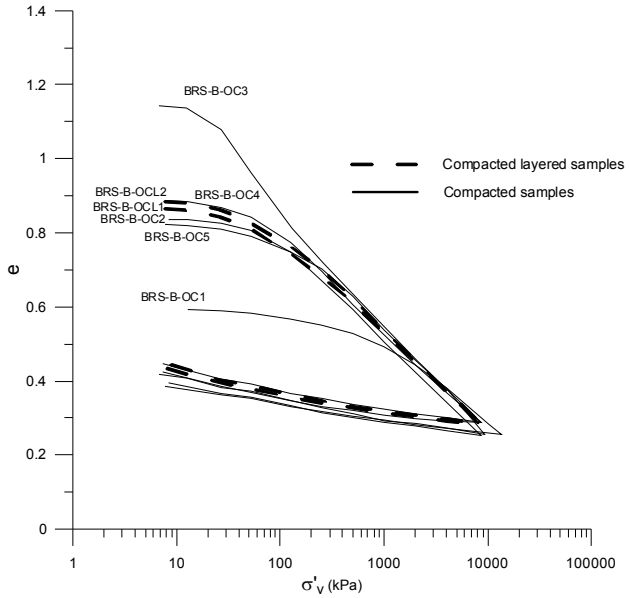

Figure 5.6 Oedometer compression of the remoulded compacted samples of the BRS-B

In Chapter 4, it was described that some of the BRS-B intact samples tested in the oedometer had vertical holes inside. In order to simulate the possible effect of these holes on the compression behaviour, a few oedometer tests were conducted on statically compacted samples with vertically drilled and pushed holes (Table 5.2) (Figures 3.8 to 3.9). The vertical holes were randomly distributed across the specimens. The main difference between the drilled and pushed holes was that a drilled hole was created by extracting material from the sample and a pushed one by displacing the material inside the sample, possibly creating a more dense structure around the holes. A top platen was used to avoid any volume change during the drilling and pushing procedures. A more detailed description of the sample preparation technique was carried out in Section 3.7.1.

Figure 5.7 shows the compression curves for all the samples with holes together with that of a remoulded compacted specimen without holes, BRS-B-OC3, which was included for comparison. Although different structures were expected to be created by each method, a clear unique NCL was identified showing that the vertical holes had no significant effect on the compression response of the BRS-B. Another important conclusion was that the number of holes created for the same procedure had no effect either as can be observed when comparing the compression lines for samples BRS-B-OCH1 (3 drilled holes) and BRS-B-OCH3 (17 drilled holes). Moreover, the comparison of the compression lines of the remoulded

compacted sample without holes, BRS-B-OC3, with the remoulded compacted specimens with holes, BRS-B-OCH4 and BRS-B-OCH5, showed that for a similar average initial void ratio there was no significant effect of the holes on the soil behaviour. Consequently, it could be concluded that the root holes, by themselves, found in some natural samples are most unlikely to have any significant impact on their behaviour, unless some local bonding occurred around them in the intact specimens.

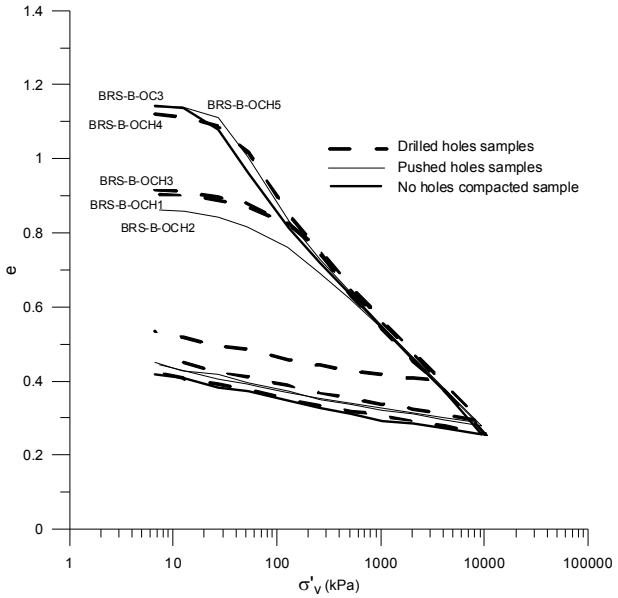

Figure 5.7 Oedometer compression of the remoulded compacted samples of the BRS-B with holes

Figure 5.8 shows the compression lines for all the remoulded compacted samples tested. As can be observed, the specimens with the highest e values displayed a stiff response at the start of the compression stages followed by an abrupt change in their compressibility after yield. For stresses beyond yield, all the curves converged towards a unique NCL, regardless of the initial structure. The abrupt change in the stiffness after yield might be a consequence of a meta-stable structure created during compaction. As the initial density of the specimens increased this meta-stable structure was less evident. The effect of the initial structure of the compacted samples will be discussed later in Section 5.2.4, where their behaviour will be compared with the unique 1D-ICL* defined by the slurry specimens.

Traditionally, for reconstituted fine-grained materials, the yield stress (σ'_y) observed during one-dimensional compression has been associated with the maximum stress level that the soil has been subjected to during its history, called the preconsolidation pressure (σ'_p) (e.g. Figure 5.2). In the case of uncemented

coarse-grained materials the yield stress occurs at the onset of major particle breakage. As described in Section 3.7.1, during the preparation process of the statically compacted samples it was possible to measure the maximum vertical stress applied to some of the specimens. The yield stress for each test was estimated using the Onitsuka (1995) method, the values being compared with the maximum compaction stresses in Table 5.2. It can be seen that there was no correlation between the maximum vertical stress applied during compaction and the yield stress, meaning that the soil did not remember its maximum stress that it had been subjected to. In fact, the maximum vertical stress applied during compaction can not be compared with the yield stress because during compaction the samples were not saturated and therefore the vertical effective stress applied was not known.

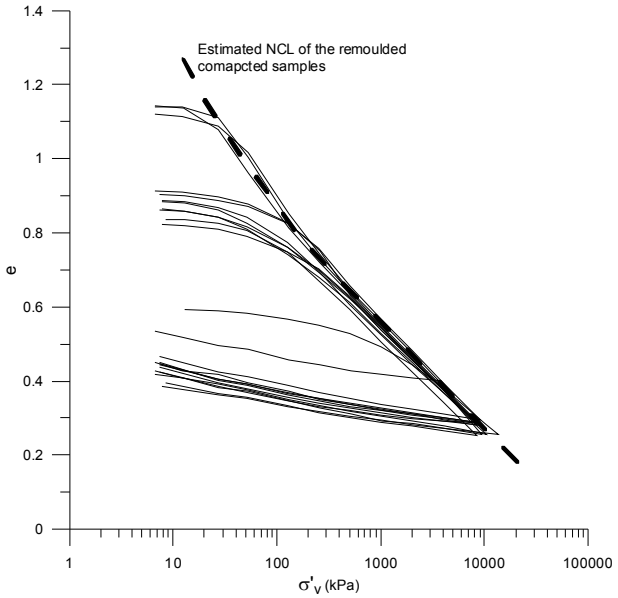

Figure 5.8 Oedometer compression lines of all the remoulded compacted samples of the BRS-B soil

Figure 5.9 shows an attempt to correlate the initial void ratio of each sample after soaking with the measured yield stress on a logarithmic scale. Although there was some of scatter in the results, a relatively good correlation was found with an R^2=0.98 and σ^2=0.0004. The slope of the linear regression on the e:logσ'_y plane was 0.34 which is equivalent to the average value of the slope of the estimated unique NCL of the compacted samples plotted in Figure 5.8. It could be said, that the comparison of both slopes is another way of trying to check the uniqueness of the NCL for the compacted samples of the BRS-B. It also showed that the yielding stress of the compacted samples could be correlated with the initial density or void ratio.

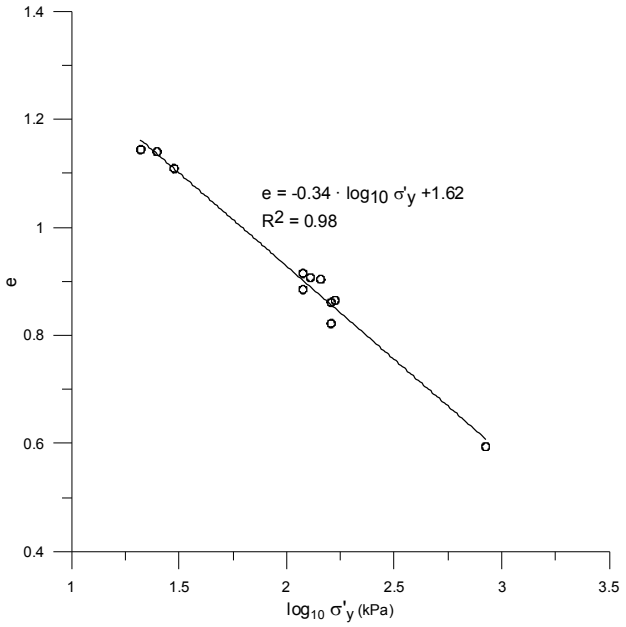

Figure 5.9 Correlation between initial void ratio after soaking anf yield stress for all the remoulded compacted samples of the BRS-B

The M_{oed}-σ'_v relationship of some of the remoulded compacted samples of the BRS-B is shown in Figure 5.10. It can be seen that the values of M_{oed} converged onto a single line for stress levels beyond yield. The differences on stiffness observed at the start of the tests reflect the effect of the initial structure of each specimen. In fact, the minimum values of M_{oed}-σ'_v exhibited by the loosest samples tends to disappear as the initial density increases.

- **Intact samples**

One of the main objectives of this research project was to investigate the effect of the in-situ structure of recently deposited alluvial materials like the BRS-B soil. As described in Section 4.3, Nocilla & Coop (2008) found that intact samples of a clayey silt with a very similar grading and geological origin to the BRS-B soil showed transitional behaviour in terms of the CSL, but they could not confirm this behaviour in compression.

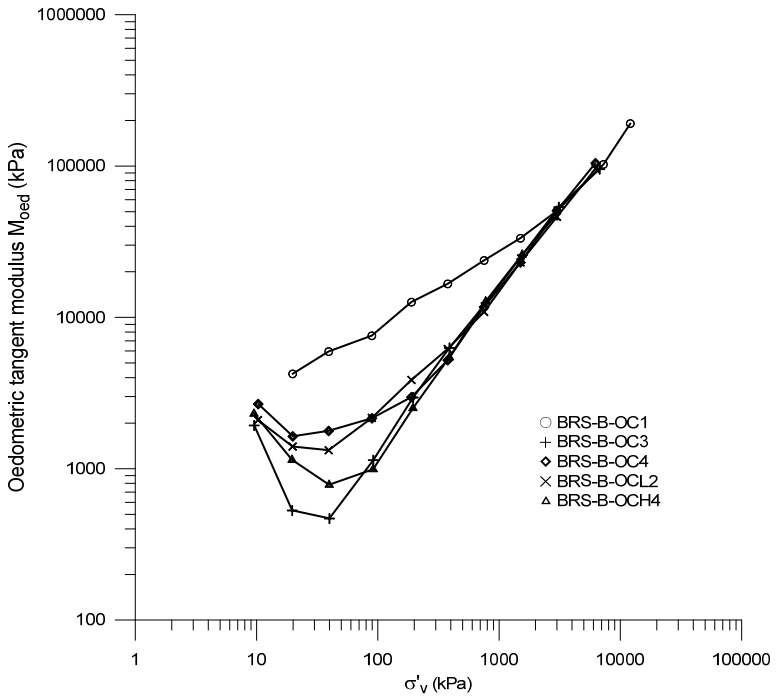

Figure 5.10 Oedometer tangent moduli (M_{oed}) of the remoulded compacted samples of the BRS-B

A series of oedometer tests on intact samples of the BRS-B were carried out to see the effect of its naturally occurring structure on its one-dimensional compression behaviour. Table 5.3 summarises the details of each test. All the samples were carefully trimmed from the block as described in Section 3.7.1. Although the intrinsic index properties of the BRS-B were the same for each of the samples tested, its in-situ structure seemed to be slightly more heterogeneous as revealed by the difference of the measured initial void ratio, which ranged from 0.713 to 0.808 with an average value of 0.751. This observed variability in the initial void ratio might be associated to a combination of different factors such as a possible heterogeneous initial structure inside the block, the error introduced in calculating e, and the structural damage induced to the samples during the preparation process. It is also interesting to recall that during the trimming of the specimens, the granulometry inside them was very homogeneous with the absence of layering which involves layers of materials with different gradings.

Test	** σ_{vi} (kPa)	$\sigma_{v(max)}$ (kPa)	w_i (%)	e_i	σ'_y (kPa)	I_L	*Swelling (%)
BRS-B-OI1	7.7	9505	19.7	0.808	300	-0.49	0.1
BRS-B-OI2	7.7	8505	21.6	0.765	300	-0.32	0.03
BRS-B-OI4	7.4	8505	20.8	0.713	345	-0.35	0.26
BRS-B-OI5	7.7	8530	18.5	0.748	230	-0.62	0.16
BRS-B-OI6	52	9042	20.6	0.778	365	-0.42	0
BRS-B-OI7	1.86	8005	19.5	0.721	300	-0.53	1.15
BRS-B-OI8	11.2	16532	16.2	0.723	400	-0.85	0.03

Table 5.3 Summary of the oedometer tests carried out on intact samples of the BRS-B. * Measured swelling of samples after flooding the cell with water once the initial vertical load was applied. ** Samples were soaked after applying this stress. * Water flushed throughout sample OI8 during 1 week under a back pressure of 10kPa after applying first load.**

The compression behaviour of the intact samples is shown in Figure 5.11. As can be observed, the initial parts of the compression curves run almost parallel to each other, with a very stiff response similar to the behaviour of a coarse-grained material, where the initial structure controls the compression response. Therefore, in the range of engineering stress levels (<1MPa) a non-unique compression path could be identified. After yield, all the compression curves tended to converge towards to a unique NCL at high stresses. This convergence was slower than in the case of the compacted samples (Figure 5.8). The location of each compression curve seemed to depend on the initial void ratio and elevated stresses were required to remove the initial structure of the samples to move towards a unique NCL.

The intact samples were initially partially saturated with a degree of saturation that varied from 62 to 80%. A suction of 90kPa was measured in a couple of samples using the suction probe technique (Ridley & Burland, 1999). In order to saturate the samples, the oedometer cell was flooded with water after applying the first load. A different procedure was followed with specimen BRS-B-OI8, where it was subjected to a circulation of water with 10kPa pressure difference across the sample during one week after applying the first load and flooding the oedometer cell. Figure 5.12 shows the comparison of the compression behaviour between samples BRS-B-OI8 and BRS-B-OI4 that were saturated using the two procedures described above. It can be seen that both samples showed the same behaviour regardless of the saturation method.

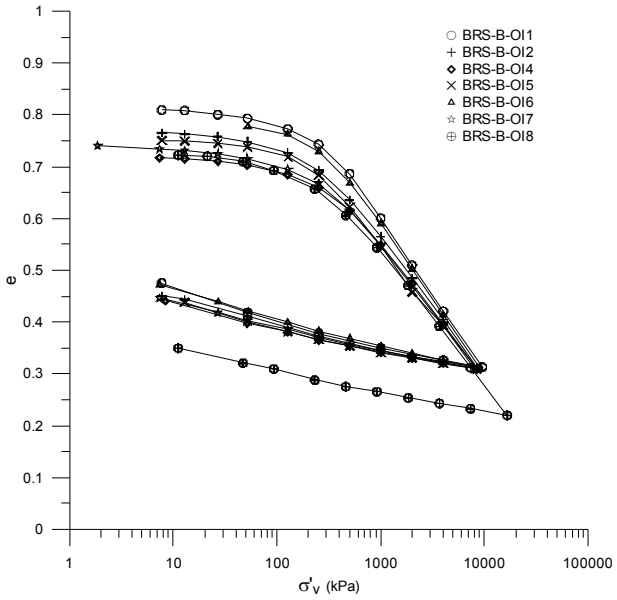

Figure 5.11 Oedometer compression of the intact samples of the BRS-B

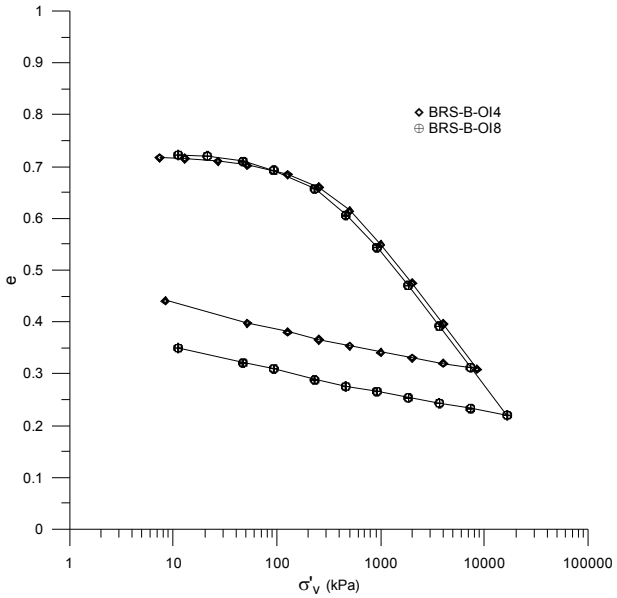

Figure 5.12 Oedometer compression of a sample saturated by flooding the oedometer cell (BRS-B-OI4) and another sample saturated by circulating a back pressure of 10kPa for one week (BRS-B-OI8)

The initial swelling response of the intact samples was also measured by monitoring the axial displacement of the specimens after the first load was applied and the oedometer cell was flooded with water. This was also done with the remoulded compacted samples of the BRS-B. The results are shown in Tables 5.2 and 5.3. As

can be observed, the swelling of the intact samples was much lower than those of the compacted, for a similar initial water content, initial applied stress and initial void ratio. For example, when comparing sample BRS-B-OI1 with BRS-B-OC5, it can be seen that for similar initial conditions the swelling was much higher for the compacted sample, 1.82%, compared with the intact one, 0.1%. Figure 5.13 shows a comparison of the compression behaviour for both samples. Initially, the compression line of the intact sample was stiffer and displayed a higher yield stress compared with that of the compacted specimen. After yield, the compression line of the intact sample runs quasi-parallel to the compacted, showing a very slow convergence towards a unique NCL. This difference in behaviour could be associated with an initial structure of the intact sample that probably consisted of a bonding together with a fabric that was not totally erased during compression over the range of stresses reached. The effect of the initial structure of the natural intact samples on the compression behaviour of the BRS-B will be analysed in Section 5.2.4.

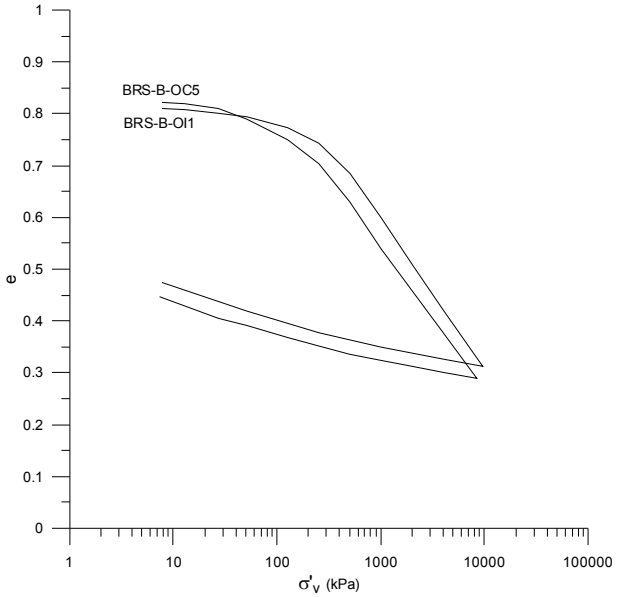

Figure 5.13 Comparison of the one-dimensional compression behaviour of an intact sample (BRS-B-OI1) with a compacted sample (BRS-B-OC5)

The yield stresses for the intact samples were also estimated, which values ranged from 230 to 400kPa, as shown in Table 5.3. All the yield stresses were much higher than the estimated in-situ vertical effective stress of the block sample σ'_v=75kPa. The yield stress ratio (YSR) associated to these values varied from 3 to 5.3. It is very unlikely that the in-situ sample had a maximum past stress level of the same value as the measured yield stress and therefore the measured yield stresses could not be correlated to the pre-consolidation pressure. One factor that could have had an important effect on the high values of the yield stress could have been

desiccation processes due to the shallow depth (1.4m) from where the block was retrieved. The yield stresses of the intact samples are plotted in Figure 5.14 together with the values measured for the compacted samples. In this case a slightly larger scatter in the results can be seen compared with the reconstituted compacted samples that could be a consequence of the in-situ structure.

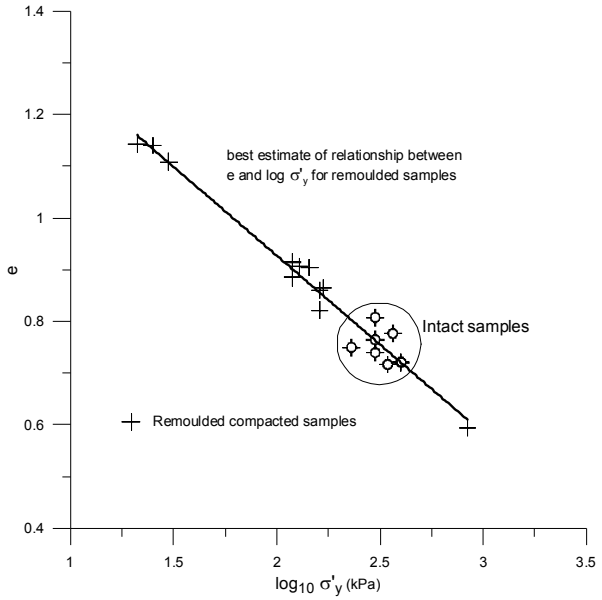

Figure 5.14 Correlation between the initial void ratio after soaking and the yield stress for all the remoulded compacted and intact samples of the BRS-B

As has been done for the slurry and compacted samples, Figure 5.15 shows the relationship between M_{oed} and σ'_v of all the natural intact samples of the BRS-B. It can be observed that all the M_{oed}-σ'_v curves converged onto a single line at stresses higher than the estimated yield values. The effect of the initial swelling during the flooding of the oedometer cell on the compression response is shown in Figure 5.16. As can be seen, the initial in-situ structure of the intact samples was weakened during swelling with a consequently reduction on the initial stiffness as the swelling increased. This showed that part of the initial structure was disturbed during swelling but it appeared to have little effect at high stresses. Comparing the M_{oed}-σ'_v relationships of the intact specimens with that of the slurry sample BRS-B-OS4 plotted in Figure 5.4, it could be observed that no correlation could be established between the M_{oed}-σ'_v relationship and the yield stress. While in the slurry sample the yield stress was clearly defined after a maximum value of the stiffness followed by a sudden decrease, in the case of the intact samples this type of M_{oed}-σ'_v relationship was not seen. This could help to support the idea that the yield stresses of the intact samples are not a consequence of unloading processes but a post-depositional behaviour.

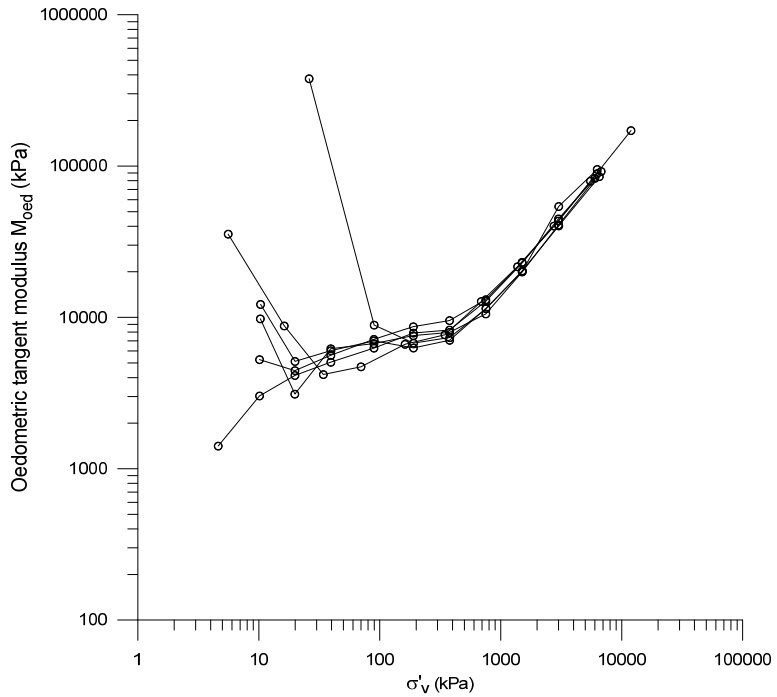

Figure 5.15 Oedometer tangent moduli (M_{oed}) of the intact samples of the BRS-B

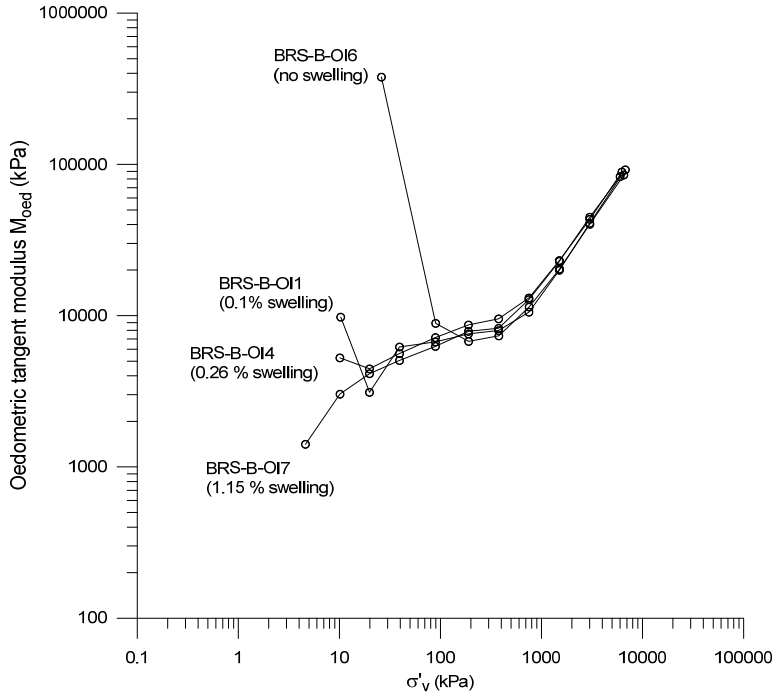

Figure 5.16 Oedometer tangent moduli (M_{oed}) of the intact samples of the BRS-B. Effect of initial sweeling on the compression behaviour

5.2.3 Compression behaviour of the Bormida sandy silt (BRS-E)

Only a small quantity of material of the BRS-E was available to test in this research project. This imposed a limitation on the number of oedometer tests that could be performed.

- **Slurry samples**

Three oedometer tests were carried out on slurry samples of the BRS-E. As in the case of the clayey silt (BRS-B), the objective was to investigate the effect of the initial structure on the compression behaviour of the BRS-E. The slurries were created at different initial water contents, which varied from 1 to 1.5 times the liquid limit, as shown in Table 5.4.

Test	w_i (%)	I_L	$\sigma_{v(max)}$ (kPa)
BRS-E-OS1	29.5	2	8163
BRS-E-OS2	37.7	3.9	12523
BRS-E-OS3	25.7	1.1	12523

Table 5.4 Summary of the oedometer tests carried out on slurry samples of Bormida sandy silt (BRS-E).

The compression behaviour of the BRS-E specimens tested in this research project is shown in Figure 5.17 together with the results obtained by Radici (2006). Apart from tests BRS-E-OS1 and BRS-E-OS3, the compression lines did not show any tendency to converge onto a unique NCL despite being tested to high stress levels. The position of each compression line depended on the initial void ratio meaning that the initial structure could not be erased during compression even at high stresses and therefore showing a transitional behaviour. This behaviour was previously anticipated by Radici (2006). However, the compression lines of samples BRS-E-OS1 and BRS-E-OS3 converged onto a unique NCL. In the case of a relatively small difference in the initial void ratio, an apparent convergence could be found but this does not mean that for larger differences in initial void ratios there will be the same convergence as shown with the other specimens. Consequently, it is very important to create samples with larger differences in the initial void ratio in order to check the possible transitional behaviour of a soil.

Figure 5.18 shows a comparison of the compression response of the slurry samples of the two BRS materials. It can be clearly seen that while the compression curves of the clayey silt (BRS-B) converged onto a unique 1D-ICL* regardless of the

initial structure, the response of the sandy silt (BRS-E) displayed a transitional behaviour. In addition, the slope of the BRS-B compression lines was slightly higher that those of the BRS-E, as well as the swelling lines. This change in slope could be due to a higher plasticity of the BRS-B compared with the BRS-E.

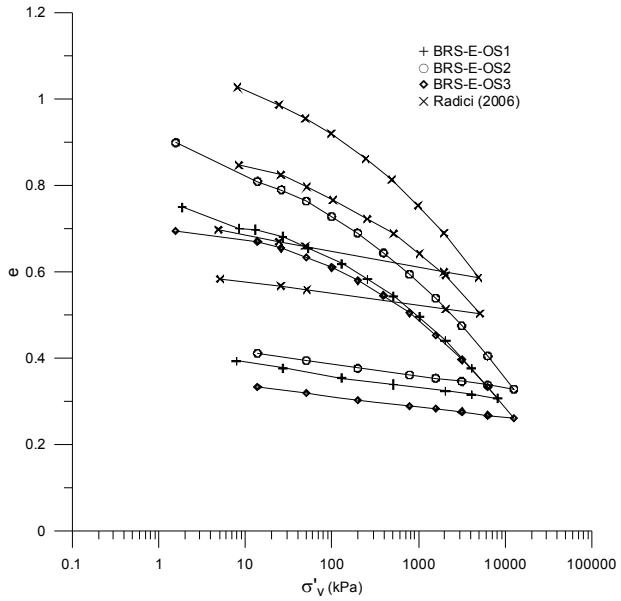

Figure 5.17 Oedometer compression of the slurry samples of the BRS-E

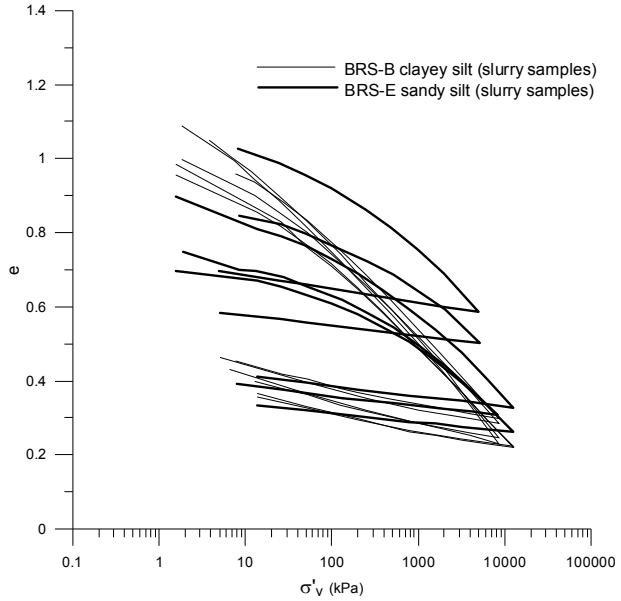

Figure 5.18 Comparison of the oedometer compression lines of the slurry samples of the clayey silt (BRS-B) and sandy silt (BRS-E)

- **Compacted samples**

Two tests were carried out on compacted specimens of the BRS-E to investigate the possible effect of the sample preparation method on the compression behaviour. The samples were compacted dynamically by hand. The details of each test are shown in Table 5.5.

Test	**σ_{vi} (kPa)	$\sigma_{v(max)}$ (kPa)	w_i (%)	e_i	σ'_y (kPa)	*swelling (%)	Comments
BRS-E-OC1	13	9681	19	0.635	900	0.8	Dynamic wet compaction by hand
BRS-E-OC2	7.9	8163	1.3	0.793	250	0.25	Dynamic air-dried compaction by hand

Table 5.5 Summary of the oedometer tests carried out on compacted samples of the BRS-E. *Measured swelling of samples after flooding the cell with water once the initial vertical load was applied. **Samples were soaked after applying this stress.

Figure 5.19 shows the compression response of the BRS-E samples together with the results of two more tests carried out by Radici (2006). It can be observed that, regardless of the compaction method, all the compression curves converged onto a unique NCL, with a compression index of C_c=0.29. This result contrasts with the behaviour of the slurry samples, where it was not possible to find a unique NCL during compression for the same range of applied stresses (Figure 5.17). Consequently, and according to the results presented above, it can be concluded that the sample preparation technique produced different initial structures which resulted in a non-convergence of the compression curves and therefore determined whether there is transitional behaviour of the Bormida sandy silt (BRS-E). This conclusion was anticipated from a review of the literature of some other soils that displayed transitional behaviour (Section 2.5.3).

The relative breakage (Br) of sample BRS-E-OC1 was measured using the method proposed by Hardin (1985) and assumes that the fines are supposed not to contribute to the breakage of the material. The relative breakage measured was Br=0.1 at a maximum stress of 9.7MPa.

Figure 5.20 shows the M_{oed}-σ'_v relationship plotted on a logarithmic scale, of the compacted and slurry samples of the BRS-E soil. It can be seen that the values of the M_{oed} converged onto a single line regardless the sample preparation method and regardless of whether the behaviour was transitional or not.

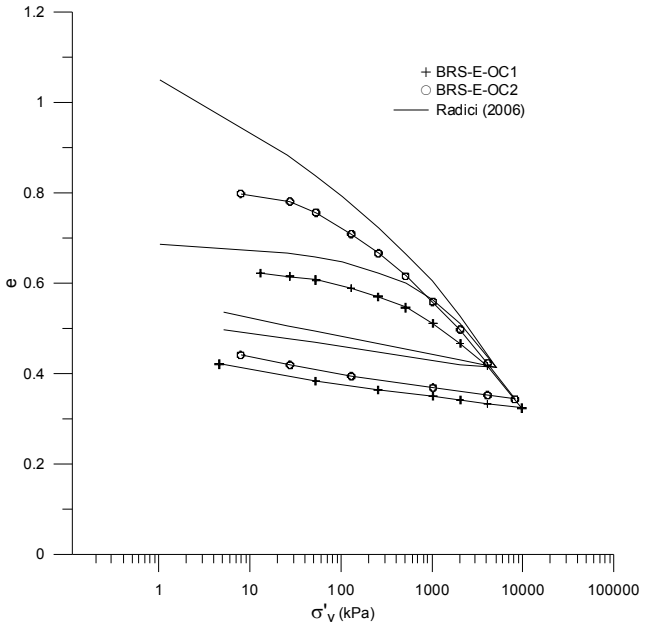

Figure 5.19 Oedometer compression of the compacted samples of the BRS-E

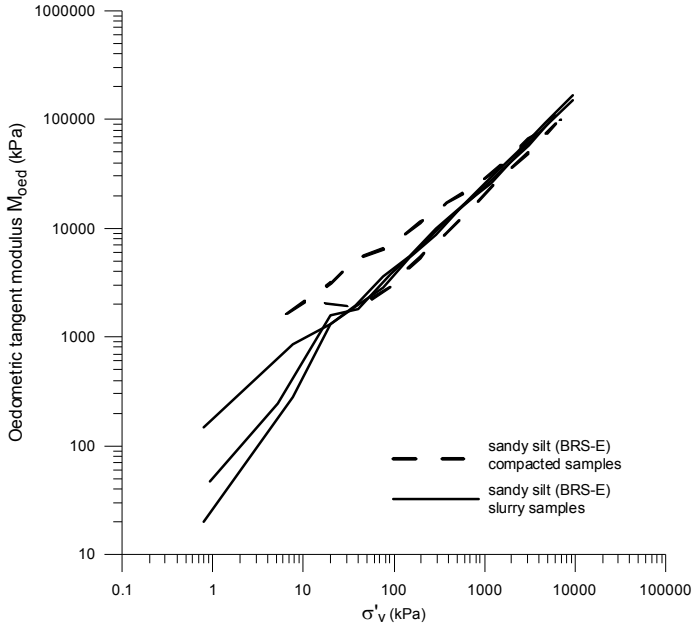

Figure 5.20 Oedometer tangent moduli (M_{oed}) of the slurry and compacted samples of the BRS-E

5.2.4 Influence of the initial structure on the compression behaviour of the BRS soils

- **Clayey silt (BRS-B)**

In order to evaluate the effects of the in-situ structure of the natural intact samples on the one-dimensional compression behaviour, a commonly accepted method is to compare the intact soil response with its reconstituted state (e.g. Burland, 1990). In this comparison it is assumed that, for reconstituted materials, there exists a unique intrinsic normal compression line (ICL) (Burland, 1990). In the case of the BRS-B, a unique intrinsic compression line was found for the slurry specimens and it was taken as the one-dimensional 1D-ICL* to be used as the reference line for comparison with the other samples (Figure 5.1). This 1D-ICL* was normalized by volume using the void index (I_v) (Burland, 1990) and is plotted in Figure 5.21. Burland suggested an equation for the ICL when data are not available. This equation is also plotted in Figure 5.21. As can be observed, the 1D-ICL* measured for the BRS-B slightly deviates from the curved ICL defined by the Burland.

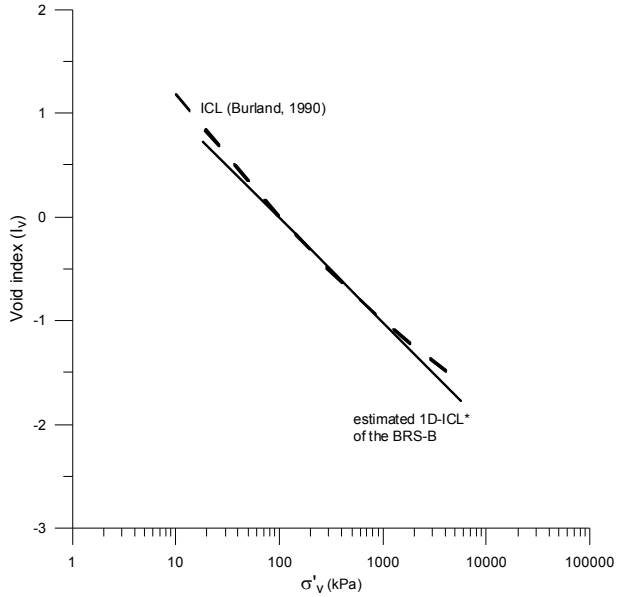

Figure 5.21 Comparison between the intrinsic compression line 1D-ICL* of the BRS-B and the ICL proposed by Burland (1990)

Figure 5.22 shows the comparison between the normalized compression curves of the natural intact samples, the 1D-ICL* of the BRS-B clayey silt and the sedimentary compression line (SCL) (Burland, 1990). As can be seen, all the normalized compression curves of the intact specimens crossed the 1D-ICL* and yielded at different stress levels in between the 1D-ICL* and the SCL. The ratio of

the yield stress (σ'_y) to the equivalent effective stress on the intrinsic compression line (σ'_{ve}) was defined by Cotecchia & Chandler (2000) as the stress sensitivity ($S_\sigma=\sigma'_y/\sigma^*_{ve}$). In the case of the intact specimens of the BRS-B, the stress sensitivity varied from 1.2 to 2.5 with the lowest and highest values corresponding to the densest and loosest samples respectively. The post-yield behaviour showed a very slow convergence towards the 1D-ICL*, displaying a robust effect of the initial structure that could not be easily removed during one-dimensional compression. Burland et al. (1996) suggested that in cases where the yielding stress is located between the 1D-ICL* and the SCL in a σ'_v:I_v plane, the main difference in the compression behaviour between reconstituted and intact samples is due to different fabrics, with a small influence of the particle bonding. It is believed that this is the case of the intact specimens of the Bormida clayey silt (BRS-B).

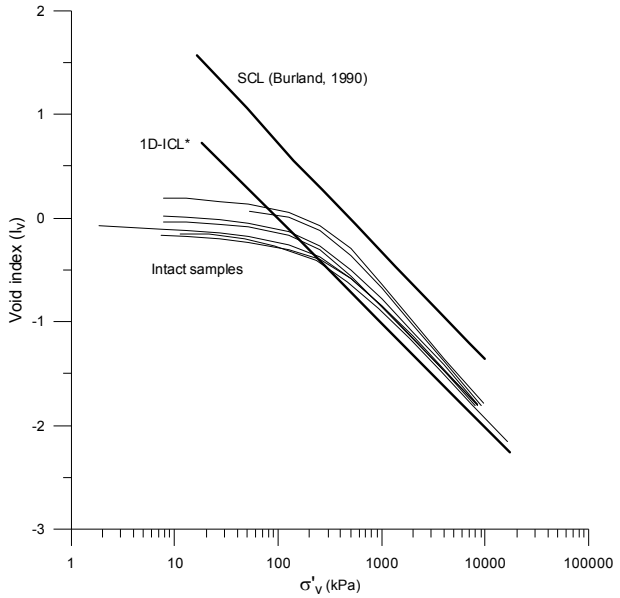

Figure 5.22 Comparison between the normalized compression lines of the BRS-B intact samples, the measured 1D-ICL* and the SCL

The normalized compression curves of the intact BRS-B samples are plotted together with other Holocene materials such as the Sibari silty clay and the Bothkennar clay in Figure 5.23. The normally consolidated Sibari silty clay is a coastal and alluvial Holocene sedimentary soil, rapidly deposited in a changing environment (Coop & Cotecchia, 1995, 1996). It has a stable sedimentation structure with a low strength sensitivity and little post-yield convergence towards the ICL meaning that the initial fabric controlled the compression behaviour even at large strains (Cotecchia & Chandler, 2000). On the other hand the Bothkennar clay is a recently deposited Holocene material which appeared to have a meta-stable sedimentary structure with a stress sentivity of about 6 and rapid post-yield

convergence towards the ICL due to destructuration (Burland, 1990; Smith et al.,1992; Cotecchia & Chandler, 2000). As can be observed from Figure 5.23, the normalized compression behaviour of the BRS-B clayey silt is very similar to that exhibited by the Sibari silty clay, where fabric had the major effect on the compression behaviour with a minor effect of bonding.

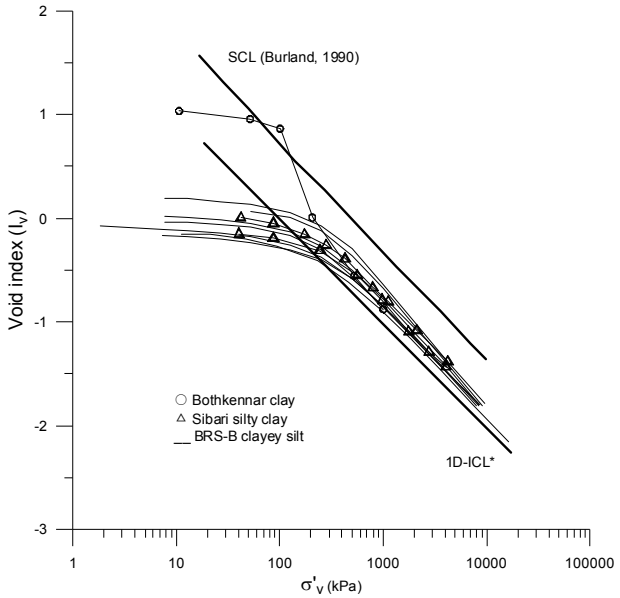

Figure 5.23 Comparison between the normalized compression lines of the BRS-B intact samples and two other Holocene natural materials (data from Burland, 1990; Smith, 1992 and Coop & Cotecchia, 1995)

The normalised compression response of the compacted specimens is shown in Figure 5.24. As can be seen, the compression curves also crossed the estimated 1D-ICL* showing an effect of the initial structure created during compaction. This effect was more important as the initial density increased. In fact, the samples with higher initial void ratios reached the SCL with stress sensitivity values of around 5, displaying a rapid post-yield convergence towards the 1D-ICL* as a consequence of the meta-stable structure created during compaction. At very high stress levels the compression lines plotted slightly above the 1D-ICL*. The observed effect of the initial structure of the remoulded compacted samples proved that the structure level found was larger compared with the slurry samples and therefore this justified that they could not be used as a reference for the analysis of the effects of the initial structure of the natural intact samples.

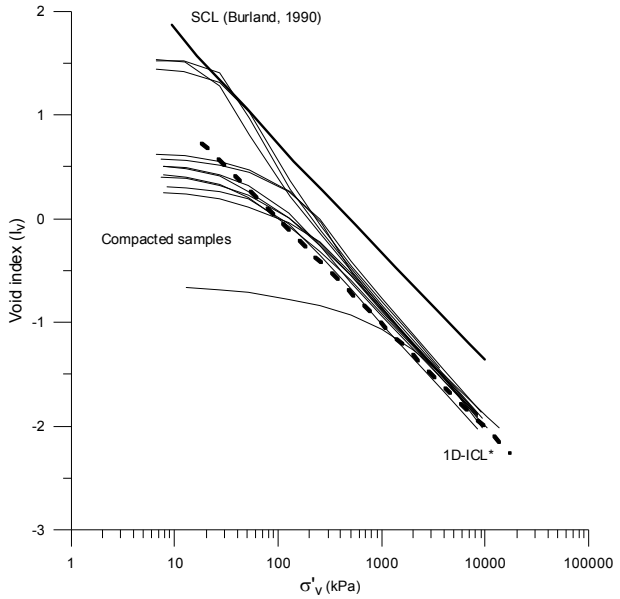

Figure 5.24 Comparison between the normalized compression lines of the BRS-B compacted samples, the measured 1D-ICL* and the SCL

Figure 5.25 shows a comparison of the variation of the oedometric tangent moduli with the effective stress of the intact specimens together with the estimated M_{oed}-σ'_v relationship along the 1D-ICL* defined by the slurry samples. It can be seen that for stresses below yield, the stiffness of the intact samples was higher showing the effect of the initial structure, which was also affected by the swelling experienced by the specimens during the soaking in the oedometer cell. For stresses beyond yield, all the lines converged onto a unique relationship with values of the stiffness slightly lower than those of the slurries for a given effective stress level. This response shows that although the structure of the intact samples was stronger than that of the slurries for a given e (e.g. Figure 5.22), the stiffness was slightly smaller.

The stiffness of the remoulded compacted samples is compared with the slurries in Figure 5.26. A clear effect of the meta-stable structure created in the remoulded compacted specimens with very high initial void ratios, BRS-B-OC3, BRS-B-OCH4 and BRS-B-OCH5 can be observed. The yield stresses for these samples were located on the SCL and after yield they collapsed towards the 1D-ICL* (Figure 5.24). The stiffness of these specimens after yield was lower compared with those of the slurry samples and they eventually reached the same unique relationship between M_{oed} and σ'_v as the other samples. At very high stress levels, the lines also converged onto the unique relationship defined by the slurries.

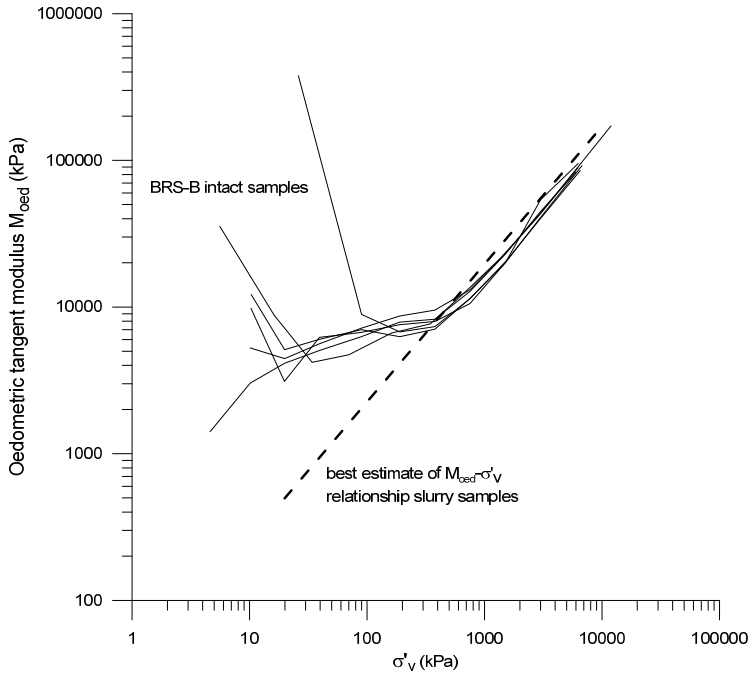

Figure 5.25 Comparison of the oedometric tangent moduli (M_{oed}) for intact and slurry samples of the BRS-B

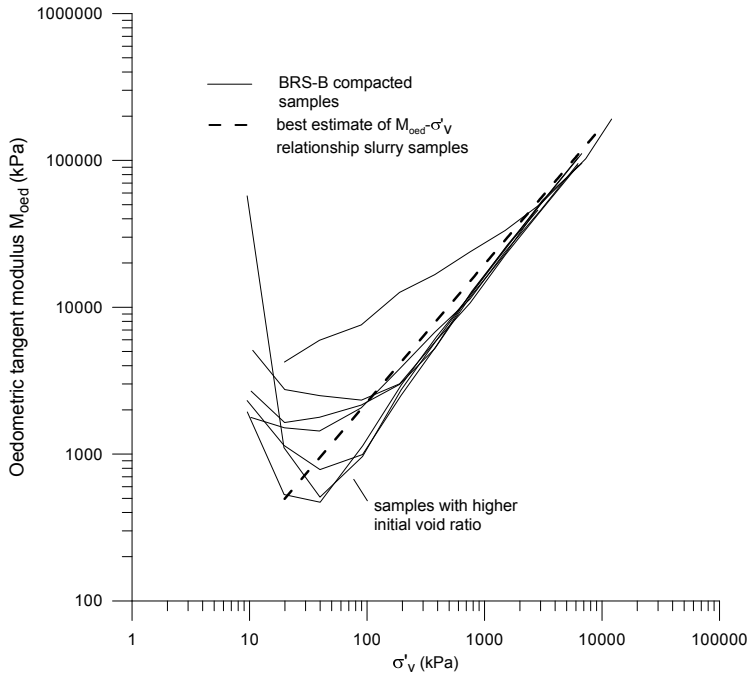

Figure 5.26 Comparison of the oedometric tangent moduli (M_{oed}) for remoulded compacted and slurry samples of the BRS-B

- **sandy silt (BRS-E)**

In the case of the Bormida sandy silt (BRS-E), only slurry and remoulded compacted samples were tested during this research project with no intact specimens available. As shown in Figure 5.17, for the slurry samples it was found that a different NCL was obtained for each initial water content, showing a clear transitional behaviour in one-dimensional compression. The slope of each NCL defined at high stresses was essentially the same, as shown in Figure 5.27. This lack of uniqueness of the NCL would make any comparison between natural intact samples and slurry samples to determine the effects of structure impossible, and the concept of intrinsic compression line as a reference line can not be used. On the other hand, a unique NCL was identified for the remoulded compacted samples (Figure 5.19) that had a very similar slope to the compression paths of the slurry samples as shown in Figure 5.27. Consequently, for the Bormida sandy silt (BRS-E) it could be concluded that the sample preparation technique has an important effect on the presence of transitional behaviour in one-dimensional compression.

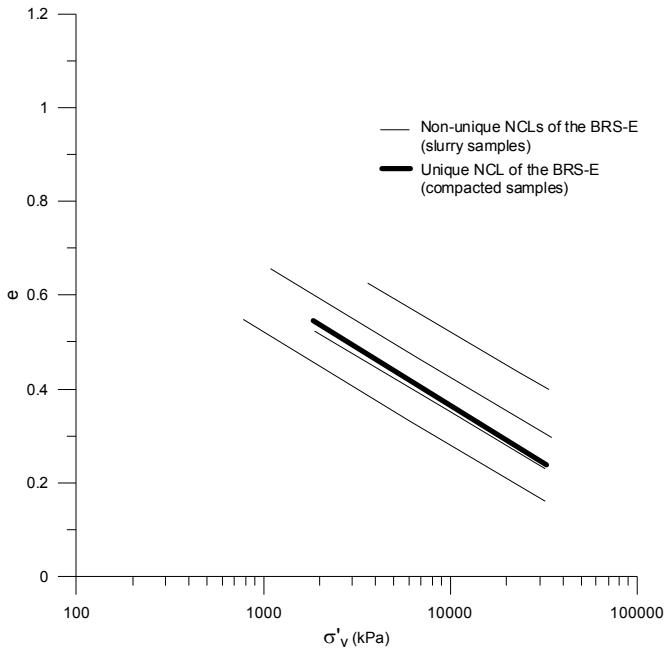

Figure 5.27 Effect of the sample preparation method on the uniqueness of the normal compression lines of the BRS-E sandy silt

Finally Figure 5.28 shows the M_{oed}-σ'_v relationship along the NCL in a logarithmic plot for the slurry and reconstited samples of the Bormida clayey silt (BRS-B) and the sandy silt (BRS-E). It can be seen that for the same vertical effective stress the stiffness of the sandy silt was larger compared with the clayey silt up to a stress

level of around 3MPa. For stresses beyond 3MPa the M_{oed}-σ'_v relationships crossed making the clayey silt stiffer. This might be due to the onset of major particle breakage in the more sandy material compared with the clayey silt. Data from the Venetian silty soils (Simonini et al., 2007) are also plotted in Figure 5.28. It can be seen that the Bormida River silty soils showed a similar trend compared with those of the Venetian materials.

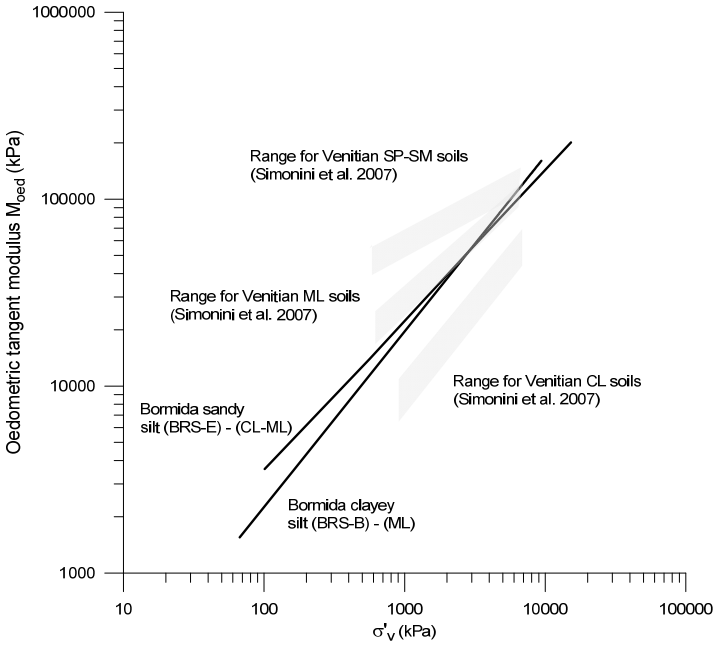

Figure 5.28 Comparison of the oedometric tangent moduli for the clayey silt (BRS-B), the sandy silt (BRS-E) and soils from the Venice lagoon (data redrawn from Simonini et al., 2007)

5.2.5 Summary of the compression behaviour

In the previous sections the one-dimensional compression behaviour of the Bormida silty soils (BRS) was investigated. Two different soil gradings were tested; the Bormida clayey silt (BRS-B) classified as ML and the sandy silt (BRS-E) classified as ML-CL. The main important features of their behaviour are summarised in the following paragraphs.

- **Clayey silt (BRS-B)**

A unique normal compression line was found for the slurry samples regardless of the initial water content, defining the one-dimensional intrinsic compression line (1D-ICL*) of the BRS-B. This 1D-ICL* was used as a reference for analysing the

effect of the initial structure of the compacted and the intact specimens of the BRS-B.

In the case of the compacted samples, a unique NCL was also found at high stress levels, regardless of the compaction method, the number of soil layers created during compaction and the presence of vertical holes. Their normalized compression lines were located to the right of the 1D-ICL* and below the SCL, showing the effect of the initial structure created during compaction. The specimens with the highest initial void ratios reached the SCL, exhibiting a meta-stable structure with a rapid post-yield convergence towards the 1D-ICL*. In the case of the densest samples, the effect of the initial structure was less noticeable, and that could be due to an artefact of the normalisation process. At high stress levels, the deformation induced during compression was almost sufficient practically to erase the differences of the initial structure of the samples as they tended to converge onto the unique 1D-ICL*.

The observed effect of the initial structure of the remoulded compacted samples justified that their unique NCL could not be used as a reference for the analysis of the effects of initial structure of the natural intact samples.

The effect of the in-situ structure of the intact block material was clear as the normalized compression curves crossed the 1D-ICL* and yielded at different stress levels in between the 1D-ICL* and the SCL. The stress sensitivity varied from 1.2 to 2.5 with the lowest and highest values corresponding to the densest and loosest samples respectively. The post-yield behaviour showed a very slow convergence towards the 1D-ICL*, displaying a robust effect of the initial fabric that could not easily be removed during one-dimensional compression. It appeared that the in-situ structure of the Bormida clayey silt was slightly heterogeneous in terms of void ratio, where fabric had the major effect on the compression behaviour with a minor effect of bonding.

- **Sandy silt (BRS-E)**

In the case of the BRS-E sandy silt, only slurry and remoulded compacted samples were tested during this research project due to the lack of intact specimens.

For the case of the slurry samples it was found that a different NCL was obtained for each initial water content, where the position of each compression line depended on the initial void ratio, meaning that the initial structure could not be erased during compression even at high stresses and therefore showing a clear transitional behaviour. This lack of uniqueness of the NCL would make impossible any

comparison between natural intact samples and slurry samples to determine the effects of structure and the concept of intrinsic compression line then has no meaning.

Contrary to the transitional behaviour observed on the slurry samples a unique NCL was identified for the remoulded compacted specimens regardless the compaction method. Consequently, it could be concluded that, in the case of the Bormida sandy silt (BRS-E), the sample preparation technique has an important effect on the presence of transitional behaviour in one-dimensional compression.

5.3 Triaxial behaviour of the Bormida River clayey silt (BRS-B)

The triaxial test is the most widely used apparatus to investigate the stress-strain behaviour of all types of soil. As described in Section 3.3, two different triaxial apparatus were used in this research project; a conventional Bishop & Wesley stress path cell and a modified 7MPa triaxial cell. A computer controlled software called TRIAX was used to monitor the pressures and displacements, and control the stresses and strains.

Three types of specimens were tested; slurry, remoulded compacted and intact samples. All the specimens had a 38mm diameter apart from those tested in the 7MPa cell which were 50mm in diameter. The same length/diameter ratio of 2 was used for all the samples sizes. As mentioned in Section 4.2, a small quantity of the BRS-E sandy silt was available for testing and only oedometer tests could be carried out. Therefore this material was not tested in the triaxial.

5.3.1 Calculations

The stress-strain behaviour of the samples tested in the triaxial apparatus was represented by using the stress invariants and the corresponding conjugate strain invariants defined by the following equations:

$$p' = \frac{\sigma_a + 2 \cdot \sigma_r}{3} - u \qquad 5.9$$

$$q = \sigma_a - \sigma_r \qquad 5.10$$

$$\varepsilon_v = \varepsilon_a + 2 \cdot \varepsilon_r \qquad 5.11$$

$$\varepsilon_s = \frac{2}{3} \cdot (\varepsilon_a - \varepsilon_r) \qquad 5.12$$

where:

p’	mean effective stress
q	deviator stress
ε_v	volumetric strain
ε_s	deviator/shear strain
σ_a	total axial stress
σ_r	total radial stress
u	pore water pressure
ε_a	axial strain
ε_r	radial strain

In soil mechanics, compressive stresses are taken as positive by convention. Therefore a negative sign is required to make compressive strains positive. This was the convention followed in this thesis. The axial strain (ε_a) was calculated measuring the change in axial length (δl) over the initial sample length or gauge length (l_o). As described in Section 3.4.2, δl was measured using external and local axial displacement transducers. The average axial strain was calculated using the measurements of the local transducers until they went out of range. After this, the external transducer was used.

$$\varepsilon_a = \frac{-\delta l}{l_o} \qquad 5.13$$

The volumetric strain (ε_v) was obtained directly by measuring the change of water entering or leaving the volume gauge (δV) and the initial volume of the sample (V_o).

$$\varepsilon_v = \frac{-\delta V}{V_o} \qquad 5.14$$

The radial strain (ε_r) was calculated from the volumetric strain and axial strain by Equation 5.15. In this equation and in Equation 5.12 it is implicitly assumed that the radial and circumferential strains are equal and therefore it is also imposed that the sample properties are either isotropic or cross-anisotropic.

$$\varepsilon_r = \frac{\varepsilon_v - \varepsilon_a}{2} \qquad 5.15$$

However, when a radial belt was used, the radial strain was also obtained by measuring the change in diameter (δD) using the local transducer and the initial sample diameter (D_o).

$$\varepsilon_r = \frac{-\delta D}{D_o} \qquad 5.16$$

The volumetric strain could also be calculated from measurements of the axial and radial strain by using the local transducers. For small strains, there was a very good agreement with the value obtained using Equation 5.14. In the case of intermediate to large strains the volumetric strain calculated with the local transducers introduced large errors due to unrealistic measurements of the radial strain due to the barrelling shape experienced by the samples during shearing.

The deviator stress (q) was obtained from the deviator force (P) measured by a submersible load cell and the current cross-sectional area of the sample A_c.

$$q = \frac{P}{A_c} \qquad 5.17$$

Figure 5.29 shows the deformation mechanism of the some specimens of the BRS-B material tested in this project. As can be seen the typical mode of deformation of the slurry and compacted samples was mainly of a barrelling type. In the case of the intact specimens, the samples also barrelled but developed more clear shear bands compared with those of the slurry and compacted samples.

Although the stress-strain behaviour at large strains calculated from boundary measurements may not be adequate when shear bands occur, it was decided not to apply the shear band area correction to the samples due to the difficulties in obtaining the real geometry of the shear mechanism. It was considered that the current cross-sectional area of the sample should be calculated using Equation 5.18 assuming that the sample deforms as a right cylinder (Bishop & Henkel, 1957),

$$A_c = A_o \frac{1-\varepsilon_v}{1-\varepsilon_a} \qquad 5.18$$

where A_o is the initial cross-sectional area of the sample.

The initial void ratio of the samples was calculated using Equations 5.1 to 5.4 as described in Section 5.2.1. As mentioned before, accurate initial values of the initial void ratio were essential to ensure the correct location of the compression and

critical state lines in the v:logp' plane. The estimated maximum error in calculating the initial void ratio was less than ±0.025.

(a)

(b)

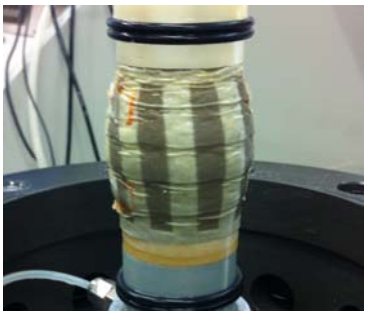

(c)

(d)

(e)

(f)

Figure 5.29 Deformation mechanisms during shearing of (a) slurry sample BRS-B-TS7 (b) slurry sample BRS-B-TS8-ko (c) compacted sample BRS-B-TC2 (d) intact sample BRS-B-TI7 (e) intact sample BRS-B-TI4 and (f) intact sample BRS-B-TI9

5.3.2 Compression behaviour of slurry and compacted samples

A series of triaxial tests were carried out on slurries and remoulded compacted samples from trimmings of the BRS-B block. As described in Section 3.7.2, the

slurry samples were created at different initial water contents to investigate the effect of the initial structure on the compression behaviour as was done with the oedometer specimens. Once the slurry was prepared, it was compressed in a floating ring consolidometer (Figure 3.10) to a targeted stress level (Table 5.6). After consolidation was complete, the samples were extruded from the consolidometer and trimmed to reach the required dimensions. Remoulded statically compacted specimens were also tested to see the influence of the sample preparation technique on the soil behaviour. Table 5.6 shows the details of all the samples tested.

The specimens were isotropically or anisotropically compressed after a back pressure was applied to ensure saturation. Initially, a small isotropic compression was carried out to reach a mean effective stress of 20kPa in the samples before starting to connect the suction cap (Section 3.7.2). Compression was re-started after the suction cap was connected.

Test	e_i	σ'_v (kPa)*	p'_o (kPa) Before shearing	OCR	Type of test	Comments
BRS-B-TS1	0.928	40	400	1	CIU	
BRS-B-TS2	0.862	80	500	1	CIU	Only compression data available
BRS-B-TS4	0.840	113	500	1	CID	Test had to be stopped at ε_a=8%
BRS-B-TS5	0.821	113	200	1	CID	
BRS-B-TS6	0.738	200	100	4	CIU	
BRS-B-TS7	0.843	135	200	1	CIU	
BRS-B-TS8-ko	0.825	100	518	1	CKo	
BRS-B-TC1	0.966		400	1	CIU	
BRS-B-TC2	0.760		545	1	CIU	
BRS-B-TC3	0.765		770	1	CIU	Only compression data available
BRS-B-TC4	0.836		500	1	CIU	
BRS-TC5-ko	0.768		448	1	CKo	Only compression data available

Table 5.6 Summary of the triaxial tests carried out on slurry (TS) and remoulded compacted (TC) samples of the BRS-B clayey silt. (*) Maximum vertical stress applied to the slurry samples in the floating ring consolidometer.

• Isotropic behaviour

The isotropic compression behaviour of the slurry samples can be seen in Figure 5.30. Samples were compressed to a maximum mean effective stress that ranged from 200 to 500kPa and then sheared with an OCR=1. Only sample BRS-B-TS6

was overconsolidated, to an OCR=4. In this case, the term OCR is defined in terms of p'.

Although it can be observed that there is some scatter in the compression lines, a tendency towards a unique isotropic intrinsic compression line (ICL*) can be seen regardless of the initial water content of the samples. This result is in agreement with the oedometer behaviour where a unique 1D-ICL* was also found for the slurry specimens. In the case of sample BRS-B-TS6, a higher difference in the initial void ratio was created compared with the other samples. Its compression line did not reach the ICL* but showed a slow tendency to converge towards it.

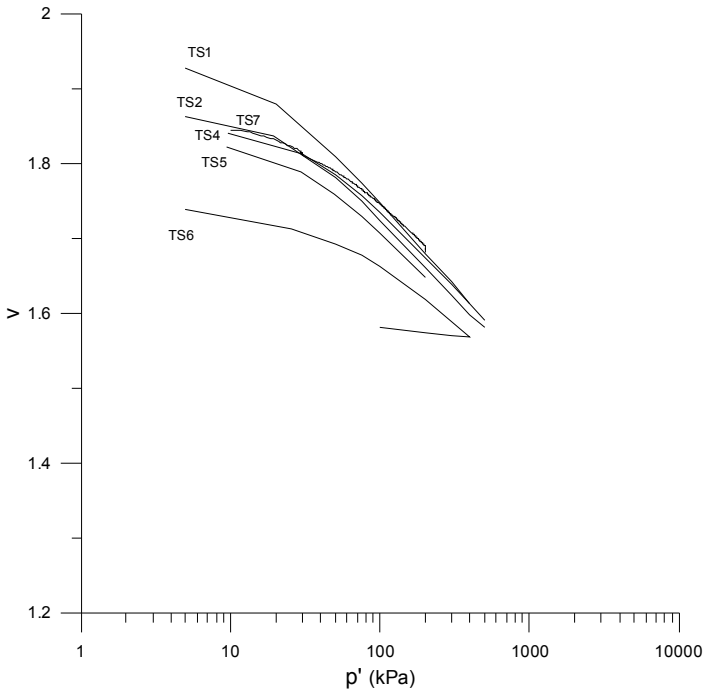

Figure 5.30 Isotropic compression of the slurry samples of the BRS-B clayey silt

As was mentioned above, the slurry samples were initially compressed in a floating ring consolidometer to a target vertical effective stress level (Table 5.6). This initial anisotropic compression imposed a stress history on the samples that created an anisotropic structure. Measurements of the strains during the isotropic compression of the samples provided an excellent way to validate the assumption of isotropy of the samples in order to locate the isotropic ICL*. In the case of an isotropic material, the value of $(\delta v/\delta \varepsilon_a - 3)$ should be equal to zero. Burland (1967) suggested an equivalent quantity, Equation 5.19, as a measure of the isotropy. Equation 5.19 gives an immediate indication of the relative magnitude of the shear strain ($\delta\varepsilon$) in comparison with the volumetric strain (δv), where $\delta\varepsilon_1$ is the axial strain. For an isotropic compression stress increment Burland proposed that if the

value of Equation 5.19 is ±0.05 or smaller it could be assumed that the sample is isotropic.

$$\frac{\delta\varepsilon}{\delta v} = \frac{\delta\varepsilon_1}{\delta v} - \frac{1}{3} \qquad 5.19$$

Figure 5.31 shows values of Equation 5.19 measured for each increment of stress in isotropic compression applied to the slurry samples BRS-B-TS4, BRS-B-TS5 and BRS-B-TS6. The axial strains were calculated using local LVDT's attached to the sample whereas the volumetric strains were measured by an Imperial College designed volume gauge. Specimens BRS-B-TS4 and BRS-B-TS5 were initially compressed in the consolidometer under the same vertical stress of 113kPa and sample BRS-B-TS6 under a vertical stress of 200kPa. Assuming that the coefficient of earth pressure at rest for the normally consolidated samples ($k_{o(NC)}$) is equal to 0.53 (this value is justified in the following paragraphs), these vertical stresses are equivalent to a p'≅76kPa and 136kPa respectively.

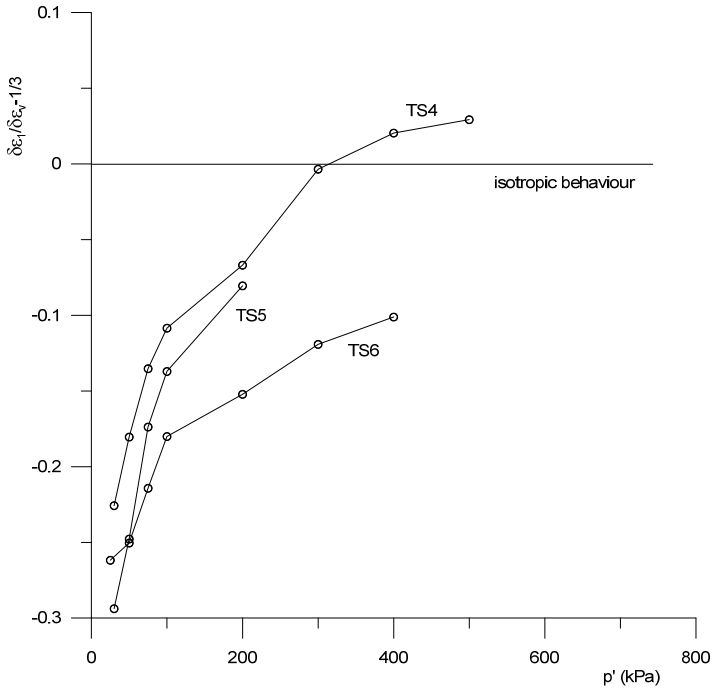

Figure 5.31 Strain ratio measured during the isotropic compression of the slurry samples BRS-B-TS4, BRS-B-TS5 and BRS-B-TS6

From Figure 5.31, it can be observed that initially the samples showed a clearly anisotropic structure that induced anisotropic deformations under the isotropic stress increments. Although the samples were subjected to mean effective stresses

higher than those applied in the consolidometer, only sample BRS-B-TS4 could be considered to have reached a reasonable state of isotropic deformation. Moreover, it can be seen from Figure 5.31 that a mean effective stress of 300kPa was necessary to be applied to sample BRS-B-TS4 to bring it to an isotropic deformation behaviour. This value was four times higher that of the maximum mean effective stress applied during the anisotropic compression in the consolidometer. In the case of samples BRS-B-TS5 and TS6, the ratio between the applied anisotropic mean effective stress and the final isotropic mean effective stress at the last stage of compression was around 2.6 and 2.9 respectively. For these stress ratios, the shear strain measured in the samples due to an isotropic stress increment was around 10% of the volumetric strain and the assumption of the samples being isotropic was questionable. Consequently it could be said that a higher isotropic mean effective stress was necessary to bring these latter samples to a reasonably isotropic state of deformation. This conclusion agrees with the observed tendency in the compression lines to converge onto a unique ICL* at higher stresses for samples BRS-B-TS5 and BRS-B-TS6 (Figure 5.30).

Based on the previous analysis, a unique isotropic intrinsic compression line for the slurry samples was estimated and drawn in Figure 5.32, representing an upper bound for the location of the ICL*. The measured slope of the estimated ICL* in the compression plane v:logp' was C^*_c=0.24, equivalent to a λ^*=0.104 when using the natural logarithmic scale. This value was very close to the slope of the intrinsic one-dimensional compression line obtained in the oedometer tests, C^*_c=0.25. In terms of the swelling behaviour of the triaxial samples, only sample BRS-B-TS6 was overconsolidated, with an OCR=4. An average slope of the swelling line C^*_s=0.024 was measured in the range of stress applied. Obviously, this value was smaller than that measured in the oedometer, where the average slope of the swelling line was calculated over a larger OCR. The relationship between v and p' along the estimated ICL* in the v:lnp' plane is given by Equation 5.20, where N is the extrapolated specific volume at p'=1kPa.

$$v = N - \lambda^* \cdot \ln p' = 2.238 - 0.104 \cdot \ln p' \qquad 5.20$$

Figure 5.33 shows the compression lines of the statically compacted samples together with the slurries. It can be observed that all the compression lines converged towards the same unique compression line regardless of the sample preparation method. Consequently, the sample preparation technique appears to have no influence on the location of the unique isotropic ICL* of the BRS-B clayey silt. This result agrees with the conclusions obtained in the oedometer where all the compression lines converged onto a unique NCL at very large stresses for the slurry and compacted samples. However in the oedometer tests, at lower stress levels, it

could be seen an effect of the initial structure created in the compacted samples at high void ratios that eventually was erased.

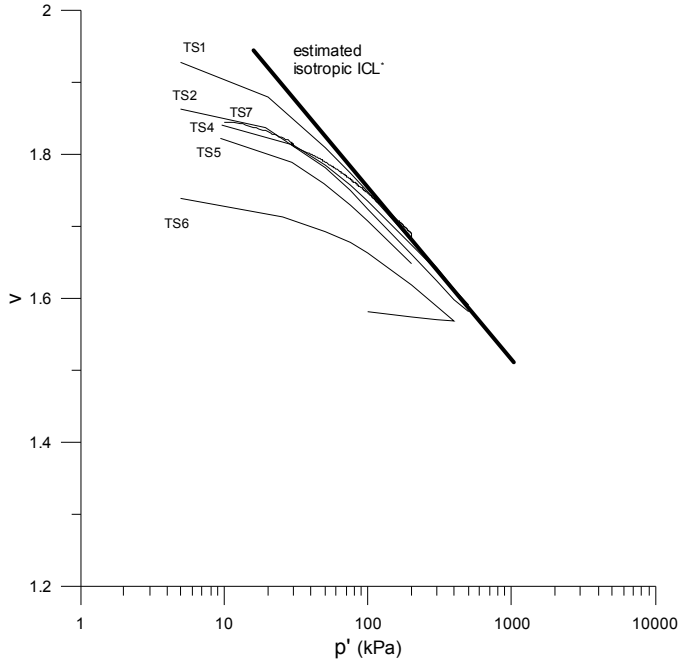

Figure 5.32 Estimated isotropic intrinsic compression line (ICL*) of the slurry samples of the BRS-B clayey silt

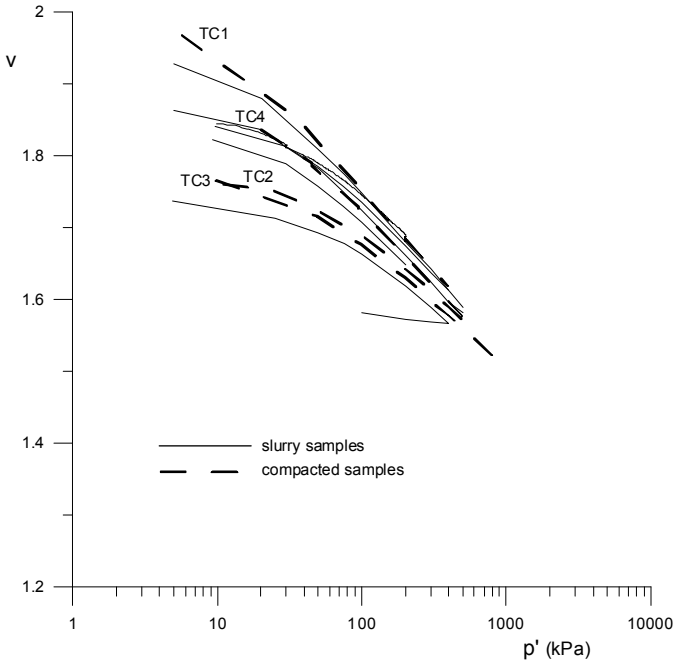

Figure 5.33 Isotropic compression lines of the slurry and compacted samples of the BRS-B clayey silt

• Behaviour under k_o conditions

Two samples, BRS-B-TS8-k_o and BRS-B-TC5-k_o, were anisotropically tested in the triaxial under zero lateral deformation conditions in order to estimate the coefficient of earth pressure at rest (k_o) and the location of the one-dimensional intrinsic compression line (1D-ICL*) in the v:logp' plane. The tests were carried out using a local radial strain transducer attached to the sample as described in Section 3.4.2. Figure 5.34 shows the stress paths followed during k_o conditions of both samples. After an initially isotropic compression stage, the stresses were increased at constant p' until an estimated initial coefficient of earth pressure at rest for normally compressed soils ($k_{o(NC)}$). Subsequently, the radial stress was increased at constant rate under a k_o condition, that was controlled by measuring the radial strain. In addition, sample BRS-B-TS8-ko was subjected to a cycle of unloading and reloading stresses.

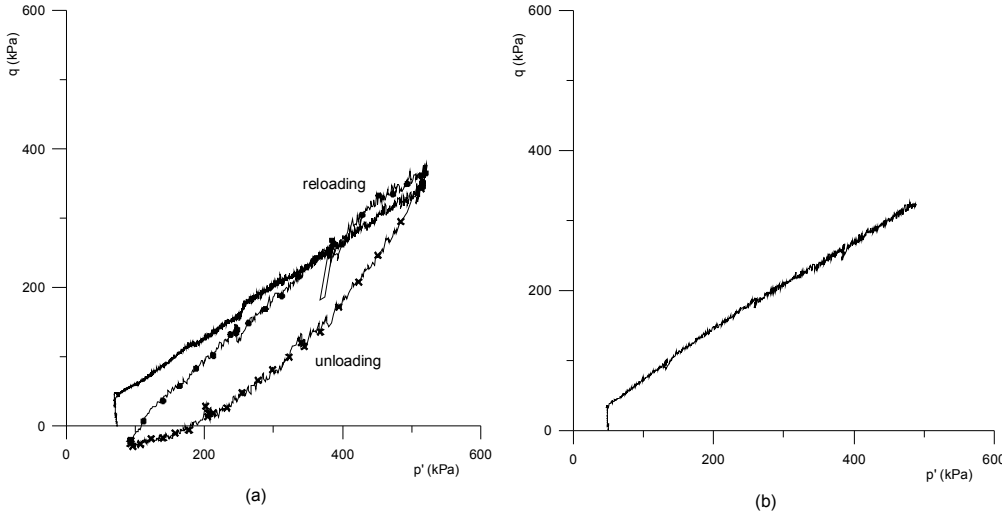

Figure 5.34 Anisotropic stress path under ko conditions of (a) slurry sample BRS-B-TS8-ko and (b) compacted sample BRS-B-TC5-ko

Figure 5.35 shows the stress paths during the first compression stage for both samples. The radial strains throughout the first normal compression stage are plotted in Figure 5.36, showing a clear condition of zero lateral deformation of the specimens. The ratio of the stress components in the p':q plane ($\eta_{ko(NC)}$=q/p') was constant along the normal compression line with a measured value of 0.67 equivalent to an earth pressure coefficient at rest for a normally consolidated state of $k_{o(NC)}$=0.53.

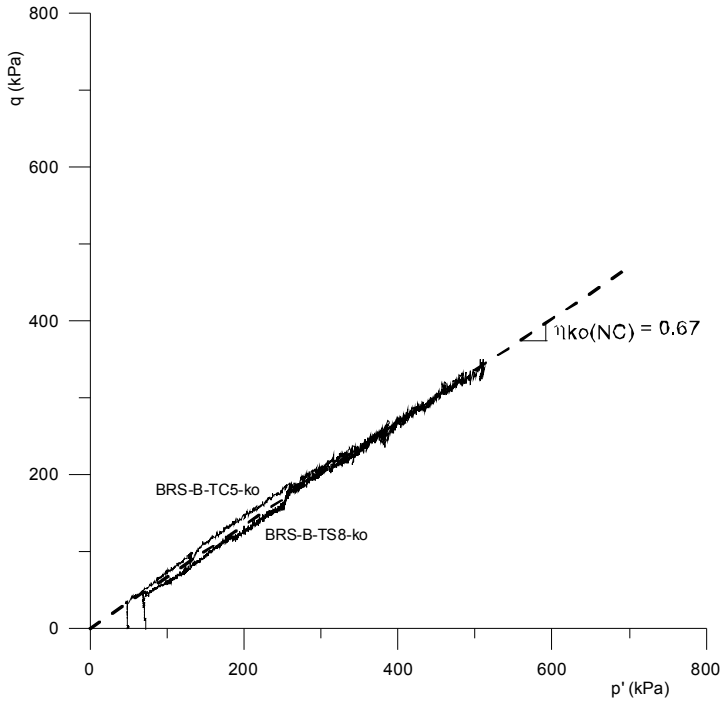

Figure 5.35 ko compression stress path of slurry sample BRS-B-TS8-ko and compacted sample BRS-B-TC5-ko

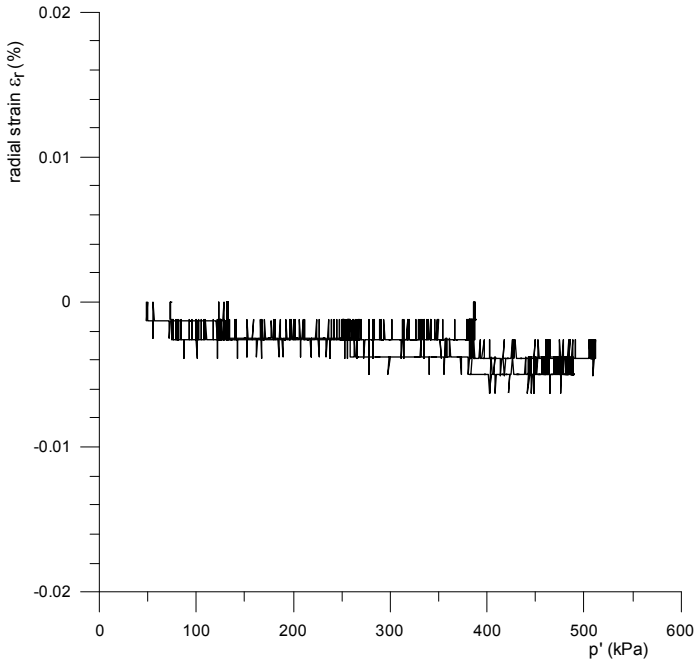

Figure 5.36 Radial strains measured during ko compression of slurry sample BRS-B-TS8-ko and compacted sample BRS-B-TC5-ko

The variation of $k_{o(NC)}$ with p' during the normal compression stage is shown in Figure 5.37. It can be said that, despite the small initial variation, the value of $k_{o(NC)}$ was found to be constant as expected, with an average $k_{o(NC)}$=0.53. One of the most successful semi-empirical expression to estimate the $k_{o(NC)}$ value is that proposed by Jáky (1944), which is $k_{o(NC)}$=1-sinϕ'. As will be shown later, the angle of shear resistance of the BRS-B is equal to ϕ'= 31.5º and by using Jáky's formula a value of $k_{o(NC)}$=0.48 is obtained. This value is slightly smaller than the measured $k_{o(NC)}$=0.53 from the tests.

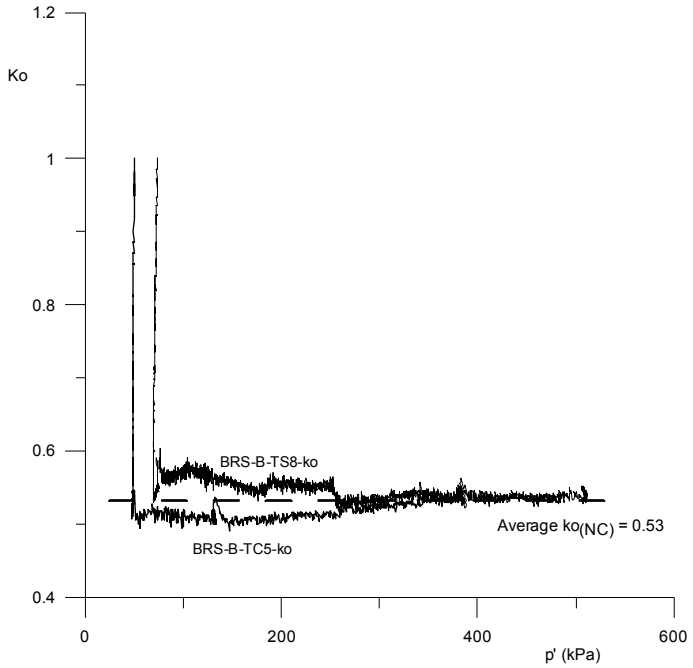

Figure 5.37 Variation of the coefficient of earth pressure at rest during the anisotropic normal compression of slurry sample BRS-B-TS8-ko and compacted sample BRS-B-TC5-ko

As mentioned above, the estimation of the coefficient of earth pressure at rest for normally consolidated soils can be made with a simple equation such as that suggested by Jáky. On the other hand, in the case of overconsolidated soils, the determination of $k_{o(OC)}$ is without any doubt a more complicate task as a consequence of its dependence on whether the sample is on an unloading or reloading stress path. In order to evaluate the dependency of k_o on the stress path and the OCR, sample BRS-B-TS8-ko was subjected to a stress cycle of unloading-reloading as can be seen in Figure 5.38. From the theory of elasticity, if the soil behaves isotropically and elastically immediately on unloading, the initial stress path should be a straight line in the p':q plane. As can be seen in Figure 5.38, in

the case of sample BRS-B-TS8-ko, the unloading produced a clearly curved stress path in the p':q plane even immediately on unloading.

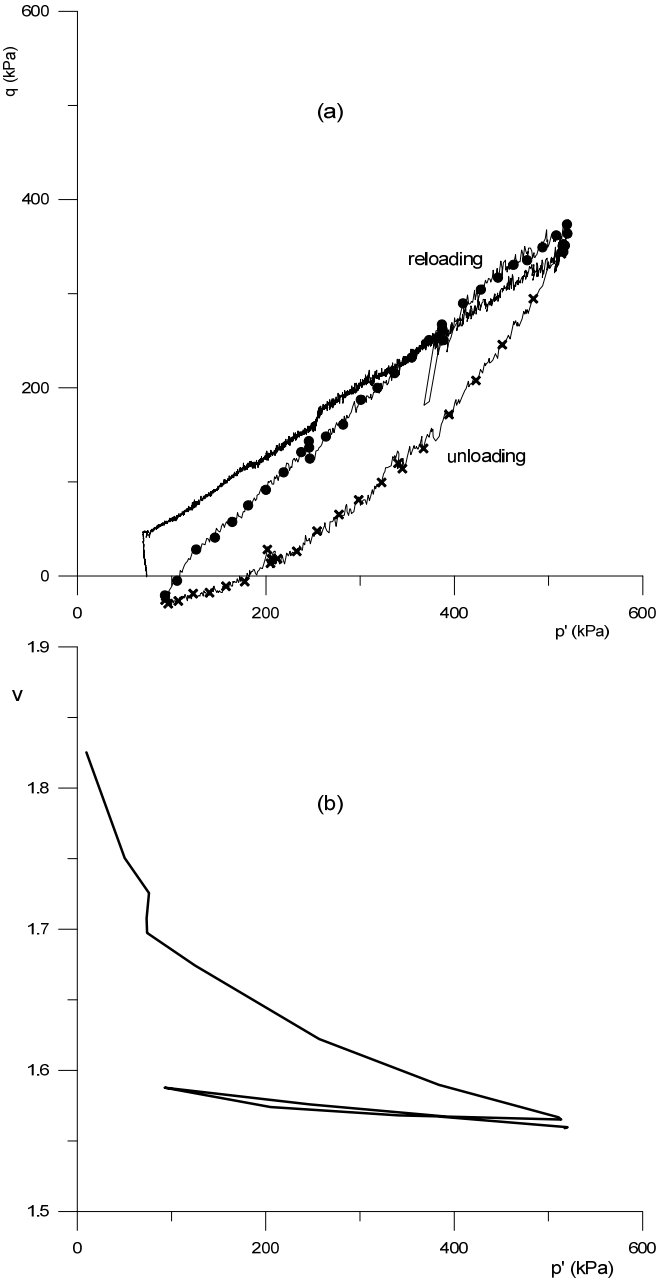

Figure 5.38 Anisotropic stress path under ko conditions of slurry sample BRS-B-TS8-ko in the planes (a) q:p' and (b) v:p'

Based on experimental findings, Wroth (1972, 1975) proposed that the unloading stress path could be represented by a straight line given by Equation 5.21, where m

is the inverse of the gradient of the unloading stress path in the η:ln(p'/p'$_{(NC)}$) plane. A correlation of m with the plasticity index was also suggested by Wroth. Equation 5.21 can be rewritten in the form of Equation 5.22 and therefore the coefficient of earth pressure at rest during unloading $k_{o(OC)}$ can be estimated for a given soil with an effective angle of shear strength ϕ', a plasticity index IP and an OCR.

$$m \cdot (\eta - \eta_{(NC)}) = \ln\left(\frac{p'}{p'_{(NC)}}\right) \qquad 5.21$$

$$m \cdot \left(\frac{3 \cdot \left(1 - k_{o(NC)}\right)}{1 + 2 \cdot k_{o(NC)}} - \frac{3 \cdot \left(1 - k_{o(OC)}\right)}{1 + 2 \cdot k_{o(OC)}}\right) = \mathrm{Ln}\left(\frac{OCR \cdot \left(1 + 2 \cdot k_{o(NC)}\right)}{1 + 2 \cdot k_{o(OC)}}\right) \qquad 5.22$$

Figure 5.39 shows the unloading and reloading stress paths of sample BRS-B-TS8-ko in the η:(p'/p'$_{(NC)}$) and η:log(p'/p'$_{(NC)}$) planes. It can be observed that the unloading stress path in the η:log(p'/p'$_{(NC)}$) plane showed an initial curvature followed by an approximately straight line with a value of m=1.8. This value is higher than the estimated m=1.45 obtained by using the correlation with the plasticity index proposed by Wroth. The unloading stress path was also represented in a natural plane η:(p'/p'$_{(NC)}$) and in this case two clearly straight lines with different slopes could be fitted. The change in slope happened at a stress ratio of around $\eta \cong 0$. When the sample was reloaded from an overconsolidated state, the effective stress path in Figure 5.38(a) rose very steeply and then followed an approximately straight path until the initial $k_{o(NC)}$ was reached. During this reloading path a sudden failure in the control of the test occurred that resulted in a drop of the k_o value. The stresses were then raised again under zero lateral strain to reach the previous condition. It is well known that a very small lateral deformation of the sample could affect the value of k_o and consequently this could be the reason to explain why the reloading stress path crossed $\eta_{ko(NC)}$ and then moved parallel to it with a slightly higher value of η. The reloading stress path was also plotted in the η:(p'/p'$_{(NC)}$) and η:log(p'/p'$_{(NC)}$) planes as shown in Figure 5.39. In both cases, the stress path was clearly curved all along the reloading stage.

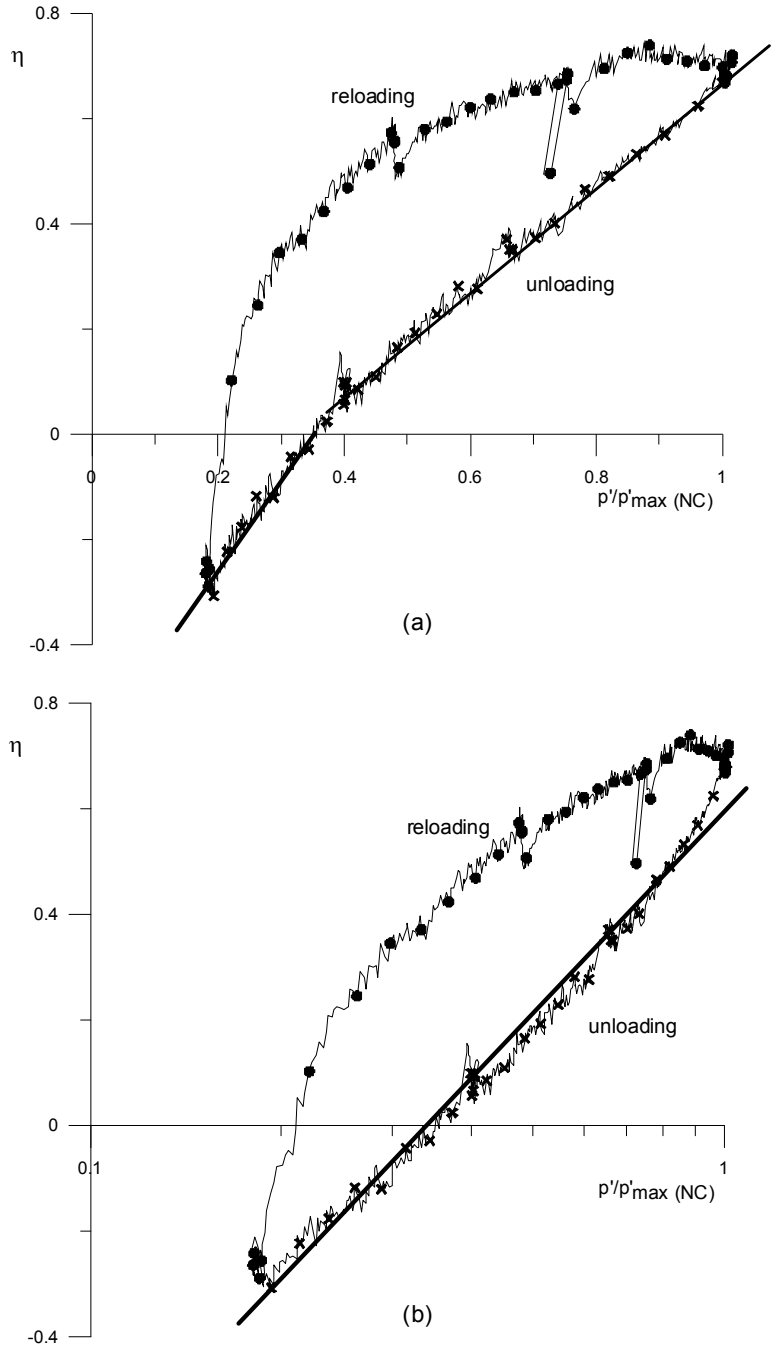

Figure 5.39 Unload-reload stress paths under ko conditions of slurry sample BRS-B-TS8-ko in the planes (a) η:p'/p'$_{max(NC)}$ and (b) η:log(p'/p'$_{max(NC)}$)

The variation of k_o with p' during the whole test is plotted in Figure 5.40. As shown in the previous paragraph, the value of $k_{o(NC)}$ remained constant along the

normal compression stress path. However, when the sample was unloaded, and therefore became overconsolidated, the OCR had a pronounced effect on the value of $k_{o(OC)}$ and also during the reloading stress path. Several empirical correlations have been proposed to calculate $k_{o(OC)}$ through the unloading stress path. One of the most widely used formulas was that given by Schmidt (1966). He found a linear relationship of the form of Equation 5.23 between $k_{o(OC)}$ and the OCR when both values are plotted on logarithmic scales. A number of expressions were suggested for the parameter α.

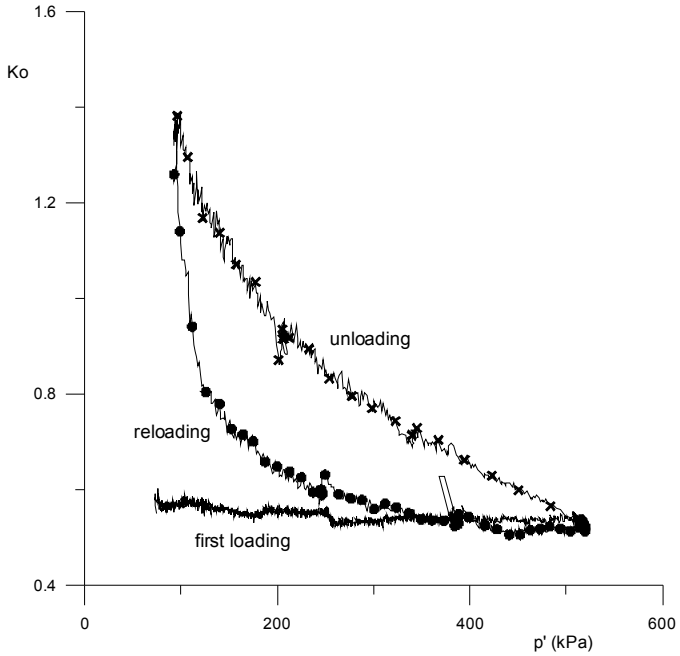

Figure 5.40 Variation of the coefficient of earth pressure at rest with p' for slurry sample BRS-B-TS8-ko

Mayne and Kulhawy (1982) proposed that the best value of α which fitted the experimental data they analysed was $\sin\phi'$. Figure 5.41(a) shows the experimental data of the variation of k_o with the OCR using logarithmic axes for both. It can be observed that during the unloading path, the relationship between k_o and OCR was approximately linear suggesting that an expression of the form of Equation 5.23 could be applied to calculate the value of k_o. Equation 5.22 and Equation 5.23 with $\alpha=\sin\phi'$ were used to estimate the value of k_o. The comparison of the experimental with the computed results can be seen in Figure 5.41(b). Even considering that Equations 5.22 and 5.23 yielded very similar results, none of them provided a good fit with the measured values of k_o. The curvature of the variation of k_o with OCR along the reloading path invalidated any possible matching of the experimental results with Equations 5.22 or 5.23. It could be risky to draw general conclusions about the variation k_o of the BRS-B during the unloading-reloading stress path

based on only one sample, so more tests should be carried out to confirm the observed behaviour.

$$k_{o(OC)} = k_{o(NC)} \cdot OCR^{\alpha} \qquad 5.23$$

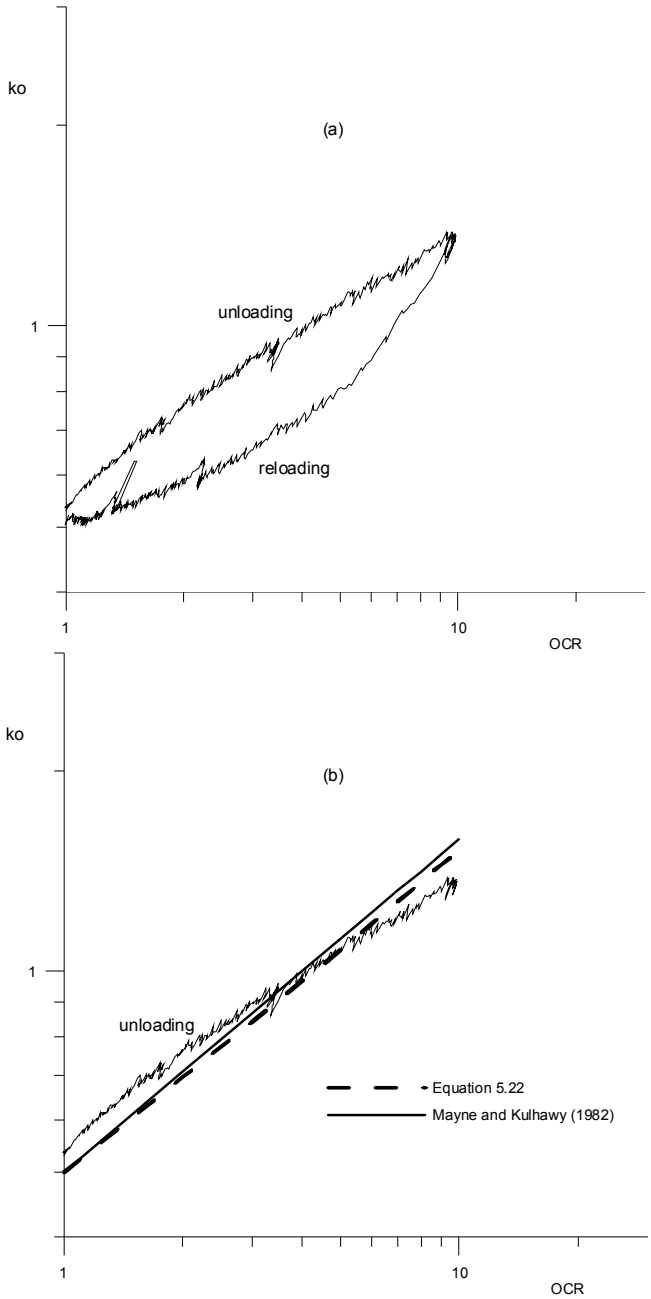

Figure 5.41 Variation of the coefficient of earth pressure plotted against the OCR for slurry sample BRS-B-TS8-ko (a) unload-reload cycle (b) comparison of computed and experimental data

Figure 5.42 shows the one-dimensional compression and swelling lines of samples BRS-B-TS8-k_o and BRS-B-TC5-k_o in the v:logp' plane, where they were compared with the estimated isotropic ICL*. Both k_o compression lines converged into a single line regardless of the sample preparation method. In addition, the oedometer compression line of slurry test BRS-B-OS1 and the estimated 1D-ICL*, defined by Equation 5.6, were also plotted in Figure 5.42. In doing so, the mean effective stress was calculated by using the measured value of $k_{o(NC)}$=0.53. Comparing all the compression lines shown in Figure 5.42, it could be said that the slope of the triaxial k_o samples was smaller compared with the oedometer results for the same range of stresses. The slope of the 1D-ICL* was obtained using the last part of the oedometer compression lines, where the stresses were very high compared with the triaxial and this could be the reason for the difference observed in slope between the ICL* and the 1D-ICL*.

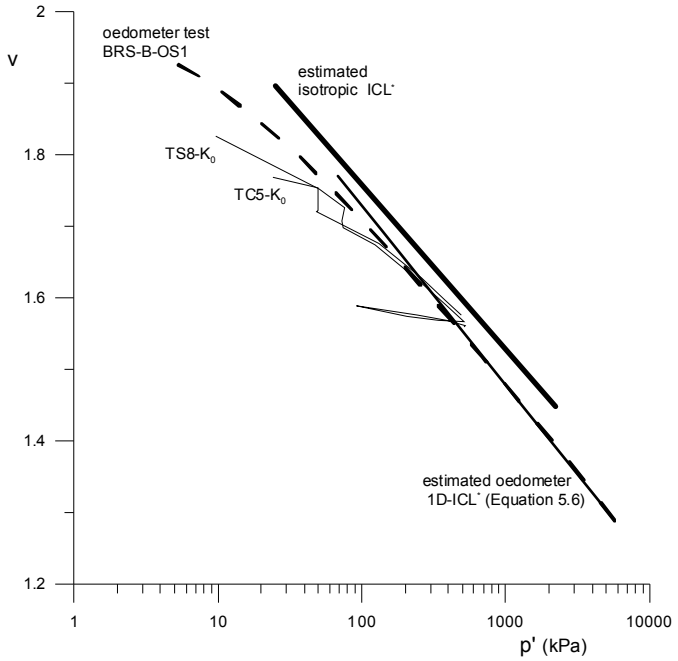

Figure 5.42 ko and isotropic compression lines of the slurry and compacted samples of the BRS-B clayey silt. Comparison with the estimated ICL* and 1D-ICL*

In terms of swelling index, an average slope of C^*_s=0.035 was measured in the k_o unloading-reloading stress path that was a little higher than the isotropic value of 0.024 obtained for a smaller overconsolidation ratio. In order to make a comparison between the isotropic and anisotropic behaviour during swelling, the mean effective stress and the specific volumes of the isotropic BRS-B-TS6 and anisotropic BRS-B-TS8-ko samples were normalised by the maximum mean effective stress (p'_{max}) and corresponding $v_{max(NC)}$ before unloading (Figure 5.43). The results showed that the normalised swelling lines were almost identical and both curved confirming the

unique dependence on p' of the volume changes during unloading. The same behaviour was found by Gens (1982). The curvature of the unloading path did not agree with the habitually assumed straight line in the critical state framework. It was very difficult to give a definitive average value of C^*_s based only on one cycle of unloading or unloading-reloading stress path as in this case. This is due to the influence of the size of the hysteretic loop and also of the maximum p' applied before unloading the sample.

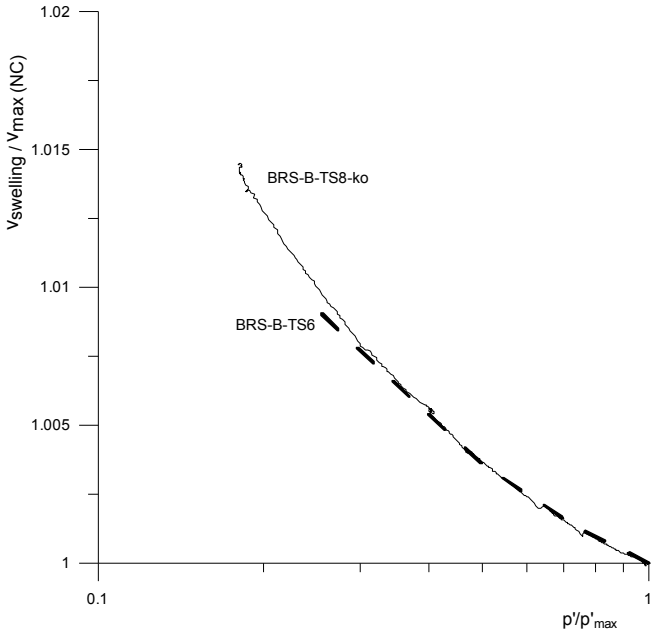

Figure 5.43 Normalized swelling lines of isotropic BRS-B-TS6 and anisotropic BRS-B-TS8-ko samples

5.3.3 Shearing behaviour of the slurry and compacted samples

In this section the influence of the sample preparation technique on the shearing behaviour of slurry and compacted specimens of the BRS-B clayey silt will be examined. In particular, the uniqueness of the critical state line will be investigated. Table 5.6 shows the details of the triaxial tests carried out.

• Large strain behaviour of slurry samples

The stress-strain behaviour of the slurry samples are shown in Figures 5.44 to 5.47. All samples were normally consolidated except BRS-B-TS6 that was overconsolidated with an OCR=4. Before shearing, the samples were isotropically compressed apart from BRS-B-TS8-ko that was subjected to an unloading-

reloading stress path under a k_o condition as shown in Figure 5.38. A barrelling mechanism of failure was observed in all samples at the end of the tests, for which conventional rough ends were used. No clear evidence of slip failure surfaces was visible in any case as can be seen in Figure 5.29(a)(b).

The variations of deviator stress (q), increment of pore water pressure (Δu) and mean effective stress (p') during undrained shearing are plotted in Figure 5.44. The behaviour of the normally consolidated samples was initially contractant, which corresponded to an increase in the pore water pressure. This behaviour changed to a dilatant mode at axial strains of about 5.5%, where the Δu reached a very smooth peak and the mean effective stress was at its minimum value. The point where the soil changes from a contractant to a dilatant behaviour is termed the phase transformation (Ishihara et al. 1975) and is a characteristic response of clean sands and granular soils with a relatively low quantity of fines (e.g. Georgiannou et al. 1990). After the phase transformation point, the mean effective stress increased and finally reached a constant value that could be associated to a critical state. This behaviour can also be observed in Figure 5.45. The undrained effective stress paths initially curved to the left associated to a contractant behaviour and then reached the phase transformation point where the soil started to dilate, climbing at a constant stress ratio until the end of the test.

The same dilatant response was also observed in slurry samples of a silty soil tested by Nocilla et al. (2006) and shown in Figure 4.24. As was described in the detailed literature review in Section 4.3, Nocilla's soil has the same origin and mineralogy as the BRS-B clayey silt. Moreover, one of the four gradings tested in her research, the 25% clay content, also has a very similar particle size distribution to the BRS-B clayey silt.

In Figure 5.44, during shearing the deviator stress in all tests was increasing until reaching a steady value at large deformations. Only sample BRS-B-TS8-ko exhibited a slight peak deviator stress before the end of the test.

In terms of pore water pressure, the ratio of $\delta(\Delta u)/\delta\varepsilon_s$ tended towards zero at the end of the test in all cases, apart from the overconsolidated sample BRS-TS6. Initially, this sample showed a very small positive Δu followed by a dilatant response until the end of the test. The deviator and mean effective stresses seemed to reach constant values at large strains whereas the increment of pore water pressure was still decreasing, suggesting that the critical state was not achieved at the level of strains reached at the end of the test.

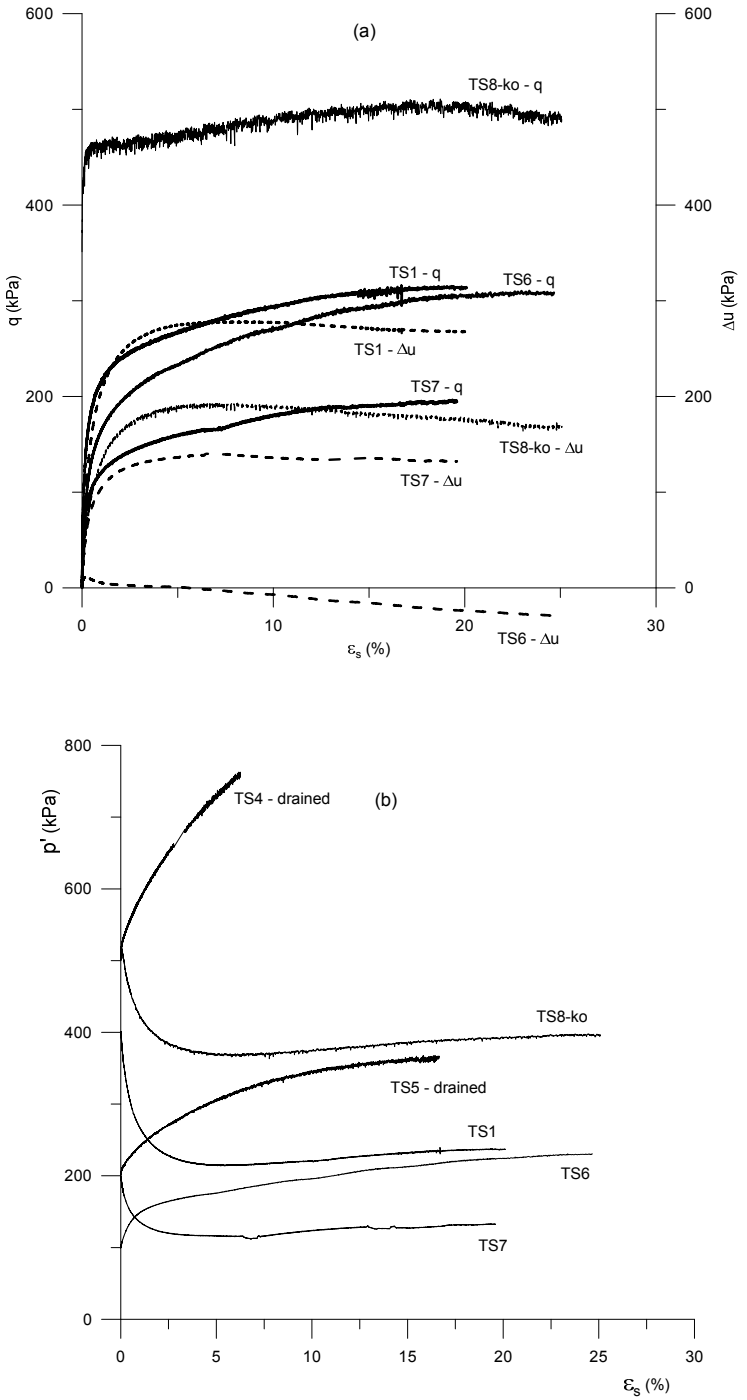

Figure 5.44 Variation of (a) deviator stress and increment of pwp and (b) mean effective stress during undrained shearing of BRS-B slurry samples

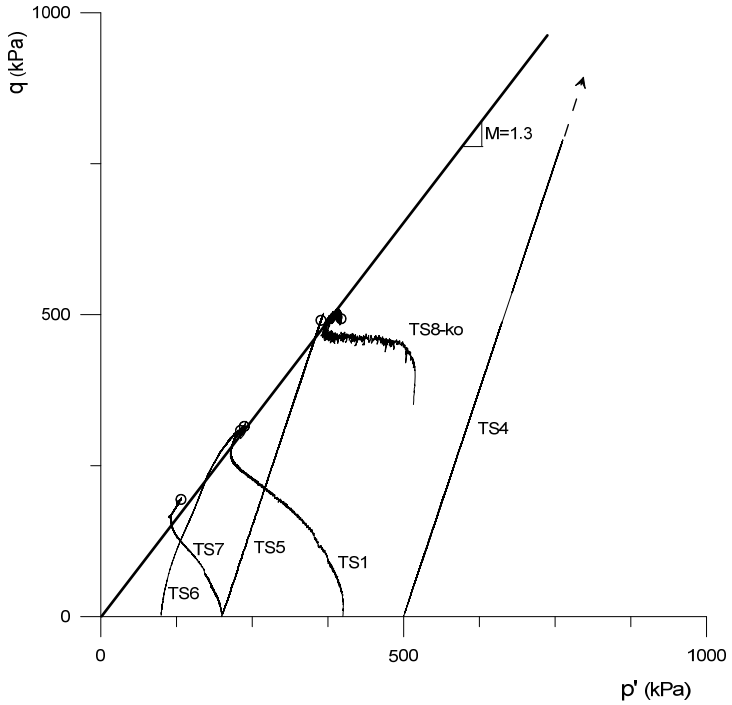

Figure 5.45 Undrained and drained stress paths of slurry samples of the BRS-B

In addition to the undrained tests described above, two drained tests were performed on samples BRS-B-TS4 and BRS-B-TS5. Both samples were normally consolidated before shearing. Figure 5.46 shows the deviator stress and volume strain during shearing. In both cases the behaviour was contractant as expected. For the case of sample BRS-B-TS5, it can be observed that the deviator stress and volume strain seemed to reach a fairly constant value at the end of the test which could be associated to a critical state. The variation of the mean effective stress during the test for this sample was also plotted in Figure 5.44(b) where the value of p' was slightly increasing at the end of the test. Unfortunately, the test on sample BRS-B-TS4 had to be stopped at an early axial strain of around 8% and the deviator stress and volume strain were clearly increasing at the end of the test. The stress paths for these tests are shown in Figure 5.45 where the arrow indicates the incompleteness of test BRS-B-TS4. The location of the intrinsic critical state line (CSL*) in the p':q plane was constructed using the stress state at the end of the tests as shown in Figure 5.45. The slope of the estimated CSL* was M=1.3 which is equal to the value obtained by Nocilla et al. (2006) for their silty samples (Figure 4.24).

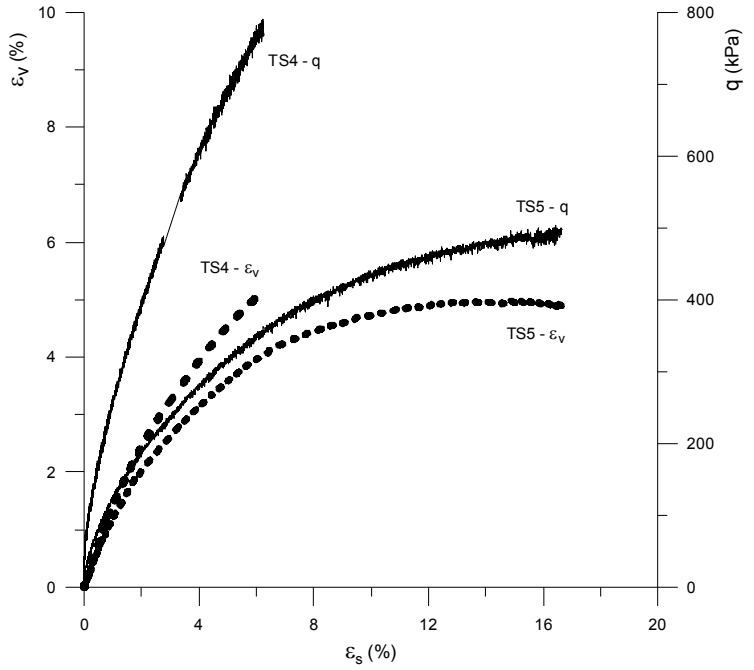

Figure 5.46 Variation of deviator stress and volume strain during drained shearing of samples BRS-B-TS4 and BRS-B-TS5

The stress ratio (η=q/p') is plotted against shear strain in Figure 5.47 for all the slurry samples. Despite of the higher value of η observed for sample BRS-B-TS7, the overall behaviour in undrained shearing was similar and tended towards to the same stress ratio at the end of the test. As expected, the initial stiffness of the overconsolidated sample BRS-B-TS6 was higher than those of the normally consolidated. Its stress ratio showed a very smooth peak at a shear strain of around 10% and then started to decrease towards a critical state which confirmed the ongoing dilatant response observed in Figure 5.44, where the increment of pore water pressure was still decreasing at the end of the test. The anisotropically compressed sample BRS-B-TS8-ko exhibited an initially stiffer response similar to that of the overconsolidated sample BRS-B-TS6. It also showed a smooth peak, followed by a very slow decrease of the stress ratio until the end of the test, where the final value of η was slightly lower compared with the other specimens. In terms of the drained tests, only sample BRS-B-TS5 was sheared to a sufficient shear strain to reach an apparent critical state. The stress ratio at the end of the test was equal to that observed for the undrained samples. The estimated average value of the stress ratio at the critical state (M=q/p') was again equal to 1.3, the same as the estimated slope of the critical state line in the p':q plane.

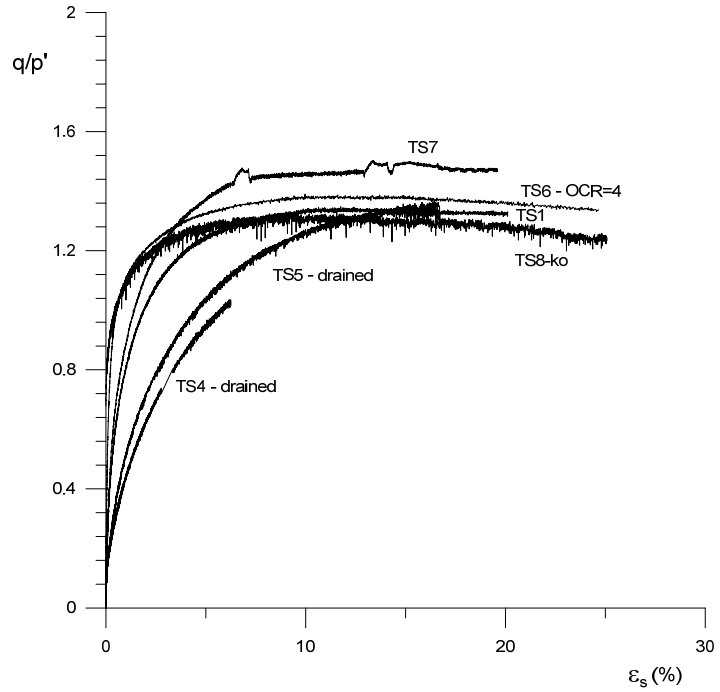

Figure 5.47 Normalized stress-strain behaviour for the slurry samples of the BRS-B

The shearing data of all the triaxial tests for the slurry specimens are plotted in Figure 5.48 together with the estimated isotropic intrinsic compression line (ICL*). The end of test points are represented by a circle and the small arrows indicate the direction that incomplete tests were travelling in when the tests were stopped. Based on the discussion presented above, the location of the end of the tests and the direction in which the incomplete tests were moving in, it could be said that a unique critical state line could be found in the v:logp' plane for the slurry samples. This intrinsic critical state line (CSL*) is parallel to the estimated ICL* for the range of stress applied, which agrees with the critical state framework. The intercept of the estimated CSL* with the v axis at a p'=1kPa was equal to Γ=2.179. Equation 5.24 represents the specific volume at the critical state for each p' in the v:lnp' plane.

$$v_{cs} = 2.179 - 0.104 \cdot \ln p' \qquad 5.24$$

Figure 5.49 shows the measured undrained shear strength (s_u=q/2) as a function of the specific volume at the end of the undrained tests, together with the estimated CSL* and ICL* in the v:logp' plane. It can be observed that, for the normally consolidated samples that reached the critical state, s_u plots along a line that is parallel to the CSL* and ICL*. Sample BRS-B-TS7 showed a slightly higher value of s_u compared to that expected. This difference was due to the fact that the value

of M measured at the end of the test was above the average M=1.3. In the case of the overconsolidated sample BRS-B-TS6, the measured s_u at the end of the test was lower than expected due to the fact that the sample did not reach the critical state. Although more tests should be carried out to confirm this behaviour, it could be said that there is a unique relationship between undrained shear strength and the specific volume for the BRS-B clayey silt, as the critical state framework would predict. Based on the above results, it could be added that this unique relationship is independent of the compression path followed before shearing, as demonstrated by the s_u measured for the k_o compressed sample BRS-B-TS8-k_o.

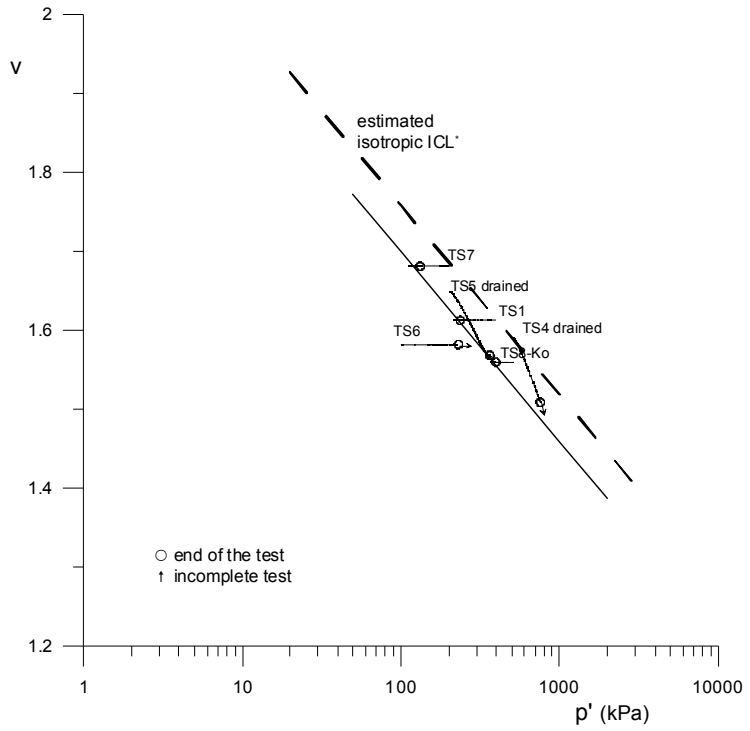

Figure 5.48 Shearing stress paths in the v:logp' palne for the slurry samples of the BRS-B

An attempt to normalise the shearing data was carried out in Figure 5.50. Assuming uniqueness of the CSL* in the v:lnp' plane, the stress path for each sample was normalised by using the equivalent mean effective pressure on the critical sate line (p'_{cs}) as suggested by Atkinson (1993) and defined in Equation 5.25.

$$p'_{cs} = e^{\left(\frac{\Gamma - v}{\lambda}\right)} \qquad 5.25$$

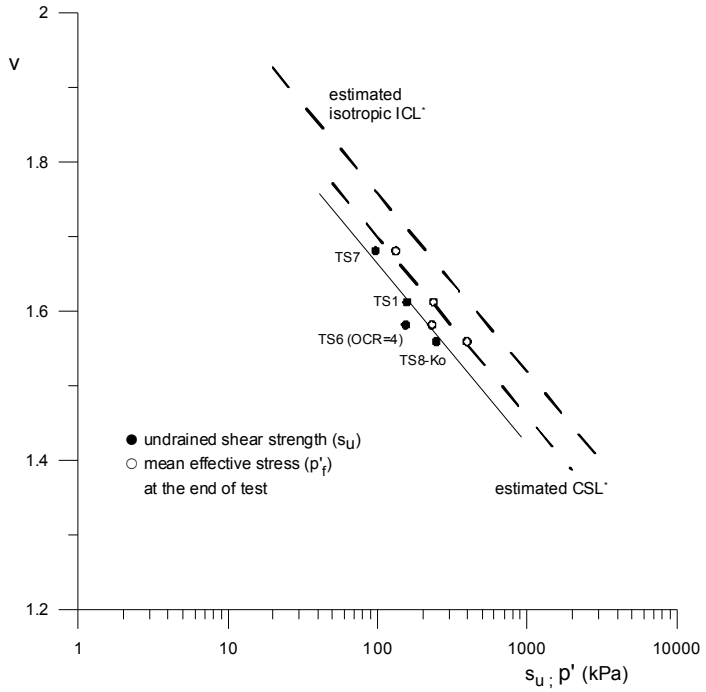

Figure 5.49 Relationship between undrained shear strength and specific volume for the slurry samples of the BRS-B

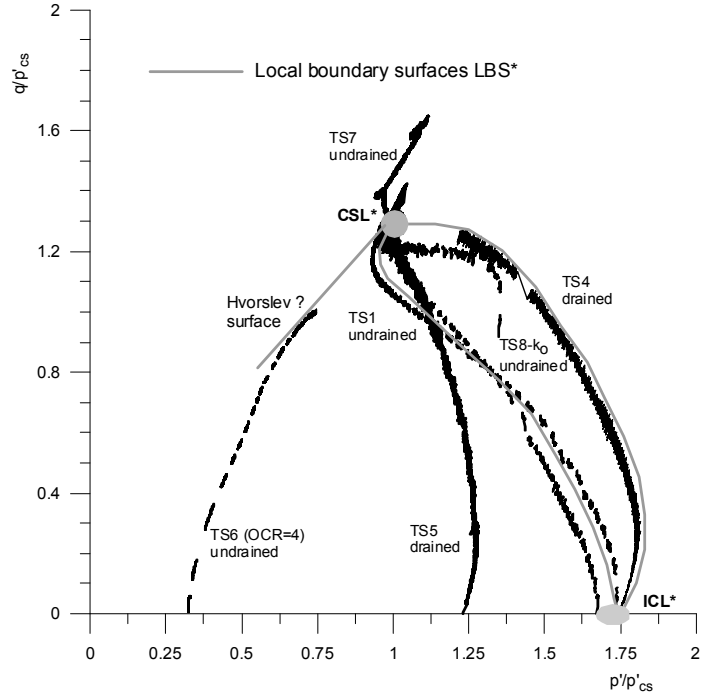

Figure 5.50 Normalized triaxial shearing data of slurry samples of the BRS-B using equivalent pressures on the intrinsic critical state line (CSL*)

As can be observed in Figure 5.50, even though all tests on the wet side of the CSL* were normally consolidated, the shearing started from different distances to the CSL*, depending whether their corresponding isotropic compression lines ended on the unique ICL* or were still moving towards it, as in the case of sample BRS-B-TS5 (Figure 5.32). In addition, it should be taken into account the small scatter observed in the location of the compression lines, due to small errors in estimating the initial void ratio. The normalised paths for samples BRS-B-TS1, BRS-B-TS5 and BRS-B-TS8-ko showed that a unique critical state was reached at the end of the tests with a value of $q/p'_{cs} \cong 1.3$ at $p'/p'_{cs}=1$. As mentioned above, the drained test BRS-B-TS4 had to be stopped at a low axial strain, but its normalised path tended to move towards the unique critical state define by the other samples. In the case of sample BRS-B-TS7, initially, its response was similar to the isotropic undrained sample BRS-B-TS1. At larger strains, the dilatant "tail" of the stress path was moving towards a slightly different critical state. For the case of the overconsolidated sample BRS-B-TS6, the normalised path showed that the sample was still clearly dilating and perhaps moving along the Hvorslev surface towards the critical state. More tests should be performed on heavily overconsolidated specimens to define properly the Hvorslev surface.

Another aspect of the BRS-B clayey silt response was that Rendulic's principle did not apply, as the normalised path of the drained BRS-B-TS4 and undrained BRS-B-TS8-ko samples plotted outside those of the isotropically normally consolidated undrained specimens BRS-B-TS1 and BRS-B-TS7. The local sate boundary surface (LBS*) defined by tests BRS-B-TS1 and BRS-B-TS7 was pushed out, showing the dependency of the LBS* on the type of test. This feature was observed initially by Gens and Potts (1982) for a well-graded glacial till. Nocilla et al. (2006) also found the same behaviour for their silty soil (Figure 4.26). Therefore, a more extensive programme of drained tests at different stress ratios should be carried out to identify more accurately the intrinsic state boundary surface (SBS*) for the BRS-B soil. Unfortunately only one test was carried out on the dry side of the CSL* and that was not enough to locate the Hvorslev surface as mentioned above. Finally, and based on the set of tests performed, an estimate of the intrinsic local boundary surfaces is drawn in Figure 5.50.

• Large strain behaviour of the compacted samples

The stress-strain behaviour of the statically compacted samples is shown in Figure 5.51. All the samples were normally consolidated and sheared undrained. As in the case of the slurry specimens, the failure mechanism was of a barrelling type,

showing no evidence of slip failure surfaces (Figure 5.29c). The details of each test are summarized in Table 5.6.

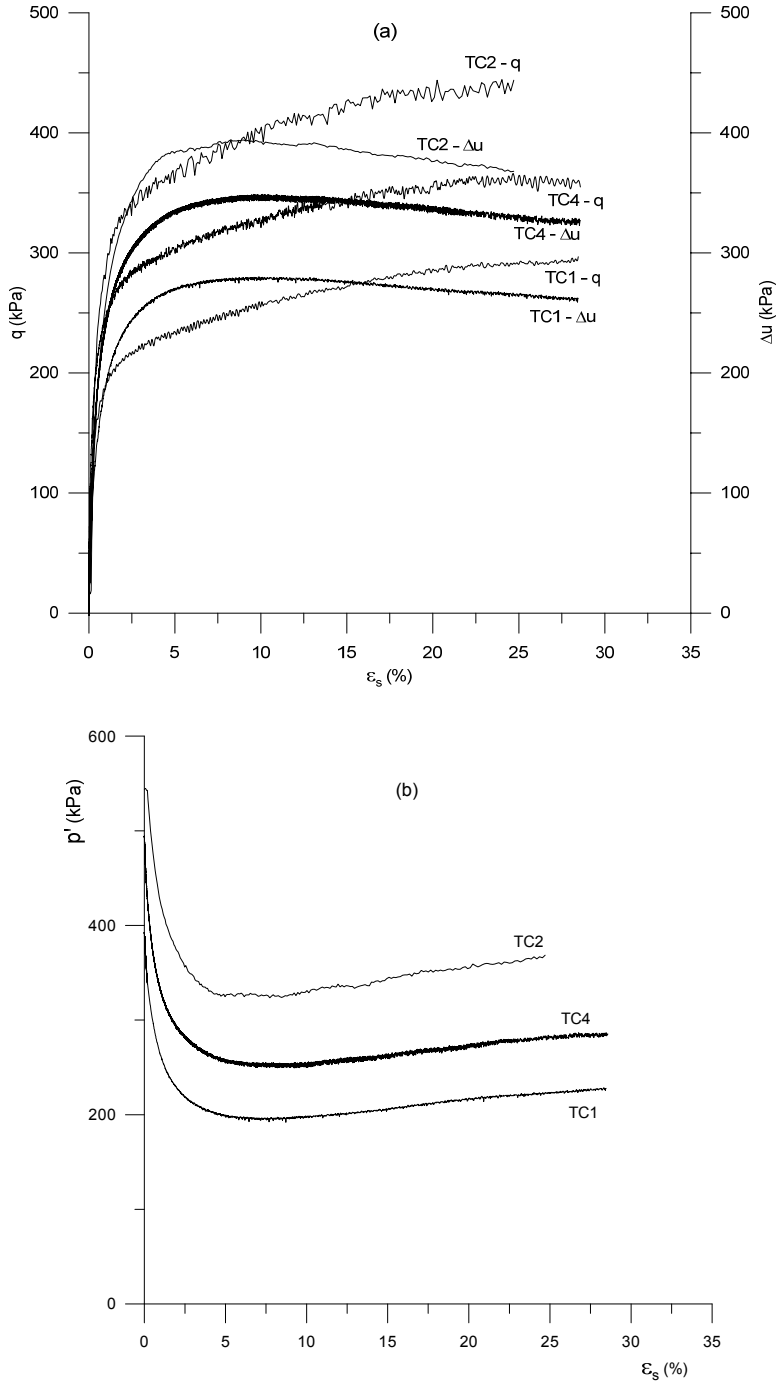

Figure 5.51 Variation of (a) deviator stress and increment of pwp and (b) mean effective stress during undrained shearing of compacted samples of the BRS-B

The overall stress-train behaviour of the compacted samples was the same as the slurry samples. Initially all samples displayed a contractant response followed by a change to a dilatant mode after the phase transformation point (Figures 5.51b and 5.52). The shear strain at the phase transformation point was around 9% for the three samples as can be observed in Figure 5.51. This value was higher than the 5.5% measured for the normally consolidated slurry samples. In terms of critical state, the deviator stress reached a clearly steady value for sample BRS-B-TC4 while for the other two samples it was still slightly increasing. The ratios of $\delta(\Delta u)/\delta\varepsilon_s$ and $\delta p'/\delta\varepsilon_s$ tended towards zero at the end of the tests although some small increment could also be observed.

Figure 5.52 shows the undrained stress path in the p':q plane. As in the case of the slurry samples, the stress paths curved to the left associated to a contractant behaviour and then reached the phase transformation point where the soil started to dilate, climbing at a constant stress ratio until the end of the test. The shape of the stress paths was essentially the same for tests BRS-B-TC1 and BRS-B-TC4, while sample BRS-B-TC2 displayed a stiffer behaviour at small strains. This may be due to the fact that, at the start of the shearing stage, the rate of shearing was four times higher than the other two samples. After the samples reached a shear strain of 0.2%, the rate of shearing was the same for the three samples and the stress paths were homothetic until the ends of the tests. The estimated intrinsic CSL* defined by the slurry samples is also included in Figure 5.52 as a reference for comparison with the compacted samples. It can be seen that, apart from sample BRS-B-TC2, the stress ratios at the end of the tests plotted along the CSL*. In the case of sample BRS-B-TC2 the value of M was slightly lower as can also be observed in Figure 5.53, where η was plotted against the shear strain.

Many authors concluded that for sandy soils the slope of the critical state line in the p':q plane is approximately the same as the line defined by the stress ratio at the phase transformation point (e.g. Been et al, 1991; Ishihara, 1993). In the case of the compacted samples of the BRS-B clayey silt, the stress ratio at the phase transformation point did correspond approximately to the value at the critical state for samples BRS-BTC1 and BRS-B-TC4 (Figure 5.52). This feature was also observed in the case of the slurry samples (Figure 5.45).

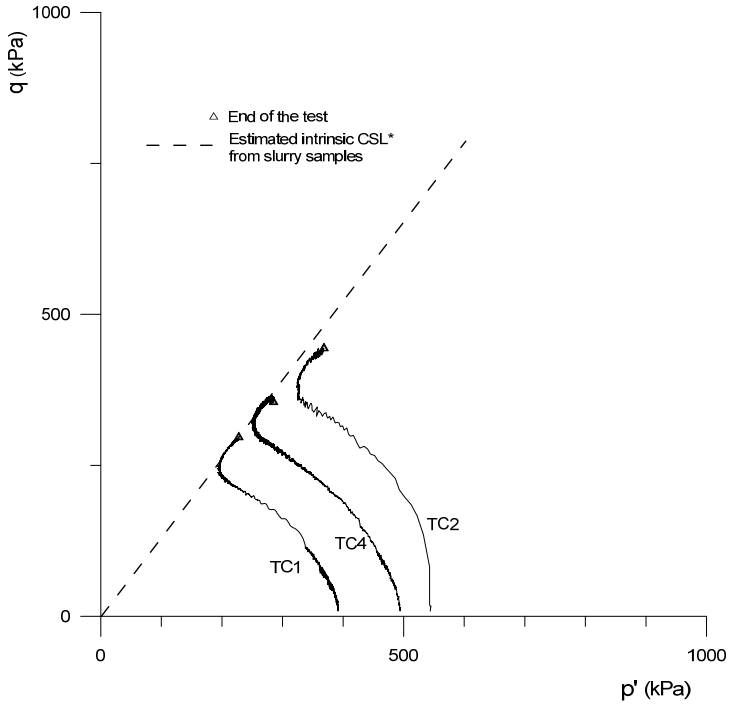

Figure 5.52 Undrained stress paths of compacted samples of the BRS-B

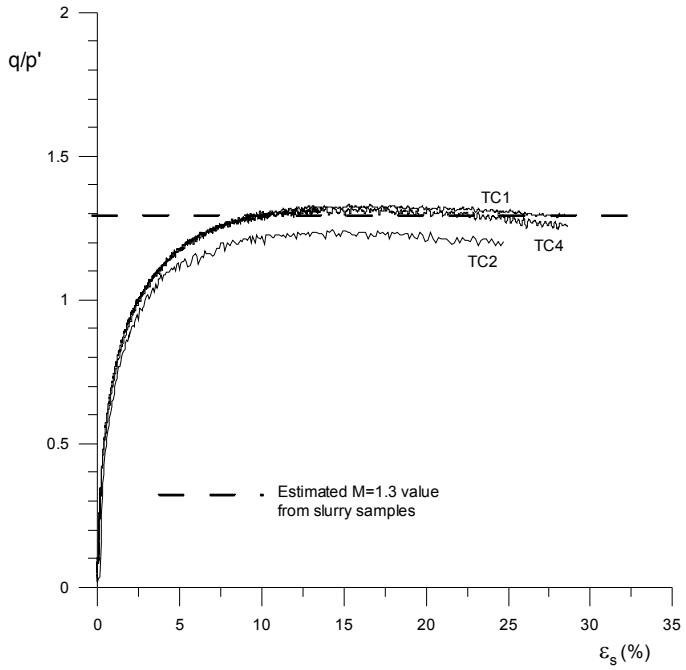

Figure 5.53 Normalized stress-strain behaviour for the compacted samples of the BRS-B

One of the questions to be answered in this research project was about the influence of the sample preparation technique on the behaviour of the BRS-B clayey soil, in particular the effect on the uniqueness of the CSL in the compression plane. Figure 5.54 shows the stress-volume states at the ends of the tests in the v:logp' plane for all the slurry and compacted samples. The line represents the estimated intrinsic CSL* defined by the slurry specimens. As can be observed, and having taken into account possible small errors in calculating the initial void ratio, the stress states for the compacted samples lie on the CSL*, proving that there exists a unique intrinsic critical state line in the compression plane despite the sample preparation technique.

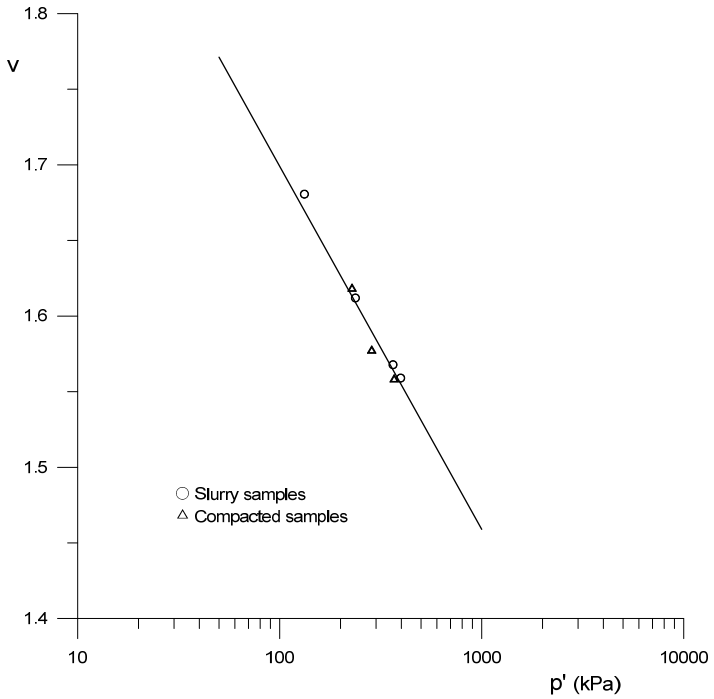

Figure 5.54 Unique critical state line for the slurry and compacted samples of the BRS-B

As was done with the slurry samples, the undrained shear strength (s_u) at the end of the test was measured for the compacted samples and compared with the values obtained for the slurry specimens. Figure 5.55 shows the values of the measured s_u as a function of the specific volume at the end of the test. The unique intrinsic CSL* defined in Figure 5.54 was also include in the figure. It can be seen that apart from the slurry sample BRS-B-TS7 tested at a higher specific volume and analysed in the previous paragraphs, a unique line could be fitted. This line is also parallel to the unique CSL* as would be expected from the critical state framework.

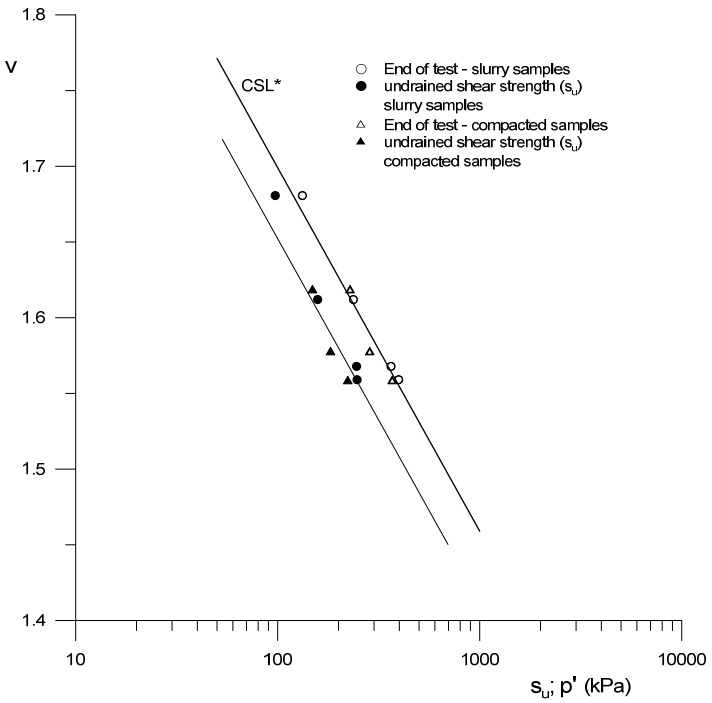

Figure 5.55 Relationship between undrained shear strength and specific volume for the slurry and compacted samples of the BRS-B

5.3.4 Compression behaviour of intact samples

As was mentioned in Section 5.2.2, one of the main objectives of this research was to investigate the effect of the in-situ structure on the compression and shearing behaviour of the recently deposited alluvial BRS-B clayey silt. In doing so, a series of triaxial tests on intact samples were carried out. The specimens were trimmed from the block sample as described in Section 3.7.1. Table 5.7 summarises the details of each test.

Figure 5.56 shows the compression lines for all the isotropically compressed intact samples in the v:logp' plane. The observed variability in the initial void ratio was also seen in the oedometer tests performed on intact samples and, as discussed in previous sections, it was related to an in-situ heterogeneous structure. In Figure 5.56 it can be seen that the initial parts of the lines run quasi-parallel to each other with small slopes indicating a high stiffness. This behaviour was also identified in the oedometer tests on intact samples (Figure 5.11).

Test	e_i	p'$_o$ (kPa) Before shearing	OCR	Type of test	Comments
BRS-B-TI1	0.799	400	1	CIU	
BRS-B-TI2	0.721	200	1	CIU	
BRS-B-TI3	0.872	500	1	CIU	Hole in the sample
BRS-B-TI4	0.673	2000	1	CIU	50mm sample 7 MPa cell
BRS-B-TI7	0.721	300	1	CIU	
BRS-B-TI9	0.690	4000	1	CIU	50mm sample 7 MPa cell
BRS-B-TI10	0.730	300	1	CID	Test had to be stopped at ε_s=7.5%
BRS-B-TI11	0.764	100	1	CID	Only compression data avalaible

Table 5.7 Summary of the triaxial tests carried out on intact samples of the BRS-B clayey silt.

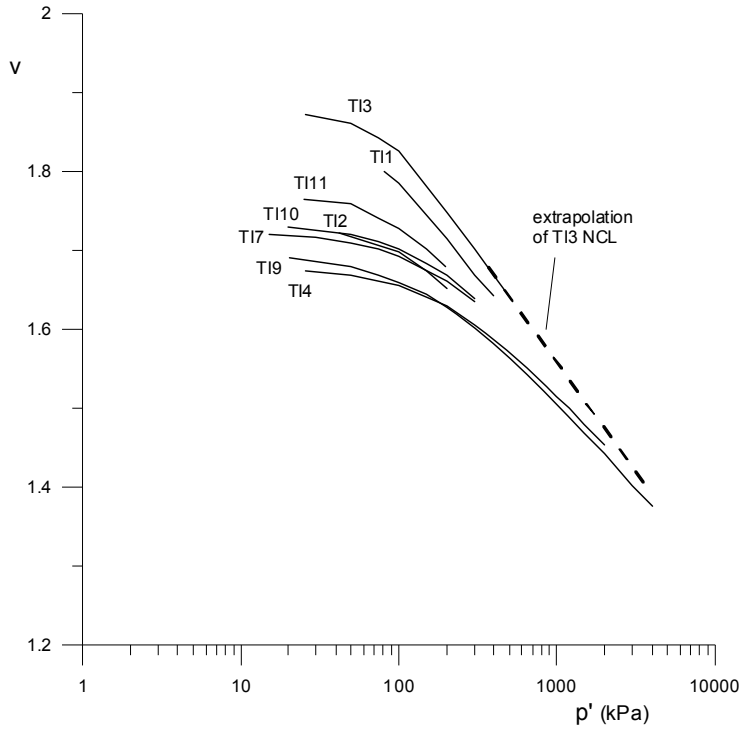

Figure 5.56 Isotropic compression lines for the intact samples of the BRS-B

It is interesting to point out that, for the stress levels reached commonly in conventional triaxial cells, where the maximum mean effective stress is usually lower than 500kPa, the compression lines do not converge onto a unique isotropic NCL. This characteristic soil response, that is generally a feature of granular materials, could lead to the erroneous idea of a possible transitional behaviour where the location of the compression lines in the v:logp' plane depends on the initial density of the samples. However, it seems that following the slope of the last part of the compression line of sample BRS-B-TI3, and extrapolating its behaviour to larger stresses (dashed line), it will eventually converge onto a unique NCL. Consequently, it could be said that very large stresses of several MPa would be required to make the compression lines to converge onto a unique isotropic normal compression line. In fact, this was also the case of the intact samples tested in the oedometer, where the convergence towards a unique normal compression line took place at very high stress levels (Figure 5.11).

The comparison of the compression lines of the intact samples with the estimated isotropic ICL*, defined by the slurry specimens, is shown in Figure 5.57. The compression lines of samples BRS-B-TI1 and BRS-B-TI3 clearly crossed the ICL*, and after yield, they remained quasi-parallel to the ICL* showing the effect of the in-situ structure of the intact samples on the compression behaviour. As pointed out above, it seemed that the compression line of sample BRS-B-TI3 will eventually converge onto a unique normal compression line, that apparently correspond to the isotropic ICL*. This hypothesis seems to be confirmed by the compression lines of samples BRS-B-TI4 and BRS-B-TI9, that were tested to higher stresses and appeared to have reached the ICL*. In the case of the other specimens, with initial densities between the densest and the loosest, it can not be concluded whether their compression lines would have crossed the ICL* or followed the ICL* at higher stress levels. It also appears that the effect of the in-situ structure reduces as the void ratio decreases e.g. samples BRS-B-TI4 and TI9. This feature of the soil behaviour has been observed by others researchers and they concluded that it may be an artefact of the method of comparison (e.g. Gaspare, 2005 and Hosseini Kamal et al, 2014).

In any case, the compression behaviour of samples BRS-B-TI1 and BRS-B-TI3 showed a clear effect of their in-situ structure compared with the slurry samples. Moreover, the fact that the compression lines of these two samples did not show any sign of convergence towards the ICL* during the post-yield behaviour, in the range of stresses applied, could be a sign of a stable structure. As originally suggested by Coop et al. (1995), stable structures in soils are mainly due to the effect of fabric. Consequently, the main difference in the compression behaviour between these two intact samples and the ICL* could be associated to an initial robust fabric that could not be erased in the range of stresses applied. According to

this hypothesis, it could be said that any possible initial bonding in the samples had a minor impact on the soil response.

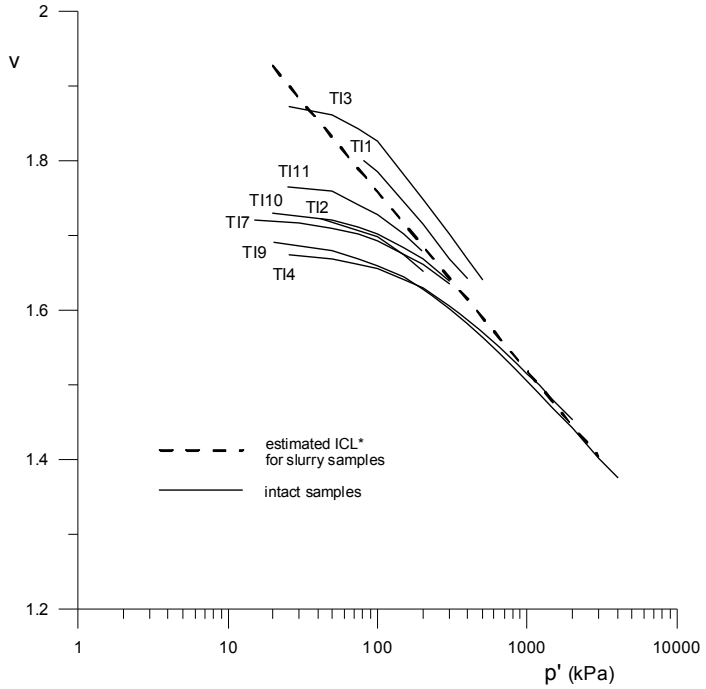

Figure 5.57 Isotropic compression lines of the intact samples of the BRS-B. Comparison with the isotropic ICL* defined by the slurry samples

In terms of the sensitivity framework (Cotecchia & Chandler, 2000), it was found that the stress sensitivity of samples BRS-B-TI1 and BRS-B-TI3 varies from 1.5 to 2 respectively. These values were similar to those measured in the oedometer tests where the stress sensitivity was around 1.2 to 2.5. A more detailed analysis of the effects of structure on the compression and shearing behaviour of the intact samples will be carried out in the following sections.

An attempt to estimate the in-situ anisotropy of the intact samples was carried out by applying Equation 5.19 during the isotropic compression stages. Two samples were selected, the dense BRS-B-TI2 and the loose BRS-B-TI3. Figure 5.58 shows the measured increments of axial and volumetric strains for each mean effective stress level. It can be observed that the initial degree of anisotropy of the two intact samples was different. It is also interesting to point out that, despite the initial differences in the deformation response, the intact sample BRS-B-TI3 followed a similar trend compared with the slurry BRS-B-TS4. According to the criterion proposed by Burland (1967) both samples were assumed to be in a reasonably isotropic state before shearing whereas sample BRS-B-TI2 was not in an isotropic state.

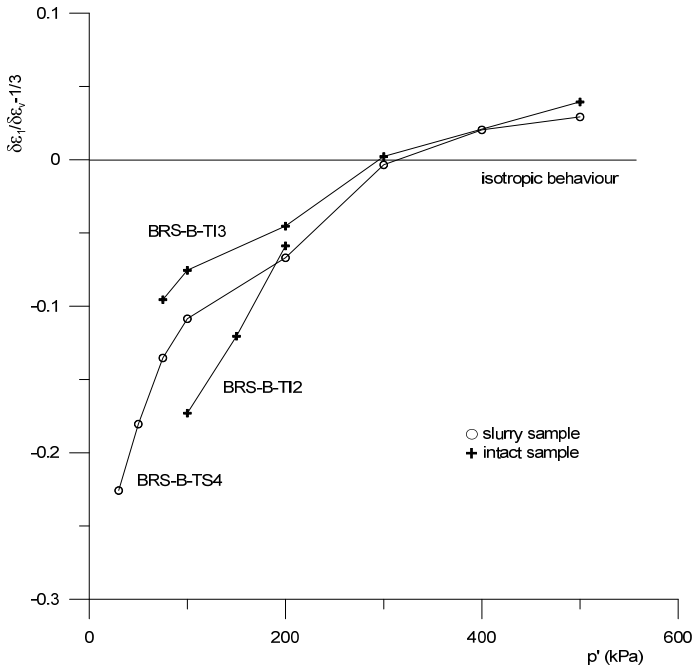

Figure 5.58 Strain ratios measured during isotropic compression of two intact samples BRS-B-TI2 and BRS-B-TI3. Comparison with slurry sample BRS-B-TS4

5.3.5 Shearing behaviour of intact samples

• Large strain behaviour

A series of undrained compression tests were performed on intact samples of the BRS-B clayey silt. Two drained tests were also carried out but unfortunately they were incomplete for different reasons. Most of the tests were performed on 38mm diameter specimens apart from samples BRS-B-TI4 and BRS-B-TI9 that were tested in the 7MPa triaxial cell using 50mm diameter samples. Before shearing, all samples were isotropically compressed to a range of stresses that varied from 200 to 4000kPa. Table 5.7 summarises the tests details. The failure mechanism was of the barrelling type together with shear bands observed in some specimens at large strains which induced non-homogeneous deformations in the samples (Figure 5.29d,e,f).

Figure 5.59 shows the undrained stress-strain behaviour in the $q:\varepsilon_s$, $\Delta u:\varepsilon_s$ and $p':\varepsilon_s$ planes for the tests performed at lower stresses. The high pressure tests on samples BRS-B-TI4 and BRS-B-TI9 are plotted in a separate figure for clarity (Figure 5.60). Looking at Figure 5.59, it can be seen that, apart from test BRS-B-TI2, the deviator stress was clearly increasing at the end of the tests that means the critical state was not reached. It is interesting to point out that the deviator stress for

sample BRS-B-TI7 plotted above that of sample BRS-B-TI1 which was tested at a higher confining pressure, showing the possible effect of the different initial degree of in-situ structure observed in Figure 5.57.

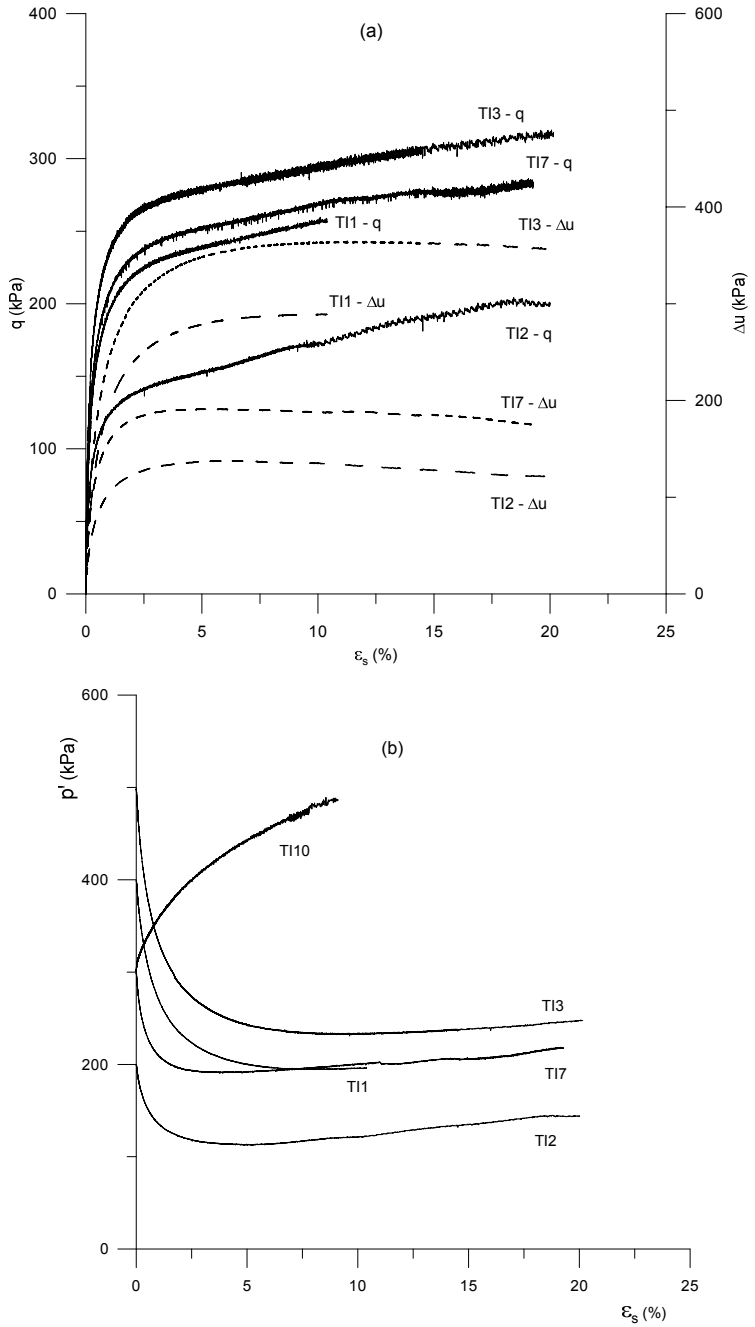

Figure 5.59 Variation of (a) deviator stress and increment of pwp and (b) mean effective stress during undrained shearing of intact samples of the BRS-B

The initial positive increment of pore water pressure of all samples corresponded to a clear contractant response until the phase transformation point, where the increment of pore water pressure reached its maximum value and thereafter started to decrease very smoothly, related to a dilatant response, and eventually reaching an almost steady value. It is interesting to see how the phase transformation point started at different shear strain levels. In the case of sample BRS-B-TI3, the change from the contractant to dilatant behaviour occurred at an axial strain of around 10% while in samples BRS-B-TI7 and BRS-TI2 it happened at around 4 and 6% respectively. In terms of mean effective stress, and apart from sample BRS-B-TI2, it can be observed how all samples showed a very slight ongoing increment at the end of the test.

The stress-strain response of the specimens tested at high confining stresses is shown in Figure 5.60. These samples were tested to larger shear strains that ranged from 27 to 30% compared with the average of 20% reached in the Bishop & Wesley triaxial cell. The samples initially displayed a strain-hardening response reaching a very smooth peak at shear strains of around 17 to 20%. After the peak, the deviator stress decreased slightly, reaching a more stable value at the ends of the test compared with the behaviour observed in Figure 5.59, in particular for the case of sample BRS-B-TI4. Looking at the variation of the increment of pore water pressure, phase transformation points were also clearly identified at shear strains of around 7.5 to 10%. The increment of pore water pressure and the mean effective stress for both specimens eventually reached an apparent steady value at the end of the tests. It is important to recall that the shearing mechanism exhibited by these samples included barrelling plus clear shear bands, in particular test BRS-B-TI4 (Figure 5.29e,f). This caused non-homogeneous deformation states throughout the samples and therefore the stresses and strains calculated from the boundary measurements at the ends of the tests should be taken with caution, specially when plotting the points corresponding to the ends of the tests in the q:p' and v:p' planes.

Two drained tests were carried out on samples BRS-B-TI10 and BRS-B-TI11. Unfortunately these tests were incomplete and shearing data were only available for sample BRS-B-TI10 as can be seen in Figure 5.61. The deviator stress and volume change were both still increasing when the test had to be stopped. The mean effective stress during shearing is plotted in Figure 5.59(b) and it was also increasing at the end of the test.

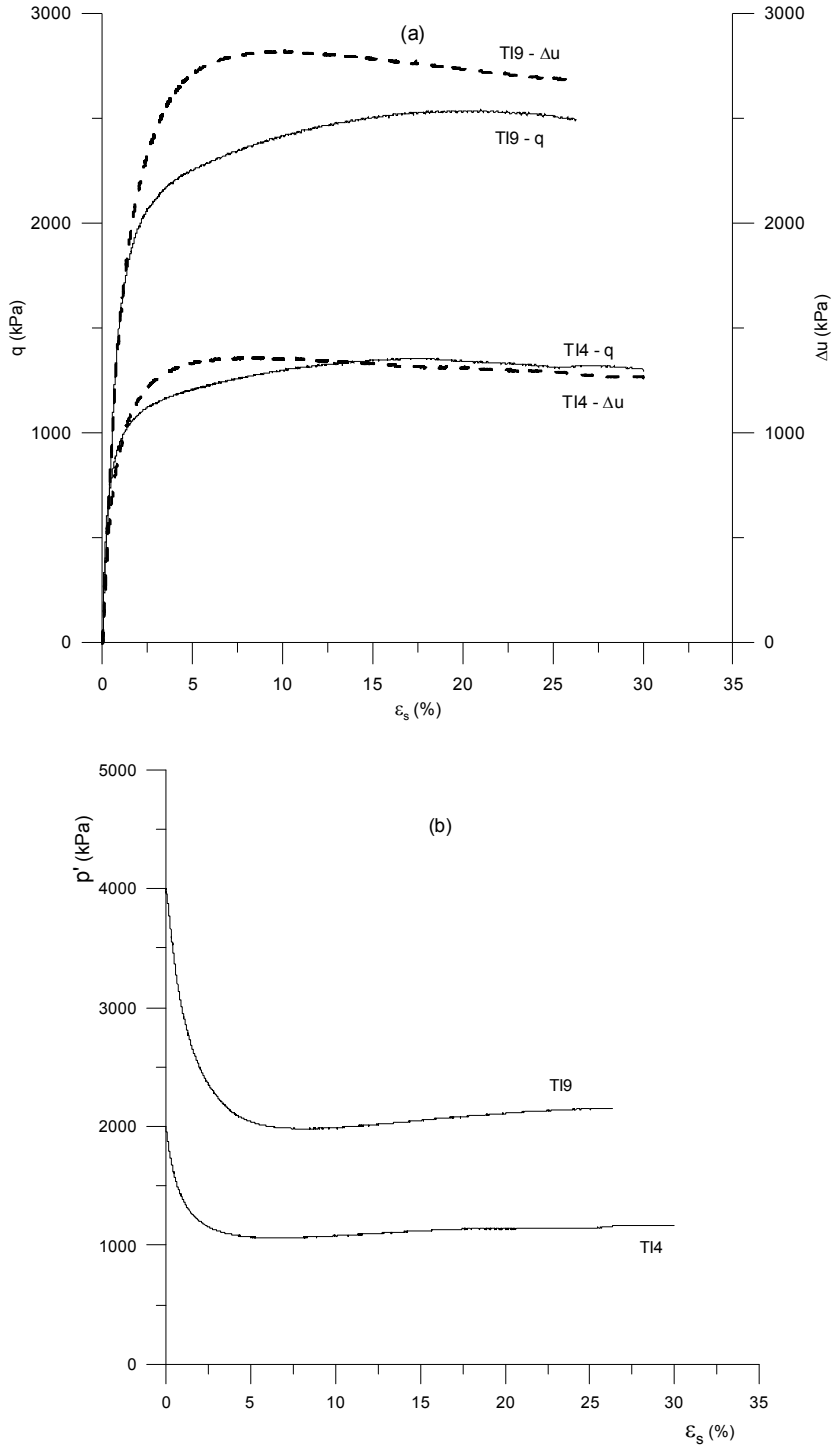

Figure 5.60 Variation of (a) deviator stress and increment of pwp and (b) mean effective stress during undrained shearing of intact samples of the BRS-B at high confining stresses

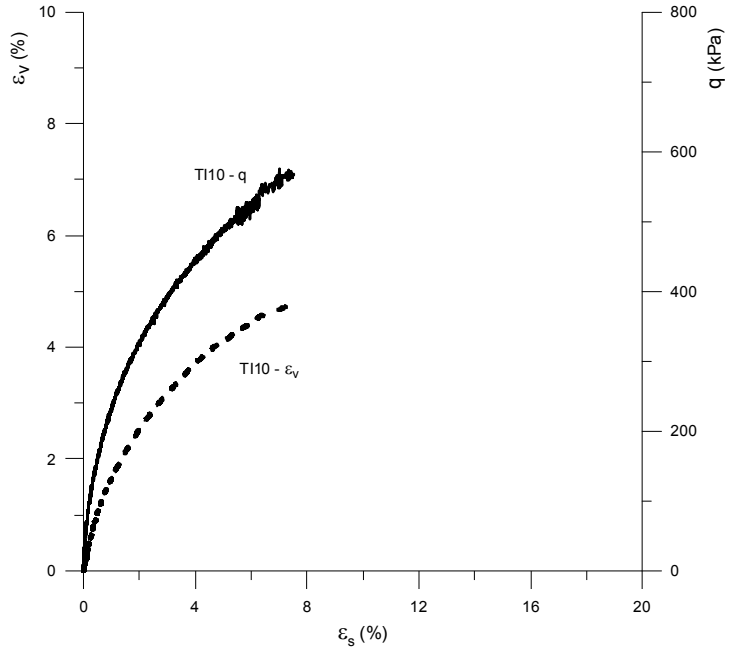

Figure 5.61 Variation of deviator stress and volume strain during drained shearing of intact sample BRS-B-TI10

The stress paths of the intact samples in the p':q plane are plotted in Figures 5.62 and 5.63. Figure 5.62 only shows the stress paths of samples sheared at lower confining stresses, in order to view more clearly the soil behaviour. The undrained stress paths of all samples showed an initially contractant response, corresponding to a positive increment in the pore water pressure, followed by a phase transformation point that changed the behaviour into a dilatant mode. As in the case of the slurry samples, after the phase transformation point, the stress paths climbed at a reasonably constant stress ratio until the end of the tests. It is interesting to point out that the paths followed by samples BRS-B-TI1, BRS-B-TI2 and BRS-B-TI3 had a slight different shape compared with sample BRS-B-TI7. This latter test showed a more stiff response at small strains.

The stress state at the end of each test was compared with the estimated intrinsic CSL* defined by the slurry samples. It can be observed that all the end of the test points for the undrained tests plot along the CSL*, apart from sample BRS-B-TI2, which had an end point of the stress path that was slightly above the CSL*. The drained test BRS-B-TI10 is also plotted in Figure 5.62, where the arrow indicates the incompleteness of the test.

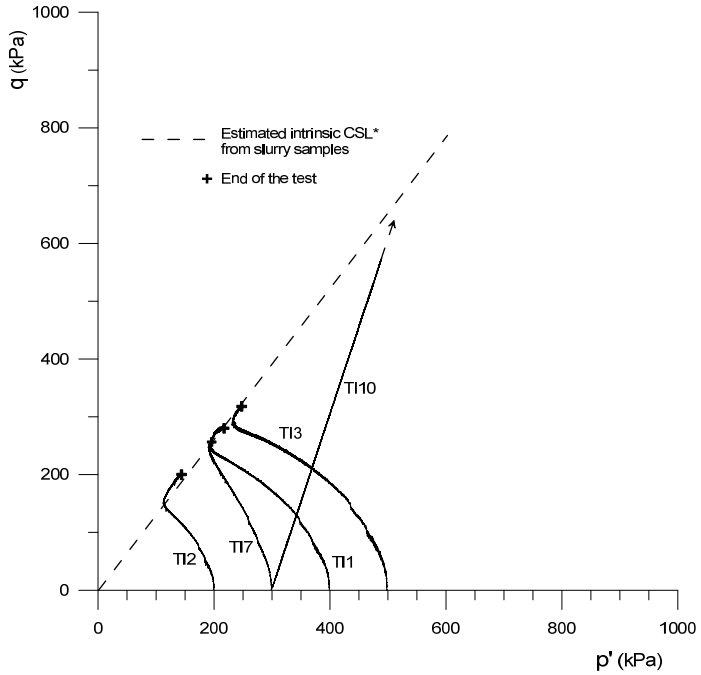

Figure 5.62 Undrained and drained stress paths of intact samples of the BRS-B at lower confining stresses

Figure 5.63 shows the stress paths of samples BRS-B-TI4 and BRS-B-TI9. They also displayed an initially contractant behaviour followed by a dilatant response after the phase transformation point. Comparing the stress paths of all the intact samples plotted in Figures 5.62 and 5.63, it is interesting to point out that a peak value was observed in the deviator stress for the two samples tested at high confining pressures. Moreover, these samples also experienced larger strains during undrained shearing, around 30 and 27% respectively. After the peak in the deviator stress, the stress paths changed in direction and moved downwards. This behaviour was more accentuated in the case of sample BRS-B-TI4, where the shear strain at the end of the test was around 30%, the largest for all the tests carried out. On the other hand, in the case of the samples sheared in the conventional cell, at lower confining pressures, the tests reached shear strains of around 20% and the stress paths did not show any peak value in the deviator stress. As mentioned above, the deformation mechanism of specimens BRS-B-TI4 and BRS-B-TI9 at larger shear strains produced a clearly non-homogeneous shear strain distribution that made the stress-strain data questionable. This could be one of the reasons to explain the differences between the stress paths of samples tested in the Bishop & Wesley triaxial cell and in the 7MPa cell. It would have been interesting to be able to reach larger strains in the tests at lower confining pressures in order to check the tendency of the stress paths but unfortunately it was impossible due to the limited maximum movement of the axial ram in the Bishop & Wesley triaxial cells.

The stress states at the end of the tests for samples BRS-B-TI4 and BRS-B-TI9 were located well below the estimated CSL* giving a smaller M value with respect to the samples tested at lower stresses. Although the stress states at the ends of the tests were doubtful, the stress paths before peak still plotted below the CSL*, which could lead to the possibility of a curved CSL* in the p':q plane at high stresses.

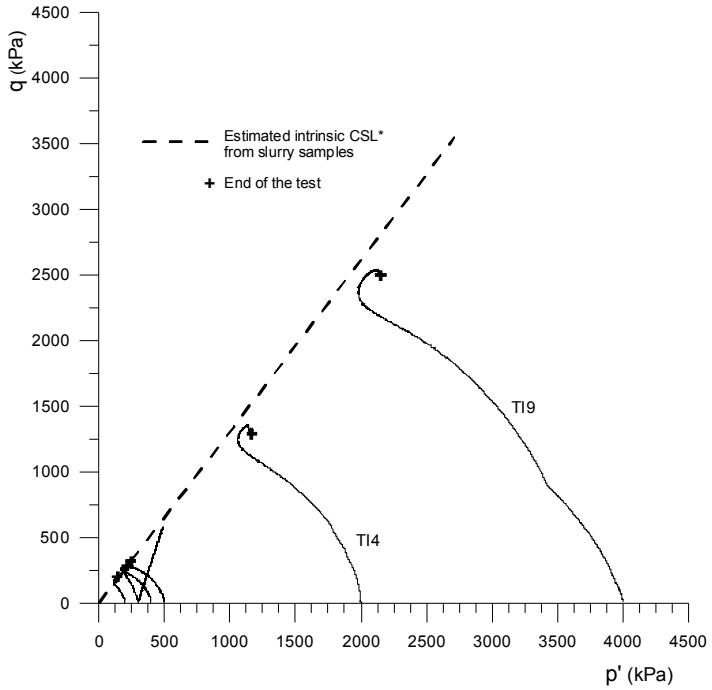

Figure 5.63 Undrained and drained stress paths of intact samples of the BRS-B

The normalised stresses (q/p') plotted against the shear strain for all the intact samples are shown in Figure 5.64, together with the estimated average critical state value M*=1.3 for the slurry specimens. A stiffer response of samples BRS-B-TI2 and BRS-B-TI7 can be seen compared with the others specimens. This agrees with the more vertical stress paths observed in Figure 5.62. Moreover, the M value measured at the end of test BRS-B-TI2 was slightly higher, however, it showed a tendency towards the constant value obtained for samples BRS-B-TI3 and BRS-B-TI7 that matched the estimated M*=1.3. In the case of the high confining stress tests BRS-B-TI4 and BRS-B-TI9, the stress ratio reached a peak and then decreased towards a much lower value at large strains, displaying a very smooth strain-softening response which could have favoured the formation of the observed shear bands on these two specimens, in particular test BRS-B-TI4 (Figure 5.29e).

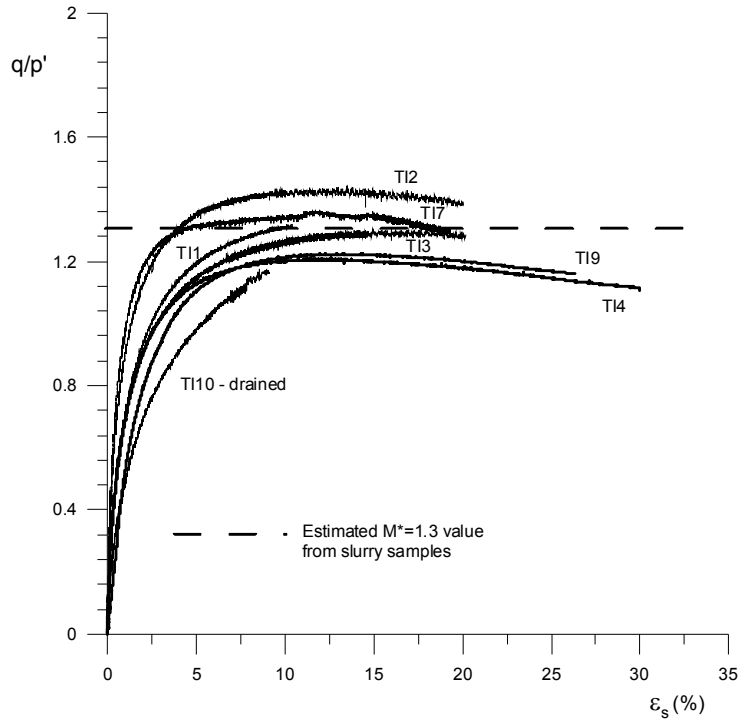

Figure 5.64 Normalized stress-strain behaviour for the intact samples of the BRS-B

Figure 5.65 shows the stress paths and the stress states at the ends of the tests in the v:logp' plane. Additionally, the estimated isotropic ICL* and CSL* are also included in the figure as references to compare with the behaviour of the intact samples. As shown before, in the case of samples BRS-B-TI1 and BRS-B-TI3, the compression lines clearly crossed the isotropic ICL* showing the effect of their in-situ structure. This structure could not be erased during isotropic compression and, in fact, the compression lines run parallel to the ICL* without showing any sign of convergence towards the ICL* for the range of stresses applied. As described in the previous paragraphs, a robust fabric was the possible cause of this stable effect of structure observed during compression. The destructuration induced in these samples during undrained shearing was not enough to reach the CSL*, and therefore their stress states at the ends of the tests were located to the right of the CSL*, in particular sample BRS-B-TI3.

It could be argued that the shear strains reached during the tests were insufficient to arrive at the critical state, especially in the case of sample BRS-B-TI1. However, looking at the tendency of the mean effective stress at the end of the tests (Figure 5.59), it can be seen that a small positive increase would be expected for larger shear strains but, in any case, this would not change very much the position of the end of the test point with respect to the CSL*, mainly because of the logarithmic scale in the x-axis. In addition, the "tail" of the stress path in the p':q plane after

the phase transformation point of sample BRS-B-TI1, was very short compared with the other samples as a consequence of the limited strain (10%) induced during shearing. Therefore, it would be expected that at larger strains the end of the test point will move to the right of the current position.

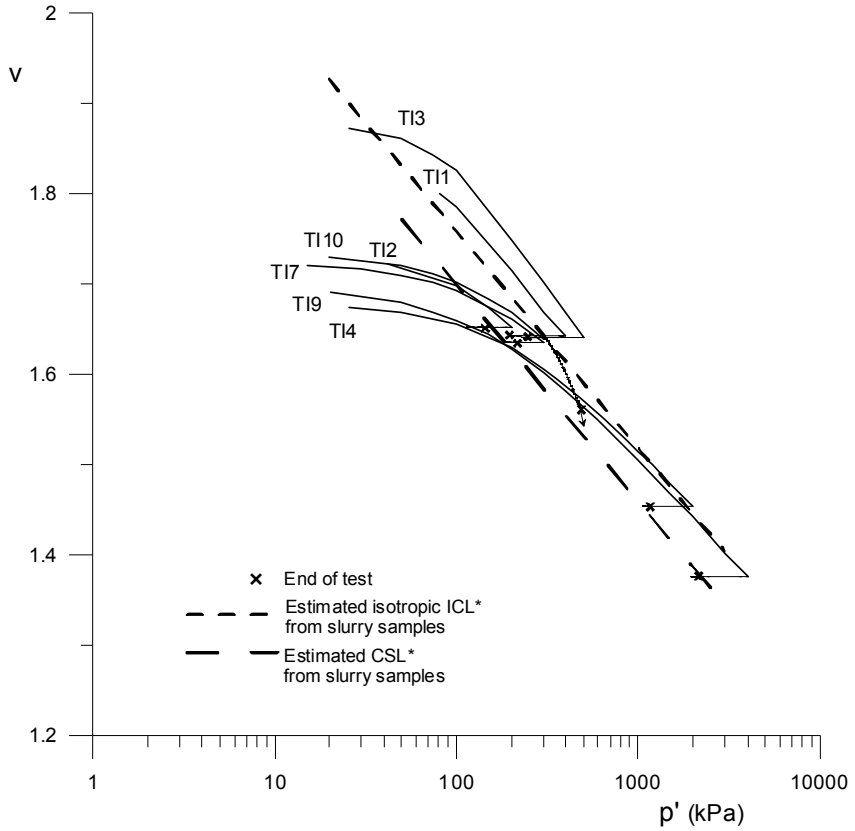

Figure 5.65 Compression and shearing stress paths in the v:logp' plane for the intact samples of the BRS-B

The stress path for the drained test BRS-B-TI10 is also plotted in Figure 5.65. Unfortunately the test had to be stopped at an early shear strain where the deviator stress and volume strain were still clearly increasing (Figure 5.61). The end of test point in the v:logp' plane reflected the incompleteness of the test. An arrow is included to indicate the direction of the stress path when the test was stopped.

In order to quantify the effect of the in-situ structure of the intact samples during shearing, the data were normalised using the equivalent mean effective pressure on the estimated unique CSL* defined by the slurry samples. Figure 5.66 shows the normalised data of all intact samples together with those of the slurries. In addition, the estimated intrinsic local boundary surfaces (LBS*) are included in the

figure. Apart from sample BRS-B-TI7, the shapes of the normalised undrained paths of the intact samples are almost the same with different sizes. Starting with the tests performed at high confining pressures, samples BRS-B-TI4 and BRS-B-TI9, it can be seen that a critical state corresponding to the CSL* was clearly reached by sample BRS-B-TI9 (Figure 5.65) whereas in the case of sample BRS-B-TI4 the final state plotted slightly to the right of the CSL*. As mentioned above, the final stress state of sample BRS-B-TI4 could be affected by the non-homogeneous deformation observed at the end of the test. Both specimens exhibited lower values of M as shown in Figures 5.62 and 5.63.

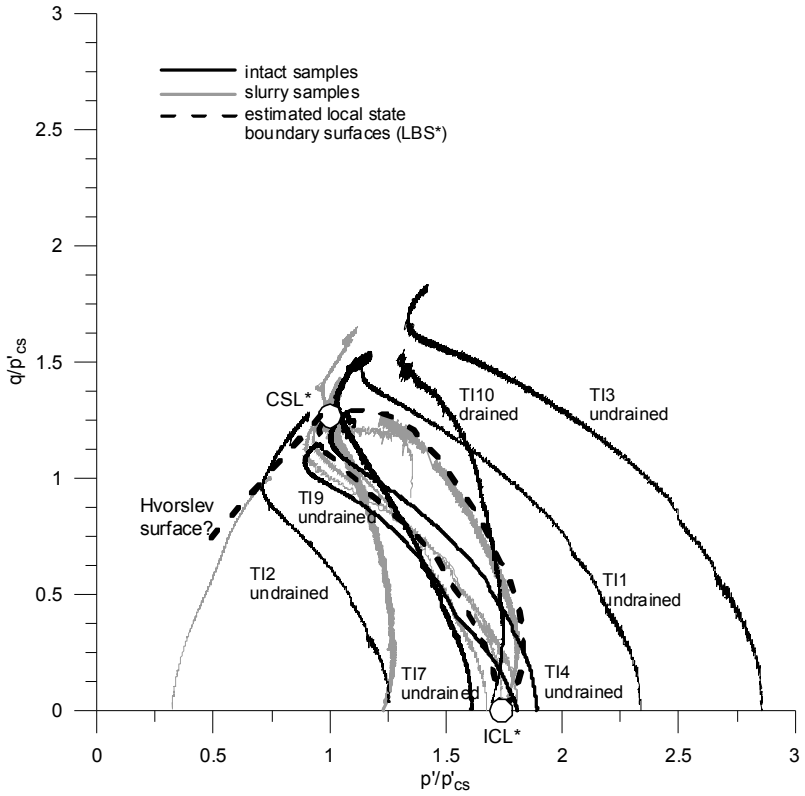

Figure 5.66 Normalized triaxial shearing data of intact samples of the BRS-B using the equivalent pressure on the intrinsic critical state line (CSL*)

The rest of the normalised paths plotted in Figure 5.66 correspond to tests performed in the Bishop & Wesley triaxial cell, where the compression stresses ranged from 200 to 500kPa and the maximum shear strains were around 20%, lower than the 27 to 30% reached in the high confining pressure tests. As described before, during the isotropic compression of samples BRS-B-TI1 and BRS-B-TI3, it was observed that their compression lines crossed the ICL* and remained parallel to it (Figure 5.65). As can be seen in Figure 5.66, their normalised stress paths during shearing plotted well to the right of the intrinsic behaviour with no sign of

converging towards the intrinsic critical state. The dilatant "tail" of sample BRS-B-TI1 was shorter probably due to the relatively small strain of 10% reached during shearing, as mentioned before. At the end of the tests, the normalised paths moved towards a different critical state, in particular sample BRS-B-TI3, but with the same M value as the slurry samples. Moreover, the shapes of the intact boundary surfaces of these isotropically compressed samples were the same as the intrinsic surface defined by the undrained tests on the slurry samples, but larger due to the possible effect of the stable structure, in particular a probably robust fabric that could not be destroyed during undrained shearing. These results agree with the conclusion obtained by Cotecchia & Chandler (2000) for structured clays with stable fabrics, where they found that intact boundary surfaces had the same shape as the intrinsic surface but larger in size.

In the case of sample BRS-B-TI2, the stress path looked like it was moving along the estimated Hvorslev surface towards the critical state. On the other hand, sample BRS-B-TI7 showed a stiffer response compared with the other undrained specimens and at the end of the test it tended to move to a different critical state. The normalised path of drained test BRS-B-TI10 crossed some undrained paths and also the drained path of the slurry sample that defined the outer limit of the LBS*. Unfortunately, the test was incomplete but, in any case, it appears the stress path was moving towards a different critical state.

In summary, and although the location of the normalised stress paths with respect to the CSL* could be affected by small errors in estimating the initial specific volumes of the specimens, it appears that a robust fabric is the main part of the in-situ structure that had a noticeable effect on the shearing behaviour of the intact BRS-B soil. The effect of the in-situ structure was seen only in some samples that showed a clear effect on the compression behaviour. On the other hand, samples with denser in-situ structure which did not show structure effects in compression did not in shearing either, in contrast to what was found by Hosseini Kamal et al. (2014). The robust fabric exhibited by some of the specimens seemed to produced different critical states in the normalised p'/p'_{cs}:q/p'_{cs} plane. This behaviour could not be clearly identified in Figure 5.65 because of the logarithmic scale used for the mean effective stress, although test BRS-B-TI3 did anticipate it.

5.3.6 Stiffness data

In the following paragraphs the stress-strain behaviour of the BRS-B clayey silt at small strains is analysed. A comparison between the slurry, compacted and intact samples is carried out, as an attempt to evaluate the effect of the sample preparation technique and the in-situ structure on the stiffness at small strains. All

samples were sheared at the same rate and the stiffness was measured using internal local transducers attached to the sample as described in Section 3.4.2. For the sake of simplicity, the stiffness of the soil is defined by the secant Young's modulus.

- **Slurry samples**

The tests on samples BRS-B-TS1, BRS-B-TS7 and BRS-B-TS6 were chosen to show the stiffness degradation during undrained shearing of the BRS-B clayey silt. The samples were isotropically compressed to mean effective stresses of 400, 200 and 100kPa respectively. Samples BRS-B-TS1 and BRS-B-TS7 were normally consolidated, whereas sample BRS-B-TS6 was overconsolidated, with an OCR=4.

Figure 5.67 shows the variation of the undrained secant Young's modulus (Eu_{secant}) with the axial strain at small strains for the three selected samples. As was expected, the stress-strain behaviour was highly non-linear in the small strain region and the stiffness varied with the strain, mean effective stress level and the overconsolidation ratio.

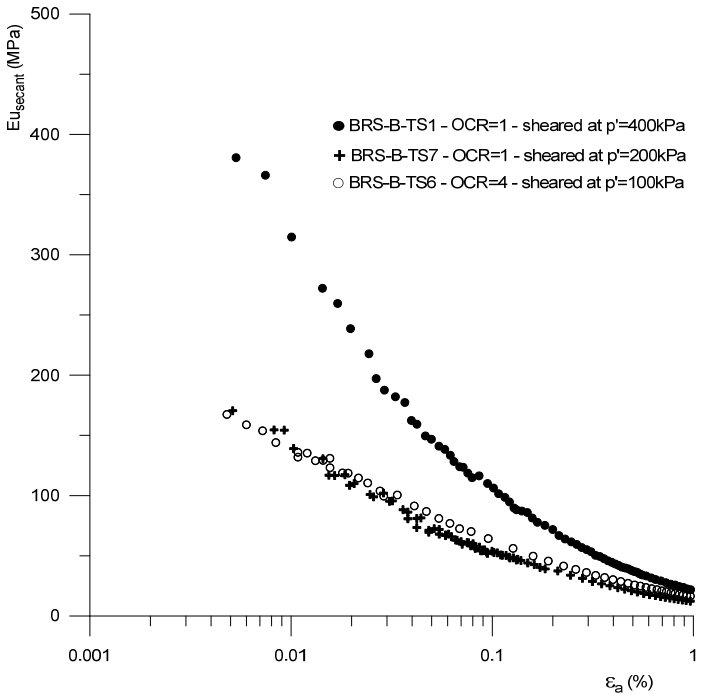

Figure 5.67 Degradation of undrained secant Young's modulus with strain for the normally consolidated slurry samples BRS-B-TS1, BRS-B-TS7 and overconsolidated sample BRS-B-TS6 sheared at different mean effective stress levels

The effect of the overconsolidation ratio on the stiffness at small strains can be seen more clearly in Figure 5.68, where the undrained secant Young's modulus plotted in Figure 5.67 was normalised by using the current mean effective stress (Eu_{secant}/p'). In the case of the normally consolidated samples, a non-linear unique relationship between Eu_{secant}/p' and the axial strain could be found. Moreover, it can be observed that, for a given axial strain, the value of Eu_{secant}/p' depended on the degree of overconsolidation as expected. Using the results of several investigations on different soils carried out at Imperial College, Jardine (1995) plotted the ratio of $(Eu_{secant}/p')^{OC}/(Eu_{secant}/p')^{NC}$, measured at a shear strain of 0.01%, against the OCR (Figure 5.69). Based on the results of Figure 5.68, in the case of the BRS-B clayey silt, the measured ratio was around 1.7 for an OCR=4, which fitted well within the range of values for reconstituted sands and silts shown in Figure 5.69.

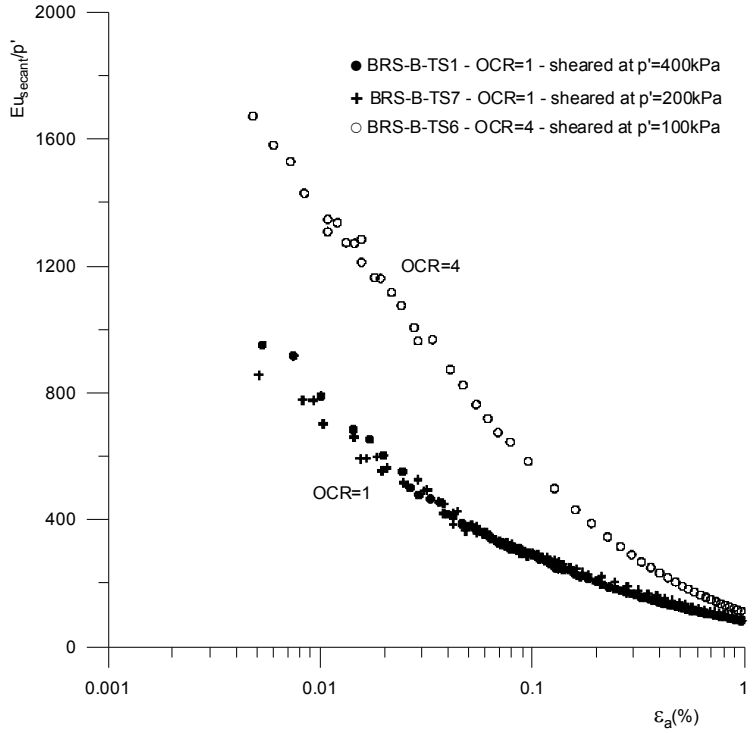

Figure 5.68 Effect of the OCR on the normalized undrained secant Young's modulus for the slurry samples of the BRS-B

• Compacted samples

The variation of Eu_{secant} with the axial strain for the two compacted samples BRS-B-TC1 and BRS-B-TC4 is plotted in Figure 5.70. Both samples were isotropically compressed to mean effective stresses of 392 and 500kPa respectively. In this case,

and due to some scatter observed in the values of the deviator stress at very small strain levels, the first reliable value of stiffness considered for the analysis was at 0.01%. As in the case of the slurry samples, the stress-strain behaviour was non-linear.

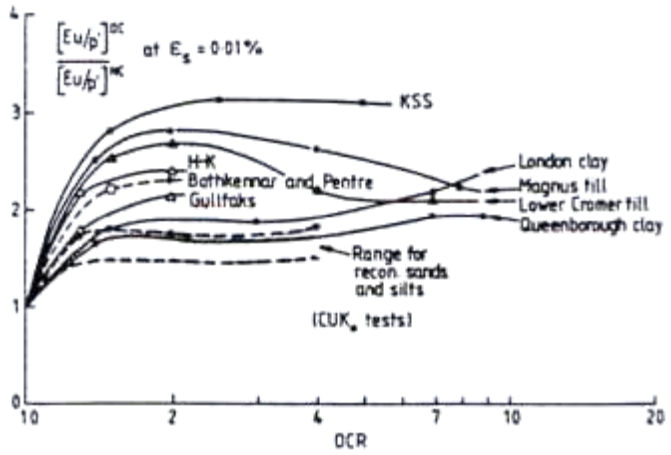

Figure 5.69 Effect of the OCR on the undrained compression stiffness (Jardine,1995)

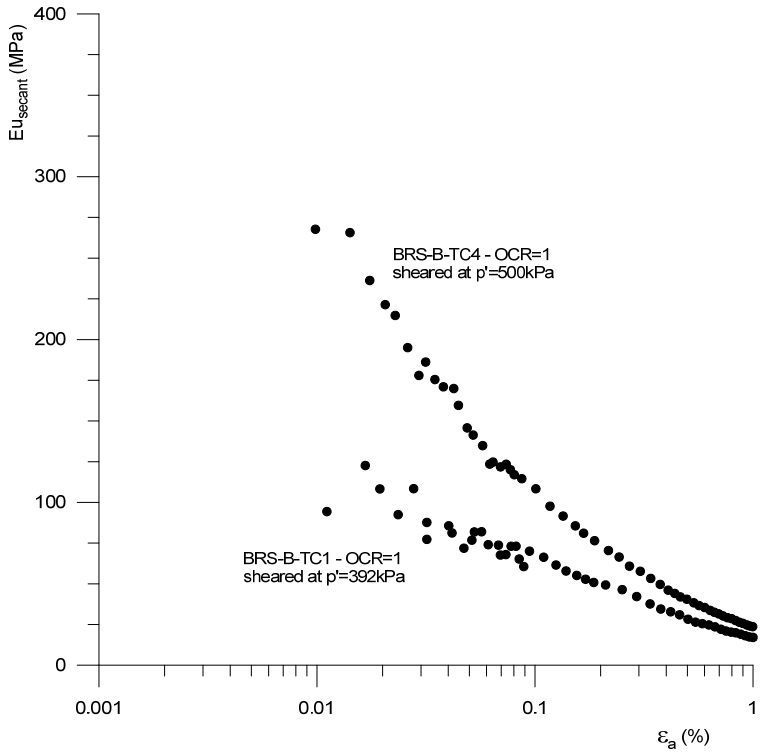

Figure 5.70 Degradation of undrained secant Young's modulus with strain for the normally consolidated compacted samples BRS-B-TC1 and BRS-B-TC4 sheared at different mean effective stress levels

The undrained Young's modulus of the compacted samples was also normalised by using the current mean effective stress. The results are plotted in Figure 5.71 together with the normalised values of the normally consolidated slurry samples. In contrast to the observed unique non-linear relationship between Eu_{secant}/p' and the axial strain for the slurry samples, the stiffness of the compacted samples was lower for the same level of strain, in particular for sample BRS-B-TC1. As the shearing continued the stiffness degradation curves tended towards a unique relationship at axial strains of around 1%. Although more tests should be carried out to confirm this behaviour, it could be said that the sample preparation technique seems to have an effect on the stiffness at small strains, where the compacted samples showed a less stiff fabric compared with the slurry for the same level of strain and mean effective stress.

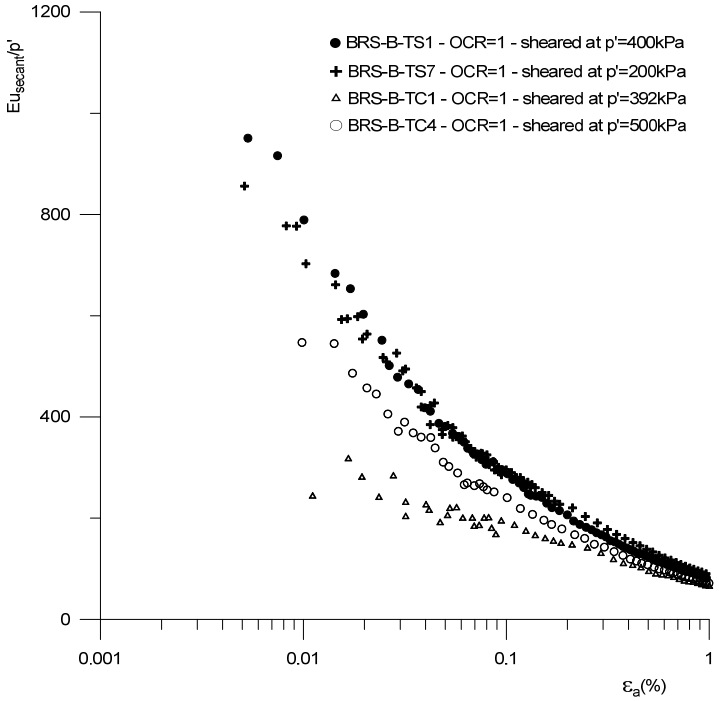

Figure 5.71 Comaprison of the normalized undrained Young's modulus between normally consolidated slurry (TS) and compacted (TC) samples of the BRS-B

• Intact samples

Figure 5.72 shows the variation of the undrained secant Young's modulus with the axial strain for the intact samples BRS-B-TI1, BRS-B-TI2, BRS-B-TI3, BRS-B-TI4 and BRS-B-TI7. The samples were isotropically compressed to a mean effective stress higher than their estimated in-situ stress level and in general their stress state before shearing plotted on the ICL* or crossed it, as shown in Figure 5.57.

The behaviour was highly non-linear with an influence of the confining pressure before shearing. Although the overall trend was that the stiffness increased as the confining pressure was higher, the comparison of sample BRS-B-TI7 with sample BRS-B-TI1, contradicted this behaviour. Samples BRS-B-TI7 and BRS-B-TI1 were isotropically compressed to mean effective stresses of 300 and 400kPa respectively before shearing and their Eu_{secant} were very similar at each strain level.

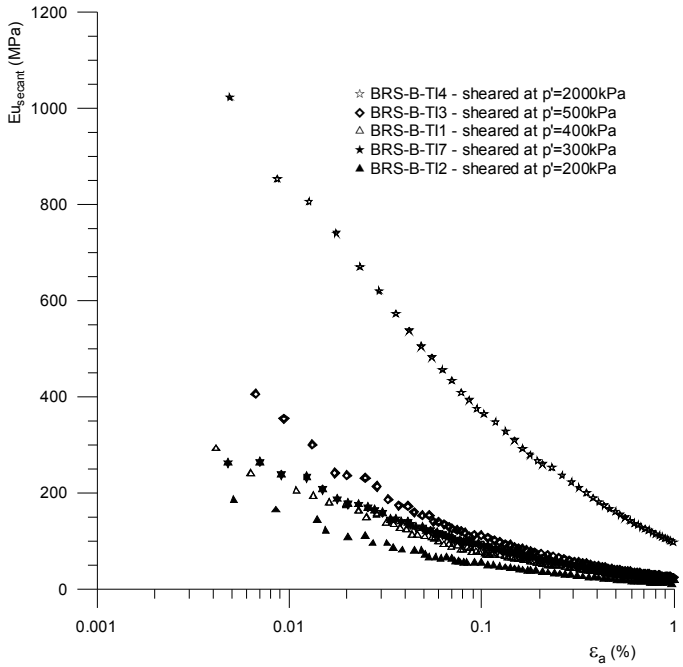

Figure 5.72 Degradation of undrained secant Young's modulus with strain for the intact samples of the BRS-B sheared at different mean effective stress levels

At this point, it is interesting to recall that the intact samples BRS-B-TI1 and BRS-B-TI3 exhibited a clear effect of their in-situ structure during isotropic compression when their compression lines crossed the ICL* and ran parallel to it, displaying a clearly stable fabric as shown in Figure 5.57. In order to evaluate the possible effect of the in-situ structure of the intact samples on the stiffness at small strains, a comparison between intact, compacted and slurry samples was carried out. As was done during the analysis at large strains, the slurry behaviour was taken as a reference for the comparison due to the more homogeneous structure developed during the sample preparation.

Figure 5.73 shows a comparison between the intact sample BRS-B-TI1 with the slurry BRS-B-TS1 and the compacted BRS-B-TC1 samples. The samples were isotropically compressed to the same mean effective stress of 400kPa. The specific volume of each sample, before undrained shearing started, was quite similar with a

value of 1.610 for sample BRS-B-TS1, 1.618 for sample BRS-B-TC1 and 1.640 for sample BRS-B-TI1. The slightly higher value of the intact specimen was due to the effect of the in-situ structure, in particular its stable fabric which could not be removed during compression. It can be observed that for a given strain level, the stiffness of each sample was different, where the slurry displayed the higher values of Eu_{secant}. The comparison between the intact with the compacted samples showed that the undrained Young's modulus was very similar for axial strains higher than 0.1% and eventually they converged onto a unique line with the slurry sample at axial strains of around 0.7%. Based on the results of this comparison, it seems to be clear that there is an effect of the in-situ structure of the intact sample and also and effect of the sample preparation technique on the stiffness at small strains. The structure of the intact sample made it less stiff compared with the slurry specimen in contrast with the literature.

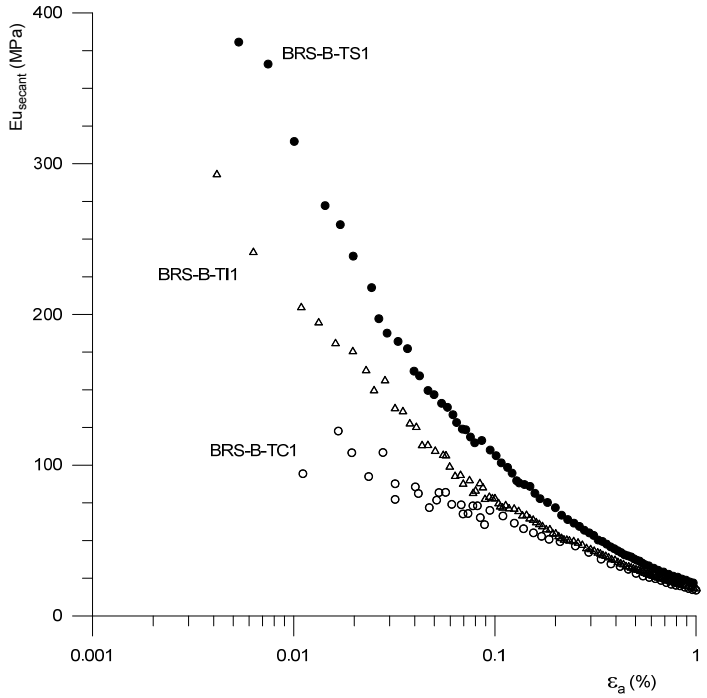

Figure 5.73 Effect of the in-situ structure on the stiffness of the BRS-B. Comaprison between intact (TI), compacted (TC) and slurry (TS) samples sheared at p'=400kPa

In Figure 5.74, the comparison was carried out between the intact sample BRS-B-TI3 and the compacted sample BRS-B-TC4. Both samples were isotropically compressed to a mean effective stress of 500kPa. The specific volumes of the samples before shearing started were 1.64 and 1.577 respectively. Unfortunately, in this case the slurry test BRS-B-TS2 carried out at the same mean effective stress had to be stopped due to a failure in the system and only compression data were

available. Although the state of each sample at the start of shearing was different in terms of specific volume, the stiffness was the same for both samples in the range of axial strains analysed.

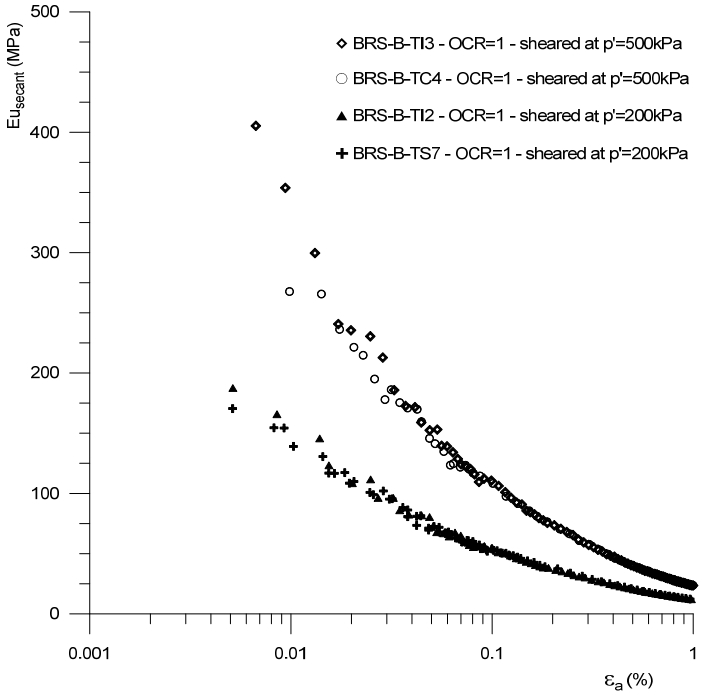

Figure 5.74 Effect of the in-situ structure on the stiffness of the BRS-B. Comaprison between intact (TI), compacted (TC) and slurry (TS) samples sheared at p'=200kPa and p'=500kPa

Additionally, another comparison between the intact sample BRS-B-TI2 and the slurry sample BRS-B-TS7 is included in Figure 5.74. In this case, both samples were isotropically compressed to a mean effective stress of 200kPa with specific volumes of 1.650 and 1.680 respectively. It can be seen that the stiffness degradation curve was the same for both samples and therefore it could be said that in this case the in-situ structure did not have any effect on the stress-strain behaviour at small strains. This result is opposite to the conclusion obtained from the comparison in Figure 5.73 where the slurry sample was stiffer than the intact. However it should be noticed that the sate of the intact sample BRS-B-TI2 was slightly overconsolidated as shown in Figure 5.65 and this may have increased the stiffness for a given p' and shear strain with respect to a normally consolidated state. Therefore the expected higher stiffness of the slurry sample BRS-B-TS7 might have been cancelled by an effect of the overconsolidated state of the intact sample BRS-B-TI2.

It has been long established that the stiffness of a material is related to the mean effective stress level and state by an expression of the type of Equation 5.26, where p_{ref} is a reference pressure to make Equation 5.26 dimensionless, YSR is the yield stress ratio expressed in terms of p' and A, n and m depend on the nature of the soil and on the strain level.

$$E = p_{ref} \cdot A \cdot \left(\frac{p'}{p_{ref}} \right)^{n} \cdot YSR^{m} \qquad 5.26$$

Figure 5.75 shows the relationship between the undrained secant Young's modulus and the current mean effective stress during shearing at various levels of axial strain for the intact, slurry and compacted samples, in a double logarithmic scale. The overconsolidated slurry sample BRS-B-TS6 was excluded from the comparison. For each strain level, a regression line was derived and the slope, which corresponds to the value of the parameter n, was measured. The coefficient of correlation (R^2) ranged from 0.92 to 0.97 and the values of n varied from 0.76 to 0.88. As expected, the value of n increased towards unity with the strain level as suggested by many authors (e.g. Porovic & Jardine, 1994; Viggiani & Atkinson, 1995; Jovicic & Coop, 1997). Consequently, this confirms the tendency towards a linear dependency of the stiffness with the mean effective stress at large strains.

In summary, it could be said that, although an apparent effects of the in-situ structure and sample preparation technique on the stiffness at small strains was observed in Figure 5.71, it would be inappropriate to draw a general conclusion based on the limited number of comparison tests available. On the other hand, when all the tests are compared in Figure 5.75, it seems that the in-situ structure of the intact samples had no a large effect on the stiffness of the BRS-B clayey silt at small strains.

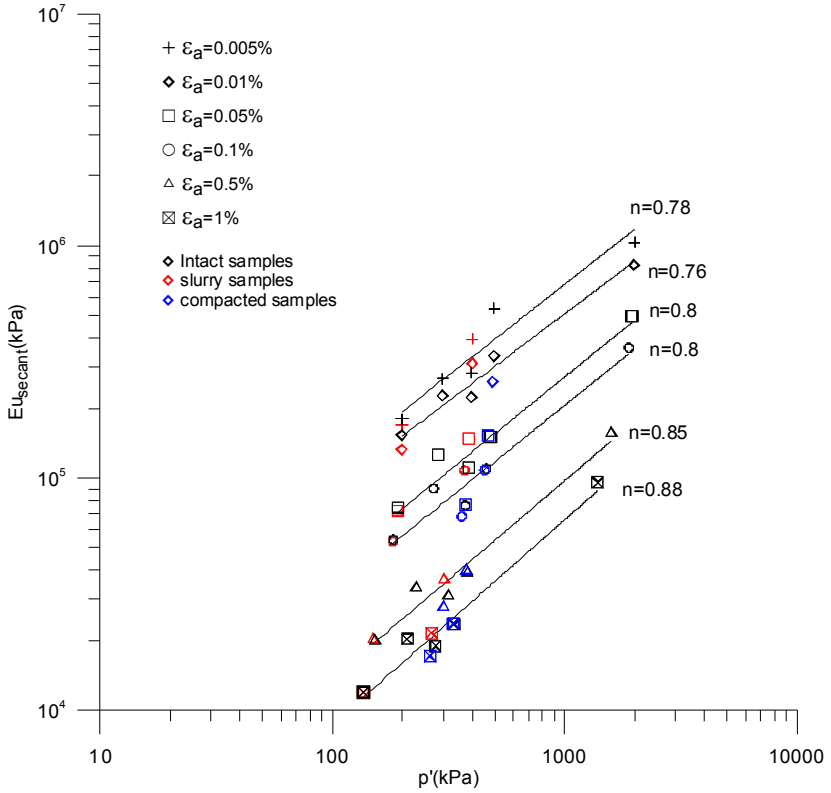

Figure 5.75 Undrained secant Young's modulus as a function of the current mean effective stress at various strsin levels for the slurry, compacted and intact normally consolidated samples of the BRS-B

Chapter 6
The Valencia Silty Soils

6.1 Introduction

The second materials investigated in this research project were the Valencia silty soils (VSS). In this chapter a detailed characterisation of the index properties of the VSS is presented.

6.2 The Valencia silty soils

Figure 6.1 shows a geomorphological map of the Turia River coast plains as described by Carmona & Ruiz (2011), where the city of Valencia was founded. The geomorphology of the area is characterised by levels of Pleistocene and Holocene alluvial fans and plains deposited along a littoral subsiding tectonic NNE-SSW axis (Simon, 1984). A detailed analysis of the historical morphogenesis and stratigraphy of the Turia River coastal plains has been carried out by many researchers (e.g. Carmona, 1990; Carmona & Ruiz, 2011).

The Valencia silty soils tested in this research project are made up of Holocene alluvial deposits with different particle size distributions that ranged from silty sands to silty clays, retrieved from the flood plain of the Turia River, at two different locations in the city of Valencia (Figure 6.2).

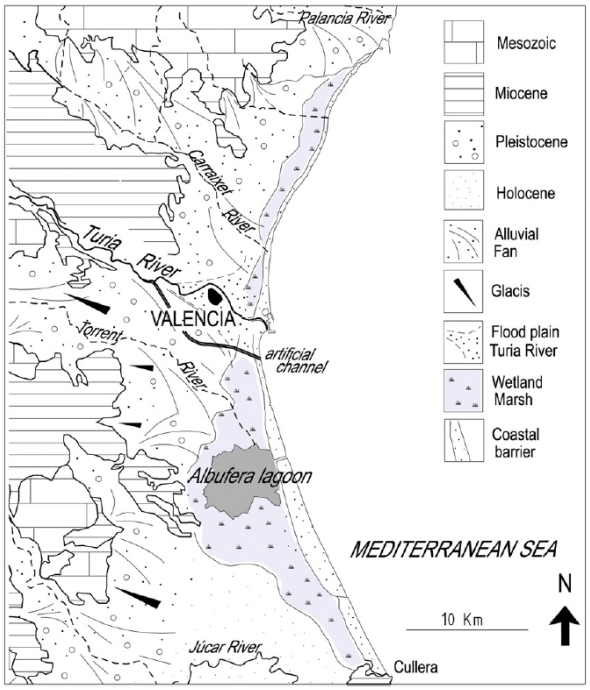

Figure 6.1 Geomorphological map of the Turia River coastal plains (Carmona & Ruiz, 2011)

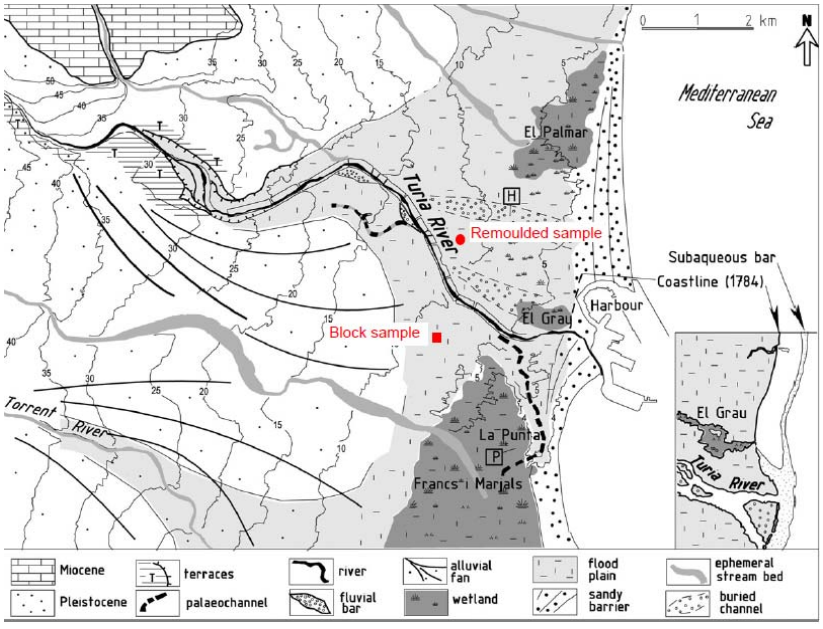

Figure 6.2 Geomorphological map of the Turia River coastal flood plains and location where the block and remoulded samples of the VSS tested in this research project were retrieved (modified Carmona & Ruiz, 2011)

Two types of samples were obtained. The first type was a block sample obtained during the excavation works of the T2 underground line extension to the southeast of the city. The sample was taken from a depth of 4.5m below ground level at the new General Urrutia underground station. Figure 6.3 shows the soil profile at the location where the block sample was retrieved. Alternating layers of "cohesive" and granular materials are commonly found in the area with a cover of anthrophic debris at the surface level. The water table was located 6m below ground level. As will be described later, the material in the block sample was made up of a silty clay with aggregates of particles of different sizes cemented by calcium carbonate, randomly distributed in the block. Figure 6.4 shows the sampling process of the block. The second type of sample was two remoulded specimens taken at different depths from the excavation site of a new underground car park at Chile Street. The remoulded material consisted of sandy silt/clay and silty sand.

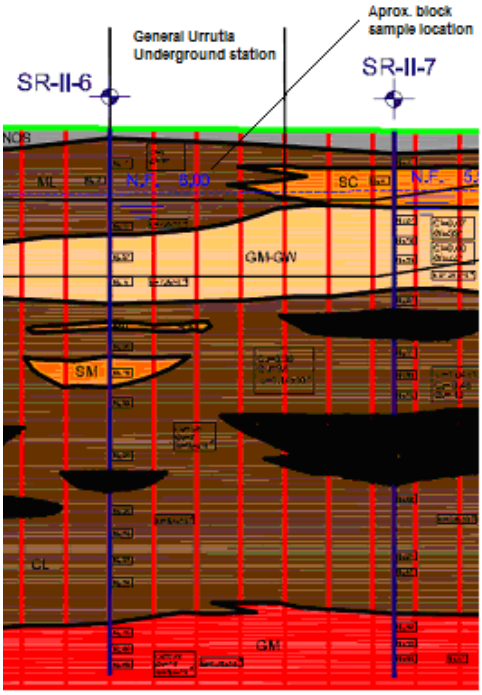

Figure 6.3 Soil profile at the General Urrutia underground station where the block sample of the VSS was retrived

6.2.1 Characterization of the Valencia silty soils: index properties

In this section the index properties of the VSS will be presented. The procedures for their determination followed the British BSI and Spanish UNE recommendations.

- **Particle size distribution**

Figure 6.5 shows the grading curves of all the Valencia soils tested in this research project. The average contents of clay-sized, silt and sand particles are presented in Table 6.1, together with the characteristic median particle size (D_{50}), according to the MIT classification system. Three grading curves were identified, the silty clay (VMClay) that formed the material contained in the block sample, the silty sand (VMSand) and the sandy silt (VSSilt) that corresponded to the remoulded samples. The VMSand and VSSilt were taken from the same location at different levels.

Figure 6.4 Sampling process of the intact block of the VSS obtained from the excavation works of the T2 underground line extension to the south of the city of Valencia at the General Urrutia underground station

In the case of the VMClay material, the quantity of clay-sized particles varied from 28 to 40%, with a silt content that ranged from 55 to 64%. This showed that the material contained in the block sample had basically the same quantity of fine particles but with some samples being more silty than others. Moreover, during the sieving analysis it was be observed that there were very hard aggregates of cemented particles with sizes that ranged from 0.6mm to 1.2cm, with angular to

sub-angular shapes (Figure 6.6). Part of the 5 to 8% sand content of the VMClay corresponds to these aggregates.

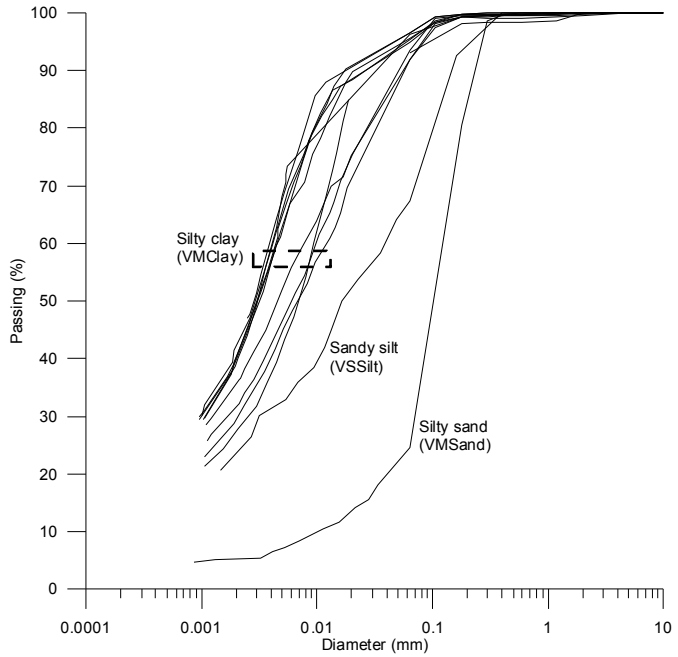

Figure 6.5 Particle size distributions of the Valencia silty soils tested in this research project

Soil	Clay-sized (%)	Silt (%)	Sand (%)	D_{50} (mm)
VMSand	5	20	75	0.1
VSSilt	25	43	32	0.07
VMClay	28-40	55-64	5-8*	0.003-0.007

Table 6.1 Average content of clay-sized, silt and sand particles and median particle size (D_{50}) according to MIT classification systems. * Part of the sand content corresponds to the aggregates of cemented particles with the size of sand.

Figure 6.6 Samples of the aggregates of cemented particles found in the clayey silt block sample

In order to determine the mineralogy of the aggregates, energy dispersive X-ray spectroscopy (EDX) analyses from scanning electron microscopy images were performed at two different locations as shown in Figure 6.7. The results of the EDX analyses presented in Figure 6.8 proved that the aggregates were made up of calcium carbonate cement that surrounds silt-sized particles. As mentioned before, these aggregates were randomly distributed in the block samples and in some cases their occurrence complicated the trimming of the intact specimens (Figure 3.12).

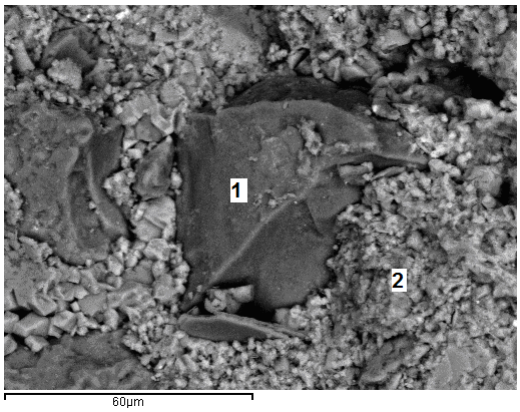

Figure 6.7 Back scattered electron microscopy image of an aggregate of particles cemented by calcium carbonate with EDX analysis locations

In the case of the remoulded samples of the silty sand (VMSand) and the sandy silt (VSSilt), the material was very homogeneous in comparison with the silty clay (VMClay) and a unique grading curve was obtained in each case. The VMSand is a uniform sand with a coefficient of uniformity of Cu=17 whereas the VSSilt represents a grading distribution that is a mix of the VMClay and the VMSand.

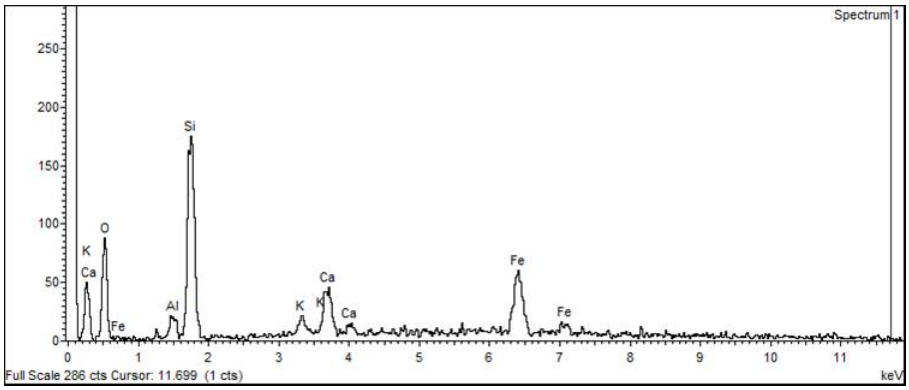

(a)

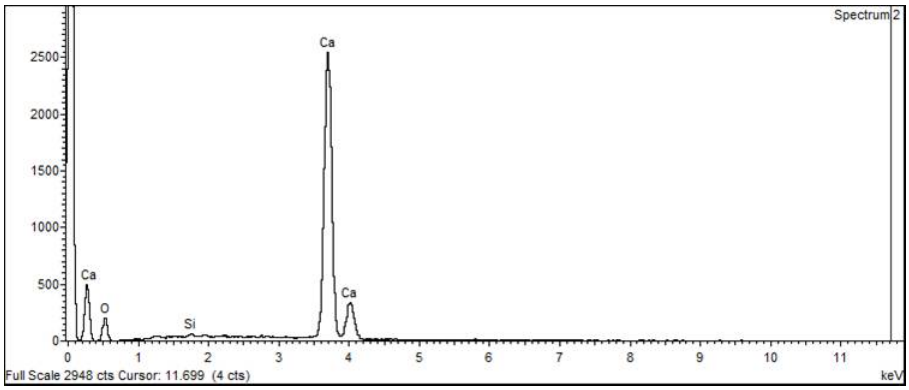

(b)

Figure 6.8 Energy dispersive X-ray spectroscopy (EDX) analysis of the aggregate shown in Figure 6.7 at different locations: (a) silt particle (location 1) and (b) calcium carbonate cement (location 2)

• Particle shape

The particle shape of the Valencia silty soils was analysed by using digital microscope photos of samples that had been previously sieved. Only photos of the Valencia silty sand (VMSand) were taken. Figures 6.9 and 6.10 show the retained material on the 180μm sieve and the material passing through the 63μm sieve. The shape of the bulk particles was sub-angular to sub-rounded. A comparison with the photos of the Italian Bormida River silts (BRS-B) material shows that both soils have very similar particle shapes.

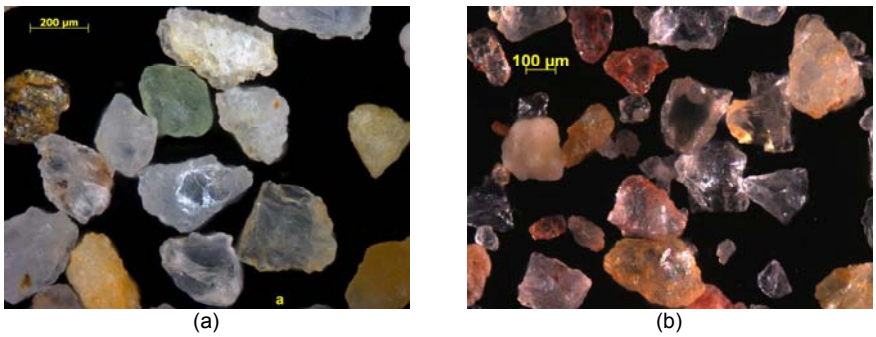

(a) (b)

Figure 6.9 Comparison of digital microscope photos of soil particles with 180µm<D<300µm: (a) Italian clayey silt (BRS-B) and (b) Valencia silty sand (VMSand)

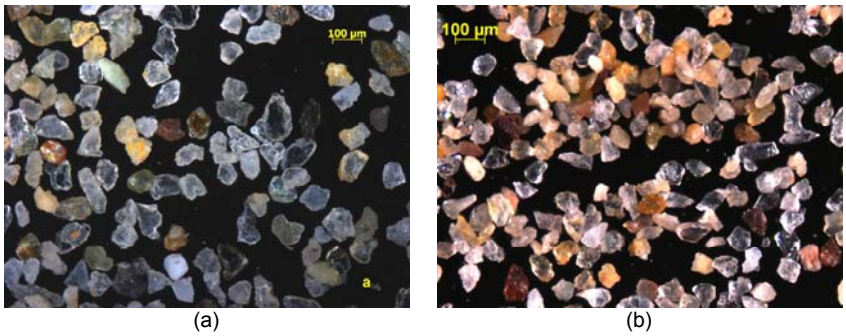

(a) (b)

Figure 6.10 Comparison of digital microscope photos of soil particles passing 63µm sieve: (a) Italian clayey silt (BRS-B) and (b) Valencia silty sand (VMSand)

• Specific gravity Gs

The specific gravity of the particles (Gs) was measured on several samples from different locations in the block of the VMClay and on samples from the remoulded material VMSand and VSSilt. The measured values are shown in Table 6.2. As can be seen Gs varied slightly with the grading distribution. An average value of 2.744 will be used for the analysis of the VMClay tests.

Soil	Gs (20ºC)
VMSand	2.703
VSSilt	2.719
VMClay	2.745
	2.743
	2.746

Table 6.2 Specific gravity values of the Valencia silty soils VMClay, VMSand and VSSilt.

• Atterberg limits

The results of the liquid and plastic limit tests carried out on several samples from the intact block and from the remoulded material are summarised in Table 6.3. In the case of the Valencia silty sand (VMSand) the material was non-plastic. Figure 6.11 shows the Casagrande plasticity chart with the points associated to the samples in Table 6.3. It could be observed that all points plotted above and parallel to the A line that confirmed the same origin of all soils tested. According to the unified soil classification system (USCS), the material contained in the intact block sample and identified as Valencia silty clay (VMClay) was classified as a low plasticity silty clay (CL). The remoulded Valencia sandy silt (VSSilt) was classified as silt/clay of low plasticity with sand (CL-ML) and in the case of the Valencia silty sand (VMSand) the material was classified as a non-plastic silty sand (SM).

Sample	w_l (%)	w_p (%)	I_p (%)	w_n (%)	I_L	USCS	Material
VMClay-TI4	29.5	17.7	11.8	19.2	0.13	CL	
VMClay-TIH2	30.8	17.9	12.9	18.4	0.04	CL	
VMClay-OI6	27	19.1	7.9	21.5	0.3	CL	Block sample
VMClay-OI5	25	16.4	8.6	18.3	0.22	CL	
VMClay-Cake	30	18.7	11.3	-	-	CL	
VSSilt	23.6	17	7	-	-	CL-ML	Remoulded
VMSand	Non-plastic			-	-	SM	Remoulded

Table 6.3 Atterberg limits and liquidity index measured on some intact oedometer (O) and triaxial (T) samples and on a slurry cake (Cake) samples of the Valencia silty soils

The average activity (A) of the plastic soils was also calculated. The values for the VMClay and VSSilt were 0.31 and 0.28 respectively. These similar results proved that the mineralogy of the clay particles contained in all the Valencia silty soils was the same and classified as inactive.

• Natural water content

The range of in-situ natural water contents measured on samples from the intact block varied from 18 to 22%, with an average of 19.5%. Table 6.3 shows the results of some of the samples tested in the triaxial and in the oedometer. It can be observed that the natural water content of all the samples was between the plastic limit and the liquid limit, with a liquidity index that ranged from 0.04 to 0.3 with

an average value of 0.17. These values of the liquidity index were associated to a plastic condition of the samples with a firm to soft state of consistency. Although the intact block sample was retrieved from 1m above the position of the water table, high degrees of saturation were measured as expected. The values ranged from 89 to 95%, with an average of 92%.

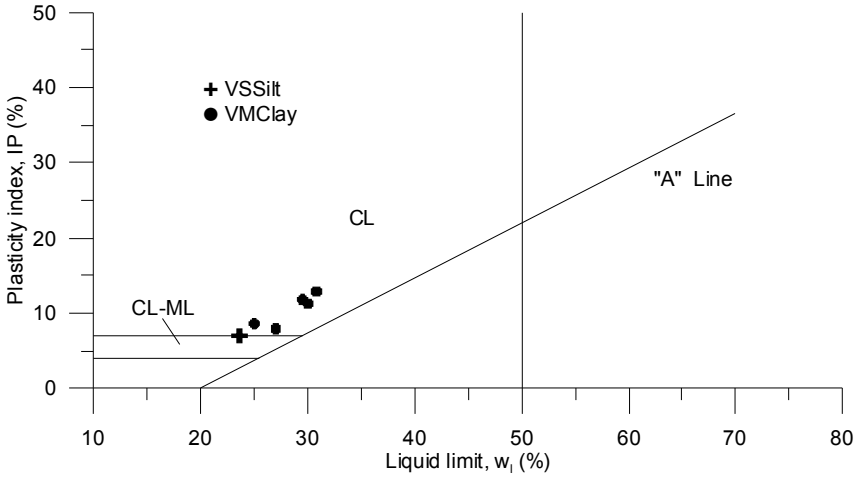

Figure 6.11 Casagrande plasticity chart of the Valencia silty soils for the samples included in Table 6.3

• Organic matter content

Several organic matter content tests were performed on samples of the Valencia silty soils. Only the tests on samples from the intact block of the VMClay contained a very small quantity of organic matter. The values measured varied from 0.11 to 0.2% with an average quantity of 0.16%. The organic matter on the remoulded samples from the VMSand and VSSilt was negligible.

• Carbonate content

As in the case of the Bormida River silts, the Bernard Calcimeter procedure was followed to measure the calcium carbonate ($CaCO_3$) content of the Valencia silty soils. Two tests were performed on samples from the intact block of the VMClay plus one more test was directly carried out on an aggregate of particles similar to those shown in Figure 6.6. Another test was conducted on a sample from the cake prepared with trimmings of the intact block sample. Two more tests were also performed on remoulded samples of the VMsand and VSSilt. Table 6.4 summarises the results of all the tests.

Material	$CaCO_3$ (%)
VMSand	30
VSSilt	33.4
VMClay-TIH2	50
VMClay-OI5	48
VMClay-Cake	51.3
Aggregate of particles	67.6

Table 6.4 Content of calcium carbonate ($CaCO_3$) measured on samples of the Valencia silty soils

From the results in Table 6.4, it can be seen that the quantity of $CaCO_3$ was very homogeneous for each location from where the samples were retrieved, with a higher concentration in the case of the block sample, the average value of which was 49.5% compared with 31.7% for the VMSand and VSSilt. Moreover, the aggregates of cemented particles found in the block samples showed a very high content of $CaCO_3$=67.6% that confirmed the observed peak of the spectroscopy (EDX) analyses in Figure 6.8. In any case, the high content of calcium carbonate found for the soil contained in the intact block sample of the VMClay could be a source of inter-particle bonding as shown in Figure 6.12. Certainly, this bonding will enhance the strength of the intact samples with respect to the reference slurry samples.

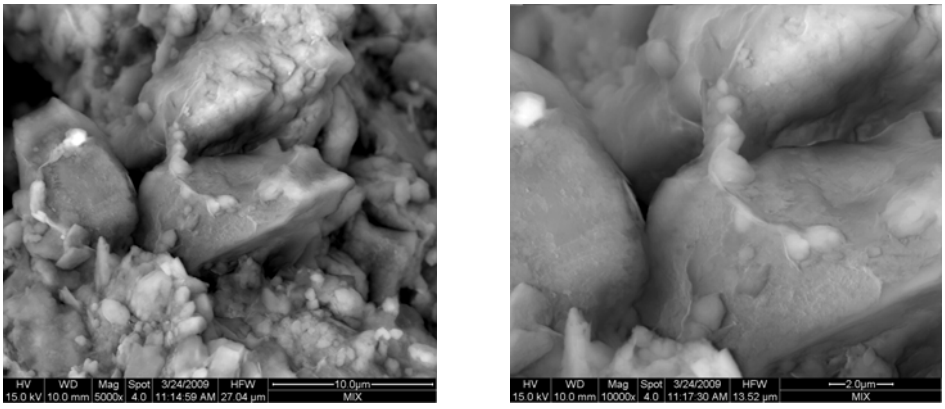

Figure 6.12 Electron microscopy images of silt particles nonded by calcium carbonate found in an intact sample of the silty clay soil (VMClay) from the block

6.2.2 Summary of the index properties of the Valencia silty soils

Based on the results shown in the previous paragraphs, the VSS soils tested in this research project can be classified as follows:

- **VMClay** (material from the block sample)

  This soil consists of an inorganic light-brown low plasticity silty clay with aggregates of cemented particles.

  - 28 – 40% clay-sized
  - 55 - 64% silt
  - 5 - 8% fine to medium sand
  - Average $CaCO_3$=50% in soil
  - Proportion of mass of aggregates ranged from 0.3 to 4% with an average value of 1.5%. $CaCO_3$=67.6%
  - Average w_l=28.5% and I_p=10.5%
  - Average natural water content=19.5%
  - Average degree of saturation=92%
  - Average Liquidity index=0.17
  - Average Activity A=0.31
  - Unified soils classification system: CL

- **VSSilt** (remoulded material)

  In this case, the soil consists of an inorganic light-brown low plasticity silt/clay with sand.

  - 25% clay-sized
  - 43% silt
  - 32% fine to medium sand
  - Average w_l=23.6% and I_p=7%
  - $CaCO_3$=33.4%
  - Average Activity A=0.28
  - Unified soils classification system: ML-CL

- **VMSand** (remoulded material)

  The soil consists of an inorganic yellow non-plastic silty sand.

  - 5% clay-sized
  - 20% silt
  - 75% fine to medium sand
  - Non-Plasctic
  - $CaCO_3$=30%
  - Unified soils classification system: SM

6.3 Previous investigations on the mechanical behaviour of the Valencia silty soils

A review of previous works on the mechanical behaviour of the Valencia silty soils was carried out. All the available information was based on commercial geotechnical reports specifically done for the design and construction of the underground lines of the Valencia metro. Unfortunately, there was not any research work performed that focussed on the influence of the in-situ structure on the mechanical behaviour and on any possible transitional behaviour of the Valencia silty alluvial soils.

In terms of particle size distribution, three fundamental types of gradings were identified and named by Celma (1990, personal communication) as:

- Cohesive layers A and F that consist mainly of mixtures of clay/silt soils, where the A material is normally the first alluvial cohesive layer that could be found in the boreholes. In many cases, aggregates of particles cemented by calcium carbonate could be also found in these cohesive layers. In general the soils are classified as CL or ML-CL.

- Transitional layers of silty sands that are found as a transition between the cohesive and the granular material. In many cases they could appear as alternating layers in the cohesive soils. This material is normally classified as SM.

- Granular layers G that are formed of silty gravels.

The presence or absence of any of these materials on the boreholes depends on the erratic movement experienced by the Turia River that makes the soil's profile very heterogeneous throughout the city of Valencia.

Due to the common heterogeneity of gradings that can be found in each of these layers, it was considered not appropriate to provide geotechnical properties associated to these materials in this thesis because of their variability from one site to the other.

The intact block sample tested in this research project was taken from a layer of cohesive soil that was assumed to correspond to the A material described above. Based on the information available from the geotechnical report (Estudio geológico-geotécnico para la Línea T2 Metro Sur, Tramo Xativa – Nazaret, Gestec 2005), the A layer, from which the intact block sample was retrieved, was considered to be lightly overconsolidated with OCRs that ranged from 1.17 to 1.47. No explanation was provided to prove the reason for these OCRs.

Chapter 7
The mechanical behaviour of the Valencia Silty Soils

7.1 Introduction

The Valencia silty soils (VSS) from the Turia River flood plain were the second materials studied in this research project. As in the case of the Bormida River silts, the aim of this chapter is to give answers to the following questions: *(a) Is it possible to find a unique NCL for the VSS? (b) Is it possible to find a unique CSL? (c) How does the sample preparation technique influence the mechanical behaviour in terms of a possible transitional response? (d) How does the in-situ structure influence the behaviour of these soils?* To answer these questions a similar experimental programme to that for the BRS was defined based on oedometer and triaxial tests.

7.2 Oedometric behaviour

A series of oedometer tests were carried out to investigate the uniqueness of the NCL and the effect of the in-situ structure on the compression behaviour of the VSS. In the case of the silty clay soil (VMClay), tests were performed on slurry, compacted and intact samples, whereas in the case of the silty sand (VMSand) and sandy clay/silt (VSSilt) materials, only compacted and slurry samples were tested due to the lack of intact specimens. The initial void ratio of the samples was

obtained using Equations 5.1 to 5.4, where the maximum error in calculating e was less than ±0.02. The effect of the system compliance was checked and it was found that for stresses higher than 4MPa, the difference between corrected and un-corrected compression lines was significant.

7.2.1 Oedometric behaviour of the Valencia silty clay soil (VMClay)

As described in Chapter 6, the intact block sample of the Valencia silty clay soil that was classified as CL was taken from a depth of 4.5m below ground level. The water table was located 1.5m below the point from where the block was retrieved. The estimated in-situ vertical effective stress at the depth of sampling was σ'_v=105kPa. The average index properties of this soil were summarised in Section 6.2.2. In the following sections the results of the oedometer tests carried out on slurry, compacted and intact samples are presented.

• Slurry samples

Two types of slurry samples were prepared from the trimmings of the intact block. The first type was the conventional slurry sample created by mixing distilled water with the material obtained when the intact specimens were trimmed for testing. After the slurry was created, it was directly poured into the oedometer ring and the test was performed. The second type was named a "cake" sample. In this case, the slurry was first placed in a large consolidometer cell and compressed to a maximum vertical stress level of 100kPa (Figure 3.11). Once the cake sample was removed from the cell, it was cut into small pieces from which specimens were trimmed to be tested in conventional oedometer apparatus. A more detailed description of the procedure to create the cake sample was given in Section 3.7.2. Table 7.1 summarises the details of the oedometer tests carried out. From Table 7.1 it can be observed that the slurry samples were identified as OS, the cake as OSC and the compacted as OC.

Test	w_i (%)	$\sigma_{v\,max}$ (kPa)	Comments
VMClay-OS1	40.7	2006	Slurry prepared at $1.4 \cdot w_l$
VMClay-OS2	37.9	1993	Slurry prepared at $1.3 \cdot w_l$
VMClay-OS3	43	9013	Slurry prepared at $1.5 \cdot w_l$
VMClay-OSC1	26	5102	Cake sample
VMClay-OC1	17	13263	Wet compacted sample

Table 7.1 Summary of the oedometer tests carried out on slurry samples of the Valencia silty clay (VMClay)

Figure 7.1 shows the compression lines of three slurry samples prepared at three different water contents, which varied from 1.3 to 1.5 times the average liquid limit of the VMClay soil. The size distribution of the materials used for the preparation of the slurry specimens covered the range of gradings shown in Figure 6.5. In Figure 7.1, it can be seen that all the compression lines were slightly concave upwards and although the grading was slightly different for each sample, a unique intrinsic normal compression line (1D-ICL*) could be identified, regardless of the initial water content and size distribution. The average value of the intrinsic compression index for the estimated 1D-ICL* was C^*_c=0.158. This value was very close to that calculated from the correlation with the void ratio at the liquid limit proposed by Burland (1990), which gave a compression index of 0.160. The swelling behaviour was very similar in all the samples with an average value of the swelling index of C^*_s=0.025 and a ratio of C^*_s/C^*_c=0.16. These values will be used as a reference for the analysis of the in-situ structure of the intact samples from the block.

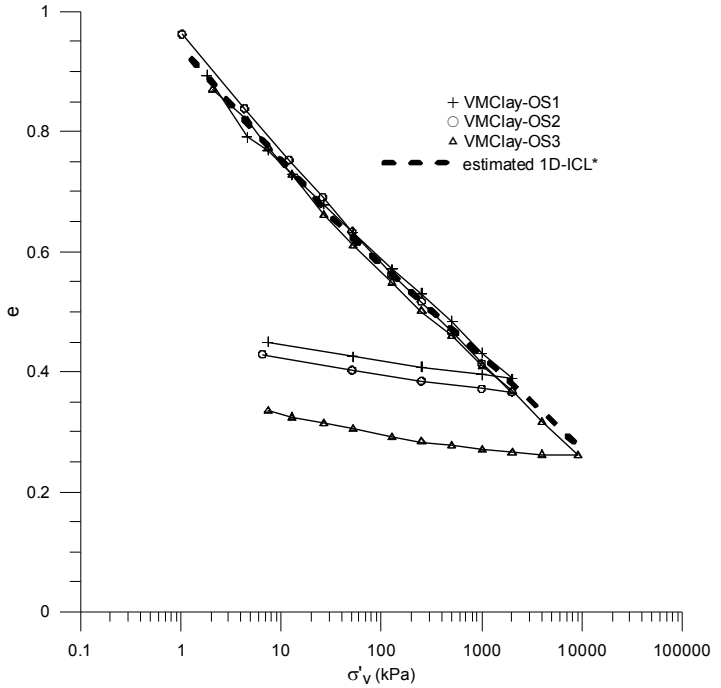

Figure 7.1 Oedometer compression of the slurry samples of the Valencia silty clay (VMClay)

The compression behaviour of a cake specimen and a dynamically compacted sample are plotted in Figure 7.2 and compared with the slurries. Sample VMClay-OSC1 was trimmed directly from a piece of the cake block. The compression line of this "intact" cake specimen crossed those of the slurries and plotted slightly above, suggesting the possibility of a small effect of the initial structure on the soil

behaviour. An estimation of the yield stress was carried out which gave a value of 100kPa. This stress was equal to the maximum previous vertical effective stress that the cake was subjected to in the consolidometer, clearly showing that the sample remembered its stress history during the recompression test. After yielding, the compression line tended to converge slowly towards the unique 1D-ICL* at high stresses. A small double arrow line is included in Figure 7.2 that shows the maximum estimated error in measuring the initial void ratio. Although it is believed that the sample preparation technique might have created a slightly different structure, unfortunately, the accuracy in measuring e was of the same order of magnitude as the observed difference in the position of the compression lines so it could not be concluded if the difference in behaviour was due to a real effect of the initial structure of the cake sample with respect to the slurries.

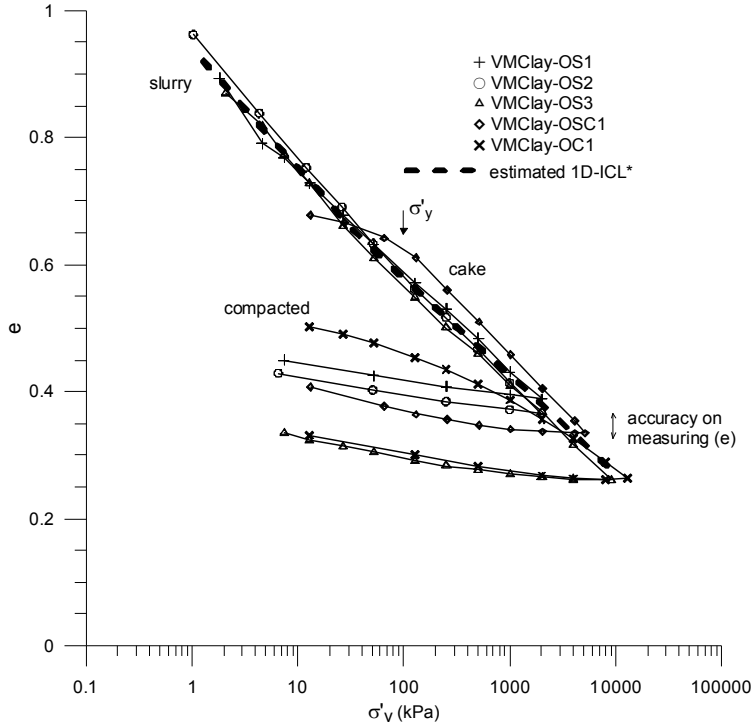

Figure 7.2 Comparison of the compression of the slurry (OS), cake (OSC) and compacted (OC) samples of the VMClay

On the other hand, a comparison of the compression behaviour of the compacted sample VMClay-OC1 with the slurries showed that the compression index was slightly lower, even at very high stresses, pointing to the possibility of an effect of the sample preparation technique on the compression behaviour as seen in other silty soils (e.g. Santucci de Magistris et al., 1998).

The oedometric stiffness of the slurry, cake and compacted samples was analysed and plotted in Figures 7.3 and 7.4, using a logarithmic scale for both axes. Figure 7.3 shows the relationship between the oedometric tangent modulus (M_{oed}) and the vertical effective stress, during loading and unloading, for the three slurry samples tested. It can be observed that apart from the scatter observed in the measured values at the start of the compression stage, all the samples converged onto a unique straight line along the normal compression and swelling lines. A regression analysis was carried out to estimate the relationship between the M_{oed} and σ'_v. Equations 7.1 and 7.2 express the stiffness for stress levels along the normal compression and swelling lines respectively. Their coefficients of correlation were very good in both cases, with values of R^2=0.995 and 0.994.

$$M_{oed}(NC) = 26.2 \cdot \sigma_v^{'\,1.012} \ (kPa) \qquad 7.1$$

$$M_{oed}(OC) = 101.3 \cdot \sigma_v^{'\,1.082} \ (kPa) \qquad 7.2$$

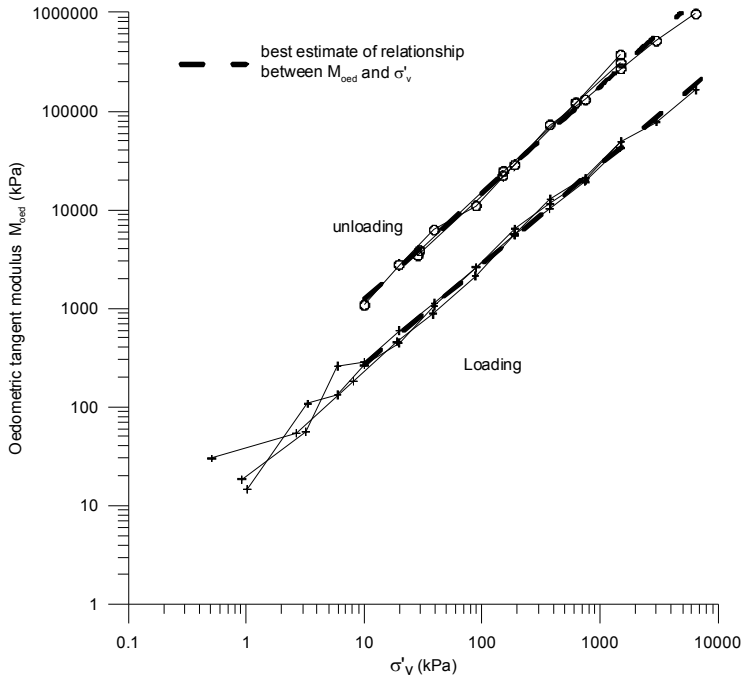

Figure 7.3 Oedometric tangent moduli (M_{oed}) of the slurry samples of the VMClay

Figure 7.4 shows a comparison between the stiffness of the cake, compacted and slurry samples. The estimated unique relationship between the M_{oed} and σ'_v for the slurry was taken as a reference for the comparison. It is interesting to point out how, in the case of the "intact" cake sample, there was a clear change in the slope of the relationship between the M_{oed} and σ'_v at around a vertical stress of 100kPa,

which corresponded to the yield stress measured in the oedometric curve. After yield, the stiffness increased linearly with the stress level, the values being slightly lower than those along the reference line defined by the slurry samples, although the structure of the cake sample was slightly stronger than that of the slurry at the same e value. The compacted sample showed higher stiffness compared to the other samples due to the effect of its denser initial state but at elevated stress levels the oedometric modulus was slightly lower than the reference values of the slurries.

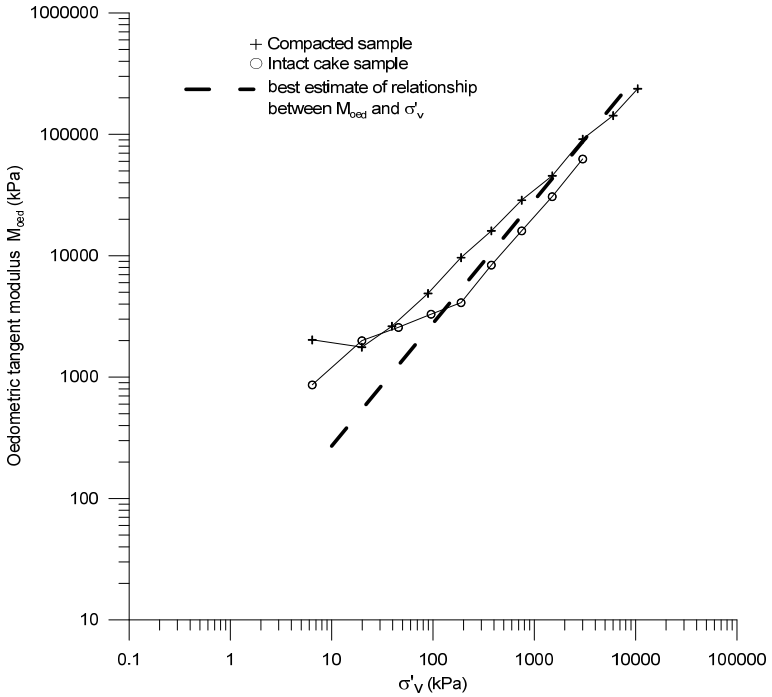

Figure 7.4 Comparison between oedometric tangent moduli (M_{oed}) of the slurry, cake and compacted samples of the VMClay

• Intact samples

A series of oedometer tests were performed on intact samples from the silty clay block. Table 7.2 summarises the details of each test carried out. One of the first things to pay attention to in Table 7.2 is the variability on the values of the initial void ratio that ranged from 0.593 to 0.687. This variability can be associated to a combination of different factors such as a possible heterogeneous initial structure inside the block sample, the heterogeneity in the grain size distribution, the error introduced in calculating e, which was estimated to be ±0.02, and possibly some structural damage induced to the samples during the sampling and preparation process. In fluvial environments, the rates and modes of deposition are likely to vary considerably during the formation of sedimentary soils due to changes in the

course of the river, as is the case of the Turia River. Although each of the above factors could have played a part in the initial void ratio, it was consequently believed that the most important and likely one was a heterogeneous in-situ structure due to variations in depositional conditions. In fact during the trimming of the intact samples for testing some specimens exhibited parts with slightly higher contents of silt than others.

Test	$*\sigma_{vi}$ (kPa)	$\sigma_{v(max)}$ (kPa)	w_i (%)	I_L	e_i	σ'_y (kPa)
VMClay-OI1	26.8	7989	18.8	0.08	0.593	600
VMClay-OI2	20.7	13753	17.0	-0.10	0.596	550
VMClay-OI3	20.9	14432	19.6	0.15	0.636	555
VMClay-OI5	7.3	9039	18.4	0.04	0.629	340
**VMClay-OI6	7.7	9013	22.6	0.40	0.687	425

Table 7.2 Summary of the oedometer tests carried out on intact samples of the Valencia silty clay (VMClay). * Samples were soaked after applying this stress. ** Water flushed throughout the sample during 24h under a back pressure of 10kPa after applying first load.

The compression behaviour of all the samples is shown in Figure 7.5. It can be observed that in the range of typical engineering stress levels (<1MPa) all the compression lines run almost parallel to each other, with a stiff response. In this region of stresses, non-unique compression lines were found. This is an important feature to be highlighted because, in routine commercial oedometer tests, it is very common to compress the samples to a maximum stress level lower than 1MPa with a consequent misunderstanding of the fundamental soil behaviour in terms of compressibility. The same behaviour was seen in the intact specimens of the BRS-B.

The yield stress was estimated for each test and the results are shown in Table 7.2. As can be seen, the values ranged from 340 to 600kPa with an average of 494kPa. Despite the assumed error involved in the procedure to calculate the yield stress, it seemed that there was no clear correlation between the initial void ratio and the yield stress level and all the yield stresses were much higher than the estimated current in-situ vertical effective stress of σ'_v=105kPa. These values would be equivalent to OCRs in the range of 3.2 to 5.7, which were very unrealistic because it is known that such high values of the geological preconsolidation stresses did not occur in the area. On the other hand, suction during the tests could be expected to be acting in the samples that could have influenced the values of the yield stress if the specimens had not been soaked before starting the test. Consequently the effect of the suction on the yield stress was expected to be negligible. Another factor that

could have had an important effect on these high values of yield stress could have been processes associated with seasonal volume changes, causing historical suction through desiccation and/or current suction in-situ due to the fact that the sample was retrieved from a relatively swallow depth of 4.5m. In fact, and shown in Table 2, the liquidity indices of all the samples were very close to zero or negative, supporting the idea that part of the measured yield stress could be due to a certain degree of overconsolidation as a result of desiccation. In any case, it appeared that the higher values of the yield stress measured on the intact samples of the Valencia silty clay soil (VMClay) could be associated to a more complex post-sedimentation structure.

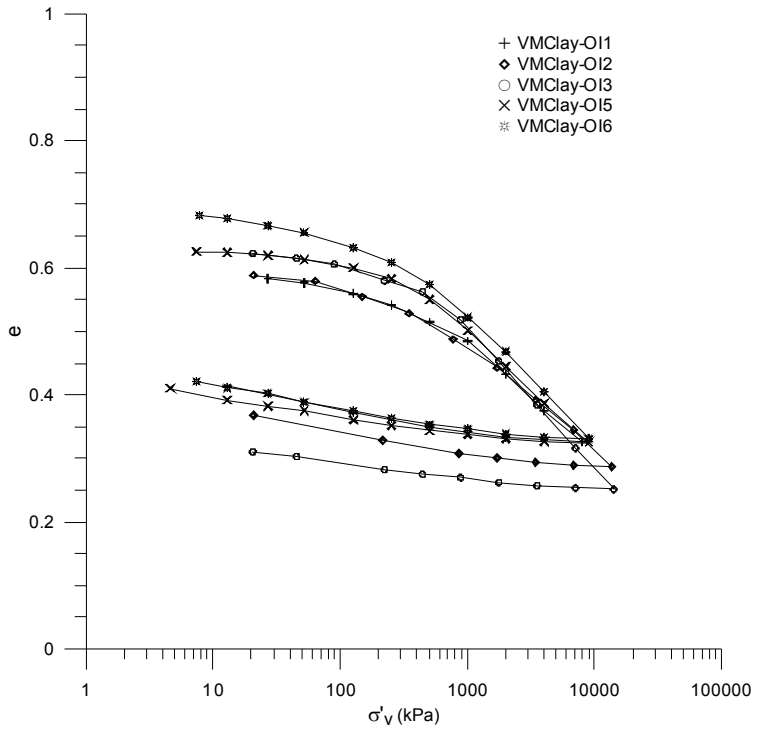

Figure 7.5 Oedometer compression of the intact samples of the VMClay

Although some scatter could be observed, after yielding, the compression curves seem to converge towards a unique normal compression line at high stresses regardless of their initial structure. Only the final part of the compression line of sample VMClay-OI3 showed a greater slope compared to the other curves. The behaviour during unloading showed that all the swelling lines run nearly parallel with very similar slopes. The swelling of the intact samples was also measured at the start of the oedometer tests, after the first load was applied and the cell was flooded with water. As shown in Table 7.2, the flooding was carried out at different

vertical stress levels, which ranged from 7.3 to 26.8kPa, well below the estimated in-situ stress level. No measurable swelling or collapse was observed in any of the samples.

As was described in Chapter 6 and shown in Figure 6.5, the silty clay soil that formed the material contained in the block had basically the same quantity of fines particles (average 93%) but with some samples being more clayey than others. In fact, the clay-sized content varied from 28 to 40% between specimens. In order to check the possible effect on the compression behaviour of the clay-sized content on the soil, a comparison between the samples with the higher content of clay-sized and silt-sized particles is made in Figure 7.6. It appears that both samples converge onto the same normal compression line at high stress with the same response during unloading, despite the fact that their initial structure was different, as was their yield stress. Consequently, it again seems that the variability in grain size distribution of the material contained in the block did not have a significant effect on the compression behaviour of the VMClay soil, so the observed differences of the initial void ratio can be attributed to differences in structure.

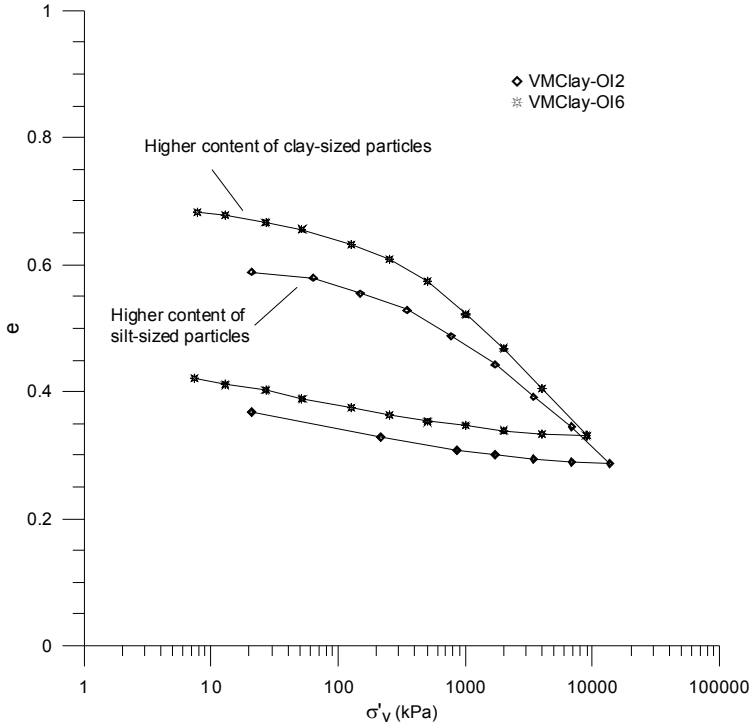

Figure 7.6 Oedometer compression of some intact samples of the VMClay with different grading curves

• Effect of the in-situ structure of the intact samples on the compression behaviour

The one-dimensional compression behaviour of the intact samples is compared with the slurries in Figure 7.7. As can be seen, all the compression curves of the intact samples crossed those of the slurries, showing a clear effect of their in-situ structure on the compression behaviour. In terms of swelling behaviour, the swelling lines were almost parallel to the slurries resulting in a swell sensitivity index of around unity. This suggests that any possible initial bonding affecting the in-situ structure had little effect at the end of the tests.

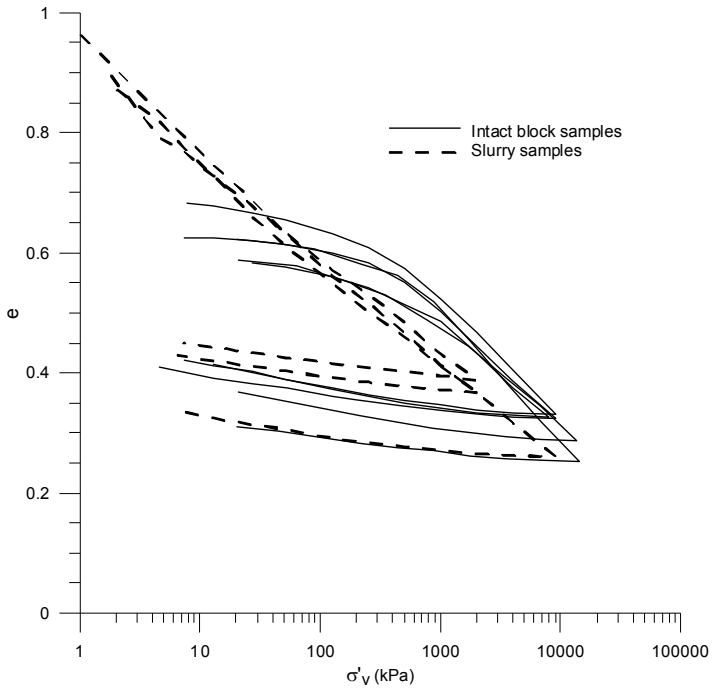

Figure 7.7 Comparison between the oedometer compression of the intact and slurry samples of the VMClay

Figure 7.8 shows the compression curves and in-situ state normalised for volume by means of the void index (Iv), using as a reference the best estimate unique intrinsic compression line (1D-ICL*), defined in Figure 7.1 by the slurry samples. In addition, the intrinsic (ICL) and sedimentation compression (SCL) lines (Burland, 1990) are also plotted in the same figure. The first point to note from the comparison of the ICL with the best estimate unique 1D-ICL* is that, for the range of stresses applied, the shape of the latter deviated from the curved shape of the ICL of Burland at stresses lower than 40kPa and higher than 1500kPa.

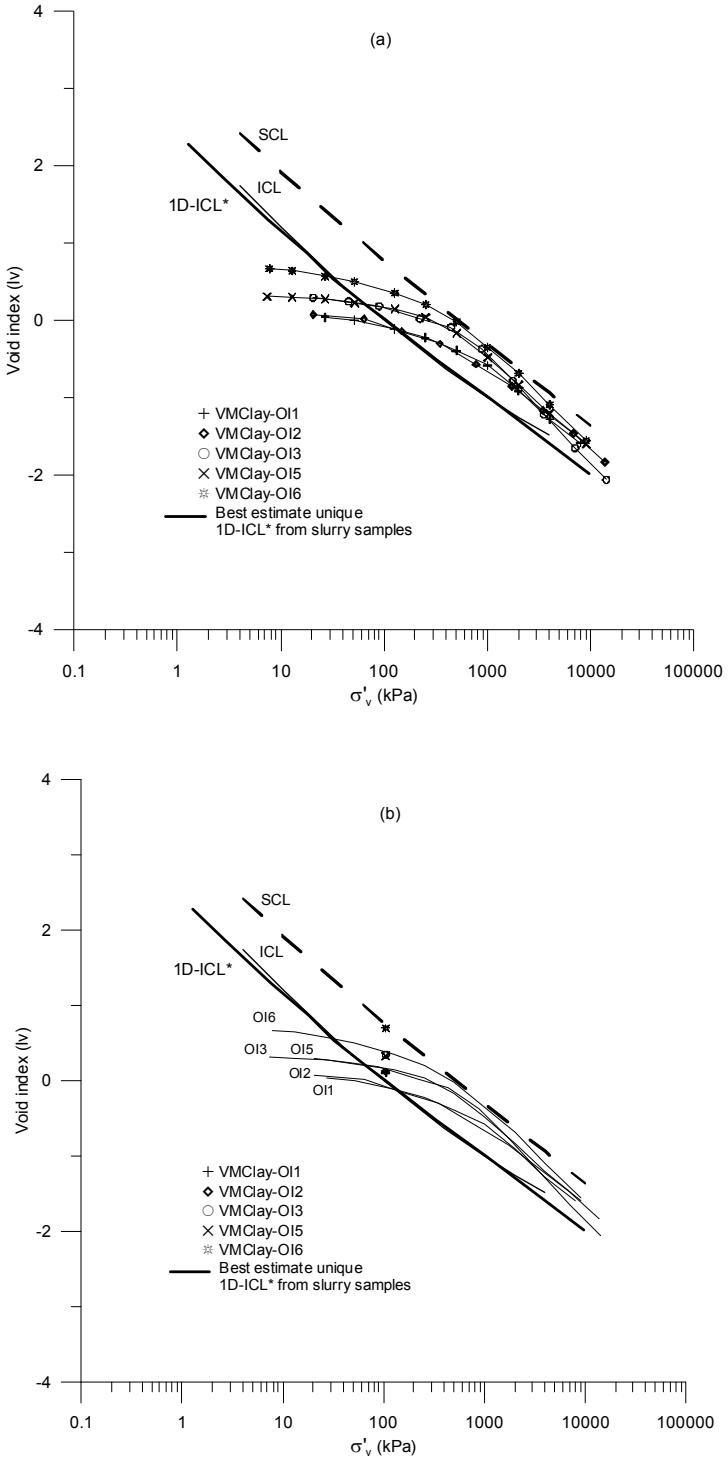

Figure 7.8 Normalized data (a) oedometer compression of the intact samples and (b) in-situ states of the VMClay

From the comparison in Figure 7.8, it can be seen that the normalised compression curves of the intact samples crossed the 1D-ICL* and yielded at different stress levels in between the 1D-ICL* and the SCL, with the looser specimens plotting on or very close to the SCL. The stress sensitivity values ranged from 2.0 to 4.8 with an average of 3.0, where the higher values corresponded to the higher initial void ratios. The post-yield behaviour was slightly different depending on the initial void ratio. In the case of the denser samples VMClay-OI1 and VMClay-OI2, the normalised lines run almost parallel to the 1D-ICL* line after yielding, showing a robust effect of the initial fabric even at very high stresses, with little effect of transient features of structure such as bonding.

On the other hand, the loosest sample VMClay-OI6 reached the SCL and thereafter tended to converge slowly onto the same unique normal compression line as the denser samples. The effect of an initial bonding in this sample might be slightly larger compared with the denser samples. A similar behaviour was seen in sample VMClay-OI5. The behaviour of sample VMClay-OI3 was slightly different to the other specimens. In this case its normalised compression line almost reached the SCL and after that, it converged faster than the other samples towards the 1D-ICL*, with an apparent total removal of its initial structure at the end of the test. This response suggests a more noticeable effect of bonding in the initial structure, with a smaller influence of more robust fabric effects.

In conclusion, it seems that in general, and apart from sample VMClay-OI3, fabric had the most important effect on the compression behaviour of the intact block samples despite the high carbonate content in the soil. It is important also to point out that although some of the specimens tested did have different initial void ratios, they apparently reached very similar stable structures at the end of the test, where the initial fabric was not totally erased and with stress sensitivities larger than unity.

The normalised in-situ stress state of each intact sample is plotted in Figure 7.8(b). It can be seen that all the stress states lay in-between the 1D-ICL* and the SCL but with different locations depending on the estimated in-situ void ratio of each sample, again confirming a clear heterogeneous in-situ structure of the material contained in the block sample, since any influence of grading should be normalised by Iv. Unfortunately the sedimentation compression curve (SCC) (Terzaghi, 1941) of the VMClay is unknown and therefore the current OCR can not be estimated to be compared with the yield stress ratio measured for each sample, which ranged from 3.2 to 5.7. In addition, and as mentioned before, OCRs equals to these calculated YSRs would be totally unrealistic because it is known that such high values of the geological preconsolidation did not occur in the area. As was described in Chapter 6, Section 6.3, and based on previous commercial geotechnical

reports, the soil layer from which the intact block sample was retrieved was lightly overconsolidated with OCRs that varied from 1.17 to 1.47. No explanation was given to justify these OCRs. In any case, and as said above, it seems that the higher values of the yield stress ratios measured on the intact samples of the Valencia silty clay soil (VMClay) might be associated to a post-sedimentation structure, resulting from diagenetic processes more complex than simple mechanical unloading, which controlled the soil behaviour.

The variation of the oedometric modulus (M_{oed}) with the vertical effective stress of the intact samples is shown in Figure 7.9, together with the estimated unique relationship between M_{oed} and σ'_v along the 1D-ICL*, defined by the slurries. It can be observed that for stresses below yield, all the samples exhibited higher stiffness than the slurries, reflecting the effect of the initial structure on the soil behaviour. Moreover, and apart from a couple of points for the initial loading of sample VMClay-OI6, all the M_{oed}-σ'_v lines plotted in a narrow band with the same trend. A break in the slope of the stiffness increase appears to occur at around a vertical stress which coincided with the position where most of the lines crossed the estimated unique M_{oed}-σ'_v relationship for the slurries. For stresses beyond yield, the M_{oed}-σ'_v lines tended to converge onto a unique relationship defining the increase of the stiffness with the stress level at yield stress ratios of 1. It is important to point out that for YSR=1, the stiffness of the intact samples was smaller than the corresponding value of the slurries for the same stress level. This behaviour proved that, although beyond yield, the structure of the intact samples was stronger than that of the slurry for the same e, as shown in Figures 7.7 and 7.8, so the stiffness was smaller and decreasing as the in-situ structure was being erased during compression.

Finally, it could also be interesting to highlight that the change in stiffness from a pre-yield to a post-yield state of stress happened without any maximum in the stiffness, which is normally followed by a sudden decrease of M_{oed} for overconsolidated soils (e.g. Davison & Atkinson, 1990 and Figure 5.4). This latter argument could help to support the hypothesis that the yield stresses measured on the intact samples did not correlate with any previous maximum pressure, but was related to post-depositional processes.

7.2.2 Oedometric behaviour of the Valencia silty sand (VMSand)

The second material of the VSS studied in this chapter was the non-plastic Valencia silty sand (VMSand) that was classified as SM. A remoulded sample was excavated from a very homogenous layer at a depth of 3m below ground level, well above the water table. The average index properties were summarised in Section

6.2.2. In this case no intact samples were available for testing and only air-dried and wet compacted samples were tested to avoid any possible segregation that could happen when using slurries. The details of each test are shown in Table 7.3.

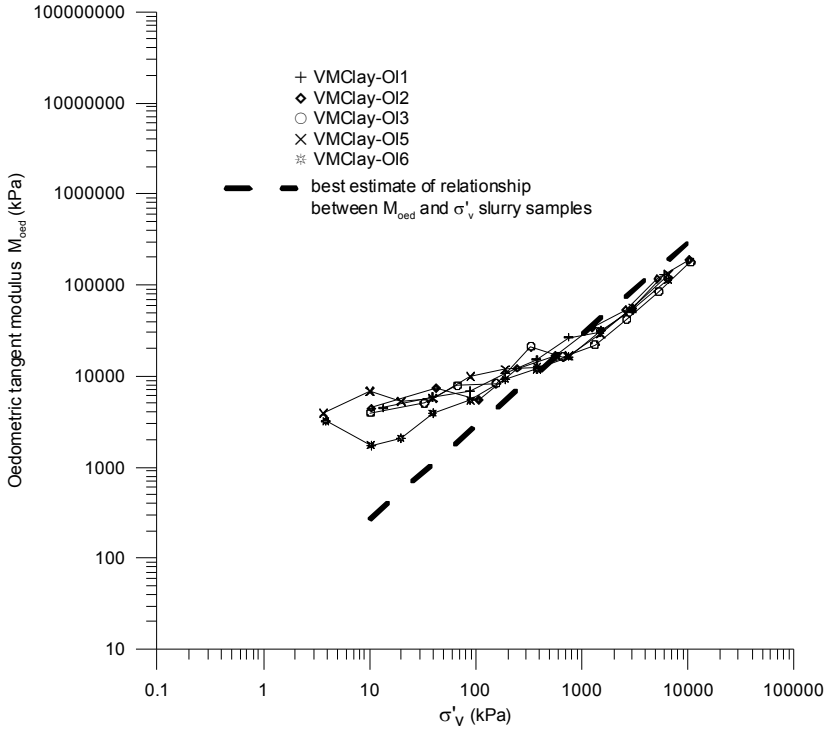

Figure 7.9 Oedometric tangent moduli (M_{oed}) of the intact samples of the VMClay

test	w_i (%)	e_i	σ_{vmax} (kPa)	Comments
VMSand-ODC2	1.5	0.781	13800	
VMSand-ODC3	1	0.725	2008	
VMSand-ODC4	1	0.934	13800	
VMSand-OWC1	26.8	0.790	13800	
VMSand-OWC2	14.3	0.821	28892	Only used for breakage analysis
VMSand-OWC3	28.9	0.802	28892	

Table 7.3 Summary of the oedometer tests carried out on compacted samples of the Valencia silty sand (VMSand) (notation OWC: oedometer wet compaction; ODC: oedometer air-dried compaction)

The one-dimensional compression behaviour of the VMSand is shown in Figure 7.10. It can be observed that in the range of typical engineering stress levels (<1MPa), the compression lines run nearly parallel to each other, showing no sign of convergence towards a unique NCL, so the initial density controlled the compression behaviour of each sample. None of the compression lines showed an abrupt change in compressibility, so although it was not easy to determine the exact point where each sample yielded, it was apparent that the yield stress was higher for the denser samples, as might be expected due to their higher coordination numbers. As the stresses increased the compression lines tended to converge very slowly onto a unique normal compression line at very elevated levels of stress, regardless of the initial void ratio. A best estimate unique normal compression line (1D-NCL) for the compacted samples of VMSand is drawn in Figure 7.10 with a slope C_c=0.371. The behaviour during swelling was very similar with an average value of the swelling index C_s=0.017, giving a ratio of C_s/C_c=0.046.

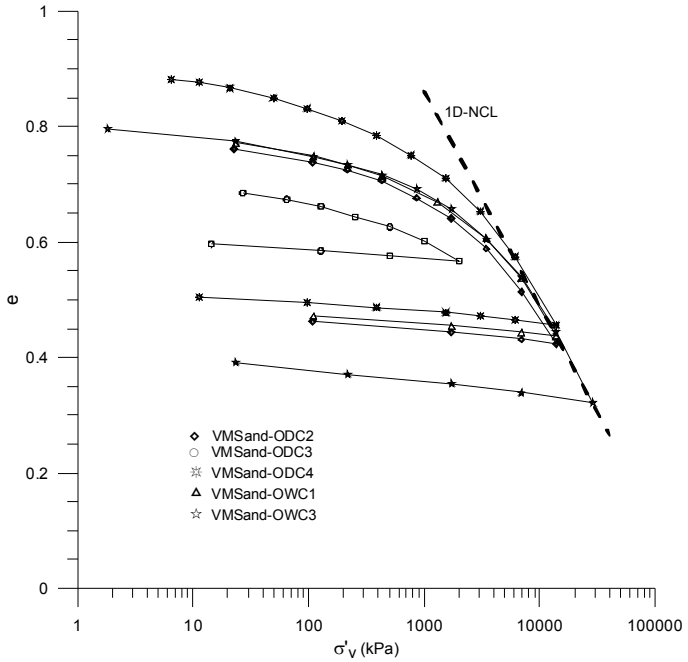

Figure 7.10 Oedometer compression of the compacted samples of the Valencia silty sand (VMSand). Notation OWC: oedometer wet compaction; ODC: oedometer air-dried compaction

The particle breakage of a material can be analysed by different methods (e.g. Hardin, 1985; Einav, 2007). The simplest and perhaps the most used is Hardin's method. In this method, the relative particle breakage (Br) is measured by comparing the grading curves above the 74μm sieve before and after testing (Figure 2.4). The method ignores the fines, based on the assumption that they do not

contribute to the breakage. Although this hypothesis is not correct (e.g. Altuhafi and Coop, 2011), it was considered valid to apply Hardin's method to evaluate the possible particle breakage of the VMSand due to its simplicity and facility to compare literature results with those obtained in this research project.

The particle size distribution of each sample before and after the oedometer tests was determined by the conventional mechanical sieving method, the results of which are plotted in Figure 7.11. As expected, the particle breakage increased with stress level. The effect of the initial void ratio on the amount of particle breakage at the same stress levels of 13.8 and 28.9MPa was checked in Figure 7.11(b). The relative breakage was essentially the same in the case of the samples tested to a maximum stress level of 28.9MPa. These two samples had nearly the same initial void ratio. On the other hand, and contrary to the findings of Altuhafi and Coop (2011), for the case of the tests at 13.8MPa, the loosest sample showed the lowest value of the relative breakage. It is important to point out that the quantification of the breakage using Hardin's method is sensitive to the number of sieves used during the sieving process and repeatability in the number and size of them is of importance. Unfortunately, one of the sieves used to analyse the grading size distribution of the loosest sample VMSand-OWC3 (13.8MPa) did not coincide with those used with the other samples (Figure 7.11a). This might have slightly affected the value of the breakage of this sample because of the assumed linear variation of sizes between sieves.

Figure 7.12 shows the variation of the oedometric modulus with the vertical effective stress during loading and unloading. A larger scatter in the results can be observed compared with the Valencia silty clay (VMClay) slurry samples (Figure 7.3). During compression, it appears that the slope of the M_{oed}-σ'_v relationship slightly changed at a stress level of around 900kPa where the scatter of the data reduced considerably and a unique line could be defined. It was therefore considered to split the M_{oed}-σ'_v relationship into two parts. A regression analysis was performed and the best estimate lines for the M_{oed}-σ'_v relationship during loading were represented by a power law in Equation 7.3. The coefficients of correlation were 0.94 and 0.98 respectively. During unloading, a larger scatter in the results was again seen. Equation 7.4 represented the best estimate M_{oed}-σ'_v line for unloading.

$$M_{oed} = 383.9 \cdot \sigma'^{\,0.663}_v \quad (\text{kPa}) \quad \sigma'_v < 900\text{kPa}$$
$$M_{oed} = 814 \cdot \sigma'^{\,0.55}_v \quad (\text{kPa}) \quad \sigma'_v > 900\text{kPa} \qquad 7.3$$

$$M_{oed} = 371.3 \cdot \sigma'^{\,0.91}_v \quad (\text{kPa}) \qquad 7.4$$

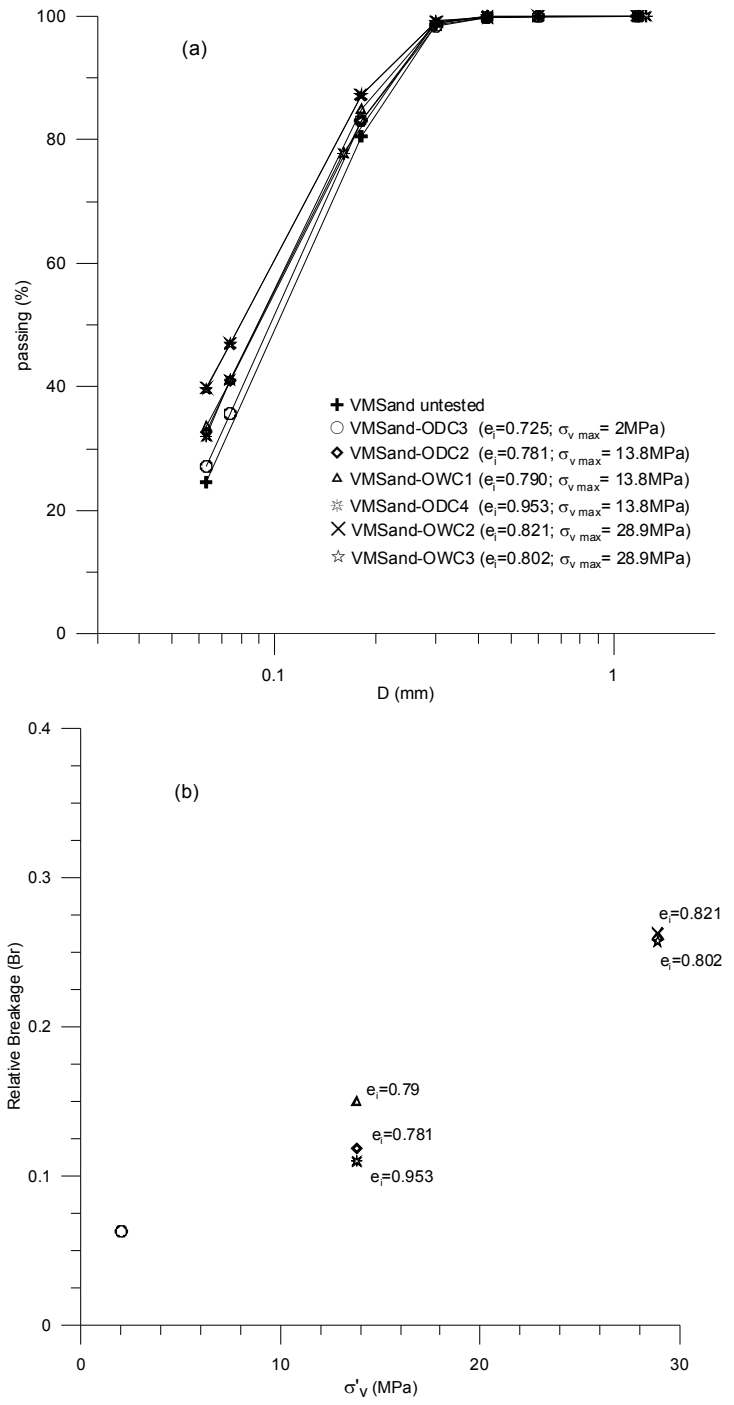

Figure 7.11 Particle breakage of the VMSand: (a) grading curves before and after the oedometer test and (b) relative breakage based on Hardin (1985) definition

In coarse grained materials like the VMSand, where the stiffness increases with the stress, the positive locking effect due to densification of the soil during compression overcomes the unlocking negative effect caused by the particle breakage that reduces the stiffness. This type of soil behaviour was called Type C by Mesri & Vardhanabhuti (2009).

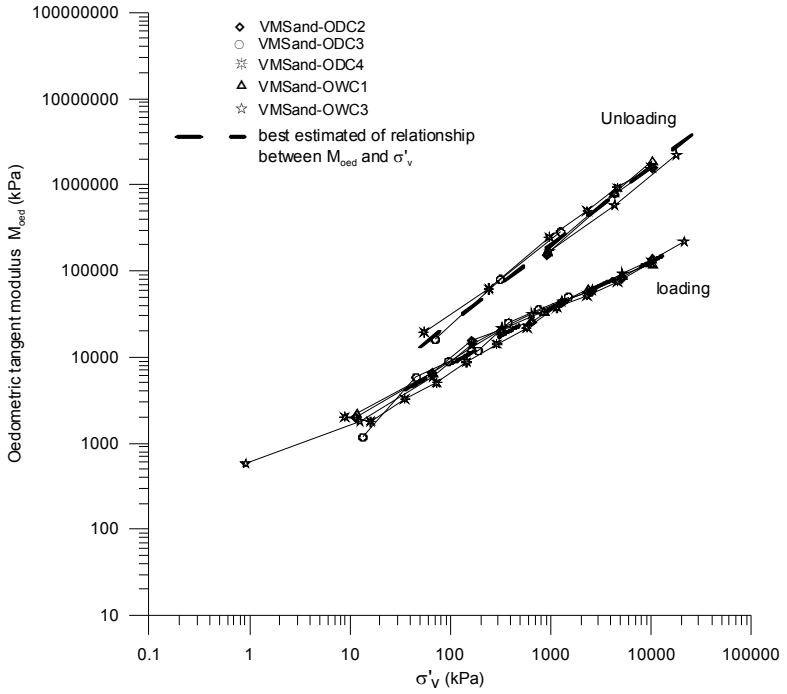

Figure 7.12 Oedometric tangent moduli (M_{oed}) of the compacted samples of the VMSand

One of the topics reviewed in Chapter 2 was the debate about the definition of the normal compression line of sands. Some researchers state that for a given sand there exists many different NCLs, each corresponding to a different initial density, regardless of the stress level (e.g. Ishihara et al., 1975; Jefferies & Been, 2000). Other researchers considered that a unique NCL exists for any particular sand and it only occurs at the onset of particle breakage at high stress level (e.g. Vesic & Clough, 1968; Coop & Lee, 1993; Pestana & Whittle, 1995). The main point to consider in the definition of the NCL could be the stress level, which will control the behaviour of the soil. If the tests carried out, for example by Jefferies & Been, would have been taken to very high stress levels, it is likely that a unique normal compression line would have been obtained and the conclusions would have been the same as those obtained, for example, by Coop & Lee. The results obtained for the one-dimensional compression behaviour of the Valencia silty sand (VMSand), and shown in Figure 7.10, agree with both arguments.

7.2.3 Oedometric behaviour of the Valencia sandy silt/clay (VSSilt)

The last material of the VSS studied in this chapter was the Valencia sandy silt/clay (VSSilt) that was classified as CL-ML. A remoulded sample was excavated at the same location as the VMSand from a homogenous layer at a depth of 1.5m below ground level. The soil profile at the sampling site showed that the VSSilt soil was deposited over the VMSand material. The average index properties were summarised in Section 6.2.2. As in the case of the VMSand, no intact samples were available for testing and only wet compaction and slurry samples were tested. The details of each test are shown in Table 7.4.

Test	w_i (%)	$\sigma_{v\,max}$ (kPa)	Comments
VSSilt-OS1	27.1	4904	Slurry prepared at $1.15 \cdot w_l$
VSSilt-OS2	38.8	15956	Slurry prepared at $1.6 \cdot w_l$
VSSilt-OS3	46.7	13800	Slurry prepared at $2 \cdot w_l$
VSSilt-OWC1	20.4	4904	Wet compacted sample

Table 7.4 Summary of the oedometer tests carried out on slurry and compacted samples of the Valencia sandy silt/clay (VSSilt)

Figure 7.13 shows the compression behaviour of three slurry samples prepared at different initial water contents, which varied from 1.15 to 2 times the average liquid limit of the VSSilt. It can be seen that a clear unique intrinsic compression line (1D-ICL*) could be defined regardless of the initial water content. In addition, the compression behaviour of a wet compacted sample was also plotted in Figure 7.13 to investigate the possible effect of the sample preparation technique on the soil response. As can be observed, the compression line converged onto the same unique normal compression line as that defined by the slurry samples, showing no effect of the sample preparation technique on the position of the intrinsic compression line. The measured intrinsic compression index was equal to 0.144. This value was slightly higher compared with the estimated one of 0.124 using the correlation proposed by Burland (1990).

The M_{oed}-σ'_v relationships during compression and unloading are plotted in Figure 7.14. Despite the initial scatter in the results, during compression all the samples converged onto a unique M_{oed}-σ'_v line defined by the power relationship of Equation 7.5. A larger scatter was observed during unloading, where the best estimated M_{oed}-σ'_v relationship was expressed by Equation 7.6.

$$M_{oed} = 29.1 \cdot \sigma'_v \quad (\text{kPa}) \qquad 7.5$$

$$M_{oed} = 103 \cdot \sigma_v^{'\,1.05} \quad (kPa) \qquad 7.6$$

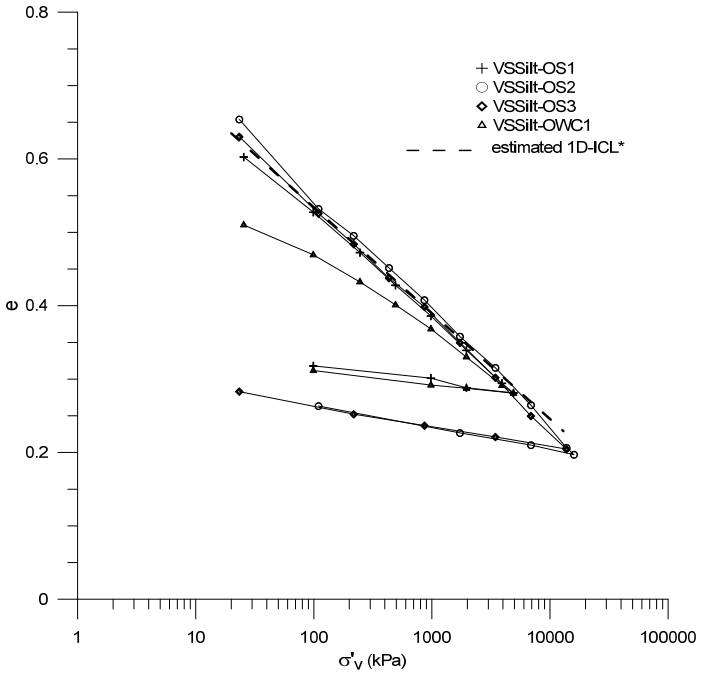

Figure 7.13 Oedometer compression lines of the slurry (OS) and compacted (OWC) samples of the Valencia sandy silt/clay (VSSilt)

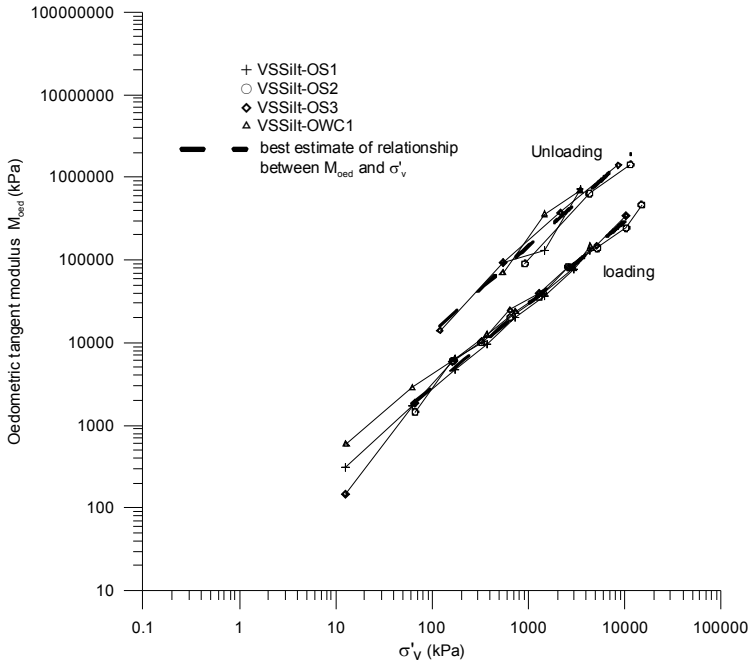

Figure 7.14 Oedometric tangent moduli (M_{oed}) of the slurry and compacted samples of the VSSilt

7.2.4 Summary

In the previous sections of this chapter, the oedometric compression behaviour of the Valencia silty soils from the alluvial plains of Turia River was investigated. Three different materials were studied; the silty clay (VMClay), the silty sand (VMSand) and the sandy silt/clay (VSSilt).

Figure 7.15 shows a comparison of the slurry/reconstituted unique normal compression lines indentified for each of the Valencia silty soils (VSS). It is important to note that the unique normal compression line of the VMSand was defined at very high stresses, whereas in the range of typical engineering stress levels (<1MPa) a non-unique NCL could be identified. The stiffness of the compression lines of the VMSand in this region was much higher compared with the other two soils. Despite the above explanation, it can be seen that as the fines content increased the position of the unique NCL of the VSSilt moved downwards and flattened but with an additional increase of fines the movement of the NCL of the VMClay changed direction, moving upwards with respect to the VSSilt, with a very small increase in the slope of the NCL. This behaviour suggests that there must be a transitional or limiting fines content in the VSS when the soil response changes from a coarse-grained dominated mode to fine-grained. Table 2.3 summarises the transitional fines contents reported by many researchers, the values of which varied from 25 to 35%, with the exception of the 50 to 70% found by Carrera et al. (2011). In the case of the VSS, the transitional fines content seems to be higher than those presented in Table 2.3 and similar to that obtained by Carrera et al. in their mixtures of sand with silt.

In terms of compressibility, a comparison of the M_{oed}–σ'_v relationships during loading for each grading is shown in Figure 7.16. It can be seen that in the case of the VMClay and VSSilt soils, the M_{oed}–σ'_v lines were essentially the same. The effect of grading was more noticeable in the case of the VMSand soil. As can be observed, for a given vertical effective stress the oedometric modulus of the VMSand was higher compared with those of the VMClay and VSSilt, up to a vertical effective stress level of around 1500kPa where the M_{oed}–σ'_v lines crossed. Beyond this point the stiffness of the VMSand was lower compared to the other soils. A justification for this behaviour could be the onset of a major particle breakage for the Valencia silty sand (VMSand) for stresses higher than 1500kPa that reduced the stiffness considerably.

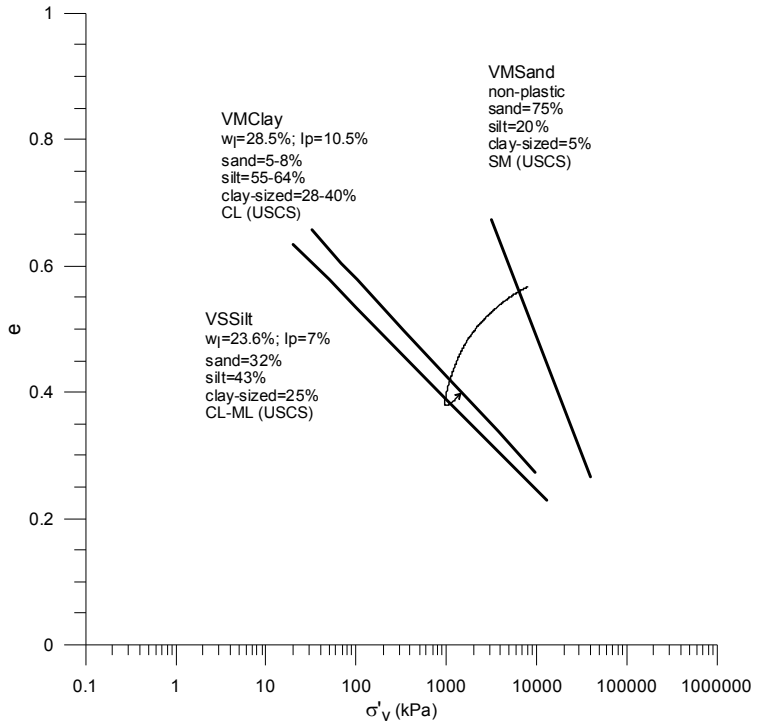

Figure 7.15 Unique normal compression lines of the Valencia silty soils (VSS)

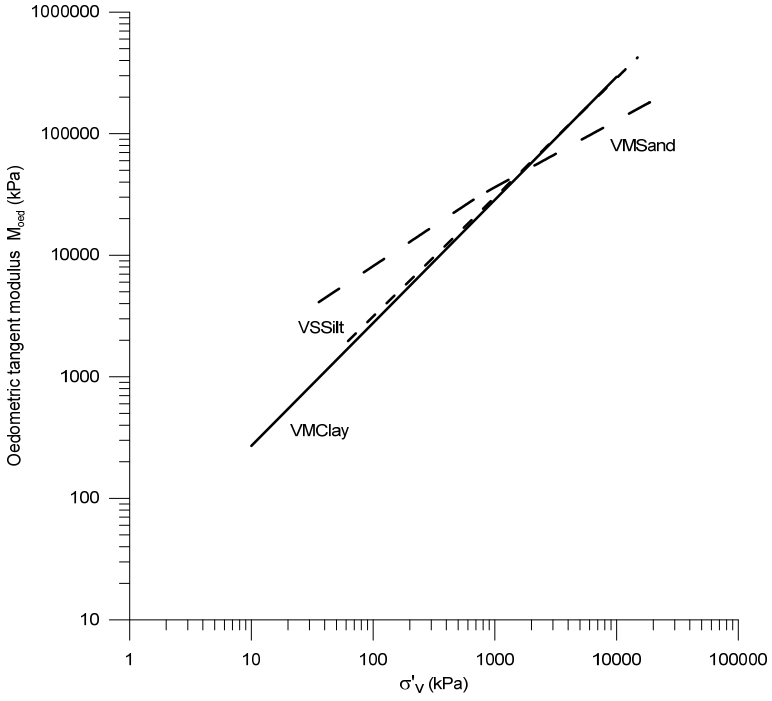

Figure 7.16 Oedometric tangent moduli (M_{oed}) of the Valencia silty soils (VSS)

Finally, the comparison between the one-dimensional behaviour of the slurry and the intact samples of the Valencia silty clay (VMClay) showed a clear effect of a heterogeneous in-situ structure. This heterogeneous in-situ structure found in the intact block sample is believed to be due to variations in depositional conditions of the Turia River together with different degrees of bonding (Figure 6.12), which might be associated to a post-sedimentation structure, resulting from diagenetic processes and more complex than simple mechanical unloading, which controlled the soil behaviour.

7.3 Triaxial behaviour of the Valencia silty clay (VMClay)

In the following sections the triaxial behaviour of the Valencia silty clay (VMClay) is presented. Slurry and intact specimens were tested to investigate the effect of the in-situ structure on the compression and shearing response of the VMClay.

7.3.1 Compression behaviour of the slurry samples

A series of triaxial tests were performed on slurry specimens trimmed from the cake sample prepared using the material from the intact block of the VMClay. Table 7.5 summarises the details of each test carried out.

test	e_o	σ'_v (kPa)*	p'_o (kPa) before shearing	OCR	Type of test
VMClay-TSC1	0.692	100	300	1.7	CIU
VMClay-TSC2	0.697	100	400	1	CIU
VMClay-TSC3	0.696	100	100	4	CIU
VMClay-TSC-$k_0$1	0.691	100	288	1	Ck_0U
VMClay-TSC-$k_0$2	0.694	100	200	1	Ck_0U

Table 7.5 Summary of the triaxial tests carried out on slurry cake samples of the Valencia silty clay (VMClay). (*) Maximum vertical stress applied to the slurry cake sample in the consolidometer when the cake was consolidated.

• Isotropic compression

Figure 7.17 shows the compression curves of three slurry samples that were compressed isotropically to a maximum mean effective stress which ranged from 400 to 500kPa. Two of the samples were unloaded, before shearing them at OCRs of 1.7 and 4. As was described in Section 7.2.1, the cake sample, from which the specimens were trimmed for testing, was anisotropically compressed to a maximum vertical stress level of 100kPa in the consolidomer. As will be shown later, the

estimated coefficient of earth pressure at rest of the VMClay for a normally consolidated state is equal to 0.48 and therefore the maximum vertical effective stress of 100kPa is equivalent to a mean effective stress of p'=66kPa. This anisotropic compression imposed a stress history that created an initial anisotropic structure in the cake.

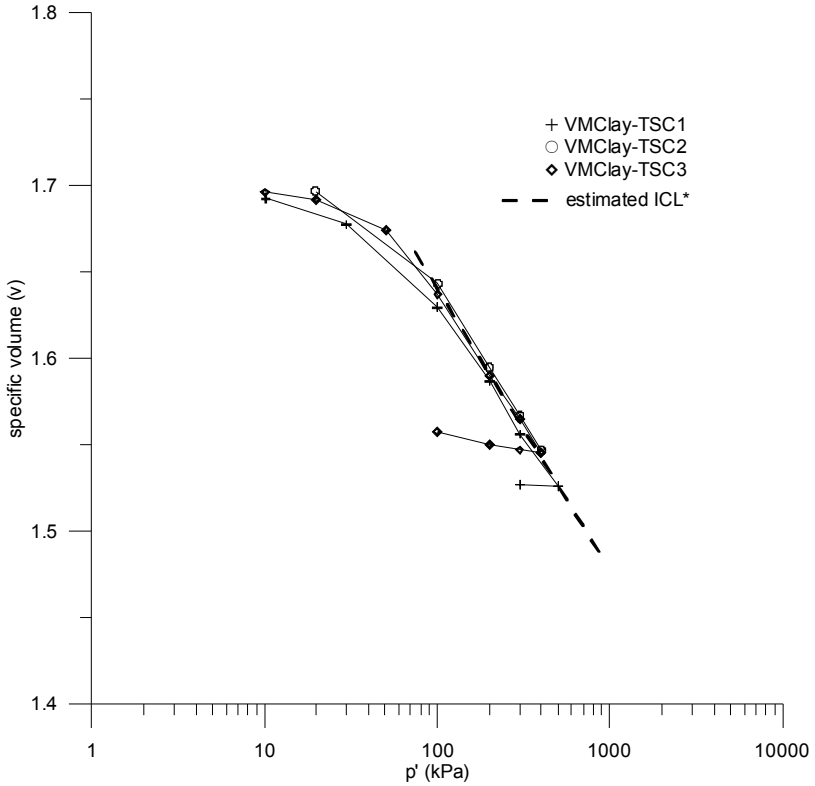

Figure 7.17 Isotropic compression of the slurry cake samples of the VMClay

Figure 7.18 shows the stress-strain response of sample VMClay-TSC3 during the isotropic loading and unloading stress increments, where the strains where calculated using Equation 5.19. The axial strains were measured using local LVDT's attached to the sample while the volumetric strains were calculated by using an Imperial College designed volume gauge. Looking at the results plotted in Figure 7.18, it can be seen that the anisotropic structure induced to the sample during the one-dimensional compression in the consolidometer resulted in a clear anisotropic deformation under the isotropic stress increments. The anisotropic mode of deformation decreased as the mean effective stress level increased and eventually reached a nearly pure state of isotropic deformation at a stress of p'=400kPa at the end of the compression stage. This stress level at which sample VMClay-TSC3 reached a nearly pure isotropic deformation state corresponds to approximately six times the maximum previous stress of p'=66kPa, applied to the

cake in the consolidometer. As described in Section 5.3.2, Burland (1967) proposed a criterion, where it can be assumed that a sample deforms isotropically under an isotropic stress increment for values of $\delta\varepsilon_1/\delta v\text{-}1/3$ equal to ±0.05 or smaller. Applying this criterion to the behaviour of sample VMClay-TSC3, it can be seen that this strain ratio condition is reached at p'=300kPa, which is equal to about 4.5 times the maximum previous value of p'=66kPa. These measured stress ratios required to bring an initially anisotropic sample to an isotropic state of deformation under an isotropic stress increment are in a similar range to those observed in the Bormida silty soils (BRS) and those frequently found in the literature (e.g. Mitaritonna et al. 2013).

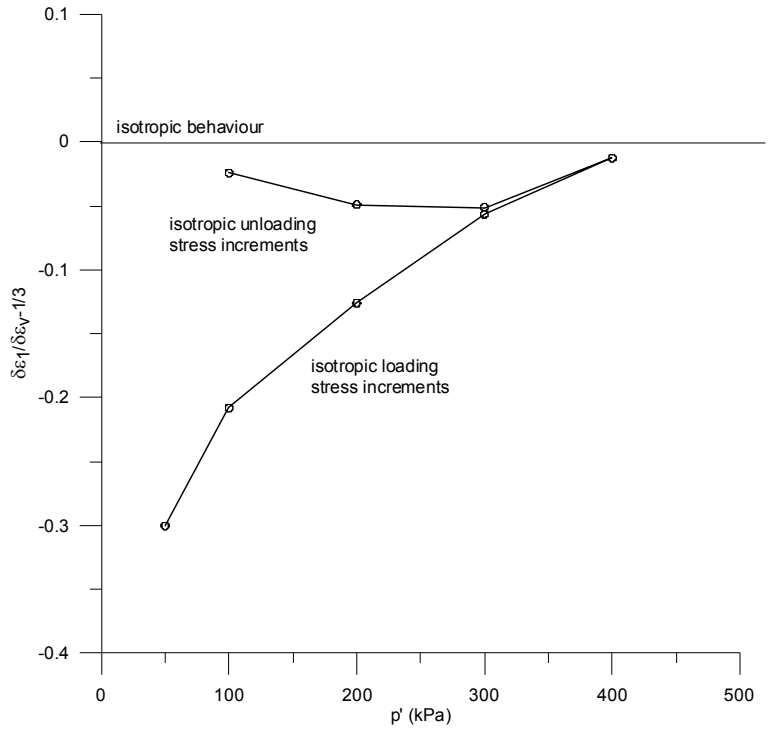

Figure 7.18 Strain ratio measured during isotropic loading and unloading stress increments of the slurry cake samples of the VMClay

A unique isotropic intrinsic compression line (ICL*) was estimated and drawn in Figure 7.17, based on the assumed isotropic state of the samples at the end of the compression stages as discussed above. The compression index of the estimated ICL* was C^*_c=0.160, equivalent to a λ^*=0.069 when using the natural logarithmic scale. This value was essentially the same as that measured in the oedometer tests, C^*_c= 0.158, performed on the slurry samples of the VMClay. Equation 7.7 represents the relationship between the specific volume and the mean effective stress along the estimated ICL* in the v:lnp' plane. An average swelling index of C^*_s=0.021 was estimated using the unloading curve of sample VMClay-TSC3 as its

OCR was the largest of the two overconsolidated specimens tested. A very similar value of 0.025 was obtained in the oedometer tests.

$$v = N - \lambda^* \cdot \ln p' = 1.960 - 0.069 \cdot \ln p' \qquad 7.7$$

• Behaviour under k_o conditions

In order to estimate the coefficient of earth pressure at rest (k_o), two slurry samples, VMClay-TSC-k_o1 and VMClay-TSC-k_o2, were anisotropically consolidated under zero lateral deformation conditions. The tests were performed using a local radial strain transducer attached to the samples. After an initial isotropic compression stage, both samples were subjected to a constant p' stress path to reach an initial estimated k_o. Figure 7.19 shows the stress paths followed during the k_o compression stages of each sample.

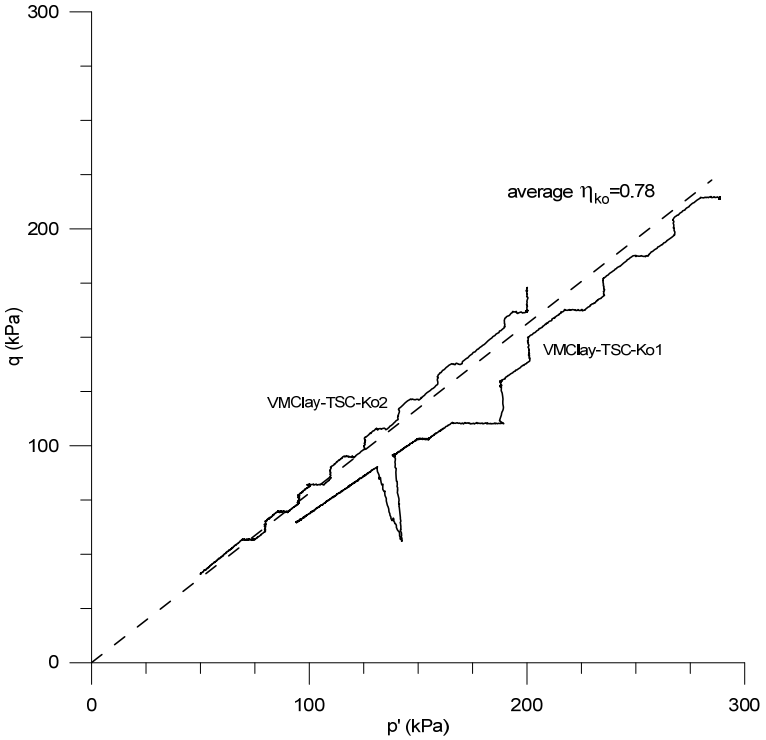

Figure 7.19 Anisotropic compression stress paths under ko conditions of two slurry cake samples of the VMClay

A temporary power cut happened during the compression of sample VMClay-TSC-k_o1 that could be clearly identified with the observed sudden drop in its stress path. An average value of the stress ratio at zero lateral deformation (η_{ko}) was estimated which gave a value of the coefficient of earth pressure at rest for a

normally consolidated state of $k_{o(NC)}$=0.48. As will be shown later, the angle of shear resistance of the VMClay is equal to 32.3º. Using the empirical equation proposed by Jáky (1944), the coefficient of earth pressure at rest is 0.47, just slightly lower than the average measured value on Figure 7.19.

Figure 7.20 shows the k_o compression paths of samples VMClay-TSC-k_o1 and VMClay-TSC-k_o2, together with those of the isotropically compressed specimens. As can be seen, the compression lines of the two k_o specimens are located very close to those of the isotropic samples, meaning that the distance between the normalised k_o line and the ICL* will be very small along the p'/p'$_{cs}$ axis. In addition, the estimated unique 1D-ICL* obtained in the oedometer tests is plotted in the same figure. It can be observed that although the slope was the same as the isotropic and triaxial k_o lines, its position was well below them with an offset in the specific volume of 0.08 for a given p'. No reason was found to justify this large difference.

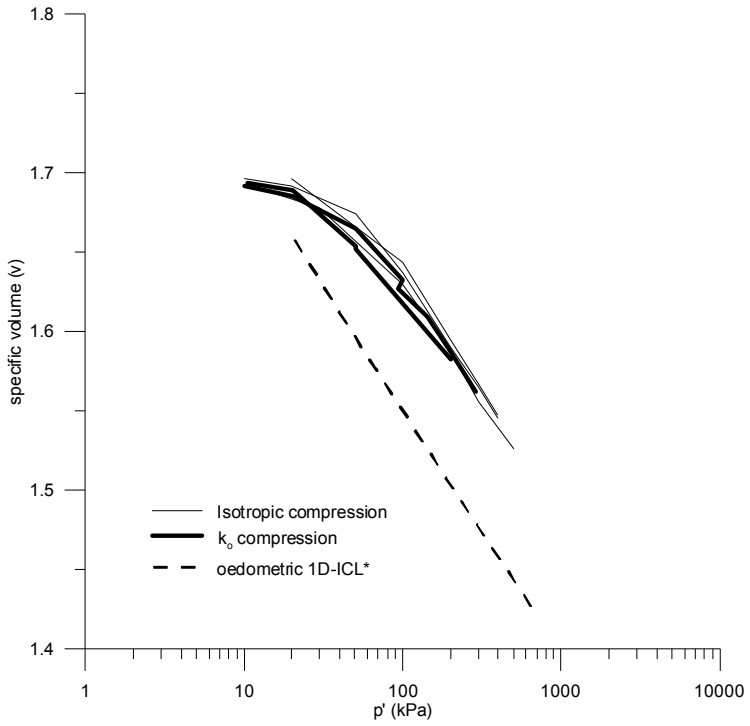

Figure 7.20 Comparison between the isotropic, ko and oedometric compression paths of the slurry cake samples of the VMClay

7.3.2 Large strain behaviour of the slurry samples

The stress-strain behaviour during undrained shearing of the slurry cake samples of the VMClay is shown in Figures 7.21 to 7.26. The failure mechanism observed in all the samples at the end of the tests was mainly of a barrelling type with some slight evidence of conjugate shear bands (Figure 7.29).

Overall, the undrained response in the $q:\varepsilon_s$ plane of the isotropic specimens was strain-hardening up to a shear strain of around 11 to 12% where the deviator stress reached a peak value followed by a smooth strain-softening behaviour until the end of the test (Figure 7.21a). A phase transformation point is seen in samples VMClay-TSC1 and VMClay-TSC2 at a shear strain of around 6.5%, where the contractant behaviour changed to a dilatant mode (Figures 7.21 and 7.22). After the phase transformation point, the dilatant "tails" of the stress paths were very small and nearly vertical, with a very little increment of p' as can be seen in Figures 7.21(b) and 7.22.

In the case of the heavily overconsolidated sample VMClay-TSC3, a clear dilatant response was displayed practically since the start of shearing as seen in Figures 7.21 and 7.22. A very smooth peak was observed in the deviator stress compared with the other two isotropically compressed samples (Figure 7.21a). The increment of pore water pressure reached a minimum negative value at a shear strain of around 1.25%. After a shear strain of 5%, the pore water pressure kept constant until the end of the test. Contrary to the observed behaviour, this sample was expected to show a dilatant stress path that would reach the Hvorslev surface and then move along it until reaching the critical state. During this process a continuous decrease of the pore water pressure would be expected, associated to the dilatant response of the soil skeleton. The state of stresses at the end of each test for all the isotropically consolidated samples appeared to have reached a critical state condition where the deviator stress, pore water pressure and mean effective stress could be considered constant (Figure 7.21).

The stress-strain behaviour of the k_o compressed samples VMClay-TSC-k_o1 and VMClay-TSC-k_o2 is also shown in Figures 7.21 and 7.22. Several different features of behaviour can be observed when comparing with the shearing response of the isotropically compressed samples. The stress-strain curves show a clear and well defined peak in the deviator stress followed by a sudden reduction in q as the shear strain increased. This clear undrained brittleness was not seen for the isotropic specimens. The ultimate state of stresses of both tests, which were considered to have reached critical states, plotted along the same stress ratio (η=q/p') line in the p':q plane as the other isotropically compressed specimens (Figure 7.22). On the

other hand, the η values measured at the peak deviator stresses were lower than those at the critical state in the p':q plane, while in the case of the isotropic samples both, peak and critical state were essentially on the same line.

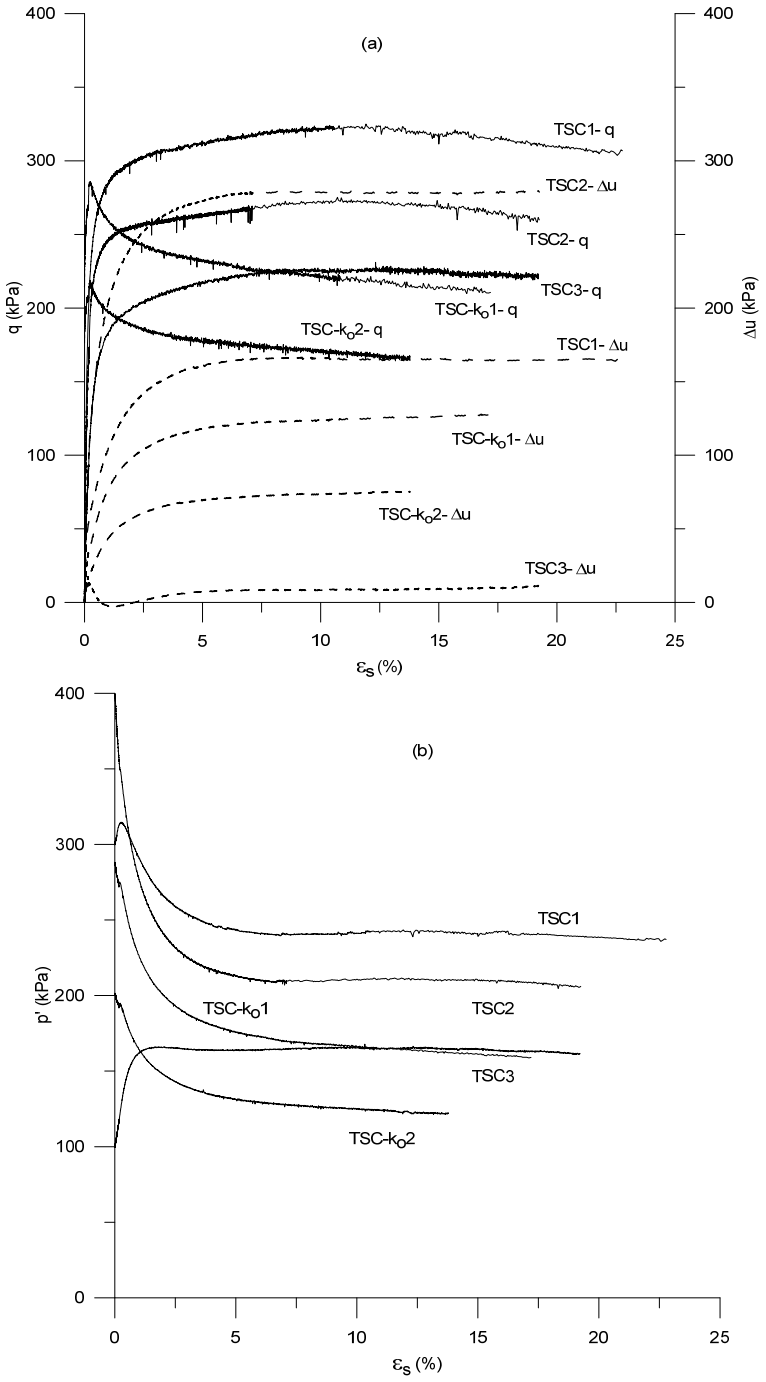

Figure 7.21 Variation of (a) deviator stress and increment of pwp and (b) mean effective stress during undrained shearing of the slurry cake samples of the VMClay

The brittleness of the stress path for anisotropically compressed samples has been associated to the rate of shearing, where the brittleness increased with the rate of shearing (e.g. Gens, 1985). In this thesis the shearing rate was the same for all the tests, but in order to reduce the duration of each test, the shearing rate was gradually increased during the shearing stage. The effect of changing the shearing rate during a test can be seen on the stress paths plotted in Figure 7.22, where a sudden change in the slope of the stress path is noticeable at the start of a new rate of shearing. This procedure would not have any effect on the critical state stress ratio because its value would be independent of the shearing rate.

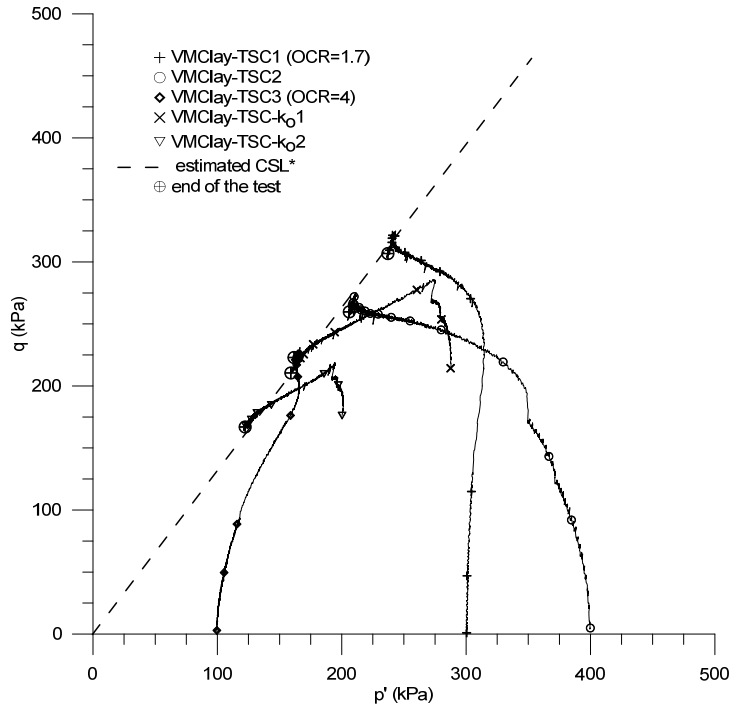

Figure 7.22 Undrained stress paths of the slurry cake samples of the VMClay

In Figure 7.21, the pore water pressure generated during shearing of the k_o samples increased continuously, with a consequent reduction of the mean effective stress. At the ends of the tests the variations of the pore water pressure and mean effective stress with shearing were nearly zero, associated to a critical state, as was mentioned above.

Figure 7.23 shows the variation of the stress ratio (η) with the shear strain for all the slurry samples. The η values of the isotropically compressed specimens displayed a strain-hardening response up to the peak deviator stress followed by a very smooth strain-softening that agrees with the behaviour shown in Figure 7.21. In the case of the k_o specimens, although the deviator stress was reducing with the

shear strain after peak, the stress ratio was increasing, meaning that the soil was strain-hardening as can be seen with the continuous increase of the pore water pressure. Moreover, it can also be seen that for the isotropically compressed samples the initial stiffness was higher as the OCR increased. The values of η at the ends of the tests were slightly scattered with an average value of M*=1.32.

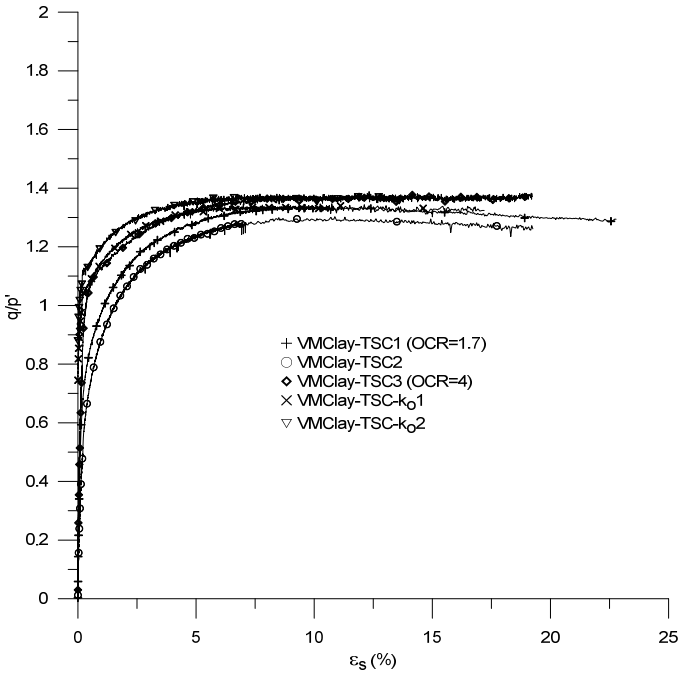

Figure 7.23 Normalized stress-strain behaviour of the slurry cake samples of the VMClay

Although it would be desirable also to have drained tests to define the CSL, in Figure 7.22 a unique intrinsic CSL* can be defined in the p':q plane by the undrained tests performed on slurry samples of the Valencia silty clay (VMClay). The slope of the estimated unique CSL* is M*=1.32, which was the same as the average measured in the q/p':ε_a plane.

The undrained stress paths for the slurry samples are plotted in the v:logp' plane in Figure 7.24. As can be seen, the stress states at the ends of the tests define a unique intrinsic critical state line (CSL*) which is parallel to the estimated intrinsic isotropic compression line (ICL*) for the range of stresses applied. This result agrees with the critical state framework. Equation 7.8 represents the relationship between the specific volume and the mean effective stress on the CSL* in the v:lnp' plane.

$$v_{cs} = 1.910 - 0.069 \cdot \ln p' \qquad 7.8$$

The undrained shear strength (s_u=q/2) was measured at the end of each test as shown in Figure 7.25. It can be observed that the best estimate relationship between s_u and v is parallel to the CSL* and ICL*. The s_u values were also predicted using the Cam Clay model, the results for which are plotted as small black circles in the same figure. As can be seen, the prediction was very good except in the case of test VMClay-TSC-ko2, where the measured value was slightly higher than that predicted.

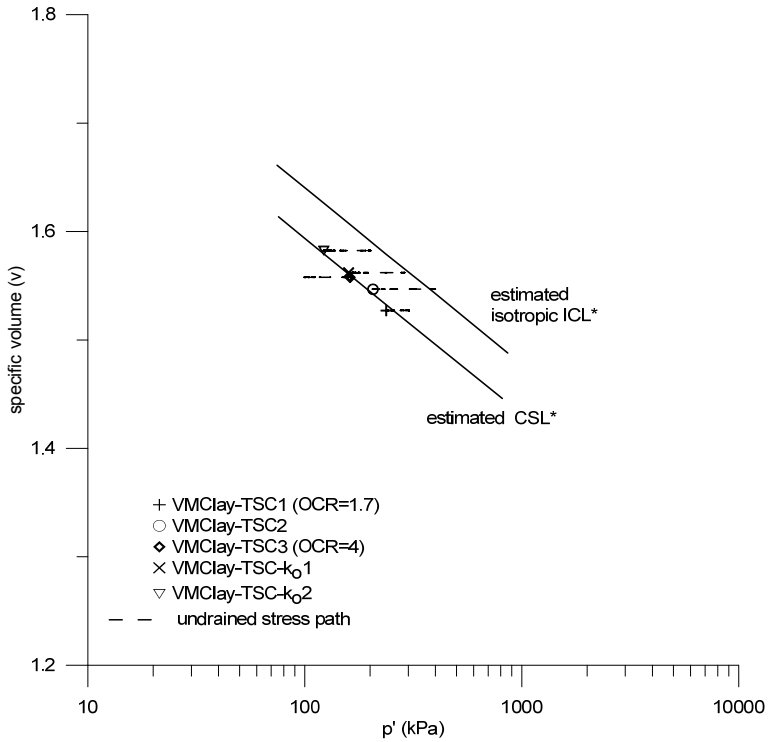

Figure 7.24 Undrained shearing stress paths and critical state line in the v:logp' plane of the slurry cake samples of the VMClay

Figure 7.26 shows the normalised undrained shear stress paths of the slurry samples of the VMClay. As in the case of the Bormida silty soils, the normalising parameter was the equivalent mean effective pressure on the unique CSL*, as defined by Equation 5.25. It can be seen that, essentially, all the stress paths converged onto a unique state at the end of the tests which represents the critical state with a stress ratio of q/p'_{cs}=1.32 at p'/p'_{cs}=1. In the case of sample VMClay-TSC1, the M value in the p':q plane was the same as the others but with a stress state located slightly to the left of the CSL* in the v:logp' plane (Figure 7.24). The distance from the ICL* to the CSL* was slightly higher than the value of 2 that would be expected from the Modified Cam Clay model.

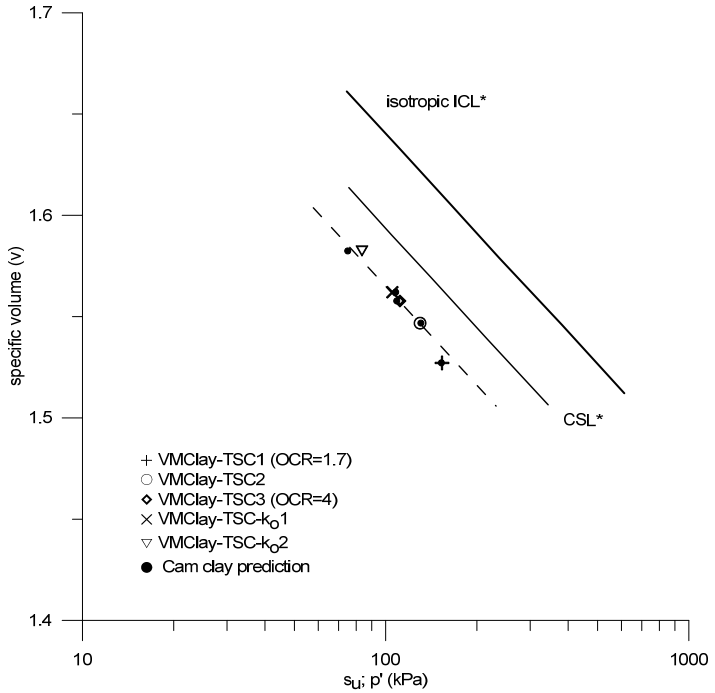

Figure 7.25 Comparison of the undrained shear strengths predicted by the Cam clay model and the experimental results for the slurry cake samples of the VMClay

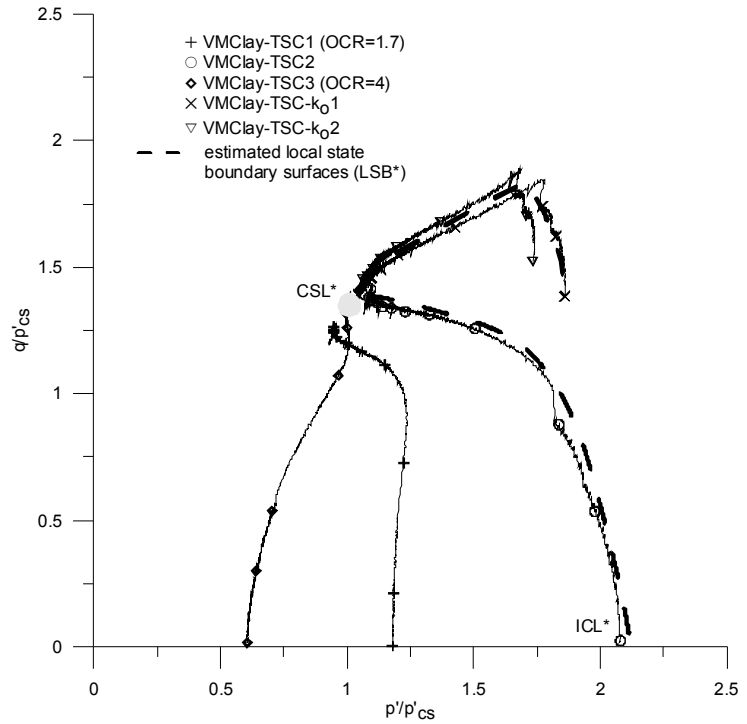

Figure 7.26 Normalized undrained shearing stress paths of the slurry cake samples of the VMClay using an equivalent pressure on the intrinsic critical state line (CSL*)

Looking at the normalised stress paths of the wet side samples, the local state boundary surface defined by the isotropically normally consolidated specimen VMClay-TSC2 was pushed out by the k_o samples resulting in a state boundary surface that is dependent on the mode of compression prior to shear. This behaviour was also seen in the normalised stress paths of the Bormida silty soils. For the dry side of the critical state line, only one test was performed, and as a result it was not possible to define the Hvorslev surface since that test followed a path beneath that surface. A more extensive programme including isotropically and anisotropically consolidated drained tests should be carried out to identify more comprehensively the intrinsic state boundary surfaces (SBS*) of the VMClay on the wet and dry sides of the critical state. Having said this, an estimation of the local undrained state boundary surfaces (LBS*) was drawn in Figure 7.26, based on the tests available. As can be seen the LSB* changes in shape depending on the test performed.

7.3.3 Compression behaviour of the intact samples

In this section the isotropic compression response of the intact samples that were trimmed from the block of the VMClay is explored. Vertically and horizontally cut samples were tested. Table 7.6 shows the details of each of test. As in the case of the intact oedometer specimens, there was a small variation in the measured values of the initial void ratio, which, as was mentioned before, is believed to be associated to heterogeneous in-situ structure. However the differences in the e values for the triaxial samples are lower than those measured in the oedometer specimens.

test	e_o	p'_o (kPa) before shearing	OCR	Type of test	Comments
VMClay-TIV1	0.558	300	1	CIU	(V)Vertical sample
VMClay-TIV2	0.583	1500	1	CIU	
VMClay-TIV3	0.620	200	1	CIU	
VMClay-TIV4	0.549	400	1	CIU	
VMClay-TIH1	0.558	300	1	CIU	(H) Horizontal sample
VMClay-TIH2	0.547	200	1	CIU	

Table 7.6 Summary of the triaxial tests carried out on intact samples of the block of the Valencia silty clay (VMClay).

Figure 7.27 shows the isotropic compression behaviour of the intact samples, where the vertical sections found in some of the lines represent stages of excess pore pressure dissipation. It can be observed that for the range of stresses applied no convergence is seen in the compression lines, although it appears that the tendency

is to do so at high stresses. In the case of the densest sample VMClay-TIV4, its compression line exhibited a higher compressibility compared with the other dense specimens and runs nearly parallel to sample VMClay-TIV2. Figure 3.12(b) shows a photo of this sample while being trimmed. As can be observed some aggregates of cemented particles were found in the sample. One of these aggregates was removed to be able to reach the final dimensions and the hole was filled with trimmings from the same sample. Without any doubt, this heterogeneous structure and the remoulding of it during trimming is expected to have an important role on the compression and shearing behaviour of sample VMClay-TIV4. Another aggregate of particles was found in sample VMClay-TIV3, but in this case the specimen could be trimmed without the necessity of removing it. No more aggregates of cemented particles were noticeable in any of the other intact samples, but this does not mean that they could not have been present in the specimens.

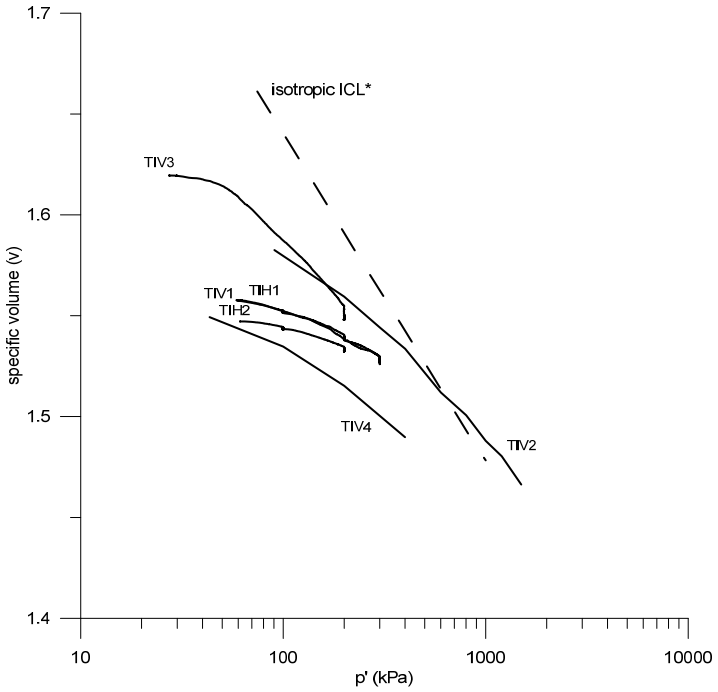

Figure 7.27 Isotropic compression of the intact samples of the VMClay

One the intact samples, VMClay-TIV2, was tested in the 7MPa triaxial cell where it was possible to reach a higher isotropic compression stress of p'=1500kPa. Its compression line crossed the intrinsic ICL* defined by the slurry samples, showing a clear effect of the in-situ structure as seen in the oedometer tests (Figures 7.7 and 7.8). In the case of the other samples, they were tested in the conventional stress path triaxial cell, where the maximum isotropic compression stresses applied were smaller and therefore it can not be concluded whether their compression lines

would have crossed the ICL* at higher stresses. Apart from sample VMClay-TIV3, none of the specimens showed a clear yield stress. In the case of sample VMClay-TIV3, a clear change in the slope of the compression line can be seen at a mean effective stress of 60kPa, which would be equivalent to a vertical effective stress of 90kPa. This value is well below the yield stresses measured in the oedometer tests, although the compression conditions were not the same.

An attempt to evaluate the in-situ anisotropic structure of the intact samples and its evolution during isotropic compression was carried out in Figure 7.28, applying Equation 5.19. As in the previous Section 7.3.1, the axial strains were calculated by using a pair of LVDTs attached to the samples and a volume gauge for the volumetric strains. Overall, the axial strains measured by each of the LVDTs during isotropic compression were slightly different and average values were used for the calculation. Only in the case of the highest p' compression test VMClay-TIV2, the differences were large and so it was not included in Figure 7.28. This heterogeneous strain response is attributed to the observed heterogeneous structure of the intact samples. The strains were calculated at the end of each compression increment when the samples reached a state where all the excess pore water pressure generated was dissipated. Two samples, VMClay-TVI1 and VMClay-TIV3, were compressed at a slow continuous rate until the final p' without intermediate stops for excess pore water pressure dissipation. Therefore, for these two samples the strain ratio plotted in Figure 7.28 represents the state at the end of the compression stage after all the remaining excess pore water pressure was dissipated.

The strain ratios measured at the start of the tests showed a clear initial in-situ anisotropic structure in all the samples with an apparent different initial degree and evolution depending on the orientation of the specimens (Figure 7.28). In fact, the strain ratios for the horizontally cut samples plot above those of the vertically cut specimens, with the exception of sample VMClay-TVI3. The behaviour of the slurry sample VMClay-TSC3, which was initially compressed anisotropically in the consolidometer before being tested isotropically in the triaxial, is also included in Figure 7.28 for comparison. Overall, the degree of anisotropy measured on the intact samples during isotropic compression was higher compared with that of the slurry specimen for the same p' which most likely reflects the higher resistance of the anisotropic in-situ structure to be erased during isotropic compression. More tests should be carried out to confirm the effect of the orientation of the specimens on the degree and evolution of the anisotropic structure of the intact samples of the Valencia silty clay (VMClay).

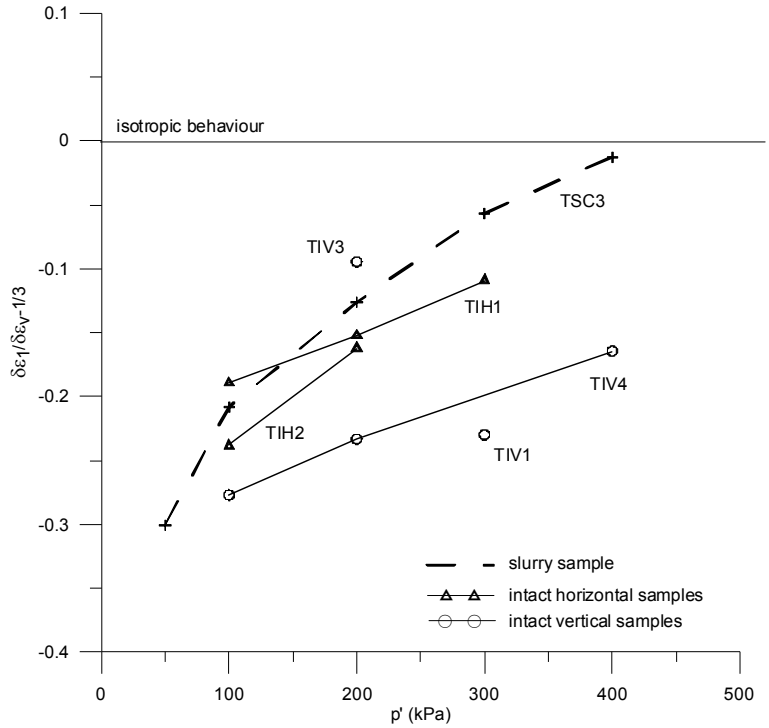

Figure 7.28 Strain ratios measured during isotropic loading stress increments for the intact samples of the VMClay

7.3.4 Large shearing behaviour of the intact samples

The stress-strain behaviour of the intact samples of the VMClay is shown in Figures 7.30 to 7.35. The failure mechanism of all the specimens consisted of a mix between barrelling and clear shear bands, compared with the mainly barrelling mechanism observed in the slurry samples (Figure 7.29). For the clarity of the plots, the undrained stress-strain response of sample VMClay-TIV2, which was tested at high confining pressure, is represented in separate figures.

Figure 7.30 shows the undrained behaviour of the specimens tested in the Bishop & Wesley triaxial cell where the samples were isotropically compressed at stresses that ranged from 200 to 400kPa. As can be seen, in general, the deviator stress increased with the shear strain until the end of the test in all the samples. Only sample VMClay-TIV1 displayed a transient peak value at a low shear strain followed by a further continuous increase of the deviator stress. The variation of the pore water pressure showed that, initially, the specimens exhibited a contractant response which increased the pwp until it reached a peak value. After the peak value, the samples started to display a dilatant mode of shearing with a

consequent reduction of the pwp as the shear strain increased, which caused a p' increase until the end of the test.

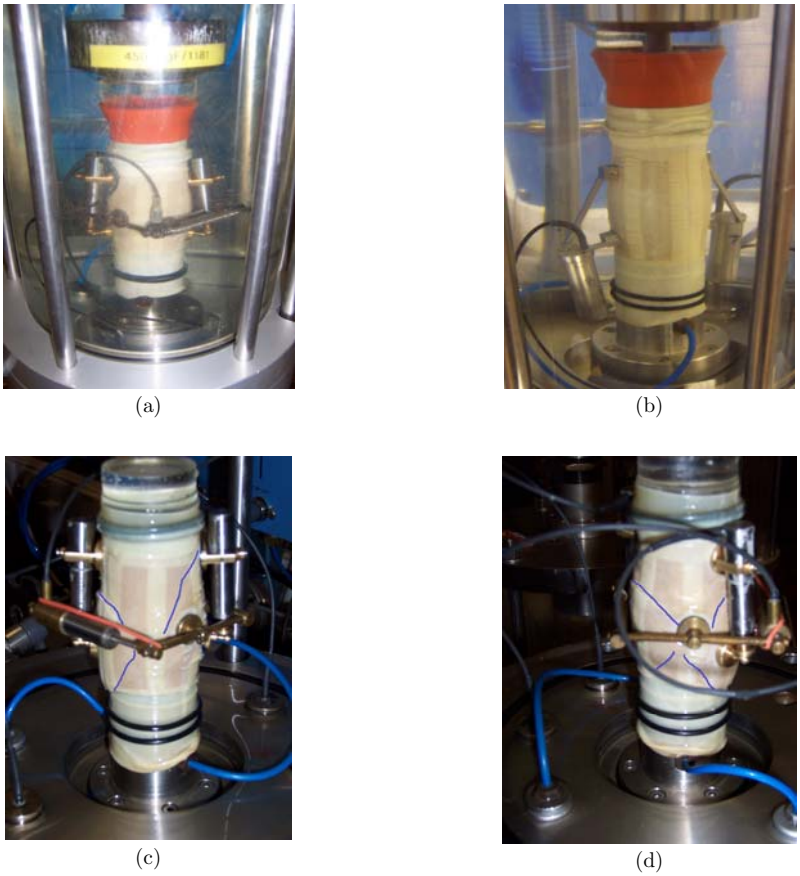

(a) (b) (c) (d)

Figure 7.29 Shear mechanisms of (a) slurry sample VMClay-TSC1 (b) slurry sample VMClay-TSC2 (c) and (d) intact sample VMClay-TIV4

The undrained shear response of sample VMClay-TIV2, which was isotropically compressed to a p'=1500kPa and crossed the ICL*, is shown in Figure 7.31. In this case, the deviator stress exhibited a very smooth peak value at a shear strain of around 15% compared with the other specimens. The variation of the excess pwp during shearing represented a contractant behaviour, with a very smooth maximum compared with those values observed in the samples tested at lower confining pressures. After the maximum, the soil started to be dilative until it reached a constant pore water pressure at the end of the test.

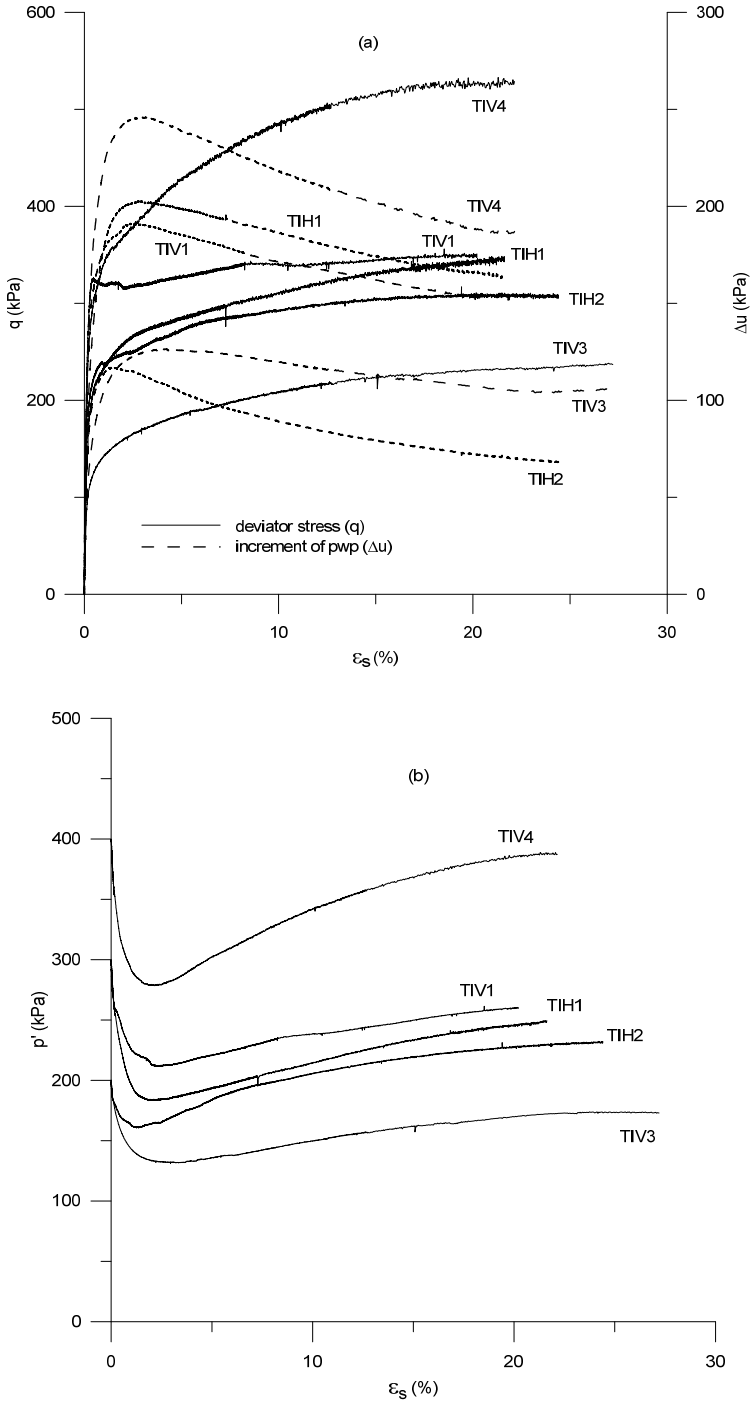

Figure 7.30 Variation of (a) deviator stress and increment of pwp and (b) mean effective stress during undrained shearing of the intact samples of the VMClay

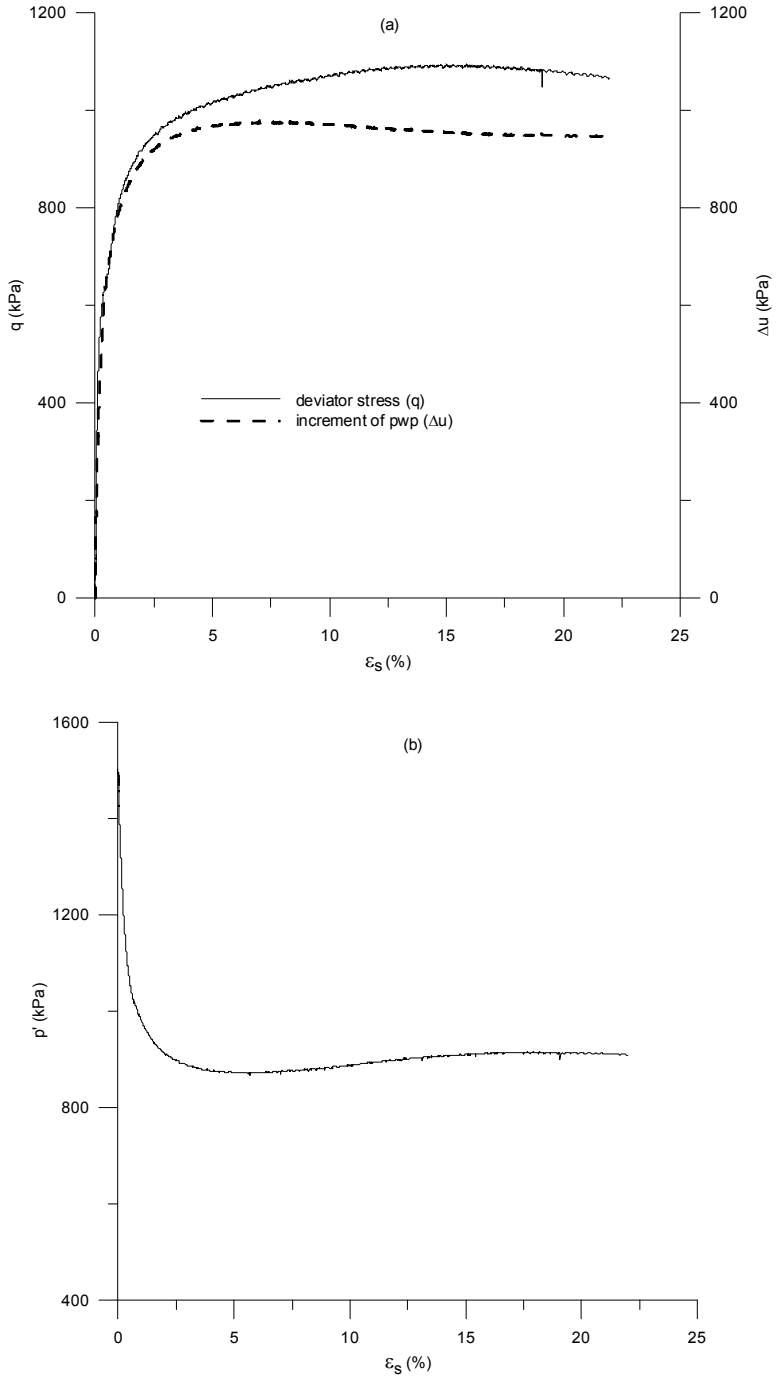

Figure 7.31 Variation of (a) deviator stress and increment of pwp and (b) mean effective stress during undrained shearing of the intact sample VMClay-TIV2 at a high confining pressure

Figure 7.32 shows the increment of pore water pressure normalised by the maximum mean effective stress reached during the isotropic compression stage (p'_o). It can be observed that apart from sample VMClay-TIV2, the overall soil response was similar in all samples where a peak value was clearly noticeable for the samples tested at lower confining pressures. In addition, an effect can be seen of the rotation of specimen VMClay-TIH2 on the normalised increment of pwp.

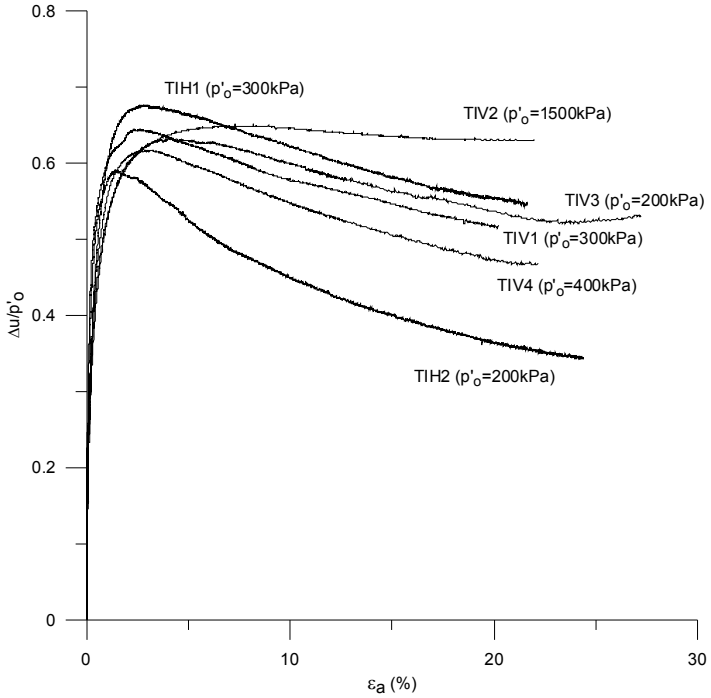

Figure 7.32 Normalized increment of pore water pressure during undrained shearing of the intact samples of the VMClay

Figure 7.33 shows the stress paths in the p':q plane only for the specimens tested at lower stress levels. As described above, initially all the samples displayed a contractant response up to the phase transformation point where the soil's skeleton started to dilate with a consequent increase of p' as the shear strain increased. After the phase transformation point, the stress paths climbed at a reasonably constant stress ratio that was above the estimated CSL*. Although the stress-strain behaviour plotted in the q:ε_s plane apparently showed a strain-hardening response, the real behaviour of the soil skeleton after the peak value of the pwp, which corresponded with the phase transformation point, was strain-softening as can be seen in Figure 7.35. In natural soils, heterogeneities are always present as is the case of the intact samples of the VMClay. These heterogeneities play an important role when the soil dilates due to the concentration of strains during shearing, favouring the likely formation of shear bands in the sample. The dilatant "tails"

observed in each stress path for the intact samples showed the effect of the strain-softening observed in the Δu:ε_s, q/p':ε_s planes (Figures 7.30a and 7.35), which may have triggered the shear bands seen in the specimens. It is interesting to point out that, in the case of the slurry samples, the dilatant "tails" of the stress paths were insignificant compared with those of the intact samples (Figure 7.35). This behaviour agrees with the mainly barrelling type of failure mechanism exhibited by the slurry specimens compared with the shear bands observed in the intact samples (Figure 7.29).

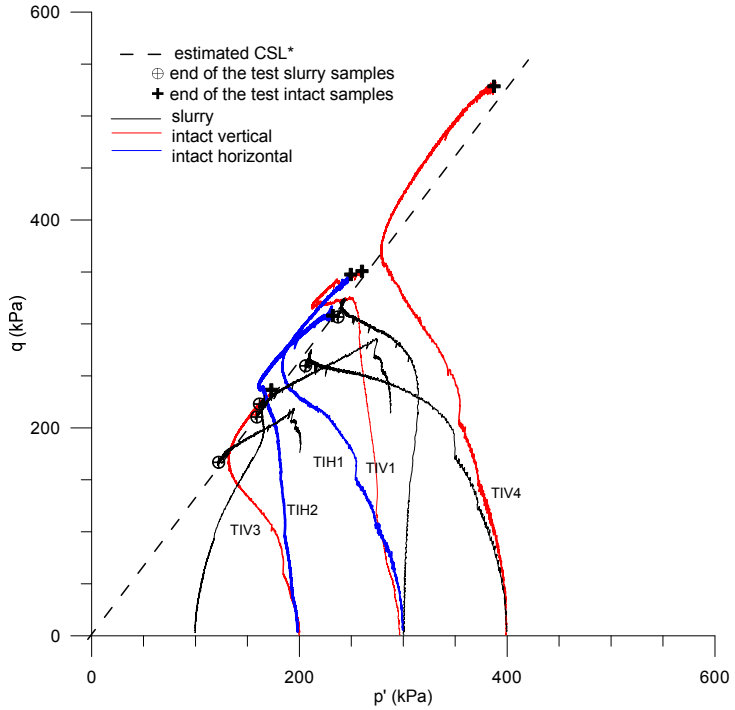

Figure 7.33 Undrained stress paths of all the samples of the VMClay. Sample VMClay-TIV2 is not included in this plot

A common way to asses the effect of the anisotropy on the shear strength behaviour is based on testing vertically and horizontally cut samples. Figure 7.33 shows the stress paths of two horizontally cut specimens where their behaviour is compared with the vertical samples. In the case of samples VMClay-TIV1 and VMClay-TIH1, before shearing the stress state in the compression plane v:logp' was the same, as can be seen in Figure 7.27. The stress paths of the two samples were clearly different and, as will be shown later, at small strains sample VMClay-TIV1 exhibited a stiffer response. At large strains both specimens reach a very similar undrained shear strength showing no effect of the rotation of the sample but a direct dependency on the initial specific volume as would be expected from the critical state framework. The comparison between specimens VMClay-TIV3

and VMClay-TIH2 shows that, again, there was a clear effect of the rotation of the sample on the stress path but in this case the vertical specimen displayed a higher stiffness, contrary to the behaviour observed in the comparison of samples VMClay-TIV1 and VMClay-TIH1. Moreover, it can be seen that the stress path of sample VMClay-TIV3 plotted only slightly above the intrinsic CSL* compared with sample VMClay-TIH2, the stress path of which plotted well above the CSL* before reaching the CSL* at the end of the test. Although the values of the specific volume before undrained shearing were slightly different between these two specimens, the ratio of undrained shear strength was of the order of 1.3, with the larger value for the horizontal sample showing a clear effect of the anisotropic structure. More tests on horizontally cut samples should be performed in order to draw general conclusions on the effect of the rotation of the specimens.

Figure 7.34 shows the stress path of sample VMClay-TIV2, which was isotropically compressed to a p'=1500kPa in the 7MPa triaxial cell. As in the case of the other specimens, the sample exhibited a contractant response followed by a phase transformation point where the soil's skeleton started to dilate, displaying a short dilative "tail" before reaching a peak value of deviator stress. The abrupt changes observed in the slope of the stress path were associated to the change of the shearing rate, as mentioned before.

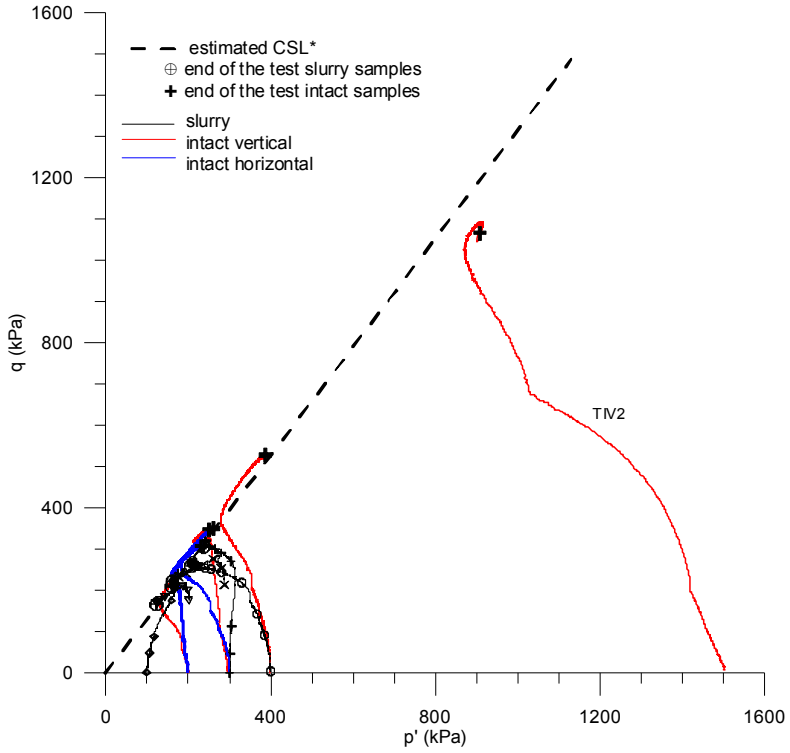

Figure 7.34 Undrained stress paths of all the samples of the VMClay

Overall, the stress states of the intact samples at the ends of each test plotted slightly above the intrinsic CSL* defined by the slurry specimens in the p':q plane (Figures 7.33 and 7.34). At high confining pressure, the stress state of sample VMClay-TIV2 was slightly below the CSL*, suggesting a possible curved CSL in the p':q plane at high stresses. This behaviour was also seen in the tests carried out with the Bormida silty soils (Figure 5.63).

Figure 7.35 shows the variation of the stress ratio (q/p') with the shear strain for all the intact samples together with those of the slurry specimens. It can be seen that apart from sample VMClay-TIV2, the normalised curves of the intact samples plot above those of the slurry and show a peak value which decreased as the maximum mean effective stress applied during isotropic compression increased, as would be expected for an overconsolidated sample. Only in the case of sample TIV3 was the behaviour more similar to that of the slurry specimens. It is important to point out that this sample displayed a clear yield stress during isotropic compression which might justify this normalised behaviour. After the peak, all the curves tended towards the estimated average M* value except sample VMClay-TIV2, the curve for which plotted well below those of the slurries, as shown in Figure 7.34.

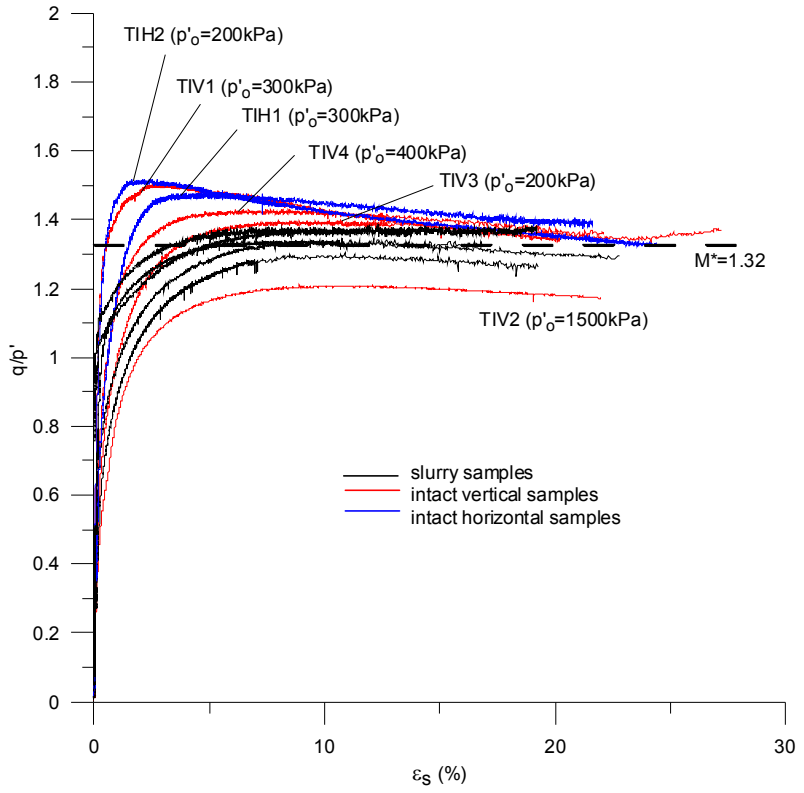

Figure 7.35 Normalized stress-strain behaviour of all the samples of the VMClay

The undrained stress paths are plotted in the v:logp' plane in Figure 7.36. As can be seen, apart from sample VMClay-TIV2, the stress state at the end of the tests plot along, or very close to the estimated CSL*. When shear bands develop during shearing the soil can not be considered as a continuum and the results of the tests could lead to erroneous interpretation when using boundary measurements. Having said that, it appears that the in-situ structure of the specimens seems to have been erased during compression and shearing and a unique critical state was reached.

In the case of sample VMClay-TIV2, the compression line crossed the ICL* showing the effect of its in-situ structure. The destructuration induced to the sample during shearing was, however, still not enough to reach the CSL* and the stress state at the end of the test plots well to the right of the CSL*.

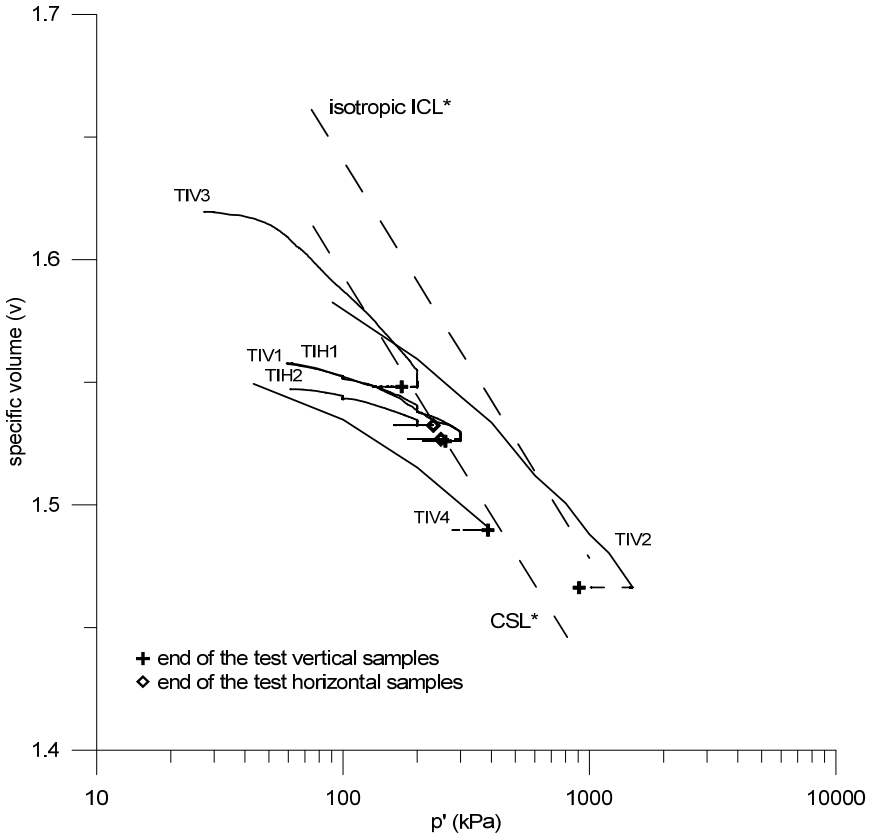

Figure 7.36 Undrained shearing stress paths in the v:logp' plane for the intact samples of the VMClay

In order to quantify the effect of the in-situ structure of the intact samples on the shearing response, the undrained stress paths were normalised by the equivalent pressure on the critical state line and plotted together with those of the slurry specimens in Figure 7.37. As described above, the intrinsic local state boundary

surface of the slurry samples was compression path dependent. Unfortunately the Hvorslev surface for the slurries was not defined as tests on specimens at even higher overconsolidation ratios would have been required to locate it. Having said this, the normalised stress paths of the intact samples sheared from stress states close to the CSL* probably have a little effect of their in-situ structure, in particular the bonding component, as a consequence of the close location of their estimated Hvorslev surface to the CSL* slope (Figure 7.37). At the end of the test the majority of the samples reached the unique CSL* apart from specimens VMClay-TIV3 and VMClay-TIV4 that were moving towards it as seen in Figure 7.36. In the case of sample VMClay-TIV2, the compression line of which crossed the ICL*, the normalised stress path plotted to the right of the isotropic intrinsic local state boundary surface showing no sign of convergence towards the CSL*. This soil response might be attributed to a stable structure, in particular the in-situ fabric component, which could not be removed by shearing even at large shear strains. More tests at even higher compression stresses would have been required to confirm this behaviour.

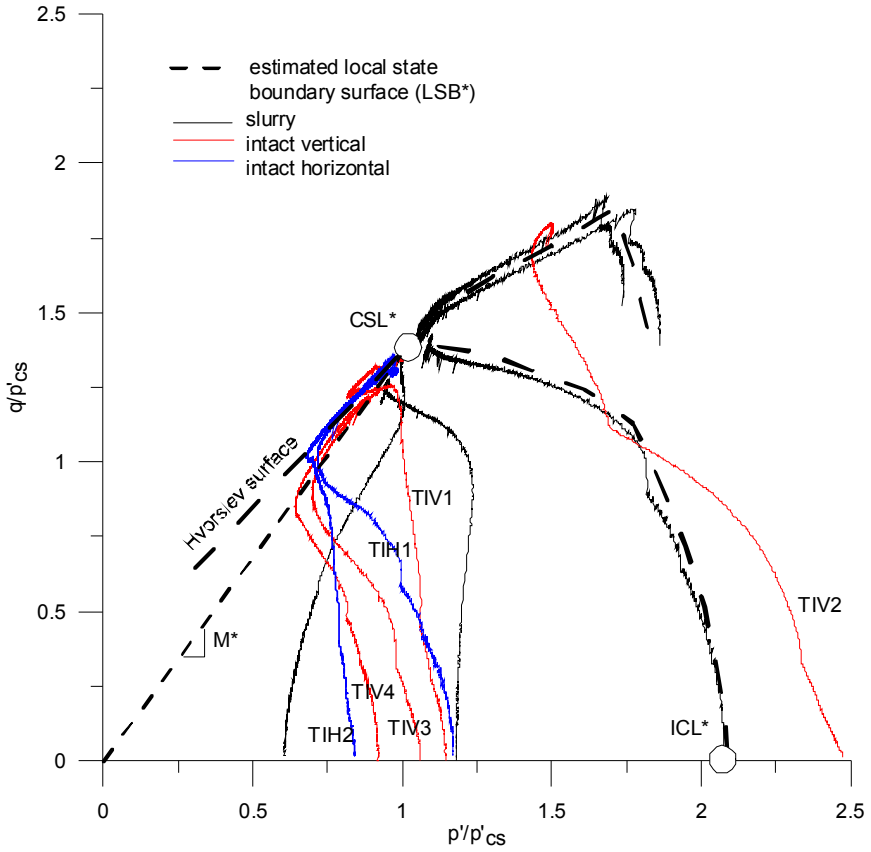

Figure 7.37 Normalized undrained shearing stress paths of all the samples of the VMClay using the equivalent pressure on the intrinsic critical state line (CSL*)

In summary it appears that fabric is the main part of the in-situ structure that had a noticeable effect on the behaviour of the VMClay, however its influence on the soil response at large strains was very small.

7.3.5 Stiffness data

In this section the stiffness at small strains of the VMClay material is analysed. All the samples were sheared at the same rates and the strains were measured using internal local transducers. As was done with the BRS soils, the stiffness of the material was analysed in terms of the secant Young's modulus.

• Slurry samples

Figure 7.38 shows the stiffness-strain curves normalised by the current mean effective stress for the three slurries compressed isotropically before shearing. Sample VMClay-TSC2 was normally consolidated whereas samples VMClay-TSC1 and VMClay-TSC4 were overconsolidated with OCRs of 1.67 and 4 respectively. As can be seen, the stiffness is highly non-linear at small strains and the values depended on the strain and on the overconsolidation ratio, where for a given p' and shear strain, the stiffness increased with the OCR as expected.

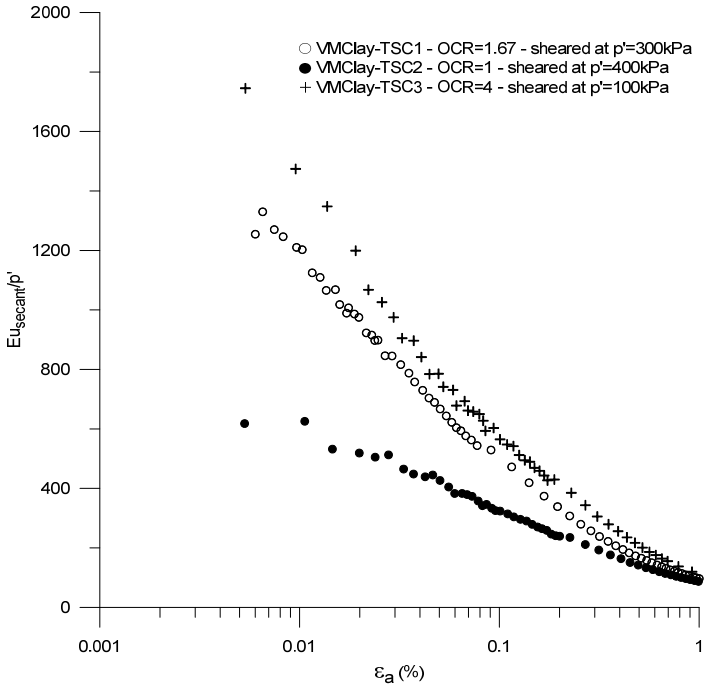

Figure 7.38 Normalized undrained secant Young's modulus degradation curves for the slurry samples of the VMClay compressed isotropically

The normalised stiffness-strain curves of the two samples normally compressed under k_o conditions are plotted in Figure 7.39. It can be seen that the normalised curves nearly converged onto a unique relationship for Eu_{secant}/p' at axial strains beyond 0.01%. The stiffness-strain curve of the isotropically compressed sample VMClay-TSC2, with an OCR=1, is compared with those of the k_o specimens in the same figure. It can be observed that the stiffness is lower for the anisotropically compressed samples as would be expected.

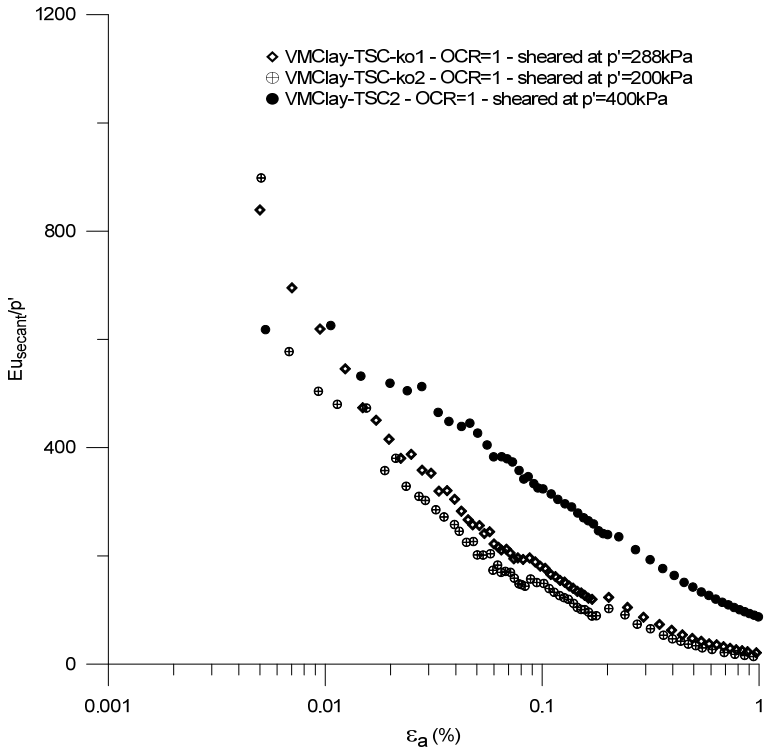

Figure 7.39 Normalized undrained secant Young's modulus degradation curves for the slurry samples of the VMClay compressed under ko conditions. Comaprison with the isotropically compressed specimen VMClay-TSC2

• Intact samples

Figure 7.40 shows the normalised stiffness-strain curves of three vertically cut intact samples. Before shearing, the specimens were isotropically compressed to stresses that ranged from 200 to 400kPa and at the end of the compression stage the state of stress of all the compression curves plotted to the left of the ICL*, implying a certain degree of overconsolidation (Figure 7.36). As shown in Figure 7.27, the compressibilities of these samples during compression were very different, where specimen VMClay-TIV3 displayed a clear yield stress during compression and sample VMClay-TIV1 exhibited the stiffer response. Those responses are

reflected in the stiffness-strain behaviour observed during undrained shearing, where samples VMClay-TIV3 and VMClay-TIV1 displayed the lowest and highest stiffnesses respectively for a given p'.

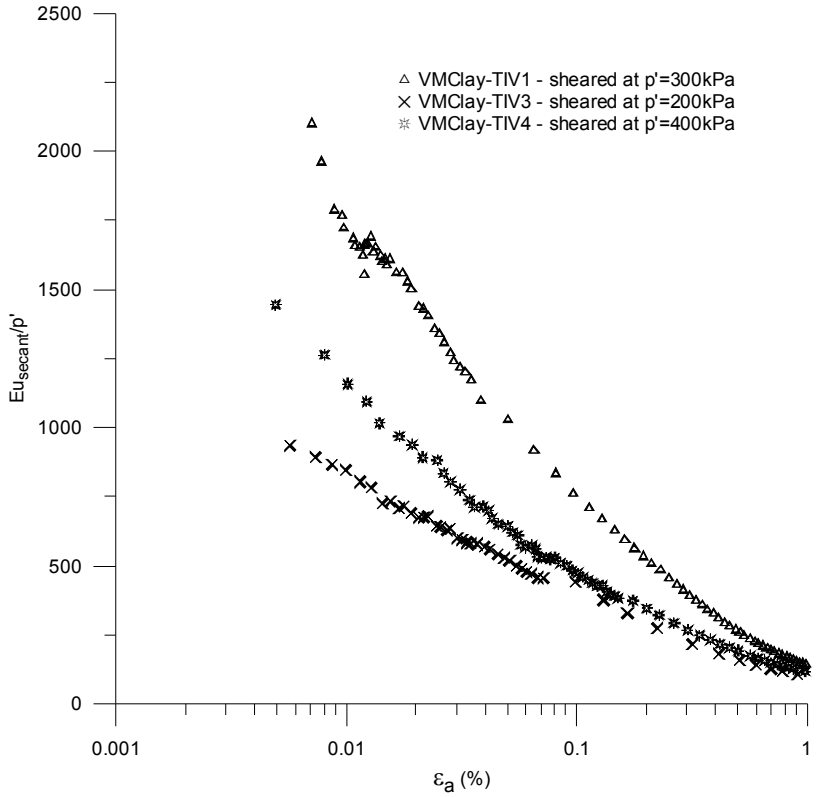

Figure 7.40 Normalized undrained secant Young's modulus degradation curves for the intact samples of the VMClay

A comparison of the stiffnesses between the vertically and horizontally cut samples is shown in Figures 7.41. As can be seen, in the case of specimens VMClay-TIV1 and VMClay-TIH1, the stiffness of the vertical sample was higher than the horizontal. However, when the other two samples VMClay-TIV3 and VMClay-TIH2 were compared, the stiffness of the horizontal specimen was higher than that of the vertical. It is interesting to recall again that in this latter comparison sample VMClay-TIV3 exhibited a clear yield stress during isotropic compression which probably affected its stiffness during shearing. Aditionally, the vertical sample underwent significant perturbation during its trimming due to the presence of an aggregate of cemented particles which had to be partially removed. Having said this and due to the small number of comparison tests, it would be too risky to draw a general conclusion on the effect of the rotation of the samples on the stiffness at small strains. Moreover, it can be observed that at around an axial strain of 0.07% the stiffness-strain curves of the samples compressed to a higher p'

converged onto a unique relationship with the stress-strain curves of those compressed to lower p' in pairs of vertical with horizontal specimens.

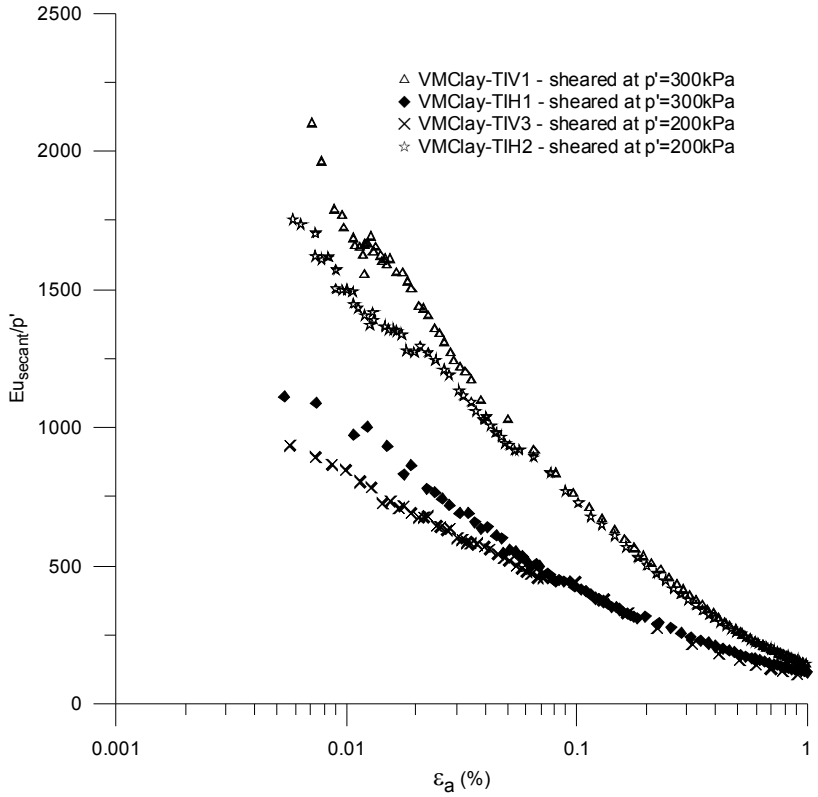

Figure 7.41 Comparison of the normalized undrained secant Young's modulus degradation curves for the vertical and horizontal intact samples of the VMClay

Figure 7.42 shows the relationship between Eu_{secant} and the current p' during undrained shearing at different levels of axial strain in the range of small strains for the intact and slurry samples using a double logarithmic scale. Only the isotropically compressed samples are included in the figure. Although it is known that the stiffness at small strains of a material depends on many factors such as stress level, OCR and structure, a regression line was derived for each strain level the slope of which corresponded to the stress level exponent (n) value in Equation 5.26. The coefficient of correlation (R^2) varied from 0.52 to 0.67 with a mean square error (MSE) that ranged from 0.12 to 0.03 at the lowest and highest shear strains measured, reflecting the observed scatter on the data. Though there was a relatively poor correlation of the data, the stress level exponent (n) increased with the strain level, tending towards unity as suggested by many researchers (e.g. Porovic & Jardine, 1994; Viggiani & Atkinson, 1995; Jovicic & Coop, 1997).

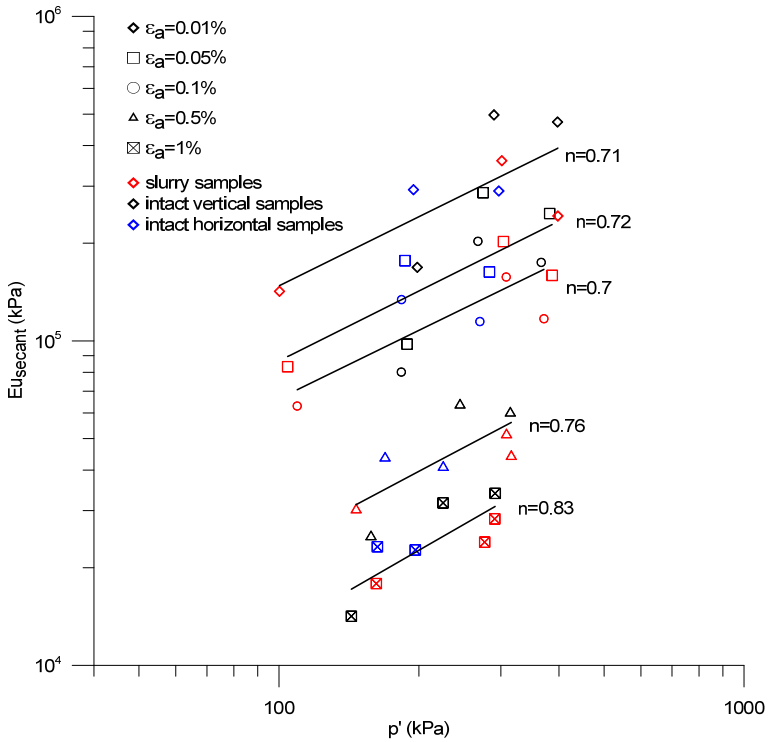

Figure 7.42 Undrained secant Young's modulus as a function of the current mean effective stress at various strain levels for the slurry and intact samples of the VMClay

In summary it appears that the scatter observed in Figure 7.42 might be partly associated to the state of the samples before shearing and partly to the effect of the in-situ heterogeneous structure of the VMClay. In any case, it could be concluded that no clear effects of the in-situ structure on the small stiffness could be seen which might agree with the hypothesis proposed before that no significant bonding was present in the intact samples of the VMClay.

Chapter 8
Discussion

8.1 Introduction

The materials tested in this research project consist of Holocene alluvial soils, recently deposited and retrieved from the alluvial plains of the Bormida River at Castellazo Bormida, Italy and Turia River at Valencia, Spain. These materials were named the Bormida River silts (BRS) and the Valencia silty soils (VSS).

Traditionally much of the research carried out to investigate the natural structure of soils has been focused on geologically old materials but less attention has been paid to young Holocene deposits. In this respect one of the main objectives of this research project was to explore the effects of the naturally occurring structure in shallow young alluvial sediments like the BRS and VSS materials. In this chapter the effects of the natural structure on the mechanical behaviour of these two soils are compared and the new results are also put in context with previous studies on young Holocene sediments, in particular with the Sibari and Pisa soils.

As described in Section 2.5, a transitional soil is defined as one where a non-unique NCL and/or CSL can be defined even at high stress levels and large strains. Transitional behaviour is therefore associated to a stable initial structure of the soil, in particular its fabric, which can not be removed by compression and shearing. This behaviour was found in a large range of materials with very different gradings and mineralogy. The conclusions obtained from the analysis carried out in Section 2.5.3 showed that, contrary to what was stated in the literature, the sample

preparation method appears to have a clear effect on materials that displayed transitional behaviour. Consequently, another objective of this study was to investigate the effect of the initial structure of slurry and compacted samples of the BRS and VSS on the uniqueness of their compression and critical state lines.

8.2 Index properties

Figure 8.1(a) shows the size distributions of all the materials studied in this research project together with the soils tested by Nocilla et al. (2006), which has the same geological origin as those of the BRS. It is worth to recall that two of the soils tested by Nocilla, in particular those with the lower clay-sized particles content, showed transitional behaviour in compression and shearing. In addition, and as a comparison, Figure 8.1(b) represents the range of materials that displayed transitional behaviour according to Shipton (2010).

As described in Chapter 4, the BRS materials consist of a BRS-B block specimen and a remoulded BRS-E sample retrieved from the foundation level of the river embankments. A unique size distribution for each soil was found as can be seen in Figure 8.1(a). On the other hand, the VSS are made up of a wide range of soils with different gradings that varied from silty sands to silty clays as described in Chapter 6. In this case, an intact block specimen (VMClay) together with two remoulded samples, the VSSilt and VMSand, were taken from the alluvial plains of the Turia River near to the Mediterranean Sea. The VSSilt and VMSand materials exhibited a unique grading curve for each soil whereas the material inside the block sample was more heterogeneous displaying the range of grading distributions shown in Figure 8.1(a). In addition, it is interesting to recall that during the trimming process of the intact samples of the VMClay it was observed that in some specimens the granulometry was not the same within them and some parts were more clayey/silty than others, creating a certain degree of layering. This in-situ structural feature is characteristic in fluvial environments where the rates and modes of deposition are likely to vary rapidly during the formation of the sedimentary soils as is the case of the Turia River. That heterogeneous structure found in some samples of the VMClay was not seen in any of the BRS-B intact specimens which might reflect the different fluvial dynamics and sedimentation conditions from where the samples were retrieved.

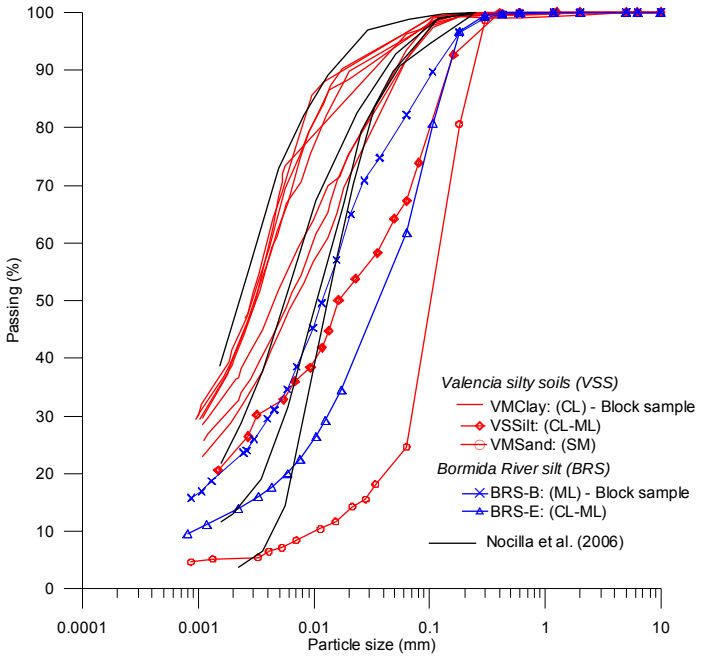

(a)

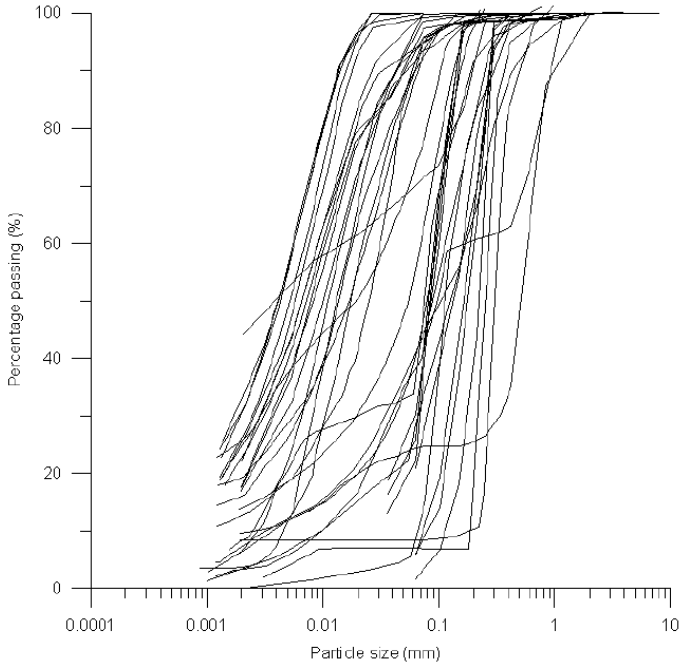

(b)

Figure 8.1 Particle size distributions of (a) the BRS, VSS and Nocilla et al. (2006) and (b) soils that displayed transitional behaviour (Shipton, 2010)

Table 8.1 summarises the index properties of the BRS and VSS soils. It can be seen that the plasticity of all the materials is low. In general the BRS plotted below and very close to the "A" line in the plasticity chart whereas the VSS were located above it. The activity is also low with slightly higher values for the BSR. Moreover, for the given location the activity is very similar in the case of the VSS soils, which reveals a common mineral origin. In the case of the BRS materials the activity values are different although the samples were retrieved from the same location. Large contents of calcium carbonate were found in the VSS compared with those of the BRS. One of the direct effects of the high content of $CaCO_3$ on the index properties is to reduce the plasticity of the soil.

Material	Clay-size (%)	Silt (%)	Sand (%)	w_l (%)	w_p (%)	PI (%)	USCS	A	OM (%)	$CaCO_3$ (%)
BRS-B	22	60	18	35.2	24.9	10.3	ML	0.47	1.1	10.4
BRS-E	13	50	37	25.3	21.1	4.2	CL-ML	0.33	-	12
VMClay	28-40	55-64	5-8	28.5	18	10.5	CL	0.31	0.16	50
VSSilt	25	43	32	23.6	16.6	7.0	CL-ML	0.28	-	33.4
VMSand	5	20	75	Non-plastic			SM	-		30

Table 8.1 Summary of index properties of the BRS and VSS

8.3 Oedometric compression behaviour

A simple comparison between the grading curves shown in Figure 8.1 indicates that part of the materials which comprise the BRS and VSS are in the range of soils that displayed transitional behaviour according to Shipton (2010). A priori, this makes the BRS and VSS potential transitional materials.

As mentioned above, an objective of this investigation was to study the effect of the initial structure of the samples on the possible transitional behaviour of the BRS and VSS materials. In addition, to evaluate the effect of the in-situ structure on the compression behaviour of natural intact samples, as is the case of the BRS-B and VMClay block specimens, a commonly accepted method is to compare the response of the intact material with that of the reconstituted (slurry), assuming that for a given soil there exists a unique intrinsic normal compression line (e.g. Burland, 1990). Consequently a key factor to make possible this comparison was to determine if there exists a unique NCL defined by the slurry samples of the BRS and VSS materials.

8.3.1 Slurry and compacted behaviour

The one-dimensional compression behaviour of the BRS and VSS was investigated in Chapters 5 and 7 respectively. Apart from the BRS-E soil, in all the slurry and compacted specimens tested, a unique normal compression line could be defined as shown in Figure 8.2. It is interesting to point out that the unique normal compression line of the compacted specimens of the BRS-B, which included samples with vertical holes, is located slightly above that defined by the slurries although at high stress levels they tended to converge onto a unique line. This difference might be associated to a very small effect of the sample preparation method and/or possibly to the small errors in calculating the initial void ratio, which in fact is of the same order of magnitude as the observed distance between the lines. In any case, it appears that at high stress levels, the sample preparation technique does no have a noticeable effect on the uniqueness of the NCL lines of the BRS and VSS materials apart from BRS-E as is shown below.

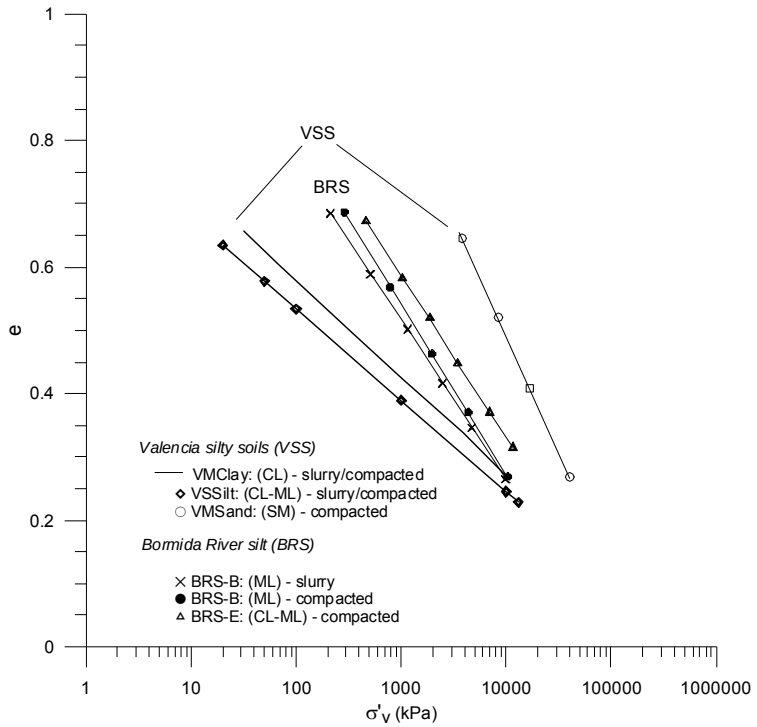

Figure 8.2 One-dimensional normal compression lines of the BRS and VSS

The variability in size distribution observed in the material contained in the block of the VMClay had no effect on the location and slope of the NCL, giving a unique intrinsic line regardless of the clay-size content of the samples. It also appears that, as a general trend, the increment in fines content caused a reduction in the void

ratio and flattened the normal compression lines. At a certain fines content, the increment of fines in the soil did not have an apparent effect in changing the slope of the NCL but its position in the compression plane varied depending on the size distribution. Although it has to be pointed out that the number of data were scarce, an attempt to correlate the measured intrinsic compression index (C^*_c) with the liquid limit was made. Equation 8.1 gives the relationship found with an R^2=0.88. This equation is essentially the same as that proposed by Skempton (1944).

$$C_c^* = 0.0096 \cdot (w_l - 10) \qquad 8.1$$

It is also important to recall that the NCLs shown in Figure 8.2 were estimated using the last parts of the compression lines at high stresses. However, in the range of typical engineering stress level (<1MPa) the effect of increasing the fines content resulted in a increase of the slope of the NCL, as was observed in the VSS materials when comparing the VMSand with the VSSilt and VMClay. The reason for this effect is the onset of particle breakage in the sandy soil at high stresses which controls the compression behaviour.

In the case of the BRS-E soil, it was found that the sample preparation technique had a clear effect on the uniqueness of the compression line as can be seen in Figure 8.3. The compression lines of the slurry specimens did not show any sign of convergence towards a unique NCL for the range of stresses applied. In fact, the lines run parallel to each other and the locations appeared to depend on the initial structure of each sample. This behaviour means that the soil "remembered" its initial structure during compression even at large stresses. As was discussed in previous sections, the two samples that did converge only had a small difference in their initial void ratio, but this does not mean that for larger differences in initial void ratio there will be the same convergence, as shown with the others samples. It also could be argued that the error in calculating the initial void ratio had an effect on the location of the compression lines, but this error was very small in comparison with the large differences measured in the samples tested. On the other hand, the compacted samples converged onto a clear unique NCL regardless of the value of the initial void ratio. The slope of the unique NCL defined by the compacted specimens was essentially the same as those of the slurries as shown in Figure 8.3. The non-uniqueness of the NCLs for the slurry samples shows the lack of meaning of the term "intrinsic" behaviour as a reference framework.

It can be seen from Table 8.1 that the fines content of the BRS-E and VSSilt is basically the same with a higher quantity of clay-sized particles of 12% for the case of the VSSilt. As shown above the BRS-E displayed a clear transitional behaviour

for slurry samples whereas in the case of the VSSilt a unique NCL was found regardless of the sample preparation technique. In order to try to find a reason for that different behaviour, a comparison of their index properties was carried out. The plasticity of both samples is very similar while the activity is slightly higher in the case of the BRS-E, exhibiting the effect of the different mineralogy of the fines. The content of calcium carbonate in the BRS-E was much lower (12% compared to 33.4%) than that of the VSSilt which confirms what was said above about the different natures of the fines contents. It would have been very interesting to analyse the evolution of the structure during compression of these two materials using SEM photos and porosimetry tests but unfortunately this was not carried out in this research project.

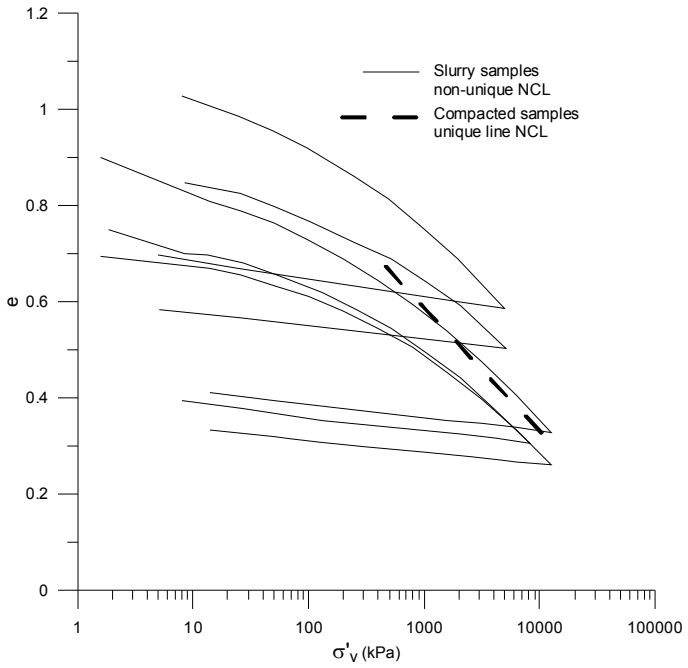

Figure 8.3 One-dimensional compression lines of slurry and compacted samples of the BRS-E

Many researchers working specifically on the transitional behaviour of soils concluded that the sample preparation method alone does not create different initial structures which can result in a non-convergence of the NCLs (e.g. Nocilla et al., 2006; Ferreira & Bica, 2006; Shipton, 2010). In Chapter 2, Section 2.5.3, an investigation was carried out of the effect of the sample preparation method on materials that displayed transitional behaviour. The one-dimensional compressions lines were redrawn grouping samples prepared by the same method. Transitional behaviour was observed in slurry specimens whereas a unique normal compression line was found for wet or air-dry compacted samples (Figures 2.61 to 2.63). Figures

2.61 and 2.62 represent the compression lines associated to the grading curves shown in Figure 8.1(a) and labelled as by Nocilla et al. (2006), in particular those with the lower clay-sized particle content of 3.5 and 8%, which exhibited transitional behaviour. Consequently and contrary to what was concluded, the sample preparation methods appeared to have a clear effect in triggering the transitional response, at least in the soils analysed.

As described above, for a given material, compacted samples always converged onto a unique NCL at high stress levels, so the remaining question was to compare their behaviour to that of the slurry samples. An extensive comparison was made in Chapter 5, Section 5.2.2, where statically and dynamically compacted samples of the BRS-B trimmings were tested in the oedometer. Heterogeneous "layered" specimens were created where each layer had a different initial void ratio. It is important to recall that in this case the term "layered" sample is not the same as the one that can be usually found in the literature, where a layered sample consist of soils with different gradings. Moreover, a series of compacted samples with vertical holes were also produced, trying to simulate the holes found in some intact specimens of the BRS-B. Figure 8.4 shows the compressions lines of all the compacted samples, normalised using the void index (Burland, 1990), with the intrinsic parameters measured on the unique 1D-ICL* defined by the slurry specimens.

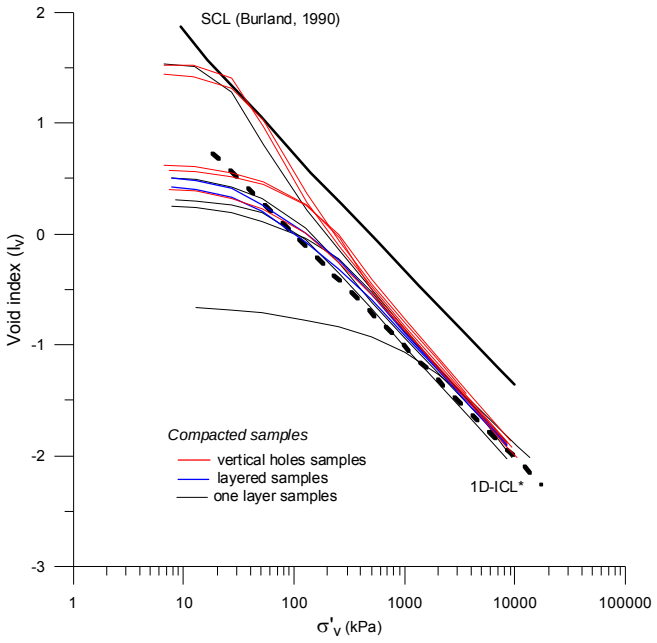

Figure 8.4 Normalized one-dimensional compression behaviour of the compacted samples of the BRS-B

It can be seen that the normalised compression lines crossed the estimated 1D-ICL*, showing the effect of the initial structure created. This effect was more noticeable with increasing the initial void ratio of the specimens, where a clear meta-stable structure could be observed, regardless of the type of sample (i.e. holes and layered). After yield, all the compression lines moved towards the 1D-ICL*, as was also shown in Figure 8.2. This behaviour confirmed that the initial structure was practically erased by compressing the samples to very high stress levels where the stress sensitivity values were close to unity. In the case of the BRS-E material this comparison was not possible due to the transitional behaviour of the slurry samples. Only a few dense samples were available for the comparison between slurry and compacted specimens of the VSSilt soil. The behaviour was similar to that observed in Figure 8.4. These results agree with the conclusions obtained by others researcher for silty soils (e.g. Santucci de Magisttri et al. 1998).

8.3.2 Intact behaviour

The effect of the in-situ structure on the compression response of the intact block specimens of the Bormida River silt (BRS-B) and Valencia silty clay (VMClay) materials was investigated in Chapters 5 and 7.

As described above the soil contained in the block sample of the BRS-B was very homogeneous in terms of size distribution compared with the variability observed in the VMClay block specimen (Figure 8.1a). In addition, the granulometry within some samples of the VMClay was not the same producing a certain degree of layering . This feature was not seen in the BRS-B specimens. In Section 6.2.1, it was shown that part of the sand fraction encountered in the VMClay consisted of aggregates of particles cemented by calcium carbonate, which appear randomly distributed inside the block. It is important to recall that the variability of size distributions in the VMClay materials contained in the block sample had no effect on the location and slope of the normal compression line in their reconstituted states, the intrinsic 1D-ICL* of which was unique regardless of the clay-sized content of the samples (Figures 7.2 and 8.2).

The index properties for both materials are summarised in Table 8.1. The main difference between them is the content of calcium carbonate which is 50 and 10.4% for the VMClay and BRS-B respectively. This higher content of $CaCO_3$ in the VMClay could be a source of inter-particle bonding that would enhance the strength of the intact material with respect to that of the slurry specimens. In terms of size distribution, the BRS-B is more sandy with a content of 18% compared with the 5-8% of the VMClay. As mentioned above part of the 5-8% of supposedly sand particles was associated to the aggregates.

Figure 8.5 shows a comparison of the normalised compression lines of the intact samples in plane I_v:σ'_v plane. The SCL and the ICL proposed by Burland (1990) are also plotted in the same figure with the extended range of stresses as modified by Chandler (2000). As was pointed out in previous chapters, the first thing to note is the slightly deviation of best estimate unique 1D-ICL* of the BRS-B and VMClay from that of the curved shape of the ICL proposed by Burland at lower and higher stress levels. Comparing the normalised lines, both materials exhibited variability in the initial void ratio, which was slightly larger in the case of the VMClay. It was believed that in the case of the VMClay this variability represents a heterogeneous in-situ structure mainly due to variations in the depositional conditions that produced, for example, the range of gradings observed in the material contained in the block sample. On the other hand the different initial void ratios observed in the BRS-B were not associated to differences in the size distribution of the specimens. It is also obvious that other factors such as small errors in estimating the initial void ratio could have affected this observed variability in void ratio. Another aspect to notice from the comparison is that, in general, the in-situ structure of the BRS-B samples was denser than that of the VMClay although the BRS-B was taken from a more swallow depth (1.4m) compared to the VMClay (4.5m).

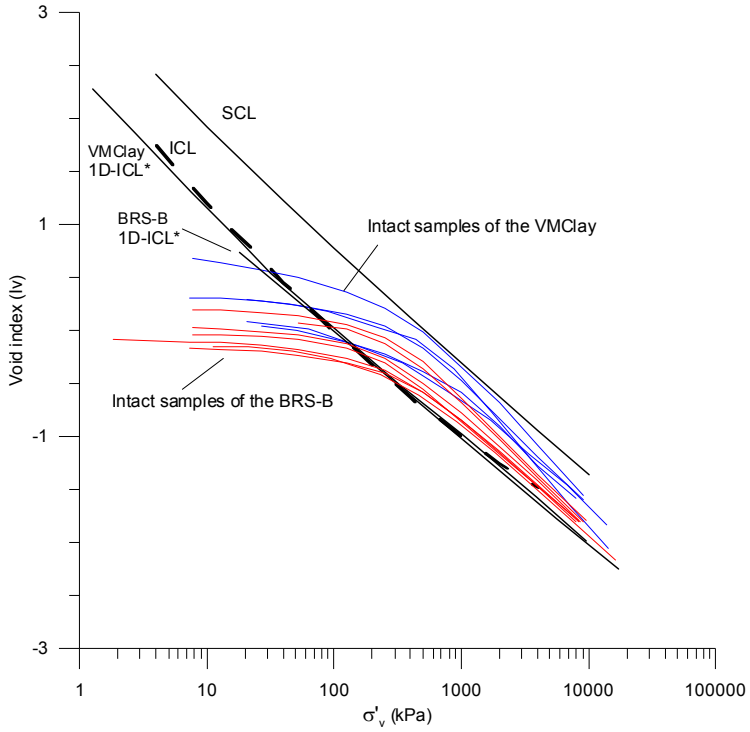

Figure 8.5 Normalized one-dimensional compression behaviour of the intact samples of the BRS-B and VMClay

As can be seen from Figure 8.5 all the compression lines crossed the 1D-ICL* showing the effect of the in-situ structure on the compression behaviour. In all cases, the samples yielded at different stress levels in between the 1D-ICL* and the SCL with stress sensitivities that ranges from 2.0-4.8 and from 1.2-2.5 for the VMClay and BRS-B respectively. In both cases, after yield, the compression lines moved towards the 1D-ICL* very slowly and at very high stress levels the stress sensitivity was still higher than unity, exhibiting a stable structure that could not be totally removed during compression. This stable structure was more noticeable in the case of the VMClay material. The absence of a clear and abrupt change in the slope of the compression lines could be associated to there being only a small effect of the initial bonding on the soil behaviour for both materials. The apparent higher effect of the in-situ structure observed for the VMClay in the compression behaviour may be also affected by the method of normalisation which may de-emphasise the effect for denser samples (e.g. Gaspare & Coop, 2008; Hosseini Kamal et al., 2014).

Figure 8.6 shows a comparison between the normalised compression behaviour of the Sibari clay and Pisa clayey silts with those of the BRS-B and VMClay. The Sibari clay is a layered Holocene alluvial and coastal deposit, the in-situ structure of which is characterised by intercalation of silt and fine sands (Coop & Cotecchia, 1995). They associated this mesoscopic in-situ structure to a rapidly fluctuating depositional environment at the site. All the normalised compression lines of the Sibari intact samples tested by Coop & Cotecchia were located in a band between the ICL and SCL. For clarity of the figure, only a few of the compression tests are plotted in Figure 8.6. Coop and Cotecchia concluded that the slow post-yield convergence towards the intrinsic line was a consequence of the heterogeneous grading inside the samples. Moreover it was proposed that the location of each normalised compression line with respect to the ICL increased with the degree of heterogeneity inside the samples. The compression curves of the Pisa soils correspond to tests carried out on shallow samples (<6m) of recent alluvial Holocene clayey silts from the flood plain of the Arno River (Rampello & Callisto, 1998). These samples were retrieved from the surrounding area of the Leaning Tower of Pisa. Although the sensitivity of the Pisa soils is higher than that of the other materials, the normalised compression curves showed a clear stable structure after yield, with very little tendency to converge towards the ICL.

The normalised behaviour of the BRS-B and VMClay materials appears to display a similar trend as that of the Sibari and Pisa soils. Looking at Figure 8.6 it can be seen that, for each material, the normalised compression lines plotted in a relatively narrow band with a higher distance to the 1D-ICL* for the VMClay. As was recalled above, at a meso-structure level the material inside the VMClay block sample was heterogeneous in terms of size distributions and during the tests some

of the samples exhibited parts with a higher content of silt/clay than others creating a certain layering in the specimens. This heterogeneous in-situ structure of the block was also associated to changes in the rates and modes of deposition of the Turia River. In the case of the BRS-B block sample, and during the trimming of the specimens for testing, the in-situ structure seemed more homogeneous than those of the VMClay. This could explain the smaller offset of the lines with respect to the 1D-ICL* according to the conclusions obtained by Coop & Cotecchia (1995).

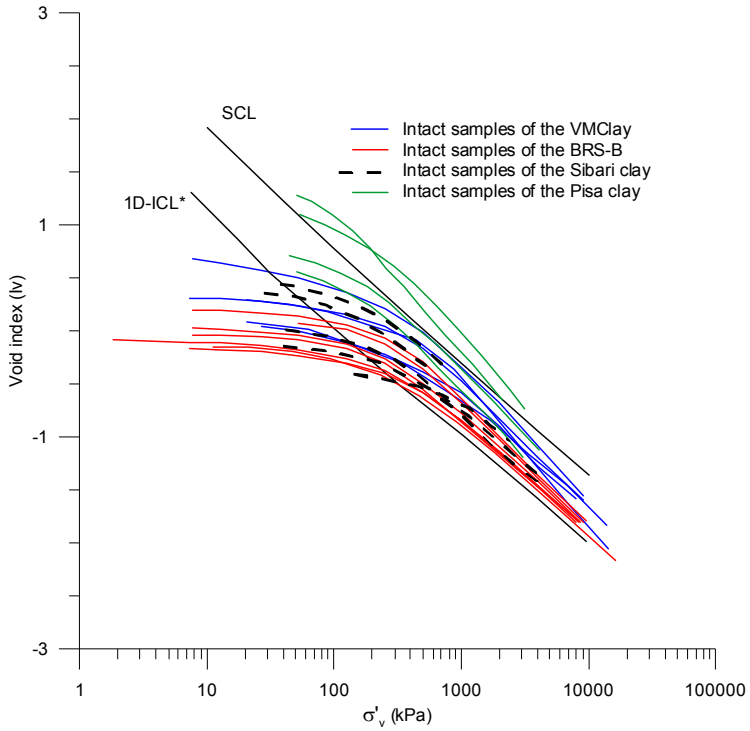

Figure 8.6 Comparison of the normalized one-dimensional compression behaviour of the intact samples of the BRS-B, VMClay, Sibari clay and Pisa clay (Sibari and Pisa clay data redrawn from Coop & Cotecchia, 1995 and Rampello & Callisto, 1998 respectively)

Micro-structure studies were carried by using SEM images taken from different specimens of the BRS-B and VMClay in order to find an explanation for the observed differences in compression behaviour between the reconstituted and intact samples. Figures 8.7 to 8.9 show the initial micro-structure of the slurry, intact and compacted samples of the BRS-B soil. The micro-structure of the intact sample shown in Figure 8.8 is characterised by a fabric where clear aggregates of particles can be identified, which in some cases are bonded by bridges of particles of smaller sizes. In the case of the slurry sample (Figure 8.7) a more homogeneous structure can be distinguished, so it appears that the aggregates of particles found in the intact specimen were destroyed during the reconstitution process to create the slurry. The destructuration of the intact samples seems to be less efficient in the

case of the compacted specimen (Figure 8.9), the intact material of which was remoulded at its natural water content by hand-mixing with a spatula. Correlating the micro-structure observed in the intact sample with the normalised behaviour shown in Figure 8.6 it seems that the aggregates of particles had a positive effect on the compression behaviour which contrasts with the results found in the literature (e.g. Fearon & Coop, 2002).

The micro-structure of the VMClay material is shown in Figures 8.10 to 8.12. The first thing to notice is the higher content of clay-sized particles contained in the sample compared with that of the BRS-B soil. In this case only images of intact and slurry samples were taken. A clear homogeneous micro-structure can be observed for the case of the slurry sample where silt particles are contained in a clay-sized matrix (Figure 8.10). In previous paragraphs it was described that a certain degree of layering was seen during the trimming of some intact specimens of the VMClay. Obviously, this meso-structure feature can not be identified at a micro-scale level as that seen in the SEM images. The micro-structure of an intact sample is shown in Figure 8.11. The two images were taken from the same sample at two different locations and essentially the structure was the same in both cases. Perhaps one difference between the two images could be a higher content of silt particles in Figure 8.11(a) which could be associated to the layering. No clear differences can be observed when the intact and slurry samples are compared. Finally, Figure 8.12 shows SEM imagines of silty particles bonded by calcium carbonate which, as mentioned before, appeared to have only a small positive effect of the in-situ structure on the compression response. This latter conclusion is based on the absence of a clear and abrupt change in the slope of the compression lines which would be the case for materials with large effects of bonding.

In summary, and based on the above discussion, it might be concluded that fabric is the part of the in-situ structure which had the most important effect on the compression behaviour of the intact samples of the VMClay and BRS-B materials, with only small effects of bonding. Although very high stresses were reached during compression, the initial structure, and in particular the fabric, was not totally erased, with stress sensitivity values still larger than unity. This effect appears to be more noticeable in the case of the VMClay.

8.4 Shearing behaviour at large strains

The shearing behaviour of the materials tested in this research project was investigated using the triaxial apparatus. The study was focused on the shear response of the materials contained in the block samples of the VMClay and BRS-B. A detailed description of their behaviour was given in Chapters 5 and 7.

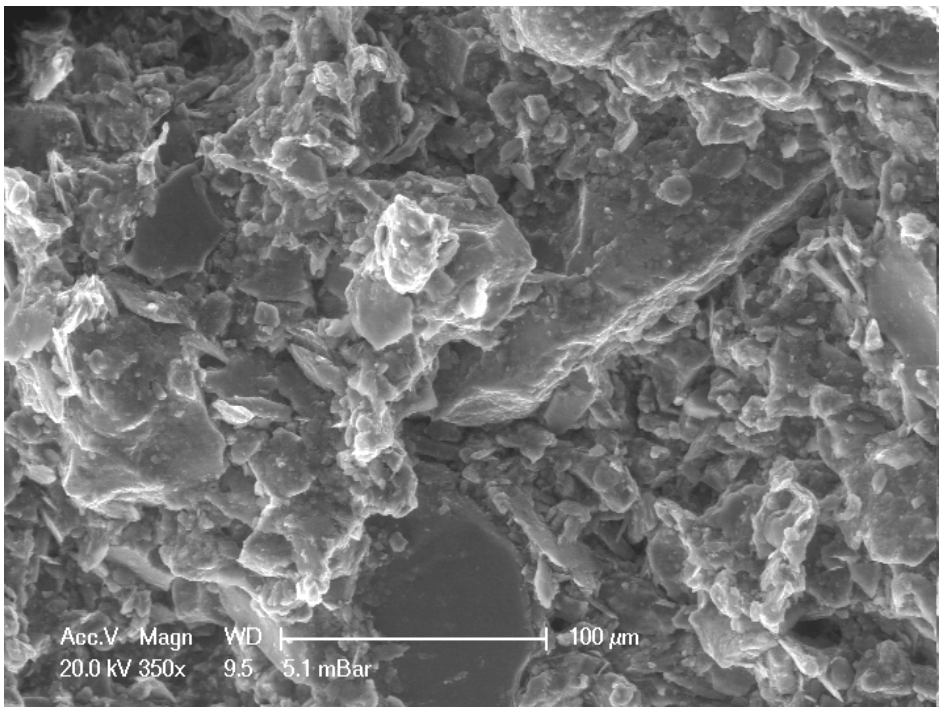

(a)

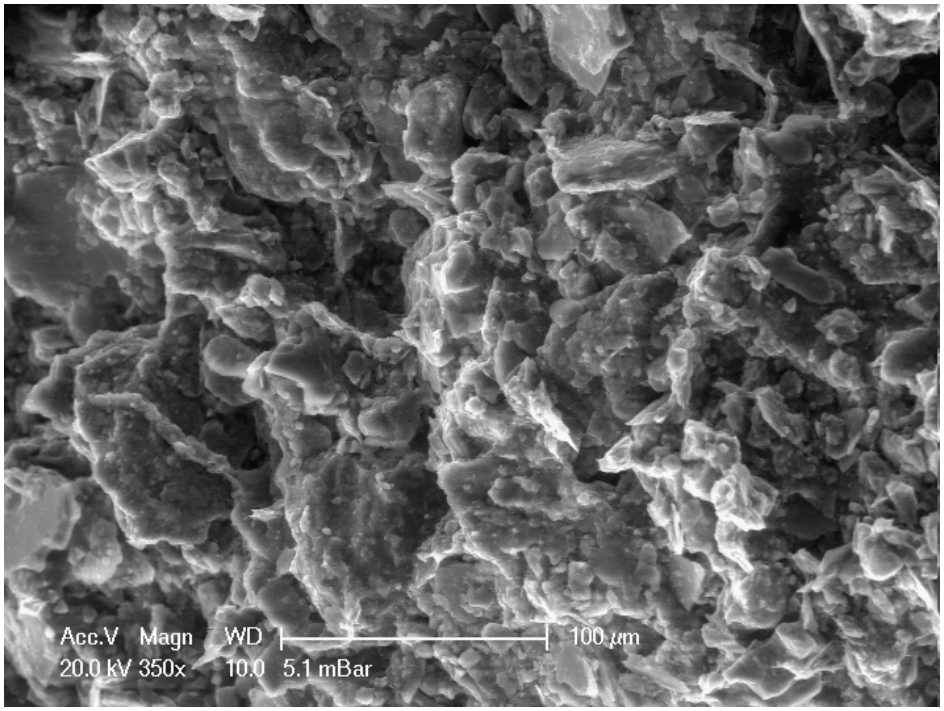

(b)

Figure 8.7 Electron microscopy images of a slurry sample of the BRS-B

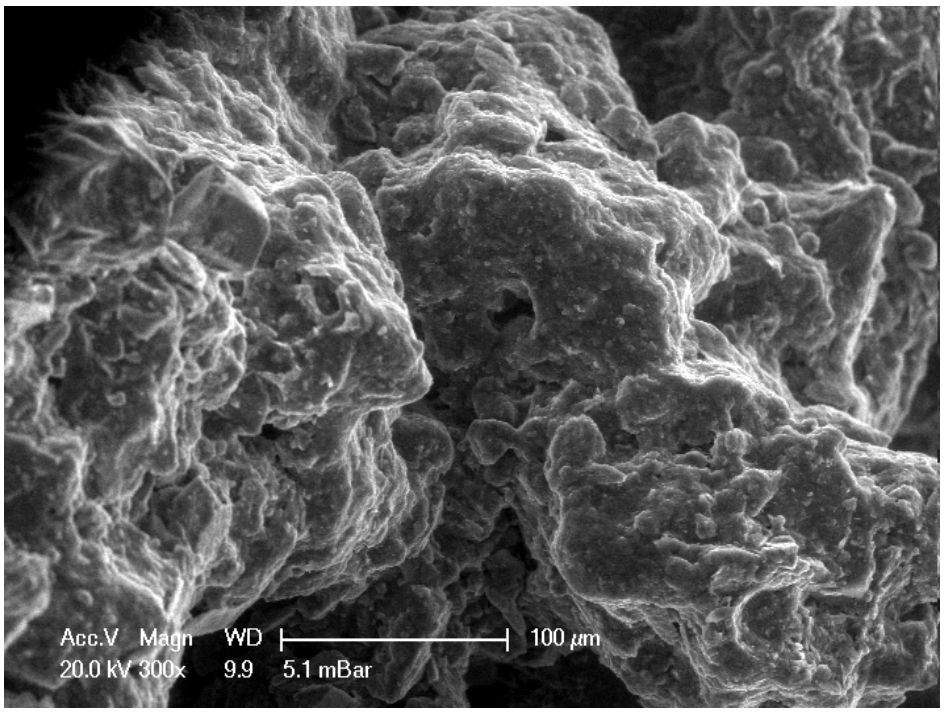

(a)

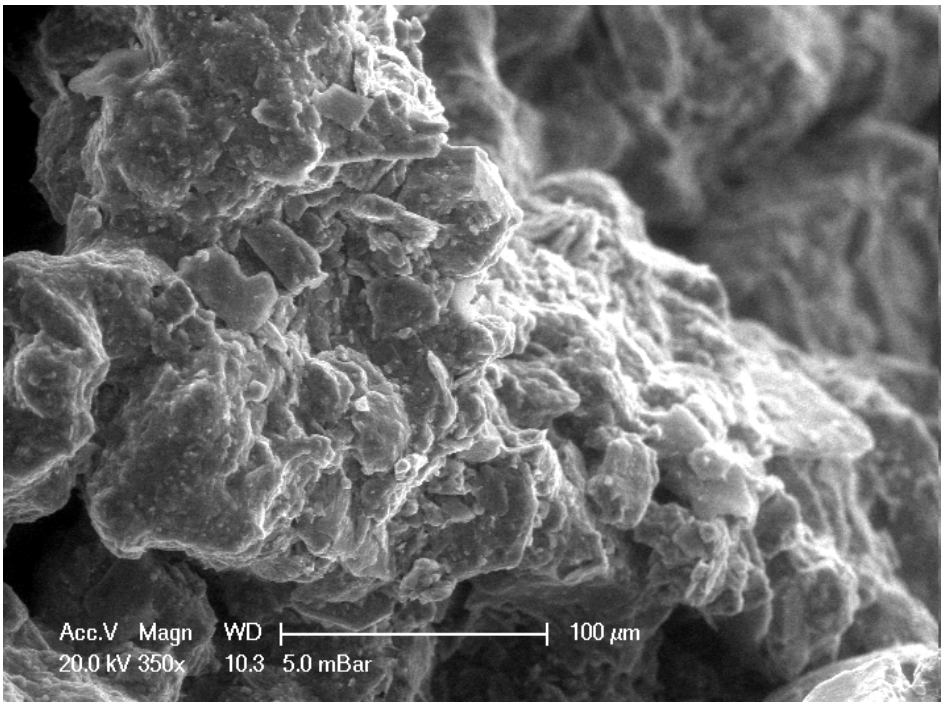

(b)

Figure 8.8 Electron microscopy images of an intact sample of the BRS-B

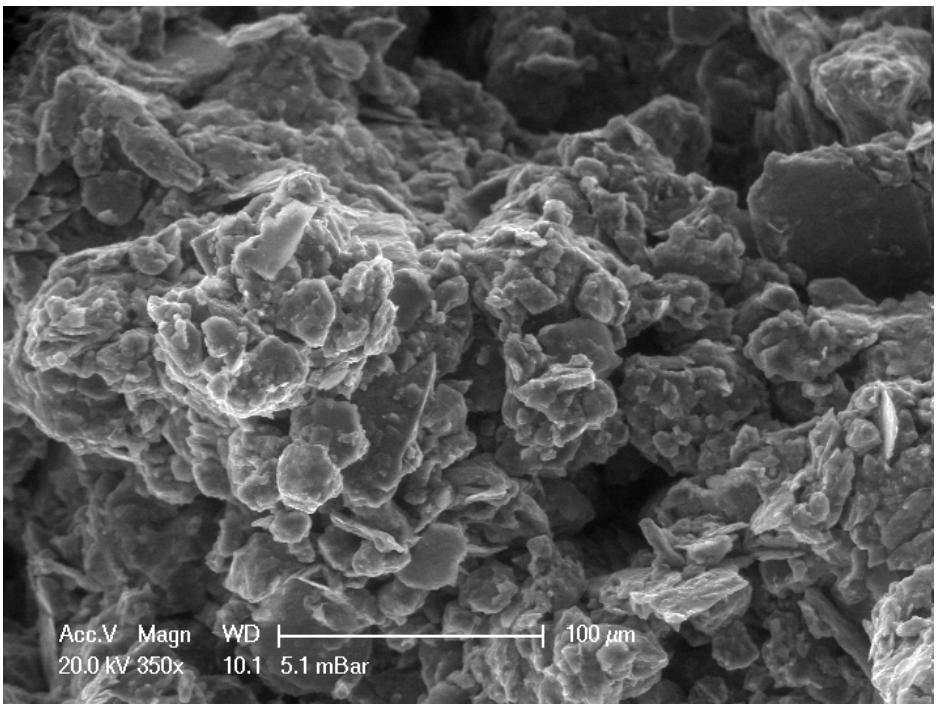

(a)

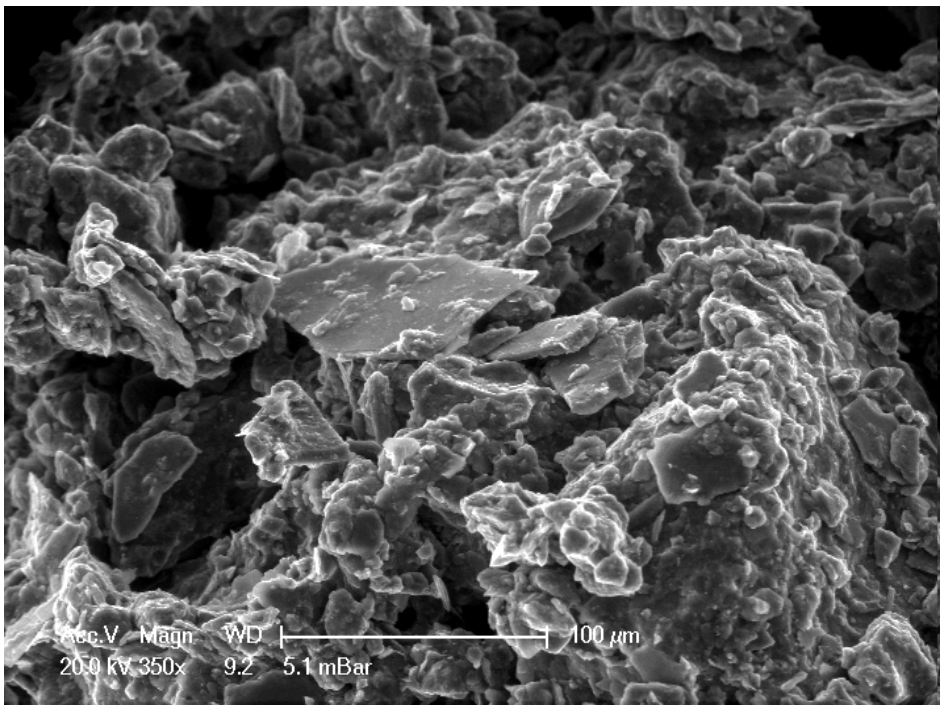

(b)

Figure 8.9 Electron microscopy images of a compacted sample of the BRS-B

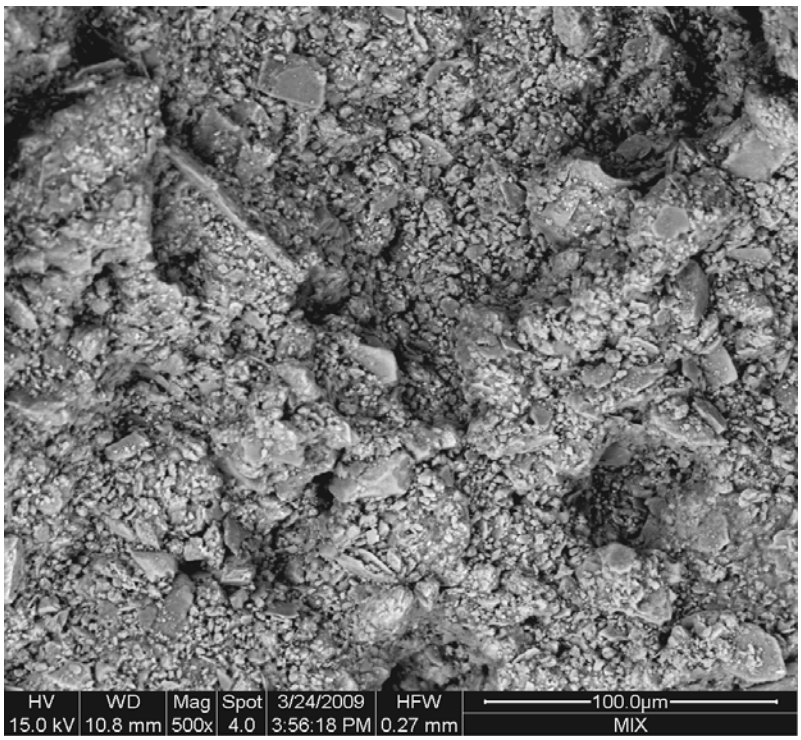

(a)

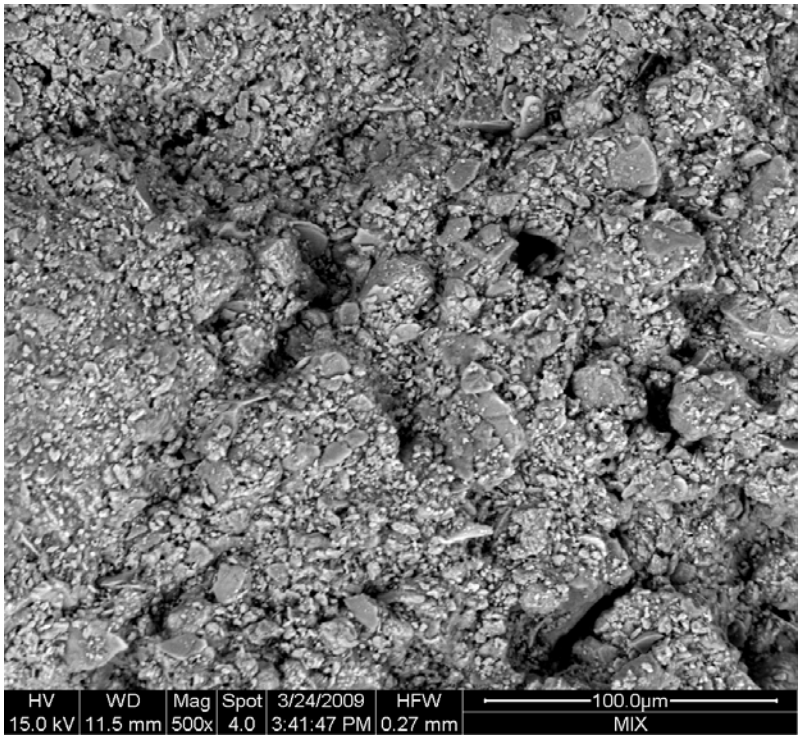

(b)

Figure 8.10 Electron microscopy images of a slurry sample of the VMClay

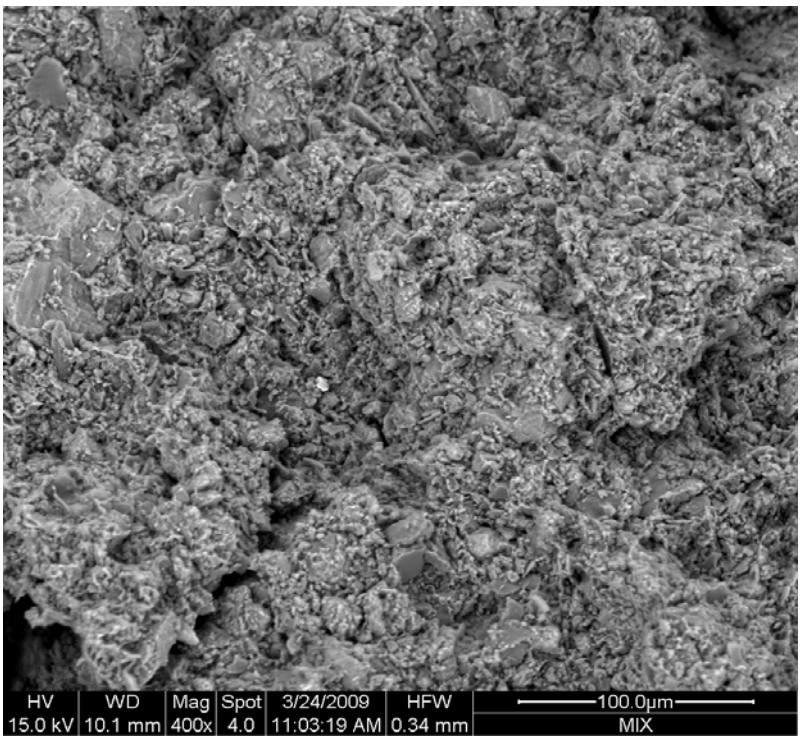

(a)

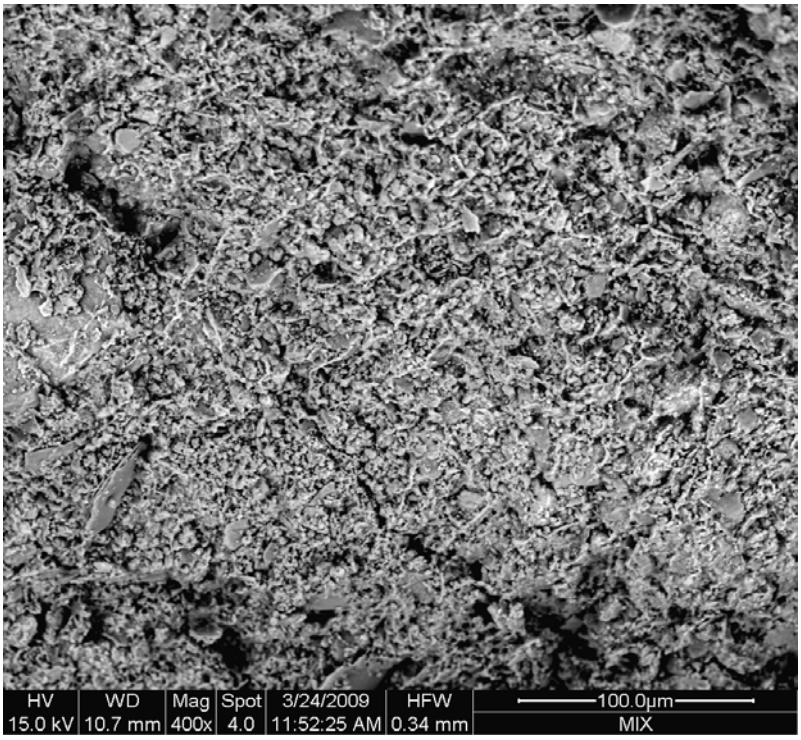

(b)

Figure 8.11 Electron microscopy images of an intact sample of the VMClay

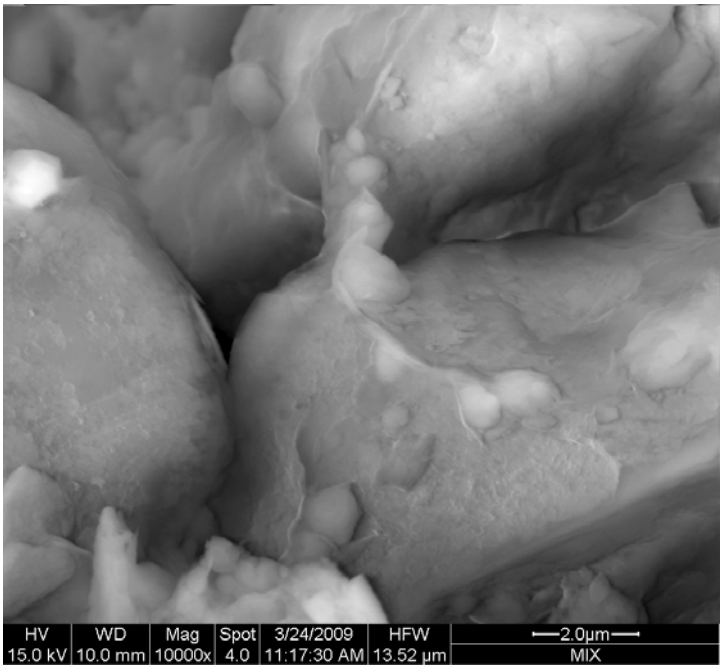

(a)

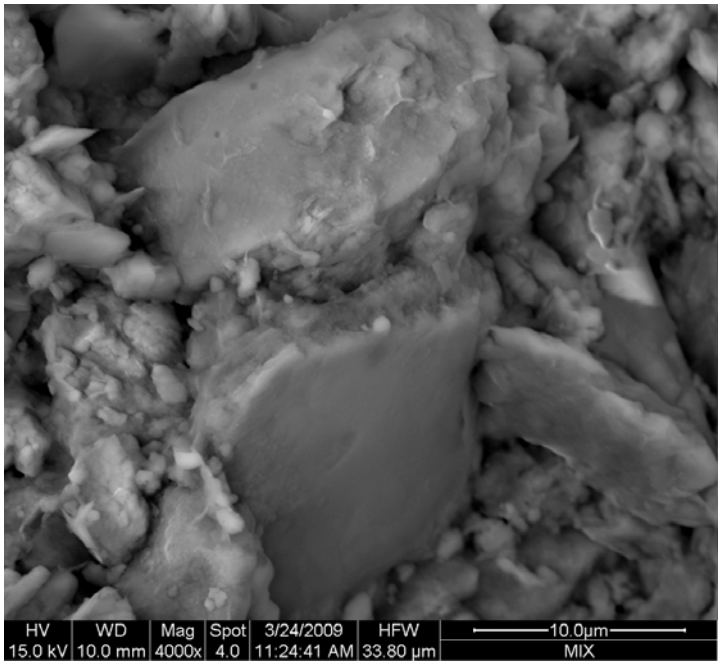

(b)

Figure 8.12 Electron microscopy images of silty particles bonded by calcium carbonate taken from two intact samples of the VMClay

8.4.1 Slurry and compacted behaviour

A unique isotropic ICL* and CSL* were found for both materials regardless of the sample preparation method and these are shown in Figure 8.13. For a given material the ICL* and CSL* were parallel to each other in the range of stresses applied as expected from the critical state framework. As was concluded above, it can also be observed that the slope of the compression line decreased with an increase of the fines content, although the mineralogy of the VMClay and BRS-B was different. The stress ratio between the estimated ICL* and the CSL* was 2.02 and 1.75 for the VMClay and BRS-B respectively. These values are very close to those of clays whose stress ratios (p'/p'_{cs}) are often around 2. Moreover, the value for the BRS-B is essentially the same as that measured on samples of the material tested by Nocilla et al. (2006), which did not show transitional behaviour and corresponded to the gradings with 25 and 45% of clay-sized particles, plotted in Figure 8.1(a).

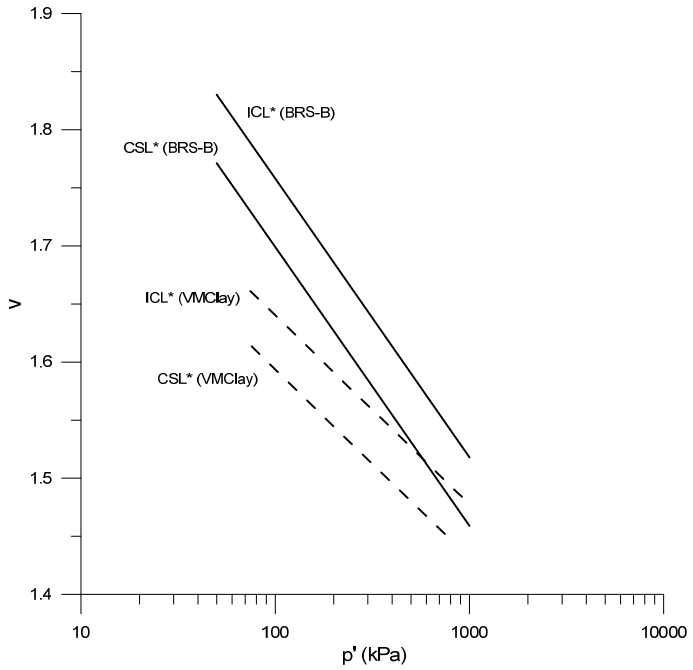

Figure 8.13 Isotropic ICLs* and CSLs* for samples of the BRS-B and VMClay

The normalised stress paths of the slurry samples for each material are shown in Figure 8.14. The stress paths were normalised by using the equivalent mean effective pressure on the critical state line. In both cases, the normalised stress paths defined a unique critical state. Some samples such as the drained test and also the highly overconsolidated undrained tests of the BRS-B were still moving towards it at the ends of the tests.

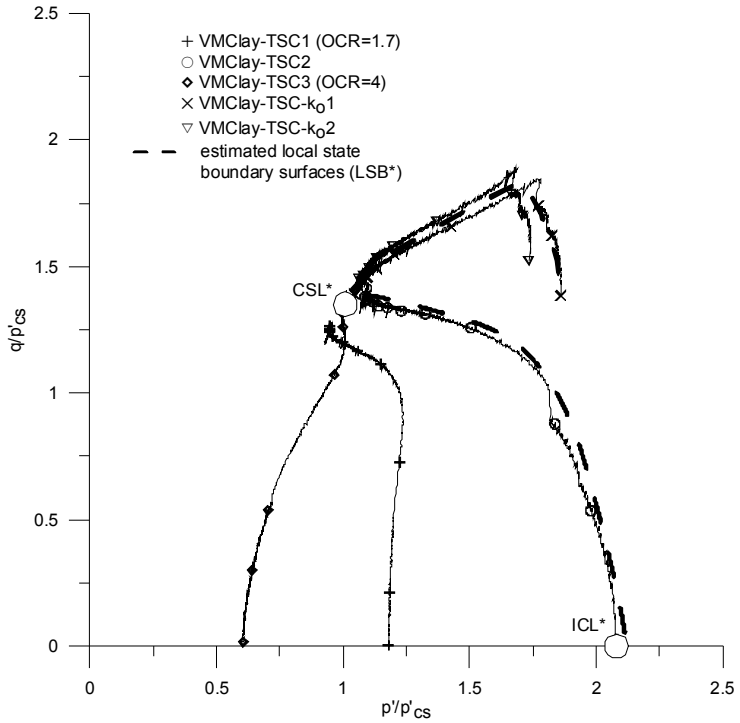

(a)

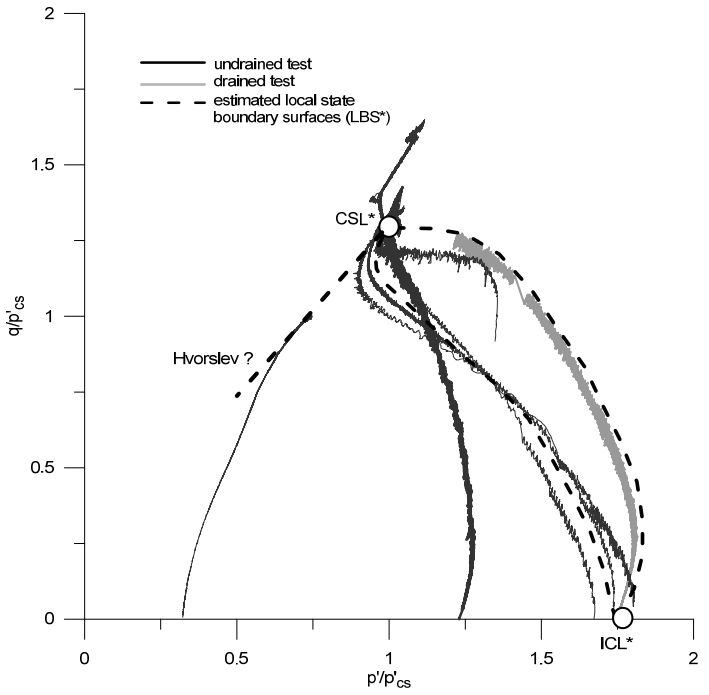

(b)

Figure 8.14 Normalized shearing data for the slurry samples of the (a) VMClay and (b) BRS-B

The final average M* values were 1.3 and 1.32 for the BRS-B and VMClay respectively. However, one of the undrained tests of the BRS-B was moving to a slightly higher value. One clear difference between the two normalised plots is the length of the dilatant "tails" of the stress paths after the phase transformation point. It can be observed that a more clear and larger dilatant tail was developed in the case of the undrained tests on the BRS-B compared with the VMClay. This shows that the dilatant response after the phase transformation point reduced with the increase of fines content. Another difference in behaviour between the BRS-B and VMClay was seen in the normalised stress paths of the k_o compressed specimens. A clear brittle response was observed in the samples of the VMClay, the peak undrained strength of which occurred at a smaller q/p' value compared with the final average M* value. On the other hand the stress path of the BRS-B did not show any brittle behaviour and its final undrained strength coincided with the critical state. It appears that the undrained brittleness increased with the fines content as proposed, for example, by Georgiannou et al. (1990).

In terms of the intrinsic state boundary surface, it can be seen that Rendulic's principle did not work, as for example the drained path for the normally consolidated sample of the BRS-B plotted outside those of the undrained specimens. In addition, the local state boundary surface (LBS*) was dependent on the type of test as can be observed for the case of the k_o compressed samples in both materials. This was a feature observed by Gens (1982) and also seen in other materials like those tested for example by Nocilla et al. (2006). Unfortunately the Hvorslev surfaces for both materials could not be defined properly due to the lack of enough tests on heavily overconsolidated samples. Figure 8.15 shows the estimated local state boundary surfaces for the BRS-B and VMClay material based on the tests performed on this research project. A more extensive programme of drained tests at different stress ratios should be carried out to identify the intrinsic state boundary surface (SBS*) more comprehensively.

8.4.2 Intact behaviour

The effect of the in-situ structure of the intact samples on the shearing behaviour at large strains was investigated by normalising their stress paths with respect to the p'_{cs} on the unique CSL* of each material. Figure 8.16 shows the normalised stress paths of the intact samples compared with those of the slurry specimens for both soils.

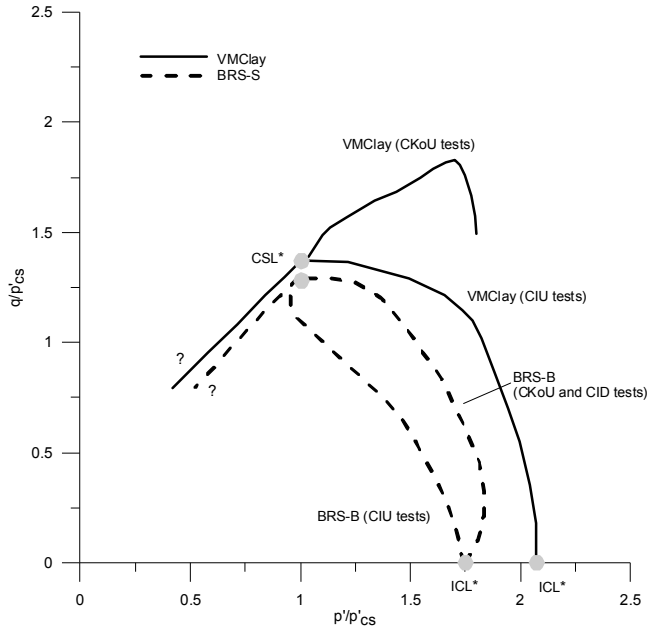

Figure 8.15 Intrinsic local state boundary surfaces (LBS*) of the VMClay and BRS-B

In the case of the VMClay material, the normalised paths moved directly towards the unique CSL* at the ends of the tests for the samples where shearing started slightly above or below the CSL*, which implied a certain degree of overconsolidation. Only one sample plotted outside the intrinsic local state boundary surface on the isotropic axis, showing a stable structure at large strains and where no convergence was seen towards the unique CSL*. Apart from this latter sample, it appears that the destructuration induced during compression and shearing in the triaxial was enough to remove the stable in-situ structure observed in Figure 8.5 during one-dimensional compression. Another interesting feature to notice was the dilatant tail exhibited mainly by the overconsolidated intact samples compared to the lack of it in the slurries. These samples displayed a clear strain-softening behaviour during shearing favouring the formation of shear bands as shown in Figure 7.29. The behaviour of the BRS-B is represented in Figure 8.16(b). In this case the normalised stress paths for the specimens that crossed the ICL* during compression exhibited a clearer stable structure that could not be removed during shearing. The drained test also showed a clear stable structure although the test had to be stopped at a shear strain of 10%. The values of M were very similar to those of the slurry, except in the cases of specimens BRS-B-TI4 and BRS-B-TI9 tested at high pressures which exhibited lower values at the ends of the tests. In both materials, the values of M for the samples tested at higher confining pressures were lower than those measured at lower stresses pointing to the possibility of a curved CSL in the p':q plane.

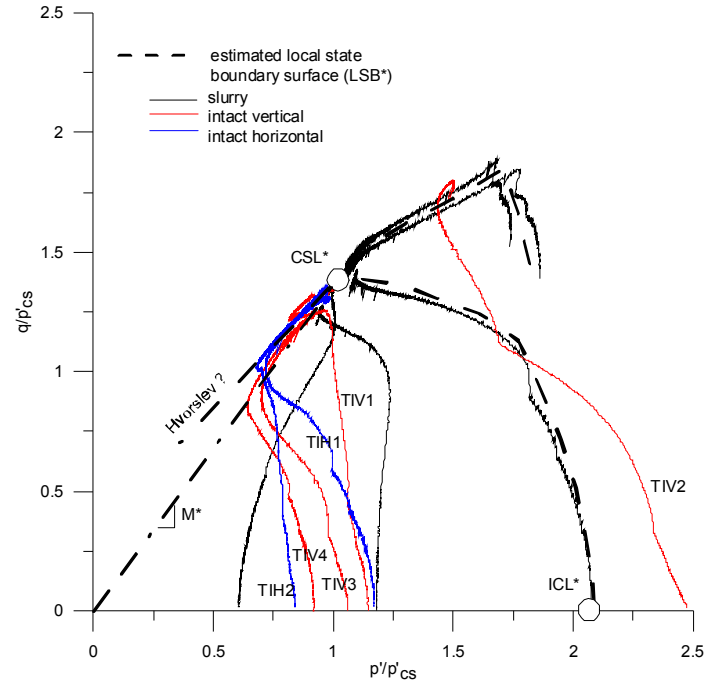

(a)

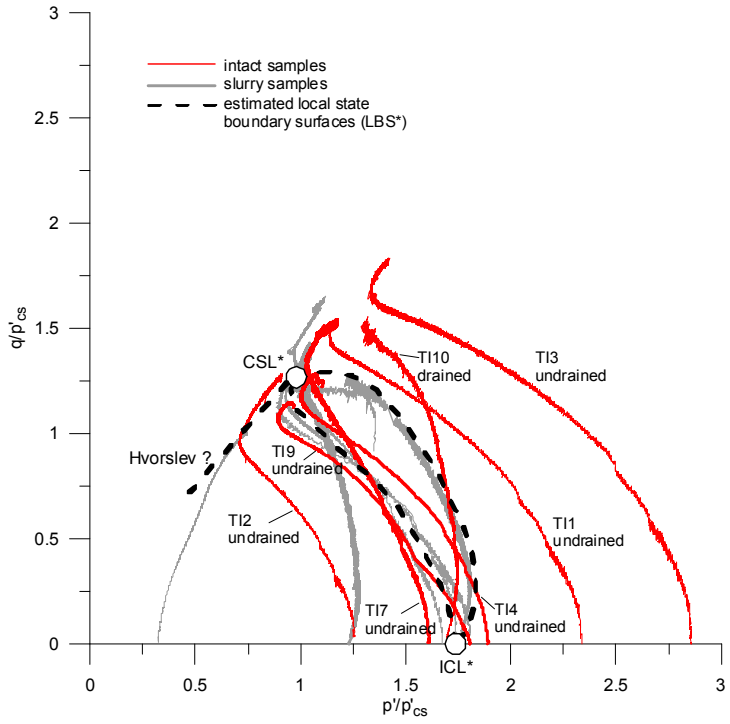

(b)

Figure 8.16 Normalized shearing data of the slurry and intact samples of the (a) VMClay and (b) BRS-B

In Figure 8.16, and for both materials, it can be observed that none of the samples displayed any clear effect on the dry side of the critical state. In summary it appears that some elements of stable structures, in particular fabric, is the main part of the in-situ structure that had a noticeable effect on the shearing behaviour of the VMClay and BRS-B materials, however its influence on the soil response at large strains was relatively small. Comparing these results with those obtained by Coop & Cotecchia (1995) for the Sibari layered clay shows that the possible layering affecting the intact samples of the VMClay had a much smaller influence on the soil response at large strains.

8.5 Shearing behaviour at small strains

Although it was not the main subject of this research project, the influence of the initial structure on the stiffness at small strains of the BRS-B and VMClay materials was analysed in Chapters 5 and 7 respectively. Figure 8.17 shows the relationship between the undrained secant Young's modulus and the current mean effective stress at various levels of axial strain for both materials. A regression analysis was performed for each strain level. As can be seen, a larger scatter in the results was observed for the case of the VMClay samples (Figure 8.17b). The coefficient of correlation for the BRS-B varied from 0.92 to 0.97 whereas in the case of the VMClay the correlation was relatively poor with values that ranged from 0.52 to 0.67. Part of this poor correlation seen in the VMClay material might be explained by the higher yield stress ratios of the intact and slurry samples before starting shearing (Figure 8.16a). A comparison of the stiffnesses for both materials is shown in Figure 8.18. As can be observed the undrained Young's moduli of the VMClay are higher than those of the BRS-B for a given axial strain.

Figure 8.19 shows the variation of the effective stress level exponent of the stiffness (n) with the shear strain for the BRS-B and VMClay. As can be seen the values of n increased with the strain level moving towards unity for both materials as suggested by many authors (e.g. Viggiani & Atkinson, 1995; Jovicic & Coop, 1997). Slightly lower values were measured for the case of the VMClay which might reflect the different mineralogy between the VMClay and BRS-B.

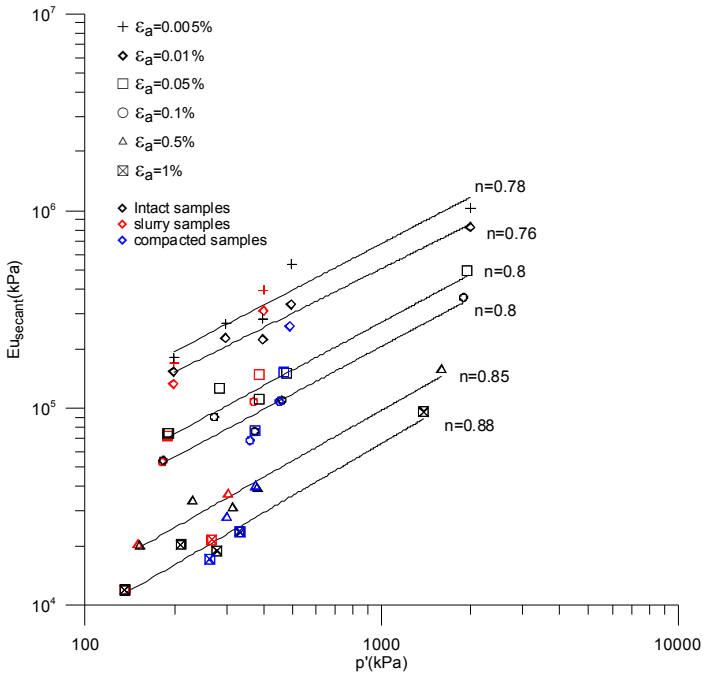

(a)

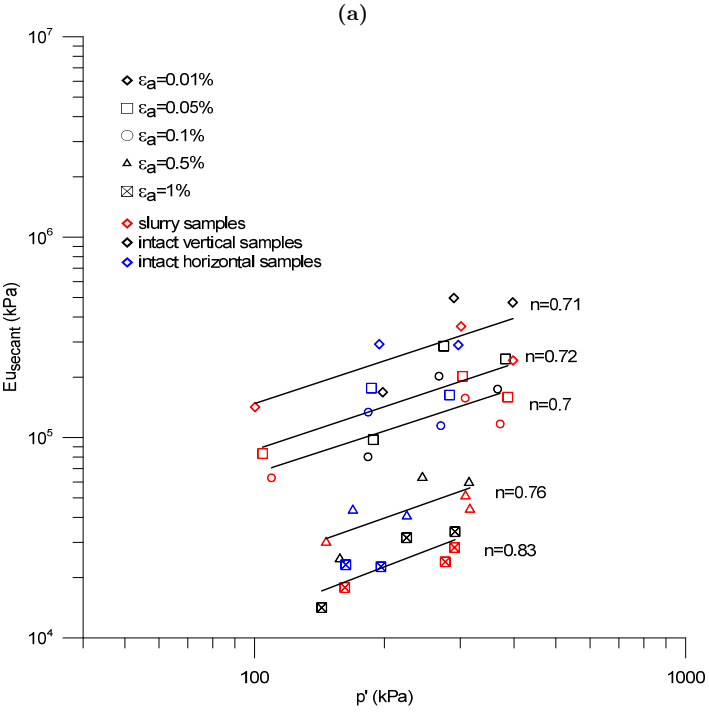

(b)

Figure 8.17 Undrained secant Young's modulus as a function of the current mean effective stress at different strain levels for samples of the (a) BRS-B and (b) VMClay

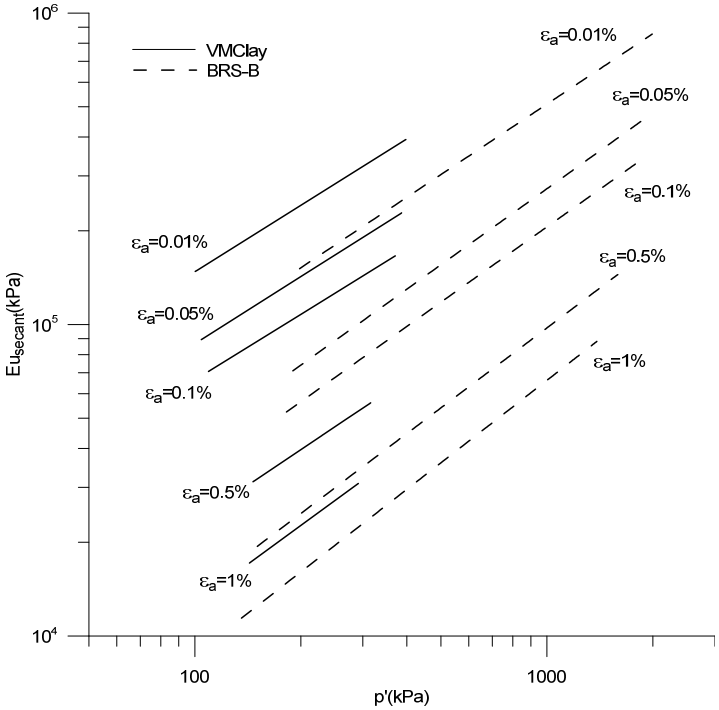

Figure 8.18 Comaprison of the undrained secant Young's modulus as a function of the current mean effective stress at different strain levels for samples of the BRS-B and VMClay

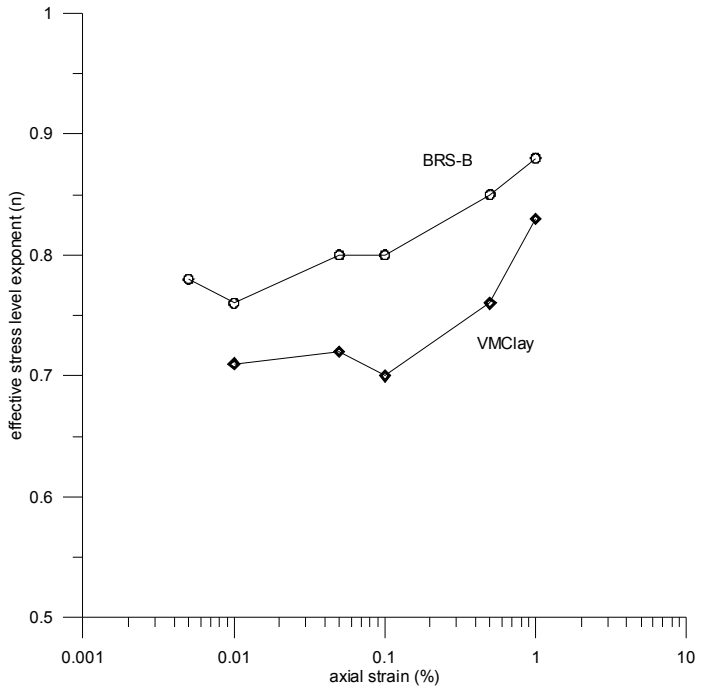

Figure 8.19 Comparison of the variation of the effective stress level exponent of stiffness (n) with axial strain for the VMClay and BRS-B

The effect of the sample preparation method and the in-situ structure of the BRS-B samples is shown in Figure 8.20 where the stiffnesses of samples compressed to the same mean effective stress are compared. Unfortunately only one comparison between slurry, compacted and intact specimens was available which is at p'_0=400kPa. From this comparison it can be seen that the more homogeneous structure of the slurry sample exhibited the highest stiffness and the compacted specimen the lowest. It is interesting to recall that the intact sample involved in this comparison is BRS-B-TI1, the compression line of which crossed the ICL* as shown in Figure 8.16(b). The strength enhancement due to its stable in-situ fabric resulted in a lower stiffness compared with the slurry state. The differences in stiffness between these three samples reduced with shear strain.

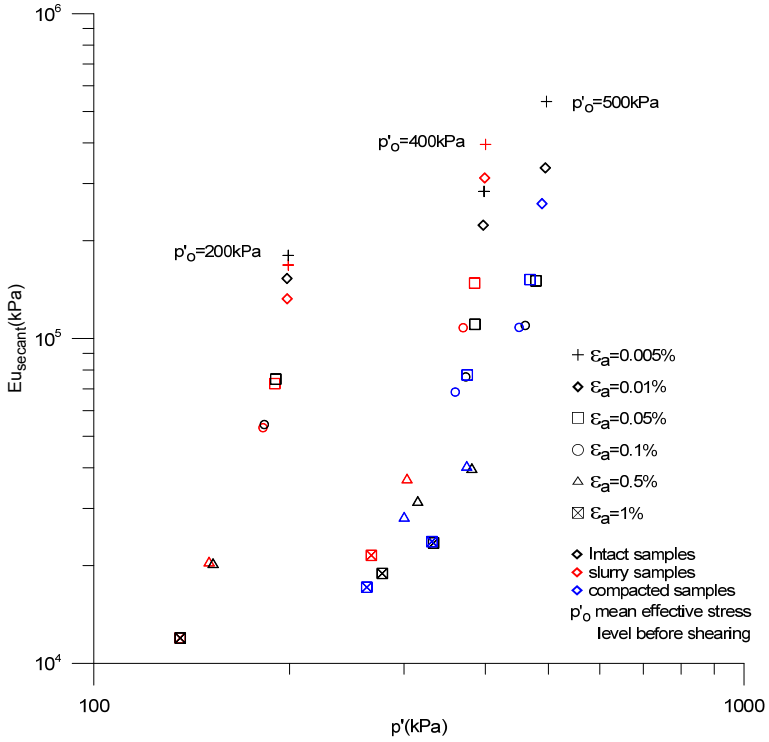

Figure 8.20 Effect of the sample preparation method and in-situ structure on the stiffness at different strain levels of the slurry, compacted and intact specimens of the BRS-B

Another interesting comparison in Figure 8.14 is that at p'_0=500kPa. In this case a compacted and an intact sample were compared. Unluckily the test on the slurry specimen had to be stopped due to a failure in the system and only compression data were available. From this comparison, it can be seen that the stiffnesses were essentially the same apart from the initial values where the intact specimen was stiffer. The intact sample involved in this comparison, and labelled as BRS-B-TI3, also showed a clear stable fabric after crossing the ICL* (Figure 8.16b). It might

be expected that, as in the case of the intact specimen BRS-B-TI1, its more open fabric would lead to lower stiffnesses compared with a slurry sample.

The last comparison in Figure 8.20 was carried out at p'_0=200kPa. In this case a slurry and an intact sample were compared. As can be seen, the stiffness for both specimens was essentially the same. This result is the opposite to what was found in the comparison at p'_o=400kPa. However, a possible explanation of this might be the overconsolidated state of the intact sample before shearing as shown in Figure 8.16(b). For a given stress state the stiffness is higher for an overconsolidated sample compared to that of a normally consolidated one so this might have cancelled the expected higher stiffness of the slurry sample. Having said that, and due the insufficient number of comparison tests available, it could be too ambitious to draw a general conclusion on the effect of the sample preparation method and the in-situ structure on the stiffness at small strain.

A comparison between the stiffness of vertically and horizontally cut intact specimens of the VMClay was carried out and plotted in Figure 8.21. Two pairs of tests were compared for samples compressed isotropically at 200 and 300kPa before shearing. The results from each comparison give opposite conclusions. It might be argued that this inconsistent behaviour could be attributed to the in-situ heterogeneity of the samples. However, an important factor that might have influenced the soil response was the perturbation induced to the samples during the trimming process. In fact, the vertical sample compressed to a p'=200kPa, underwent a significant perturbation during its trimming due to the presence of an aggregate of cemented particles which had to be partially removed. As in the case of the BRS-B material, more tests should be performed to draw a general conclusion on the effect of the in-situ structure of the VMClay on the stiffness at small strains.

In summary, no clear effects of in-situ structure could be observed on the behaviour of the VMClay and BRS-B at small strains. A more specific testing programme should be carried out to identify more comprehensively the effect of the naturally occurring structure of these materials.

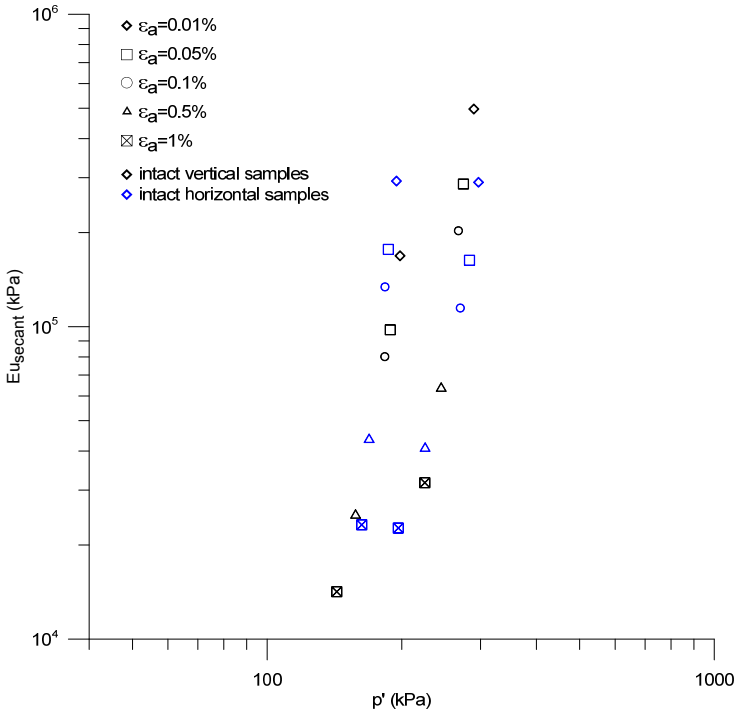

Figure 8.21 Undrained secant Young's modulus as a function of the current mean effective stress at different strain levels for vertically and horizontally intact cut samples of the VMClay

Chapter 9
Conclusions and recommendations for future work

9.1 Conclusions

The work presented in this thesis focused on investigating the effects of the naturally occurring structure on the mechanical behaviour of two young Holocene alluvial materials, the Italian Bormida River silts (BRS) and the Valencia silty soils (VSS) from the Turia River. Not much information about the effects of structure of young Holocene deposits can be found in the literature so this thesis was intended to provide more knowledge about the behaviour of this type of materials. It also provides the first example of a comparison between two young shallow (less than 5m deep) Holocene alluvial materials deposited in clearly different sedimentary conditions as a result of the different fluvial dynamics at each location. The samples of the BRS were retrieved from the foundation level of the river embankments in a meandering area which suggests alluvial depositional conditions subjected to frequent flooding events such as a natural levee. On the other hand the specimens of the VSS were taken far from the active river channel suggesting an alluvial depositional setting such as a flood plain.

A large number of examples could be found in the literature where stable forms of the initial structure created on reconstituted samples controlls the mechanical behaviour of the material in compression and shearing to large strains. In these cases a non-unique NCL or CSL can be defined for the reconstituted state which makes the term "intrinsic" lose its meaning. This soil behaviour was defined as "transitional". Another important objective of this thesis was to explore if this type of behaviour is affecting the soils analysed in this thesis which would invalidate any possible analysis of the effects of the natural structure.

An experimental programme was specifically defined where oedometer and triaxial tests on slurry, compacted and natural intact samples were carried out. The BRS materials tested consisted of an intact block sample (BRS-B) and a remoulded sample (BRS-E). The size distributions were different and unique for each soil and classified as clayey silt ML (BRS-B) and sandy silt CL-ML (BRS-E). In the case of the VSS an intact block sample was also retrieved (VMClay) together with two remoulded samples (VSSilt and VMSand) taken from a different location to that of the block. The size distribution of the material contained in the block sample VMClay was not unique and even more important the granulometry was not the same even within some of the specimens tested creating a certain degree of layering at a meso-structure scale. The remoulded samples VSSilt and VSSand were essentially homogeneous in terms of gradings and both yield a unique size distribution for each soil. The VSS were classified as a silty clay with aggregates of cemented particles CL (VMClay), silt/clay with sand CL-ML (VSSilt) and non-plastic silty sand SM (VMSand).

As described above, a large range of soils with different size distributions from sands to clays were tested in this thesis. In general a unique intrinsic normal compression line was found in all soils for slurry and compacted samples showing that the sample preparation technique had no effect on the uniqueness of the NCL. Only in the case of the BRS-E soil a clear transitional behaviour was found for the slurry specimens where the soil "remembered" its initial structure displaying a set of parallel compression lines until the ends of the tests, the location on the compression plane of which depended on the initial density. However, the compacted samples of the same soil converged onto a unique NCL in contrast to the transitional behaviour observed for the slurry specimens. Consequently and contrary to what was concluded in the literature, the sample preparation technique had a clear effect in triggering the transitional response, at least in one of the soils analysed in this thesis. This finding also agrees with the results obtained after re-analysing the transitional behaviour of other soils from the literature in which it had previously been concluded that the sample preparation technique does not create different structures which can result in non-convergence of the NCLs. The transitional behaviour observed in the BRS-E breaks down traditional concepts of

the uniqueness of the intrinsic compression line for slurry samples that has been used as a reference framework for evaluating the effect of structure in natural intact specimens in the oedometer. Unfortunately, no intact samples of the BRS-E were available for testing in this thesis, the effect of the structure of which would have been impossible to be investigated due to the non-uniqueness of the intrinsic compression line.

In terms of the intact samples of the VMClay and BRS-B materials, a clear effect of their naturally occurring structure was observed in the oedometer tests after normalisation, using the intrinsic compression line defined by the slurry samples in each case. A stable structure was found in both cases, even at very high stresses with stress sensitivity values still larger than unity at the ends of the tests. Very small effects of bonding, thought as a solid link, were exhibited by the samples despite the high quantity of calcium carbonate contained in the VMClay. The effect of the in-situ structure was more noticeable in the case of the VMClay where a higher degree of heterogeneity was observed inside the samples. This heterogeneity was characterised by a certain degree of layering observed within some samples at a meso-structure level, where parts of the specimens were more clayey/silty than others. In the case of the BRS-B intact samples no layering was observed, instead a heterogeneous micro-fabric that consisted of aggregates of particles was clearly identified by using SEM images. It is believed that the layering observed in the VMClay specimens had its origin on the dramatic changes in the rate and mode of deposition of the sediments of the Turia River which was very much influenced by seasonal flow and the variable proximity of the coast.

The one-dimensional compression behaviour of other late Holocene alluvial deposits like the Sibari and Pisa soils were compared with the VMClay and BRS-B materials. The normalised compression behaviour of the VMClay and BRS-B showed a similar trend on the effect of the in-situ structure as that of the Sibari and Pisa soils in which stable structures were found at high compression stresses. The stable structures displayed by the Sibari soils were related to the effect of layering, the effect of which was larger as the degree of heterogeneity inside the samples increased. As mentioned above, the effect of the in-situ structure of the VMClay, which exhibited a certain degree of layering at meso-structure scale in some specimens, was more noticeable compared with that of the BRS-B material, the structure of which was characterised by a heterogeneous fabric of aggregates of particles. These different structural features might be responsible for the higher offset of the normalised compression lines of the VMClay with respect to the BRS-B.

Only samples of the materials inside the block samples VMClay and BRS-B were tested in the triaxial apparatus. The mechanical behaviour at large strains of the

slurry and compacted samples, prepared with the trimmings of the intact specimens, showed that there exists a unique normal compression line and critical state line regardless of the sample preparation technique for both materials. Both lines were parallel in the range of stresses applied, as expected from the critical state framework. The normalised stress paths exhibited a clear dependency of the local state boundary surface on the type of test, that is, isotropic and anisotropic compression paths showed different local state boundary surfaces. Moreover, it was also found that the Rendulic's principle did not work. On the other hand, and although the mineralogy of both materials was different, an increased fines content reduced the dilatant response after the phase transformation point and, in the case of the anisotropically compressed samples, increased the undrained brittleness of the stress paths, the stress ratios q/p' of which were lower than those at the critical state.

The stress-strain behaviour of the intact samples was evaluated using the intrinsic response as a reference framework. The values of the stress ratio q/p' at the ends of the tests were essentially the same as the intrinsic values for both materials. It was also observed that in the case of the high pressure tests the values of q/p' were slightly lower than the intrinsic stress ratios for both materials, suggesting the possibility of a curved critical state line in the p':q plane at high stress levels.

The effect of the in-situ structure of the intact samples on the shearing behaviour at large strains was investigated by normalising their stress paths with respect to the p'_{cs} on the unique intrinsic critical state line of each material. On the wet side of the CSL*, a few samples of the BRS-B plotted outside the intrinsic local state boundary surface moving towards a different CSL in the compression plane, displaying the effect of the in-situ structure at large strains. In the case of the VMClay only one specimen plotted outside the intrinsic behaviour. On the dry side no significant effects of the in-situ structure were seen in any of the samples. It appears that fabric is the main part of the in-situ structure that had a noticeable effect on the behaviour of the VMClay and BRS-B, but its influence on the soil response at large strains was relatively small. This relatively small effect of the in-situ structure of the BRS-B and VMClay contrasts with that of the Sibari soils, the state boundary surfaces of which plotted well to the right of that of the reconstituted material, displaying a very robust and stable structure, in particular fabric, in shearing even at large strains.

At small strains, no clear effects of the in-situ structure or the sample preparation methods could be observed on the behaviour of the VMClay and BRS-B. However, and as a general trend, the undrained secant Young's moduli of the VMClay were higher than those of the BRS-B for a given mean effective stress and strain level. The variation of the effective stress level exponent of the stiffness (n) with the

shear strain increased with the strain level, moving towards unity for both materials as suggested by many authors. Slightly lower values were measured for the case of the VMClay which might reflect the different mineralogy and plasticity between the VMClay and BRS-B.

In summary it can be concluded that:

- Contrary to what was believed, the transitional behaviour of alluvial deposits at their reconstituted state is not that common as suggested by Nocilla et al. (2006). In fact only one material from the large range of soils tested in this thesis displayed that behaviour and it was triggered by the sample preparation technique. This latter result also contrasts with the statement that the sample preparation technique does not create different structures which can result in a transitional behaviour (e.g. Martins et al., 2001; Nocilla et al., 2006; Shipton 2010)

- The naturally occurring in-situ structure, in particular the fabric, of the intact shallow samples of the BRS-B and VMClay material was more robust and stable than those in their reconstituted states in compression. This robust stable structure does not imply that the intact behaviour is transitional but a clear effect of the in-situ structure which could not be removed by compression in the oedometer even at high stress levels. Similar results were found in other soils like for example the shallow samples of the Pisa clayey silt.

- Small effects of the in-situ structure were observed at large shearing strains and only on the wet side of the critical state. This suggests that the effects of any possible layering at a meso-structure scale of the VMClay as well as the effects of the heterogeneous fabric of the BRS-B characterised by the aggregates of particles of the BRS-B were practically removed during shearing.

- In general the mechanical behaviour of the soils tested in this thesis could be well described within a critical state framework.

9.2 Recommendations for future work

As was concluded above, the sample preparation method had a clear effect in creating stable initial structures, in particular in slurry specimens, which were not removed even at high stress levels in the oedometer tests for the BRS-E soil. It would be very interesting to investigate the evolution of the initial structure comparing slurry samples that displayed transitional behaviour with compacted specimens that converged onto a unique NCL. For doing so it is proposed to carry out porosimetry tests together with SEM photos at different stress levels.

Another possible recommendation for future work is continuing with the research on the effects of the natural occurring structure of the VMClay material. As described in Chapter 6 and shown in Figure 6.3, the block sample of the VMClay was taken from a shallow depth where alternating cohesive layers could be found. All these cohesive layers consist of clay/silt soils but buried at different depths. It would be interesting to investigate the effect of the depth on the structure of the soils.

References

Atkinson, J. H.; Fookes, P.G.; Miglio, B. F. and Pettifer, G. S. (2003). Destructuring and disaggregation of Mercia Mudstone during full-face tunnelling. Quarterly Journal of Engineering Geology and Hydrogeology, 36, pp. 293-303.

Alarcon-Guzman, A. and Leonards, G.A. (1988). Discussion: Liquefaction evaluation procedure. Journal of Geotechnical Engineering, ASCE 114, No. 2, 232-236.

Alarcon-Guzman, A., Leonards, G.A. and Chameau, J.L. (1988). Undrained monotonic and cyclic strength of sands. Journal of Geotechnical Engineering, ASCE 114, No. 10, 1089-1108.

Altaner, S.P. and Ylagan, R. (1997). Comparison of structural models of mixed-layer illite/smectite and reaction mechanisms of smectite illitization. Calys and clay minerals, 45, No. 4, 517-533.

Altuhafi, F. (1997). On the mechanical behaviour of glacial sediments. PhD thesis, University College London.

Altuhafi, F.N and Coop, M.R. (2011). Changes to particle characteristics associated with the compression of sands. Geotechnique 61, No. 6, 459-471.

Atkinson, J.H. (1993). The mechanics of soils and foundations. McGraw-Hill, London.

Bandini, V. and Coop, M.R. (2011). The influence of particle breakage on the location of the critical state line of sands. Soils & Foundations, in print.

Baudet, B. and Stallebrass, S. (2004). A constitutive model for structured clays. Geotechnique 54, No. 4, 269-278.

Been, K. and Jefferies, M. (1985). A state parameter for sands. Geotechnique 35, No. 2, 99-112.

Been, K., Jefferies, M.G. and Hachey, J. (1991). The critical state of sands. Geotechique 41, No. 3, 365-381.

Booth, J.S and Dahl, A.G. (1986). A note on the relationships between organic matter and some geotechnical properties of marine sediments. Marine Geotechnology, 6 (3), 281-297.

Bouckovalas, G.D., Andrianopoulos, K.I. and Papadimitriou (2003). A critical state interpretation for the cyclic liquefaction resistance of silty sands. Soil Dynamics and Earthquake Engineering 23, No. 2, 115-125.

Burland, J.B. (1967). Deformation of soft clay. PhD thesis, University of Canmbridge.

Burland, J.B. (1990). On the compressibility and shear strength of natural clays. Geotechnique 40, No. 3, 329-378.

Burland, J.B., Rampello, S., Georgiannou, V.N. and Calabresi, G. (1996). A laboratory study of the strength of four stiff clays. Geotechnique 46, No. 3, 491-514.

Butterfield, R. (1979). A natural compression law for soils (an advance on e-logp'). Geotechnique 29, No. 1, 62-65.

Callisto, L. and Rampello, S. (2004). An interpretation od the structural degradation for three natural clays. Canadian Geotechnical Journal, 41, 392-407.

Carrera, A. (2008). Mechanical behaviour of Stava tailings. PhD thesis. Poitecnico di Torino.

Carrion, M.A. (2006). Influence of the aggregated fabric on the behaviour of the Mercia mudstone. Msc thesis. Imperial College, University of London.

Casagrande, A. (1936). Characteristics of cohesionless soils affecting the stability of slopes and earth fills. Journal of Boston Society of Civil Engineers 23, No. 1, 13-32.

Chandler, H.W. (1985). A plasticity theory without Drucker's postulate, suitable for granular materials. J. Mech, Phys. of Solids 33, 215-226.

Chang, N., Heymann, G. and Clayton, C. (2011). The effect of fabric on the behaviour of gold tailings. Geotechnique 61, No. 3, 187-197.

Cheng, Y.P., Nakata, Y. and Bolton, M.D. (2005). Grain crushing and critical states observed in DEM simulations. Powders and Grains, Taylor and Francis, London, Vol. 2, 1393-1397.

Chuhan, F.A., Kjeldsatd, A., Bjorlykke, K., Hoeg, K. (2003). Experimental compression of loose sands: relevance to porosity reduction during burial in sedimentary basins. Canadian Geotechnical Journal 40, No. 5, 995-1011.

Coop, M.R. (1990). The mechanics of uncemented carbonate sands. Geotechnique 40, No. 4, 607-626.

Coop, M.R. and Cotecchia, F. (1995). "The Compression of Sediments at the Archaelogical Site of Sibari. Proceedings of the XI European Conference on Soil Mechanics and Foundation Engineering, Copenhagen, 8.19-8.26. Danish Geotechnical Society.

Coop, M.R. and Cotecchia, F. (1997). The geotechnical settlements of the archaeological site of Sibary. Proceedings of the Arigo Croce Memorial Symposium, Geotechnical Engineering for the Preservation of Monuments and Hostoric Sites, Naples. 138-149. Balkema,Rotterdam.

Coop, M.R. and Lee, I.K. (1993). The behaviour of granular soils at elevated stresses. In G.T. Houlsby and A.N. Schofield (Eds.), Proceedings Wroth Memorial Symposium – Predictive Soil Mechanics, Oxford, 186-198. Thomas Telford.

Coop, M.R., Sorensen, K.K., Bodas Freitas, T. and Georgoutsos, G. (2004). Particle breakage during shearing of a carbonate sand. Geotechnique 54, No. 3, 157-163.

Coop, M.R., Atkinson, J.H. and Taylor, R.N. (1995). Strength, yielding and stiffness of structured and unstructured soils. Proceedings 11th ECSMFE, Copenhagen, Vol. 1, 55-62.

Costa-Filho, L.M. (1980). A laboratory investigation of the small strain behaviour of London Clay. PhD thesis, Imperial College, University of London.

Cotecchia, F. (1996). The effects of structure on the properties of an Italian Pleistocene clay. PhD thesis, Imperial College, University of London.

Cotecchia, F. and Chandler, R.J. (2000). A general framework for the mechanical behaviour of clays. Geotechnique 50, No. 4, 431-447.

Davison, L.R. and Atkinson, J.H. (1990): Continuous loading oedometer testing of soils. Quarterly Journal of Engineering Geology 23, 347-355.

DeGregorio, V.B. (1990). Loading systems, sample preparation, and liquefaction. Journal of Geotechnical Engineering, ASCE, 116, No. 5, 805-821.

Dennis, N.D. (1988). Liquefaction evaluation procedure: Discussion, Journal of Geotechnical Engineering, ASCE, 114, No. 2, 241-243.

Desrues, J., Lanier, J. and Stutz, P. (1985). Localization of the deformation in tests on sand sample. Eng. Fract. Mech., 21, No. 4, 909-921.

Desrues, J. (1992). Strain localisation in geomaterials: experimental basis. Programma di Istruzione Permanente, Politecnico di Milano.

Dumbleton, M.J. (1967). Origin and mineralogy of African red clays and Keuper Marl. Quarterly Journal of Engineering Geology, 1, pp. 39-45.

Einav, Itai. (2007). Breakage mechanics – Part I: theory. Journal of the Mechanics and Physics of Solids, 55 No. 6, 1274-1297.

Einav, Itai. (2007). Breakage mechanics – Part II: Modelling granular material. Journal of the Mechanics and Physics of Solids, 55, No. 6, 1298-1320.

Fearon, R. and Coop, M.R. (2000). Reconstitution: what makes an appropriate reference material? Geotechnique 50, No. 4 471-477.

Fearon, R. and Coop, M.R. (2002). The influence of landsliding on the behaviour of a structurally complex clay. Quarterly Journal of Engineering Geology and Hydrogeology 35, No. 1, 25-32.

Ferreira, P.M.V. and Bica, A.V.D (2006). Problems on the identification of structure in a soil with transitional behaviour. Geotechnique 56, No. 7, 445-454.

Finno, R.J. and Rechenmacher, A.L. (2003). Effects of consolidation history on critical state of sand. Journal of Geotechnical and Geoenvironmental Engineering, ASCE 129, No. 4, 350-360.

Finno, R.J., Harris, W.W., Mooney, M.A. and Viggiani, G. (1996). Strain localization and undrained steady state of sands. Journal of Geotechnical Engineering 122, No. 6, 462-473.

Fraser, H.J. (1935). Experimental study of the porosity and permeability of clastic sediments. Journal of Geology 43, No. 8, 910-1010.

Gasparre, A. (2005). Advanced laboratory characterisation of London clay. PhD thesis, Imperial College, University of London.

Gens, A. (1982). Stress-strain and strength characteristics of a low plasticity clay. PhD thesis, Imperial College, University of London.

Georgiannou, V.N., Hight, D.W., Burland, J.B. (1990). The undrained behaviour of clayey sands in triaxial compression and extension. Geotechnique 40, No. 3, 431-449.

Hardin, B.O. (1985). Crushing of soils particles. Journal of Geotechnical and Geoenvironmental Engineering, ASCE 111, No. 10, 1177-1192.

Hesseini Kamal, R. (2012). Experimental study of the geotechnical properties of UK mudrocks. PhD Thesis, Imperial College, London.

Hosseini Kamal, R., Coop, M.R, Jardine, R.J., Brosse, A. (2014). The post-yield behaviour of four Eocene-to-Jurassic UK stiff clays. Geotechnique 64, No. 8, 620-634.

Ishihara, K. (1993). Liquefaction and flow failure during earthquakes. Geotechnique 43, No. 3, 351-415.

Ishihara, K., Cubrinovski, M. and Nonaka, T. (1998). Characterization of undrained behaviour of soils in the reclaimed area of Kobe. Soils and Foundations 37, No. 3, 33-46.

Ishihara, K., Tatsuoka, F. and Yasuda, S. (1975). Undrained deformation and liquefaction of sand under cyclic stresses. Soils Foundations 15, No. 1, 29-44.

Jaky (1944). The coefficient of earth pressure at rest. Journal of the Society of Hungarian Architects and Engineers, 355-358.

Jefferies, M. and Been, K. (2000). Implications for critical state theory from isotropic compression of sands. Geotechnique 50, No. 4, 419-429.

Jefferies, M.G. (1993). Nor-Sand: a simple critical state model for sand. Geotechnique 43, No. 1, 91-103.

Jovicic, V. and Coop, M. R. (1997). Stiffness of coarse –grained soils at small strains. Geotechnique 47, No. 3, 545-561.

Konrad, J.M. (1998). Sand state from cone penetrometer tests: a framework considering grain crushing stress. Geotechnique 48, No. 2, 201-215.

Kuerbis, R., Negussey, D. and Vaid, Y.P. (1998). Effect of gradation and fines content on the undrained response of sand. In Van Zyl, D.J.A and Vick, S.G. (Eds.), Hydraulic Fill Structures, Geotechnical Special Publication 21, ASCE, 330-345.

Kwag, J.M., Ochiai, H. and Yasufuku, N. (1999). Yielding stress characteristics of carbonate sand in relation to individual particle fragmentation strength. In Engineering for calcareous sediments. Al-Shafei, K.A. (Ed). A.A. Balkema, Rotterdam, the Netherlands, 79-87.

Lade, P.V. and Yamamuro, J.A. (1997). Effects of non-plastic fines on static liquefaction of sands. Canadian Geotechnical Journal 34, 918-928.

Lade, P.V., Liggio, C.D. and Yamamuro, J.A. (1998). Effects of non-plastic fines on minimum and maximum void ratios of sand. Geotechnical Testing Journal 21, No. 4, 336-347.

Leonard, G.A. and Ramiah, B.K. (1959). Time effects in the consolidation of clay. ASTM Special Technical Publication. No. 254, Philadelphia, 116-130.

Leroueil, S. and Vaughan, P.R. (1990). The general and congruent effects of the structure in natural soils and week rocks. Geotechnique 40, No. 3, 467-488.

Martins, F.B., Bressani, L.A., Coop, M.R. and Bica, A.V.D. (2001). Some aspects of the compressibility behaviour of a clayey sand. Canadian Geotechnical Journal 38, No. 6, 1177-1186.

Mayne, P.W. and Kulhawy, F.H. (1982). Ko-OCR relationships in soils. Journal of the Geotechnical Engineering Division, ASCE, vol. 108, 851-872.

McDowell, G.R. and Bolton, M.D. (1998). On the micromechanics of crushable aggregates. Geotechnique 48, No. 5, 667-679.

McDowell, G.R., Bolton, M.D. and Robertson, D. (1996). The fractal crushing of granular materials. Journal of the Mechanics and Physics of Solids, 44, 2079-2102.

McGeary, R.K. (1961). Mechanical packing of spherical particles. Journal of the American Ceramic Society 44, No. 10, 513-522.

Mesri, G. and Vardhanabhuti, B. (2009). Canadian Geotechnical Journal 46, No. 4, 369-392.

Mitaritonna, G., Amorosi, A., Cotecchia, F. (2013). Experimental investigation of the evolution of elastic stiffness anisotropy in a clayey soil. Geotechnique 64, No. 6, 463-475.

Mitchel, J.K. and Soga, K. (2005). Fundamentals of Soils Behaviour. 3rd ed. Wiley and Sons., New Jersey.

Mitchell, J.K. (1976). Fundamental of soils behaviour. Wiley, New York.

Mitchell, J.K. (1993). Fundamentals of Soils Behaviour. 2nd ed., Wiley, New York.

Mooney, M.A. (1996). An experimental study of strain localization and the mechanical behaviour of sand. PhD thesis, Northwestern University, Evanston, I11.

Mooney, M.A., Finno, R.J. and Viggiani, G. (1998). A unique critical state for a sand?. Journal of Geotechnical and Geoenvironmental Engineering 124, No. 11, 1128-1138.

Muir Wood, D. (2008). Critical states and soil modelling. In Burns, Mayne, and Santamarina (Eds.), Deformation Characteristics of Geomaterials, Vol. 1, IOS Ansterdam, 51-72.

Muir Wood, D. and Maeda, K. (2008). Changing grading of soil: effect on critical states. Acta Geotechnica, online.

Murthy, T.G., Loukidis, D., Carraro, J.A.H., Prezzi, M. and Salgado, R. (2007). Undrained monotonic response of clean and silty sands. Geotechnique 57, No. 3, 273-288.

Naeini, S.A. and Baziar, M.H. (2004). Effect of fines content on steady-state strength of mixed and layered samples of a sand. Soil Dynamics and Earthquake Engineering 24, No. 3, 181-187.

Negussey, D. and Islam, M.S. (1994). Uniqueness of steady state and liquefaction potential. Canadian Geotechnical Journal 31, 132-139.

Ni, Q., Tan, T.S., Dasari, G.R., and Hight, D.W. (2004). Contribution of fines to the compressive strength of mixed soils. Geotechnique 54, No. 9, 561-569.

Nocilla, A., Coop, M.R. and Colleselli, F. (2006). The mechanics of an Italian silt; and example of "transitional" behaviour. Geotechnique 56, No. 4, 261-271.

Pestana, J.M. and Whittle, A.J. (1995). Compression model for cohesionless soils. Geotechnique 45, No. 4, 611-631.

Polito, C.P. (1999). The effects of non-plastic and plastic fines on the liquefaction resistance of soils. PhD thesis, Department of Civil Engineering, The Virginia Polytechnic Instituted and State University, Blacksburg, Va.

Polito, C.P. and Martin J.R. (2001). Effects of nonplastic fines on the liquefaction resistance of sands. Journal of Geotechnical and Geoenvironmental Engineering 127, No. 5, 408-415.

Poulos, S.J. (1981). The steady state of deformation. Journal of Geotechnical Engineering Division, ASCE 107, No. 5, 553-562.

Poulos, S.J., Castro, G. and France, J.W. (1988). Liquefaction evaluation procedure: Reply. Journal of Geotechnical Engineering, ASCE, 114, 232-256.

Porovic, E and Jardine, R.J (1994). Some observation on the static andd dynamic shear stiffness of Ham River sand. Proc. IS-Hokkaido, Balkema, Rotterdam, Vol. 1, 25-30.

Radici, F. (2006). Analisi sperimentale del comportamento dei terreni di fondazione degli argini del Po. Tesi di laurea specialistica. Univerisita Degli Studio di Brescia. Faculta di Ingegneria. In Italian.

Rahman, M.M., Lo, S.R. and Gnanendran, C.T. (2008). On equivalent granular void ratio and steady state behaviour of loose sand with fines. CanadianGeotechnical Journal 45, 1439-1456.

Rampello, S. and Callisto, L. (1998). A study on the subsoil of the Tower of Pisa based on the results from standard and high-quality samples. Canadian Geotechnical Journal, 35, 1074-1092.

Riemer, M.F. and Seed, R.B. (1997). Factors affecting apparent position of steady-state line. Journal of Geotechnical and Geoenvironmental Engineering Division, ASCE 123, No. 3, 281-288.

Riemer, M.F., Seed, R.B., Nicholson, P.G. and Jog, H.L. (1990). Steady state testing of loose sands: Limiting minimum density. Journal of Geotechnical Engineering 116, No. 2, 332-337.

Roberts, J.E. and de Souza, J.M. (1958). The compressibility of sands. Proceedings of the American Society for Testing and Materials 58, 1269-1272.

Roscoe, K.H. (1970). The influence of strain in soil mechanics. Geotechnique 20, No. 2, 129-170.

Roscoe, K.H., Schofield, A.N. and Wroth, C.P. (1958). On the yielding of soils. Geotechnique 8, No. 1, 22-52.

Russell, A.R. and Khalili, N. (2004). A bounding surface plasticity model fro sands exhibiting particle crushing. Canadian Geotechnical Journal 41, 1179-1192.

Sadrekarimi, A. and Olson, S.M. (2009). A new ring shear device to measure the large displacement shearing behaviour of sands. Geotechnical Testing Journal 32, No. 3, 197-208.

Sadrekarimi, A. and Olson, S.M. (2011). Yield strength ratios, critical strength ratios, and brittleness of sandy soils from laboratory tests. Canadian Geotecnical Journal 48, 493-510.

Sandroni, S.S. (1977). The sthrenght of London Clay in total and effective shear stress terms. PhD thesis, Imperial College, University of London.

Santucci de Magistris, F., Silvestri, F. and Vinale, F. (1998). The influence of compaction on the mechanical behaviour of a sitly sand. Soils and Foundations 38, No. 4, 41-56.

Sarti, G., Rossi, V. and Amorosi, A. (2012). Influence of Holocene stratigraphic architecture on ground surface settlements: A case study from the City of Pisa (Tuscany, Italy). Sedimentary Geology 281, 75-87.

Shipton, B. (2010). The mechanics of transitional soils. PhD thesis, Imperial College London.

Schmertmann, J.H. (1969). Swell sensitivity. Geotechnique 19, No. 41, 530-533.

Smith, P.R. (1992). The behabiour of natural high compressibility clays with special reference to consolidation on soft ground. PhD thesis, Imperial College, University of London.

Thevanayagam, S. (1998). Effect of fines and confining stress on undrained shear strength of silty sands. Journal of Geotechnical and Geoenvironmental Engineering, ASCE 124, No. 6, 479-491.

Thevanayagam, S. and Mohan, S. (2000). Intergranular state variables and stress-strain behaviour of silty sands. Geotechnique 50, No. 1, 1-23.

Thevanayagam, S., Shenthan, T., Mohan, S. and Liang, J. (2002). Undrained fragility of clean sands, silty sands, and sandy silts. Journal of Geotechnical and Geoenvironmental Engineering 128, No. 10, 849-859.

Vaid, Y., Chung, E.K.F and Keurbis, R.H. (1990). Stress path and steady state. Canadian Geotechnical Journal 27, No. 1, 1-7.

Verdugo, R. and Ishihara, K. (1996). The steady state of sandy soils. Soils and Foundations 36, No. 2, 81-91.

Vesic, A.S. and Clough, G.W. (1968). Behaviour of granular materials under high stresses. Journal of Soil Mechanics and Foundation Division, ASCE 94, No. 3, 661-668.

Viggiani, G and Atkinson, J.H. (1995). Stiffness of fine-grained soil at very small strains. Geotechnique 45, No. 1, 149-154.

Vilhar, G., Jovicic, V., Coop, M.R. (2013). The role of particle breakage in the mechanics of a non-plastci silty sand. Soils and Foundations, 53, 91-104.

Vitone, C. and Cotecchia, F. (2011). The influence of intense fissuring on the mechanical behaviour of clays. Geotechnique 61, No. 12, 1003-1018.

Wang, Z., Dafalias, Y.F., Li, X.S. and Makdisi, F.I. (2002). State pressure index for modelling sand behaviour. Journal of Geotechnical and Geoenvironmental Engineering, ASCE 128, No. 6, 511-519.

Wroth, C.P. (1972). General theories of earth pressures and deformations. Proceedings of the 5th European Conference on Soil Mechanics and Foundation Engineering, Madrid, Vol 2, 33-52.

Wroth, C.P. (1975). In-situ measurements of critical stresses and deformations characteristics. Proceedings of Specialty Conference on In-situ Measurements of Soils Properties, ASCE, Raleigh, 181-230.

Wroth, C.P, & Basset, R.H. (1965). A stress-strain relationship fro the shearing behaviour of sand. Geotechnique 15, No. 1, 32-56.

Yang, S.L., Lacase, S. and Sandven, R. (2006). Determination of the transitional fines content of mixtures of sand and non-plastic fines. Geotechnical Testing Journal, ASTM 29, No. 2, 102-107.

Yang, S.L., Sandven, R. and Grande, L. (2006). Steady-state lines of sand silt mixture. Canadian Geotechnical Journal 43, No. 11, 1213-1219.

Ying, J.H. (1999). Properties and behaviour of Hong Kong marine deposits with different clay contents. Canadian Geotechnical Journal 36, No. 6, 1085-1095.

Zlatović, S. and Ishihara, K. (1995). On the influence of nonplastic fines on residual strength. In Ishihara, K. (Ed.), Proceedings of International Conference on Earthquake Geotechnical Engineering, Balkema, Rotterdam, The Netherland, 239-244.